Analysis & Tools to Spur Increased Deployment of "Waste Heat" Rejection/Recycling Hybrid Ground-source Heat Pump Systems in Hot, Arid or Semiarid Climates Like Texas

Final Report

September 2013

DoE Award Number: DE-EE0002803
Sponsor: U.S. Department of Energy, Recovery Act

Co-PI: Glenn Y. Masada, University of Texas at Austin
masada@mail.utexas.edu (512) 471-3061
Co-PI: Paul Ballentine, University of Rochester
Co-PI: Tess J. Moon, University of Texas at Austin
Partners: ClimateMaster Geothermal Heat Pump Systems
Good Company Associates
ToolWerks
Sollenium

This material is based upon work supported by the U.S. Department of Energy's Office of Energy Efficiency and Renewable Energy's (EERE) Building Technologies Program under Award Number EE-0002803.

TABLE OF CONTENTS

LIST OF ACRONYMS AND ABBREVIATIONS

ASHRAE	American Society of Heating, Refrigerating, and Air Conditioning Engineers
COP	Coefficient of performance
CWCT	Wet closed cooling tower
DNI	Direct normal irradiance
EER	Energy efficiency ratio
EWT	Heat pump entering water temperature
GHP	Ground source heat pump
GLHEPRO	Ground Loop Heat Exchanger Program
HAMBASE	Heat Air and Moisture model for Building And Systems Evaluation program
HGHP	Hybrid ground source heat pumps
HVAC	Heating, ventilation and air-conditioning
SHR	Supplemental heat rejection/recovery
TRNSYS	TRaNsient SYstem Simulation program
TMY	Typical meteorological year data
VAV	Variable-air-volume
VCC	Vapor compression cycle

NOMENCLATURE

T - temperature (°C)
ϕ - relative humidity
h - enthalpy (kJ/kg)
$\dot{m}$ - mass flow rate (kg/s)
$\dot{Q}$ - energy rate (kJ/s)
$\dot{Q}_{Latent}$ - Rate of latent cooling (kJ/s)
ω - humidity ratio
c,C - heat capacity (kJ/kg/K)
H - borehole length (m), humidity ratio
q - heat flux (kJ/m^2)
t - time (seconds)
r_b - radius of borehole (m)
α - thermal diffusivity (m^2/s)
R_{BH} - equivalent borehole thermal resistance
t_s - steady state time (seconds)
z - distance along depth of borehole (m)
V - volumetric flow rate of water (m^3/s)
v_w -specific volume (m^3/kg)
G -mass velocity on minimum area (kg/(s m^2))
k -mass transfer coefficient (kg/(s m^2))
k_w -mass flow rate (kg/s)
m -mass transfer coefficient (kg/(s m^2))
q - rate of heat transfer (W)
α -convective heat transfer coefficient (W/(m^{2}K))
P - pressure (Pa)
η - efficiency
W - pump work (W)
EWT - heat pump entering water temperature (°C)
TMY -typical meterological year weather data

Subscripts

db - dry bulb
wb - wet bulb
DA - dry air
WV - water vapor
IN - at inlet
OUT - at exit
cond - condensation
BH - borehole
rad - radiation/wall
w - water
fg -latent heat vaporization
a -air
L -latent heat
sh -sensible heat
c -cooling water
e -evaportation
s -spray
1,2 -inlet, outlet

ACKNOWLEDGEMENTS

The financial support from the Department of Energy, Recovery Act, is greatly appreciated. The cost-share and technical support from ClimateMaster, Good Company Associates, ToolWerks, and Sollenium were instrumental in the successful completion of this work. Individuals that contributed to this work include:

Paul Ballentine	Sollenium, Austin, TX
Mike Hammond, Paul Bony, and Dee Brower	ClimateMaster, Oklahoma City, OK
Chris Winland	Good Company Associates, Austin, TX
Mel Riser	ToolWerks, Austin, TX
Jeffrey Spitler	Oklahoma State University, Stillwater, OK

Students who participated directly in this work include:

Jonathan Gaspredes	Graduate research assistant
Siddharth Balasubramanium	Graduate research assistant
Jacob Blair	Graduate research assistant
Siddharth Shah	Undergraduate research assistant

Also, 21 mechanical engineering senior students in seven different design project groups investigated various aspects of the project.

ABSTRACT

This project team analyzed supplemental heat rejection/recovery (SHR) devices or systems that could be used in hybrid ground source heat pump (HGHP) systems located in arid or semi-arid regions in southwestern U.S. Identification of effective SHR solutions would enhance the deployment of ground source heat pumps (GHP) in these regions. In a parallel effort, the team developed integrated GHP models that coupled the building load, heat pump, and ground loop subsystems and which could be applied to residential and commercial office buildings. Then GHP and HGHP performances could be compared in terms of operational performance and life-cycle costs.

Several potential SHR devices were analyzed by applying two strategies: 1) to remove heat directly from the water in the ground loop before it enters the ground and 2) to remove heat in the refrigerant loop of the vapor compression cycle (VCC) of the heat pump so less heat is transferred to the water loop at the condenser of the VCC. Cooling towers, adsorption coolers, and thermoelectric liquid coolers were included in strategy 1, and expanded desuperheaters, thermosyphons, and an optimized VCC were included in strategy 2. Of all SHR devices analyzed, only the cooling tower provided a cost-effective performance enhancement.

For the integrated GHP model, the project team selected the building load model HAMBASE and its powerful computational Simulink/MatLab platform, empirical performance map models of the heat pumps based upon manufacturers' performance data, and a ground loop model developed by Oklahoma State University and rewritten for this project in Simulink/MatLab. The design process used GLHEPRO, also from Oklahoma State University, to size the borehole fields. The building load and ground loop models were compared with simulations from eQuest, ASHRAE 140-2008 standards, EnergyPlus, and GLHEPRO and were found to predict those subsystems' performance well. The integrated GHP model was applied to a 195m^2 (2100ft^2) residential building and a 4,982m^2 (53,628ft^2) three-story commercial office building, and it ran 10-15 year simulations. The integrated GHP model and its Simulink platform provided residential data, ranging from seconds to years, and commercial office building data, ranging from minutes to years.

A cooling tower model was coupled to the base case integrated GHP model for the residential building and the resulting HGHP system provided a cost-effective solution for the Austin, TX location. Simulations for both the residential and commercial building models were run with varying degrees of SHR (device/system not identified) and the results were found to significantly decrease installation costs, increase heat pump efficiency (lower entering water temperature), and prolong the lifetime of the borehole field. Lifetime cycle costs were estimated from the simulation results.

Sensitivity studies on system operating performance and lifetime costs were performed on design parameters, such as construction materials, borehole length, borehole configuration and spacing, grout conductivity, and effects of SHR. While some of the results are intuitive, these studies provided quantitative estimates of improved performance and cost. One of the most important results of this sensitivity study is that overall system performance is very sensitive to these design parameters and that modeling and simulation are essential tools to design cost-effective systems.

1.0 EXECUTIVE SUMMARY

Despite their potential to reduce residential and commercial electricity consumption by 40–70%, ground–source (or ground–coupled) heat pump (GHP) systems have made few inroads into the hot, arid or semi–arid climates of Texas and, more generally, the southwestern United States. In these regions severe geology and hydrology issues, such as relatively high ground temperatures and limited ground water, require ground loops over 91.4 meters (300 feet) deep to satisfy the cooling-dominated building thermal loads for more than 10-15 years of operation. The key technical and economic issues that impede the deployment of GHPs systems include high initial installation costs, engineering required to size system components, and space requirements needed to avoid ground coupling heating imbalance that can reduce heat pump efficiency after 7-10 years [Fisher & Rees, 2005; Navigant, 2009]. One approach to reduce initial costs and balancing the net heat to the ground is to add supplemental heat rejection/recycling (SHR) devices, such as cooling towers; these hybrid ground-source heat pump (HGHP) are often employed in commercial buildings.

This project's fundamental aim was to develop integrated models capable of accurately representing (1) building loads of various building types and sizes (*e.g.,* residential, commercial, government, schools and universities), (2) HVAC and commercially-available GHPs, (3) local climate history (*e.g.,* temperature, humidity, irradiation, etc.), (4) building site characteristics (*e.g.,* geology, hydrology), and (5) proposed SHR strategies. These models were then used to estimate the effects of 'waste heat' from SHR devices and assess the technical and economic feasibility of deploying GHP and HGHP systems in hot, arid or semi-arid regions. The accomplished tasks from this project are as follows.

- **SIMULINK-BASED INTEGRATED GHP/HGHP SYSTEM MODEL**

Component models for (1) building thermal loads, (2) ground source heat pumps, (3) vertical borehole-ground, and (4) SHR devices were coupled into integrated GHP/HGHP models using the MatLab/Simulink® environment to take advantage of Simulink®'s powerful built-in computational and integration algorithms [Mathworks, 2011]. The integrated models can simulate responses every 30 seconds to 20 years of operation. Each model is summarized below.

Building Load Thermal Model: HAMBASE (**H**eat **A**ir and **M**oisture model for **B**uilding **A**nd **S**ystems **E**valuation), developed at the Eindhoven University of Technology, was selected as the building load model [de Wit, 2006]. It is implemented as a Simulink® function block and is

based on zones, with each zone governed by coupled mass and heat transfer differential equations for temperature and humidity. Typical Meteorological Year, version 3 (TMY) data sets are used for environmental inputs.

The building load model was validated with the ASHRAE140-2007 standard [ASHRAE, 2007] and with eQuest simulations for residential applications and with open-loop comparisons with EnergyPlus for DoE's Commercial Reference Building Models [US DoE, 2010] for a commercial building application.

Ground Source Heat Pump: An empirical model was developed based upon available manufacturer's data for the ANSI/ASHRAE/ARI/ISO 13256-1 standard for rating and testing water source heat pumps. The model calculates heat pump latent and sensible cooling capacities and heat exchange with the ground loop.

Vertical Borehole-Ground: The vertical borehole-ground model was based on Eskillson's hybrid analytical-numerical approach using g-functions for long-time responses (10-20 years) and Oklahoma State University modification of the Eskillson's approach by Xu to allow short-term responses (30 seconds) [Ekillson, 1987; Xu, 2007]. The borehole lengths were sized with GLHEPRO (**G**round **L**oop **H**eat **E**xchanger **P**rogram [Spitler, 2000; Oklahoma State, 2010]. The coupled ground source heat pump and vertical borehole-ground loop model was validated with GLHEPRO simulations.

SHR Device: Several SHR devices and approaches were analyzed for GHP applications, including enhanced desuperheater, thermosyphons, cooling towers, optimized refrigeration cycle, thermoelectrics, and storage tanks. A compact cooling tower model was coupled to the integrated GHP model for residential applications.

- **INTEGRATED RESIDENTIAL BUILDING APPLICATION**

The integrated building load-GHP model that coupled the building load, ground source heat pump, and vertical borehole-ground models (see above) was applied to a base case residential house using a limiting ground loop sizing criterion of using the heat pump shutoff temperature of 48.9^{o}C (120^{o}F) as the maximum heat pump entering water temperature (EWT). This criterion provided the shortest possible borehole lengths. Various model parameters were then varied from the base case values to assess their effects on GHP performance; these parameters included borehole length, borehole configuration, grout thermal conductivity, ground temperature, and SHR heat rejection.

Base Case: A 195m^2 (2100ft^2) one-story, single family, four occupant, residential building model was developed for operation in cooling-dominated Austin, TX (construction details and ground properties are given in the main text—Section 4.6). The GHP system used a 14.6kW (4-ton) ClimateMaster Tranquility 20 Series single speed heat pump and the ground loop was sized using GLHEPRO for 10-year operation with the maximum heat pump EWT at 48.9C (120F), which resulted in four in-line boreholes, spaced on 4.6 meters (15 feet) centerlines and each 68.6 meters (225 feet) deep. The heating and cooling temperature set points were 21^{o}C and 25^{o}C, respectively, with a 1^{o}C deadband. The model uses 30 second time steps for the entire model except for the ground loop model, which is updated every five minutes. Results show that over a 15-year period, despite increases in local ground temperature due to the imbalance in energy transfer to the ground, the system controlled the condition space temperatures to set point within the allowable ASHRAE standards.

Sensitivity Studies: Based upon the base case above, sensitivity studies were conducted on borehole length, borehole configuration (in-line vs square and centerline spacing), grout thermal conductivity, ground temperature, and amount of SHR heat rejection. Performance criteria included the heat pump EWT (affects heat pump efficiency) and the number of unmet hours (300 hours)—number of hours/year where the hourly-averaged temperatures exceeded the set point limits. The main results of these studies are summarized below:

Borehole Length (Base case: 68.6m/borehole (225ft/borehole), 4 boreholes)

a) The base case borehole length provided the lower limit for adequate performance.
b) A 5% decrease in length resulted in an under-designed system—number of unmet hours exceeded limits; results a) and b) show that the limiting borehole sizing criterion used is valid.
c) Increasing borehole length from the base case to 91.4m (300ft)/borehole, typical of Austin, TX, and 100.6m (330ft)/borehole decreased the maximum heat pump EWT from 48.9^{o}C (120^{o}C) to 41.7^{o}C (107^{o}F) and 40^{o}C (104^{o}F), respectively, after 15 years of operation.

Borehole Length Conclusion: Borehole lengths longer than the base case length lowered heat pump EWT, improved heat pump efficiency, significantly lowered electricity costs, and increased borehole lifetime. Even with the increased initial drilling costs, the net savings with subsidies can be significant.

Borehole Configuration and Spacing (Base case: 4 boreholes, in-line with 4.6m (15ft) centerline spacing: e.g. notation 1x4x15—in-line, four boreholes and15ft centerline spacing)

Comparisons were made between boreholes configured in-line (1x4) and square (2x2) and

varying centerline spacing between boreholes.

a) For the in-line configuration, the base case centerline spacing provided the lower limit for adequate performance. Borehole spacing less than 4.6m (15ft) resulted in an under-designed system. For 3.04m (10ft) centerlines, the cooling capacity (in MWh) of the heat pump was reduced by 1.4% compared to the base case capacity in year 10 of operation.
b) For the square configuration (2x2), centerline spacing of 4.6m (15ft) resulted in an under-designed system. For the 2x2x15 and 2x2x10 cases, the total yearly cooling capacity (in MWh) of the heat pump was reduced by 0.7% and 3.3%, respectively, in year 10 of operation. The minimum spacing for the 2x2 configuration that provided adequate GHP performance was 6.1m (20ft).
c) For a given centerline spacing, the in-line configuration was more efficient than the square configuration. Compared to the base case at 10 years of operation, increasing spacing to 6.1m (20ft) increased the heat pump EER by 3% for the in-line configuration while the square configuration case yielded the same EER as the base case.

Borehole Configuration and Spacing Conclusion: Using the in-line configuration with maximum allowable centerline spacing lowered heat pump EWT, improved heat pump efficiency, lowered electricity costs, and increased borehole lifetime for virtually no additional costs.

Grout Thermal Conductivity (Base case: Bentonite grout with 0.744 W/m/K (0.43 Btu/(hr ft F)) thermal conductivity)

a) For improper backfilling, represented by 0.50 W/m/K (0.29 Btu/(hr ft F)) thermal conductivity, the resulting GHP system was under-designed.
b) Compared to the base case, using thermally enhanced grouts of 1.00 W/m/K (0.58 Btu/(hr ft F)), 1.333 W/m/K (0.78 Btu/(hr ft F)) (ground thermal conductivity), and 1.500 W/m/K (0.87 Btu/(hr ft F)) reduced the mean hourly averaged heat pump EWT in year 10 of operation by 0.5^{o}C, 1^{o}C, and 2^{o}C (1^{o}F, 2^{o}F, and 4^{o}F), respectively.

Grout Thermal Conductivity Conclusion: Increasing the grout thermal conductivity lowered heat pump EWT, improved heat pump efficiency, moderately lowered electricity costs, and increased borehole lifetime, but the added cost of enhanced grout may be greater than the savings in electricity cost.

Ground Temperature (Base case: 22.8^{o}C (71.2^{o}F))

Ground temperatures in Texas range from 15.6^{o}C (60^{o}F) in the Panhandle area to 27.2^{o}C (81^{o}F) in the border regions. While ground temperatures are location specific, this study looked at the effects of different ground temperatures from the base case.

a) For ground temperatures above the base case, the GHP system was under-designed and the heat pump could not maintain conditioned temperatures at set point. For 27.2°C (81°F) ground temperature, the total yearly cooling capacity (in MWh) of the heat pump was reduced by 3.8% compared to the base case in year 10 of operation.
b) For ground temperatures at 19.4C (67F) and 16.7C (62F), the heat pump EER increased by 4.8% and 10.0%, respectively, compared to the base case in year 10 of operation.

Ground Temperature Conclusion: Operation of GHPs is very sensitive to local geological conditions (temperature, in this study) and site-specific analyses should be done to design efficient systems.

Supplemental Heat Rejection (Base case: no SHR devices, 68.6m/borehole (225ft/borehole))

Simulated reductions, from 250W to 5000W, in heat rates carried from the house to the ground were run, which corresponded to 1.4% to 28.5% of the 17,500W heat rate normally rejected to the ground during cooling periods with a heat pump EWT of 32.2°C (90°F). The reduction in heat rates using SHRs is also reflected by reduced borehole lengths.

a) For the reduction range of 250W to 5000W, the SHRs reduced the heat rejected to the ground by 2.1% to 41.3% with corresponding reductions in borehole lengths of 66.8m/borehole (219ft/borehole) to 42.1m/borehole (138ft/borehole).
b) For a 5000W SHR in year 10 of operation, the annual average ground temperature decreased by 6.4°C (12°F), compared to the base case.
c) The total cooling hours in year 10 of operation was reduced by 1.5% to 7.5% for SHRs of 250W to 5000W.

Supplemental Heat Rejection Conclusion: SHRs are effective means of significantly lowering heat pump EST, improving heat pump efficiency, significantly lowering electricity costs, and increasing borehole lifetime. However, with the exception of a cooling tower, an effective and cost effective SHR device was not found in this study (see next section).

- **SUPPLEMENTAL HEAT REJECTION SYSTEM STUDY**

This study investigated several potential SHR devices/systems focusing on two strategies: 1) to remove heat directly from the water in the ground loop before it enters the ground, and 2) to remove heat in the refrigerant loop of the vapor compression cycle (VCC) of the heat pump so less heat is transferred to the water loop at the condenser of the VCC. Devices investigated for strategy 1 included water capacity devices (adsorption coolers, evaporative coolers, and cooling towers, ponds, tanks) and novel thermoelectric liquid coolers, heat pipes, thermo-magnetic/acoustic coolers. Devices investigated for strategy 2 included thermosyphons, an

expanded desuperheater and an optimized VCC. Of the proposed SHR devices, only the cooling tower was an effective and cost effective device/system. The cooling tower and optimized VCC are summarized below.

Heat Rejection—Compact Cooling Tower on Residential Building Application (HGHP system with heat pump capacity held constant): A steady-state compact cooling tower model was used to iteratively solve a series of thermal fluid governing equations [Hasan & Siren, 2002]. This model was coupled to the integrated residential building application using the smallest capacity commercial cooling tower found. The 7kW (2ton) tower model consisted of 12 rows of bank of tubes, each bank with 19 tubes, and each tube was 1.2m (4.7ft) long with an outer diameter of 10mm (0.39in). The longitudinal and transverse spacing of the tubes were 20mm (0.79in) and 60mm (2.4in), respectively. The width of the tower was 0.6m (2.4ft). Water flow in the tubes was 0.8kg/s (12gpm), 0.23m^3/s (8.12ft^3/s) air flow rate, and 1.37kg/s (21.7gpm) spray flow. The cooling tower only operated during the cooling periods when the exit water temperature leaving the heat pump is greater than 35^{o}C (95^{o}F) and rejected approximately 80% of the heat removed from the water and the ground loop removed the other 20%.

a) The addition of the cooling tower SHR decreased the length of each of the four boreholes from the base case of 58.6m/borehole (225ft) to 26.5m/borehole (87ft/borehole).
b) The average heat pump EWTs in years 1 to 10 for the GHP base case were 40^{o}C (104^{o}F) to 45^{o}C (113^{o}F), respectively, and for the HGHP case were 30.3^{o}C (86.5^{o}F) to 33.1^{o}C (91.5^{o}F). The significant amount of energy not dissipated into the ground loop significantly increased heat pump efficiency (EER of 11.5 versus base case of 7.5 in year 10) and the borehole lifetime.
c) The heat pump ran for approximately 1893 hours/year for the 10 years of operation.
d) The total costs (fixed and variable) for 10 years of operating the HGHP case showed a savings of $2,900 compared to the GHP case, mainly due to the decreased drilling costs associated with the shorter boreholes.

Optimized Vapor Compression Cycle (VCC) on Residential Building Application:

In the cooling mode, the VCC removes heat from the conditioned space at the evaporator and the heat pump water loop removes heat at the condenser before returning to the ground loop. The condenser conditions depend upon the heat pump EWT and water flow rates (constant at 12gpm). Manufacturer's heat pump data shows for a given EWT and flow rate, there are ranges in operation for the resulting discharge pressure, superheat, subcooling and rise in water temperature. The strategy employed here attempted to optimize the VCC

thermodynamic parameters to minimize the heat rejected in the condenser while satisfying the cooling load requirements at the evaporator and preventing compressor floodback, thereby reducing the water loop temperature before the water returned to the ground. The three parameters optimized were suction superheat (at the compressor), condenser subcooling (before the expansion valve), and refrigerant flow rate.

The results show a minimum suction superheat (minimizes compressor work) and the maximum subcooling for the given expansion valve will provide the lowest heat rejection to the compressor (minimum heat absorbed by the water in the GHP loop). However, the resulting water loop temperature decrease was minimal. Use of electronic expansion valves, variable speed compressors, and flooded evaporators can provide more degrees of freedom and should be investigated.

Desuperheater on Residential Building Application: This study investigated the use of existing desuperheaters to remove additional superheat from the refrigeration cycle at the exit of the compressor so less heat would be rejected to the water loop in the condenser. The effects of using 50%, 75% and 100% of the available superheat on the amount of hot water and water temperature showed that while the amount of hot water can be increased significantly, the resulting water temperatures do not decrease by more than a few degrees.

- **INTEGRATED COMMERCIAL OFFICE BUILDING APPLICATION**

The integrated building load-GHP model that coupled the building load, ground source heat pump, and vertical borehole-ground models was applied to a base case commercial office building using the maximum heat pump EWT of 32.2.^{o}C (90^{o}F).

Base Case: A commercial office building was modeled to represent the Medium Office from DoE's Commercial Reference Building Models [US DoE, 2010]. The building is a 4,982m^2 (53,628 ft^2), three-story office building with rectangular dimensions of 49.91m (163.8 ft) long, 33.3m (109.2 ft) wide, and 11.9m (39 ft) high and 33% of the total vertical exterior surface area are windows. Each floor is divided into six zones: four perimeter (East/West—floor area 131m^2/ea (1,413 ft^2/ea), North/South—floor area of 207m^2/ea (2,232 ft^2/ea)) zones, one core zone (floor area 2,698m^2 (10,587 ft^2) and one unconditioned plenum zone (floor area 1661m^2 (17,876ft^2)). Inlet and outlet water vaults combine the inlet and outlet water flows from and to the ground loops. The base case model has the borehole field as a matrix of 10x16 boreholes, each on 6.1m (20ft) centers, and 171m (561ft) deep. Separate Climate Tranquility Series heat pumps control each zone: 14.6kW (4-ton) units for the East zones, 17.6kW (5-ton) units for each North and West zones, 24.6kW (7-ton) units for the South zones, and 35.2kW (10-ton) units for the

Core zones of floors 2 and 3, and a 52.8kW (15-ton) unit for the Core zone of floor 1 (due to elevator equipment). The model uses one minute time steps for the entire model except for the ground loop model, which is updated every hour.

Comparison of the base case building load model, HAMBASE with EnergyPlus simulations for fifteen open-loop tests showed good steady state temperature agreements, but the HAMBASE transient temperature responses were faster with time constants half those of EnergyPlus. EnergyPlus had faster and more pronounced humidity responses than HAMBASE.

Results for the base case model show that over a 15-year period the base case design controlled the condition space temperatures to set point within the allowable ASHRAE unmet hours.

Sensitivity Study: Two SHR sensitivity studies were simulated to show the effects of %SHR (0%, 10%, and 25%) heat removal and use of the heat pump shutoff temperature, 48.9^{o}C (120^{o}F), as the maximum heat pump EWT used by GLHEPRO to size the boreholes. This choice of EWT would yield a limiting constraint on the design with minimal borehole depths and minimal heat pump performance. The first study kept the borehole lengths constant with 9.1m (30ft) centerline spacing at the 0%SHR value of 50.3m/borehole (165ft); only the 25%SHR case was able to control the zonal temperatures. The second study used 10.7m (35ft) centerline spacing and recomputed the borehole lengths depending upon the % SHR. All design cases were able to control zonal temperatures with significant savings in installation costs.

1.5 GHP Residential Building Design Study

A project objective was to develop an interactive web-based program to provide users with design decisions based upon technical GHP performance and life-cycle costs, however this task was not done because of the complexity of the integrated GHP model and long simulation times; a 15 year simulation for the commercial building took a minimum of five days running on a 2 dualcore, hyperthreadign 3.73 GHz Xenon processor. Instead, a residential building construction design study was performed for three cities in the southwest region: Austin, Albuquerque and Phoenix. Using the 195m^2 (2100ft^2) base case residential house (brick exterior, asphalt shingle roof, minimum insulation (per code) in exterior walls/windows) described in Section 2, this study investigated the extent to which the following house construction parameters improved GHP performance while being cost-effective: 1) exterior wall construction (brick, stone, wood, and cement), 2) roof (shingle and metal), 3) exterior wall insulation (code minimum up to maximum based upon spacing), and 4) window fenestration/solar gain (code minimum and maximum insulating). Both new house construction

(seven case perturbations from the base case with heat pump capacity and borehole length resized for each perturbation) and retrofit (four case perturbations from the base case with heat pump capacity and borehole length constant at base case values) cases were considered. For example, one perturbation case had brick exterior, asphalt shingle roof, minimum window insulation, but with maximum wall insulation.

New Construction: For a given city, the heat pump capacity was the same and borehole lengths did not vary significantly, since the design changes did not vary the peak heating/cooling loads used to size the boreholes using GLHEPRO. The costs associated with the exterior wall type varied significantly (from brick to concrete) while wall type effects on GHP efficiency was very small. Using the maximum exterior wall insulation and the maximum window thermally insulating properties showed the greatest improvements in GHP performance, but the latter was more expensive to implement than the former. In general, from a cost and GHP efficiency point of view, using wood exterior walls and maximum wall insulation appeared to be the most cost effective choices.

Retrofit Construction: Since the heat pump capacity and borehole lengths were constant in all cases, the most cost effective retrofit was to maximize wall insulation.

2. INTRODUCTION

Section 2 provides the motivational background on GHP and HGHP systems, how they affect the energy landscape, and why their widespread deployment face issues in hot, arid or semi-arid regions. Later, the objectives of the work, project scope, and tasks are presented along with the underlying strategies.

2.1 BACKGROUND

Despite their potential to reduce residential and commercial electricity consumption by 40–70%, ground–source (or ground–coupled) heat pump (GHP) systems have made few inroads into the hot, arid or semi–arid climates of Texas and, more generally, the southwestern United States. In these regions severe geology and hydrology issues, including relatively high ground temperatures and limited ground water (Figure 2.1), require ground loops over 91.4m (300 feet) deep to satisfy the cooling-dominated building thermal loads for more than 10 years of operation. The key technical and economic issues that impede the deployment of GHPs systems include high initial installation costs, engineering required to size system components, and space requirements needed to avoid ground coupling heating imbalance that can reduce heat pump efficiency after 7-10 years [Fisher & Rees, 2005; Navigant, 2009]. As a result, GHP systems are generally viewed as not being economically viable—curiosities only for the wealthy; consequently the average Texas (as well as national) consumer knows relatively little about GHP systems—in spite of their potential long–term economic and environmental benefits to individual consumers, as well as society [Hughes, 2008].

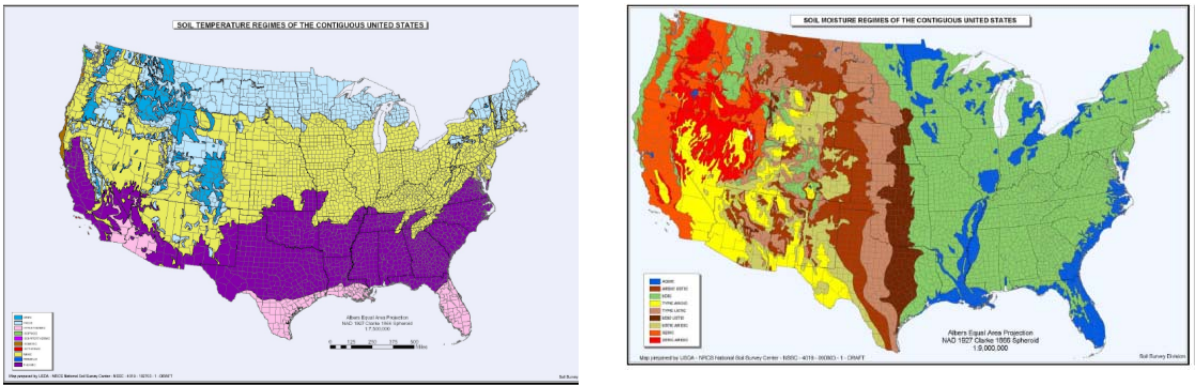

Figure 2.1: Soil Temperature (Left) & Moisture (Right) Regimes of the Contiguous U.S. [USDA, 2009]

Temperature: Pink (hyperthermic), Purple (Thermic), Yellow (Mesic)

Moisture: Yellow (Typic Aridic), Light Brown (Typic Ustic), Light Green (Ustic Aridic), Red-Brown (Aridic Ustic)

One approach to reduce initial costs and balance the net heat to the ground is to reduce 'waste heat', the instantaneous difference between the building's thermal load and the GHP system's thermal "off–loading" capacity. In the southwestern regions of the United States, 'waste heat' accumulates over time, gradually heating the ground resources while concomitantly reducing GHP system efficiency. Reducing "waste heat" sent underground using supplementary heat rejection (SHR) techniques will reduce the deleterious effects of ground heating and offer the potential to improve the economic and technical viability of GHPs systems in Texas. In several industrial building applications, Austin Energy discovered that, after just a few years, the GHP system had to be retrofitted with an auxiliary cooling tower in order to maintain acceptable GHP system efficiency [Yerba, 2009]. In fact, the hybrid approach has been demonstrated in a U.S. Department of Energy (DoE) study to yield greater energy saving benefits in warmer (higher cooling load) locations [US DoE, 2001]. It has been demonstrated using auxiliary cooling towers in industrial applications that, for heavily cooling–dominated sites like Texas, "hybrid GHPs can result in heat pump and system energy savings compared to full GHPs when the supplementary heat rejecter is operated enough hours to reduce the average heat pump entering fluid temperature during the cooling season" [Yavuzturk & Spitler, 2000].

Texas—the Nation's 2nd most populated state—is hot and only getting hotter. 2011 was the hottest year in Texas; Austin had 90 triple digit days, smashing the previous record of 69 days set in 1925. On August 3, 2011, the Electric Reliability Council of Texas, Inc. (ERCOT), the electric grid operator for 85% of the state, announced that Texans set a new daily usage record with an hourly average of 68,305 megawatts (MW) of power [ERCOT, 2011]. In fact, the most pressing short-term policy concern in Texas is the rapid growth in peak electricity demand. According to ERCOT, it expects peak demand to increase by 2.3% annually from 2007 through 2012. ERCOT has raised the prospect that, in the near future, the state may not have sufficient generation capacity to meet peak demand, suggesting new generation sources need to be secured [Elliot, 2007].

Deployment of GHPs and HGHPs in Texas has the potential to impact electricity usage. According to independent reports, if a conventional air–to–air heat pump was replaced with a hybrid GHP system in a Texas home, it would reduce a typical Texas home's heating– and cooling–related electricity consumption by 40-70%, while also preheating domestic water [Frontier Assoc, 2008; TexasIsHot, 2009]. If deployed throughout ERCOT's service region, they could cut peak demand in summer months by upwards of 20%, or alternatively eliminate over 80% of forecasted electric load growth at costs substantially cheaper than securing additional electric supply [US DoE, 2009; Nat Res Def Council, 2007]. For example, present value of first

costs plus electricity costs of a ground–coupled heat–pump system has been demonstrated to be reduced by more than 50% for very highly cooling dominated applications such as the small office building in Houston, which has a cooling-to-heating load ratio of 24:1 [US DoE, 2001]. Thus, there is an urgent need—as well as great cost–, energy– and emissions–saving potentials—for increased deployment of SHR–augmented GHP systems in Texas and, more generally, the southwestern and western U.S.

2.2 PROJECT OBJECTIVES

The project objective is to develop engineering data, analysis, modeling and decision–support tools to enable the identification, selection, design, specification, and construction of supplementary heat rejection (SHR) systems/devices that, when added to conventional ground–source heat pump (GHP) systems, make the resulting hybrid GHP system technically and economically viable in hot, arid or semiarid climates typical of the southwestern and western United States given: (1) various building types and sizes; (2) historical and predicted installation and maintenance costs; (3) local climate history; (4) building site characteristics; (5) resource availability; (6) various ground resources/designs; and (7) electricity sources along with related costs and greenhouse gas (GHG) emissions. An implicit objective is demonstration that SHR systems/devices are *central* to the viability of GHP systems in these demanding environmental, geological and hydrological conditions, all which have an impact on installation cost and feasibility. An ancillary objective is to develop and distribute web–based information and tools that provide engineering guidance to building owners and designers regarding which SHR–augmented GHP systems offer the best performance at the lowest life–cycle cost.

2.3 PROJECT SCOPE

This project is aimed at “waste heat” rejection/recycling strategies for GHP systems that are technically and economically viable for various building applications and ground resource designs in heavily cooling–dominated climates like those found in the southwestern and western United States. As they currently stymie widespread GHP system deployment, particular attention will be paid to aggravating factors, such as limited access to ground and/or surface water, extensive hard underlying rock and limited land availability. Engineering analysis and modeling will be provided to enable the design, selection and sizing of SHR–augmented GHP systems that offer the best performance and lowest life–cycle cost at these sites. Several SHR system alternatives will be examined: (1) evaporative fluid/air coolers or pre–conditioners, which liberates thermal energy from the working fluid before it enters the ground loop/resource; (2)

desuperheaters, which recycle some of the waste heat to preheat hot water; and (3) two–phase thermosyphons, which are passive refrigeration devices that transfer heat against gravity. Other SHR systems will be examined as they are identified, if evidence suggests that they may be technically and economically viable.

As GHP systems offer substantial energy efficiency by leveraging earth's intrinsic thermal storage, they could play a pivotal role in reducing building energy consumption and limiting GHG emissions in heavily cooling dominated states which are experiencing large increases in population and correspondingly, in peak electricity demand.

2.4 TASKS TO BE PERFORMED

The objectives and scope outlined above were incorporated into the following implementation plan. Sections of this report that focus on the Tasks are provided.

Task 1: "Waste Heat" Rejection/Recycling Estimation

Purpose: Estimate the "waste heat" that an auxiliary SHR device/system must reject/recycle (in order to mitigate against ground heating) as a function of all relevant parameters. This estimate will provide the first indication of the potential need for and viability of an auxiliary SHR device/system for a given application, and provides critical guidance for the SHR device/system selection and sizing.

Project Results: Section 5 and Appendix D address the SHR devices/systems considered, modeled, and analyzed in this project. Section 4.8.5 presents a sensitivity study for a base case residential building (Section 4.6) to illustrate the effects of adding an SHR (device/system not specified) and its effects on the heat pump operating performance and on the installation and operating costs of the system for 10-15 years of operation. Section 6.5.1 presents the same study for a base case commercial office building (Section 6.1). Addition of SHR devices decreases the installation costs significantly, increases heat pump efficiency, and increases the lifetime of the borehole field; it is cost effective if a SHR device can be identified. The SHR study revealed that of the systems considered, only the cooling tower yielded operational and cost performance effective for a HGHP system. As such, Section 5.1.3 implements the cooling tower model (Section 5.1.1) to the base case residential building and illustrates a successful performance and cost implementation.

Task 2: Technical Performance Analysis & Modeling

Purpose: Assess the technical performance and relative merits/demerits of different auxiliary SHR devices/systems for use in conjunction with GHP systems as a function of all relevant

parameters. Key performance metrics include heating– and cooling–related daily energy and/or electricity use; building air temperature and humidity; working fluid and ground resource temperature; industry standard coefficient of performance (COP), seasonal energy efficiency ratio (SEER, residential) or integrated part load value (IPLV, commercial); and GHG emissions. These metrics will provide guidance for assessment of the technical viability and relative merits/demerits of the various auxiliary SHR devices/systems.

Project Results: In order to assess technical performance, accurate models of the building loads, heat pump, ground loop, and SHR devices were developed. Section 3 provides the detailed models of the generic building loads (HAMBASE-Section 3.1), heat pump (Performance Map-Section 3.2), and ground loop (GLHEPRO and Oklahoma State-Section 3.3) and validation of these component models. The IBL-GHP model, coupling the three component models above, were applied to base case residential and commercial office buildings in Sections 4 and 6, respectively, along with validation studies comparing ASHRAE standards, eQuest, GLHEPRO, and EnergyPlus data/simulations. Performance metrics and base case designs are provided in each building application. SHR models were developed for cooling towers and thermosyphons in Sections 5.1 and Appendix D.1, respectively, and detailed analyses completed for vapor compression cycle optimization and desuperheaters in Sections 5.2 and 5.3, respectively. Analyses for other potential SHR devices are presented in Appendix D.2-D.6.

Task 3: Life–Cycle Cost Analysis & Modeling

Purpose: Assess overall life–cycle cost, as well as the cash–flow timeline, of different auxiliary SHR devices/systems for use in conjunction with GHP systems as a function of all relevant parameters. Estimates of the data's degree of uncertainty will be included, because they are vital in determining the "robustness" of a given SHR–augmented GHP project's economic viability, i.e., whether the system is economically viable even if certain assumptions are only marginally valid or simply invalid. Ultimately, demonstration of economic feasibility under multifactorial uncertainty will translate to higher consumer confidence in purchase decisions, as well as to more widespread deployment of SHR–augmented GHP systems. Key uncertainties that will be tracked include electricity costs, sources and emissions; prevailing interest rates; potential regulatory tariffs; SHR–augmented GHP system performance reliability; local weather and water availability. These costs and attendant uncertainties will provide guidance for assessment of the economic feasibility and relative merits/demerits of the various auxiliary SHR devices/systems.

Project Results: The operational performances of the base case models for the residential and commercial office buildings are presented in Sections 4.7 and 6.4, respectively, and show

temperatures, humidities, heat pump EWTs and efficiencies, and installation and operating costs (electricity, water, etc.). Section 4.8 presents the effects on operation and cost on the base case residential building of varying designer-specified parameters such as borehole length, grout conductivity, borehole filed configuration and spacing, and application of a SHR device. Section 5.1.2 provides the performance and life-time costs associated with the HGHP residential system.

Task 4: Web–Based Decision–Support Tools Development

Purpose: *Create novel and robust, web–based, decision–support tools that enable prospective GHP system customers and financiers to compare life–cycle costs and technical performances for purchase and design decisions of GHP systems with and without auxiliary SHR devices/systems. Make these tools available to the public via the National Geothermal Database System (NGDS) and other consumer education sites.* In order to secure the capital necessary for GHP system installation, customers need to be able to quantify their project's intrinsic value and degree of uncertainty, as well as demonstrate its short– and long–term technical and economic feasibility.

Project Results: This task was not done because of the complexity of the integrated GHP model and the large time needed to simulate a 10-15 year operating period—a reasonable real-time interactive Web-based program could not be accomplished. Instead, a residential building construction design study was performed for three cities in the southwest region: Austin, Albuquerque and Phoenix. Using the base case residential building (Section 4.6), Section 7 investigated the extent to which house construction parameters improved GHP performance and overall costs. Both new house construction and retrofit cases were considered.

3. SIMULINK-BASED INTEGRATED GHP/HGHP SYSTEM MODELS

Section 3 describes the component models coupled into the integrated GHP system models for residential and commercial building applications and the Simulink environment. The main component models are: (1) building thermal loads (Section 3.1—HAMBASE) (2) ground source heat pumps (Section 3.2—ClimateMaster Tranquility 20 Series), and (3) vertical borehole-ground (Section 3.3—Hellstrom/Ekillson/Xu). The Simulink® environment has powerful built-in computational and integration algorithms that easily couples the component models and provides multi-time-step computations needed for the fast (building and heat pump) and slow (ground loop) dynamics of the total system. The integrated models can simulate responses every 30 seconds to 20 years of operation. Each model is summarized below. Validation of individual component models and combinations of component models are provided.

3.1 BUILDING LOAD THERMAL MODEL

The creation of the integrated build GHP model first began with the selection of the building thermal load model, since that model would dictate the modeling environment that would be used for the rest of the project. The complexity of building load models in combination with the large number of available models led to the decision to use an existing model as opposed to creating a new one. To reduce implementation time and reduce possible errors, the building load model would be used in its developed environment. That is, if EnergyPlus was chosen for the building load model, the rest of the combined model would be implemented using the EnergyPlus format. This constraint increases the complexity of the model selection processes because different formats of the other sub-models must be considered, as well as the benefits (computation, coupling, flexibility) of the modeling environment.

3.1.1 Model Requirements

For clarity the building load model requirements are divided into environment requirements and building load requirements. Understanding and satisfying these requirements allows for the selection of the models and environments that are best suited for the project.

3.1.1.1 Environment Requirements

One key goal of the overall project is to evaluate possible methods to reject heat using SHR devices to reduce the net yearly load on the ground loop. Various methods were evaluated such as cooling towers and desuperheaters. Evaluating these SHR devices requires modeling their operation and control in the chosen environment. This implies two requirements. First, the environment must support the addition of user definable components. Second, the components

will be created in the environment, therefore it is preferred that the programming language of the environment be known by the research group aprior. These include Matlab, Simulink, C, and C++. The computing resources available also dictate that the model be run at least on Windows-based operating systems, but it would be preferable for the modeling environment to run on Macintosh and Linux operating systems as well.

Another key goal of the research project is to show the effects of ground heating on the conditioning provided to the house. Therefore, the building load model must interface with a ground source heat pump model to model the response of the building load and internal conditioned air temperatures to reductions in heat pump capacity due to long term ground heating. This requires coupling between the heat pump and the building load models. As the ground temperatures rise, the heat pump EWT also increases, which in turn reduces the cooling capacity and efficiency of the heat pump. If the capacity is reduced significantly the heat pump will not be able to maintain the set point temperatures in the conditioned spaces of the building. Therefore, the combined model must couple the building model with the heat pump and ground loop at every time step [Crawley et al., 2001].

Localized ground heating due to GHPs manifests itself over many years, so the model must be able simulate many years of operation (10-20 years) in a reasonable amount of computation time. The model must also handle the different dynamic responses of the various components that make up the combined model; heat pump responses on the order of seconds/minutes and the ground responses on the order of hours/months/years.

The model must be able to perform parametric studies such as the effects of the undisturbed ground temperature, ground conductivity, building material properties, internal building loads, and SHR capacity. The model also must be easily reconfigurable to compare the placement, type, and capacities of the SHRs. The ability to add/move/change/remove components without significant reprogramming of the model would be very beneficial. The implementation and development of various SHR models must be completed independently from the combined model to simplify development and validation as well as allow for parallel model development.

A summary of the environment requirements are:

- Ability to add user defined components (thermostats, water pumps, SHRs)
- Preference to programming languages known apriori (Matlab, Simulink, C, C++)
- Full coupling of building load, heat pump and ground loop models
- Multi-year simulations, with a reasonable simulation time
- Ability to make significant model configuration changes without significant reprogramming

- Independent component model development
- Run off different computer platforms and operating systems
- Simulate the range of dynamic response characteristics of the many components

3.1.1.2 Building Load Model Requirements

Another key goal of the project is to determine cost-effective methods to reduce the energy rejected into the ground while providing cooling/heating across a range of building types. The cooling/heating profiles of commercial facilities and residential structures differ greatly, which present different opportunities for possible SHR methods. This requires that the model be accurate for a wide range of buildings from large multi-zone commercial buildings to single family residences.

The building load model must not only account for the temperature of the air in the structure, it also must account for the moisture in the structure. In climates with high levels of outdoor humidity the ability of the heating, ventilation and air-conditioning (HVAC) system to remove moisture from the air plays a large role in the overall comfort in the occupants of the structure. If the HVAC system can reduce the amount of moisture during cooling, the thermostat can be set at a higher temperature, which reduces the cooling energy needed. To account for the perceived comfort level of the occupants, the building load must account for both the moisture and the temperature of the air [Crawley et al., 2008; de Wit, 2006]. The model must also use industry-accepted weather data such the Typical Metrological Year (TMY) data [NREL, 2008].

Due to the time required to develop and validate a new building load model, an existing model that has been validated would be preferred. This strategy will reduce the model implementation time and allow for more time to be spent modeling the heat pump and/or ground loop.

A summary of the building load model requirements are:

- Accurately model building loads of the residential and commercial buildings
- Model the relative humidity in the building
- Perform hourly or sub-hourly load calculations for the entire year
- Previously validated

3.1.2 Building Load Model Literature Review

Based on the requirements listed above, the following building load models/modeling environments were considered and briefly summarized below: eQuest, EnergyPlus, TRANSYS, and HAMBASE.

3.1.2.1 eQuest/DOE-2.2

eQuest provides a user-friendly graphical interface to create building models using the DOE 2.2 building simulation program, based upon Fortran, and provides hourly data results. Two key limitations are the difficulty to add user-defined component models and the lack of simultaneous coupling between the heat pump-ground loop system and the building load [Hirsch, 2009].

3.1.2.2 EnergyPlus

EnergyPlus also uses DOE 2.2 without a user-interface, although third-party interfaces are available. The heat pump-ground loop is fully coupled to the building load computations and it accepts user-defined component models. However, user-defined models are only functional in Energy Plus. In contrast, the IBL-GHP model allows user-defined components to be written in different languages including C, Fortran, and Matlab, allowing for easy expansion of the model as well as be simulated independently from the combined model for validation and independent analysis. In Energy Plus, computations are nominally on 15-minute time steps but smaller time steps are used to compute temperature responses during the 15 minute intervals [Crawley et al. 2001l; US DoE, 2011].

3.1.2.3 TRNSYS

TRNSYS (TRaNsient SYstem Simulation) allows simultaneous coupling of modular components from a library of models (or user-defined models in any programming language) using a graphical user interface, which makes running parametric studies very simple. TRNSYS also features the ability to turn an entire model into a stand-alone application that can be used by non-expert users to run parameter studies [Duffy, et al., 2009].

3.1.2.4 HAMBASE

HAMBASE (Heat Air and Moisture model for Building And Systems Evaluation) is a building load model that was developed at the Eindhoven University of Technology. The version of the model considered is implemented as a Simulink function block. The Simulink environment is excellent for multi-domain simulation of dynamic systems. It incorporates a graphical interface, Matlab functionality and built-in solvers. Using the Simulink environment to develop the combined model will allow for easy creation of different model components due to the built-in functions of the MatLab programming language as well as the prior familiarity of the research group with it. Simulink also allows for independent component model development, which allow the custom component model to be tested and evaluated independently from the combined model. The graphical interface allows for changes to be made to the model such as adding a SHR device to the ground loop with just a few clicks [de Wit, 2006]. HAMBASE does not

include a graphical user interface and there are no commercially available interfaces, so the creation of the building model must be completed in a text file. This is more difficult than using a graphical user interface such as eQuest, however the user knows exactly what is being modeled. HAMBASE has not had a complete third-party validation study performed on it, but the developers performed the first test of ASHRAE's 140-2007 Standard (discussed in Section 4) with good results.

HAMBASE utilizes a modeling procedure based on zones. A zone is the smallest simulated volume of the structure. Each zone represents a single room or a group of rooms that have similar thermal and moisture conditions. The Simulink implementation of HAMBASE defines two differential equations for each zone, one for the heat transfer and the other for the mass transfer. The heat transfer model includes radiation, convection, and conduction on the exterior and internal zonal walls of the building, heat losses or gains from infiltration and ventilation, and internal heat loads (people, lights, equipment, etc.). The mass transfer model includes moisture gains from internal latent loads, infiltration, ventilation, and storage in various materials. The heat and mass transfer models are coupled because the saturation vapor pressure needed for the hydric model depends on air temperature and the amount of heat released during condensation. Using the Simulink environment allows for each zone to have its own HVAC system or share a common system with the other zones. Using zones allows accurate modeling of areas of the structure with very different climates. The zones also allows for the internal heat and moisture gains to be placed in the proper area of the structure, such as the zone associated with the kitchen in a residential house [de Wit, 2006].

The Simulink environment allows for full coupling between all ~~of~~ the different components. Since the model is based on differential equations the Simulink implementation of HAMBASE can take advantage of user-defined controllers and HVAC system components. The HVAC system components can then be coupled to a ground loop model, allowing for the ground loop water temperature to effect to provided cooling and efficiency of the HVAC system. The Simulink environment has built-in solvers to determine the time step which can either be a variable time step that is used to reduce error or a user defined fixed time step. Having control of the time steps allows for the user to trade accuracy for speed, or vise versa, when needed. Simulink also allows for multi-rate simulations, i.e. part of the model can be simulated at one time step and a different part of the model can be simulated at a different time step. The Simulink environment also allow for running simulations of any desired length. Simulink/Matlab is available on Windows, Mac, and Linux [Mathworks, 2011].

3.1.3 Model and Environment Selection

After comparing the simulation programs and associated environments with the model requirements previously discussed, a decision matrix showed TRNSYS and HAMBASE to be the best options [Gaspredes, 2011]. The HAMBASE/Simulink® combination was selected primarily because the built-in features and functionality of Simulink® are significantly better than those found in the other environments considered.

3.1.4 Validation of HAMBASE Building Load Model

The ASHRAE (American Society of Heating, Refrigeration and Air-Conditioning Engineers) 140-2007 standard provides a series of cases with standardized building, load and weather parameters that can be used to validate proposed building load models based on comparisons with tabulated results from eight different models, including EnergyPlus, TRNSYS, and DoE2. Since there is no exact solution for each case, the user must interpret the results and determine if the proposed model is sufficiently accurate [ASHRAE, 2007].

The ASHRAE 140-2007 standard is divided into several cases that vary specific building parameters. The basis for all of the test cases is case 600. The rest of the tests use modified versions of this case. The inputs and results of case 600 will be discussed in detail here for illustrative purposes. Over 17 case variations were run and details can be found in [Gaspredes, 2011].

3.1.4.1 Case 600 - Model Details

Case 600 is a rectangular building, located in Denver, CO, with a flat roof and south facing windows as depicted in Figure 3.1. The building is oriented so that each exterior wall faces a cardinal direction. The building is composed of materials with low thermal masses. The standard provides: specific material properties of the external walls, roof, and floor; values for the heat transfer properties of the building materials, such as the overall heat transfer coefficient for each exterior surface and properties for the windows; infiltration rates and internal loads; set point temperatures, and HVAC capacity [ASHRAE, 2007].

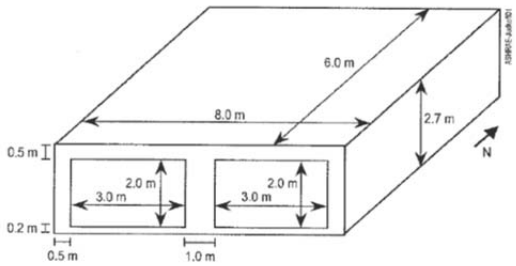

Figure 3.1: Case 600 building dimensions Source: ASHRAE 140-2007 [ASHRAE, 2007]

3.1.4.2 Case 600 - Selected Results

Case 600 in ASHRAE 140-2007 provides a variety of data sets designed to test and troubleshoot different parts of the building load model. The standard suggests that when validating a model the user should get good agreement for all of the case 600 data sets and then move on to the additional tests.

The validation begins by looking at the solar load on the surfaces of the building. Figure 3.2 compares the incident radiation on the west wall of the building for every hour on July 27th. The line represents the results from HAMBASE and diamonds is the mean of the eight values reported by 140-2007, with the error bars indicating the maximum and minimum values reported by the standard. This format is used for all plots of this type. The results show good agreement between HAMBASE and the reported values. Similar plots for the south wall, as well as, for March 5th are available in [Gaspredes, 2011].

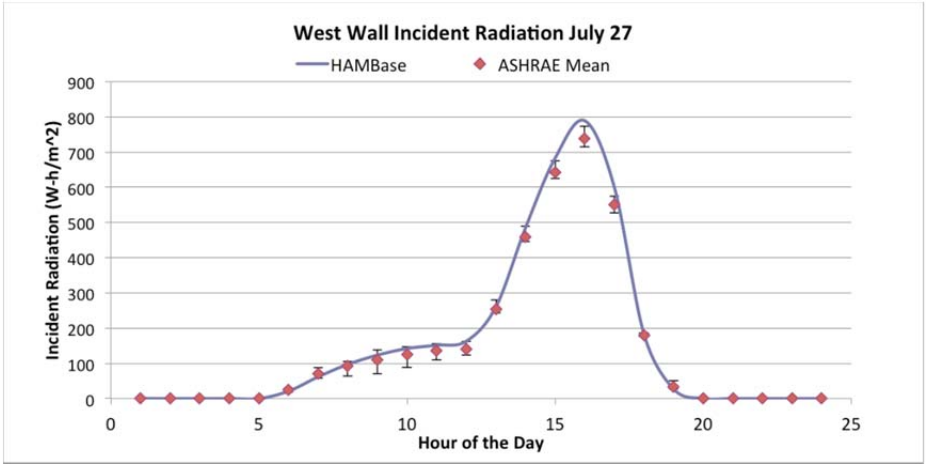

Figure 3.2: Hourly Incident Radiation on West Wall for July 27

Table 3.1: Annual Solar Radiation Loads on Case 600

	140-2007 Reported Values			HAMBASE
	Minimum	Average	Maximum	
Annual Incident Radiation (kWh/m^2)				
North	367.4	428.8	457	441.8
East	959	1079.9	1217.3	1156.2
West	856.5	1018.4	1090	1084.2
South	1456	1490.0	1566	1590.8
Horizontal	1797	1826.8	1832	1839.4
Annual Transmitted Radiation (kWh/m^2)				
	914	962.5	1051	1001.5
Annual Transmissivity Coefficient				
	0.623	0.646	0.671	0.629

Next, the total annual loads on each surface of the building and the radiation transmitted through the glazing are compared. Table 3.1 shows annual incident radiation values for each surface of the building. The values for HAMBASE are within the reported range for the north, east and west walls, while the south wall and the roof (horizontal) are just outside of the reported maximum range. All of HAMBASE's values are higher than the mean reported values. Table 3.1 also compares the annual radiation transmitted through the glass and the annual transmissivity coefficient. The annual transmissivity coefficient is the fraction of the incident radiation on the south wall that is transmitted through the glazing on the south wall. Both of these values fall within the reported ranges.

The hourly HVAC system loads and the hourly interior air temperatures are compared for January 4th in Figure 3.3. The heating loads are represented as positive loads (adding energy to the building) while cooling loads are represented as negative (removing energy from the building). The figure shows that HAMBASE results are just outside of the reported range for seven hours; HAMBASE predicts more cooling during hours 11, 12, 13 and 14 and it predicts more heating for hours 19, 20, and 21.

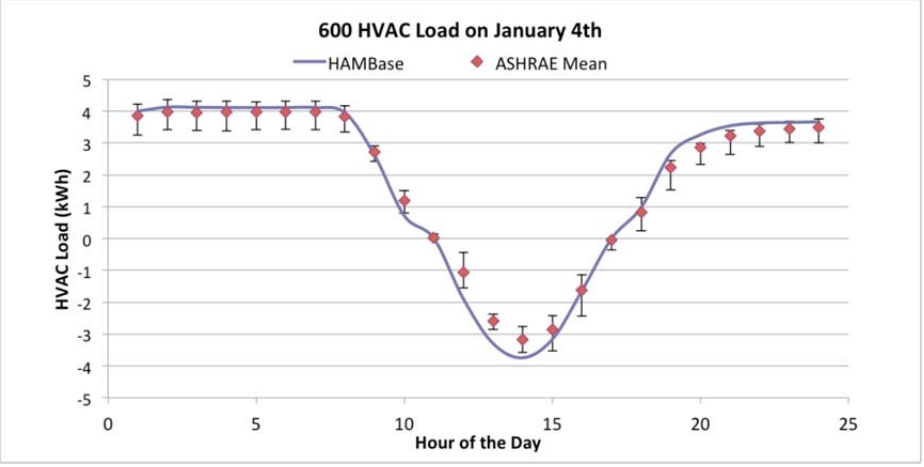

Figure 3.3: Hourly HVAC Load for January 4th

Figure 3.4 shows the hourly "free floating" temperature (HVAC turned off) for January 4th for Case 600FF. HAMBASE accurately predicts the interior air temperatures of the building; all of HAMBASE's values are within the range of reported values.

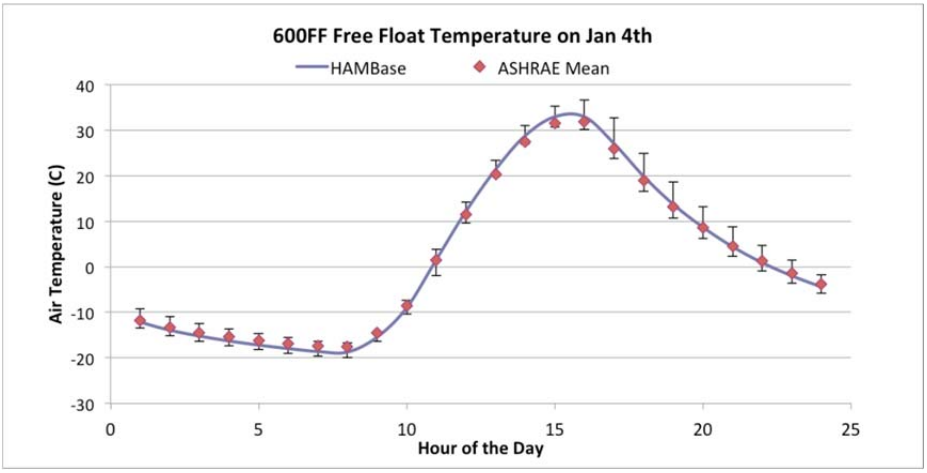

Figure 3.4: Hourly Air Temperature Values for the 600FF case

A final comparison for Case 600 is shown in Figure 3.5. This chart compares the total annual heating and cooling loads, in MW-h, and the peak heating and cooling loads (in kW) for the eight models and HAMBASE (far right of each section). HAMBASE predicts values within the range of the reported values.

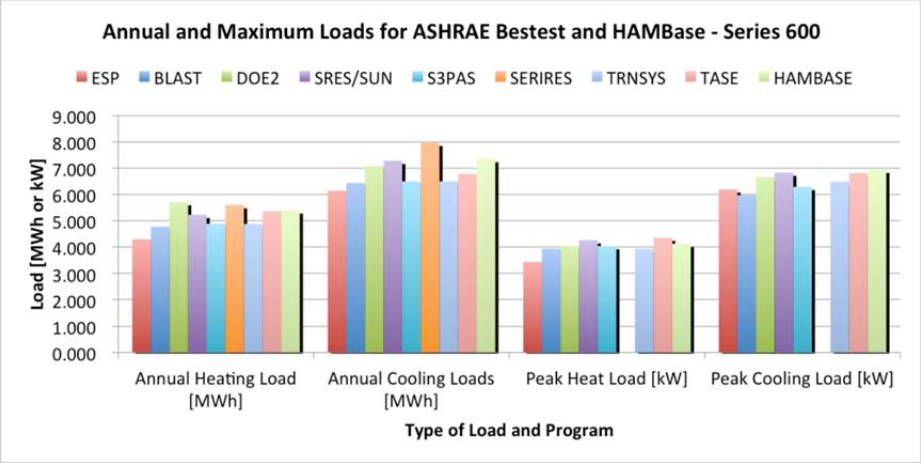

Figure 3.5: Annual and Peak Heating and Cooling Loads

Based on the results presented, it was determined that HAMBASE was in good agreement with the reported values for Case 600. Additional cases of the 140-2007 standard where completed to further validate HAMBASE.

3.1.4.3 Sensitivity Study

The additional cases specified by ASHRAE 140-2007 are used to determine the sensitivity of the model to various changes. Each additional case has a single change from its base case as summarized in Table 3.2. For example, case 620 moves the south facing windows of case 600 to the east and west faces of the building, while all other parameters are exactly the same.

In addition, case 630 then adds shading around the east and west facing windows of its base case 620. In total, 16 additional cases where simulated as listed in Table 3.2.

Table 3.2: Summary of Sensitivity Study Cases

Case	Base Case	Changes
610	600	Add shading over south facing windows
620	600	Remove the 12m^2 of windows from the south wall and add 6m^2 of shading to the east and west walls
630	620	Add shading above and around the widows on east and west walls
640	600	Heater thermostat is setback to 10^{o}C between 2300 and 0700 hrs then at 20^{o}C between 0700 and 2300 hrs
650	600	Night time ventilation added between 1800 and 0700 hrs, heat is always off and cooling is only provided between 0700 and 1800 hrs
900	600	Construction materials changed with higher heat capacities
910	610	Same as 900
920	620	Same as 900
930	630	Same as 900
940	640	Same as 900
950	650	Same as 900
960	900	Add unconditioned sunspace on the south side of house
600FF	600	No heating or cooling provided to the building
650FF	650	Same as 600FF, still has night time ventilation
900FF	900	Same as 600FF
950FF	950	Same as 600FF, still has night time ventilation

The results of all additional cases except for the free floating temperature cases (600FF, 900FF, 650FF, and 950FF) were compared to the reported values by determining the change in annual heating and cooling and peak loads between the case and it's basis. For example, Figure 3.6 shows HAMBASE prediction for Case 610, which adds shading over the south facing windows of the 600 case; 1.6 MW-h less annual cooling than case 600, while the annual heating and peak loads did not change much. Comparing these results to the reported values it is seen that the heating load changes were very small for all models and the annual cooling value changes agree. The change in the peak cooling load for the HAMBASE model was less than the reported range of values for the models, but was close to the minimum value. Results of additional tests are found in Appendix A (HAMBASE Validation).

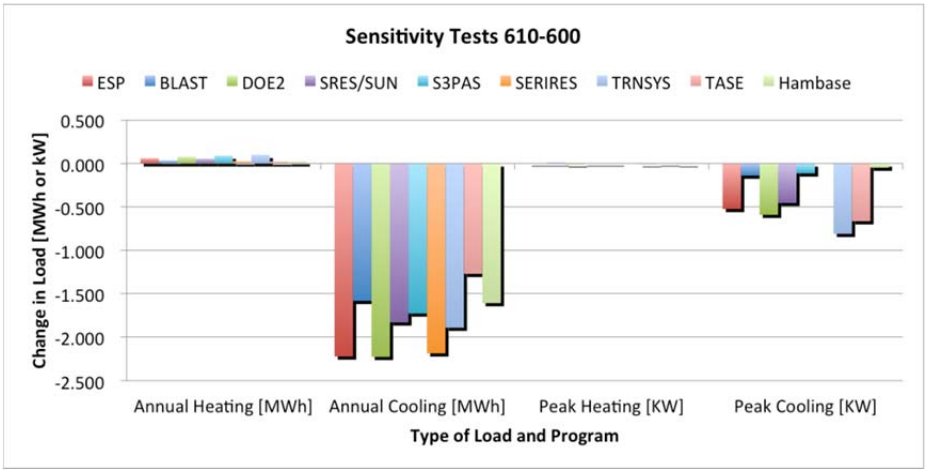

Figure 3.6: Changes in building loads from case 600 to case 610, addition of shading over south facing windows

3.1.5 Conclusion: Validation of HAMBASE Building Load Model

ASHRAE 140-2007 does not provide criteria to determine if the simulation results are in agreement or not. The standard provides a set of guidelines for comparing the results and lets the user determine whether not the model is accurate. Based on the results of the case 600 model presented in Sections 3.1.3 and the 16 sensitivity studies run (Appendix A and Gaspredes, 2011) it was determined that HAMBASE simulated the ASHRAE cases with sufficient accuracy for the research group to use it as the building load model.

3.2 HEAT PUMP MODEL

An air-to-water heat pump model is an integral part of the GHP system that contains the refrigerant loop that extracts/rejects heat from/to the conditioned air space and rejects/extracts heat to/from the water circulating though the ground loop for cooling/heating, respectively. The heat pump unit consists of the compressor, expansion valve, refrigerant-to-air fin and tube heat exchanger, and refrigerant-to-water concentric tube heat exchanger.

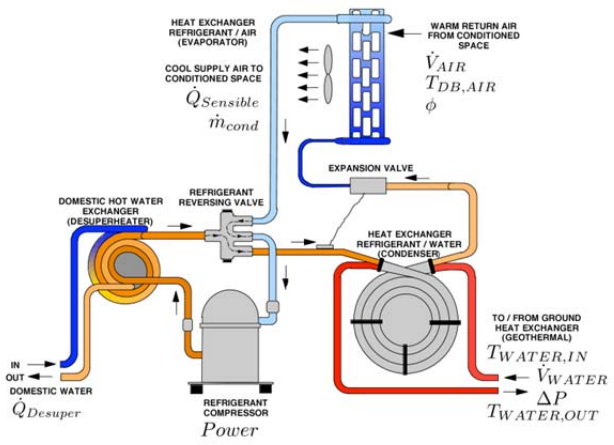

Figure 3.7: Operation of heat pump during cooling with model variables [Oklahoma State University, 2010]

Figure 3.7 is a schematic of a water source heat pump in the cooling mode with the inputs and outputs of the model labeled as shown in Table 3.3. The model inputs are: temperatures of the air, $T_{DB,AIR}$, and water, $T_{WATER,IN}$ at the inlet to the heat pump unit; the volumetric flow rates of air, $\dot{V}_{AIR}$, and water, $\dot{V}_{WATER}$, through the unit; the heat removed by a SHR device, $\dot{Q}_{Desuper}$; and the water content of the entering air in terms of the relative humidity, φ. The model needs to calculate: the sensible, $\dot{Q}_{Sensible}$, and latent, $\dot{m}_{cond}$, output of the heat pump; the electrical power consumed by the unit, *Power*; the water outlet temperature, $T_{WATER,OUT}$; and the pressure drop of the water as it flows through the refrigerant to water heat exchanger, ΔP.

Table 3.3: Heat Pump Model Inputs and Outputs

Inputs		Outputs	
$\dot{V}_{AIR}$	$[m^3/s]$	$\dot{Q}_{Sensible}$	$[W]$
$T_{DB,AIR}$	$[^oC]$	$\dot{m}_{cond}$	$[kg/s]$
ϕ		Power	[W]
$\dot{V}_{WATER}$	$[L/s]$	$T_{WATER,OUT}$	$[^oC]$
$T_{WATER,IN}$	$[^oC]$	ΔP	[KPa]
$\dot{Q}_{Desupr}$	$[W]$		

First-principle modeling was not attempted due to the lack of detailed component geometric, material, and construction data (considered proprietary by manufacturers). Instead, empirical models were used based upon a series of equations that curve fit input/output relations (called performance mapping) to design or experimental data [Spitler, 2000; ClimateMaster, 2010]. While these models lose process physical details, they are computationally efficient, data is

readily available for a wide range of heat pumps, and the results are very accurate when the heat pump operates in the provided data range. A detailed review of current first-principles and empirical models can be found in [Gaspredes, 2011].

3.2.1 Performance Maps

A performance map model is based on data published by heat pump manufacturers, such as ClimateMaster [ClimateMaster, 2010] and Water Furnace [WaterFurnace, 2010] and based on the ANSI/ASHRAE/ARI/ISO 13256-1 standard for rating and testing water source heat pumps [ClimateMaster, 2010]. The data relates the inlet conditions of the heat pumps to the exit conditions and operating parameters; an example performance map data is shown in Figure 3.8.

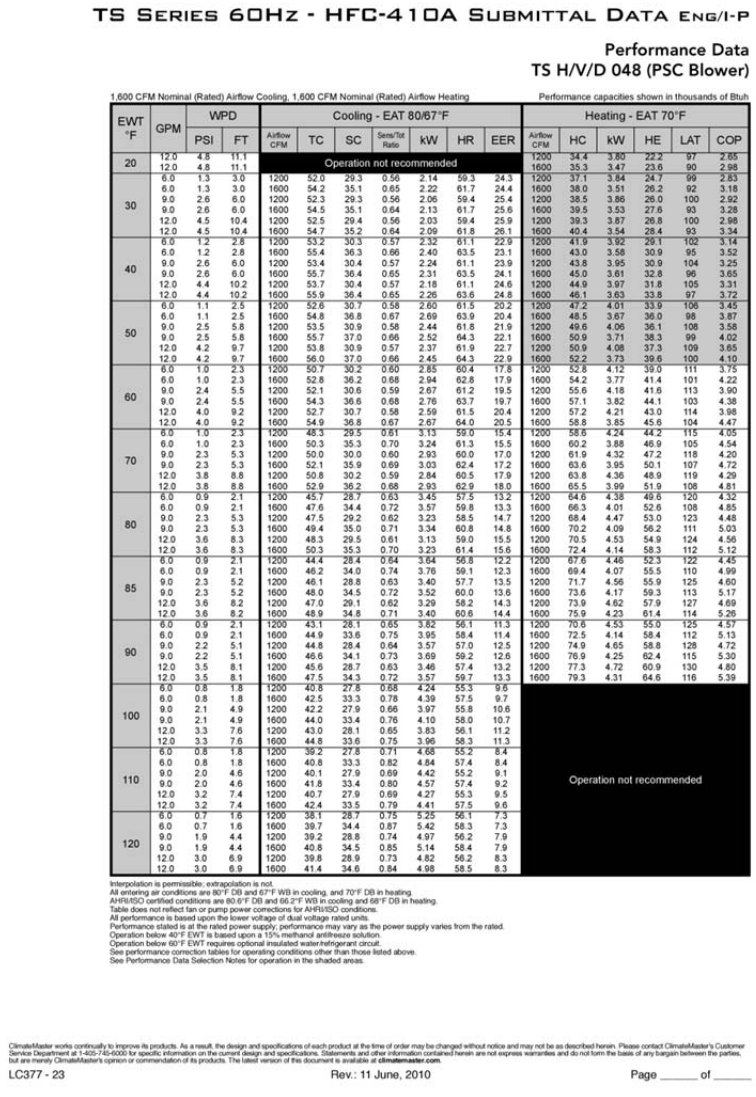

TS SERIES 60Hz - HFC-410A SUBMITTAL DATA ENG/I-P

Performance Data
TS H/V/D 048 (PSC Blower)

1,600 CFM Nominal (Rated) Airflow Cooling, 1,600 CFM Nominal (Rated) Airflow Heating — Performance capacities shown in thousands of Btuh

EWT °F	GPM	WPD		Cooling - EAT 80/67°F							Heating - EAT 70°F					
		PSI	FT	Airflow CFM	TC	SC	Sens/Tot Ratio	kW	HR	EER	Airflow CFM	HC	kW	HE	LAT	COP
20	12.0	4.8	11.1	Operation not recommended							1200	34.4	3.80	22.2	97	2.65
	12.0	4.8	11.1								1600	35.3	3.47	23.6	90	2.98
30	6.0	1.3	3.0	1200	52.0	29.3	0.56	2.14	59.3	24.3	1200	37.1	3.84	24.7	99	2.83
	6.0	1.3	3.0	1600	54.2	35.1	0.65	2.22	61.7	24.4	1600	38.0	3.51	26.2	92	3.18
	9.0	2.6	6.0	1200	52.3	29.3	0.56	2.06	59.4	25.4	1200	38.5	3.86	26.0	100	2.92
	9.0	2.6	6.0	1600	54.5	35.1	0.64	2.13	61.7	25.6	1600	39.5	3.53	27.6	93	3.28
	12.0	4.5	10.4	1200	52.5	29.4	0.56	2.03	59.4	25.9	1200	39.3	3.87	26.8	100	2.98
	12.0	4.5	10.4	1600	54.7	35.2	0.64	2.09	61.8	26.1	1600	40.4	3.54	28.4	93	3.34
40	6.0	1.2	2.8	1200	53.2	30.3	0.57	2.32	61.1	22.9	1200	41.9	3.92	29.1	102	3.14
	6.0	1.2	2.8	1600	55.4	36.3	0.66	2.40	63.5	23.1	1600	43.0	3.58	30.9	95	3.52
	9.0	2.6	6.0	1200	53.4	30.4	0.57	2.24	61.1	23.9	1200	43.8	3.95	30.9	104	3.25
	9.0	2.6	6.0	1600	55.7	36.4	0.65	2.31	63.5	24.1	1600	45.0	3.61	32.8	96	3.65
	12.0	4.4	10.2	1200	53.7	30.4	0.57	2.18	61.1	24.6	1200	44.9	3.97	31.8	105	3.31
	12.0	4.4	10.2	1600	55.9	36.4	0.65	2.26	63.6	24.8	1600	46.1	3.63	33.8	97	3.72
50	6.0	1.1	2.5	1200	52.6	30.7	0.58	2.60	61.5	20.2	1200	47.2	4.01	33.9	106	3.45
	6.0	1.1	2.5	1600	54.8	36.8	0.67	2.69	63.9	20.4	1600	48.5	3.67	36.0	98	3.87
	9.0	2.5	5.8	1200	53.5	30.9	0.58	2.44	61.8	21.9	1200	49.6	4.06	36.1	108	3.58
	9.0	2.5	5.8	1600	55.7	37.0	0.66	2.52	64.3	22.1	1600	50.9	3.71	38.3	99	4.02
	12.0	4.2	9.7	1200	53.8	30.9	0.57	2.37	61.9	22.7	1200	50.9	4.08	37.3	109	3.65
	12.0	4.2	9.7	1600	56.0	37.0	0.66	2.45	64.3	22.9	1600	52.2	3.73	39.6	100	4.10
60	6.0	1.0	2.3	1200	50.7	30.2	0.60	2.85	60.4	17.8	1200	52.8	4.12	39.0	111	3.75
	6.0	1.0	2.3	1600	52.8	36.2	0.68	2.94	62.8	17.9	1600	54.2	3.77	41.4	101	4.22
	9.0	2.4	5.5	1200	52.1	30.6	0.59	2.67	61.2	19.5	1200	55.6	4.18	41.6	113	3.90
	9.0	2.4	5.5	1600	54.3	36.6	0.68	2.76	63.7	19.7	1600	57.1	3.82	44.1	103	4.38
	12.0	4.0	9.2	1200	52.7	30.7	0.58	2.59	61.5	20.4	1200	57.2	4.21	43.0	114	3.98
	12.0	4.0	9.2	1600	54.9	36.8	0.67	2.67	64.0	20.5	1600	58.8	3.85	45.6	104	4.47
70	6.0	1.0	2.3	1200	48.3	29.5	0.61	3.13	59.0	15.4	1200	58.6	4.24	44.2	115	4.05
	6.0	1.0	2.3	1600	50.3	35.3	0.70	3.24	61.3	15.5	1600	60.2	3.88	46.9	105	4.54
	9.0	2.3	5.3	1200	50.0	30.0	0.60	2.93	60.0	17.0	1200	61.9	4.32	47.2	118	4.20
	9.0	2.3	5.3	1600	52.1	35.9	0.69	3.03	62.4	17.2	1600	63.6	3.95	50.1	107	4.72
	12.0	3.8	8.8	1200	50.8	30.2	0.59	2.84	60.5	17.9	1200	63.8	4.36	48.9	119	4.29
	12.0	3.8	8.8	1600	52.9	36.2	0.68	2.93	62.9	18.0	1600	65.5	3.99	51.9	108	4.81
80	6.0	0.9	2.1	1200	45.7	28.7	0.63	3.45	57.5	13.2	1200	64.6	4.38	49.6	120	4.32
	6.0	0.9	2.1	1600	47.6	34.4	0.72	3.57	59.8	13.3	1600	66.3	4.01	52.6	108	4.85
	9.0	2.3	5.3	1200	47.5	29.2	0.62	3.23	58.5	14.7	1200	68.4	4.47	53.0	123	4.48
	9.0	2.3	5.3	1600	49.4	35.0	0.71	3.34	60.8	14.8	1600	70.2	4.09	56.2	111	5.03
	12.0	3.6	8.3	1200	48.3	29.5	0.61	3.13	59.0	15.5	1200	70.5	4.53	54.9	124	4.56
	12.0	3.6	8.3	1600	50.3	35.3	0.70	3.23	61.4	15.6	1600	72.4	4.14	58.3	112	5.12
85	6.0	0.9	2.1	1200	44.4	28.4	0.64	3.64	56.8	12.2	1200	67.6	4.46	52.3	122	4.45
	6.0	0.9	2.1	1600	46.2	34.0	0.74	3.76	59.1	12.3	1600	69.4	4.07	55.5	110	4.99
	9.0	2.3	5.2	1200	46.1	28.8	0.63	3.40	57.7	13.5	1200	71.7	4.56	55.9	125	4.60
	9.0	2.3	5.2	1600	48.0	34.5	0.72	3.52	60.0	13.6	1600	73.6	4.17	59.3	113	5.17
	12.0	3.6	8.2	1200	47.0	29.1	0.62	3.29	58.2	14.3	1200	73.9	4.62	57.9	127	4.69
	12.0	3.6	8.2	1600	48.9	34.8	0.71	3.40	60.6	14.4	1600	75.9	4.23	61.4	114	5.26
90	6.0	0.9	2.1	1200	43.1	28.1	0.65	3.82	56.1	11.3	1200	70.6	4.53	55.0	125	4.57
	6.0	0.9	2.1	1600	44.9	33.6	0.75	3.95	58.4	11.4	1600	72.5	4.14	58.4	112	5.13
	9.0	2.2	5.1	1200	44.8	28.4	0.64	3.57	57.0	12.5	1200	74.9	4.65	58.8	128	4.72
	9.0	2.2	5.1	1600	46.6	34.1	0.73	3.69	59.2	12.6	1600	76.9	4.25	62.4	115	5.30
	12.0	3.5	8.1	1200	45.6	28.7	0.63	3.46	57.4	13.2	1200	77.3	4.72	60.9	130	4.80
	12.0	3.5	8.1	1600	47.5	34.3	0.72	3.57	59.7	13.3	1600	79.3	4.31	64.6	116	5.39
100	6.0	0.8	1.8	1200	40.8	27.8	0.68	4.24	55.3	9.6	Operation not recommended					
	6.0	0.8	1.8	1600	42.5	33.3	0.78	4.39	57.5	9.7						
	9.0	2.1	4.9	1200	42.2	27.9	0.66	3.97	55.8	10.6						
	9.0	2.1	4.9	1600	44.0	33.4	0.76	4.10	58.0	10.7						
	12.0	3.3	7.6	1200	43.0	28.1	0.65	3.83	56.1	11.2						
	12.0	3.3	7.6	1600	44.8	33.6	0.75	3.96	58.3	11.3						
110	6.0	0.8	1.8	1200	39.2	27.8	0.71	4.68	55.2	8.4						
	6.0	0.8	1.8	1600	40.8	33.3	0.82	4.84	57.4	8.4						
	9.0	2.0	4.6	1200	40.1	27.9	0.69	4.42	55.2	9.1						
	9.0	2.0	4.6	1600	41.8	33.4	0.80	4.57	57.4	9.2						
	12.0	3.2	7.4	1200	40.7	27.9	0.69	4.27	55.3	9.5						
	12.0	3.2	7.4	1600	42.4	33.5	0.79	4.41	57.5	9.6						
120	6.0	0.7	1.6	1200	38.1	28.7	0.75	5.25	56.1	7.3						
	6.0	0.7	1.6	1600	39.7	34.4	0.87	5.42	58.3	7.3						
	9.0	1.9	4.4	1200	39.2	28.8	0.74	4.97	56.2	7.9						
	9.0	1.9	4.4	1600	40.8	34.5	0.85	5.14	58.4	7.9						
	12.0	3.0	6.9	1200	39.8	28.9	0.73	4.82	56.2	8.3						
	12.0	3.0	6.9	1600	41.4	34.6	0.84	4.98	58.5	8.3						

Interpolation is permissible; extrapolation is not.
All entering air conditions are 80°F DB and 67°F WB in cooling, and 70°F DB in heating.
AHRI/ISO certified conditions are 80.6°F DB and 66.2°F WB in cooling and 68°F DB in heating.
Table does not reflect fan or pump power corrections for AHRI/ISO conditions.
All performance is based upon the lower voltage of dual voltage rated units.
Performance stated is at the rated power supply, performance may vary as the power supply varies from the rated.
Operation below 40°F EWT is based upon a 15% methanol antifreeze solution.
Operation below 60°F EWT requires optional insulated water/refrigerant circuit.
See performance correction tables for operating conditions other than those listed above.
See Performance Data Selection Notes for operation in the shaded areas.

Figure 3.8: Example of data provided by the Manufacturer [ClimateMaster, 2010]

Figure 3.9 shows the inputs and outputs of the performance maps. Comparing the inputs and outputs of the model shown in Table 3.3 to those shown in the black box diagram shows that the desired inputs and outputs of the overall model do not completely match the inputs and outputs of the performance maps. For example, the integrated model uses φ, relative humidity, to represent the moisture content of the air and the performance maps uses $T_{WB,AIR}$, the wet bulb temperature of the air.

Figure 3.9: Black box of performance map model

3.2.2 Assumptions

The performance map model makes two categories of assumptions about the heat pump: operational and computational assumptions. The latter assumptions are associated with model calculations and are discussed throughout the document where applicable as well as listed in Table 3.4. The operational assumptions are based on the operation of the heat pump, such as the heat pump has a single speed fan and a single stage compressor. Multi-speed fans and two stage compressors are ultra-efficient, but they were not considered due to the increase in the complexity of the control algorithms; these additions represent a desirable improvement for future work. The model currently assumes that the air flow rate, $\dot{V}_{AIR}$, is constant throughout the simulation. Constant air flow was assumed due to the lack of model information associated with pressure drops in the distribution systems of the conditioned air. This assumption could be relaxed by implementing a resistance model of the air ducts.

Table 3.4: Performance Map Model Assumptions

Assumptions	Related Section
Linear interpolation for performance map data	Section 3.2.3.1
Calculate T_{WB} based on empirical equations	Section 3.2.4
Air and water vapor are ideal gases for condensation calculations	Section 3.2.5
Condensation and leaving water temperature calculations assume that the processes are steady state, steady flow	Section 3.2.5

3.2.3 Model Calculations

The performance map calculations are divided into two steps. The first step uses interpolation to determine the operating conditions based on the inlet water temperature, $T_{WATER,IN}$, and the volumetric water flow rate, $\dot{V}_{WATER}$, based on nominal volumetric air flow rates and inlet air conditions. The second step then uses correction factors to account for the actual volumetric air flow rate, $\dot{V}_{AIR}$, the inlet air dry bulb and wet bulb temperatures, $T_{DB,AIR}$ and $T_{WB,AIR}$ and the concentration and type of antifreeze. A set of example performance map calculations can be found in Table 3.5. As previously mentioned the performance map model inputs are different from the inputs from the integrated model. In order for the models to work together the inputs to the performance map model need to be calculated. Since the performance map model is a steady state model a method has been implemented to represent the transient response of the system.

3.2.3.1 Interpolation

To determine the operating conditions based on the inlet water temperature, $T_{WATER,IN}$, and the volumetric water flow rate, $\dot{V}_{WATER}$, a double interpolation method is used. The performance map provides data over a range of inlet water temperatures from 20−120$^{\circ}F$, and for each inlet water temperature three different volumetric water flow rates are given. The data is provided for a set of nominal airflow rates that vary by the capacity of the heat pump and the nominal inlet air conditions set at 68$^{\circ}F$ dry bulb for heating and 80$^{\circ}F$ dry bulb and 67$^{\circ}F$ wet bulb for cooling. An example performance map data was shown in Figure 3.8

The model uses linear interpolation to determine the values of operating conditions between the reported operating conditions. The linear interpolation assumes that the relationship between the independent, *x*, and dependent, *y*, values are linear with a slope determined by the closest known operating conditions. The formula used for this calculation is given in Equation 3.1.

$$y = y_1 + (x - x_2)\frac{y_2 - y_1}{x_2 - x_1} \text{ where } y_1 = f(x_1) \ \& \ y_2 = f(x_2) \tag{3.1}$$

The model first interpolates based on the inlet water temperature and then interpolates based on the volumetric water flow rate. Since each reported inlet water temperature has multiple reported volumetric water and air flow rates associated with it, the model interpolates over the range of reported volumetric water and air flow rates values. An example of this is shown in Table 3.5 under Step 1. The next step is to interpolate the values based on the volumetric flow rate of water, which is performed similarly to previous step and shown in Table 3.5 under Step

2. The result of completing the interpolation is a complete set of operating conditions for the specified inlet water temperature and flow rate and the nominal inlet air conditions and flow rates.

Table 3.5: Example Calculations - Interpolation and Correction Factors

Entering Air Temp DB	75 F	NOTES: 1) Correction Factors are From Matlab and Table Values are directly taken from the provided correction factor tables 2)All Interpolation is done in the Excel Spreadsheet 3) Error on Correction Factors includes error on curve fitting	
Entering Water Temp	65 F		
GPM	9 GPM		
Airflow	1313.2 CFM		
Entering Air Temp WB	66.23 F		

Interpolation Data

EWT F	Water Flow Rate GPM	Air Flow Rate CFM	Heating Capacity kBtuh	Power kW	Heat Extracted kBtuh	Cooling Total Capacity kBtuh	Sensible Capacity kBtuh	Power kW	Heat Rejected kBtuh
60	5.5	1050		43	3.15	32.3	40.6	26	2.17	48
60	5.5	1400		44.1	2.88	34.3	42.3	31.1	2.24	49.9
60	8.3	1050		45.1	3.19	34.2	41.9	26.4	2.06	48.9
60	8.3	1400		46.3	2.91	36.3	43.6	31.7	2.13	50.9
60	11	1050		45.7	3.2	34.8	42.5	26.6	1.99	49.3
60	11	1400		46.9	2.93	36.9	44.3	31.9	2.05	51.3
70	5.5	1050		47.6	3.24	36.6	38	24.8	2.37	46.1
70	5.5	1400		48.9	2.96	38.8	39.6	29.7	2.45	48
70	8.3	1050		49.9	3.29	38.6	39.6	25.5	2.25	47.3
70	8.3	1400		51.2	3.01	41	41.3	30.6	2.33	49.2
70	11	1050		51.1	3.33	39.7	40.4	25.9	2.19	47.9
70	11	1400		52.5	3.04	42.1	42.1	31	2.26	49.8

Step 1: Interpolation for $T_{WATER,IN}$

EWT	Water Flow Rate	Air Flow Rate	Heating Capacity	Power	Heat Extracted	Cooling Total Capacity	Sensible Capacity	Power	Heat Rejected
65	5.5	1050		45.3	3.195	34.45	39.3	25.4	2.27	47.05
65	5.5	1400		46.5	2.92	36.55	40.95	30.4	2.345	48.95
65	8.3	1050		47.5	3.24	36.4	40.75	25.95	2.155	48.1
65	8.3	1400		48.75	2.96	38.65	42.45	31.15	2.23	50.05
65	11	1050		48.4	3.265	37.25	41.45	26.25	2.09	48.6
65	11	1400		49.7	2.985	39.5	43.2	31.45	2.155	50.55

Step 2: Interpolation for V_{WATER}

EWT	Water Flow Rate	Air Flow Rate	Heating Capacity	Power	Heat Extracted	Cooling Total Capacity	Sensible Capacity	Power	Heat Rejected
65	9	1050	47.7333	3.2465	36.6204	40.9315	26.0278	2.1381	48.2296
65	9	1400	48.9963	2.9665	38.8704	42.6444	31.2278	2.2106	50.1796

Step 3: Correction Factors for V_{AIR}

	Air Flow Ratio	Heating Capacity	Power	Heat Extracted	Cooling Total Capacity	Sensible Capacity	Power	Heat Rejected
Correction Factor	0.9380	0.9940	1.0169	0.9880	0.9924	0.9583	0.9907	0.9920
Table Values		0.9940	1.0167	0.9880	0.9923	0.9578	0.9906	0.9920
Error		0.00%	-0.02%	0.00%	-0.01%	-0.05%	-0.01%	0.00%
Corrected Value	1313.2	48.7023	3.0166	38.4039	42.3203	29.9256	2.1900	49.7782

Step 4: Correction Factors for Entering Air Conditions

	Heating - Based on $T_{AIR,DRY}$			Cooling- Based on $T_{AIR,WET}$			
	Capacity	Power	Heat Extracted	Total Capacity	Sensible Capacity	Power	Heat Rejected
Correction Factor	0.9892	1.0558	0.9719	0.9860	0.8137	1.0003	0.9873
Table Values	0.9883	1.0556	0.9706	0.9882	0.8152	0.999	0.9903
Error	-0.09%	-0.02%	-0.13%	0.22%	0.18%	-0.13%	0.30%

3.2.3.2 Correction Factors

To account for conditions other than the nominal inlet air conditions and flow rates a set of correction factors are used to scale the operating conditions. The correction factors are valid for all of the GHPs in a single model line; i.e. the correction factors are valid for all Tranquility 20 heat pumps regardless of the capacity. The corrections factors are provided in tabular form as shown in Tables 3.6 and 3.7. The correction factors were implemented using two different methods; one based on curve fitting and the other was specifically designed for the sensible capacity correction factors in Table 3.7.

3.2.3.2.1 Curve Fitting Method

All correction factors, except the sensible cooling correction factor, are a function of a single variable. For example, in Table 3.6 the correction factors are based on the % of rated airflow. To implement these correction factors in the model an equation was fit to each set of values. Figure 3.10 shows a plot of the airflow correction factors for heating that are in Table 3.6 with the curve fits and the resulting equations. All curve fits are based on polynomials and achieved good agreement with the data as represented by the R^2 value in the plot. Table 3.5 was used to verify the accuracy of the curve fits and that the model was calculating the correction factors correctly. The test inlet conditions were chosen to correspond to values reported in the correction factor tables. For example, the volumetric air flow was chosen to be 1313.2 CFM which is 93.75% of the rated airflow. This allows for the correction factor to be calculated in the model and compared directly with the values in the table, and based on these two values an error was calculated. Table 3.5 shows that the error is significantly less that 1% for all correction factors.

Table 3.6: Correction Factors for Airflow [ClimateMaster, 2010]

PSC Fan Motor

Airflow	Cooling					Heating		
% of Rated	Total Capacity	Sensible Capacity	S/T	Power	Heat of Rejection	Heating Capacity	Power	Heat of Extraction
68.75%	0.9465	0.8019	0.8472	0.9614	0.9496			
75%	0.9602	0.8350	0.8696	0.9675	0.9617	0.9740	1.0936	0.9425
81.25%	0.9724	0.8733	0.8981	0.9744	0.9728	0.9810	1.0635	0.9582
87.50%	0.9831	0.9149	0.9306	0.9821	0.9829	0.9876	1.0379	0.9744
93.75%	0.9923	0.9578	0.9653	0.9906	0.9920	0.9940	1.0167	0.9880
100%	1.0000	1.0000	1.0000	1.0000	1.0000	1.0000	1.0000	1.0000
106.25%	1.0062	1.0392	1.0328	1.0102	1.0070	1.0057	0.9878	1.0105
112.50%	1.0109	1.0733	1.0617	1.0211	1.0130	1.0112	0.9800	1.0194
118.75%	1.0141	1.1001	1.0848	1.0329	1.0180	1.0163	0.9705	1.0284
125%	1.0159	1.1174	1.0999	1.0455	1.0220	1.0211	0.9614	1.0368
130%	1.0161	1.1229	1.1050	1.0562	1.0244	1.0247	0.9554	1.0430

Black area denotes where operation is not recommended.

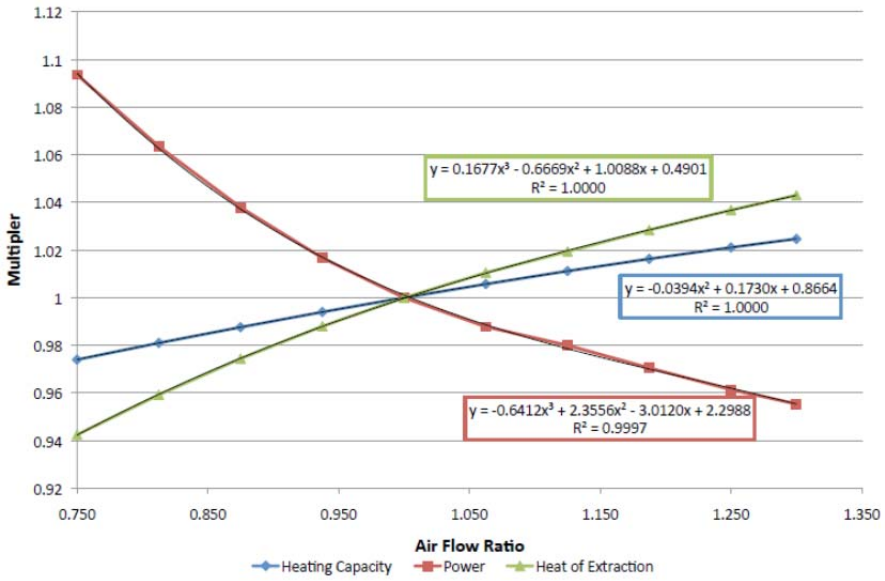

Figure 3.10: Plot of correction factors for airflow fraction during heating

3.2.3.2.2 Wet Bulb Corrections for Cooling

The correction factors for the sensible cooling capacity are based on both the wet bulb and dry bulb temperatures as shown in Table 3.7. To implement this into the model, MATLAB's built in interpolation command, *interp2(Z, XI, YI)*, was used. Since the correction factors are not defined for every wet bulb and dry bulb temperature combination in the table two boundary functions were determined based on the table. These allow for the model to determine if the particular combination of inlet conditions is not recommended, blacked out in Table 3.7, or if it is too dry for any latent cooling to occur, starred in Table 3.7.

Table 3.7: Correction Factors for Wet Bulb Temperature [ClimateMaster, 2010]

Cooling												
Entering Air WB°F	Total Capacity	Sensible Cooling Capacity Multiplier - Entering DB °F									Power	Heat of Rejection
		60	65	70	75	80	80.6	85	90	95		
50	0.7432	0.9111	*	*	*	*	*	*	*	*	0.9866	0.7901
55	0.8202	0.7709	0.8820	1.0192	*	*	*	*	*	*	0.9887	0.8527
60	0.8960		0.6702	0.8540	1.0473	*	*	*	*	*	0.9924	0.9146
65	0.9705			0.6491	0.8657	1.0809	1.1066	*	*	*	0.9975	0.9757
66.2	0.9882			0.5939	0.8152	1.0333	1.0592	1.2481	*	*	0.9990	0.9903
67	1.0000			0.5559	0.7801	1.0000	1.0261	1.2158	*	*	1.0000	1.0000
70	1.0438				0.6377	0.8645	0.8913	1.0847	1.2983	*	1.0042	1.0362
75	1.1159	Operation not recommended				0.6008	0.6289	0.8323	1.0578	1.2773	1.0123	1.0959

* = Sensible capacity equals total capacity
AHRI/ISO/ASHRAE 13256-1 uses entering air conditions of Cooling - 80.6°F DB/66.2°F WB, 1 and Heating - 68°F DB/59°F WB entering air temperature

3.2.4 Wet-Bulb Calculations

In order to implement the performance maps the wet bulb temperature of the incoming air is required, and the integrated building-GHP model provides φ, the relative humidity. During the creation of the model two different methods of calculating the wet bulb temperature where explored. The first method, based on the Clausius-Clapeyron equation, Equation 3.2, used the saturation pressure of water and the volume fraction of water, Equation 3.3, in the air to calculate the relative humidity [Schmidt et al., 2006].

$$ln(P_{SAT}) = \frac{21.4T + 494.41}{T + 273.15} \tag{3.2}$$

$$y = \frac{(T_{DB,AIR} - T_{WB,AIR})c_p^{AIR} - L_V(P_{WB,SAT}/P)}{-(T_{DB,AIR} - T_{WB,AIR})c_p^{VAPOR} - L_V} \tag{3.3}$$

This model was useful since it is valid for any atmosphere pressure.

The second method uses a series of empirically determined curves based on a psychometric chart (U.S. Department of Commerce, Weather Bureau). Equations that relate the dry bulb temperature to the wet bulb temperature of the form shown in Equation 3.4 were found for constant relative humidity values.

$$T_{WB} = aT_{DB}^2 + bT_{DB} + c \tag{3.4}$$

For a given dry bulb temperature a range of wet bulb temperatures are calculated for the range of relative humidity specified. The actual wet bulb temperature is then interpolated based on the actual relative humidity. A disadvantage of this model is that it is only valid for a given altitude. Therefore the equations need to be updated as the altitude of the simulation changes.

To ensure the accuracy of these conversions, the calculated relative humidity values, φ, was compared to a table published by NOAA that converts dry bulb and wet bulb temperatures into relative humidity based on psychometric charts [US Dept Commerce, 2010] The results are shown in Figures 3.11 and 3.12. Figure 3.11 shows that the error for the Clausius-Clapeyron equation is large at low temperatures and high φ. In comparison Figure 3.12 shows the error based on the curve fit equations, which is significantly less than the Clausius-Clapeyron equation. Based on these results the curve fitting method was chosen.

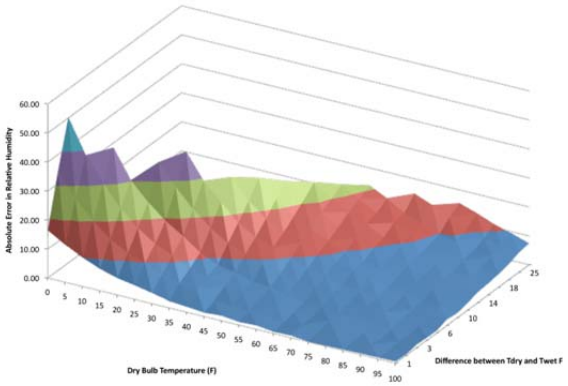

Figure 3.11: Absolute error for relative humidity to wet bulb temperature calculations based on Clausius-Clapeyron equation

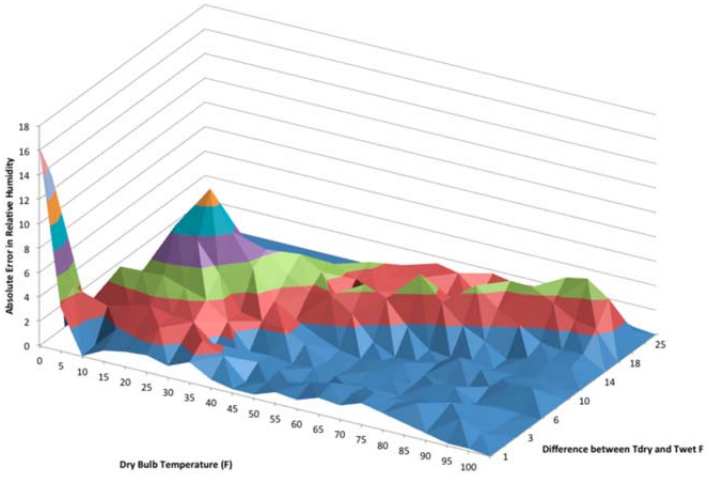

Figure 3.12: Absolute error for relative humidity to wet bulb temperature calculations based on curve-fitted equations

3.2.5 Condensation Calculations

The dehumidification of the conditioned air space is important for occupant comfort. The building model accounts for this by allowing the mass flow rate of water removed from the air to be specified. The performance map calculates the latent cooling capacity, which is the amount of cooling associated with water condensing out of the air. Assuming that water vapor and air are ideal gases and that the process is in a steady state, steady flow process an energy balance for the air/water vapor mixture flowing through the heat pump can be written as shown in Equation 3.5 [Schmidt et al., 2006].

$$h_{DA,IN} + \omega_{IN} h_{WV,IN} + \frac{\dot{Q}}{\dot{m}_{DA}} = h_{DA,OUT} + \omega_{OUT} h_{WV,OUT} \tag{3.5}$$

In the equation h_{DA} and h_{WV} are the enthalpies of the dry air and water vapor, ω is the humidity ratio, $\dot{Q}$ is the energy added to the system, and $\dot{m}_{DA}$ is the mass flow rate of dry air. Realizing that $\dot{Q}$ has been determined from the performance maps in the form of Equation 3.6 the portions of Equation 3.5 associated with the dry air can be removed reducing it to Equation 3.7.

$$\dot{Q} = -(\dot{Q}_{Latent} + \dot{Q}_{Sensible}) \tag{3.6}$$

$$\omega_{IN} h_{WV,IN} + \frac{-\dot{Q}_{Latent}}{\dot{m}_{DA}} = \omega_{OUT} h_{WV,OUT} \tag{3.7}$$

Assuming that the enthalpy of the water vapor is constant over the process Equation 3.7 reduces to Equation 3.8.

$$\omega_{OUT} = \omega_{IN} + \frac{-\dot{Q}_{Latent}}{\dot{m}_{DA} h_{WV}} \tag{3.8}$$

Recognizing that ω is defined as shown in Equation 3.9, the mass balance of the water vapor for the process can be rewritten as shown in Equation 3.10.

$$\omega = \frac{\dot{m}_{WV}}{\dot{m}_{DA}} \tag{3.9}$$

$$\dot{m}_{cond} = \dot{m}_{DA}(\omega_{IN} - \omega_{OUT}) \tag{3.10}$$

Combining Equation 3.8 and Equation 3.10 gives Equation 3.11, which relates the rate of water condensation, $\dot{m}_{cond}$, to the rate of latent cooling, $\dot{Q}_{Latent}$, and the enthalpy of the water vapor in the air, h_{WV}.

$$\dot{m}_{cond} = \frac{\dot{Q}_{Latent}}{h_{WV}} \tag{3.11}$$

3.2.6 Leaving Water Temperature Calculations

The performance map calculates the amount of heat rejected/extracted into/from the ground loop water, but does not directly calculate the temperature change of the water. An option would be to assume that all of the heat rejected/extracted into/from the water was then rejected/extracted into/from the ground. This is true most of the time but it does not account for the temperature change in the ground loop water which will affect the efficiency the heat pump and the rate of heat transfer into the ground. Therefore, the temperature rise of the ground loop water as it passes through the heat pump needs to be calculated. Performing a energy balance assuming steady state, steady flow gives Equation 3.12.

$$u_{IN} + \frac{\dot{Q}}{\dot{m}} = u_{OUT} \tag{3.12}$$

$$T_{OUT} = T_{IN} + \frac{\dot{Q}}{\dot{m}c} \tag{3.13}$$

By assuming that the heat capacity, *c*, is constant and rearranging Equation 3.12 to solve for T_{OUT} in Equation 3.13.

3.3 VERTICAL BOREHOLE-GROUND LOOP MODEL

The vertical borehole-ground loop model computes temperatures inside the borehole and the ground outside the borehole. A schematic of a single borehole is shown in Figure 3.13. The model must properly interface with the rest of the combined building-GHP model so must meet the following requirements:

- Calculate the heat transferred into the ground by specifying only the inlet water (or antifreeze) temperature and flow rate and the previous ground loop loads.
- Be computationally efficient.
- Model the effect of multiple boreholes in close proximity to compute ground coupling.
- Accommodate time steps at least smaller than an hour and preferably on the minute time scale.
- Be validated.

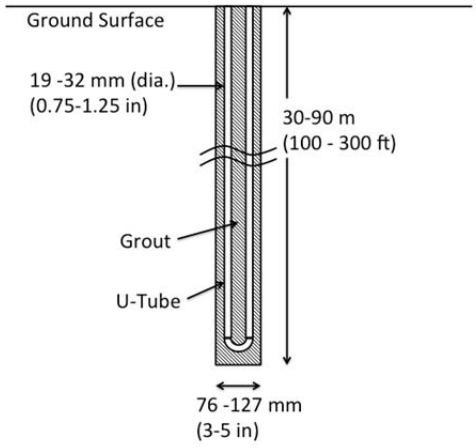

Figure 3.13: Drawing of vertical borehole ground loop with approximate dimensions

3.3.1 Borehole Models: Review

In general, the heat transfer in the bulk ground outside the borehole is typically treated as a heat conduction problem with a line or cylindrical source in an infinite or semi-infinite medium.

Inside the borehole, there is convection between the water and u-tube and conduction between the two legs of the u-tube, the grout, and the surrounding ground.

Hellström developed an analytical solution for the resistance network heat transfer between the two segments of the u-tube and the ground assuming uniform temperature around the circumference of the borehole [Helstrom, 1991]. Hellström's two-dimensional model was extended by Zeng et al. to create a quasi three-dimensional model by adding the heat capacity of the fluid and defining the equations over the total borehole length, H [Zeng et al., 2003].

Bennet et al. [Bennet et al, 1987] developed an analytical multipole model which calculates the conductive heat flow between pipes of different radii, does not require symmetry along the borehole axis, and uses multiple sets of line sources with line sinks at mirrored points to solve the general two-dimensional steady-state Fourier heat conduction equation. Each leg of the u-tube is represented by point heat sources and sinks and constant temperatures are assumed inside the pipe walls and the outer boundary conditions defined at, r_b, the radius of the outer region (set to 100 m). Young showed that using ten sources per pipe (10^{th}-order) gave results with at least four digits of accuracy [Young, 2004]. Xu also used the multipole model to calculate the total thermal resistance of the borehole using Equation 3.14 below and for calculating equivalent resistances for his one-dimensional borehole model [Xu, 2007]:

$$R_{BH} = \frac{T_{fluid} - T_{BH}}{q_{utube,1} + q_{utube,2}} \tag{3.14}$$

where T_{BH} is the average borehole wall temperature, T_{fluid} is the average u-tube pipe temperature, and $q_{utube,1}$ and $q_{utube,2}$ are the heat fluxes out of each leg of the u-tube, respectively.

3.3.2 Bulk Ground Models: Review

Eskillson developed an analytical solution to a finite line source model, which assumes a semi-infinite medium with a uniform initial temperature, constant heat flux, and constant surface temperature. The finite line source solution is derived by dividing the borehole into point sources and integrating their contributions to get the temperature response in the ground. The constant heat flux assumption requires that the heat transfer be calculated for the entire length of the borehole [Ekillson, 1987]. Using this solution, the borehole wall temperature is computed over time for a given heat flux. Since the model approximates a finite radius borehole with a line source with no radius, it has a lower time limit of $t = 5\,r_b^2/\alpha$, which corresponds to about 1-2 days for a 100 mm borehole in saturated clay. For times less than this limit, the model is not accurate [Ekillson, 1987].

Eskillson created a hybrid analytical-numerical technique (g-function model) to calculate ground temperatures around a borehole using a four-step approach:

Step 1: Thermal response of a single borehole is determined using a two-dimensional (radial-axial coordinates) finite volume method with a unit step heat input, assuming the ground is homogenous with constant boundary conditions. Since the time steps considered are much longer that the transient response of the borehole the thermal capacitance of the borehole is neglected [Ekillson, 1987].

Step 2: From the cylindrically symmetric response of a single borehole, the thermal response of multiple boreholes in a field is determined by spatial superposition. The ground temperature at an arbitrary point is represented by:

$$T(x, y, z, t) = T_0(z) + \sum_{i=1}^{N} T_i(r_i, z_i, t) \tag{3.15}$$

where T_i is the thermal response of borehole i, r_i and z_i are the radial distance and depth of the desired point in relation to borehole i, and $T_0(z)$ is the initial ground temperature.

Step 3: The thermal response is converted into non-dimensional response factors, which Eskillson calls "g-functions", which are functions of r_b/H, the ratio of borehole radius to borehole length, and t/t_s , the ratio of current time to the steady state time. The temperature response is given by:

$$T_b = T_0 + \frac{q}{2\pi k} g\left(\frac{t}{t_s}, \frac{r_b}{H}\right) \text{ where } t_s = \frac{H^2}{9\alpha} \tag{3.16}$$

$$\text{where } g\left(\frac{t}{t_s}, \frac{r_b}{H}\right) \approx \begin{cases} \ln\left(\frac{H}{2r_b}\right) + \frac{1}{2}\ln\left(\frac{t}{t_s}\right) & \text{for } \frac{5r_b}{\propto} < t < t_s \\ \ln\left(\frac{H}{2r_b}\right) & \text{for } t > t_s \end{cases}$$

By expressing the response in non-dimensional form, the thermal response of a particular borehole field geometry must be calculated only once and can be reused for different bulk ground properties by changing α, the diffusivity, and different borehole geometries by changing H and r_b. Selections of the resulting g-functions are shown in Figure 3.14 for the same ground properties and borehole geometry, the only difference is the number of boreholes and configuration (line or grid).

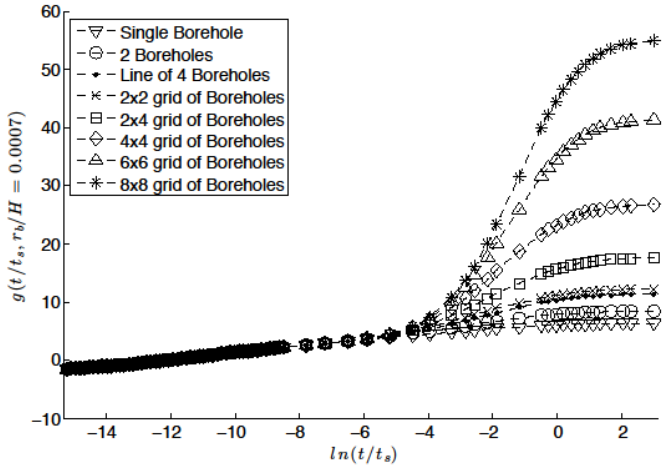

Figure 3.14: g-functions for typical borehole configurations [Oklahoma State University, 2007]

As the number of boreholes increases the interaction among them also increases causing an increase in the thermal response of each borehole, especially for values of $\ln(t/t_s) > -4$, which corresponds to approximately 8.5 months.

Step 4: The thermal response of the borehole to a time varying heat flux, $q(t)$, uses a temporal superposition technique that begins by approximating $q(t)$ with a piecewise constant function as shown in Figure 3.15 (left).

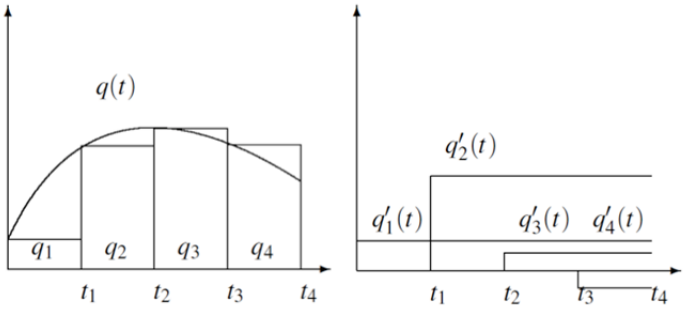

Figure 3.15: (Left) q(t) and its piecewise approximation, (right) Resulting temporal superposition of q(t)

Next, the piecewise approximation is decomposed into individual heat pulses switched on at the appropriate times and held constant until the end of the simulation as shown in Figure 3.15 (right). The heat pulses are represented as:

$$q_1'(t) = q_1 \qquad (3.17)$$

$$\sum^{n}$$

where $H(t)$ is the Heaviside step function and n is the number of time steps. Applying this decomposition to Equation 3.15 gives:

$$T_b = T_0 + \sum_{i=1}^{n} \frac{q_i - q_{i-1}}{2\pi k} g\left(\frac{t_n - t_i}{t_s}, \frac{r_b}{H}\right) \quad (3.18)$$

The total response of the borehole is a superposition of the temperature responses of n different heat fluxes, each added at a different start time, t_i [Hellstrom, 1991; Xu, 2007].

The g-function solution has a minimum time step requirement of $\Delta t > 5\, r_b^2/\alpha$. Since many building models produce hourly/sub-hourly loads the ground loop model should handle sub-hourly time steps. Xu extended the g-function model to allow for shorter time steps as described below [Xu, 2007].

3.3.3 Implemented Borehole-Ground Loop Model

Xu's one-dimensional, finite volume numerical model uses a fully implicit method to solve the discretized transient conduction equation in cylindrical coordinates, shown in Equation 3.19 [Xu, 2007].

$$\frac{1}{\alpha}\frac{\partial T}{\partial t} = \frac{\partial^2 T}{\partial r^2} + \frac{1}{r}\frac{\partial T}{\partial r} \quad (3.19)$$

The model assumes a single, centered pipe in the borehole, the effects of the ground surface and the end of the u-tube are negligible, uniform bulk ground properties, and the interaction between neighboring boreholes is negligible. The diameter of the pipe is taken as $\sqrt{2}$ times larger than a single leg of the actual u-tube to mimic the thermal mass of both the grout and water in the pipe. The model is divided into five grid sections as shown in Figure 3.16, each representing the different types of materials/heat transfer in the borehole.

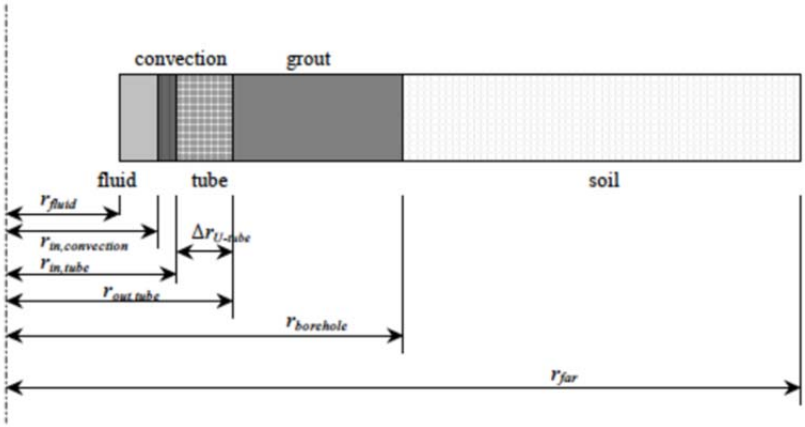

Figure 3.16: Grid method used in one-dimensional numerical model [Xu, 2007]

Each section is modeled as multiple individual finite volume cells; e.g. the far field $(r_{borehole} < r < r_{far})$ is represented by 500 cells. The two grid sections closest to the pipe centerline represent the ground loop fluid and convection between the fluid and inside of the u-tube. Equivalent heat transfer properties are used in each section. A single conductivity for the grout and the u-tube layers is calculated, as shown in Equation 2.3.7, based on the resistance of the actual two-dimensional borehole determined by the multipole method to ensure that the resistances of the one-and two-dimensional models are the same.

$$\mathrm{k_{equiv}} = \frac{\ln(\mathrm{r_b}/\mathrm{r_{tube,in}})}{2\pi \mathrm{R_{equiv}}} \tag{3.20}$$

where R_{equiv} is the resistance calculated by the multipole method and $r_{tube,in}$ is the inner radius of the single tube. The conductivity of the convection layer is calculated in a similar manner. The model performs the calculations each time step since the total borehole resistance changes with temperature.

The IBL-GHP model uses Xu's one-dimensional model for the short-term thermal response of the borehole and surrounding ground. The algorithm combines the load from each time step into larger blocks for the calculation of the g-functions [Ekillson, 1987]. The model then aggregates the loads and applies these loads to Eskillson's g-functions to calculate the long-term response as follows [Yavuzturk, 1999].

$$T_{borehole}(t) = T_{ground} + \Delta T_{one-d} + \sum_{m=1}^{M} \left[\frac{(\bar{q}_m - \bar{q}_{m-1})}{2\pi k} g\left(\frac{(t - t_m)}{t_s}, \frac{r_b}{H} \right) \right] + R_{equiv} q(t) \tag{3.20}$$

where $\bar{q}_m$ is the aggregated loads, ΔT_{one-d} is the temperature response of the one-dimensional model, and $q(t)$ is the current ground loop load. The heat rejected/extracted to the ground for each time step is calculated by:

$$Q(t) = \frac{(T_{ground} - T_{borehole})}{R_{total}} \tag{3.21}$$

$T_{borehole}$ is assumed to be the average of the inlet and outlet temperatures. The outlet temperature is then calculated using [Xu, 2007]:

$$T_{out} = 2T_{borehole} - T_{in} \tag{3.22}$$

Xu's model is computationally more complex than the line and cylindrical source models discussed previously, but it allows short time steps and a larger range of operating conditions to be considered. The use of the average borehole temperature can be problematic. If the inlet temperature changes significantly faster than the average borehole temperature can respond the outlet temperature must change significantly in the opposite direction and can cause large transient spikes in the outlet temperature, which in turn causes the ground loop temperatures to

fluctuate over the next time steps. For sufficiently large time steps the fluid in the ground loop will be completely replaced, so this assumption is never violated; for a 91.4m borehole with a 25mm diameter u-tube and 0.19 L/s water flow (typical for residential applications), this time-delay corresponds to 8.2 minutes [Xu, 2007].

4. IBL-GHP RESIDENTIAL MODEL

The integrated building load-GHP (ILB-GHP) model couples the component models described in Section 3 for the building loads, heat pump performance maps, and borehole-ground loop. In Section 4, the model was applied to a residential building and simulated to test the borehole sizing criterion using the heat pump shutoff temperature as the maximum heat pump EWT. This criterion would yield the minimum borehole length, maximum heat pump EWT, and minimum operational efficiency while still satisfying the heating/cooling needs of the building. Choosing lower heat pump EWTs would yield more conservative and more realistic actual designs.

Section 4.1 describes the Simulink computational environment. Sections 4.2-4.5 discuss the heat pump/thermostat, building load, borehole/ground, and water pump model implementations, respectively, into Simulink. Section 4.6 introduces the base case residential house used for the ILB-GHP model, specific heat pump, borehole sizing, and model validation comparisons with eQuest and GLHEPRO. Section 4.7 shows the base case simulation results. Section 4.8 presents the sensitivity studies from the base case for borehole length, borehole configuration and spacing, grout conductivity, ground temperature, and supplemental heat rejection.

4.1 SIMULINK MODELING/COMPUTATIONAL ENVIRONMENT

The MatLab/Simulink environment is designed for multi-domain simulation of dynamic systems. Simulink includes a graphical user interface that allows the user to modify the model. The model is presented in a block diagram format, with blocks that perform mathematical functions, data manipulation, or conditional statements. Simulink includes a large library of blocks for the user, as well as allowing the user to develop user-defined blocks using the functionality of MatLab. Large models can be divided into sub-models that act like sub-functions in traditional text based programming. For example, Figure 4.1 shows the main Simulink model in the graphical editor for the integrated building load-GHP model. The four largest blocks are sub-models that contain the models for HAMBASE, the performance map based heat pump model, Xu's ground loop model and the water pump model. Each block is a custom block that was created by the research team. The top level model also used some of the included blocks, such as the constant block, which outputs a constant value, and the selector, which selects a subset of an array of values [Mathworks, 2011].

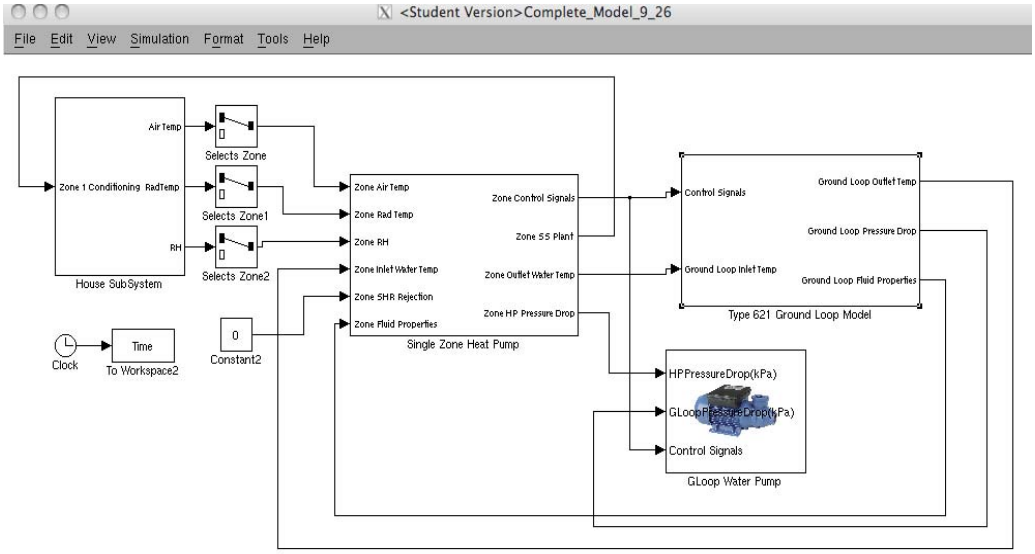

Figure 4.1: Top Level Simulink Model

The graphical model editor allows the user to easily make configuration changes to the model without rewriting the underling code. For example, a block that models a cooling tower can easily be dropped into the editor and connected into the ground loop without modifying any text-based code. The graphical environment also allows the model to be used by a non-expert user. For example, to change the size of the heat pump the user just double clicks on the heat pump model block and a menu appears that has the size of the heat pump in a drop down menu [Mathworks, 2011].

Simulink comes with built-in solvers to simulate the model. There are two types of solvers that can be used; variable time step solvers that change the size of the time step based on the integration error and fixed time step solvers. Each solver has multiple options for the order of the numerical solution. The model is solved using a 1st order, fixed step solver. An additional advantage of the Simulink environment is its ability to handle multi-rate simulations. In the integrated model the ground loop is simulated every five minutes and the rest of the model is simulated every 30 seconds. Simulink has built-in blocks to handle the required time step transitions and data manipulation [Mathworks, 2011].

The model was developed so that it could be expanded to include multiple heat pump models with a single building load model and a single ground loop model or even a case with multiple buildings and heat pumps with a single ground loop model. Therefore the model is divided into sub-models that are self-contained and can be duplicated inside of the model. The Simulink model is composed of three main sub-models, the building load model, the heat pump model and the ground loop model. The Simulink implementation of the building load, thermostat, heat pump, ground loop, and ground loop pump are shown in Figures 4.2-4.6, respectively.

4.2 HEAT PUMP IMPLEMENTATION

The heat pump sub-model, shown in Figure 4.2 contains the performance map heat pump model discussed in Section 3.2 as well as the thermostat to control the heat pump. As with all of the sub-models the inputs, which are designated by the small, numbered ovals, are defined on the left and the outputs on the right. They correspond to the connections in the top level model. For example, the heat pump sub-model has six inputs and four outputs. The large block in the middle of the sub-model contains the performance map code that was discussed previously. Figure 4.2 shows the drop-down menu which allows the user to select the heat pump size and manufacturer. The far right side of Figure 4.2 shows a large, square box labeled “HeatPumpOperation". This saves all the data that is connected to it. In the case of the heat pump sub-model the block saves all the outputs of the model as well as some selected inputs that are not saved in other sub-models. All sub-models have blocks like this to save the data.

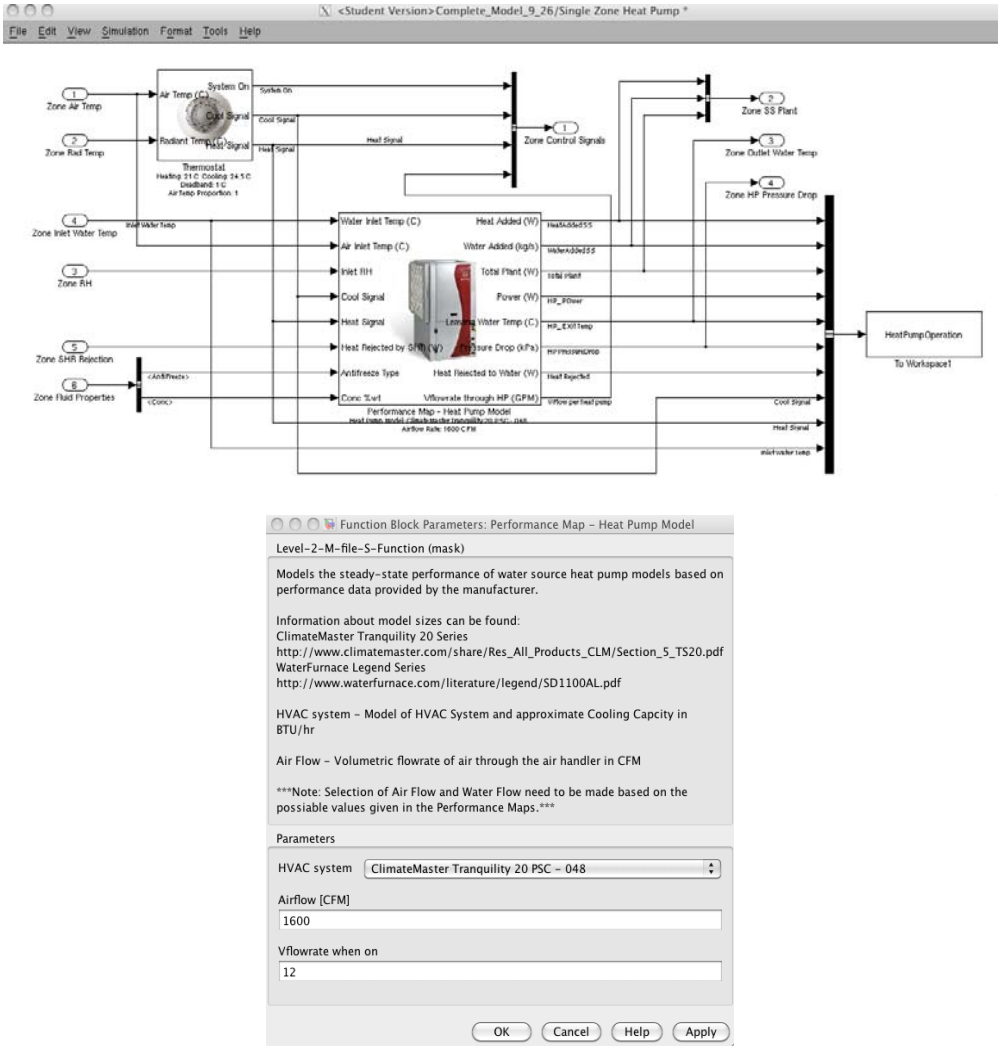

Figure 4.2: Performance map options

Thermostat Model: The heat pump is controlled by the thermostat model shown in Figure 4.2. The model determines the room temperature based on a combination of the zone air temperature, T_{air}, and the zone radiant wall temperature, T_{rad} as shown in Equation 4.1. The weighting factor, α determines how the air and radiant wall temperatures are combined.

$$T_M = \alpha T_{air} + (1-\alpha) T_{rad} \text{ where } 0 \le \alpha \le 1 \quad (4.1)$$

This equation is implemented in Simulink using the built-in blocks on the left hand side of the block diagram. The thermostat compares the temperature of the room to the user-defined temperature set points. This is accomplished by the thermostat blocks on the right hand side of the block diagram. These blocks model the deadband of the thermostats. The deadband keeps the heat pump on after the temperature has passed back through the set point until the temperature reaches a predefined value. For example, with the cooling set point at 25^{o}C and a 1^{o}C deadband the heat pump will turn on if the temperature goes above 25^{o}C and will stay on until the temperature reaches 24^{o}C. The thermostat also contains a menu that allows the user to modify the set points, deadband and α. The thermostat outputs a '1' for the proper signal when the thermostat determines that cooling or heating is needed. This signal is read by the performance map heat pump model to determine the proper state of operation, – cooling, off ('0' signal), or heating. The thermostat was modeled separately from the heat pump so that the control system could be modified separately from the heat pump model.

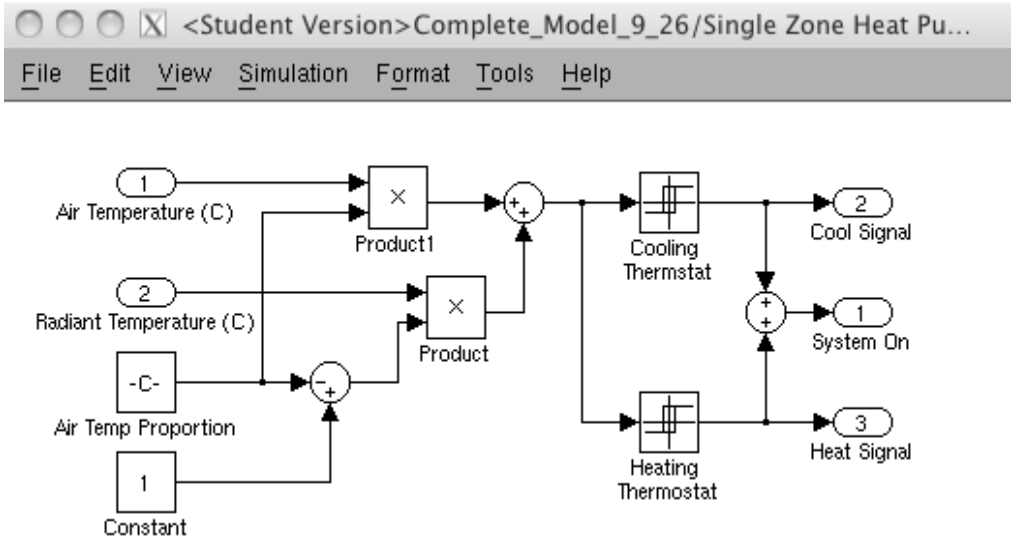

Figure 4.3 Simulink implementation of thermostat submodel

4.3 BUILDING LOAD MODEL IMPLEMENTATION

The Simulink implementation of the building load model, shown in Figure 4.4, takes the output of the heat pump model and simulates the response of the building. The HAMBASE model block takes in the sensible and latent loads from the heat pump and a ventilation rate. Each of these variables becomes an input to each zone. The model shown in Figure 4.4 has six total inputs, since there are two zones. The inputs to zone two are all zero since that zone is unconditioned. The block outputs the air temperature, radiant temperature and relative humidity for each zone as well as some additional building values that are not used, such as the wind pressure and external temperature. The building is defined in a text file that is read by the model. The text file controls the building structure, internal loads, basic ventilation, and building location. The text file referenced by the model can be changed under the menu associated with the building model block. All data is saved for the length of each simulation.

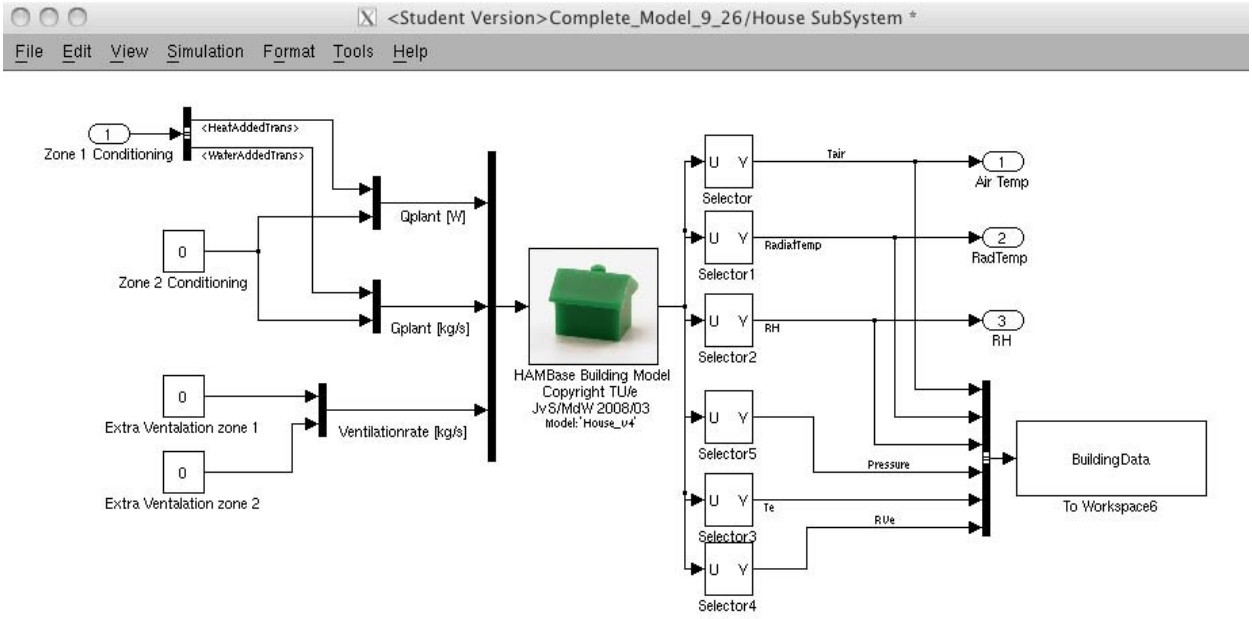

Figure 4.4: Simulink implementation of building load submodel

4.4 BOREHOLE-GROUND LOOP IMPLEMENTATION

The implementation of Xu's ground loop model is the most complex. The ground temperatures have a significantly slower response time than the building and the heat pump system, so the ground loop is simulated at larger time step intervals, every five minutes, than the rest of the model, which is simulated every 30 seconds. This multi-rate simulation capability increases the speed of the model as well as solving the issue with oscillating ground loop temperatures due to the way the outlet and inlet water temperatures are defined, as discussed

in Section 3.3.3. The model takes advantage of Simulink's built-in ability to model systems with different time steps.

The rate transition blocks shown in Figure 4.5 handle the timing and data transfer between the two time steps. The model assumes that the input water temperature and flow rate to the ground loop are the average value over the previous five minutes. The averaging is accomplished using the sub system shown on left of the ground loop model. This subsystem calculates the ground loop water flow rate over a set interval, L. To ensure that the energy content of the water represents the proper values based on the previous five minutes a weighted average of the short time step water temperatures is performed to calculate the long time step temperatures. The temperatures are weighed based on the flow rate for that time step, as shown in Equation 4.2. Where T_{long} is the long time step water temperature, V_i is a short time step water flow rate and T_i is a short time step water temperature.

$$T_{long} = \frac{\sum_{i=1}^{L} V_i T_i}{\sum_{i=1}^{L} V_i} \tag{4.2}$$

where L is a function of the differences in the time steps. The longer ground loop time step must be an integer multiple, L, of the shorter time step. For this case the long time step is equal to five minutes (300 seconds) and the short time step is equal to 30 seconds, so L is 10. The outputs of the ground loop model are only updated every five minutes so the rate transitions on the right side of the ground loop model act like zero-order holds. Due to the use of the multi-rate simulation there are two blocks that save the data from the ground loop model at the two different rates.

The ground loop parameters are specified in a text file that is created using GLHEPRO [Spitler, 2000]. GLHEPRO is a software package available from Oklahoma State University. The user must input the ground and borehole parameters into GLHEPRO to create the parameter file for the ground loop. In addition to creating the parameter files, GLHEPRO can be used to size the ground loop based on the building load and type of heat pump. See Section 4.6.3.1 for a description of how GLHEPRO is used with the Simulink model.

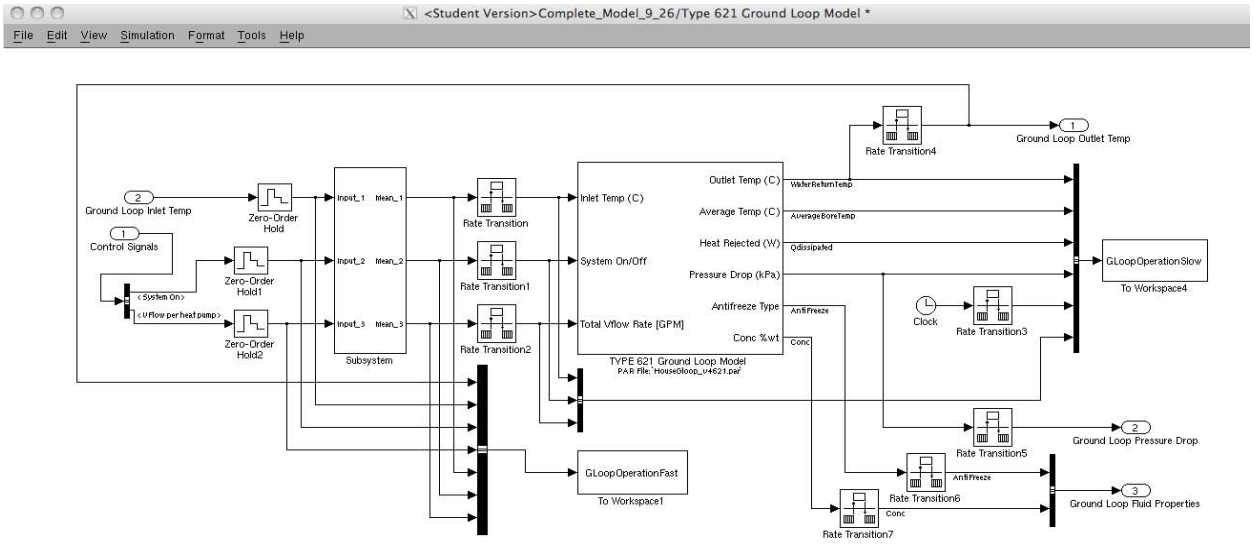

Figure 4.5: Simulink implementation of ground loop submodel

4.5 ADDITIONAL MODEL IMPLEMENTATION

A variety of data is shared between the different component model of the Simulink model. For example, the heat pump specifies the water flow rate through the ground loop. This was done so that the when the model is expanded to include multiple heat pumps, the flow rate through the ground loop depends on the number of heat pumps that are operating. The ground loop model specifies if antifreeze has been added to the ground loop water since GLHEPRO uses this information to calculate various ground loop parameters. To calculate the power needed to pump the water through the ground loop the total pressure drops for the specified flow rates are calculated in each of the component models by GLHEPRO. These pressure drops are then sent to the pump sub-model, shown in Figure 4.6, where the energy required to pump the fluid is calculated. The pumping power is calculated using Equation 4.3, where v_w is the specific volume of water, ΔP is the pressure drop across the system, and η is the pump efficiency.

$$W = \frac{v_w \Delta P}{\eta} \tag{4.3}$$

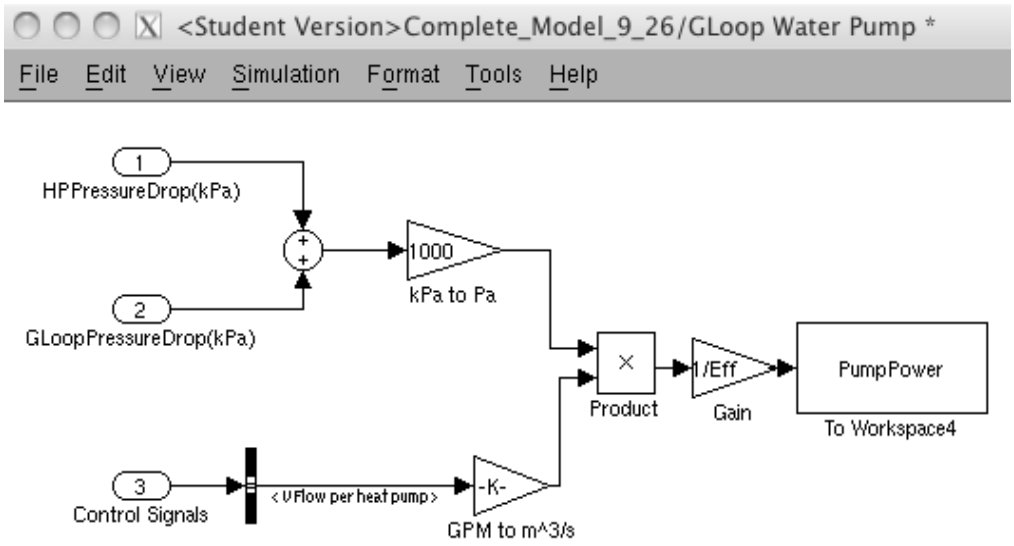

Figure 4.6: Simulink implementation of ground loop pump submodel

4.6 IBL- GHP MODEL APPLICATION TO BASE CASE RESIDENTIAL BUILDING

4.6.1 Residential Building Load

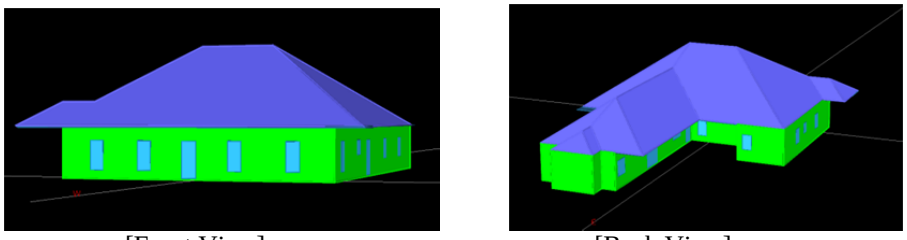

[Front View] [Back View]

Figure 4.7: Images of the modeled house

To test the IBL-GHP model, the base case study uses a 195m^2 (2100ft^2), single-story house placed in Austin, Texas. Figure 3.8 is an eQuest graphical rendering of the modeled house. It was assumed that the roof was a traditional, asphalt single roof instead of metal. The house was divided into two zones; the conditioned living area and the unconditioned attic. The conditioned zone is bounded by three different wall constructions: 1) Exterior walls—typical 2x4 construction with 100mm face brick on the outside, 13mm insulation board, 100mm of R24 batt insulation and 13mm gypsum board on interior, 2) Ceiling—an interior wall connected to the unconditioned attic constructed from 13mm gypsum board and 100mm of R24 batt insulation, and 3) Foundation—modeled as carpet on 153mm of concrete and 305mm of damp soil. The

unconditioned attic was bounded by two wall construction: 1) Ceiling and 2) Roof—constructed of 16mm plywood, felt paper and asphalt shingles. The house has a total of 24.5m^2 windows in the exterior walls with a significant amount of shading due to a wrap-around porch.

Each of the four different envelope constructions (Exterior Walls, Roof, Ceiling, and Foundation) is made up of individual materials as shown in Table 4.1. For example, the External Wall is constructed out of four different materials with defined thicknesses and material properties plus two convection resistance values for the internal and external surfaces of the wall. All material properties used in the model were taken from eQuest/DOE2.2, which provides a large database of material properties that made it easy to look up properties for specific materials [Law, 2004].

Table 4.1: Envelope Constructions and Material Properties

Material	Thickness m	Thermal Cond. $\frac{W}{mK}$	Density $\frac{kg}{m^3}$	Heat Capacity $\frac{J}{kgK}$	Resis-tance $\frac{m^2K}{W}$	Emis-sivity	Mu Diffu-sion	Ks Resis-tance
External Wall								
Conv. Resistance	-	-	-	-	0.120	-	-	-
Face Brick 4in	0.101	1.311	2082.40	919.6	-	0.90	29.0	2.00
Insul Bd 1/2 in	0.013	0.055	288.332	1254.0	-	0.90	1.30	1.00
MinWool Batt R24	0.212	0.043	9.611	836.0	-	0.90	1.30	1.00
GypBd 1/2 in	0.013	0.160	800.923	836.0	-	0.90	9.00	6.00
Conv. Resistance	-	-	-	-	0.120	-	-	-
Roof								
Conv. Resistance	-	-	-	-	0.120			
Blt-Up roof 3/8 in	0.009	0.162	1121.292	1463.0	-	0.90	500.0	0.00
Bldg Paper Felt	0.038	3.605	1121.292	1463.0	0.011	0.90	5000	0.00
Plywood 5/8 in	0.016	0.115	544.628	1212.2		0.90	150.0	99.0
Roof Cons Mat 4	-	-	-	-	0.044	-	-	-
Conv. Resistance	-	-	-	-	0.260	-	-	-
Ceiling								
Convection Resistance	-	-	-	-	0.120	-	-	-
GypBd 3/4in	0.019	0.160	800.923	836.0	-	0.90	9.00	6.00
MinWool Batt R24	0.212	0.043	9.611	836.0	-	0.90	1.30	1.00
Conv. Resistance	-	-	-	-	0.120	-	-	-
Foundation								
UFMat	-	-	-	-	3.110	-	-	-
Light Soil, Damp 12 in	0.305	0.865	1601.846	1045.0	-	0.90	7.50	2.00
Conc HW 140 lb 6in	0.152	1.730	2242.585	836.0	-	0.90	25.0	40.0
Carpet and Fiber pad	-	-	-	-	0.366	-	-	-
Conv. Resistance	-	-	-	-	0.12	-	-	-

The base case house has a total of 16 windows and a front porch shading the four windows in the front and four in the back while the remaining eight windows have awnings. The model uses two types of glazing; low-e, double-paned glazing for the 16 windows and regular double-paned glazing for the four doors that have built-in windows. As a simplifying assumption the windows were assumed to be uncovered, with no blinds or solar screens. Five windows and one door face east, six windows and one door face south, five windows and two doors face north. The front of the house faces east. The window properties are listed in Table 4.2. The building has a total of $24.5m^2$ of glazing including both the windows and the doors. Each shaded window is represented by various rectangular prisms.

Table 4.2: Glazing Properties used in HAMBASE Model

Type	eQuest ID	Gap Thickness (in)	Gap Fill	U-Value	SHGC
Double Clear	2000	0.25	Air	0.68	0.76
Double Low-E Clear	2610	0.25	Air	0.60	0.72

The building load model includes internal loads that are typically found in a house by defining maximum value for each type of load; occupancy (assume to be 4 people), lighting and equipment; and then using a schedule of scaling factors to determine the hourly building load. Figure 4.8 shows the hourly internal sensible load broken down into each component of the load. The loads where compiled from a variety of sources. The per person occupancy load is $245W/person$ sensible and $155W/person$ latent, which was taken from eQuest [Law, 2004]. ASHRAE defines the number of occupants as the number of bedrooms plus one, which give four total occupants for the modeled house [ASHRAE, 2009]. The lighting loads were taken from the EnergyPlus Reference Building Models for mid-rise apartments, which is $3.87W/m^2$ [Field et al., 2011]. The equipment load was based on the data given by the Energy Plus Reference Building Models, which specifies $5.4W/m^2$. This load was scaled down based on occupancy density. The Reference Buildings specifies a density of $35.30m^2/person$ for the apartment while ASHRAE's values for the house is $49.3m^2/person$. The ratio of these values was used to scale down the equipment load to $3.86W/m^2$ [ASHRAE, 2009; Field et al., 2011].

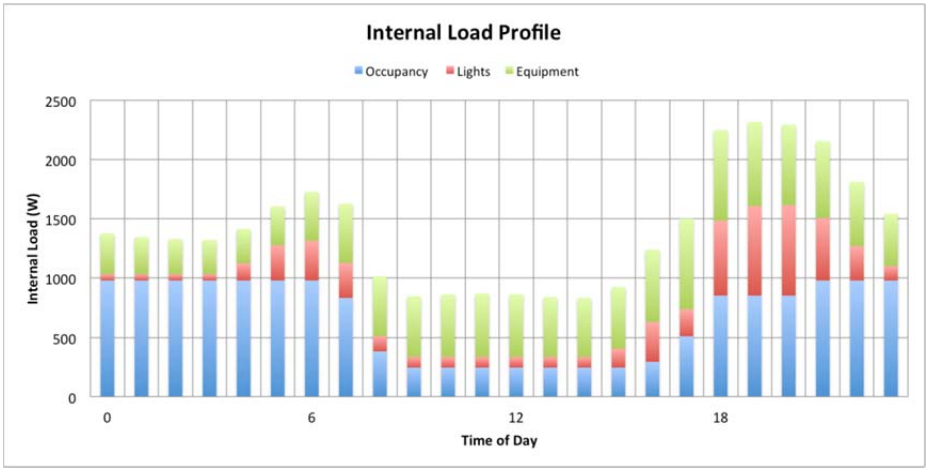

Figure 4.8: Internal Load Profiles

The hourly schedule was taken from the EnergyPlus Reference Building Models for the mid-rise apartment building. The schedule defines a multiplier for each type of load, for each hour of the day. This scales down the base values listed earlier to represent the hourly occupancy, lighting and equipment loads. For example, the full occupant load was determined to be 980 *W* for four people, which is assumed to be the load after 9 p.m. (21:00) and before 7 a.m. This is indicated by the constant loads for the occupancy loads during this time frame in Figure 4.8. After 7 a.m., the load decreases down to 25% of the full occupancy load to represent occupants leaving the house for the day. At 4 p.m. (16:00) the occupancy loads begin to increase back to the full load as occupants begin to arrive home for the evening. The lighting and equipment loads are also scaled in a similar manner [Field et al., 2011].

The infiltration rate is set at 0.5 ACH (Air Changes per Hour) for both zones which was determined from ASHRAE's values for a tight house [ASHRAE, 2009]. The house does not include any forced ventilation in either the attic zone or the main floor. The air flow between the zones was assumed to be zero as well.

The house had annual cooling and heating loads of 22.3MWh and 4.9MWh, respectively. The house experienced peak monthly cooling and heating loads of 4.3MWh and 1.5MWh, respectively. Monthly loads are given in Table 4.3 and these values were used in GLHEPRO to size the boreholes.

Table 4.3 Building Loads used to Size Base Case Ground Loop using GLHEPRO

Month	Heating Total kWh	Cooling Total kWh	Heating Peak kW	Cooling Peak kW
Jan	1743.79	24.33	10.37	2.29
Feb	1012.57	91.79	5.24	3.20
Mar	416.03	655.39	5.02	4.57
Apr	0	1601.99	0	5.70
May	0	2750.56	0	7.75
Jun	0	3708.09	0	8.39
Jul	0	4362.54	0	8.63
Aug	0	4266.12	0	8.43
Sep	0	2793.82	0	7.11
Oct	0	1545.87	0	6.10
Nov	247.57	470.52	3.02	4.48
Dec	1455.74	22.74	6.12	3.01

Month	Heating Total kBtu	Cooling Total kBtu	Heating Peak kBtu/hr	Cooling Peak kBtu/hr
Jan	5950.1	83.0	35.4	7.8
Feb	3455.0	313.2	17.9	10.9
Mar	1419.6	2236.3	17.1	15.6
Apr	0	5466.2	0	19.4
May	0	9385.3	0	26.4
Jun	0	12652.5	0	28.6
Jul	0	14885.6	0	29.4
Aug	0	14556.6	0	28.8
Sep	0	9532.9	0	24.3
Oct	0	5274.7	0	20.8
Nov	844.7	1605.5	10.3	15.3
Dec	4967.2	77.6	20.9	10.3

4.6.2 Residential Heat Pump

The water-source heat pump model parameters that needed to be specified were the type and size of heat pump to be used as well as the air and water flow rates and temperature set points. The heat pumps from ClimateMaster, Inc., the largest GHP manufacturer in the U.S., were used for all simulations. In particular, the Tranquility 20 series of single stage heat pumps with single speed fans were used. This unit was chosen as the test base case so that two-stage heat pumps and variable speed fans could be simulated in the future to assess improvements to heat pump performance [ClimateMaster, 2010].

To size the heat pump, a series of simulation trials were conducted. For each trial the model was outfitted with a different capacity heat pump and simulated for a single year. In each case, the number of hours (unmet hours) that the average building temperature was above or below

the set point temperatures was compared. The capacity of the heat pump was increased until this value did not decrease anymore. This method was used because changing the capacity of the heat pump affected the peak loads that would have otherwise been used to size the heat pump. Based on this approach, the ClimateMaster Tranquility 20 Series TS 048 single stage heat pump was chosen. The unit features a peak cooling capacity of 14,625*W* (49,900*Btu*/*h*) and peak heating capacity of 11,430*W* (39,000*Btu*/*h*) with an energy efficiency rating of 5.2 *W*/*W* (17.6*Btu*/*W*) for cooling and a COP of 3.7. The set points were set at 21°C (winter) and 25°C (cooling) with a 1°C deadband. These values were taken from the eQuest default set points. The water flow and air flow rates were assumed to be the maximum rated values for the heat pump unit. The TS 048 unit has a single stage compressor with 0.757L/s (12gpm) water flow rate and a single speed fan with 0.76m^3/s (1600CFM) of air flow.

4.6.3 Residential Borehole-Ground Loop

The ground parameters used were taken from a couple of different sources. A map of the Texas ground temperatures and ground conductivities are shown in Figures 4.9 and 4.10, respectively. The temperatures shown are for depths greater than 9.1m (30ft). Based on the maps an undisturbed ground temperature of 21.7°C (71°F) was chosen and bulk ground conductivity was chosen as 0.3895*W*/*m*/*K* (0.77*Btu ft*/*hr*/*ft*^{2}/^{o}*F*) [American Society of Petroleum Geologists, 1974]. The density of the bulk ground for Austin was chosen to be 2475*kg*/*m*^{3} (155 *lb*/*ft*^{3}) [O'Neal et al., 1994].

Figure 4.9: Undisturbed ground temperatures (F) at depths greater than 9.1 m (30 ft.), [American Society of Petroleum Geologists, 1974]

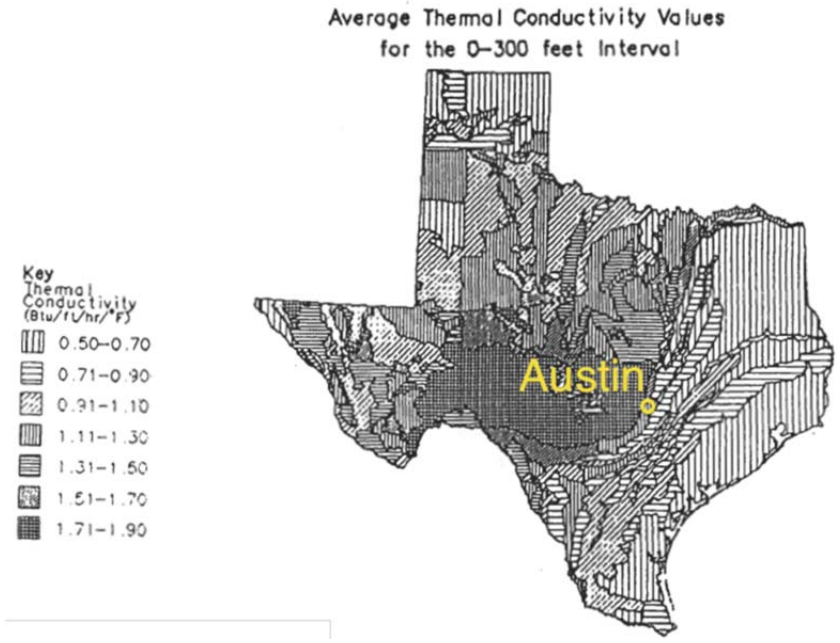

Figure 4.10: Average ground conductivity from 0-300 ft, Source [American Society of Petroleum Geologists, 1974]

The ground loop model assumes that the borehole is 127mm (5in) in diameter with 25mm (1in) SDR-11 tubing. The model assumed that regular (not thermally enhanced) bentonite grout was used to fill the borehole. The boreholes were arranged in a 1 x 4 line spaced 4.6m (15ft)

apart. Based on the ground parameters, building load, chosen heat pump, 10-year operation, and a maximum heat pump EWT of 48.9°C (shutoff temperature to prevent excessive pressure in the refrigeration loop), GLHEPRO sized the ground loops to be 68.6m/borehole (225ft). This length is significantly shorter than the typically-installed borehole length of 91.4m/borehole in Austin, Texas. This limiting shorter borehole length reflects the sizing criterion chosen of using the maximum mean heat pump EWT, which would result in the least initial cost but lower heat pump efficiency over its operating lifetime.

The ground loop properties and building load values used in GLHEPRO to size the boreholes are given in Table 4.4 and Table 4.3 (Section 4.6.1), respectively.

Table 4.4: Ground Loop Properties used for Base Case in GLHEPRO

Property	SI Units	British Units
	Geometry	**Geometry**
Length	68.6 m	225 ft
Borehole Diameter	127 mm	5 in
Shank Spacing	25.4 mm	1 in
Borehole Spacing	4.572 m	15 ft
Geometry	In-line 4	
U-Tube ID	27.33 mm	1.076 in
U-Tube OD	33.4 mm	1.315 in
	Thermal Properties	**Thermal Properties**
U-Tube Conductivity	1.333 W/m/K	0.225 Btu/hr/ft/°F
U-Tube Capacitance	1767 kJ/m^3/K	22.99 Btu/ft^3/ °F
Grout Conductivity	0.7443 W/m/K	0.43 Btu/hr/ft/ °F
Grout Capacitance	3901 kJ/m^3/K	58.17 Btu/ft^3/ °F
Ground Conductivity	0.3895 W/m/K	0.77 Btu/hr/ft/°F
Ground Capacitance	1542 kJ/m^3/K	26.35 Btu/ft^3/ °F
Ground Temperature	21.67 °C	71.01 °F
	Fluid Properties	**Fluid Properties**
Antifreeze	None	
Convection Coeff	1534 W/m^2/K	270.2 Btu/hr/ft^2/ °F
Fluid Factor	1	
Flow rate/borehole	0.1893 L/s	3 GPM
Borehole Resistance (SI)	0.2097 Km/W	0.362 °Fhrft/Btu

4.6.3.1 Sizing Borehole for Residential Building

GLHEPRO is used to size the ground loop based on total heat load on the ground as well as to create the parameter files for the Simulink R model [Oklahoma State University, 2007]. The values shown in the following screen-shots are those used for the base case model using Austin ground properties and energy loads computed for the modeled house.

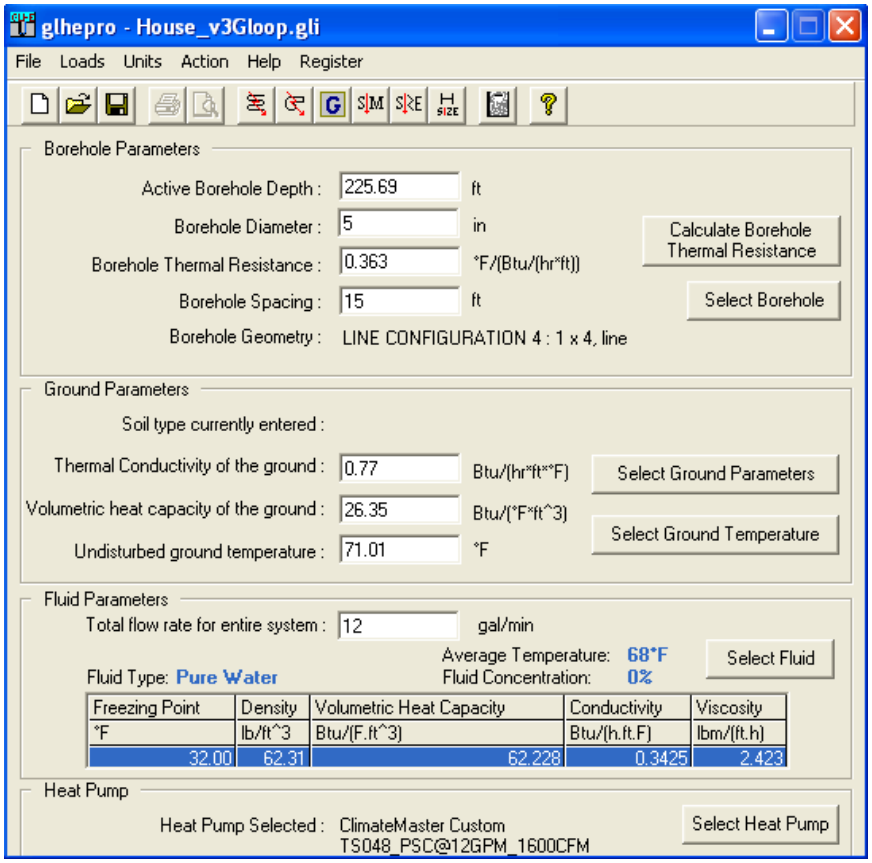

Figure 4.11: Main screen of GLHEPRO

Figure 4.11 shows the main input screen of the GLHEPRO software; the borehole field parameters such as borehole length, spacing, and geometry are entered. The borehole geometry defines how multiple borehole interact with one another. For example, the base model uses a single line of four boreholes. Other options include single boreholes and rectangular, L-shaped and U-shaped borehole fields. The undisturbed ground temperature is also entered on this screen. There is an option to pull up a map that shows the ground temperatures of the United States. The ground thermal properties can be entered on this screen as well.

The borehole thermal resistance and the g-functions for the model are calculated using the screen shown in Figure 4.12. It is accessed by clicking on the “Calculate Borehole Thermal Resistance" button on the main page. At this point the user can choose to model a single u-tube, double u-tube, or concentric tube borehole by clicking on the proper tab at the top of the screen. After selecting this, the detailed borehole geometry is entered. For the single u-tube configuration this includes the shank spacing (distance between the legs of the u-tube), the diameters of the u-tube and the volumetric flow rate in each borehole. Next the ground, grout, and pipe thermal properties are entered. Finally, the user has the option to enter a specifies

convection coefficient or use the built-in calculator to determine one. After entering all the data the user can calculate the borehole resistance and create the g-functions for the borehole. If the borehole has been properly sized the user can create the parameter file for the Simulink model by clicking on “Select G-function Print Format" and choosing to create an HVACSIM+ parameter file.

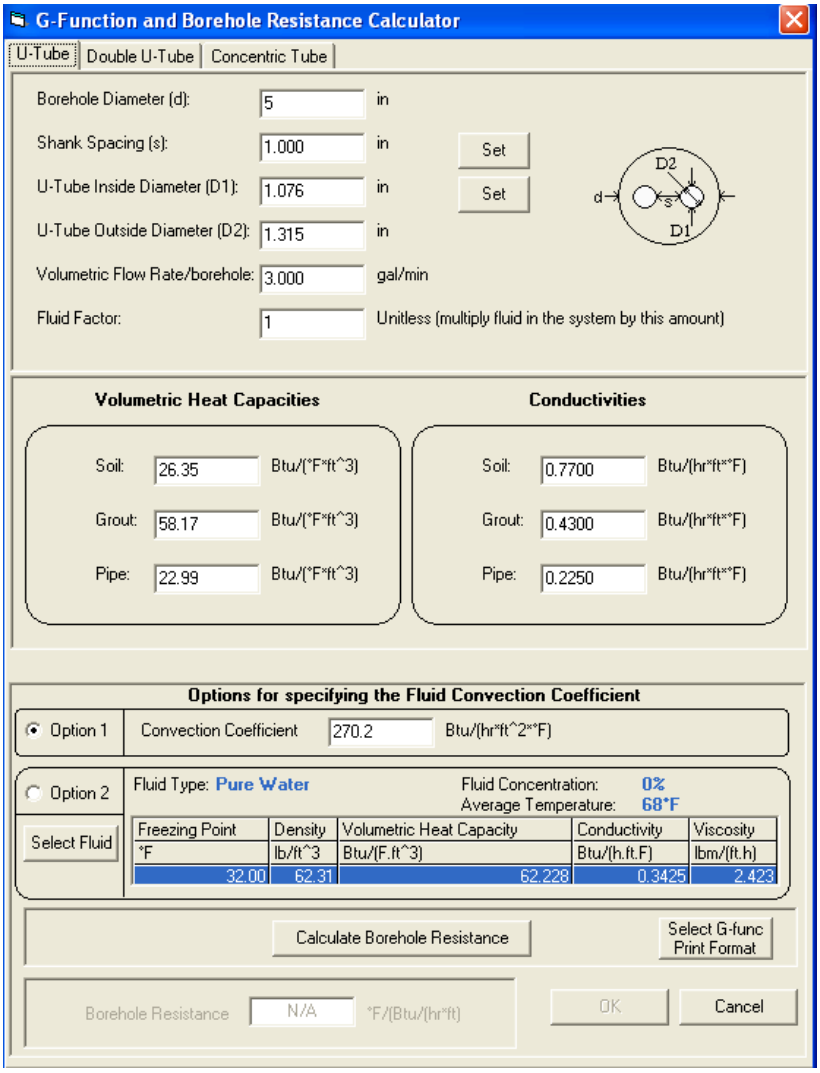

Figure 4.12: G-function and borehole resistance calculation screen

Once the borehole properties have been entered into GLHEPRO, the user can proceed to perform long term simulations or determine the proper borehole length. This requires that the monthly total and peak building loads be entered into the program as shown in Figure 4.13. This is accomplished under the Loads>Edit Heat Pump Loads menu.

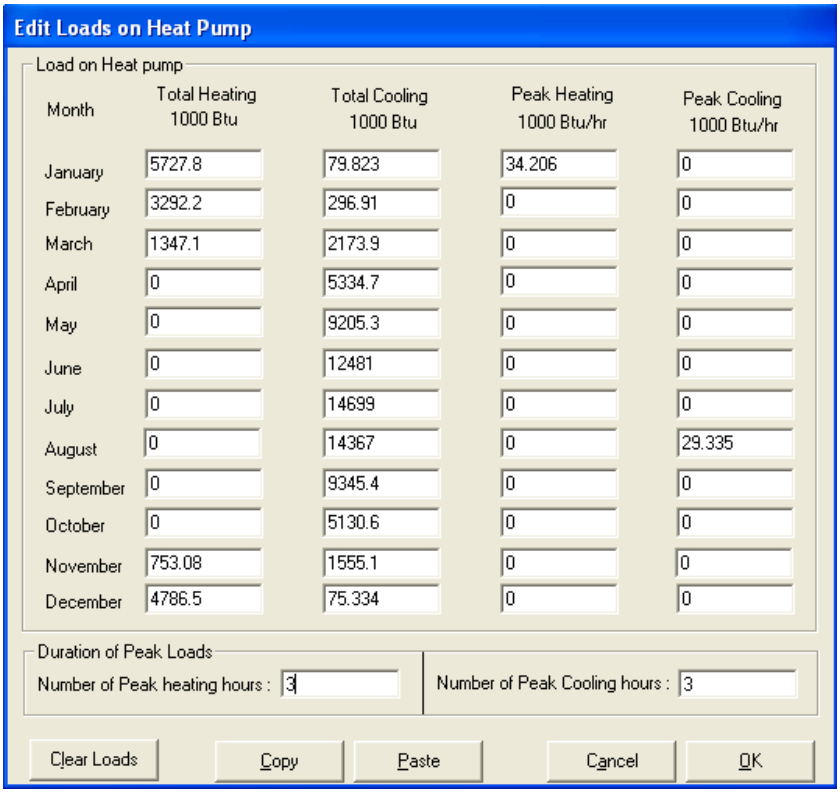

Figure 4.13: Building loads

The minimum and maximum heat pump EWT is specified as 120℉ (48.9℃) and 32℉ (0℃), respectively. This temperature is taken based on the heat pump used, Climate Master's TS048_PSC with an airflow rate of 1200 cfm (0.47 m^3/s) and 12 gpm (0.748 kg/s) water flow rate. The duration of the entire simulation (from the starting month to the end month) is entered, and in this case a 10 year run (120 months) is performed, as shown in Figure 4.14.

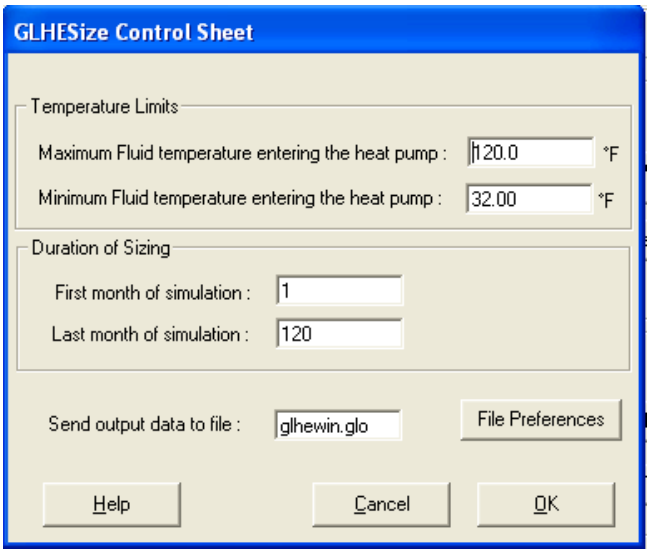

Figure 4.14: Heat pump entering water temperatures and lifetime of borehole field

Once all the parameters have been entered, GLHEPRO computes the length of the ground loop. For the given heating/cooling loads, borehole configuration and ground properties a borehole depth of 225.69 ft (68.8 m) for each one of the four loops was obtained. The average maximum and minimum temperatures of heat pump EWT calculated were 114.1 ℉ (45.6 ℃) and 64.3 ℉ (17.9 ℃), respectively, as shown in Figure 4.15.

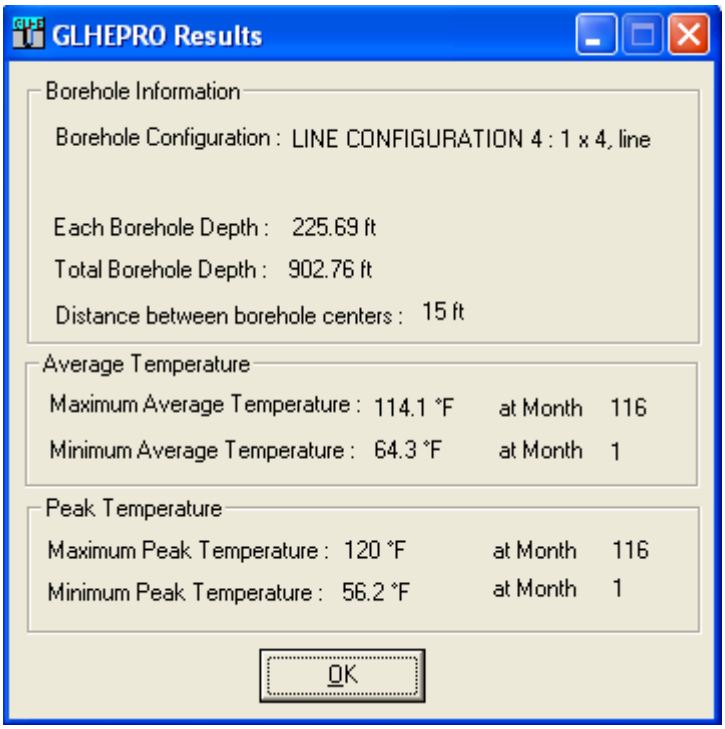

Figure 4.15: GLHEPRO final results

The user can now perform a long term simulation using the specified borehole length by selecting Action>Perform Simulation from the menu. After a simulation the monthly average, maximum, and minimum loop temperatures are reported in a csv file.

If the users only need to determine the proper length of the borehole, they can choose to perform a standard sizing or a hybrid sizing. The standard sizing is used for sizing the loop when there is not a supplemental heat rejector available. To perform the standard sizing the user selects Action>Perform Sizing from the menu. The user then selects the desired maximum and minimum loop temperatures as well as the life time of the ground loop. Based on the inputs GLHEPRO runs multiple simulations with different borehole lengths until the maximum or minimum loop temperatures are reached in the last year of the specified life time. The resulting length is then properly sized length for the ground loop based on the provided loads. The hybrid sizing procedure assumes that there is a supplementary device which can add or remove heat from the ground loop. To determine the loop length GLHEPRO determines loop lengths that will

give the user-specified maximum and minimum temperatures at the end of its lifetime. The shorter of the two lengths is chosen and the additional heat that needs to be rejected/extracted from the borehole is then calculated and reported as the proper size for the supplementary device.

4.6.4 IBL-GHP Residential Model Validation

The IBL-GHP model was validated in a two-step process. The building load submodel was compared with eQuest simulations. Then the heat pump-ground loop submodel combination was compared with GLHEPRO simulations.

4.6.4.1 Residential Building Load Validation

Besides the validation of HAMBASE provided in Section 3.1, the building load model was also validated by comparing the results of annual heating and cooling values to the results from an eQuest model. The validation criteria was taken from the ASHRAE 140-2007 standard, which showed, in Figure 3.5 and Table 4.5, variations in the eight modeled heating and cooling loads as high as 28% and 54% for the main test cases 600 and 900, respectively. Based on these values the criterion for agreement was set to be less that 25%.

Table 4.5: Range of the Reported Values for Annual Building Load for ASHRAE 140-2007 for Cases 600 and 900

Case		Minimum MWh	Maximum MWh	% Difference
600	Cooling	6.137	7.964	25.91 %
	Heating	4.296	5.709	28.25 %
900	Cooling	2.132	3.415	46.26 %
	Heating	1.170	2.041	54.25 %

An eQuest building model of the residential house used for the results presented in Section 4.6.1 was created to provide a comparison for validation. The models were simulated for two cases of internal loads: 3839 W sensible, 1085 W latent loads (values suggested by eQuest for occupancy of seven and 5.4 W/m^2 for lighting/equipment) which were assumed to be on at all times and no internal loads.

Table 4.6 shows the annual cooling and heating loads for both eQuest and the integrated Simulink model (note monthly load comparisons and comparisons of heat rejected to the ground loop can be found in [Gaspredes, 2011]. The total yearly cooling values have good agreement between the models for both the full eQuest internal loads and the no load case with 3.2% (38.7 MWh--eQuest vs 37.5 MWh) and 20.2% (18.5 MWh—eQuest vs 14.7 MWh) differences, respectively. The total heating values have large differences relative to each other because

eQuest predicts a very small amount of heating for both cases. For the full load case eQuest predicts a negligible amount of heating (0.056 kWh) while the Simulink model predicts 1.36 kWh of heating (4644 kBtu). Even though the percent difference for the full load annual heating values is large, these total heating values are still very small (≈3%) compared to the total amount of cooling provided. For the no load case the Simulink model predicts 27163 kBtu of heating while eQuest predicts 762 kBtu (7967 kWh vs 0.223 kWh for the no load case). Additional comparisons can be found in Appendix B1 (HAMBASE Validation).

Table 4.6: Comparison between Simulink Model and eQuest Building Load Results

	eQuest	Simulink	Difference	% Difference
eQuest Internal Loads				
Total Cooling (kBtu)	131801	127553	-4248	-3.2%
Total Heating (kBtu)	0.19	4644.79	4644.61	2508436%
No Internal Loads				
Total Cooling (kBtu)	62894	50190	-12703	-20.2%
Total Heating (kBtu)	762	27163	26401	3465%

For the purpose of studying ground coupling the total yearly heat that is rejected/extracted to/from the ground is important over the life cycle of the GHP system. For the internal load case the IBL-GHP model predicts 7.7% (49.3 MWh vs 45.7 MWh) more heat rejected into the ground during the year than the eQuest model. The IBL-GHP model also predicts 41% (12.6 MWh vs 21.7 MWh) less heat rejected for the no internal load case. This large difference is caused by the discrepancies between the yearly heating values for the no internal load case.

4.6.4.2 Residential Heat Pump-Ground Loop Subsystem Validation

The combination of the heat pump and ground loop models from the IBL-GHP model was used to compute the monthly heat rejection values and loop ground temperatures for four, 91.4 m boreholes. These values were compared to results calculated by GLHEPRO. The loads used as inputs into GLHEPRO were taken from the building load values calculated by the IBL-GHP model.

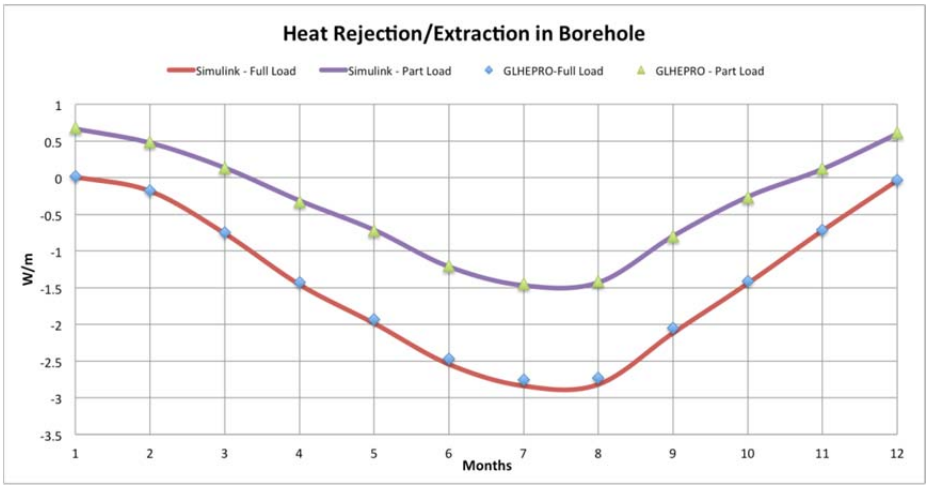

Figure 4.16: Monthly average heat rejected/extracted in the borehole, comparison between GLHEPRO and Simulink ground loop models – Jan. to Dec.

Figure 4.16 shows the heat rejected into the ground for both internal load cases. GLHEPRO, represented by the diamonds and triangles, agrees very well with the values calculated in Simulink, represented by the lines. This agreement shows that based on the same building loads the heat pump performance map model is calculating the proper temperature rise across the heat pump and that the loop water temperatures entering the ground are being averaged properly across the time step transition.

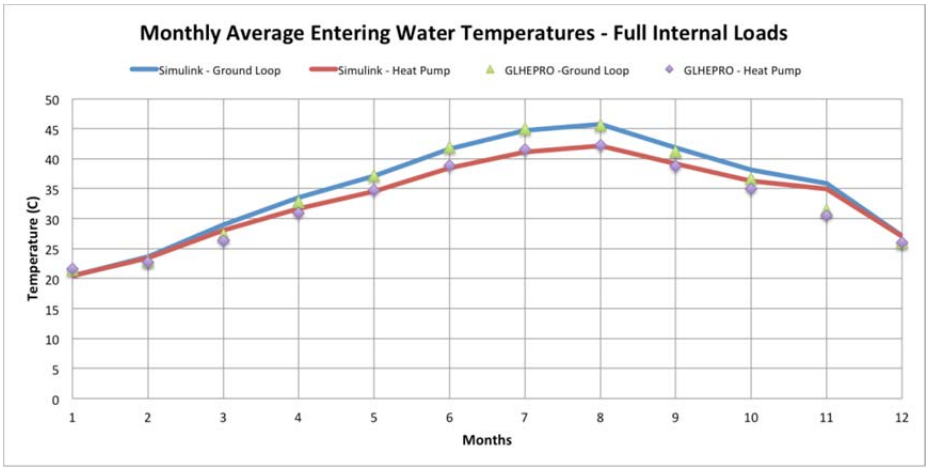

Figure 4.17: Monthly average water temperatures entering the borehole and heat pump, comparison between GLHEPRO and Simulink ground loop models,– Jan. to Dec.– full internal load, data can be found in Appendix B.2.

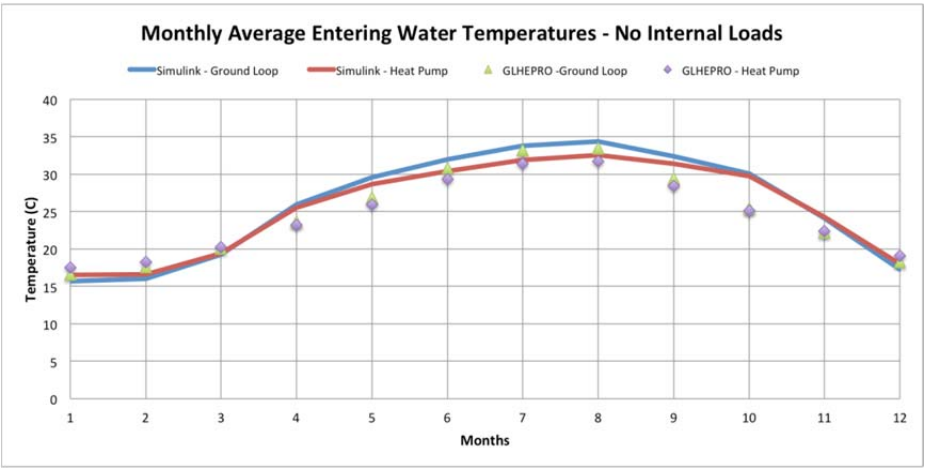

Figure 4.18: Monthly average water temperatures entering the borehole and heat pump, comparison between GLHEPRO and Simulink ground loop models,– Jan. to Dec.– no internal load

Figure 4.17 shows the monthly average water temperatures at the entrance of the ground loop and of the heat pump for full internal loads. Figure 4.18 shows the same temperatures but with no internal loads. Both figures show good agreement between the values generated by GLHEPRO and the Simulink model with the only significant difference occurring in the spring and fall when the building has lower total building loads which cause the heat pump to operate less. The difference could be a result of assumptions about the temperatures or ground loop flow rates when the heat pump is not running. For example, the Simulink model assumes that the outlet temperature is the average borehole temperature whenever there is no flow through the ground loop. If GLHEPRO assumes a different value, then the average monthly values would be different for months that have significant amounts of time when the heat pump is not running. Table 4.7 shows the yearly maximum and minimum heat pump entrance temperatures for both the full and no internal load cases. The Simulink model is predicting maximum temperatures for both loading cases within 2% (< 0.6^{o}C) of the values predicted by GLHEPRO. The minimum values that are calculated by the model do not agree as well as the maximum values, but show good agreement. Additional comparisons can be found in Appendix B.2 (HAMBASE Validation).

Table 4.7: Comparison of Maximum and Minimum Heat Pump EWT

	Maximum EWT			Minimum EWT		
	GLHEPRO ^{o}C	Simulink ^{o}C	Diff %	GLHEPRO ^{o}C	Simulink ^{o}C	Diff %
Full Load	43.98	44.54	-1.3%	17.94	15.34	14.5%
No Load	33.46	34.08	-1.9%	14.22	12.93	9.1%

Based on the comparison of the heat rejected by the Simulink ground loop model and GLHEPRO, it can be concluded that the heat pump model is correctly calculating the temperature responses across the heat pump. This also indicates that the time step transition that occurs between the heat pump and the ground loop is being performed correctly. For the months with less cooling and heat loads there are slight differences between the two models, but this can be attributed to differences in the assumptions about the loop temperatures and flow rates when the heat pump is not operating.

4.7 RESIDENTIAL BASE CASE MODEL SIMULATION RESULTS

The IBL-GHP model's wide range of time scales allow for the examination of data at different time resolutions (minute, hour, month, year) and for different purposes with representative illustrations shown below. One criterion used to assess system performance is the number of unmet hours (sum of hours per year when the heat pump cannot control the conditioned space to set point). The ASHRAE Standard 90.1-2007.G3.1.2.2 states a maximum of 300 unmeet hours [ASHRAE Standard, 2007b]. This criterion will be applied to the residential buildings even though the standard is typically applied to commercial buildings.

4.7.1 Minute Time Results

Figure 4.19 shows the building air and radiant wall temperatures, computed at every 30 second time step for zone 1, a conditioned living space, and zone 2, an unconditioned attic, for a three-hour period in the summer. Zone 1 air temperature oscillates approximately 1.5°C to reflect the required periodic cooling between the 25°C set point temperature with 1°C deadband, and zone 1 radiant wall temperature also oscillates at significantly smaller amplitudes. Zone 2 temperatures are significantly higher since it is unconditioned, and zone 2 wall temperature jumps at hrs 13 and 14 are due to changes in the hourly weather data.

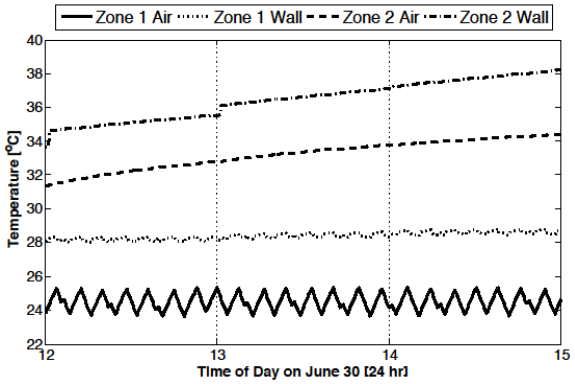

Figure 4.19: Building air and wall temperatures in zones 1 and 2 for June 30, 12:00-15:00 for base test case

Figure 4.20 shows the ground loop water temperatures at the entrance (EWT) of the heat pump (blue line) and the entrance of the ground loop (green line). The heat pump entrance temperature, which is used for the 30 second time steps, jumps when the output temperature of the ground loop model is updated, which occurs every five minutes. The heat pump entrance temperature has a great effect on the output and efficiency of the unit. On this short time scale it is not evident, but for longer time scales (on the order of months/years) this effect becomes more pronounced. The ground loop entrance temperature changes as the heat pump is switched on and off. When the heat pump is off, no heat is rejected to the water by the heat pump so both temperatures are the same. During cooling the heat pump rejects heat to the water causing the water temperature to rise.

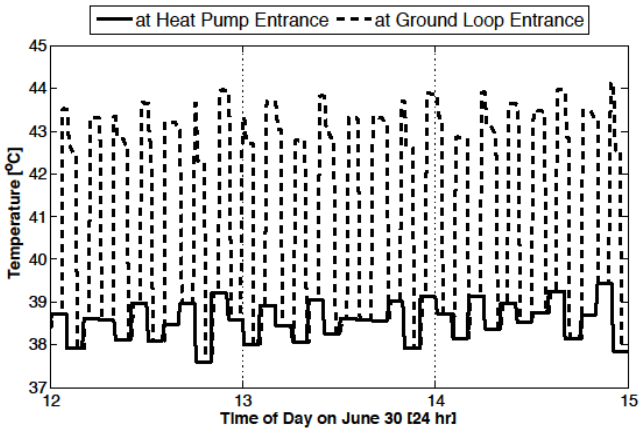

Figure 4.20: Water temperatures at the entrances to the ground loop and heat pump for June 30 of year 1, 12:00-15:00 for base test case

4.7.2 Hourly Time Results

Many of the simulation results presented are based on hourly-averages of the output data so those results can be compared to other building load models, such as eQuest and EnergyPlus, which provide hourly-averaged data. In addition, the data files that contain the results based on the 30 second time steps are approximately 78 MB per year simulated. For a 15 year simulation, 1.15 GB of data is generated. Using the hourly-averaged data brings the data file down to 1.4 MB per year simulated or 21 MB for a 15 year simulation.

Figure 4,21 shows the hourly-averaged air and wall temperatures of zone 1 and the thermostat set point temperatures during the first year of operation. The conditioned air temperature of zone 1 (blue line) remains within the thermostat set point ranges (21^{o}C (heating) and 25^{o}C (cooling) with 1^{o}C deadband—blue and red dashed lines). The wall temperature (green line) varies significantly throughout the year based on the outside weather conditions.

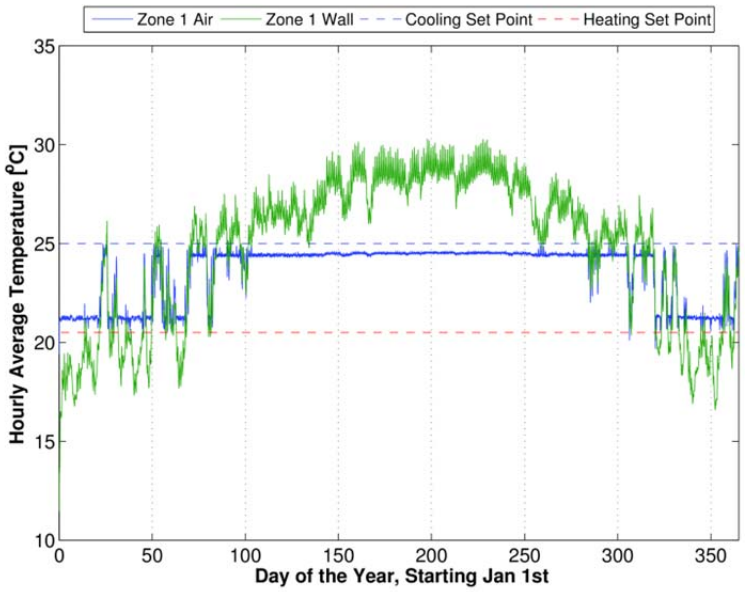

Figure 4.21: Hourly mean values of conditioned zone 1 temperatures and thermostat set points for the first year of simulation, Jan.-Dec.

Figure 4.22 shows the conditioning provided by the heat pump for each hour of the year. In the figure heating is positive and cooling is negative. The data shows significantly more total cooling than heating during the year, but the peak cooling and heating values are similar in magnitude. Figure 4.23 shows the heat rejected into the ground loop water. The positive values are associated with the heat pump adding energy to the ground loop water, which occurs when the heat pump is providing cooling to (removing heat from) the conditioned air. Comparison of Figure 4.22 and Figure 4.23 shows that the heat pump rejects more heat to the ground loop water than it removes from the conditioned air when cooling and that the heat pump extracts less heat from the ground loop water than it adds to the conditioned air when heating. This result occurs because the energy added to the refrigerant by the compressor must be rejected into the high temperature heat sink when the refrigerant is condensing. When the heat pump is cooling the high temperature sink is the ground loop water and when the unit is heating it is the conditioned air. This means that even if the annual heating and cooling building loads are the same there will still be an unbalanced heating load on the ground.

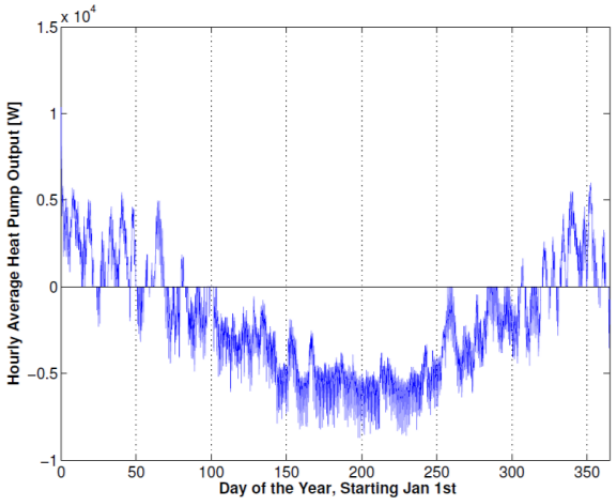

Figure 4.22: Hourly mean values of heat pump output to the conditioned zone (heating is positive), Jan.-Dec.

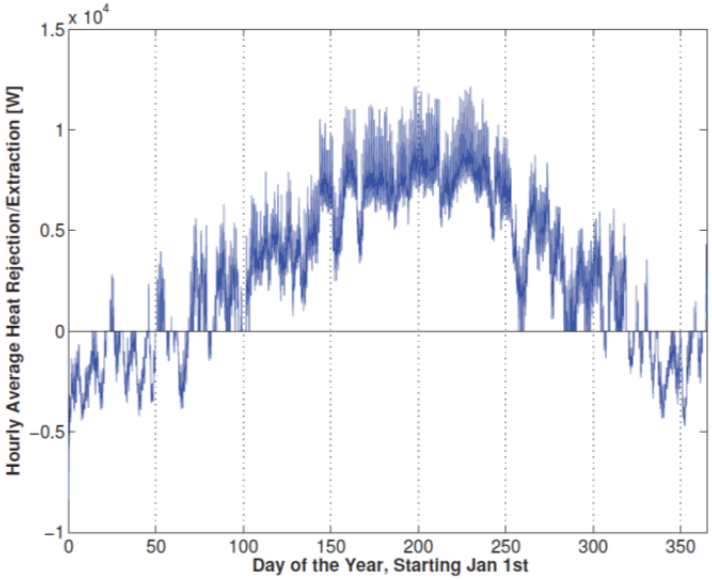

Figure 4.23: Hourly mean values of heat rejected to ground loop water by the heat pump (positive heat rejection is associated with cooling) Jan.-Dec.

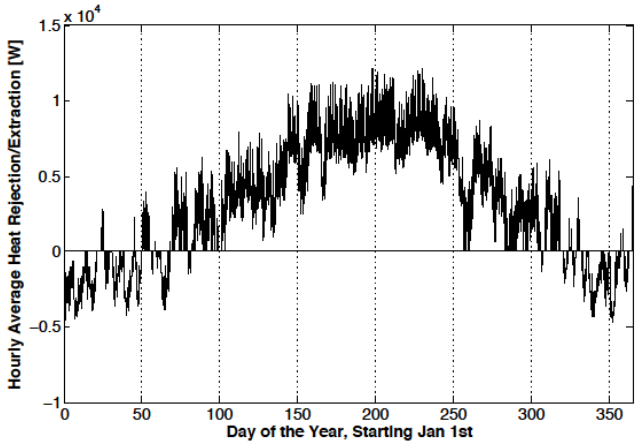

Figure 4.24: Hourly mean values of heat rejected to ground loop water by the heat pump (positive: cooling of zones), Year 1, Jan-Dec. for base test case

Figure 4.24 shows the houely averaged heat rejection rate into the ground loop water for the first year of operation. The positive (negative) values are associated with the heat pump providing cooling (heating) to the conditioned zone and rejecting (extracting) heat to the ground. Significantly more heat is rejected to than extracted from the ground during the year, which will lead to long-term ground heating.

4.7.3 Monthly Time Results

Monthly and yearly values are used to examine long term trends and normally energy, not power. Figure 4.25 shows the monthly total delivered conditioning (MWh) that the heat pump provides to the conditioned space. This figure shows that over the 15 years that were simulated the delivered cooling (blue line) was constant for each month from year to year. The delivered heating (red line) show the same results except for the first month of the simulation, which is caused by initial conditions not being at steady state.

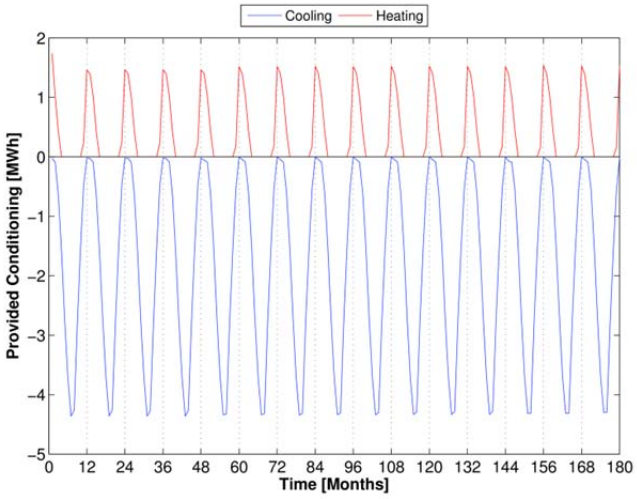

Figure 4.25: Monthly total values of heat pump output to the conditioned zone 1, 15 years

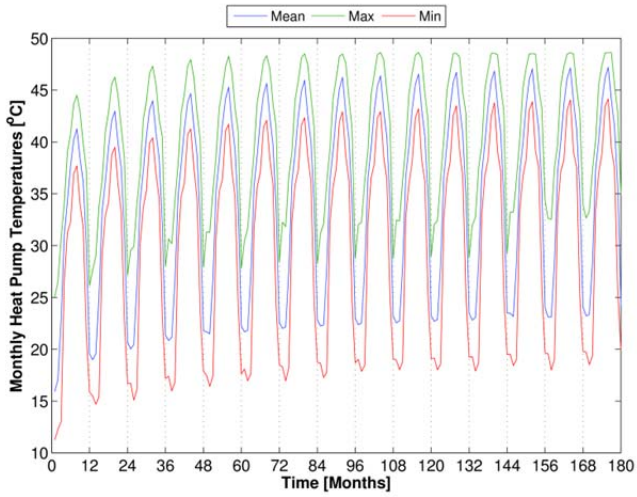

Figure 4.26: Monthly mean, max and min heat pump EWT (based on hourly averages), 15 years for base test case

Figure 4.26 shows the monthly mean, maximum, and minimum heat pump EWTs for 15 years of operation. The yearly peak mean temperature increases significantly over the first seven years, then increases much less for the remainder of the period. The yearly mean EWT temperature increases by 4.5°C to 35.0°C over the first seven years and another 1.3°C over the next eight years to 36.3°C. In turn, the higher EWT reduces the heat pump efficiency. Over the 15-year period the cooling efficiency EER decreases by 15% (from 2.80 Wh/Wh to 2.37 Wh/Wh) and the heat pump cooling time increases by 7.3% (from 2022 to 2169 hrs). Recall that the heat pump automatically shuts off if the EWT exceeds 48.9°C during cooling.

4.7.4 Yearly Time Results

Yearly values are typically used to compute operation costs and long term changes in the ground loop and heat pump operation. Over 15 years of operation, Table 4.8 shows that the number of hours that the heat pump operated in the cooling mode increased by 7%, from 2022 to 2169 hours, while remained relatively constant near 272 hours for the heating mode. The cooling/heating (MWh) provided by the heat pump remained relatively constant as expected since the weather and building internal loads are repeated every year.

Table 4.8: Heat Pump Operating Times and Cooling/Heating Provided, 15 Years of Operation

Year	Cool Time hr	Heat Time hr	Cooling Provided MWh	Heating Provided MWh
1	2022	284	-22.28	4.87
2	2056	265	-22.27	4.53
3	2075	270	-22.28	4.52
4	2087	272	-22.28	4.51
5	2095	271	-22.29	4.52
6	2104	271	-22.28	4.52
7	2111	272	-22.27	4.53
8	2116	271	-22.25	4.53
9	2122	271	-22.25	4.53
10	2128	271	-22.24	4.53
11	2135	272	-22.22	4.53
12	2147	272	-22.22	4.52
13	2156	283	-22.22	4.52
14	2164	281	-22.20	4.51
15	2169	287	-22.18	4.51

Table 4.9 shows the annual heat pump EWT and efficiency ratings. The mean heat pump EWT increased by 5.9^{o}C (10.6^{o}F) from 30.4^{o}C (86.7^{o}F) to 36.3^{o}C (97.3^{o}F). The yearly maximum EWT increased during the first seven years and leveled off at 48.5^{o}C (119.3^{o}F), which is arbitrarily close to the 48.9^{o}C (120^{o}F), the heat pump shutoff temperature and maximum EWT used to size the borehole by GLHEPRO. The mean heat pump EWT increased from 30^{o}C (87^{o}F) in year 1 to 36^{o}C (97^{o}F) in year 15. Over the 15 year operating period, the heat pump EER decreased by 15%, from 9.56 to 8.11, while the COP increased by 8%, from 4.59 to 4.95, both results reflecting the increased ground temperature and heat pump EWT.

Table 4.9: Annual Heat Pump EWT and Efficiency Ratings

Year	Mean °C	Max °C	Min °C	EER	COP
1	30.38	44.51	11.25	9.56	4.59
2	32.26	46.25	14.69	9.07	4.72
3	33.21	47.31	15.08	8.82	4.77
4	33.80	47.95	15.97	8.66	4.81
5	34.28	48.28	16.41	8.55	4.84
6	34.62	48.32	16.96	8.46	4.85
7	34.96	48.50	16.95	8.39	4.87
8	35.17	48.49	17.26	8.33	4.88
9	35.36	48.61	17.86	8.29	4.90
10	35.52	48.62	18.01	8.25	4.91
11	35.69	48.55	18.01	8.21	4.92
12	35.84	48.55	17.89	8.18	4.92
13	36.07	48.53	18.42	8.16	4.93
14	36.10	48.62	17.99	8.13	4.94
15	36.26	48.62	18.51	8.11	4.95

Table 4.10 and Figure 4.27 show the total yearly electricity used by the heat pump and the electricity used in the peak month of cooling each year. Over the 15-year period, the decreased cooling efficiency and increased operation time increased the annual electricity by 15.8%. The improved COP (8% over 15 years) decreased the annual electricity used to provide heating by 4.8%. The net effect of these changes results in a 13.7% increase in the total electricity used to operate the heat pump.

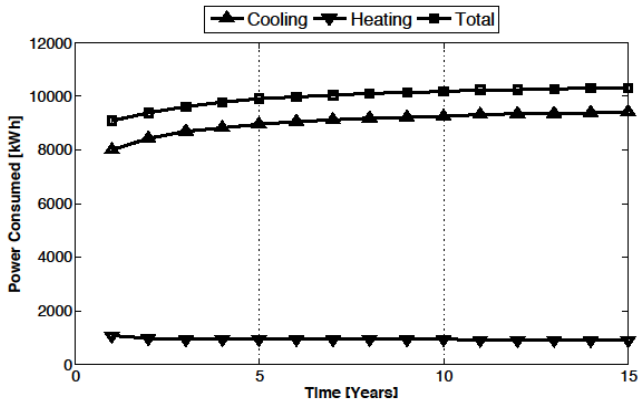

Figure 4.27: Annual and peak monthly electricity used by heat pump, 15 years for base test case.

Table 4.10: Annual and Monthly Peak Electricity Usage of the Heat Pump

Year	Cooling Elect kWh	Heating Elec kWh	Total Elec kWh	Peak Elec kWh
1	8005	1063	9068	1693
2	8427	961	9388	1776
3	8674	948	9622	1830
4	8835	940	9775	1862
5	8954	937	9890	1918
6	9047	933	9981	1932
7	9123	931	10054	1945
8	9176	929	10105	1954
9	9223	927	10150	1957
10	9259	924	10183	1961
11	9297	923	10220	1964
12	9331	920	10251	1967
13	9361	918	10280	1990
14	9382	916	10298	1991
15	9403	914	10317	1986

4.7.5 Summary: Residential Base Case Model Simulation Results

The IBL-GHP model was applied to a base case residential building and simulations run for up to 15 years of operation. The resulting simulated data illustrated the power of the model to predict system responses from seconds to years and it showed the computation and coupling power of the Simulink environment. For the base case, using the heat pump shutoff temperature as the maximum EWT for 10 years of operation as the input to the GLHEPRO ground loop sizing algorithm allowed the heat pump to maintain conditioned space temperatures to set point except for 63 unmet hours in year 10 (less than 1% of the year and represents 3% of the total cooling time of 2128 hours) and 167 unmet hours in year 15 despite ground heating effects. In other words, the use of heat pump shutoff temperature was the upper limit of EWT and the resulting 68.6m boreholes was the lower limit in length. In practice, however, longer boreholes are necessary to compensate for uncertainties in the weather, ground properties, building loads and to keep heat pump EWT below its shutoff temperature for the lifetime of the boreholes. These results are summarized by Gaspredes, et al. [Gaspredes, et al., 2012].

Simulating the model for a single year, with a single heat pump model and a two zone building, takes approximately 1.5 hrs on a 2.4 GHz Intel processor, and simulating 15 years of operation took 13 hrs to solve on a 3.73GHz Xeon processor.

4.8 RESIDENTIAL SENSITIVITY STUDY

A series of sensitivity studies was simulation and compared with the base case for the following designer-specified ground loop parameters.

- ***Borehole length***: longer boreholes increase drilling costs but reduces the heat pump EWT, which increases heat pump efficiency.
- ***Borehole configuration and spacing***: closely-spaced boreholes increase thermal coupling among boreholes and increase ground heating.
- **Grout thermal conductivity**: higher conductivity increases heat transfer rates between the borehole and ground.
- **Ground temperature**: lower ground temperatures lower heat pump EWT, which increases heat pump efficiency
- ***Supplemental heat rejection (SHR)***: SHR devices reduce the water temperature entering the ground and improve heat pump efficiencies during cooling periods.

While the general qualitative effects of these parameter changes on operating and economic performance are known, their quantitative effects are not known due to the complex coupling between building, heat pump, and ground loop. This project quantifies those effects. Recall that the boreholes were sized for a 10-year operating lifetime, so an under-designed system will reach a point in time less than 10-years where the heat pump is first turned off for more than 300 hours because its EWT exceeds the shutoff temperature and at that point, the heat pump is unable to control the conditioned space temperature.

4.8.1 Borehole Length

The model was run for six different borehole lengths with all other parameters fixed to the base case properties. The base case borehole, sized by GLHEPRO with the maximum EWT in the 10^{th} year at 48.9°C, was four boreholes, each separated by 4.6m and 68.6m deep, for a total length of 274m. A length that was 5% shorter, 65.4m per borehole, was selected to illustrate an under-designed system. In the Austin area boreholes of 91.4m are typically installed for residential applications [8]. In addition, GeoDesigner, a ground loop sizing program from ClimateMaster Inc., sized each borehole to 104m for a 39°C maximum EWT, but this length varied depending upon how other input parameters were interpreted [ClimateMaster, 2011]. Therefore 100.6m (41°C EWT) and 109.7m (38°C EWT) were used in the simulation. Finally, a length of 82.5m was chosen as an intermediate length between the sizing from GeoDesigner and the minimum length from GLHEPRO. A summary of the lengths and installation costs are shown in Table 4.11 using a price of $23/m for the Austin area [Hammond, 2011]. This price

includes drilling the boreholes, installing the u-tube, and back filling the borehole with grout to enhance the heat transfer.

The simulation results in Figure 4.28 show that the under-designed system with the shortest boreholes, as expected, caused the heat pump EWT to exceed its shutoff temperature of 48.9^{o}C within three years. For the base case that event took seven years. For the longer borehole cases, the heat pump EWT never reached the shutoff temperature in their 15-year lifetimes. For the 82.5m and 91.4m boreholes, the intermediate and typical lengths in Austin, the heat pump EWT was less than 45^{o}C and 42^{o}C, respectively, after 15 years of operation. For the two longest boreholes, the 15th-year EWT was 40^{o}C and 38^{o}C, respectively.

Table 4.11 Borehole Length Sensitivity Study Summary and Installation Cost

Length/ Borehole,m	Total Length, m	Length/Length Base Case	Installed Cost	Borehole Sizing Algorithm/Source
65.4	261.6	0.95	$6,017	Base Case-5%
68.6	274.4	1.00	$6,311	Base Case:GLHEPRO
82.5	330.0	1.20	$7,590	Intermediate
91.4	365.6	1.33	$8,409	Typical—Austin
100.6	402.4	1.47	$9,255	GeoDesigner
109.7	438.8	1.60	$10,092	GeoDesigner

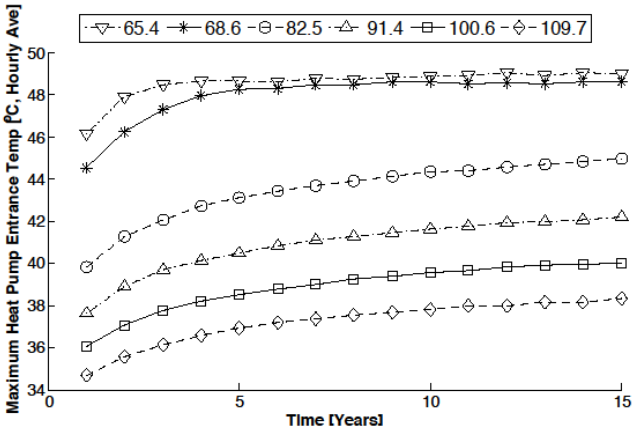

Figure 4.28: Maximum yearly heat pump entering water temperatures (EWT) for different borehole lengths, based on hourly averages (data in Appendix C.1)

Figure 4.29 shows the annual cooling, in MWh, provided by the heat pump. By year 10, the shortest and base cases (65.4m and 68.6m) had reductions in cooling provided by 0.85% and 0.15%, respectively, indicating that the heat pump could not continuously cool the conditioned zone due to its built-in thermal shutoff protections (e.g. the heat pump was shutoff for some period of time even though the temperature in the conditioned zone exceeded the set point

temperature). In contrast, all the remaining longer borehole cases maintained their required cooling capacities.

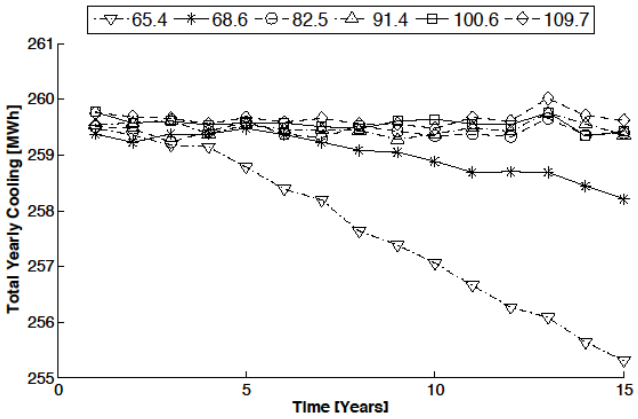

Figure 4.29: Total annual cooling for different borehole lengths (data in Appendix C.2)

The above results were supported by computing the number of unmet hours (hourly averaged) that the conditioned zone 1 temperature exceeded its set point temperatures. For the base case this value was 63 unmet hours in year 10 and 167 unmet hours in year 15. The former time is less than 1% of the year and represents 3% of the total cooling time (2128 hours), which satisfies ASHRAE Standard 90.1-2007.G3.1.2.2 and is an acceptable value considering GLHEPRO sized the borehole for 10 years of operation. For all cases with borehole lengths greater than the base case, there were zero unmet hours during the entire 15 years. As expected, the shortest borehole case was under-designed and exceeded the set point temperature by more than 200 hours, which corresponds to approximately 10% of the total cooling time in year 8. This small 5% decrease in borehole length and resulting poor performance highlights the importance of properly sizing the boreholes.

Annual EER increased with increasing borehole lengths reflecting the lower heat pump EWTs, and for a given length, the EER slowly decreased over time due to higher ground temperatures. For the 82.5, 91.4, 100.6, and 109.7 m cases, the first year EER was 9.0%, 12.9%, 15.8% and 18.2% higher, respectively, than the base case EER of 9.6. For the base case the ERR decreased by 11.8%, 16.0% and 18.3% for year 5, 10, and 15, respectively, compared to the first year.

The higher EER values result in less annual energy consumed by the heat pump to provide the same amount of cooling. Figure 4.30 shows the electricity consumption for each borehole length case. In year 5 the total electricity consumed for the 82.5, 91.4, 100.6, and 109.7 m

cases is 11.0%, 16.7%, 21.4% and 25.5% lower, respectively, than the base case usage of 9980 kWh.

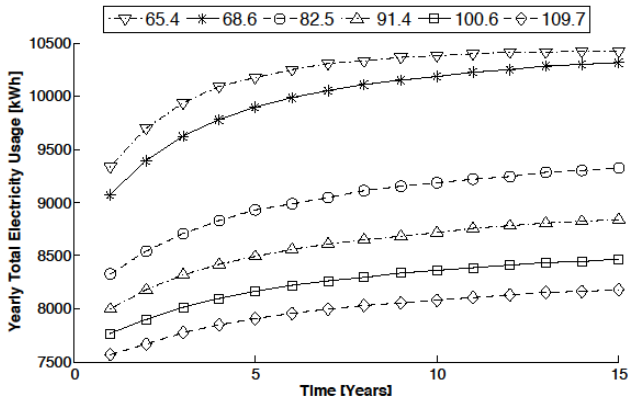

Figure 4.30: Total annual electricity use for different borehole lengths (data in Appendix C.3)

Table 4.12 shows the increased cost of drilling/installation of the longer boreholes to the energy costs (using average residential retail electricity price for Texas) over 10 years of operation (lifetime used to size base case) compared to the base case. The shortest borehole length was not considered for this analysis since it was known to be under-designed. For all cases the additional initial cost was more than the savings in reduced electricity cost—however, the initial cost did not include the 30% federal tax credit nor other potential state/local credits. If the federal credit is applied, the net cost would be less than zero for the 82.5 and 91.4 m cases over the 10-year period. For all cases to break even for the 10-year period without the tax credits, the energy rate must be at least $0.1958/kWh; the average price of electricity in New York state ($0.1921/kWh), which is the second highest in the United States [US DoE, 2011b].

Table 4.12 Comparison of Initial Borehole and Energy Costs Over 10 Years for Different Borehole Lengths; Assumes $0.1133/kWh (Texas Residential Price August 2011 [US DoE**,** 2011b]**)—Subsidies/Tax Credits not Applied**

Borehole length, m	Borehole Cost	Increase from Base Case	Operation Costs– 10 Years Without Subsidies/Tax Credits		
			Energy Cost	Savings	Net Cost
68.6	$6,311	-	$11,128	-	-
82.5	$7,590	$1,279	$10,063	$1,065	$214
91.4	$8,409	$2,098	$9,586	$1,542	$555
100.6	$9,255	$2,944	$9,226	$1,902	$1,042
109.7	$10,092	$3,781	$8,939	$2,189	$1,593

From a strictly cost perspective, longer boreholes could be a good investment, but must account for the additional installation costs, subsidies/tax credits, and the local electricity rate. Longer boreholes would compensate for differences in ground properties and provide lower heat pump EWTs to allow the units to operate more efficiently, but at the expense of higher initial costs.

4.8.2 Borehole Configuration and Spacing

This section investigates the effects of two residential borehole field configurations, a line of four (1x4) and a 2x2 square, and spacing as shown in Figure 4.31. The 2x2 configuration is less desirable due to the increased borehole thermal coupling, which results higher ground temperatures over time.

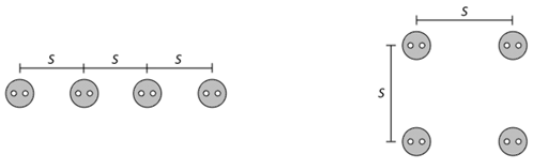

Figure 4.31: Borehole configurations (figures not to scale)

The base case has four in-line boreholes 68.6m (225ft) deep on 4.6m (15ft) centerlines. For this study the borehole length was kept constant at 68.6m but the spacing, S, was varied to 3.0m, 4.6m, 6.1m, and 7.6m. The study showed under-designed systems for borehole spacing less than 4.6m. Figure 4.32 shows reductions in the annual provided cooling for the two configurations (1x4 and 2x2) with smallest spacing (x3.0m) and the square configuration with base case spacing (2x2x4.6m). In year 10 the annual cooling provided was reduced by 0.7% for the 2x2x4.6 case, 1.4% for the 1x4x3 case, and 3.3% for the 2x2x3 case. Notice the similarity in performance between the 2x2x6.1 and 1x4x4.6 base cases.

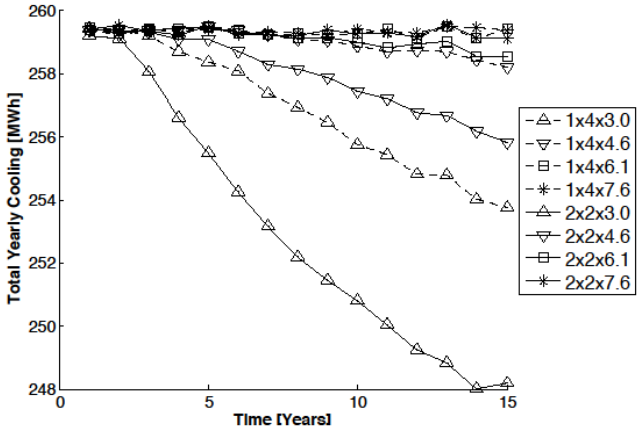

Figure 4.32: Total annual cooling for different borehole configurations (data in Appendix C.4)

Based on the annual cooling provided, it can be concluded that the all cases with 3.0m spacing and the case of the 2x2 configuration with 4.6m spacing were under-designed. The conditioned space temperatures begin to exceed the set point temperature by more than 200 hours, which corresponds to approximately 10% of the total cooling time; in year 4 for the 2x2x3 configuration, year 6 for the 1x4x3 configuration, and year 9 for the 2x2x4.6 configuration. For the remainder of the analyses in this section, the under-designed cases will not be considered.

As expected, the cases with less borehole coupling have lower heat pump EWTs, resulting in increased operating efficiency. Table 4.13 shows the increase in the EER for years 5 and 10. Increasing spacing from the base case (4.6m) by 1.5m and 3m increased the EER by approximately 2.7 and 4.5%, respectively, for all years.

Table 4.13: Comparison of EER for Years 5 and 10 Based on Different Configurations

	Borehole Configuration				
	Base Case 1x4x4.6	1x4x6.1	1x4x7.6	2x2x6.1	2x2x7.6
Year 5 EER	8.55	8.78	8.93	8.57	8.75
Increase	-	2.65%	4.51%	0.27%	2.41%
Year 10					
EER	8.24	8.46	8.63	8.24	8.42
Increase	-	2.71%	4.73%	-0.04%	2.18%

Figure 4.33 shows the annual energy consumption for each configuration and spacing of well-designed systems. As expected increased spacing for any configuration results in lower energy consumption and the in-line configuration shows the best efficiency, Notice that the 1x4x4.6 and 2x2x6.1 configuration results are similar.

When comparing these results it is important to remember that all cases have the same initial investment, the boreholes have the same 68.6m depth and the same heat pump is used. The only difference is the placement of the boreholes, and these improvements in operation are ‘free’ as long as the lot-size allows the better solution. Table 4.14 shows the total energy used and the operating cost over 10 years of operation. Increasing spacing by 1.5m and 3m saved $200 and $328, respectively, for the in-line cases and $30 and $187, respectively, for the 2x2 cases.

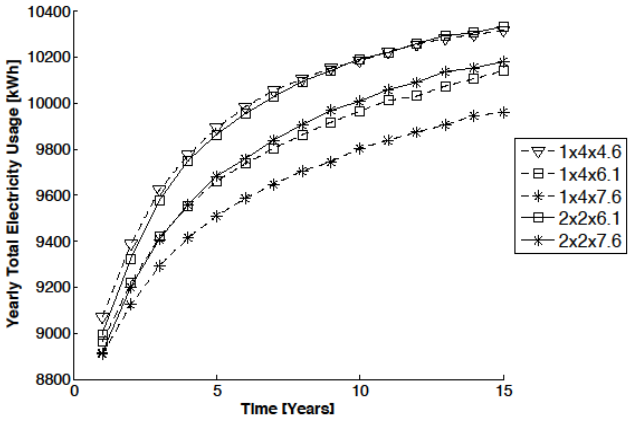

Figure 4.33: Total annual electricity use for different borehole configurations (data in Appendix C.5)

Table 4.14: **Comparison of Energy Costs for Different Configurations over 10 Years; Assumes $0.1133/kWh (Texas Residential Price, August 2011)** [US DoE, 2011b]

	Borehole Configuration				
	Base Case 1x4x4.6	1x4x6.1	1x4x7.6	2x2x6.1	2x2x7.6
Total Energy (kWh)	98217	96084	94724	97896	96220
Total Operating Cost $	$9,213	$9,013	$8,885	$9,183	$9,025
Energy Savings (kWh)	-	2132	3493	321	1996
Cost Savings $	-	$200	$328	$30	$187

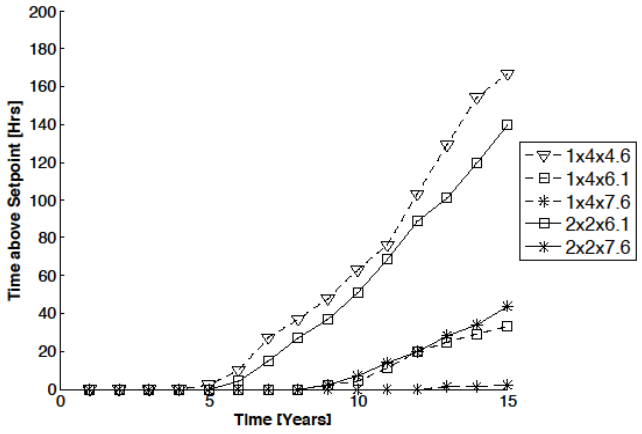

Figure 4.34: Total annual time that zone 1 air temperature exceeded cooling set point for different borehole configurations, unmet hours based on hourly averages (data in Appendix C.6)

Increasing borehole spacing reduces the operating cost and it extends the lifetime of the boreholes. Figure 4.34 shows the number of unmet hours each year that the zone 1

temperature in the building exceeded the set point temperature. In year 10 the base case had 63 unmet hours. Adding 1.5 m spacing to the base case (1x4x6.1) reduced unmet hours to four hours. In year 15 the base case reached 167 unmet hours, however, by adding 1.5 m and 3 m spacing, there were only 33 and 2 unmet hours, respectively. This result indicates that increasing the spacing significantly increases the borehole lifetime.

Based on the results presented, borehole configuration and spacing can reduce the annual energy costs and more importantly, it can significantly increase borehole lifetime by using the in-line configuration and maximum allowable spacing.

4.8.3 Grout Conductivity

Borehole performance can be enhanced by increasing the conductivity of the grout used to backfill the borehole. The packaged grout is mixed with water on-site and pumped down the boreholes. In this study, normal and thermally-enhanced grouts are tested. Normal grout is typically made with bentonite, a type of clay, with a thermal conductivity of 0.744W/m/K. In thermally-enhanced grout, silica sand is added to the base bentonite grout in varying ratios to increase conductivity up to 2.06W/m/K. If the boreholes are improperly backfilled with grout, air pockets will reduce the effective borehole conductivity.

In this study, five different grout conductivities were tested; 0.5 W/m/K (mimic improper backfill), 0.744W/m/K (standard bentonite), 1.0W/m/K (enhanced bentonite), 1.333W/m/K (local soil) and 1.5W/m/K (enhanced bentonite). All other model parameter where left identical to the base model. The results are presented as changes relative to the base case.

Table 4.15: Comparison of Maximum and Average Heat Pump EWT (^{o}C) for Years 5 and 10

	Grout Conductivity (W/m/K)				
	0.500	0.744	1.000	1.333	1.500
Year 5					
Max EWT (^{o}C)	48.8	48.3	46.7	45.5	45.1
% Change	1.2%	Base	-3.2%	-5.7%	-6.6%
Avg EWT (^{o}C)	35.4	34.3	33.7	33.3	33.1
% Change	3.1%	Base	-1.7%	-2.9%	-3.4%
Year 10					
Max EWT (^{o}C)	49.0	48.6	48.0	47.0	46.5
% Change	0.88%	Base	-1.2%	-3.4%	-4.4%
Avg EWT (^{o}C)	36.4	35.5	35.0	34.5	34.4
% Change	2.5%	Base	-1.6%	-2.8%	-3.1%

Figure 4.35 and Table 4.15 shows that increasing conductivity decreases the average heat pump EWT up to the point when the grout and ground conductivities are equal. The change in the average EWT between 0.744W/m/K and 1.333W/m/K is 1°C for years 5 and 10. For the 1.333W/m/K and 1.500W/m/K cases, it is only 0.17°C and 0.10°C for years 5 and 10, respectively. The results also show that a reduction in the conductivity has a larger effect on the average EWTs than an increase of a similar amount. In year 5, the average EWT increases by 1.1°C when decreasing the conductivity by 0.244W/m/K, but only decreases EWT by 0.6°C when the conductivity is increased by a similar amount. Similar values are seen in year 10.

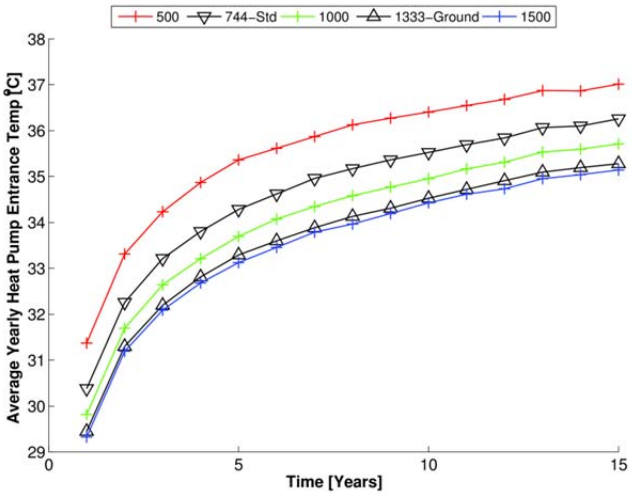

Figure 4.35: Yearly mean heat pump EWT for the grout conductivities tested (data in Appendix C.7)

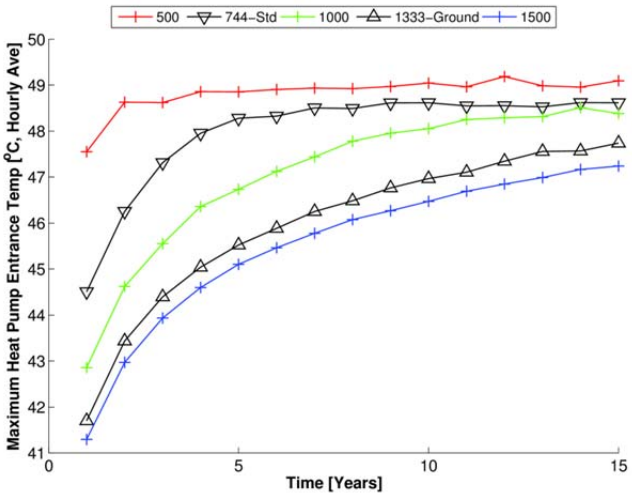

Figure 4.36: Yearly maximum heat pump EWT for the grout conductivities tested (data in Appendix C.8)

Figure 4.36 shows the effects of the grout conductivity on the annual maximum EWT temperatures. The grouts with lower conductivities reach their lifetime maximum values significantly quicker than those with higher conductivities. Here the reduced effect of increasing the grout conductivity past the ground conductivity is seen as well. Comparing this figure with the previous figure the effect of increasing the grout conductivity is more pronounced on the maximum temperatures than it is on the mean temperatures. Table 4.15 shows the change in the temperatures compared to the base case grout conductivity values. Using a grout with a conductivity of 1.333W/m/K reduces the maximum temperature by 5.7 % and 3.4% in years five and ten, when compared to the base case grout. The mean temperature is only reduced by 3.4% and 2.8% in years five and ten. Ground loops with lower conductivities reach their lifetime maximum values significantly faster that those with higher conductivities. Here the reduced effect of increasing the grout conductivity past the ground conductivity is seen as well. Table 4.15 shows that the effect of increasing the grout conductivity is more pronounced on the maximum EWT than it is on the average temperatures. Using a grout with a conductivity of 1.333W/m/K reduced the maximum EWT by 5.7% and 3.4% in years 5 and 10, when compared to the base case grout. The mean temperature is only reduced by 3.4% and 2.8% in years 5 and 10.

The total annual cooling provided by the heat pump, shown in Figure 4.37, decreased for the lowest conductivity case (by 1.6% in year 10) and the time that the zone temperature exceeded set point was more than 200 unmet hour in year 5; this case shows an under-designed system resulting from improper grout use. These results demonstrate the importance of properly backfilling the borehole during installation to ensure sufficient conductivity is attained along the entire length of the borehole.

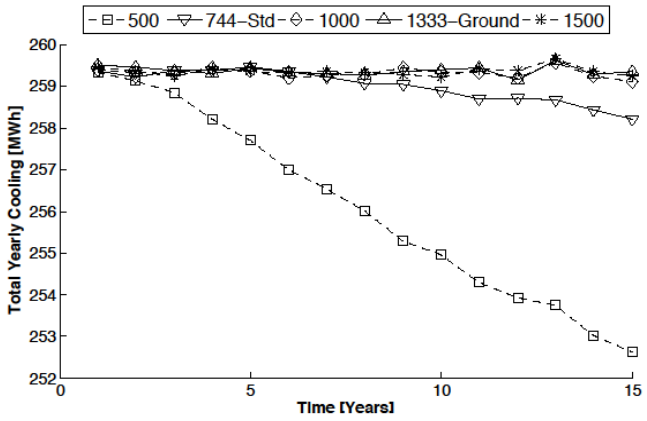

Figure 4.37: Total annual cooling for different grout conductivities (data in Appendix C.9)

For the cases with increased grout conductivity the number of unmet hours is significantly reduced. For the highest two values there are no unmet hours by the end of year 15. The 1.0 W/m/K conductivity case shows no unmet hours above the set point in year 10 and only 18 unmet hours in year 15 compared to 63 and 167 hours for the base case, respectively. These results indicate that increased grout conductivity will extend borehole lifetime.

Higher grout conductivities lower the heat pump EWT and the heat pump operates more efficiently. In year 5 the EER increases by 3.2%, 5.7% and 6.5% for each successively higher conductivity above the base case EER of 8.55. Similar increases are also seen in year 10. The higher ERRs reduce annual electricity use as shown in Figure 4.38. The total energy used over 10 years of operation is shown in Table 4.16. Increasing the conductivity of the grout to 1.0 W/m/K, 1.333W/m/K, and 1.5W/m/K reduces the total energy consumption over the 10 year period by 2.9%, 5.0%, and 5.6%, respectively, when compared to the base case of 0.744 W/m/K which consumes 98217kWh over 10 years.

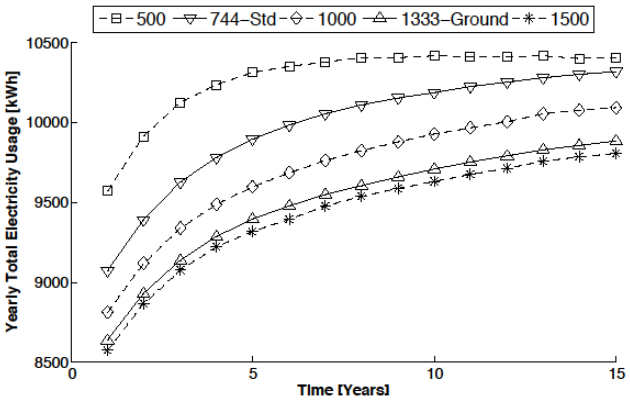

Figure 4.38: Total annual electricity use for different grout conductivities (data in Appendix C.10)

Table 4.16: Comparison of Energy Costs for Different Grout Conductivities over 10 Years; Assumes 0.1133 $\$/Kwh$ (Texas Residential Price August 2011) [US DoE, 2011b]

	Grout Conductivity (W/m/K)			
	Base Case 0.744	1.000	Ground 1.333	1.500
Total Energy (kWh)	98217	95422	93361	92675
Total Operating Cost $	$11,128	$10,811	$10,578	$10,500
Energy Savings (kWh)	-	2795	4856	5542
Cost Savings $	-	$317	$550	$628

4.8.4 Ground Temperature

One factor that sets Texas and the southwest U.S. apart from areas where ground source heat pumps are common, such as the midwest and northeast parts of the United States, is higher ground temperatures and lower ground conductivities. Figure 4.9 (Section 4.6.3) showed the ground temperatures in Texas at 9.1*m* (30*ft*) below the surface of the ground; they range from 15.5°C (60°F) in the panhandle to 27.2°C (81°F) in the most southern parts.

Table 4.17 Simulated Ground Temperatures

Celsius °C	17.3	18.8	20.3	21.7	23.3	24.8	25.3
Fahrenheit °F	63.1	65.8	68.5	71.2	73.9	76.6	79.3

To determine the effects of the ground temperatures on ground source heat pumps a sensitivity study was performed. Seven different temperatures, listed in Table 4.17, were simulated, using Austin's ground temperature, 21.7°C (71.2°F) as the base case and the temperature was increased and decreased in 1.5°C (2.7°F) increments.

As expected, the starting ground temperature affects the ground loop temperatures. As the starting ground temperatures increases across the tested range the yearly average heat pump EWTs increased by the same amounts, as shown in Figure 4.39. An interesting phenomenon occurs in year eight of the highest temperature tested. There is a significant increase in the average temperature between year seven and eight which is caused by high water temperatures during the winter that causes the heat pump to shut down. The heat pump will stop operating while it is in the heating mode if the entering water temperatures exceed 32.2°C (90°F). The yearly maximum heat pump EWT is shown in Figure 4.40. The temperatures reach the maximum designed EWT for high ground temperatures in about eight years.

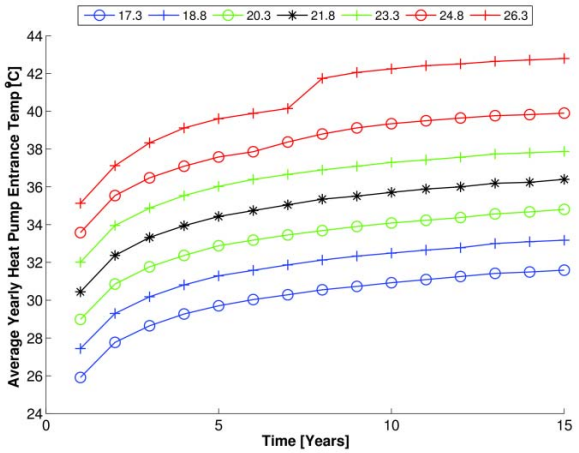

Figure 4.39: Yearly mean heat pump EWT (°C) for the different ground temperatures tested (data in Appendix C.11)

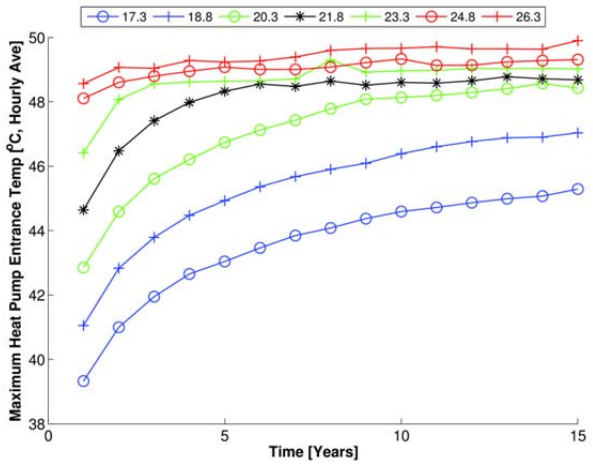

Figure 4.40: Yearly maximum heat pump EWT (°C) for the different ground temperatures tested (data in Appendix C.12)

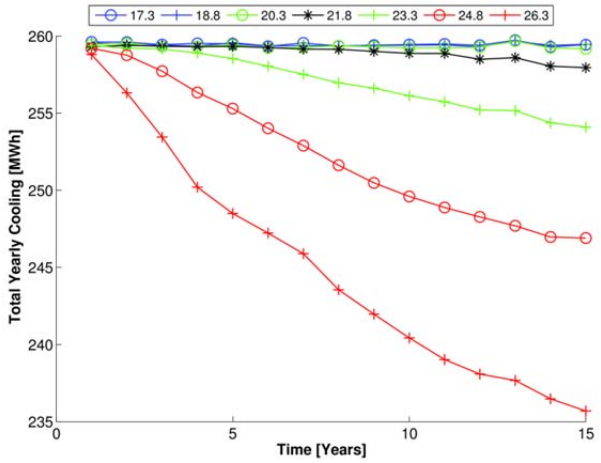

Figure 4.41: Total annual cooling (MWh) for the different ground temperatures tested (data in Appendix C.13)

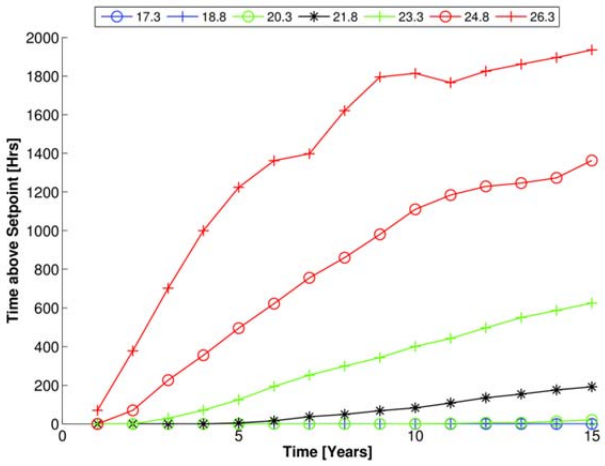

Figure 4.42: Total annual time that zone 1 air temperature exceeded cooling set point for the different ground temperatures tested, unmet hours based on hourly averages (data in Appendix C.14)

The ground temperature results were very similar to the results from the length analysis; the ground temperatures higher than Austin's ground temperature resulted in under-designed ground loops. In Figure 4.41 the total annual cooling for each year of operation is given. By year ten the annual delivered cooling is reduced by 1.3%, 3.8%, and 7.3% for the 22.3°C, 24.8°C, and 25.3°C cases, respectively. Figure 4.42 shows the number of hours each year that the building air temperature exceeded the set point temperature. The cases exceeded 200 hours of time above the set point, which corresponds to approximately 10% of the total annual cooling time, in years 7, 3, and 2 for the 22.3°C, 24.8°C, and 25.3°C cases, respectively, which point to significantly under-designed systems. The lower ground temperatures prevent the building temperature from exceeding the set point temperatures. In year fifteen, there are only 20 hours where the building temperature exceeded set point temperature for the 20.3°C case and no hours for the two lower temperatures.

The lower water temperatures associated with the reduced ground temperatures shown in Figures 4.39 and 4.40 translate into more efficient heat pump operation, as shown in Figure 4.43. In year five the EER is increased from the base case by 4.8%, 10.0% and 15.6% for the successively lower ground temperatures. Similar values are seen in year ten as well. Of all of the results presented, ground temperature had the greatest effect on the EER. The lowest ground temperature tested produced the highest EER for any of the sensitivity tests completed.

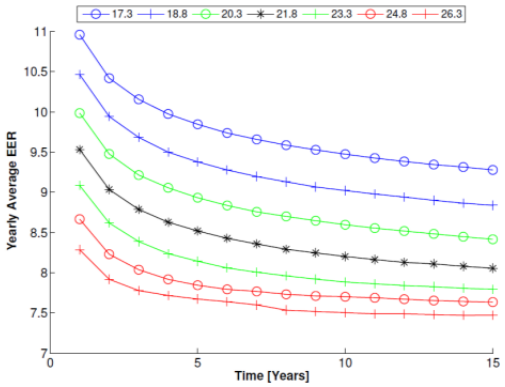

Figure 4.43: Average annual energy efficiency ratio (EER) for the different ground temperatures tested (data in Appendix C.15)

Figure 4.44 shows the total annual electricity use over the 15 years of the simulation. As shown previously, the under-designed systems actually see reductions in the annual electricity used due to the heat pump being shutdown for extended periods of time. For properly designed cases there is a 2.5% reduction in the annual energy use for every 1°C (1.8 °F) reduction in ground temperature over the range tested in years five and ten. The lowest temperature tested consumes 11.5% less energy in years five and ten than the base case.

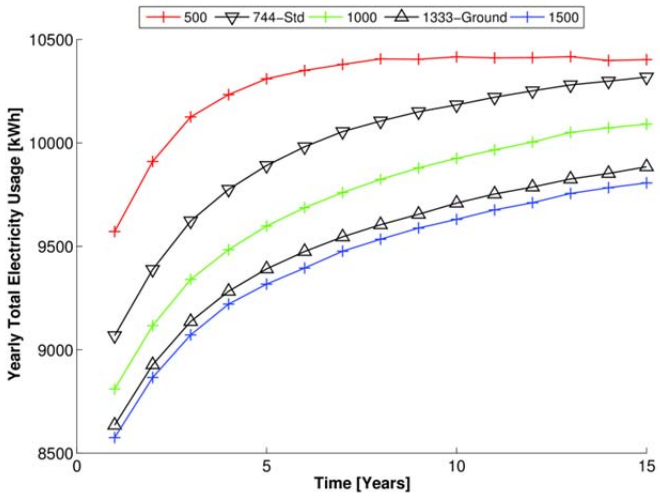

Figure 4.44: Total annual electricity use for the grout conductivities tested (data in Appendix C.16)

Table 4.17: Comparison of Operating Costs and Savings over Ten Years for the Different Ground Temperatures Tested, Assuming 0.1133 $/*kWh* (Texas residential price August 2011) [US DoE, 2011b]

	Ground Temperature [°C]			
	Base - 21.7	20.3	18.8	17.3
Total Energy (kWh)	98217	94609	90788	87137
Total Operating Cost $	$11,128	$10,719	$10,286	$9,873
Energy Savings (kWh)	-	3608	7428	11080
Cost Savings $	-	$409	$842	$1,255

Table 4.18 shows the total energy used and cost over ten years for the ground temperatures that were properly designed. There are significant reductions in the total operating cost of the ground loop as the ground temperatures decrease. For these simulations the total operating costs were reduced by $285 per °C ($155 per °F). Based on the results, ground temperature has a large effect on the operation of the heat pump. Higher ground temperatures result in lower operating efficiencies and shorter borehole life times.

4.8.5 Supplemental Heat Rejection Sizing

Supplemental Heat Rejection devices (SHRs), such as cooling towers, are used to remove heat from the ground loop water before it enters the ground loop heat exchanger, and they also reduce the total length of installed boreholes. In this study SHR devices, ranging from 250 to 5000 W, were added to assess their effects on operating performance of reducing heat rejected into the ground. For comparison the heat pump rejects 17,500 W to the ground during the cooling mode with an EWT of 32.3°C. Based on this number, the SHRs will reject 1.4% to 28.5% of the heat normally rejected to the ground. The devices were assumed to be ideal, i.e. they always reject the rated amount, and they operate any time the heat pump was cooling the building.

As shown in Figure 4.45 for all 15 years, the SHRs reduced the heat rejected to the ground by 2.1%, 8.7%, 25.7%, and 41.3% for SHRs with 250, 1000, 3000, and 5000 W, respectively. As mentioned above the 250 and 5000 W SHRs reject 1.4% and 28.5% of the heat that is generated by heat pump, so the additional reduction in the heat rejected into the ground is due to increased operating efficiency, which is reflected by the increased EER.

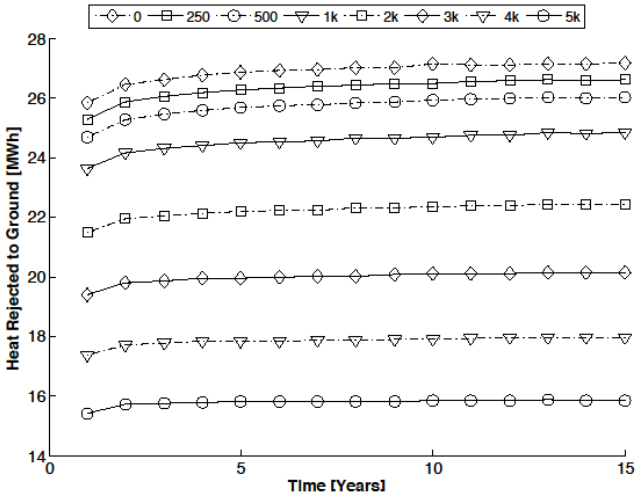

Figure 4.45: Annual net heat rejected to the ground for different capacity supplemental heat rejection

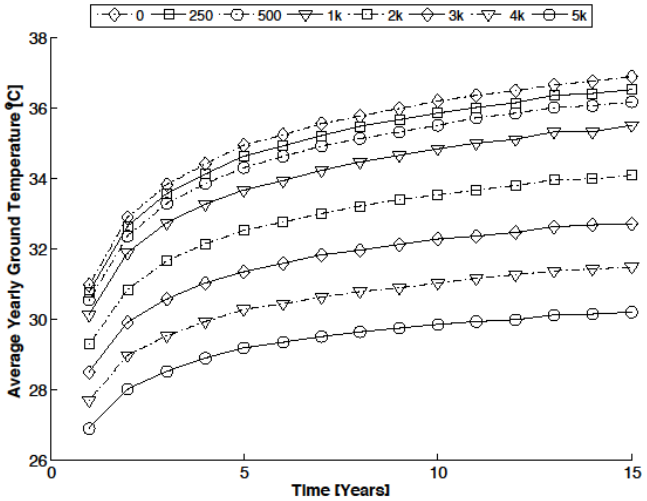

Figure 4.46: Annual mean ground temperatures near borehole for different capacity supplemental heat rejection

In year 5 the ERR was increased from the base case value of 8.54 without a SHR, to 8.94, 9.78, and 10.63 for a 1000, 3000, and 5000 W SHR, respectively. The increased efficiency due to lower heat pump EWT is directly correlated to the annual average ground temperatures shown in Figure 4.46. In year 1 there was a 4°C difference between the 5000W SHR case and the base case without a SHR. By year 10 this difference increased to 6.4 °C. In short, less heat is rejected into the ground on an annual basis due to some heat being rejected by the SHR device but also due to more efficient heat pump operation due to lower ground temperatures.

Since the heat pump operates more efficiently with larger SHRs the annual heat pump operating cost decreases as well due to lower power consumption and less total operation time. The total cooling time reduced by 1.5%, 4.5%, and 7.5% for the 1000, 3000, and 5000 W SHR

cases, respectivily. Table 4.19 shows the actual operational time for each case along with the total electricity usage, heat pump operational cost, and the total savings on electricity. Most SHR devices will have operational costs so the last column of Table 4.19 shows the break even cost for the SHR operation in dollars per hour. This was calculated taking the electricity cost savings for each case and dividing that amount over the total time the SHR unit was operational (which is also the total time the heat pump was cooling). This analysis does not consider the intial upfront cost of the unit or reoccuring fixed costs such as maintance.

Table 4.19 Total Heat Pump Operational Cost over First 10 Years of Operation, and Break Even Operational Cost for an SHR; Assumes 0.1133 $\$/Kwh$ (Texas Residential Price August 2011) [US DoE, 2011b]

SHR Size (W)	Total Electricity (kWh)	Total Cost	Savings	On Time (hr)	Break Even Operational Cost $/hr
0	98206	$11,127	Base	Base	Base
250	97278	$11,022	$105	20829	0.005
500	96317	$10,913	$214	20749	0.010
1000	94367	$10,692	$435	20609	0.021
2000	90681	$10,274	$853	20319	0.042
3000	87220	$9,882	$1,245	20019	0.062
4000	84063	$9,524	$1,602	19735	0.081
5000	8110	$9,198	$1,929	19461	0.099

Table 4.20 Reduced Length Borehole Sizes and Costs; at $23/m Borehole Cost [Hammond, 2011]

SHR Capacity (W)	Total Borehole Length (m)	Total Cost	Savings	% Savings
Base Case	261.6	$6,017	-	-
0	270.3	$6,216	-	-
250	266.5	$6,130	$86	1.4
500	264.8	$6,089	$127	2.0
1000	248.4	$5,714	$502	8.1
2000	234.0	$5,383	$834	13.4
3000	210.1	$4,833	$1,384	22.3
4000	190.5	$4,381	$1,835	29.5
5000	169.2	$3,891	$2,326	37.4

The primary benefit of adding an SHR device to a GHP is to reduce the total borehole length needed, which will reduce the initial costs and make the system more affordable without sacraficing long term performace. To explore trade offs between length and SHR size GLHEPRO was used to re-size borehole lengths using the total amount of heat rejected to the

ground by the full length case of 261.6 m for each SHR capacity tested. Table 4.20 shows the resulting lengths. As a check a 0 W SHR case was sized to determine if the method was approriate. The results show that the 0 W case was sized 3% longer than the base case (270.3 vs. 261.6 m total length). Due to this difference the 0 W case length was used to determine the cost savings of the initial borehole. As expected as the capacity of the SHR unit increases the total borehole length decreases. The cost of the boreholes was reduced by 8.1 %, 22.3 %, 37.4 % for the 1000, 3000, and 5000 W SHR cases compared to the 0 W SHR case.

With reduced borehole lengths it is important that the system maintains its ability to cool over the lifetime of the unit. Using the criteria previously discussed, the system is assumed under-designed when the total time the controlled temperature (hourly averaged) is above the thermostat set point is greater than 200 unmet hours in a given year. All cases, except the 5000W case, met this requirement up to year 10, which is the sized lifetime of the boreholes. The 5000 W SHR case had 209 unmet hours in year 10.

4.8.6 Residential Sensitivity Study Conclusions

The parameters varied in this Section 4.8 illustrated only a few possible design parameters that could be varied by the IBL-GHP model. All results show that the borehole operation is very sensitive to these parameters. The sensitivity study showed that the choice of the heat pump shutoff temperature and GLHEPRO borehole sizing algorithm yielded a limiting base case design for the GHP system that adequately controlled the building temperatures with minimum borehole length, maximum heat pump EWT, and maximum operating costs. The study showed that any perturbation ‘decrease’ from the base case parameters will result in an under-designed system that will not provide adequate control of building temperatures. This potential highlights the need to add extra borehole length to account for parameter variations since ground parameters are not typically known to precise values for residential installations. The improved results have been quantified in this study for lengths greater than the base case, as shown by the longer borehole lengths typically used in Austin, TX. With subsidies and tax credits, the longer boreholes are easily justified based on heat pump performance. Of the individual sensitivity studies performed, the most cost effective design parameter that can be addressed by the designer is the borehole configuration and spacing. As expected, placing the boreholes as far apart as possible (and with the largest aspect ratio—in the limit in-line configuration) will significantly increase heat pump efficiency and longer borehole lifetimes. While the results are intuitive, this study showed the quantitative improvements that can be expected. Finally, if the initial costs are too great and or the ground heating is significant, adding an SHR device is warranted and will improve GHP performance but with initial and yearly maintenance and

operating costs. A compact cooling tower added to the residential IBL-GHP model will be discussed in Section 5. The sensitivity study results are summarized in Gaspredes, et al. [Gaspredes, et al., 2012b].

4.9 SUMMARY: INTEGRATED RESIDENTIAL BUILDING APPLICATION

The component building load, heat pump, and borehole-ground loop models developed in Section 3 were coupled into an integrated IBL-GHP model using Simulink's powerful organization protocols. The IBL-GHP model was then sized for a base case residential house exposed to Austin, TX weather and geological conditions. One important sizing decision was the choice of the heat pump shutoff temperature as the maximum heat pump EWT used by GLHEPRO to size the ground loop. Base case simulations showed that the resulting design adequately controlled the conditioned temperatures. Simulation data showed the ability of the model to predict system performance from seconds to years. Moreover, it computed economic performance, such as heat pump electricity use, over 15 years of operation.

The sensitivity study showed that design parameters of the base case reflected a minimal adequate design. Parameter perturbations with 'smaller' design parameters from the base case showed resulting under-designed systems that were unable to achieve adequate performance and unable to meet ASHRAE 90.1 operating criterion. For example, a 5% decrease from the base case borehole length resulted in the heat pump being unable to control the conditioned temperatures and exceeded 300 unmet hours. Moreover, perturbations with 'larger' design parameters achieved improved performance measures and operating economic benefits, and the model was able to compare performance with cost implications.

The GHP system designs are very sensitive to site-specific environmental and geological conditions. Modeling and simulation are necessary tools to arrive at effective designs. With a large number of design parameters and design criteria to satisfy, it is clear that a global optimization study is needed. The IBL-GHP model can be used for such a study.

5. SUPPLEMENTAL HEAT RECOVERY/REJECTION

Section 5 focuses on the technical and economic viability of various supplemental heat rejection (SHR) devices/systems for HGHP systems to reduce the heat rejected to the ground in cooling-dominated regions. Adding an SHR device will also decrease the total required borehole length, thereby reducing the initial drilling costs, but will add the initial, maintenance and operational costs of the SHR device.

The design of a HGHP system requires sizing the borehole length and the capacity of the SHR. Figure 5.1 shows a schematic of the balance between the ground loop (borehole) length ratio (length using a HGHP/length using GHP only) and the percentage of heat added/rejected by the SHR system for commercial building [Cullin & Spitler, 2010]. The right hand side of the plot is for cooling-dominated operation and shows the ratio and the percentage of heat rejected by the SHR system. For example, point 2 denotes the case where the SHR system rejects 60% of the total heat and the the ground loop length ratio is 40%.

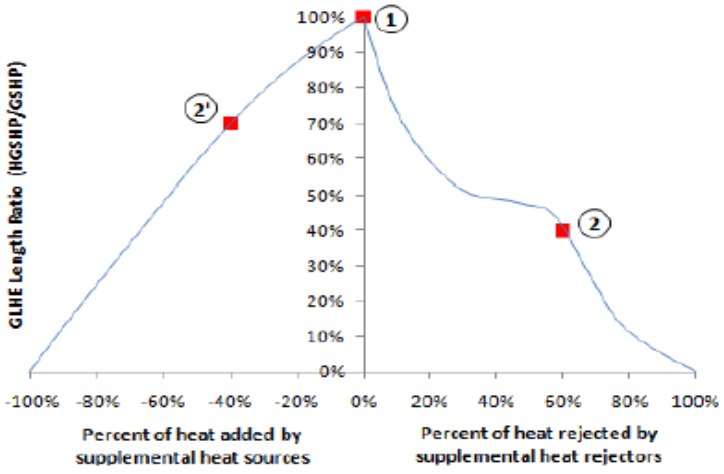

Figure 5.1: GLH length ratio vs percent heat rejected by SHR system [Cullin & Spitler, 2010]

In this report, two heat rejection strategies were followed: 1) remove heat directly from the water before it enters the ground loops and 2) remove heat from the refrigerant loop of the vapor compression cycle (VCC) of the heat pump so less heat is transferred to the water loop at the condenser of the VCC. SHR devices considered included:

Strategy 1: remove heat directly from the water before it enters the ground loops—the main obstacle facing this strategy is the low temperature of the water leaving the heat pump (approximately 5.5°C (10°F) higher than the heat pump EWT of 32-49°C (90-120°F)).

- Cooling towers

- Thermoelectric liquid coolers
- Ponds/water capacity devices
- Adsorption cooler
- Thermo-magnetic/acoustic coolers

Strategy 2: remove heat from the refrigerant loop of the heat pump VCC so less heat is transferred to the water loop at its condenser.

- Optimized VCC cycle
- Expanded desuperheater
- Thermosyphons

Of the proposed SHR devices, only the cooling tower was effective in both performance and cost. Sections 5.1-5.3 provides the cooling tower, optimized vapor compression, and expanded desuperheater models, respectively, and their implementation on the base case residential model. Other SHR strategies and analyses are contained in Appendix D (Other SHR Devices/Systems).

5.1 COOLING TOWER

Figure 5.2 shows a schematic of a HGHP using a cooling tower as a SHR device. In the cooling mode of operation, after heat is rejected to the loop water at the heat pump condenser of the refrigeration cycle, the water flows into the cooling tower, where heat in the water is rejected to the moist air flow of the tower. The cooler water then flows back into the ground loop where additional heat is rejected to the ground.

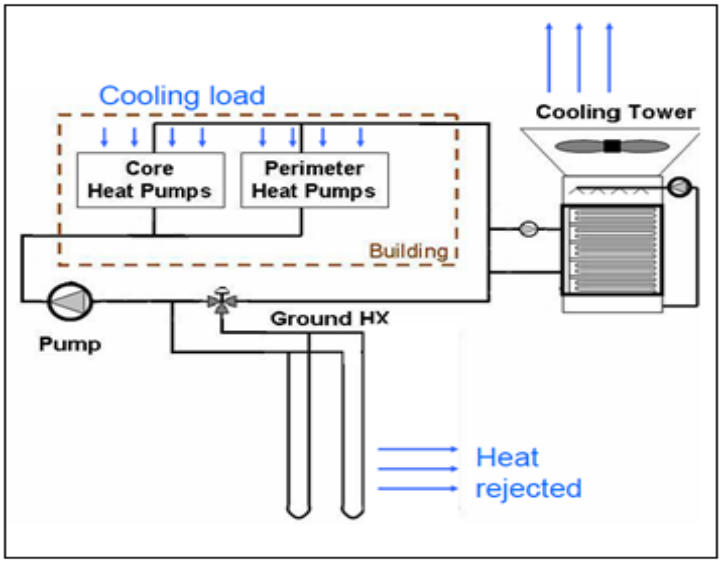

Figure 5.2: Schematic of HGHP [Hackel, 2008]

Use of cooling towers for commercial building applications have been heavily studied and shown to be cost effective for reducing initial costs while maintaining the efficiency of the heat pumps by lowering the heat pump EWT [Hackel, 2008; Cullin & Spitler, 2010]. Kavanaugh provides design guidelines for commercial buildings, but there is no industry-standard for the design or control cooling towers [Kavanaugh, 1985]. Examples of HGHP design and control algorithms are illustrated by three studies done on three stories of a 52-story office building in Houston, TX. The building had a peak heating load of 730 kW (2940 kBtu/h) and a peak cooling load of 819 kW (2794.5 kBtu/h). The number of heating hours in a year was 20 and the number of cooling hours was 1121. The number of boreholes drilled were 120, in a 10 by 12 rectangular grid. The studies by Xu, Hackel, and Cullin and Spitler are briefly described below.

Xu [Xu, 2007]; used an optimization method to minimize the life cycle cost of the HGSHP over a period of 20 years. In that method, ground loop length and the cooling tower capacity among other parameters (control of the cooling tower) were varied to determine the lowest life cycle cost (LCC). That is, for different ground loop lengths and cooling tower capacities, the LCC were calculated and the minimum among those were the optimized case. With this method, Xu obtained an optimum ground loop length of 5,544 m (18,188 ft) and a cooling tower of size 52 tons (182 kW).

Hackel et al. [Hackel et al., 2009] sized the HGSHP ground loop based on the peak heating load. This ground loop length satisfied some of the cooling needs, and the rest was satisfied by a cooling tower. The resulting ground loop length obtained was 8,061 m (26,446 ft) and a cooling tower capacity of 164 tons (574 kW). The cooling tower was sized to 130% of the unmet cooling load by the ground loop. This was obtained by varying the size of the cooling tower and optimizing the LCC.

Cullin and Spitler [Cullin & Spitler, 2010] determined the optimal HGSHP design by treating the sizing of the ground loop and the cooling tower as an optimization problem to minimize the error between the desired and the calculated maximum and minimum temperatures into the heat pump. With this strategy, they obtained a ground loop length of 5,769 m (18,920 ft) and a cooling tower capacity of 104 tons (364 kW).

The results of the three studies show that despite the same given building loads, there are wide variations in the cooling tower capacities, from 182kW to 264kW, and ground loop sizes, from 5,544m to 8,061m. Again, there is no industry-wide standards.

The focus of the discussion below investigates the use of compact cooling towers for the base case residential application (see Section 4.6) using the smallest commercially available compact cooling tower

.

5.1.1 Cooling Tower Model

Hasan and Siren developed a wet closed cooling tower (CWCT) using experimental data from a 10kW tower to define mass and heat transfer coefficients [Hasan & Siren, 2002]. That model was used as the prototype cooling tower model described below.

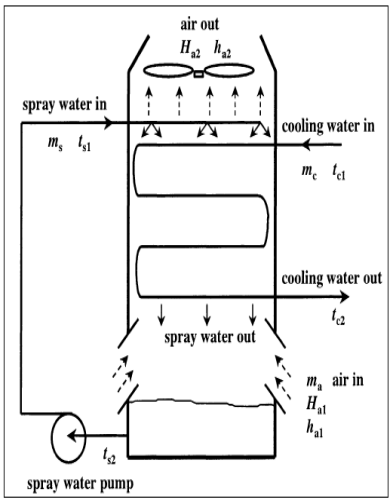

Figure 5.3: Schematic of cooling tower model [Hasan & Siren, 2002]

Figure 5.3 is a schematic of the cooling tower showing the three fluids and their initial and final conditions. The cooling water exit temperature and the heat rejected, for a given set of conditions (inlet air conditions, mass flow rate of air and spray water), are computed from the governing equations of an elemental control volume cutting across a tube cross-section, as shown in Figure 5.4 with inlet conditions of the cooling water, air and spray water.

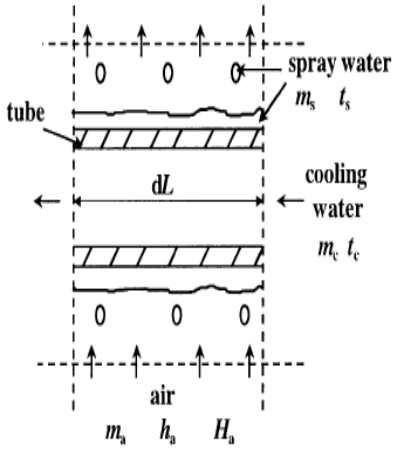

Figure 5.4: Control volume [Hasan & Siren, 2002]

Heat Transfer from Cooling Water to Spray Water

The temperature gradient between the cooling water temperature (t_c) and spray water temperature (t_s) causes heat transfer through the tube wall. The rate of heat lost by the cooling water (dq_c) is

$$dq_c = m_c C_W dt_c = -U_o(t_c - t_s)dA \tag{5.1}$$

where (U_o) is the overall heat transfer coefficient based on the outer area of the tube and C_w is the specific heat capacity of water in the control volume ($C_w = 4.186\ kJ/kgK$). U_o accounts for the heat transfer coefficient between the cooling water and the internal surface of the tube wall (α_c), the tube wall thermal conductivity (k_w) and the heat transfer coefficient between the external surface of the wall and the bulk spray water (α_s), which is a function of mass flow rate of spray water.

Heat Transfer from Air-Water Interface to the Air

Heat gained by the air stream (dq_c) from the air-water interface consists of sensible (dq_{sn}) and latent (dq_L) parts.

$$dq_a = m_a dh_a = dq_{sn} + dq_L \tag{5.2}$$

$$dq_a = m_a dh_a = \alpha_i(t_i - t_a)dA + k(H_i' - H_a')h_{fg}dA \tag{5.3}$$

where α_i is the heat transfer coefficient for the air side interface, h_{fg} is the latent heat of evaporation of water and H_i' is the humidity ratio of saturated moist air at the interface temperature t_i and k is the mass transfer coefficient, which is a function of air flow rate.

The enthalpy of air and water vapor mixture is

$$h_a = C_H t_a + h_{fg} H_a \tag{5.4}$$

where C_H is the specific heat capacity of humid air which can be considered constant. Substituting for temperature from Eq. (5.4), Eq. (5.3) yields

$$m_a dh_a = \left\{ \alpha_i \left[\frac{\left(h_i' - h_{fg} H_i'\right)}{C_H} - \frac{\left(h_a - h_{fg} H_a\right)}{C_H} \right] + k(H_i' - H_a) h_{fg} \right\} dA \tag{5.5}$$

which is rewritten as

$$m_a dh_a = \left[\frac{\alpha_i}{C_H} (h_i' - h_a) + k h_{fg} \left(1 - \frac{\alpha_i}{k C_H}\right) (H_i' - H_a) \right] dA \tag{5.6}$$

(α_i/kC_H) is the Lewis Number (*Le*), which is the ratio of thermal to mass diffusivities in a system. *Le* is taken to be equal to 1 for air and water vapor mixtures. Hence Eq. (5.6) is simplified to

$$m_a dh_a = k(h_i' - h_a) dA \tag{5.7}$$

The interface's liquid side offers negligible resistance to heat transfer, and hence the interface enthalpy (h_i') in Eq. (5.7) can be considered equal to the saturated enthalpy (h_s') at the spray water temperature (t_s). Therefore, Eq. (5.7) is rewritten as

$$m_a dh_a = k(h_s' - h_a) dA \tag{5.8}$$

Eq. (5.8) is called the Merkel equation and represents the energy transfer as the enthalpy difference between the air-water interface and the bulk air as the driving force.

Total Energy Balance of the Control Volume

The energy balance for the three fluid streams flowing through the control volume is

$$dq_a + dq_c + dq_s = 0$$

(5.9)

Expressing the heat transfer in terms of the mass flow rates, specific heats and temperatures, Eq. (5.9) becomes

$$m_c C_W dt_c + m_a dh_a + m_s C_W dt_s = 0 \tag{5.10}$$

Spray Water Temperature Distribution

The spray water temperature varies inside the cooling tower according to the height of the bank of tubes. The assumption is made that heat is transferred only by evaporation. Hence

$$t_{s1} = t_{s2} \tag{5.11}$$

Mass Balance

The spray water evaporation is calculated from the mass balance in the control volume.

$$m_e = m_a dH_a = k(H'_s - H'_a) \tag{5.12}$$

The mass transfer coefficient of air is given by

$$k = .065 * m_a^{0.773} \tag{5.13}$$

In summary, there are five known parameter values (m_a, m_w, h_{a1}, H_{a1} and t_{c1}), five unknown parameter values (t_{s1}, t_{s2}, h_{a2}, H_{a1} and tc_2), and five equations (Eqs. (5.1), (5.8), (5.10), (5.11), (5.12)) which are solved iteratively to determine the five unknowns. Each row of tubes is taken as a control volume element and two iterative loops (h_{a2} and t_{s1}) are considered. The iterative procedure is as follows :1) guess values for h_{a2} and t_{s1} in the top tube row of the tower, 2) satisfy mass and energy balances for each going down the cooling tower and at row 1, t_{s2} is finally evaluated, 3) for the given h_{a2}, vary t_{s1} in increments of 0.01 C until t_{s1} =t_{s2}, and 4) compute h_{a1} at the first row and check if it is equal to the known value specified in the problem. If not equal, change the guessed value of h_{a2} in increments of 0.01. For every new h_{a2} , the t_{s1} iteration is started afresh. The parameter values are listed in Appendix E.

Model Validation: The model described by Hasan and Siren above was implemented in MatLab and verified with experimental results mentioned in the paper. The cooling tower consisted of 12 rows of bank of tubes, each bank with 19 tubes with each tube with an outer diameter of 10 mm (0.39 in). The width of the tower was 0.6 m (1.97 ft) and each tube was 1.2 m (3.94 ft) long. The longitudinal and transverse spacing of the tubes were 0.02 m and 0.06 m, respectively. The nominal data for the cooling tower was: 3kg/s (396.8lb/min) air flow rate, 0.8

kg/s (105.8 lb/min) cooling water flow rate, 1.37kg/s (181.2lb/min) spray water flow rate, inlet cooling water temperature of 21°C (69.8°F) and an air wet bulb temperature of 16°C (60.8°F).

Figure 5.5 shows the temperature variation of spray water (green color curve) and cooling water (blue color curve). Row 12 refers the highest level of the tower and row 1 refers to the lowest level of the tower. It can be seen that the cooling water enters at 21°C (69.8°F) and as it flows along the tubes down the cooling tower, the temperature decreases to 18.3°C (65°F). The bulk of the cooling (65%) happens in the top five rows (rows 12–8). In the top five rows the water temperature decreases by 2°C (3.6°F), while it cools by only 1.6°C (2.88°F) in the bottom seven rows (1-7).

It is interesting to see the temperature profile of the spray water. It increases in the top five rows (rows 12–8) and then decreases from rows 7 to 1. The initial and final temperatures of the spray water are equal, an assumption made in the model by Equation 2.11. The profile can be explained as follows. In the top few rows of the tower, the air is almost saturated, and hence the cooling water transfers heat to the spray water, thereby increasing the latter's temperature. As the spray water moves down, it evaporates into the air by taking away latent heat. Hence, the temperature of the spray water reduces in the bottom few rows (rows 7 to 1).

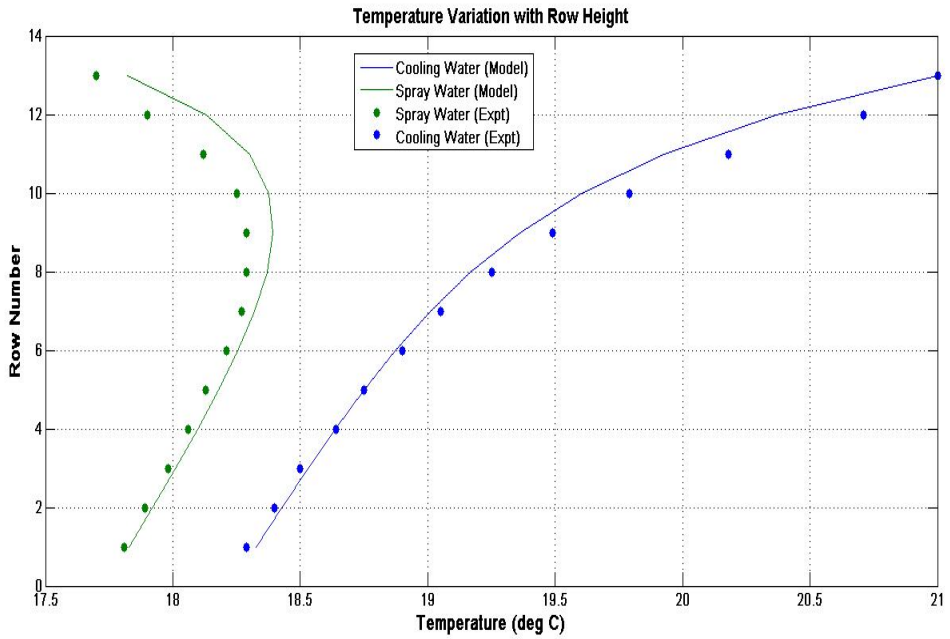

Figure 5.5: Cooling and Spray Water Temperature

Figure 5.6 shows the temperature variation of air with the row height. It is interesting to notice that although heat is being transferred to the air, its temperature decreases as it goes up

the tower. Although this seems counter intuitive, it is not. Although the temperature of the air decreases, its water vapor content increases, which leads to a higher enthalpy value as the air rises. Figure 5.7 verifies the increase in enthalpy of air with row height.

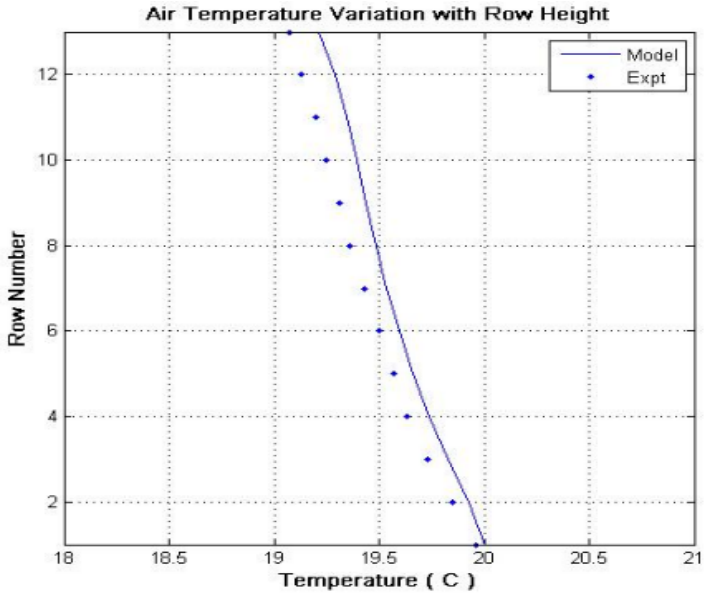

Figure 5.6: Variation of air temperature

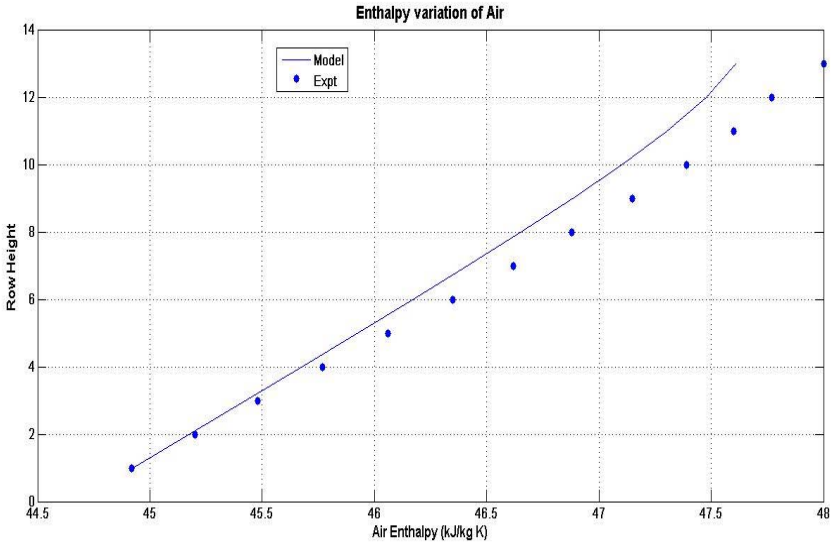

Figure 5.7: Variation of air enthalpy

This cooling tower model was selected for our study since it provides the operating values for a small sized cooling tower (9.25 kW / 2.6 tons). Most manufacturers of cooling towers do not have nominal and operating values for sizes less than 5 tons. In a residential application, typical cooling towers capacities are less than 5 tons.

Control Algorithm of Cooling Tower: The control of the cooling tower in a HGSHP is a very important aspect of the entire design. The times at which the cooling tower is started directly impacts the operation and efficiency of the heat pump. Various control strategies have been adopted depending on the ambient temperature conditions, heat pump operating limits (minimum and maximum entering water temperatures) and the operating cost of the cooling tower.

Xu adopted a strategy where the cooling tower was started when the difference between the heat pump exiting fluid temperature and the ambient wet bulb temperature was greater than 2℃ (3.6℉) [Xu, 2007]. Another control strategy used by Xu but based on a study by Yavuzturk and Spitler was to operate the cooling tower when the heat pump entering temperature was greater than 32.2℃ (90℉) [Yavuzturk & Spitler, 2000]. Hackel employed a much more detailed control strategy for the HGSHP system [Hackel, 2008]. His control strategy started the cooling tower when the difference between the temperature of the water entering the cooling tower and the ambient wet bulb temperature was greater than

- 27℉ (15℃) when ambient wet bulb temperature was greater than 70℉ (21.1℃)
- 23℉ (12.7 ℃) when ambient wet bulb temperature was between 70℉ (21.1℃) and 76℉ (24.4℃)
- 20℉ (11.1 ℃)when ambient wet bulb temperature was greater than 76℉ (24.4 ℃)

One of the reasons for selecting this algorithm is to ensure that the EWT to the heat pump never was above 95℉ (35℃), as mentioned by the heat pump manufacturer. This algorithm also resulted in the lowest 20 year life cycle cost of the HGSHP.

The control strategy employed in our analysis was a relatively simple one. The cooling tower was started whenever the water temperature entering the ground loop exceeded 35℃ (95℉) for all ambient air conditions. The reason for choosing this algorithm for all ambient conditions was that the residential building under analysis had significant cooling loads even during winter, which lead to the rise in entering water temperatures.

5.1.2 Residential Application

The cooling tower model was applied to a 7kW tower, the smallest commercial compact cooling tower available currently, and coupled to the base case Integrated Building Load-GHP model of the 195m^2 residential home in Austin, TX. While this capacity is very large compared to the base case heat pump (14.7kW), the study attempts to illustrate the performance and costs of adding such an SHR device. The tower consisted of 12 rows of bank of tubes, each bank with 19 tubes and each tube with an outer diameter of 10mm. The width of the tower was 0.6m and

each tube was 1.2m long. The longitudinal and transverse spacing of the tubes were 20mm and 60mm, respectively. The nominal data for the cooling tower were: 0.23m^3/s air flow rate, 0.8kg/s cooling water flow rate, 1.37kg/s spray water flow rate. A simple control algorithm was implemented: start the cooling tower whenever the water leaving the heat pump exceeded 35℃ for all ambient air conditions.

Since the water entering the tube is divided into 19 tubes, the computation is done only for one tube in each row (hence, mass flow rate in each tube is the total mass flow rate divided by 19. Each row of tubes is taken as a control volume element and two iterative loops (h_{a2} and t_{s1}) are considered. The iterative procedure is as follows: 1) guess values for h_{a2} and t_{s1} in the top tube row of the tower, 2) satisfy mass and energy balances for each going down the cooling tower and at row 1, t_{s2} is finally evaluated, 3) for the given h_{a2}, vary t_{s1} in increments of 0.01°C until t_{s1} =t_{s2}, and 4) compute h_{a1} at the first row and check if it is equal to the known value specified in the problem. If not equal, iterate the value of h_{a2} in increments of 0.01. For every new h_{a2} , the t_{s1} iteration is started afresh.

With this data and the cooling tower model iterative solution, the rate of cooling for a given atmospheric condition is computed. Instead of using the full cooling tower model, a simplified performance map model was coupled to the GSHP model. The map was generated as follows: three parameters and their ranges – cooling tower EWT (32.2–48.9°C), ambient air temperature (4.44–48.9°C) and ambient relative humidity (20%-100%) – were inputs to the cooling tower model described above. Four (32.2°C, 37.8°C, 43.3°C and 48.9°C), nine (4.4°C, 10°C, 15.6°C, 21.1°C, 26.**7°C**, 32.2°C, 37.8°C, 43.3°C, 48.9°C) and nine (20%, 30%, 40%, 50%, 60%, 70%, 80%, 90%, 100%) distinct values were used for the cooling tower EWT, ambient air temperature and ambient relative humidity, respectively. For all possible combinations of the input parameters (324 = 4*9*9), the power rejected, outlet temperature and power consumed by the cooling tower were calculated. For example, if the outputs are needed for 40°C cooling tower EWT, 35°C ambient air temperature and 65% relative humidity (values falling between the distinct input values used in the performance map), the function *interp3* in MATLAB is used to determine the corresponding outputs.

GLHEPRO was used to re-size the borehole length and the cooling tower capacity based on the building loads and the ground and loop properties previously listed in Table 4.3 of Section 4.6.1 and Table 4.4 of Section 4.6.2, respectively, for the base case model used in Austin. The sizing algorithm assumes that the ground loop will satisfy the peak heating load (8.63kW) and the remaining loads, as needed, will be satisfied by the cooling tower. The GHLEPRO algorithm

yielded a borehole length of 26.5m for each of the four loops, compared to the 68.6m required in the GHP base case.

5.1.2.1 Simulation Results: Performance

The HGHP model simulated operation for a 10-year period and the resulting data was averaged for every hour. The figures below compare the performances of the GHP and HGHP models. The conditioned space set point was set to 25℃ with a 1℃ deadband. Figures 5.8 and 5.9 show the minimum, average, and maximum monthly average heat pump EWTs for the HGHP and GHP cases, respectively. For the HGHP case, the average and maximum EWTs during the summers are approximately 30°C and 33°C, respectively, and the average EWT remains relatively constant over the 10 year period. In contrast, for the GHP case, the average EWT increases from approximately 40°C in the first summer to 45°C in year 10.The significant reduction in the EWTs for the HGHP case clearly translates to increased operating efficiencies and lower electricity costs.

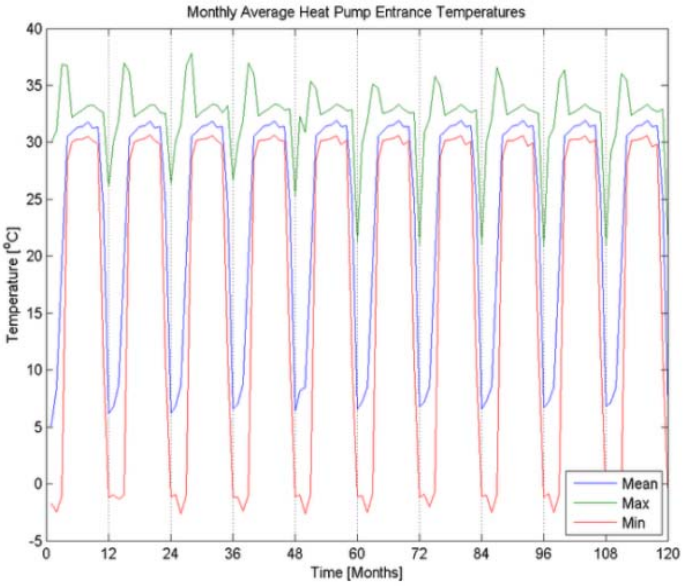

.

Figure 5.8: Monthly average heat pump EWT (°C): HGHP

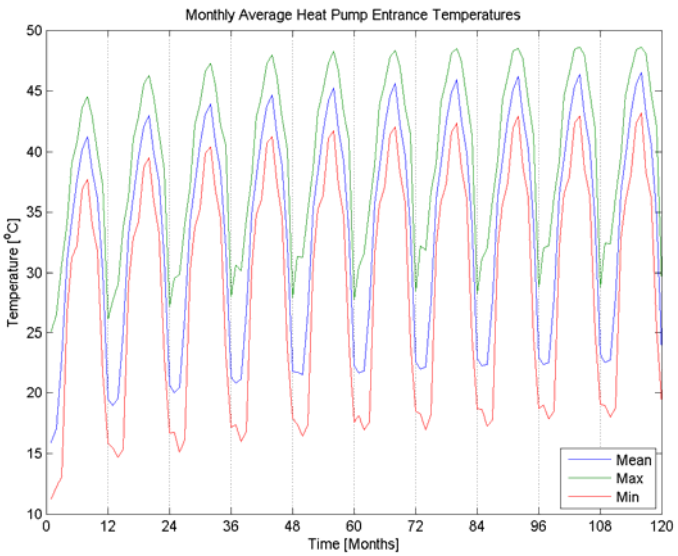

Figure 5.9: Monthly average heat pump EWT(°C): GHP

Figures 5.10 and 5.11 show the heat pump COP and EER (ratio of cooling provided to the power consumed with units Btu/Wh) over the 10 year period for the HGHP and GHP cases, respectively. For the HGHP case, the EER ranges from a high of 19.5 when the ambient temperature is low to about a nearly constant 11.5 during the summers. For the GHP case, the EER ranges from 16.0 to 8.0 in the first year and gradually decreases to 7.5 for the rest of the summers.

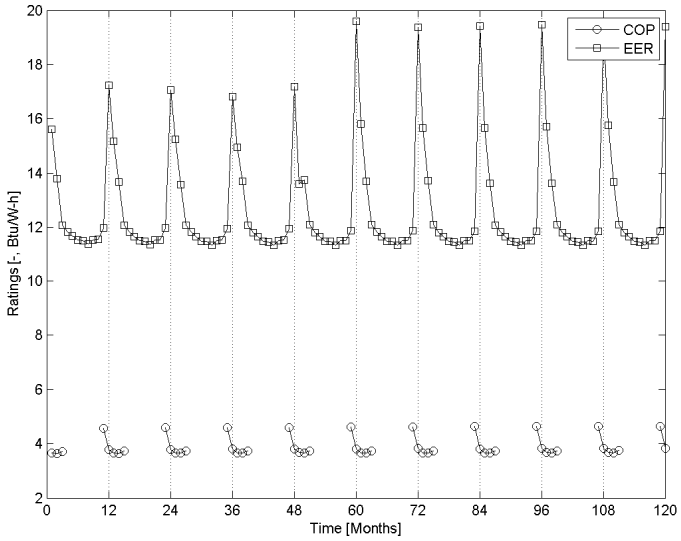

Figure 5.10: COP and EER of heat pump (Btu/Wh): HGHP

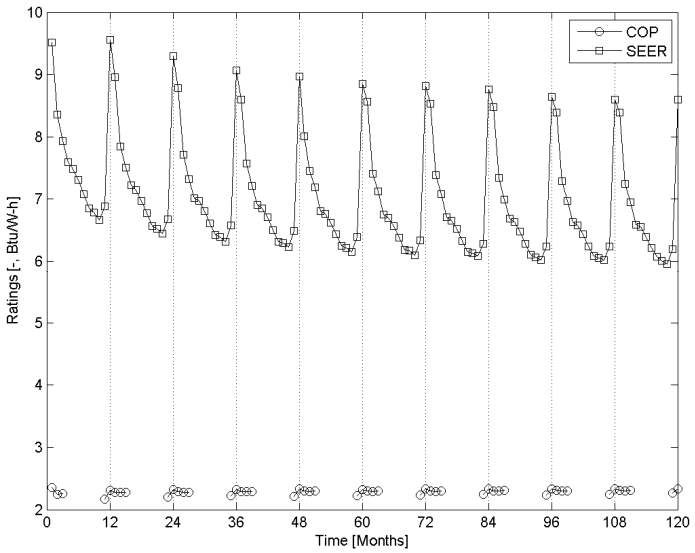

Figure 5.11: COP and EER of heat pump (Btu/Wh): GHP

Over the 10-year period, the average value of COP for the GHP case increases from an average of 4.5 to 5 due higher ground temperatures, compared to a near constant value of 4 for the HGHP case. The results of the 10-year simulations show the significant improvement in performance of the HGHP system over the GHP system due to the HGHP's ability to remove heat from the water before entering the ground loop thereby decreasing heat pump EWTs, which in turn, increases thermal efficiency.

The chosen control algorithm resulted in nearly 80% of the total heat rejected from the water (between heat pump outlet and inlet conditions) is in the cooling tower as shown in Table 5.1. Moreover, over the 10-year operating period, the cooling tower operated for a nearly constant 1,846 hours each year, while the heat pump operated in the cooling mode for a nearly constant 1,893 hours each year. The heat pump operated in the heating mode for a nearly constant 346 hours each year, and hence, it was in operation – both in cooling and heating modes – for an average of 2,239 hours each year.

Table 5.1: Energy Rejected by Cooling Tower and Ground Loop: HGHP

Year	Energy Rejected per year (kWh)		Total Energy Rejected per Year(kWh)
	Cooling Tower	Ground Loop	
1	23,099	5,609	28,708
2	23,236	5,478	28,714
3	23,294	5,414	28,708
4	23,329	5,381	28,709
5	23,359	5,372	28,731
6	23,379	5,353	28,732
7	23,366	5,346	28,712
8	23,383	5,339	28,722
9	23,398	5,326	28,724
10	23,403	5,326	28,729

5.1.2.2 Simulation Results: Economics

Adding the cooling tower lowers initial costs and adds less heat to the ground. An economic analysis was done over the 10 years for fixed and variable costs. Fixed costs include the costs of the heat pump and cooling tower, and drilling and installing the ground loop. The costs of installing the heat pump and cooling tower in the house are not included in the cost comparisons. The 14 kW heat pump cost will be the same in both the HGHP and GHP cases and are not included. Variable costs include the power needed to run the water loop pump, heat pump and the cooling tower and for the makeup water in the cooling tower.

Ground Loop and Cooling Tower

The lengths of each of the four boreholes for the GHP and HGHP cases were 68.6 m and 26.5 m, respectively. The cost of drilling and installing the ground loop in Austin was approximately $23/m [Hammond, 2011]. A 7 kW compact cooling tower for residential use from Allied Thermal Systems cost $800 ($400/3.5 kW) [Mac Word, 2011].

GHP Case

Based on the building loads computed for the base case 195 m^2 house shown in Table 4.3 of Section 4.6.1, for year 1 of operation, the heat pump ran for a total of 2022 and 284 hours in the cooling and heating modes, respectively. Over the 10-year period, it ran in the cooling and heating modes for 20,916 and 2,718 hours, respectively, and consumed 88,723 kWh and 9,493

kWh, respectively. Additionally, the water pump used to pump the water through the ground loop/heat pump consumed 1,340 kWh of energy over that period.

HGHP Case

For the HGHP case, for year 1 of operation, the heat pump ran for a total of 1891 and 383 hours in the cooling and heating modes, respectively. Over the 10-year period, it ran in the cooling and heating modes for 18,928 and 3,464 hours, respectively, and consumed 65,906kWh and 11,957kWh, respectively. Additionally, the water pumped used to pump water through the ground loop/heat pump/cooling tower consumed 928 kWh of energy was used to pump water through the cooling tower and the ground loop and 3,215kWh of energy was used to run the cooling tower fans.

Over the 10-year period cooling tower fan, rated at 0.23m^3/s (500cfm), 170W, ran for 18,458 hours over 10 years (1846/yr) was 3,215kWh. The cost analyses use an average electricity rate in Texas of $0.1082/kWh [US DoE, 2011b]. The total make-up water needed to operate the cooling tower was 71,700 gallons (tower recycles the water efficiently) and the price of water was taken from the 2011 City of Austin Water Rates [Austin, 2011]. Table 5.2 shows the 10-year cost comparison of using a GHP and a HGHP. Remember that the costs of the heat pump and installation of the heat pump and cooling towers in the house were not included.

Table 5.2: Cost Comparison of GHP and HGHP for 10 Years of Operation (excludes cost of 14kW heat pump and installation in house)

	GHP	HGHP
Fixed Cost	**$ 6,311**	**$ 3,238**
Borehole($23/m)	$ 6,311	$ 2.438
Cooling Tower ($400/ton)		$ 800
Variable Cost	**$ 10,772**	**$ 9,027**
Heat Pump ($0.1082/kWh)	$ 10,627	$ 8,425
Makeup Water	$ 0	$ 154
Fan ($0.1082/kWh)	$ 0	$ 348
Pumping ($0.1082/kWh)	$ 145	$ 100
Total Cost (10 years)	**$ 17,083**	**$ 12,265**

Based upon the items listed in Table 5.2, the 10 year HGHP system cost was $12,265, which was 28.2% lower than the $17,954 GHP system cost. The major cost reduction was the $3,873 difference in drilling costs for the two different borehole lengths (68.6 m versus 26.5 m/borehole). While the cooling tower added $800 in fixed and $502 in variable costs to the HGHP, the $3,873 in reduced fixed cost from the boreholes was more significant.

The 16.2% reduction ($1745) in the HGHP variable costs was due to the decrease in the running time of the heat pump ($2202 decrease). Note, the energy and make-up water consumed by the cooling tower added $502 to the operating costs ($348 for the fan operation and $154 for the make-up water). These cooling tower results are summarized in Balasubramanian, et al. [Balasubramanian, et al., 2012].

5.1.2.3 Simulation Results: Summary

The tower sizing algorithm assumes the ground loop satisfies the peak heating load and the remaining loads are achieved by the cooling tower, and the control algorithm turned on the tower when the water temperature exiting the heat pump (inlet to cooling tower) exceeded 35^{o}C. The sized cooling tower rejected approximately 80% of the total heat rejected from the water leaving the house. During 10 years of operation, the heat pump EWT remained relatively constant at around 30^{o}C during the summers and subsequently, its EER profile also remained constant with a value about 11.5 during the summers. The resulting lower ground temperatures increased the lifetime of the ground loop by eliminating ground coupling from the loops. In contrast, for the GSHP case, the temperatures of the water entering the ground loop and the heat pump increased, and its EER decreased over time to about 7.5 during the summers. The HGSHP's COP, however, remains constant at around 4, compared to an increase from 4.5 to 5 for the GSHP case due to higher ground temperatures.

The heat pump performance improved with a cooling tower, and the 10-year cost of operating a HGSHP was 28.2% lower than that of a GSHP case. This savings is mainly due to the reduction in drilling costs in a HGSHP, despite the additional costs associated with the cooling tower. While this 7kW-capacity cooling tower may be large for the associated 14kW heat pump, it was the smallest commercially available tower and the results show the quantitative performance of adding such an SHR device. It may be beneficial for manufacturers to develop smaller capacity cooling towers for residential applications in cooling-dominated climates.

5.2 OPTIMIZATION OF VAPOR COMPRESSION CYCLE

This section investigates the potential of rejecting heat from the refrigerant loop of the Vapor Compression Cycle (VCC) so less heat is transferred to the water loop at the condenser of the VCC. The VCC is made up of four stages: evaporation, compression, condensation and expansion, and its ideal p-h thermodynamic cycle is shown in Figure 5.12. In the cooling mode, the liquid refrigerant enters the evaporator at point 4. As it moves through the evaporator, at constant pressure P_e, the refrigerant removes heat from the conditioned space and its enthalpy increases. The refrigerant then enters the compressor suction at point 1 from where it is

compressed to high pressure and superheated vapor. The refrigerant at the compressor discharge is denoted at point 2, where it then enters the condenser. As it passes through the condenser, at constant pressure P_c, the refrigerant loses heat to either the air (air source heat pumps) or water (ground source heat pump) and becomes a subcooled liquid. This liquid refrigerant from the condenser at point 3 is then expanded through an expansion valve and the cycle repeats. This section focuses on the portion of the cycle that provides subcooling in the condenser and the superheat in the compressor suction and discharge (shown in Figure 5.12 as ΔT_{sub}, and $\Delta T_{sup,}$ respectively—note superheat at discharge not noted on figure).

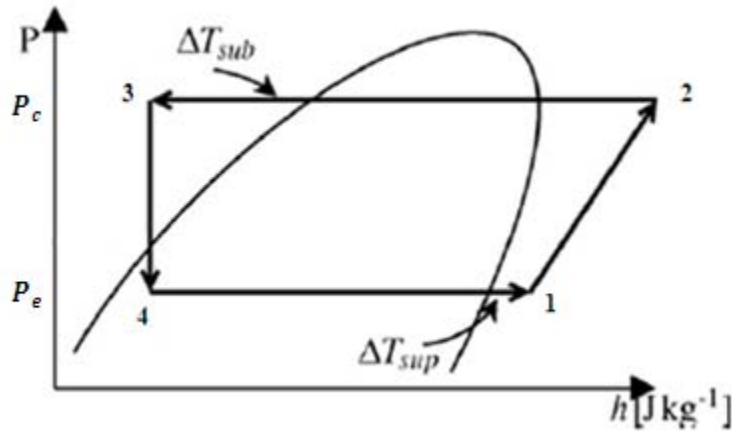

Figure 5.12: Ideal p-h diagram of Vapor Compression Cycle (VCC)

In the cooling mode, the VCC removes heat from the conditioned space at the evaporator to maintain a set point room temperature, and the heat pump water loop removes heat at the VCC condenser. On the ground loop side, the heat rejected to the condenser increases the water temperature entering the ground and subsequently increases the ground temperature. The evaporator and condenser heat loads are coupled. The condenser conditions of the VCC depend upon the ground loop water temperature entering the heat pump (EWT) and water flow rates. Figure 5.13 shows the range of VCC operating points for a heat pump EWT of 90^{o}F (32.2 ^{o}C) for ClimateMaster's Model TS048 heat pump. For a three gpm (0.187kg/s) water flow rate and 90^{o}F EWT, the data specifies a cooling load rating of 14.06kW (47.9kBtu/h) and condenser heat rejection of 16.14kW (55.1kBtu/h). Note that the heat rejected depends upon the thermodynamic operating points (suction/discharge pressures, superheat/subcoolng) shown in p-h diagram Figure 5.13.

Entering Water Temp °F	Water Flow GPM/ ton	Suction Pressure PSIG	Discharge Pressure PSIG	Superheat	Subcooling	Water Temp Rise °F	Air Temp Drop °F DB
90	1.5	138-148	396-416	7-12	7-12	19.2-21.2	18-24
	2.25	137-147	374-394	7-12	6-11	14.3-16.3	18-24
	3	136-146	352-372	7-12	4-9	9.3-11.3	18-24

Figure 5.13: Operating points of TS 048 heat pump [ClimateMaster, 2010]

The strategy 2 approach is posed as follows: can the VCC cycle's thermodynamic parameters be optimized to minimize the heat rejected to the condenser while satisfying the cooling load requirements, and thereby minimize the water loop temperature before it returns to the ground? In practice, the use of mechanical control valves and single- or two-speed compressors limit the system's ability to control the suction superheat, condenser subcooling and the mass flow rate of refrigerant. Electronic control valves and variable speed compressors can be used in to optimize the operation of a VCC. In the following sub-sections, different optimization schemes are summarized to determine the best possible operating conditions for a residential VCC. Detailed presentations and analyses of the following and other schemes can be found in [Balasubramanian, 2011].

5.2.1 Literature Review: VCC Optimization

In the following sub-sections, different optimization schemes are summarized to determine the best possible operating conditions for a residential VCC. Detailed presentations and analyses of the following and other schemes can be found in [Balasubramanian, 2011].

Minimum Power Consumption—*Larsen and Thybo*: In most analysis of VCCs, the objective is to minimize the power used by the compressor, but taking a broader picture, power is also consumed by the condenser fans, blower in the evaporator and other control valves. Larsen and Thybo minimized power consumption of an air-source heat pump from two devices, the compressor and the condenser fan, for a given cooling load [Larsen and Thybo, 2004]. The power consumed by the compressor and the condenser fan are inversely related. The objective was to reduce the total power consumption by varying the compressor discharge pressure for a given ambient temperature, evaporating temperature, suction superheat and condenser subcooling. This is a simple one degree of freedom problem, with compressor discharge pressure as the only variable.

Minimum Exergy—*Jain and Alleyne*: Jain and Alleyne developed a VCC optimization model to be used to improve performance of refrigeration systems used in trucks [Jain & Alleyne, 2011]. The model had five degrees of freedom or five parameters of the cycle: three enthalpies

$\{h_1, h_2, h_3 = h_4\}$, and either one of the three properties $\{P_1, P_3, T_1\}$, and refrigerant mass flow rate—see Figure 5.9. The four thermodynamic parameters are sufficient to describe the thermodynamic cycle. However, external conditions affect the conditions of the cycle; cooling load $\{\dot{Q}_L\}$, compressor work $\{W_s\}$ and the mass flow rate of refrigerant $\{\dot{m}\}$. The fifth parameter, the refrigerant mass flow rate is referred to as the dynamic variable. In other optimization models by Larsen the degrees of freedom considered were only thermodynamic conditions and not dynamic ones [Larsen & Thybo, 2004; Larsen et al., 2004]. Dynamic DOFs are chosen less often since they add requirements for hardware changes to the VCC cycle. If the mass flow rate is to be varied, the control valves must be changed from mechanical to electronic actuation.

The objective function used by Jain and Alleyne optimized two terms, performance and efficiency, in a weighted objective function. The performance term was the difference between the desired and actual cooling load. The efficiency term was exergy destruction. While energy is always conserved in a system, exergy is not. Exergy destruction provides a measure of how efficiently heat is transferred in both the evaporator and the condenser. Exergy destruction is small (entropy generated is low) when the temperature difference between the refrigerant and the ambient temperature is small.

Their optimization algorithm neglected some fundamental operating constraints and the optimization results showed two-phase conditions at the compressor suction and at the flow through the expansion valve. In practice there is superheat at the compressor suction to prevent floodback and there is subcooling at the expansion value to maintain stable operation.

Optimal Design versus Optimal Operation—*Jensen and Skogestad*: Jensen and Skogestad studied the optimization of an ammonia-based VCC for a storage building with an air source heat pump [Jensen and Skogestad, 2007]. In this study, the following five thermodynamic variables of the VCC were varied to minimize compressor work (see Figure 5.12 for ΔT_{sub} and ΔT_{sup}): Condenser pressure (P_c), evaporation pressure (P_e), condenser subcooling (SC)= ΔT_{sub}, suction superheat (SH)=ΔT_{sup}, and refrigeration mass flow rate (m). Three other parameters, areas of the evaporator A_{evap} and condenser A_{cond} and the pinch point of the heat exchangers, also affect the compressor work. The heat exchanger pinch point is the minimum temperature difference between the refrigerant exit temperature and the air inlet temperature, for an air-source heat pump, or the entering water temperature, for a ground-source heat pump. The study minimized compressor work but used the heat exchanger areas or pinch points as constraints in two different optimizations based on what they call, *Optimal Design* and *Optimal Operation*. In *Optimal Design*, the minimum pinch points (ΔT) of the heat exchangers are

specified and the heat exchanger areas are computed. This effectively means selecting the best heat exchanger for a specified pinch point. In *Optimal Ope*ration, the maximum heat exchanger areas are specified and the pinch points are computed. The *Optimal Operation* case is when heat exchangers have already been selected and one is trying to achieve the best performance out of the heat exchangers.

The objective function (performance index) used was:

Minimize Compressor Work

$$W_s = \dot{m}_r(h_2 - h_1) \tag{5.14}$$

The five thermodynamic variables to be optimized are subject to the following constraints:

Cooling Load: 20 kW

$$\dot{m}_r(h_1 - h_4) = 20\ kW \text{ (6.82 kBtu/h)} \tag{5.15}$$

Heat Balance at the Condenser

$$\dot{m}_r(h_3 - h_2) = UA_{condenser}(T_{rsat} - T_{air}) \tag{5.16}$$

where $UA_{condenser}$ is the heat transfer coefficient times the area of the condenser heat exchanger, $T_{rsat}$is the condensing temperature of the refrigerant and $T_{air}$is the temperature of air. This heat exchanger is an air-source heat exchanger.

Heat Balance at the Evaporator

$$\dot{m}_r(h_1 - h_4) = UA_{evaporator}(T_{revap} - T_{room}) \tag{5.17}$$

where UA_{evap} is the heat transfer coefficient times the area of the evaporative heat exchanger, $T_{revap}$is the evaporating temperature of the refrigerant and $T_{room}$is the temperature of the room.

0°C Minimum Superheat

$$T_1 > T_{1sat}$$

where $T_{1sat}$is the temperature of saturated vapor.

0°C Minimum Subcooling

$$T_3 < T_{3sat}$$

where $T_{3sat}$is the temperature of saturated liquid.

The optimization was performed for two cases: *Optimal Design* and *Optimal Operation*. The additional constraints for the heat exchanger parameters, areas and pinch point for each case are given below:

Optimal Design

Constraint on minimum pinch point

$$\Delta T > \Delta T_{min} \text{ (5ºC/9ºF)}$$

where $\Delta T = T_{r3} - EWT$

Optimal Operation

Constraint on the areas of the air source heat exchangers

$$A_{evap} \leq A_{evap\,max}$$

$$A_{cond} \leq A_{cond\,max}$$

The optimal areas obtained in the *Optimal Design* case are used as the maximum areas for the *Optimal Operation* constraint.

5.2.2 Implemented Model for VCC Optimization (UT Model)

The Jensen and Skogestad model described in Section 5.2.1 was implemented using the *fmincon* function in MATLAB [Jensen and Skogestad, 2007]. This implemented model shall be referred to as the UT Model. The five thermodynamic variables and the two heat exchanger areas were assigned initial values and then varied using the *fmincon* function of MATLAB. *fmincon* then computes the values for the five variables that minimized the compressor work.

Table 5.3 below shows the results of the UT Model in comparison with those of Jensen and Skogestad for the *Optimal Design* case; the agreement is very good. Recall for the *Optimal Design* case the minimum pinch points of 5°C (9°F) (heat exchangers were specified and the areas computed). The computed evaporator area agrees well with that of the paper, while the condenser area is 11.7% larger. The computed values for both the subcooling and superheat were 0°C, which is not common in real applications. From this case, we get the best design values of the heat exchanger areas for the given pinch point (5°C / 9°F). The minimum value for compressor work (W_s) is 4.516kW (15.4kBtu/h).

Table 5.3: Optimization Results: Optimal Design Case for 5℃ Pinch Point [Jensen & Skogestad, 2007]

	UT Model	Jensen and Skogestad
Ws (kW/kBtu)	4.516 / 15.41	4.648 / 15.86
Qc (kW/kBtu)	20 / 68.24	20 / 68.24
COP	4.43	4.30
m (kg/s) / (lb / min)	0.0181 / 2.394	0.0177 / 2.34
Superheat (℃)	0	0
Subcooling (℃)	0	0
P_evap (bar)	2.17	2.17
P_cond (bar)	11.67	11.63
Aevap (m^2) / (ft^2)	3.96 / 42.6	4 / 43
Acond (m^2) / (ft^2)	9.72 / 104.6	8.7 / 93.6

Table 5.4 compares the results of the UT and Jensen and Skogestad models for the *Optimal Operation* case that constrains the maximum size of the heat exchanger areas but allows the pinch points to vary. The maximum areas of the heat exchangers are taken from the computed areas from the *Optimal Design* results. Again, the models agree well. The minimum value for compressor work (W_s) for this case is 4.418 kW (15.1 kBtu/h).

Table 5.4: Optimization Results: Optimal Operation Case— $A_{evap} \leq A_{max}(3.96\ m^2)$ and $A_{cond} \leq A_{max}$(9.72 m^2) [Jensen & Skogestad, 2007]

	UT Model	Jensen and Skogestad
Ws (kW)/(kBtu)	4.4179 / 15.1	4.567 / 15.58
Qc (kW) /(kBtu)	20 / 68.24	20 / 68.24
COP	4.53	4.38
m (kg/s) / (lb / min)	0.0178 / 2.354	0.0173 / 2.288
Superheat (℃)	0	0
Sub-Cooling (℃) / (℉)	4.98 / 8.96	4.66 / 8.39
P_evap (bar)/(psi)	2.17	2.17
P_cond (bar)/(psi)	11.66	11.68
Aevap (m^2) / (ft^2)	4 / 43	4 / 43
Acond (m^2) / (ft^2)	9.72 / 104.6	8.7 / 93.6
Pinch Point (℃) / (℉)	0	0.49

5.2.2.1 Optimal Design versus Optimal Operation

Table 5.5 compares the results of the two optimization cases. Note that the compressor work of 4.42kW (15.1kBtu/h) in the *Optimal Operation* case is less than that of the *Optimal Design* case of 4.52kW (15.42 kBtu/h), which leads to a higher COP value of 4.53 compared to

the 4.43 value of the *Optimal Design* case. These comparisons show that it is better to constrain the heat exchanger area than to constrain the pinch point. When the pinch point is constrained (5°C/9°F in the *Optimal Design* case), the refrigerant can only be cooled to a temperature at least 5°C (9°F) greater than the ambient temperature. If the pinch point is not constrained (0°C pinch point), the refrigerant can be cooled to a temperature that is almost equal to the ambient temperature, which leads to significant subcooling that helps reduce the compressor work. In the former case, compressor work is higher due to the absence of subcooling.

Notice that in the *Optimal Design* case, both superheat and subcooling values are zero, compared to the *Optimal Operation* case, where superheat is zero but there is almost 5°C (9°F) (constraint) of subcooling. Also, the refrigerant mass flow rate in the *Optimal Operation* case of 0.0178kg/s (2.354 lb/min) is less than that of the *Optimal Design* case of 0.0181kg/s (2.394 lb/min). The reduction in compressor work of the *Optimal Operation* case is due to non-zero subcooling of the refrigerant entering the evaporator is at a lower enthalpy, and hence the refrigerant is capable of absorbing more heat from the room at a lower refrigerant mass flow rate. This leads to zero superheat needed to extract heat from the room. Zero superheat combined with a lower mass flow rate requires less power from the compressor to compress the refrigerant to the required discharge pressure. Notice that both evaporating (2.17 bar) and condensing (11.66 bar) pressures are identical for both cases.

Table 5.5: Comparison of Optimal Design (5C Pinch Point) and Optimal Operation Case — $A_{evap} \leq A_{max}(3.96\ m^2)$ and $A_{cond} \leq A_{max}(9.72\ m^2)$

	Optimal Design	Optimal Operation
Ws (kW)/(kBtu)	4.5162 / 15.41	4.4179 / 15.1
Qc (kW) /(kBtu)	20 / 68.24	20 / 68.24
COP	4.43	4.53
m (kg/s) / (lb / min)	0.0181 / 2.394	0.0178 / 2.354
Superheat (℃)	0	0
Sub-Cooling (℃) / (℉)	0	4.98 / 8.96
P_evap (bar)	2.17	2.17
P_cond (bar)	11.67	11.66
Aevap (m^2) / (ft^2)	3.96 / 42.6	4 / 43
Acond (m^2) / (ft^2)	9.72 / 104.6	9.72 / 104.6
Pinch Point (℃)/(℉)	5 / 9	0

5.2.2.2 Application to Residential Building: Air-Source Heat Pump

The UT Model, which was validated with Jensen and Skogestad's data, was applied to the 195m^2 (2100ft^2) residential building to minimize the compressor work of the VCC. It should be

emphasized that at this point, the UT model uses an air-source condenser, so the previous optimization results were for an air-source condenser. In that case the VCC operated between the room temperature of 20°C (68°F) and ambient temperature of 30°C (86°F). The refrigerant used for the residential study was R 410A and the cooling load was 14.7 kW (4 tons). Compression efficiency was taken as 65% (Copeland Compressors [Copeland, 2011]). The model of the compressor used was Copeland Scroll ZPS40K5E-PFV.

Recall that the Jensen and Stogestad study had only constraints of 0°C minimum superheat and subcooling. The base case residential study applies constraints used by heat pump manufacturers. Engineers from ClimateMaster suggest a suction superheat of 4.44-11.11°C (8-20°F) [Brower, 2011] to prevent compressor floodback, a condition where liquid refrigerant from the evaporator enters the compressor which will damage the compressor. The range of values for subcooling is 1.11-3.33°C (2–6°F). A minimum value for the subcooling of 1.11°C is specified to prevent two-phase refrigerant from being expanded in the expansion valve which would cause valve instability. Hence, the problem can be described as follows:

The objective function (performance index) used was:

Minimize Compressor Work

$$W_s = \dot{m}_r(h_2 - h_1) \tag{5.18}$$

The five variables, condenser pressure (P_c), evaporation pressure (P_e), condenser subcooling (SC)= ΔT_{sub}, suction superheat (SH)=ΔT_{sup}, and refrigeration mass flow rate (m) were subjected to the following constraints:

Cooling Load: 14 kW

$$\dot{m}_r(h_1 - h_4) = 14\,kW \text{(47.7 kBtu/h)} \tag{5.19}$$

Heat Balance at the Condenser

$$\dot{m}_r(h_3 - h_2) = UA_{condenser}(T_{rsat} - T_{air}) \tag{5.20}$$

where, $UA_{condenser} = 500\ W/K$

Heat Balance at the Evaporator

$$\dot{m}_r(h_1 - h_4) = UA_{evaporator}(T_{revap} - T_{room}) \tag{5.21}$$

where, $UA_{evap} = 1000\ W/K$

Suction Superheat

$$4.44^{o}\text{C } (8^{o}\text{F}) < T_1 - T_{1sat} < 11.11^{o}\text{C } (18^{o}\text{F}) \tag{5.22}$$

where, $T_{1sat}$is the temperature of saturated vapor.

Condenser Subcooling

$$1.11^{o}\text{C } (2^{o}\text{F}) < T_3 < T_{3sat} < 3.33^{o}\text{C } (6^{o}\text{F}) \tag{5.23}$$

where $T_{3sat}$is the temperature of saturated liquid.

The optimization was performed for same two cases as described by Jensen and Skogestad. The additional constraints for the heat exchanger parameters, areas and pinch point, for the two cases are given below:

Optimal Design

Constraint on minimum pinch point

$$\Delta T > \Delta T_{min} \text{ (5°C/9°F)} \quad (5.24)$$

where $\Delta T = T_{r3} - EWT$

Optimal Operation

Constraint on the areas of the air source heat exchangers

$$A_{evap} \leq A_{evap\,max} \quad (5.25)$$

$$A_{cond} \leq A_{cond\,max}$$

As described before, the *Optimal Design* solution yields values for the heat exchanger areas, which are then used as the maximum area values in the *Optimal Operation* constraint. The values obtained for the heat exchanger areas in the *Optimal Design* case were:

$$A_{evap} = 2.78\ m^2\ (29.9\ ft^2)$$

$$A_{cond} = 6.38\ m^2 (68.6\ ft^2)$$

The results for the *Optimal Design* case are shown in Table 5.6. It is interesting to note that the optimal values obtained for both suction superheat and condenser subcooling are the lowest in their respective ranges (4.44°C/8°F) for suction superheat and 1.11°C/2°F for condenser subcooling).

Table 5.6: Output for Residential House for *Optimal Design* Case

Ws (kW) / (kBtu/h)	2.56 / 8.73
COP	5.47
Superheat (kW) / (kBtu/h)	2.77 / 9.45
Superheat as % of load	19.78
P_{cond} (kPa)/(psi)	2191.7 / 317.7
P_{evap} (kPa)/ (psi)	1100.0 / 159.5
SH (℃) / (℉)	4.44 / 8
SC (℃) / (℉)	1.11 / 2
m (kg/s) / (lb/min)	0.0807 / 10.67
A_{evap} (m^2) / (ft^2)	2.78 / 29.9
A_{cond} (m^2) / (ft^2)	6.38 / 68.6
T_1 (℃) /(℉)	15 / 59
T_3 (℃) / (℉)	35 / 95

The results of the *Optimal Operation* case are shown below in Table 5.7.

Table 5.7: Output for Residential House for *Optimal Operation* Case

Ws (kW) / (kBtu/h)	2.38 / 8.12
COP	5.89
Superheat (kW) / (kBtu/h)	2.58 / 8.8
Superheat as % of load	18.43
P_{cond} (kPa)/(psi)	2135.9 / 308.9
P_{evap} (kPa)/ (psi)	1100.5 / 159.5
SH (℃) / (℉)	4.44 / 8
SC (℃) / (℉)	3.33 / 6
m (kg/s) / (lb/min)	0.0781 / 10.31
A_{evap} (m^2) / (ft^2)	2.78 / 29.9
A_{cond} (m^2) / (ft^2)	6.38 / 68.6
T_1 (℃) /(℉)	15.05 / 59.09
T_3 (℃) / (℉)	31.74 / 89.1

The most interesting result is that the computed suction superheat is the lowest value of its constrained range, and the computed subcooling is the highest value of its constrained range. These results are logical and can be explained as follows; with a high value of subcooling, the entering enthalpy of the refrigerant to the evaporator is lower which enables the refrigerant to absorb more heat with a smaller mass flow rate. Hence, a lower superheat is needed to provide cooling. This combination of low superheat, reduced mass flow, and maximum subcooling decreases compressor work and hence increases COP. The temperature at the exit of the condenser is 31.74^{o}C (89.1^{o}F), which gives a pinch point of 1.74^{o}C (3.13^{o}F). This is lower than the 5^{o}C (9^{o}F) that was assumed for the *Optimal Design* case, and hence leads to a lower compressor work.

Table 5.8 shows the compressor work, COP and superheat (kW) at the compressor discharge for different values of compressor suction superheat (^{o}C) for a 65% compressor efficiency and 3.33^{o}C (6^{o}F) subcooling. The data shows that as the suction superheat increases: 1) compressor work increases and hence the COP decreases, and 2) superheat (kW) at the compressor discharge, which ultimately has to be rejected into the condenser, increases. From these results, one can infer that to reduce the heat rejected to the condenser, the superheat at the compressor must be reduced by either decreasing the suction superheat or increasing compressor efficiency. In general, the model shows that a 1^{o}C (1.8^{o}F) decrease in suction superheat decreases heat rejected into the condenser by 0.11kW (0.375kBtu/h) . By reducing the suction superheat from 4.4^{o}C to 0^{o}C (8–0^{o}F), the heat rejected into the condenser is

reduced by 20.1%. However, as mentioned previously, current industry guidelines recommend a minimum 4.44°C (8°F) of suction superheat to prevent floodback. Zero suction superheat could be accomplished with the addition of a flooded evaporator, which is commonly used in Europe, but very rarely used in the United States.

Table 5.8: Variations of Compressor Work and Compressor Discharge Superheat with Suction Superheat (°C)

	Suction Superheat (°C)				
	0	**4.44**	**6**	**8**	**10**
Ws (kW) / (kBtu/h)	1.90/ 6.48	2.38/ 8.12	2.54/ 8.66	2.76/ 9.42	3.00/ 10.23
COP	7.39	5.89	5.5	5.08	4.67
Heat rejected in Condenser (kW) / (kBtu/h)	15.9/ 54.3	16.38/ 55.9	16.54/ 56.4	16.76/ 57.2	17/ 58
Compressor Discharge Superheat (kW) / (kBtu/h)	1.78/ 6.1	2.58/ 8.8	2.85/ 9.7	3.18/ 10.8	3.54/ 12.1
Compressor Discharge Superheat as % of Load	12.74	18.43	20.35	22.73	25.28
P_{evap} **(kPa) / (psi)**	1253/ 18.2	1102/ 16	1051/ 15.2	991/ 14.3	933/ 13.5
P_{cond} **(kPa) / (psi)**	2128/ 30.7	2136/ 30.98	2138/ 31	2142/ 31.1	2146/ 31.12
$\dot{m}$ **(kg/s) (lb/min)**	0.0798/ 10.6	0.0781/ 10.3	0.0775/ 10.25	0.0769/ 10.17	0.0763/ 10.1

Table 5.8 also shows the optimized thermodynamic properties of the VCC. It can be observed that the evaporating pressure of the refrigerant decreases while the condensing pressure increases with an increase in the suction superheat value. The refrigerant mass flow rate decreases as the suction superheat value increases. These results make sense since for a given cooling load the enthalpy reduction due to decreased mass flow rate is compensated for by the enthalpy increase due to increased suction superheat. Although the mass flow rate decreases with an increase in suction superheat, the compressor work increases due to the higher range of pressures through which the refrigerant must be compressed.

A flooded evaporator, shown in Figure 5.14, is a device designed like an accumulator to ensure that the refrigerant from the evaporator discharges at saturated vapor condition. Liquid refrigerant enters the flooded evaporator where it takes heat from the conditioned space (cooling mode) and changes into a two phase fluid. Once it exits the flooded evaporator, it enters a surge tank where the vapor rises to the top and the liquid accumulates at the bottom. The liquid level in the surge tank is controlled by a valve that adds liquid refrigerant to the tank.

From the surge tank, saturated vapor enters the compressor. Flooded evaporators are used for large industrial chilling stations.

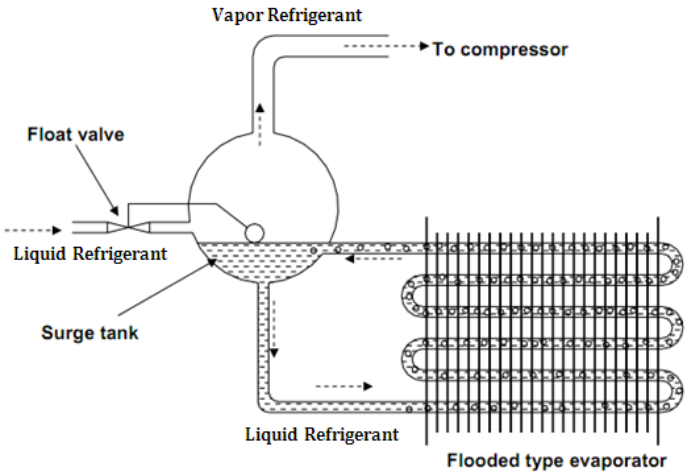

Figure 5.14: Flooded evaporator [IIT Madras, 2011]

Table 5.9 shows the results for the case where the suction superheat is fixed at 4.44°C (8°F) (the minimum) and compressor efficiency is varied from 50% to 70%. As expected, the compressor exit superheat increases as the compressor efficiency decreases in a nonlinear fashion; as compressor efficiency decreases, the superheat increases at a much higher rate, and consequently more heat must be rejected by the condenser. This analysis shows compressor efficiency and suction superheat and subcooling values are important variables in the VCC cycle.

Table 5.9: Variations of Compressor Work and Compressor Exit Superheat with Compressor Efficiency at 4.44°C Suction Superheat

Variable	Compressor Efficiency (%)				
	70%	**65%**	**60%**	**55%**	**50%**
Ws (kW) / (kBtu/h)	2.20/ 7.5	2.38/ 8.1	2.58/ 8.8	2.83/ 9.7	3.12/ 10.6
COP	6.36	5.89	5.42	4.95	4.48
Heat rejected in Condenser (kW) / (kBtu/h)	16.2/ 55.3	16.38/ 55.9	16.58/ 56.6	16.83/ 57.4	17.12/ 58.4
Compressor Exit Superheat (kW) / (kBtu/h)	2.40/ 8.2	2.58/ 8.8	2.79/ 9.5	3.03/ 10.3	3.33/ 11.4
Superheat as % of load	17.17	18.43	19.91	21.66	23.78

Table 5.10 shows the comparison between two cases of suction superheat; the ideal case (0°C) and the practical minimum case (4.44°C/ 8°F). The comparison is also shown for two values of compressor efficiency; 70% and 60%. It can be seen that for compressor efficiency of

70% and with no suction superheat, the compressor work is 20% lower (1.76kW/ 6kBtu/h compared to 2.2kW / 7.5kBtu/h) than the case with a 4.44°C/ 8°F suction superheat. With 60% efficiency, compressor work decreases by 20.1% for the no suction superheat case.

This reduction in compressor work is reflected in the heat rejected into the condenser. Using a compressor with a 70% efficiency rating, the heat rejected into the condenser is lower by 0.44kW (1.5kBtu/h) when there is no suction superheat, compared to a 4.44°C (8°F) suction superheat. This reduction is 0.52kW (1.77kBtu/h) for the compressor with 60% efficiency. It can be inferred that for a low efficiency compressor, it makes sense to have as low a suction superheat as possible to reduce condenser heat rejection.

Table 5.10: Variations of Compressor Work and Compressor Exit Superheat with Compressor Efficiency at 4.44°C Suction Superheat

Variable	Compressor Efficiency (%)			
	70%		60%	
Suction Superheat (℃)/(℉)	**0/0**	**4.44/8**	**0/0**	**4.44/8**
Ws (kW) / (kBtu/h)	1.76	2.20	2.06	2.58
COP	7.97	6.36	6.80	5.42
Heat rejected in Condenser (kW) / (kBtu/h)	15.76/ 53.8	16.2/ 55.2	16.06/ 54.8	16.58/ 56.6
Compressor Exit Superheat (kW) / (kBtu/h)	1.64/ 5.6	2.40/ 8.2	1.95/ 6.7	2.79/ 9.6
Superheat as % of load	11.75	17.17	13.91	19.91

5.2.2.3 Application to Base Case Residential Building: Ground Source Heat Pump

All the discussion and results provided in Section 5.2.2 are for air-source condensers, whose heat transfer given by:

$$Q_{cond}(Air\ Source\ Heat\ Pump) = UA_{ASHP}(T_{refcond} - T_{air}) \quad (5.26)$$

where UA_{ASHP} is the heat transfer coefficient for the condenser heat exchanger, $T_{refcond}$ is the condensing temperature of the refrigerant and T_{air} is the air temperature blowing across the heat exchanger. Note that there is only one, typically known, heat transfer coefficient. The water-source condenser will have three unknown coefficients.

A brief description of the parameters and the model are summarized below:

- Cooling load = 14kW (4tons)
- Flow rate of water in ground loop = .748kg/s (12gpm)
- Heat pump EWT= 21.1, 32.2, 43.3°C (70°F, 90°F, 110°F)—See Table 5.12
- Condition Space Room Temp = 21°C

- Compressor - Copeland Scroll ZPS40K5E-PFV

Performance Index

$$\text{Min } W_s = \dot{m}_r(h_2 - h_1) \tag{5.27}$$

Constraints

Pinch Point

$$T_3 - EWT > 5^{\circ}C \text{ (9°F)} \tag{5.28}$$

This constraint ensures that the refrigerant exit temperature is greater than the EWT by at least 5°C pinch point (see Appendix F).

Evaporator Exit Temperature

$$T_1 < 21^{\circ}C \text{ (Room Temperature)} \tag{5.29}$$

Heat Balance in the Evaporator

$$\dot{m}_r(h_1 - h_4) = UA_{evap}(T_{room} - T_1) \tag{5.30}$$

where UA_{evap} is the heat transfer coefficient times the area of the evaporative heat exchanger, $T_1$is temperature of the refrigerant at the evaporator exit and T_{room} is the temperature of the room.

Heat Balance in the Condenser

$$\dot{m}_r(h_2 - h_3) = UA_{SH}(\overline{T_{r\,SH}} - \overline{T_{w\,SH}}) + UA_{SAT}(\overline{T_{r\,SAT}} - \overline{T_{w\,SAT}}) + UA_{SC}(\overline{T_{r\,SC}} - \overline{T_{w\,SC}}) \tag{5.31}$$

where, in the superheated, saturated and subcooled regions of the condenser, UA_{SH}, UA_{SAT}, UA_{SC} are the values of heat transfer coefficient times the area; $\overline{T_{r\,SH}}$, $\overline{T_{r\,SAT}}$ and $\overline{T_{r\,SC}}$ are the average refrigerant temperatures; and $\overline{T_{w\,SH}}$, $\overline{T_{w\,SAT}}$ and $\overline{T_{w\,SC}}$ are the average water temperatures, respectively. Note that an air-source condenser has only one, typically known. heat transfer coefficient for air flow over the heat exchanger, whereas as water-source condenser has three unknown coefficients, one each to represent one of the three phases of water.

Table 5.11: Suction Superheat and Condenser Subcooling for Different EWT Ranges

EWT (°C/°F)	Superheat (°C/°F)	Subcooling (°C/°F)
21.1/70	5–7.7/9-14	2.8–5.5/5-10
32.2/90	3.9–6.7/7-12	2.2–5/4-9
43.3/110	3.9–6.7/7-12	1.7–4.4/3-8

A concentric tube counter-flow heat exchanger between the refrigerant and the water is assumed. Since manufacturers do not publish details of the heat exchanger design, performance data from heat pump performance maps are used to determine the UA (heat

transfer coefficient * Area) values of the heat exchanger at different operating conditions. Table 5.11 and 5.12 give the suction superheat and condenser subcooling ranges and performance rating of Climate Master's TT 049 model heat pump: cooling load, compressor work and the heat rejected in the condenser for three different values of entering water temperature (EWT). Figure 5.15 shows the VCC operating points for five different EWTs. It specifies the range of compressor suction and discharge pressures, suction superheat, and condenser subcooling.

Table 5.12: Rating of TT 049 Heat Pump [ClimateMaster, 2010]

EWT (^oC)/(^oF)	Cooling Load (kW)/(kBtu/h)	Compressor Work (kW)/(kBtu/h)	Heat Rejected (kW)/ (kBtu/h)	Compressor Efficiency (%)
21.1/70	15.75/53.7	2.81/9.6	18.56/63.3	64
32.2/90	14.06/47.9	3.32/11.3	17.10/58.3	71.8
43.3/110	12.13/41.4	4.00/13.6	16.14/55.1	69.2

TT049		Full Load Cooling - without HWG active					
Entering Water Temp °F	Water Flow GPM/ ton	Suction Pressure PSIG	Discharge Pressure PSIG	Superheat	Subcooling	Water Temp Rise °F	Air Temp Drop °F DB
30*	1.5 2.25 3	112-122 111-121 111-121	187-207 167-187 147-167	22-27 22-27 23-28	14-19 12-17 11-16	20.7-22.7 15.5-17.5 10.2-12.2	18-24 18-24 18-24
50	1.5 2.25 3	125-135 123-133 122-132	242-262 224-244 205-225	13-18 13-18 14-19	10-15 9-14 7-12	20.9-22.9 15.6-17.6 10.2-12.2	19-25 19-25 19-25
70	1.5 2.25 3	133-143 132-142 131-141	310-330 290-310 270-290	8-13 8-13 9-14	8-13 7-12 5-10	20.5-22.5 15.2-17.2 9.9-11.9	19-25 19-25 19-25
90	1.5 2.25 3	138-148 137-147 136-146	396-416 374-394 352-372	7-12 7-12 7-12	7-12 6-11 4-9	19.2-21.2 14.3-16.3 9.3-11.3	18-24 18-24 18-24
110	1.5 2.25 3	144-154 143-153 142-152	497-517 472-492 447-467	7-12 7-12 7-12	5-10 4-9 3-8	18-20 13.3-15.3 8.5-10.5	17-23 17-23 17-23

Figure 5.15: Performance Map – Climate Master TT 049 Heat Pump [ClimateMaster, 2010]

The only difference between the method used for water-source heat pumps and air-source heat pumps is the determination of the UA values, and the following procedure is followed. For three EWTs (70, 90 and 110^{o}F), the average operating points (suction and discharge pressures, suction superheat and condenser subcooling) are taken from the performance map (Figure 5.15). The condenser is divided into three sections as shown in Figure 5.16—superheated, saturated and subcooled—because the refrigerant temperature profile changes across the condenser; decreases across the superheated section, constant through the saturated region and again decreases through the subcooling section. This nonlinear change in refrigerant temperature and associated phase change across the condenser makes the computation of the

refrigerant and water conditions more accurate by dividing the condenser into three sections. The water temperature is approximated to increase linearly across the condenser. The refrigerant temperatures at the inlet and exit of each section are computed using the average operating points from Figure 5.16. The computation algorithm is as follows.

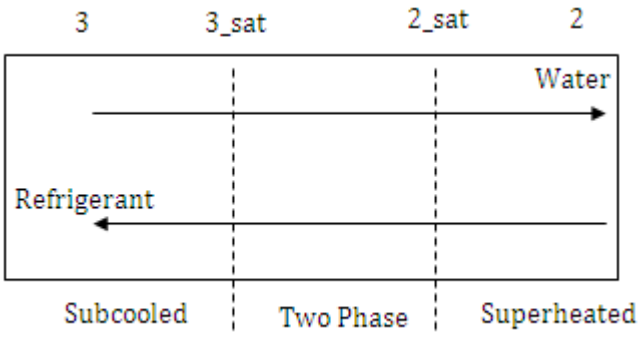

Figure 5.16: Schematic of water-source condenser heat exchanger

1) The refrigerant temperatures are computed by the optimization model
2) Heat rejected in each section is calculated then used to calculate the water temperature at the exit of each section(T_{3sat}, T_{2sat}, T_2).
3) Average temperatures of the refrigerant and water in each section are computed.
4) Average UA values in each section are calculated using the following expressions:

$$UA_{SC} = \frac{Q_{SC}}{(\overline{T_{rSC}} - \overline{T_{wSC}})} \tag{5.32}$$

$$UA_{SAT} = \frac{Q_{SC}}{(\overline{T_{rSAT}} - \overline{T_{wSAT}})} \tag{5.33}$$

$$UA_{SH} = \frac{Q_{SC}}{(\overline{T_{rSH}} - \overline{T_{wSH}})} \tag{5.34}$$

The computed UA values in each section are shown in Table 5.13.

Table 5.13: UA Values of the Water-Source Condenser (W/K)

EWT (^{o}C) /(^{o}F)	Subcooled (W/K)	Saturated (W/K)	Superheated (W/K)
21.1/70	87	2,217	168
32.2/90	77	1,904	183
43.3/110	84	1,794	210

5) The UA values are now used to solve the optimization problem.

Base Case Residential Building: Ground Source Heat Pump Results and Conclusions: The results of the optimization for the three heat pump EWTs are shown in Table 5.14. It shows the minimum compressor work attained for each EWT. For each case the suction superheat, condenser subcooling and the mass flow rate of refrigerant is also shown. In all cases, the minimum possible superheat from the specified range gives the minimum compressor work. Likewise, the subcooling values are the maximum possible in the specified range. This again confirms the previous inference that the maximum possible subcooling and minimum possible suction superheat values yield the lowest compressor work, and hence lowest heat rejection into the condenser.

Table 5.14: Optimization results for Water Source Condenser

EWT (°C)/ (°F)	Cooling Load (kW)/ (kBtu/h)	Ws (kW)/ (kBtu/h)	COP	Heat Rejected (kW)/ (kBtu/h)	SH (℃)/(F)	SC (℃)/(F)	m (kg/s)/ (lb/min)
21.1/70	15.65/53.4	2.89/9.9	5.46	18.64/63.6	5.00/9	5.55/10	0.0806/10.67
32.2/90	13.96/47.6	3.15/10.7	4.44	17.21/58.7	3.88/7	4.22/7.6	0.08/10.58
43.3/110	11.13/38	3.53/12	3.15	15.66/53.4	3.88/7	4.44/8	0.0728/9.62

Table 5.15 shows the comparison of compressor work, COP and heat rejected between the optimization results of the UT Model and ClimateMaster's performance data. It can be seen that for the 21.1°C EWT case, the UT Model is less effective than the ClimateMaster data. The UT model gives a compressor work that is 3.2% lower, a COP that is 2.5% lower and heat rejection that is 0.64% higher. The UT model gives more efficient results for the 32.2 and 43.3°C EWT cases. The compressor work for the 32.2°C EWT case is 5.1% lower, the heat rejected into the condenser is 1% lower, and the COP is 4.7% higher compared to the ClimateMaster data. The performance of VCC for the 43.3°C EWT case is significantly better than that of the 32.2°C EWT case. For the 43.3°C case, the compressor work is lower by 11.8%, the heat rejected is 2.9% lower, and the COP is 4% higher than the ClimateMaster data.

Table 5.15: Comparison between UT Model and Climate Master [ClimateMaster, 2010]

	Ws (kW) / (kBtu/h)		COP		Heat Rejected (kW) / (kBtu/h)	
EWT (°C/°F)	Model	Climate Master	Model	Climate Master	Model	Climate Master
21.1/70	2.88/9.8	2.81/9.6	5.46	5.60	18.64/63.6	18.56/63.3
32.2/90	3.15/10.7	3.32/11.3	4.44	4.24	17.21/58.7	17.38/59.3
43.3/110	3.53/12.0	4.00/13.6	3.15	3.03	15.66/53.4	16.13/55.0

This optimization shows that with optimal control of the suction superheat and condenser subcooling, the heat rejected into the condenser can be lowered by as much as 0.46kW. This heat rejected is lower than the non-optimized case by 2.9%. This 0.46kW reduction in heat rejected to the condenser is equivalent to a reduction in the exit water temperature in the ground loop by a virtually insignificant 0.15℃.

5.3 DESUPERHEATERS

Desuperheaters are devices that use the superheat of the refrigerant at the compressor discharge of the VCC to heat domestic water. During the cooling mode of operation, the heat extracted by the desuperheater is a form of supplemental heat recovery since that amount of heat would otherwise be rejected into the condenser. Desuperheaters typically capture 10 – 25 % of the total heat rejected into the condenser [Lee and Jones, 1997]. During the heating mode of operation, the heat captured for hot water heating would otherwise be used to heat the house, so the heat pump must run for a longer period to heat the house. For cooling-dominated climates, the desuperheater reduces the heat rejected into the water loop condenser, and hence decreases the amount of heat rejected to the ground. In this section, an expanded desuperheater is proposed as a SHR device to extract as much heat as possible, thereby reducing the heat rejected to the ground.

5.3.1 Cooling Mode

Figure 5.17 shows the ideal thermodynamic P-h diagram of the heat pump VCC cycle in the cooling mode with 32.2^{o}C (90^{o}F) EWT: G-B is the heat input from the building to be cooled, B-C is the compressor work and reflects its efficiency, C-F is the heat rejected in the condenser, and F-G is the expansion through the expansion valve. C-D is the region where the refrigerant is in a superheated state and where heat transfer into the desuperheater takes place in a concentric tube heat exchanger.

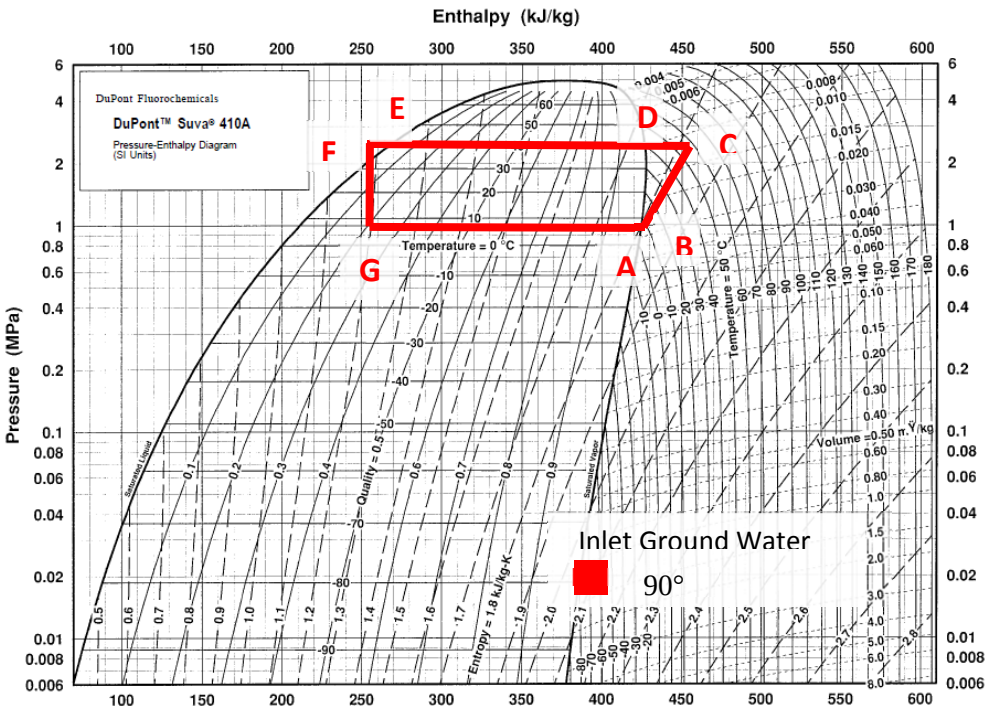

Figure 5.17: Thermodynamic cycle of heat pump in cooling mode

Table 5.16 shows the thermodynamic properties at different points in the VCC in the cooling mode for different heat pump EWTs. For the case of 32.2°C (90°F) EWT, refrigerant 410A and data from a Water Furnace Heat Pump, the average enthalpies at C and D are 455.1kJ/kgK and 427.1kJ/kgK, respectively. For a refrigerant flow rate of 0.078kg/s (10.32lb/min), the total superheat available is 2.18kW (7.44kBtu/h). This amount of superheat represents 15.9% of the cooling load. Table 5.27 shows the thermodynamic states for 21.1°C (70°F), 32.2°C (90°F) and 43.3°C (110°F) EWTS. Table 5.17 shows the superheat C-D as a percentage of cooling load, suction superheat A-B and condenser subcooling E-F for each EWT. The average suction superheat is 6.7kJ/kg, average condenser subcooling is 9.97kJ/kg and the average compressor exit superheat is 17.4% of the cooling load.

Table 5.26: Thermodynamic Values at Different Point of the VCC in Cooling Mode for Different Heat Pump EWTs

21.1°C (70°F) EWT	Pt. A	Pt. B	Pt. C	Pt. D	Pt. E	Pt. F	Pt. G
Pressure (MPa)	0.962	0.962	1.827	1.827	1.8314	1.8314	0.965
Temperature (°C)	6.1	11.9	44.2	28.9	28.9	23.9	6.1
Enthalpy (kJ/kg)	424.2	430.9	448.7	427.5	247.1	238.5	238.5
Pressure (psi)	139.5	139.5	265.0	265.0	265.6	265.6	140.0
Temperature (°F)	43.0	53.4	111.5	84.0	84.0	75.0	43.0
Enthalpy (kBtu/lb)	0.182	0.185	0.193	0.184	0.106	0.103	0.103

32.2°C (90°F) EWT	Pt. A	Pt. B	Pt. C	Pt. D	Pt. E	Pt. F	Pt. G
Pressure (MPa)	0.9894	0.9894	2.344	2.344	2.3507	2.3507	0.9915
Temperature (°C)	7	12.8	57.3	38.8	38.8	38.8	7
Enthalpy (kJ/kg)	424.4	431.1	455.1	427.1	264.9	254.9	254.9
Pressure (psi)	143.5	143.5	340.0	340.0	340.9	340.9	143.8
Temperature (°F)	44.6	55.0	135.1	101.8	101.8	101.8	44.6
Enthalpy (kBtu/lb)	0.182	0.185	0.196	0.184	0.114	0.110	0.110
43.3°C (110°F) EWT	**Pt. A**	**Pt. B**	**Pt. C**	**Pt. D**	**Pt. E**	**Pt. F**	**Pt. G**
Pressure (MPa)	0.9894	0.9894	3.102	3.102	3.1107	3.1107	0.9915
Temperature (°C)	7	12.8	73.4	50.7	50.7	45.2	7
Enthalpy (kJ/kg)	424.4	431.1	463.2	424.3	288.4	277.1	277.1
Pressure (psi)	143.5	143.5	449.9	449.9	451.1	451.1	143.8
Temperature (°F)	44.6	55.0	164.1	123.3	123.3	113.4	44.6
Enthalpy (kBtu/lb)	0.182	0.185	0.199	0.182	0.124	0.119	0.119

Table 5.17: Superheat as Percentage of Cooling Load for Different Heat Pump EWTs

EWT °C (°F)	Suction Superheat: A-B (kJ/kg)	Condenser Subcooling: E-F (kJ/kg)	Superheat as % of Cooling Load (cd/gb)
21.1°C (70°F)	6.7	8.6	11.0
32.2°C (90°F)	6.7	10	15.9
43.3°C (110°F)	6.7	11.3	25.3
Average	6.7	9.97	17.4

5.3.2 Heating Mode

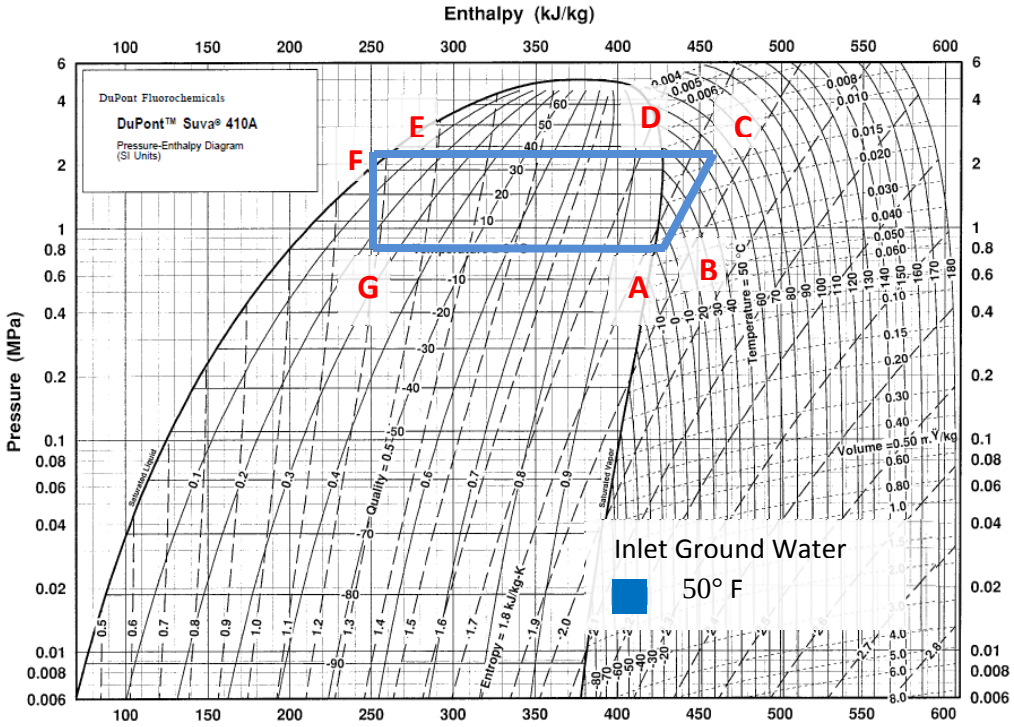

Figure 5.18: Thermodynamic Cycle of Heat Pump in Heating Mode

In the heating mode with 10°C (50°F) EWT, shown in Figure 5.18 above, G-B is the heat extracted out of the ground loop water entering the heat pump, B-C is the compressor work and reflects its efficiency, C-F is the heat supplied to the building, and F-G is the expansion through the expansion valve. Assuming 10°C EWT, refrigerant 410A and data from a heat pump manufacturer, average enthalpies at C and D are 459.1kJ/kgK and 426.3kJ/kgK (0.197kBtu/lb and 0.183kBtu/lb), respectively. For a refrigerant flow rate of 0.078kg/s, the total superheat available is 2.56kW (8.73kBtu/h). This amount of superheat is 16.2% of the heating load. Table 5.18 shows the thermodynamic states for -1.11°C, 10°C, and 21.1°C (30°F, 50°F , 70°F) EWTs. Table 5.19 shows the superheat as a percentage of heating load for each EWT. Table 5.21 also shows the superheat C-D as a percentage of cooling load, suction superheat A-B and condenser subcooling E-F for each EWT. The average suction superheat is 6.1kJ/kg, average condenser subcooling is 5.0kJ/kg and the average compressor exit superheat is 15.9% of the heating load.

Table 5.18: Thermodynamic Values at Different Points of the VCC in Heating Mode

-1.11°C (30°F) EWT	Pt. A	Pt. B	Pt. C	Pt. D	Pt. E	Pt. F	Pt. G
Pressure (MPa)	0.565	0.565	2.016	2.016	2.024	2.024	0.5666
Temperature (°C)	-10.4	-4.3	57.4	32.8	32.8	30.6	-10.4
Enthalpy (kJ/kg)	419.2	425.1	461.5	427.6	254	250.1	250.1
Pressure (psi)	81.9	81.9	292.4	292.4	293.5	293.5	82.2
Temperature (°F)	13.3	24.3	135.3	91.0	91.0	87.1	13.3
Enthalpy (kBtu/lb)	0.180	0.183	0.198	0.184	0.109	0.108	0.108
10°C (50°F) EWT	**Pt. A**	**Pt. B**	**Pt. C**	**Pt. D**	**Pt. E**	**Pt. F**	**Pt. G**
Pressure (MPa)	0.779	0.779	2.258	2.258	2.2649	2.2649	0.7871
Temperature (°C)	-0.7	6.1	59.1	37.3	37.3	34	-0.7
Enthalpy (kJ/kg)	422.35	429	459.1	426.3	262.1	256.1	256.1
Pressure (psi)	113.0	113.0	327.5	327.5	328.5	328.5	114.2
Temperature (°F)	30.7	43.0	138.4	99.1	99.1	93.2	30.7
Enthalpy (kBtu/lb)	0.182	0.184	0.197	0.183	0.113	0.110	0.110
21.1°C (70°F) EWT	**Pt. A**	**Pt. B**	**Pt. C**	**Pt. D**	**Pt. E**	**Pt. F**	**Pt. G**
Pressure (MPa)	1.0308	1.0308	2.4649	2.4649	2.5388	2.5388	1.0313
Temperature (°C)	8.3	15	60.4	42	42	37	8.3
Enthalpy (kJ/kg)	424.7	432.5	456.9	426.6	270.9	261.5	261.5
Pressure (psi)	149.5	149.5	357.5	357.5	368.2	368.2	149.6
Temperature (°F)	46.9	59	140.7	107.6	107.6	98.6	46.9
Enthalpy (kBtu/lb)	0.183	0.186	0.196	0.183	0.116	0.112	0.112

Table 5.19 Superheat as Percentage of Heating Load for Different Heat Pump EWTs

EWT °C (°F)	Suction Superheat: A-B (kJ/kg)	Condenser Subcooling: E-F (kJ/kg)	Superheat as % of Heating Load (cd/cf)
-1.1°C (30°F)	5.9	3.9	16.04
10°C (50°F)	6.7	6.0	16.16
21.1°C (70°F)	5.8	5.0	15.51
Average	6.1	5.0	15.90

The desuperheater uses the superheat portion of the compressor outlet to heat water. This section showed how much superheat is available when the heat pump is in the cooling and heating modes. These amounts will be used to determine the quantity of hot water that can be generated. The next section describes an analysis by Oak Ridge National Labs on computing the amount of hot water that can be generated by utilizing the superheat.

5.3.3 Analysis by Oak Ridge National Labs

Oak Ridge National Labs performed a detailed analysis of using desuperheaters to generate hot water for domestic use [Olszewski & Fontana, 1983]. They took a 167.2m^2 (1800ft^2) model house and calculated cost savings for a 7kW (2-ton) heat pump using refrigerant R-22. Figure 5.19 shows the p-h diagram of the VCC for different operating conditions. For the case shown by the solid line, the refrigerant condenses at a pressure of 1.774MPa (257.42psi). The region D-F is the superheated region of the condenser. The refrigerant cools down from 104^{o}C (220^{o}F) at point D to 60^{o}C (150^{o}F) at point F, and the superheat is 31% of the cooling load. For the case shown by the dashed line, the refrigerant condenses at a lower pressure, and hence the available superheat is on an average 20% of the cooling load.

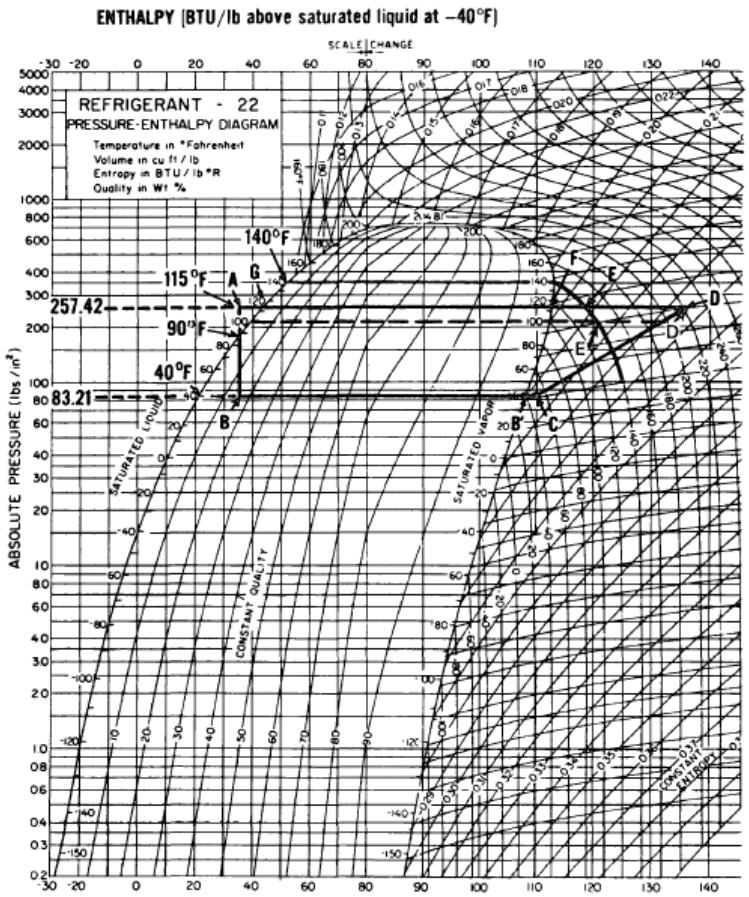

Figure 5.19: p-h Diagram of heat pump with R 22 refrigerant [Olszewski & Fontana, 1983]

Three cases of water heating consumption were analyzed: 25, 50, and 75gal/day (1.55, 3.11 and 4.68kg/s). For each case, it was assumed that the water could be heated to 60^{o}C (140^{o}F). The pinch point associated with the heat exchanger in question was 5.55^{o}C (10^{o}F). Hence, for

75 gal/day domestic hot water consumption, the maximum heat that could be used was given by:

$$Q_{max}\left(\frac{Btu}{h}\right) = 33.88 * (140 - T_{in}) \quad (5.36)$$

where, $T_{in}$was the inlet temperature of water (^{o}F) as a function of the location and time of the year.

The superheat heat available from the heat pump was given by:

$$Q_{av}\left(\frac{Btu}{h}\right) = 0.2 * \left(Q_{cyc}\right) * R_s \quad (5.37)$$

where, $Q_{cyc}$is the heat pump cooling or heating load in Btu/hr and R_s is the fraction of the time during an hour the heat pump is switched on.

The heating and cooling loads were based on the specific site analyzed, but the domestic hot water usage was assumed to be the same for all the sites (25, 50 and 75gal/day). The total energy extracted by the desuperheater was compared to the total energy needed for yearly hot water generation by either gas or electric. The difference between the two values represents the total energy saved. This analysis was done for 28 different sites. The annual energy savings was found to be the maximum in areas with long summers, where the source of reclaimed heat was mostly from the heat that was going to be rejected into the condenser. It was found that 2,848 kWh of energy per year could be saved if the desuperheater were run in Fort Worth, Texas compared to just 1,616 kWh in Chicago. The next section will discuss how the method described above will be used to extract heat out of the VCC of the base case residential building in Austin.

5.3.4 UT Desuperheater Model

The basic assumption of the Oak Ridge National Lab analysis and the subsequent UT model is that an expanded desuperheater can be designed to remove as much as 100% of the available superheat, while current desuperheater designs remove approximately 20% of the superheat.

The UT Expanded Desuperheater model analysis was applied to the base case residential house in Austin,TX ,described in Section 4.6, with a 14kW (4-ton) ClimateMaster Tranquility heat pump. The building loads were generated every two minutes for an entire year [Gaspredes, 2011]. The desuperheater is functional only when the heat pump is operating. The building load

data shows that the heat pump was in the cooling mode for 2022 hrs and in the heating mode for 277 hrs of the year, thus the heat pump was operating for a total of 2279 hrs (see Table 4.8, Section 4.7.4).

In the previous section it was calculated that the superheat represented an average of 17.4% of the cooling load and 15.9% of the heating load. The equations used to calculate the total available superheat per year were:

$$SH_{cool}\left(\frac{kBtu}{h}\right) = \sum 0.174 * Q_{cool} \quad (5.38)$$

$$SH_{heat}\left(\frac{kBtu}{h}\right) = \sum 0.159 * Q_{heat} \quad (5.39)$$

$$SH_{total}\left(\frac{kBtu}{h}\right) = SH_{cool} + SH_{heat} \quad (5.40)$$

where SH_{cool} and SH_{heat} are the superheats when the heat pump is in the cooling and heating mode, respectively, $Q_{cool}$and Q_{heat} are the cooling and heating loads in each time step (two minute steps), SH_{total} is the superheat available in the entire year.

For the 14kW heat pump, the available superheat during the cooling mode is 2.43kW (8.29 kBtu/h) and during the heating mode is 2.22kW (7.58kBtu/hr).

The next step was to determine the amount of energy required to heat the water for domestic purposes for three consumption cases: 25, 50, and 75 gal/day. The initial temperature of water in all cases was taken to be 22.2^{o}C (72^{o}F), which is the same temperature as that of the ground. The water was assumed to be heated to a temperature of 52^{o}C (125.6^{o}F) based on a 5.55^{o}C (10^{o}F) pinch point of the heat exchanger.

The pinch point was chosen by first calculating the temperatures of the refrigerant leaving the compressor for each EWT. Point C is the point where the refrigerant exits the compressor. The average compressor exit temperature was then calculated for both the heating and the cooling modes of the heat pump. The minimum average value for the two cases – heating and cooling modes – was calculated to be 57.5^{o}C (135.6^{o}F). Hence the total heat required per day for each one of the three cases is 11.6kJ, 23.2kJ and 34.8kJ (11, 22 and 33kBtu), respectively.

For each day, the total superheat that could be extracted when the heat pump was in operation was calculated. With this heat, the quantity of hot water that could be produced each day was calculated for three cases of domestic hot water consumption. The total number of days that domestic hot water needs could be satisfied by using the desueprheater was also

evaluated and plots generated. There were days when more heat was available than required to generate hot water for the three cases. The total additional quantity of water generated in a year and the cost incurred were also calculated.

5.3.4.1 UT Desuperheater on Residential Application Results: Performance

The buildings loads for the first year of operation on the base case residential building in Austin were used for the analyses [Gaspredes, 2011]. This choice is an assumption since with time, due to ground heating, more heat will be available from the heat pump when the desuperheater is used in the heating mode. Hence, calculated values will be different if the analyses were done for a different year. Table 5.20 shows the yearly available superheat from the operating heat pump and the amount of energy that can be extracted if 100%, 75% and 50% of the total available superheat were used.

Table 5.20: Energy Extracted by Desuperheater for Different Percentages of Available Superheat

Energy Extracted by Desuperheater/year	% of Available Superheat kJ (kBtu)		
	100%	75%	50%
During Cooling	13,956 (13,228)	10,467 (9,921)	6,978 (6,614)
During Heating	2,785 (2,640)	2,089 (1,980)	1,393 (1,320)
Total	16,741 (15,868)	12,556 (11,901)	8,370 (7,934)

Table 5.21 shows the number of days the desuperheater satisfied the hot water needs of a house for the 100%, 75% and 50% utilization of superheat and three hot water consumption rates (25, 50, 75gal/day). As expected, by using 100% of the superheat, the desuperheater can satisfy the hot water needs 210 days for the base case residential building for 75gal/day, 254 days for 50 gal/day and up to 303 days for 25gal/day hot water needs. For the remaining days, another source must be used to generate the required quantities of hot water. By using 75% of the superheat, the desuperheater can satisfy the hot water needs for 157, 225 and 286 days for the 75, 50 and 25gal/day requirements, respectively. By using 50% of the superheat, the desuperheater can satisfy the hot water needs only for 96, 157 and 254 days for the 75, 50 and 25 gal/day requirements, respectively.

Table 5.21: Number of Days Desuperheater can Meet Hot Water Requirements for Different % Utilization of the Available Superheat

Daily Hot Water Use kg/s (gal/day)	Energy Needed/Day kJ (kBtu)	Number of Days Hot Water Requirements Met (Days)		
		100% Superheat	75% Superheat	50% Superheat
4.68 (75)	11.6 (33)	210	157	96
3.11 (50)	23.21 (22)	254	225	157
1.55 (25)	34.8 (11)	303	286	254

Figure 5.20 to 5.22 show the quantity of water generated daily when the desuperheater uses 100% of the available superheat. The straight line (green line) in each case corresponds to the domestic consumption in each case – 75 gal/day in Figure 5.20, 50 gal/day in Figure 5.21 and 25 gal/day in Figure It can be seen that the required needs are met most of the days. Also, on the days when the required needs are met, the quantity of hot water generated is much more than needed. This excess hot water can either be stored or used for other purposes (car wash, etc).

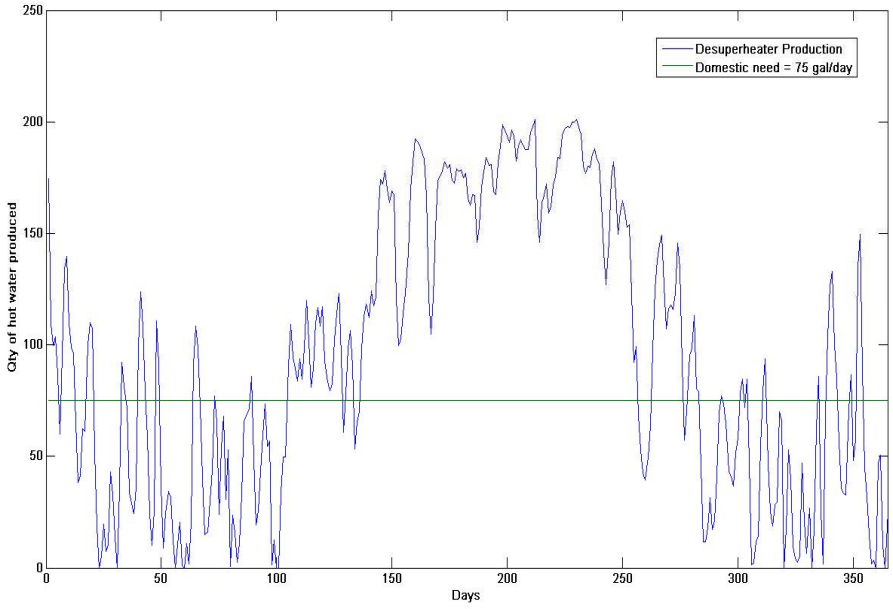

Figure 5.20: Quantity of hot water produced (in gallons) using 100% of superheat

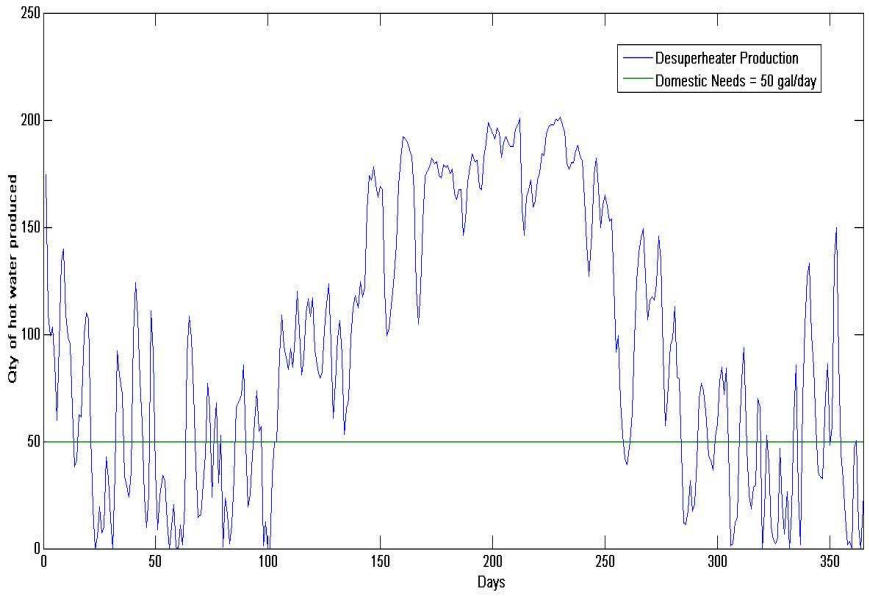

Figure 5.21: Quantity of hot water produced (in gallons) using 75% of superheat

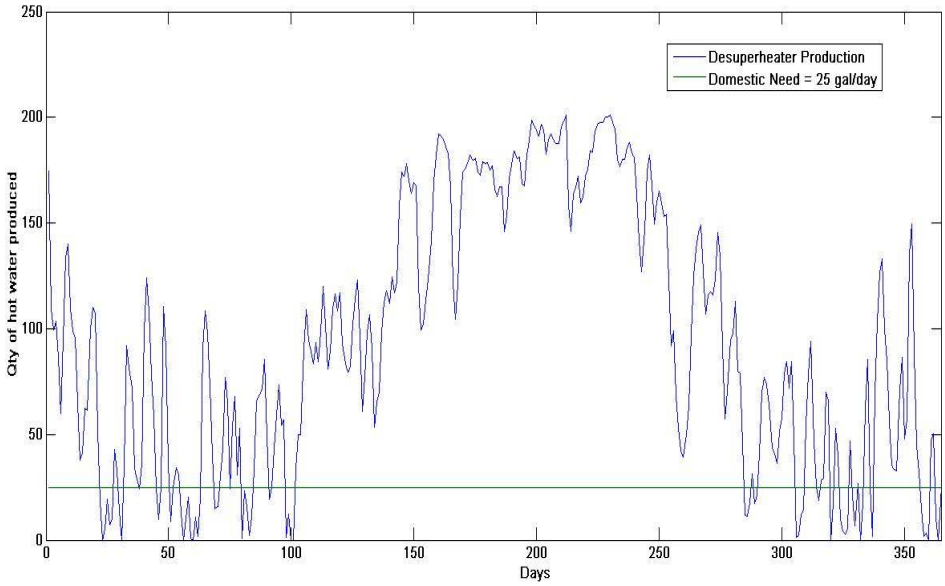

Figure 5.22: Quantity of hot water produced (in gallons) using 50% of superheat

By generating hot water in the desuperheater, heat is removed from the refrigerant loop and less heat is heat is rejected to the condenser. The average power rejected when the heat pump was in cooling mode was calculated; the heat rejected for each hour was computed and averaged over the time the heat pump operated in cooling mode (2022.2 hrs).

Table 5.22 shows the average power removed by the desuperheater in the cooling mode for the three cases of utilization of the available superheat. If 100% of the superheat were used, an average of 1.91kW (6.61kBtu/h) of power can be removed from the refrigeration loop, thereby reducing the water temperature in the ground loop by 0.61°C (1.1°F). Using 75% of the superheat removed 1.43kW (4.89kBtuh) of power and reduced the water temperature by 0.46°C (0.82°F). Using 50% of the superheat removed 0.96kW (3.23kBtuh) and reduced the water temperature by 0.31°C (0.55°F). In all cases the decrease in water temperatures at the condenser would be small.

Table 5.22: Power Removed by Desuperheater and Water Temperature Decrease in Condenser

% Superheat Utilized	Average Power Removed kW (kBtu/h)	Temperature Decrease of Water in Condenser °C (°F)
100%	1.91 (6.5)	0.61 (1.1)
75%	1.43 (4.88)	0.46 (0.82)
50%	0.96 (3.28)	0.31 (0.55)

5.3.4.2 UT Desuperheater on Residential Application Results: Economics

Turbotec manufactures desuperheaters [Turbotec, 2011] at a cost of $583 with an additional $1,000 for installation. Table 5.23 shows the additional quantity of water generated annually for the three cases of desuperheater utilization of the superheat (100%, 75% and 50%) and three domestic hot water consumption (25, 50, 75 gal/day). The negative values indicate that the desuperheater alone is not able to satisfy all the hot water needs and that an additional source is needed. For example, at 50 gal/day consumption, the 18,250 gal/year of hot water is needed. If 100% and 75% of the superheat are used, 12,833, and 6,313 gal/year additional hot water could be generated by the excess heat. At 50% superheat, no additional hot water can be generated.

Table 5.23: Additional Quantity of Hot Water that Could be Generated by the Desuperheater for Different Superheat Utilization

Daily Hot Water Usage kg/s (gal/day)	Annual Hot Water Usage gal/yr	Additional Qty of Hot Water Generated Utilizing x % of Superheat gal/yr		
		100%	75%	50%
4.68 (75)	27,375	6,208	-312	-6,833
3.11 (50)	18,250	12,833	6,313	-208
1.55 (25)	9,125	19,458	12,938	6,417

Table 5.24 shows the cost of the additional water that would be needed to generate the additional hot water. The cost in all cases is less than $25/year. The cost of the additional hot water tanks (assumed needed if stored) or that associated with using the hot water has not been included in this table.

Table 5.24: Cost of Additional Quantity of Water for Different Superheat Utilization [Austin, 2011]

Daily Hot Water Usage kg/s (gal/day)	Cost for Additional Quantity of Water Utilizing x % of Superheat $/yr		
	100%	75%	50%
4.68 (75)	7	0	0
3.11 (50)	14	7	0
1.55 (25)	21	14	7

Conclusions: The analyses presented in the previous sections show the total amount of heat that can be removed from the superheated region of the VCC. An average of 1.91kW (6.61kBtuh) of power can be removed and thereby reduce the heat rejected to the ground loop water in the condenser with a temperature drop of 0.61^{o}C (1.1^{o}F) if 100% of the available superheat were used. The power removed is 1.43kW (4.89kBtuh) with 75% superheat utilization and 0.96kW (3.23kBtuh) with 50% superheat utilization. In all cases, the economics of generating additional hot water is very favorable**.**

One problem in utilizing 100% of the available superheat is the refrigerant loses pressure in the desuperheater, which makes it difficult for the refrigerant to move through the entire length of the condenser. Hence, in practical applications, the desuperheater is run only just to satisfy the domestic heating needs. Also, when the desuperheater is run in the heating mode, more heat must be extracted out of the ground, since the heat removed by the desuperheater would normally go to heat the building. The heat pump must run for a longer time, and hence reduce the COP for the same heating provided to the building.

4.5 OTHER SHR SYSTEMS

The following list of other potential SHR systems were considered with preliminary analyses but deemed not feasible, either technically or economically, at this time for cooling dominated regions. Some of these are discussed in more detail in Appendix D (Other SHR Devices/Systems).

- Thermosyphon
- Thermoelectric liquid coolers

- Evaporative coolers
- Absorption coolers
- Thermomagnetic/Thermoacoustic cooling
- Reservoirs: swimming pools, greenhouses, city water

6.0 INTEGRATED COMMERCIAL BUILDING APPLICATION

The HAMBASE building load, heat pump, and ground loop models of the integrated IBL-GHP model developed in Section 3 and applied to a residential application in Section 4 are now used to model a medium sized commercial office building.

6.1 IBL-GHP MODEL APPLICATION TO COMMERCIAL BUILDING

The commercial building chosen for this work is the Medium Office from the Department of Energy's (DoE) Commercial Reference Building Models [US DoE, 2010]. It is a 4,982m^2 (53,628ft^2) three-story office building, that is newly built using a steel framed-wall construction approach. The envelope of the rectangular building measures 49.911m x 33.274m x 11.887m (163.75ft x 109.17ft x 39ft). An image of the building is shown in Figure 6.1.

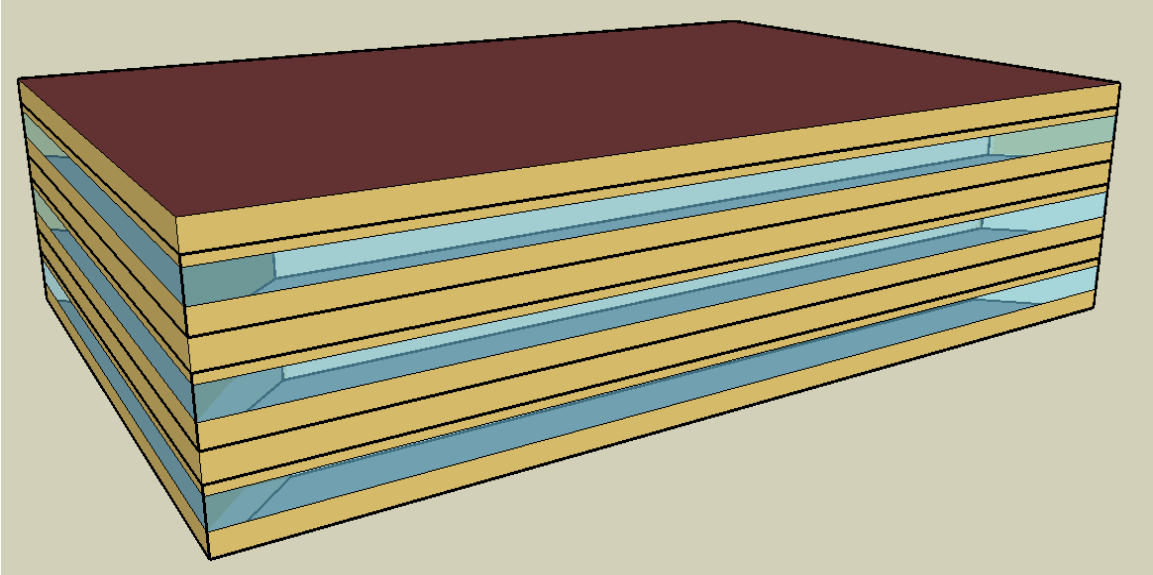

Figure 6.1: Medium office building [US DoE, 2010]

The following sections discuss the dimensions, material properties, internal loads and HVAC systems for the building.

6.1.1 Physical Layout

The building is oriented perpendicular to the cardinal-direction compass, with sides of the building directly facing north, east, south and west. Each floor of the building model consists of six zones: a core zone, four perimeter zones (north, south, east, and west) and an unconditioned plenum zone. Zones are labeled as North1, Core2, Plenum3, etc. for the first-

floor north zone, the second-floor core zone and the third-floor plenum zone, respectively. Cross-sectional views of the building are shown in Figures 6.2 and 6.3.

All perimeter zones have a single external wall that contains 1.3m (4.3ft) tall windows spanning their entire width, shown in blue. The core zones have no external walls, nor windows. The plenum zones have four external walls that extend the entire width and length of the building, but no windows. The core zones are the largest zones in the building, with a floor area of 984m^2 (10,587ft^2) and a total volume of 2,698m^3 (95,279ft^3). The east and west zones are the smallest in the building, with a floor area of 131m^2 (1,413ft^2) and a total volume of 360m^3 (12,713ft^3). The north and south zones have a floor area of 207m^2 (2,232ft^2) and a total volume of 569m^3 (20,086ft^3). Exact dimensions for each zone in the building are shown in Table 6.1.

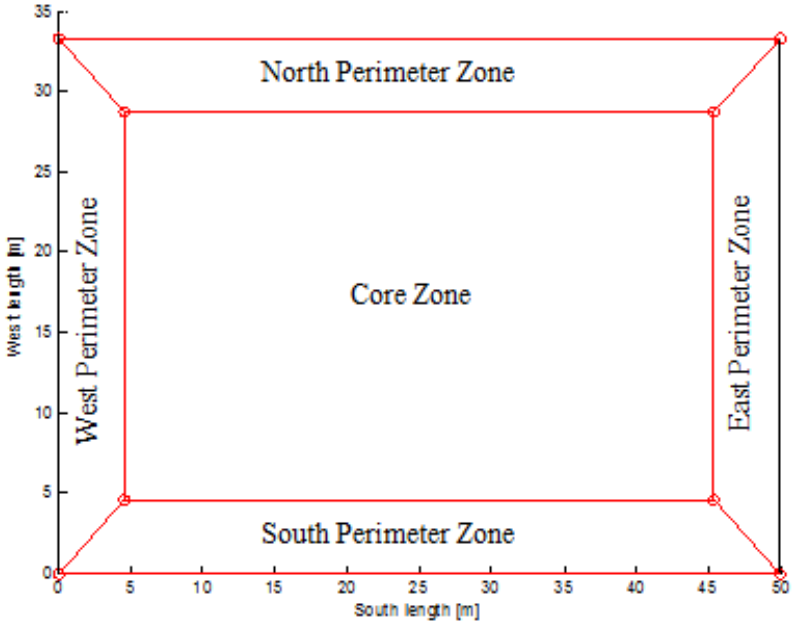

Figure 6.2: Aerial view of the first floor zones

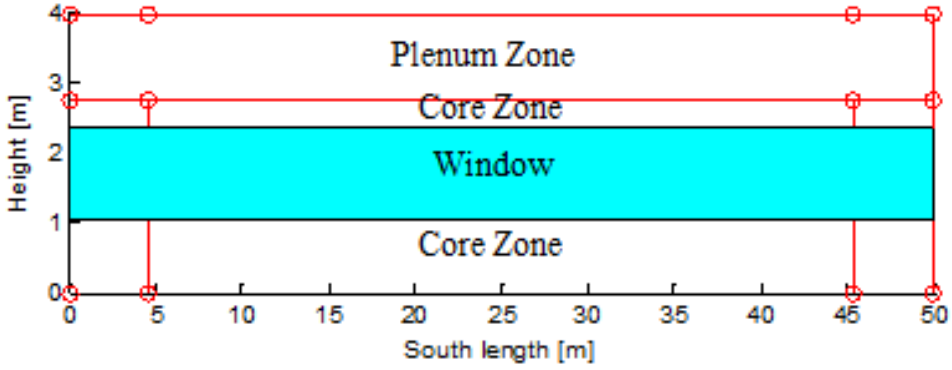

Figure 6.3: Horizontal view of the first floor zones

Table 6.1: Zone Dimensions [US DoE, 2010]

Zone Name	Floor Area (m^2)	Floor Area (ft^2)	Volume (m^3)	Volume (ft^3)	Exterior Area (m^2)	Exterior Area (ft^2)	Window Area (m^2)	Window Area (ft^2)
Core 1	984	10,587	2,698	95,280	-	-	-	-
South 1	207	2,232	569	20,086	137	1,474	65	703
East 1	131	1,413	360	12,716	91	982	44	468
North 1	207	2,232	569	20,086	137	1,474	65	703
West 1	131	1,413	360	12,716	91	982	44	468
Plenum 1	1,661	17,876	2,025	71,504	203	2,183	-	-
Core 2	984	10,587	2,698	95,280	-	-	-	-
South 2	207	2,232	569	20,086	137	1,474	65	703
East 2	131	1,413	360	12,716	91	982	44	468
North 2	207	2,232	569	20,086	137	1,474	65	703
West 2	131	1,413	360	12,716	91	982	44	468
Plenum 2	1,661	17,876	2,025	71,504	203	2,183	-	-
Core 3	984	10,587	2,698	95,280	-	-	-	-
South 3	207	2,232	569	20,086	137	1,474	65	703
East 3	131	1,413	360	12,716	91	982	44	468
North 3	207	2,232	569	20,086	137	1,474	65	703
West 3	131	1,413	360	12,716	91	982	44	468
Plenum 3	1,661	17,876	2,025	71,504	203	2,183	-	-
Building Total	9,963	107,259	19,743	697,161	3,638	39,163	653	7,027

6.1.2 Building Construction [US DoE, 2010]

The building is comprised of five separate wall constructions: exterior vertical walls, a roof, floors, interior vertical walls, and plenum drop ceilings. The exterior vertical walls use a “Steel frame wall” construction, which consists of wood siding as the outer-most layer, insulation and gypsum board as the inner-most layer for a total U-value of 0.704W/m^2·K (0.124btu/h·ft^2·°F). The roof uses an “Insulation entirely above deck” construction, which consists of a water-proof membrane as the outer-most layer, insulation, and metal decking as the inner-most layer for a total U-value of 0.358W/m^2·K (0.063btu/h·ft^2·°F). The floors consist of 4-inch concrete and a layer of carpet. Interior vertical walls consist of two layers of gypsum board. Plenum drop ceilings consist of standard drop-in ceiling tiles. Table 6.2 lists the properties of the construction materials.

Table 6.2: Properties of Construction Materials

Material	Conductivity	Density	Heat capacity	Emissivity	Moisture resistance	Moisture capacity	Vapor capacity x10^7
Wall Insulation	0.049	265	836.8	0.7	1	5	6.6
Roof Insulation	0.049	265	836.8	0.7	1	5	6.6
Wood Siding	0.11	544.6	1210	0.78	16	80	6.6
Gypsum Board	0.16	784.9	830	0.92	9	6	3.5
Concrete Floor	1.311	2240	836.8	0.7	25	40	3.7
Metal Decking	45	7680	418.4	0.7	9000000	0	0
Roof Membrane	0.16	1121	1460	0.3	5000	0	0
Carpet	0.03	112	1379	0.7	10000	0	0
Ceiling Tiles	0.057	288	1339	0.7	10	20	4.2

6.1.3 Fenestration

Windows comprise 33% of the vertical exterior surface area, or 18% of the total exterior envelope (roof included). The exact area of windows in each zone is shown in Table 6.1. The

window U-values of 6.927W/m^2·K (1.22btu/h·ft^2·°F) are based on "The highest U-values from [Standard] 90.1-1989" [US DoE, 2010]. The solar heat gain coefficient (SHGC) value of 0.25 is based on Standard 90.1-1999 [US DoE, 2010]. An additional window parameter called a "convection factor with/without sunblinds" is also required by HAMBASE, and a value of 0.04 is used based on "double glazing" [deWitt, 2009]. There are no shading devices incorporated in the building, nor does shading occur from external sources (trees, buildings, etc.).

6.1.4 Load Scheduling

The internal and external loads used in this model are all subject to hourly scheduling that varies by day of the week. At different times of day, each load will operate at some percentage of its peak value. On a weekday for example, a typical office building will experience approximately 0% people load at 5am, 10% at 6am, and 20% at 7am, and finally reaching 95% at 8am, as shown in Figure 6.4. Thus, the load generated by a particular source at a particular time is simply the product of the peak load and scheduling **load multiplier** factor. For example, the peak heat rate for Core1 is shown to be 6,355.2W (21,684.8btu/hr) in Table 6.3, so the heat rate generated by people at 7am on a weekday in Core1 is 20% (load multiplier) of the peak value, or 1,271.4W (4,338.2btu/hr).

Schedules in this model were taken from the DoE's Commercial Reference Office building, which in turn was based on, "Standard 90.1-1989 Section 13, which includes schedules for use with the Energy Cost budget Method (ASHRAE 1989)" [US DoE, 2010]. The following sections list scheduling load multiplier profiles and tables of peak loads for each heat source.

6.1.4.1 Internal Loads

The building model includes four categories of heat loads found internally within zones: people, lighting, electrical equipment and elevators. Peak heating rates and calculation methods of heat transfer are explained in detail for each category in the following sections.

6.1.4.1.1 People

Zone loads resulting from people are based upon occupancy of 18.58m^2/person as recommended by ASHRAE Standard 62.1-2004 [US DoE, 2010]. The DoE implementation uses a total heat rate of 120W/person (409.5btu/hr), which is close to the representative total heat rate of 115W (392.4btu/hr) from ASHRAE for "Seated, very light work" in an office [ASHRAE, 2009]. ASHRAE divides the total heat rate of 115W into 61% (70W, 238.8btu/hr) sensible heat and 39% latent heat (45W, 153.5btu/hr) [US DoE, 2010]. This model uses 120W/person to better match results with the DoE implementation. Table 6.3 shows the number of people in

each zone, the peak heat rate they generate, and the sensible and latent portions of the load. Figure 6.4 shows the hourly schedule used to scale the peak heat rate generated by people.

Table 6.3: Peak Heat Rates Resulting from People by Zone

Zone	Number of People	Peak Heat Rate [W]	Peak Sensible Heat Rate [W]	Peak Latent Heat Rate [W]
Core 1	53.0	6355.2	3876.7	2478.5
South 1	11.1	1336.9	815.5	521.4
East 1	7.1	846.1	330.0	516.1
North 1	11.1	1336.9	815.5	521.4
West 1	7.1	846.1	330.0	516.1
Plenum 1	0	0	0	0
Core 2	53.0	6355.2	3876.7	2478.5
South 2	11.1	1336.9	815.5	521.4
East 2	7.1	846.1	330.0	516.1
North 2	11.1	1336.9	815.5	521.4
West 2	7.1	846.1	330.0	516.1
Plenum 2	0	0	0	0
Core 3	53.0	6355.2	3876.7	2478.5
South 3	11.1	1336.9	815.5	521.4
East 3	7.1	846.1	330.0	516.1
North 3	11.1	1336.9	815.5	521.4
West 3	7.1	846.1	330.0	516.1
Plenum 3	0	0	0	0

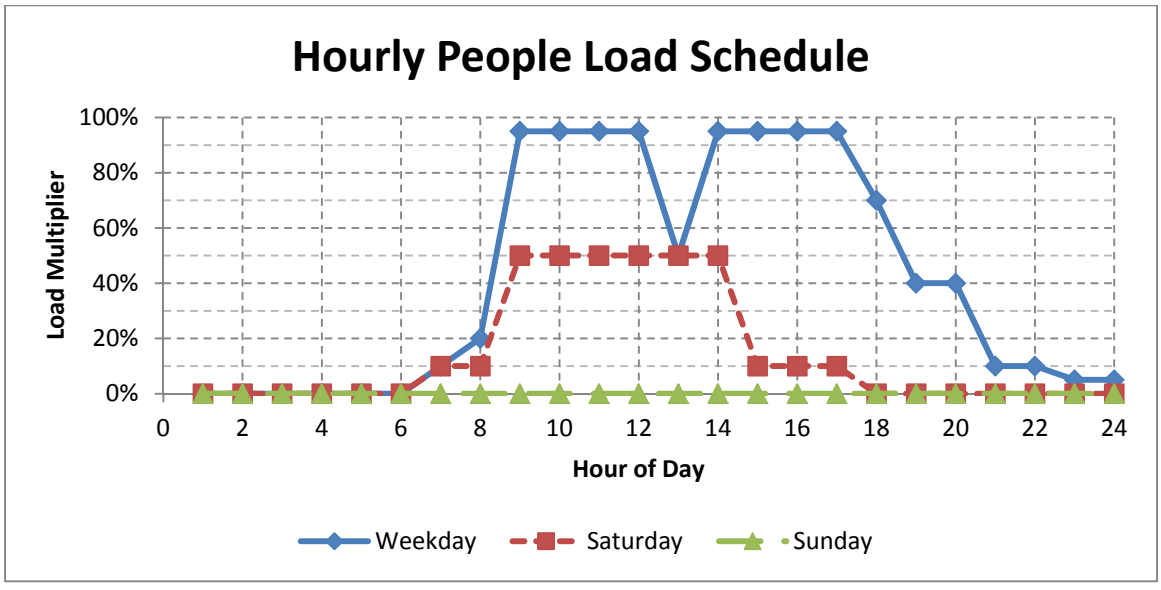

Figure 6.4: Hourly load multiplier schedule for people

6.1.4.1.2 Lighting

The DoE implementation uses "The building area method or the space-by-space method from [ASHRAE] Standard 90.1-2004" to estimate the heat rate resulting from lighting. This method estimates the lighting heat rate on a per unit area basis [US DoE, 2010]The maximum lighting power density for offices listed by ASHRAE is 12W/m^2 [ASHRAE, 2009]. The value used in the DoE implementation is 10.76W/m^2 (3.41btu/hr·ft^2). This model uses 10.76W/m^2 to better match results with the DoE implementation.

Lighting fixtures are typically located in the ceiling, which results in a load distribution between the unconditioned plenum space above the fixtures and the lighted space below the fixtures. This division results in the conditioned space receiving 60% of the load, while the plenum receives 40%. Lights do not produce latent heat, meaning that the entire load generated from lights is sensible.

Table 6.4 shows the zone areas and subsequent peak heat rates due to lighting for each zone. Figure 6.5 shows the hourly load multiplier schedule for lighting.

Table 6.4: Peak Heat Rates Resulting from Lighting by Zone

Zone	Area [m^2]	Peak Heat Rate [W]	Peak Sensible Heat Rate [W]	Peak Latent Heat Rate [W]
Core 1	984	6352.7	6352.7	0
South 1	207	1336.4	1336.4	0
East 1	131	845.7	845.7	0
North 1	207	1336.4	1336.4	0
West 1	131	845.7	845.7	0
Plenum 1	1,661	7148.9	7148.9	0
Core 2	984	6352.7	6352.7	0
South 2	207	1336.4	1336.4	0
East 2	131	845.7	845.7	0
North 2	207	1336.4	1336.4	0
West 2	131	845.7	845.7	0
Plenum 2	1,661	7148.9	7148.9	0
Core 3	984	6352.7	6352.7	0
South 3	207	1336.4	1336.4	0
East 3	131	845.7	845.7	0
North 3	207	1336.4	1336.4	0
West 3	131	845.7	845.7	0
Plenum 3	1,661	7148.9	7148.9	0

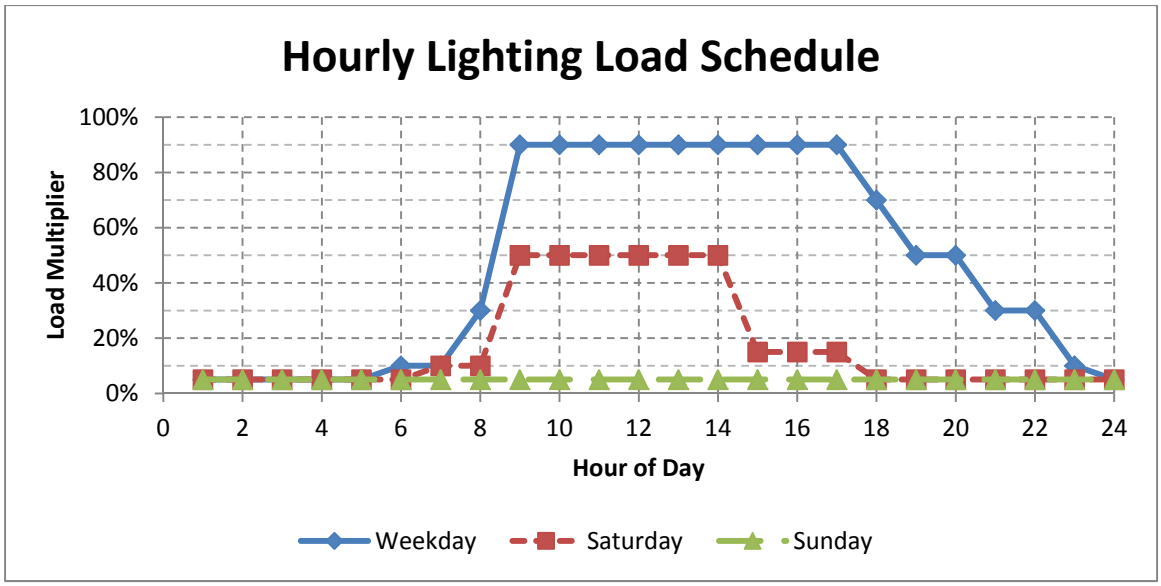

Figure 6.5: Hourly load multiplier schedule for lights

6.1.4.1.3 Equipment

Heat gains resulting from equipment (computers, printers, etc.) are based on a heat gain per unit floor area method. Acceptable heat gain values range from 4.7 to 11.6W/m^2 (1.49 to 3.68btu/hr·ft^2) with a normalized average of 8.7W/m^2 (2.76btu/hr·ft^2) [ASHRAE, 2009]. According to Wilkins and Hosni, an office with medium load density has a heat gain of 10.8W/m^2 (3.42btu/hr·ft^2) [ASHRAE, 2009]. The DoE implementation uses a load density of 10.76W/m^2 (3.41btu/hr·ft^2). This model uses 10.76W/m^2 to better match results with the DoE implementation. Typical equipment found in offices is assumed to not produce latent heat, meaning that the entire load generated from equipment is sensible. All heat loads from equipment are assumed to be generated in the conditioned spaces and not in the plenums. Table 6.5 shows the zone areas and peak heat rates from equipment for each zone. Figure 6.6 shows the hourly load multiplier schedule for equipment.

Table 6.5: Peak Heat Rates Resulting from Equipment by Zone

Zone	Area [m^2]	Peak Heat Rate [W]	Peak Sensible Heat Rate [W]	Peak Latent Heat Rate [W]
Core 1	984	10587.8	10587.8	0
South 1	207	2227.3	2227.3	0
East 1	131	1409.6	1409.6	0
North 1	207	2227.3	2227.3	0
West 1	131	1409.6	1409.6	0
Plenum 1	1,661	0.0	0.0	0
Core 2	984	10587.8	10587.8	0
South 2	207	2227.3	2227.3	0
East 2	131	1409.6	1409.6	0
North 2	207	2227.3	2227.3	0
West 2	131	1409.6	1409.6	0
Plenum 2	1,661	0.0	0.0	0
Core 3	984	10587.8	10587.8	0
South 3	207	2227.3	2227.3	0
East 3	131	1409.6	1409.6	0
North 3	207	2227.3	2227.3	0
West 3	131	1409.6	1409.6	0
Plenum 3	1,661	0.0	0.0	0

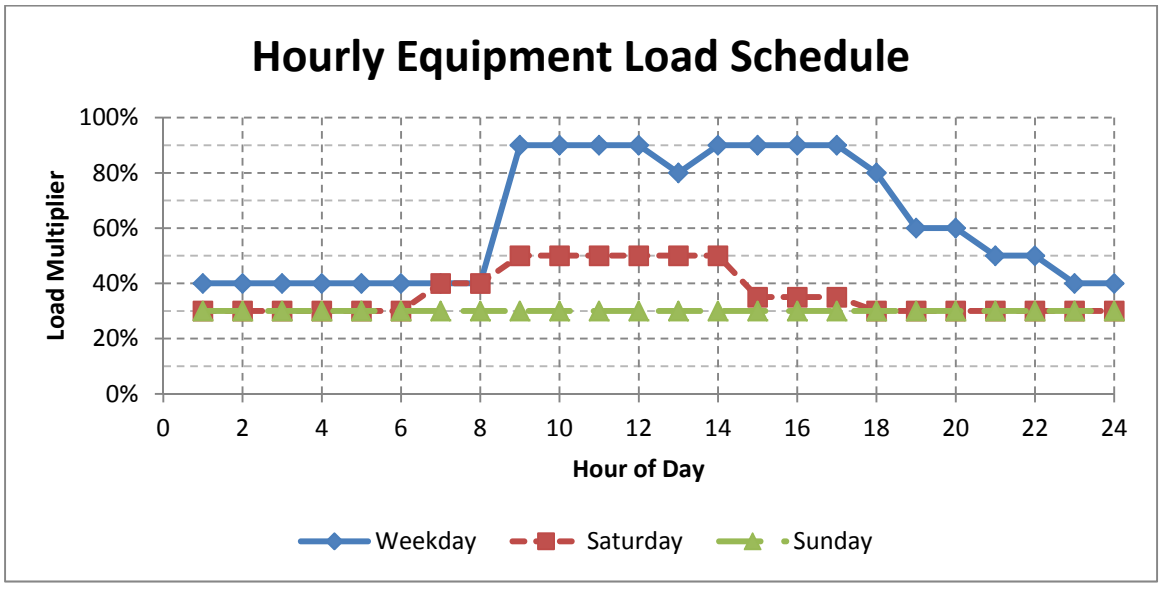

Figure 6.6: Hourly load multiplier schedule for for equipment

6.1.4.1.4 Elevators

The office building contains two elevators, each of which is assumed to "Use hydraulic motors with no counter weighting, weigh 2,500lb (1,134kg), travel 150fpm (46mpm), and have a mechanical efficiency of 58%" [US DoE, 2010]. Based on the motor power calculation from Baldor Electric Company, each motor has a power rating of 14.61kW (19.6HP), resulting in a combined power rating of 29.22kW (39.2HP) for the two elevator motors [US DoE, 2010]. The peak heat rate resulting from elevator operation used by the DoE implementation is 32.11kW (43.1HP).

Even though the elevator motors are not located in a particular zone, the heat generated by their operation will conduct through walls and eventually be handled by the building's HVAC system. As a result, this model assumes that the motors are outside of the conditioned zone, but the heat generated by their operation is entirely assigned to the first-floor core zone. In such a case, the heat equivalent generated of elevator operation is given by [ASHRAE, 2009]:

$$q_{em} = PF_{UM}F_{LM} \tag{6.1}$$

where

$q_{em} = \text{heat equivalent of equipment operation [W]}$

$P = \text{motor power rating [W]}$

$F_{UM} = \text{motor use factor}$

$F_{LM} = \text{motor load factor}$

While it is unclear what use and load factors were used in conjunction with the 29.22kW (39.2HP) total motor power rating to yield a 32.11kW internal heat gain, 32.11kW is used in this model in order to better match the DoE results. Figure 6.7 shows the hourly load multiplier schedule for the elevators.

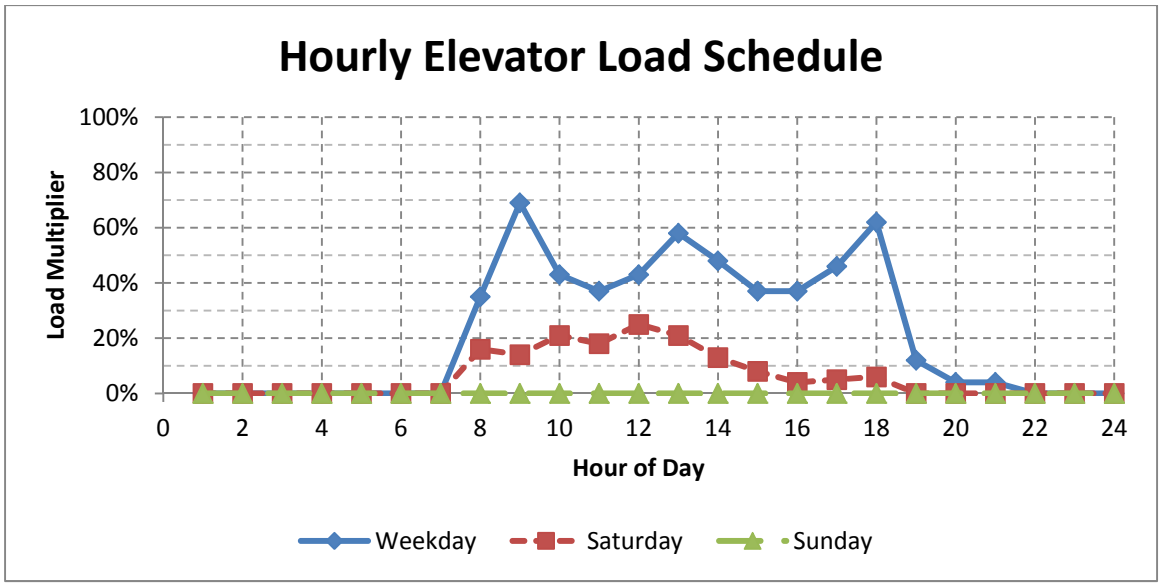

Figure 6.7: Hourly load multiplier schedule for elevators

6.1.4.1.5 Summary of Sensible and Latent Loads

EnergyPlus gives the user the option to itemize separate heat sources and automatically include each individual heat source in simulations. HAMBASE does not have this functionality. Internal loads for HAMBASE must be in the form of total sensible heat rate and total latent heat rate (in kg_{water}/s) for a given zone. As a result, all individual heat sources in each zone must be summed to create the load profile.

Table 6.6 shows the total sensible and latent loads for each zone. The latent load, originally in watts, was converted to kg_{water}/s using

$$Q_{latent} = h_{fg} \cdot \dot{m}_{water} \tag{6.2}$$

where $h_{fg} = 2440.08 \ \frac{kJ}{kg_w}$, heat of vaporization at 24°C.

Table 6.6: Total Latent and Sensible Heat Rates by Zone

Zone	Peak Heat Rate [W]	Peak Sensible Heat Rate [W]	Peak Latent Heat Rate [W]	Peak Latent Heat Rate [kg_w/s]
Core 1	55406	52927	2479	0.0010
South 1	4901	4379	521	0.0002
East 1	3101	2771	330	0.0001
North 1	4901	4379	521	0.0002
West 1	3101	2771	330	0.0001
Plenum 1	7149	7149	0	0.0000
Core 2	23296	20817	2479	0.0010
South 2	4901	4379	521	0.0002
East 2	3101	2771	330	0.0001
North 2	4901	4379	521	0.0002
West 2	3101	2771	330	0.0001
Plenum 2	7149	7149	0	0.0000
Core 3	23296	20817	2479	0.0010
South 3	4901	4379	521	0.0002
East 3	3101	2771	330	0.0001
North 3	4901	4379	521	0.0002
West 3	3101	2771	330	0.0001
Plenum 3	7149	7149	0	0.0000

6.1.4.1.6 Modeling of Sensible Loads

EnergyPlus allows sensible loads to be divided into convective and radiant components on a load-by-load basis. Since HAMBASE does not have the ability to construct multiple separate internal loads in a particular zone, dividing a particular load into convective and radiant components is not possible. Instead, HAMBASE includes a convection factor that divides the total sensible load into convective and radiant components. Example calculations for the convection factor are shown in Table 6.7 based on the loads in Core2. Values for the convection factor used for each zone are shown in Table 6.8.

Table 6.7: Example Calculation of Convective Rraction for Core 2 Zone

Heat Source	People	Lighting	Elec. Equip.	Elevator	Total	Fraction
Sensible Heat Rate [W]	3877	6353	10588	0	20818	100%
Convective Heat Rate [W]	2714	0	5294	0	8008	38%
Radiant Heat Rate [W]	1163	6353	5294	0	12810	62%

Table 6.8: Convective Factors by Zone

Zone	Peak Sensible Heat Rate [W]	Peak Radiant Heat Rate [W]	Peak Convective Heat Rate [W]	Convection Factor [%]
Core 1	52927	28865	24063	45%
South 1	4379	2695	1685	38%
East 1	2771	1705	1066	38%
North 1	4379	2695	1685	38%
West 1	2771	1705	1066	38%
Plenum 1	7149	0	7149	100%
Core 2	20817	12810	8008	38%
South 2	4379	2695	1685	38%
East 2	2771	1705	1066	38%
North 2	4379	2695	1685	38%
West 2	2771	1705	1066	38%
Plenum 2	7149	0	7149	100%
Core 3	20817	12810	8008	38%
South 3	4379	2695	1685	38%
East 3	2771	1705	1066	38%
North 3	4379	2695	1685	38%
West 3	2771	1705	1066	38%
Plenum 3	7149	0	7149	100%

6.1.4.2 External Loads

This model includes three heat flows from sources outside of the building: infiltration, “The flow of outdoor air into a building through cracks and other unintentional openings and through the normal use of exterior doors,” ventilation, “intentional introduction of air from the outside into a building” and external weather [ASHRAE, 2009]. These three inputs are described in detail in the following sections.

6.1.4.2.1 Infiltration

Infiltration rates depend on building construction, weather conditions and HVAC operation pressures. Relationships exist relating air leakage rates to pressure difference across the exterior envelope of a building, and to average envelope crack size. The pressure difference across the building envelope varies continuously with wind speed, barometric pressure and HVAC pressurization, while envelope crack size and distribution are typically unknown. As a result of these challenges, “Modeling approaches to infiltration are typically very simple” [US DoE, 2010]. In many commercial applications, it is assumed that building envelopes are airtight, but Persily and Grot found that when results are normalized by envelope area, envelope airtightness for American commercial buildings display similar levels of airflow as American houses [ASHRAE, 2009]. Another approach applies a fan pressurization test to measure flow rate through a building’s envelope at a certain supply pressure, and subsequently normalizes the flow rate by the building’s surface area. Using this method, Persily and Grot found air leakage rates, “Ranging from 1080 to 5220$cm^3/(s \cdot m^2)$ at 75Pa” [ASHRAE, 2009]. Tamura and Shaw found that air leakage values at 75Pa for tight, average and leaky walls were “500, 1500, [ASHRAE. 2009]. ASHRAE Standard 90.1-2004 proposed an ideal maximum building leakage of 2000$cm^3/(s \cdot m^2)$ for above-grade envelope area (exterior walls and roof) [US DoE, 2010]. The actual DoE implementation used a constant flow per exterior surface area value of 0.000302$m^3/(s \cdot m^2)$ (300$cm^3/(s \cdot m^2)$). This value applies only applies during times when the HVAC system is not in operation. When the HVAC system is on, the pressure exerted by the system serves to reduce infiltration into the building. As a result, it was “Assumed that the uncontrolled infiltration is reduced to 25% of the [maximum] value [US DoE, 2010]. Infiltration flow rates for each zone in the model are shown in Table 6.9. The HVAC operation schedule is shown in Figure 6.8, while the resulting infiltration load multiplier schedule is shown in Figure 6.9.

Table 6.9: Infiltration Values by Zone

Zone	Exterior Surface Area [m^2]	Infiltration, HVAC off [m^3/s]	Infiltration, HVAC off [ACH]	Infiltration, HVAC on [ACH]
Core 1	0	0.0000	0.000	0.000
South 1	137	0.0413	0.262	0.065
East 1	91	0.0276	0.276	0.069
North 1	137	0.0413	0.262	0.065
West 1	91	0.0276	0.276	0.069
Plenum 1	203	0.0613	0.109	0.027
Core 2	0	0.0000	0.000	0.000
South 2	137	0.0413	0.262	0.065
East 2	91	0.0276	0.276	0.069
North 2	137	0.0413	0.262	0.065
West 2	91	0.0276	0.276	0.069
Plenum 2	203	0.0613	0.109	0.027
Core 3	0	0.0000	0.000	0.000
South 3	137	0.0413	0.262	0.065
East 3	91	0.0276	0.276	0.069
North 3	137	0.0413	0.262	0.065
West 3	91	0.0276	0.276	0.069
Plenum 3	1864	0.5628	1.001	0.250

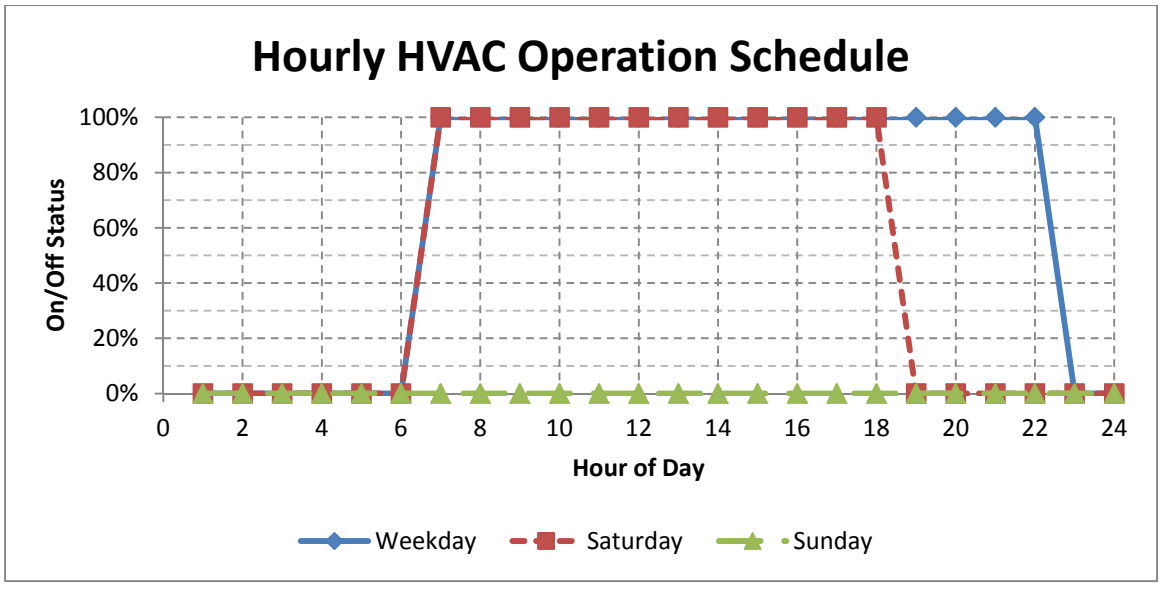

Figure 6.8: Hourly schedule for HVAC system operation

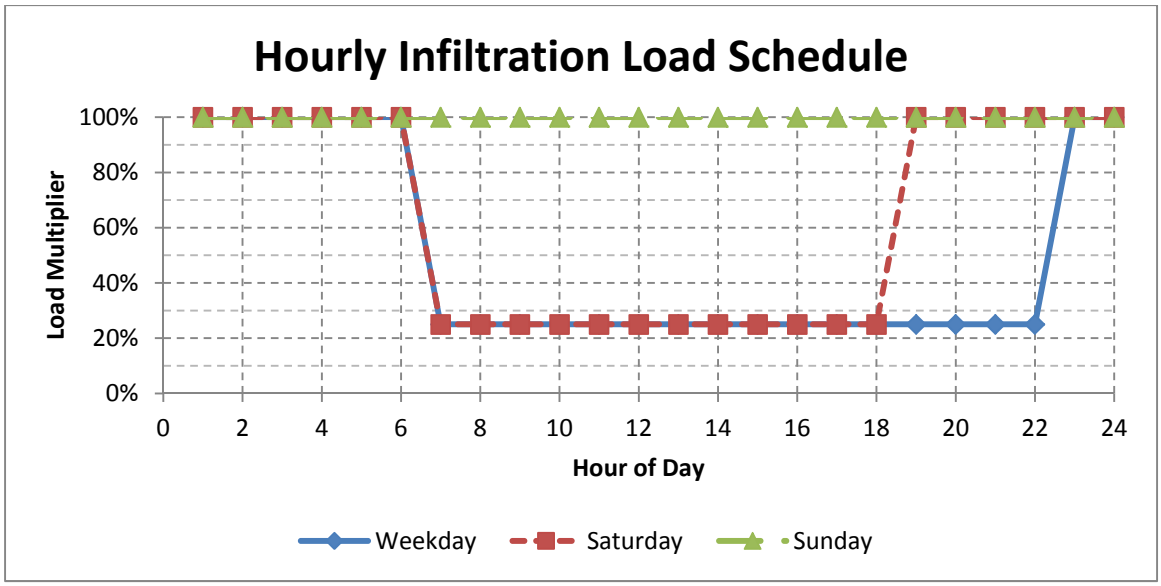

Figure 6.9: Hourly load multiplier schedule for infiltration

6.1.4.2.2 Ventilation

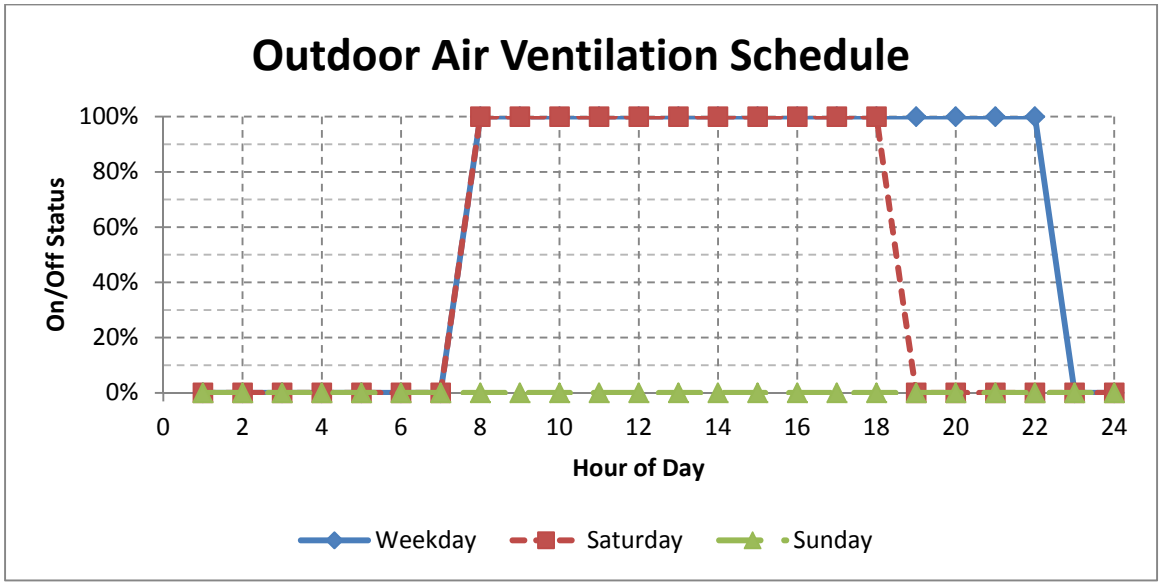

Figure 6.10: Hourly load multiplier schedule for outdoor air ventilation

6.1.4.2.3 Weather

The weather input used in this model and in the DoE implementation is the typical meteorological year (TMY) dataset produced by the National Renewable Energy Laboratory's (NREL) Electric Systems Center under the Solar Resource Characterization Project [NREL, 2009]. This dataset contains "Hourly values of solar radiation and meteorological elements for a

1-year period" [NREL, 2009]. The TMY data is in its third iteration (TMY3). It is generated by looking across years of meteorological data for a given location and choosing the best representation of typical weather for a given month. TMY3 draws from the 1961-1990 and 1991-2005 National Solar Radiation Data Base archives [NREL, 2009]. TMY3 offers data for 1020 locations in the United States and represents "Typical rather than extreme conditions," making it perfectly suited for an extended time simulation [NREL, 2009]. HAMBASE uses seven categories of weather input from the TMY3 data, which are shown in Table 6.10.

Table 6.10: Weather Inputs to HAMBASE

Weather Input	Units
Direct normal irradiance (DNI)	W/m^2
Diffuse horizontal irradiance (DHI)	W/m^2
Cloud cover	0-8
Dry bulb air temperature	°C
Relative humidity	%
Wind direction	Degrees from North
Wind velocity	m/s

6.1.4.3 Temperature Control

The temperatures in the 15 conditioned zones of the building are controlled using a dual-setpoint thermostat model. An hourly temperature control setpoint schedule for heating and cooling operation is shown in Figure 6.11 and Figure 6.12, respectively.

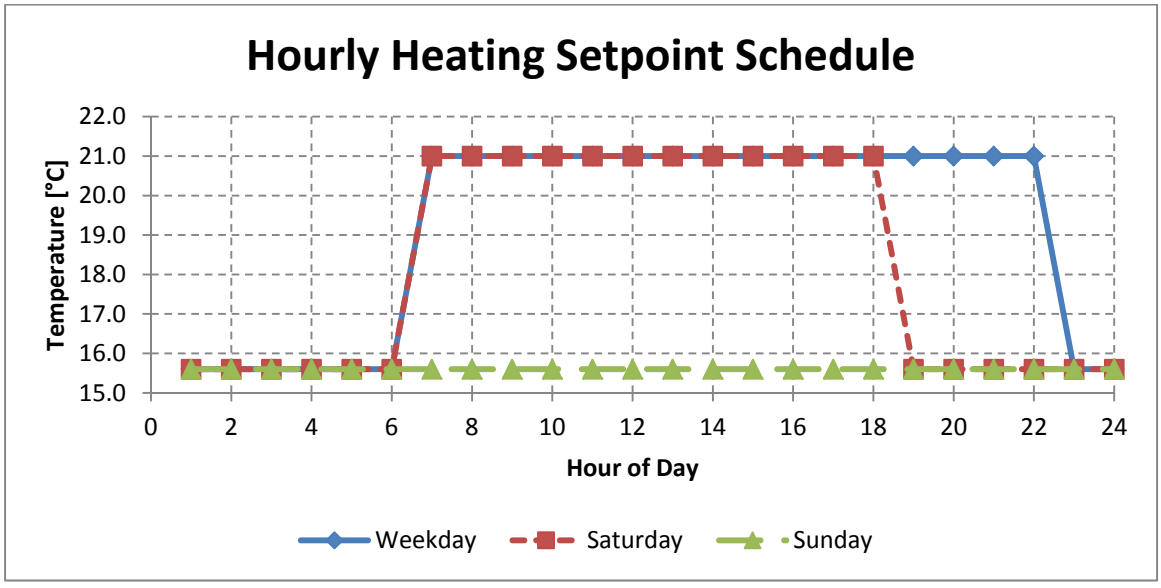

Figure 6.11: Hourly temperature control setpoint for heating

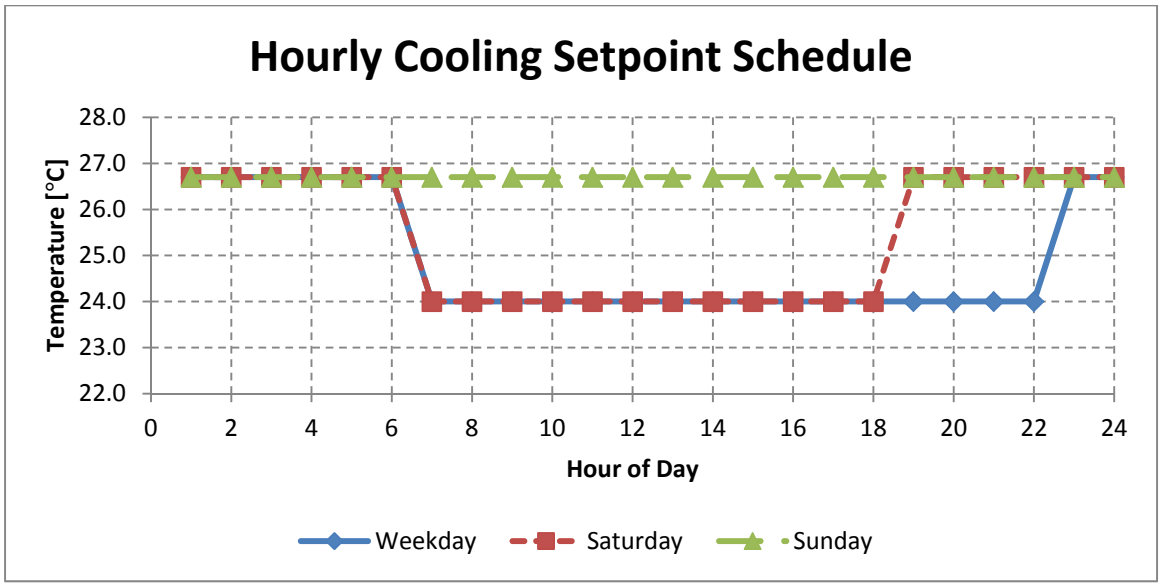

Figure 6.12: Hourly temperature control setpoint for cooling

The thermostat model includes a deadband of ±1°C (1.8°F) to eliminate the efficiency and control problems resulting from a bang-bang control. Example data

6.2 HEAT PUMP AND GROUND LOOP SIZING FOR IBL-GHP BASE CASE DESIGN OF COMMERCIAL OFFICE BUILDING

As discussed in Section 6.1, each floor has five conditioned zones (East, North, West, South, and Core) and one unconditioned plenum. Heat pump sizing for each zone was initially based on data from an EnergyPlus simulation. EnergyPlus uses design days, a worst case for cooling and a worst case for heating, to size equipment. The heat pump sizes based on EnergyPlus design days are shown in Table 6.11.

Table 6.11: Heat Pump Sizing based on EnergyPlus Design Days

	Peak Cooling Needed		Peak Heating Needed		HP Size Needed
Zone	[kW]	[tons]	[kW]	[tons]	[tons]
Core1	44.8	12.7	4.9	1.4	13.0
South1	10.0	2.9	9.5	2.7	3.0
East1	11.8	3.4	6.2	1.8	3.5
North1	9.4	2.7	9.2	2.6	3.0
West1	14.8	4.2	6.2	1.8	4.0
Core2	41.7	11.9	8.3	2.4	12.0
South2	12.0	3.4	10.5	3.0	3.5
East2	13.1	3.7	6.9	2.0	4.0
North2	11.3	3.2	10.3	2.9	3.5
West2	16.0	4.6	6.9	2.0	5.0
Core3	43.3	12.3	23.0	6.5	13.0
South3	13.0	3.7	13.8	3.9	4.0
East3	12.8	3.6	9.0	2.6	4.0
North3	13.4	3.8	13.6	3.9	4.0
West3	17.2	4.9	9.0	2.6	5.0

The EnergyPlus design day calculation estimated peak heating and cooling loads for each zone independently, but the EnergyPlus simulation did not use heat pumps in each zone. Instead, it used a variable-air-volume (VAV) HVAC system consisting of three large air conditioners, three large natural gas heaters, and one electric reheat heaters for each conditioned zone, as shown in Table 6.12.

Table 6.12: HVAC Capacity for EnergyPlus Variable Air Volume System

VAV System	Total Cooling Capacity [kW]	Total Cooling Capacity [tons]	Total Heating Capacity [kW]	Total Heating Capacity [tons]
Floor 1	139.5	39.7	21.2	0.0
Floor 2	135.9	38.7	20.9	0.0
Floor 3	151.1	43.0	20.2	0.0

EnergyPlus's floor capacities were not direct matches to HAMBASE's zonal-based approach, so the VAV heating and cooling system capacities were apportioned to the zones based on each zone's square footage. For example, the core zones represent 59% of the area of a given floor and therefore 59% of the total cooling and heating capacity of the floor's VAV system. The north and south zones each represent 12% of the area of a given floor, and east

and west zones each represent 8% of a given floor. The cooling and heating capacities resulting from this calculation are shown in Table 6.13 along with the resulting heat pump sizes.

Table 6.13: Heat Pump Sizing based on EnergyPlus HVAC Capacity

Zone	VAV Cooling Capacity [kW]	VAV Cooling Capacity [tons]	VAV Heating Capacity [kW]	Reheater Heating Capacity [kW]	Total Heating Capacity [tons]	HP Size Needed [tons]
Core1	82.7	23.5	12.6	39.9	14.9	24.0
South1	17.4	5.0	2.6	9.0	3.3	5.0
East1	11.0	3.1	1.7	10.5	3.5	3.5
North1	17.4	5.0	2.6	8.4	3.1	5.0
West1	11.0	3.1	1.7	13.2	4.2	4.5
Core2	80.5	22.9	12.4	36.4	13.9	24.0
South2	16.9	4.8	2.6	10.7	3.8	5.0
East2	10.7	3.1	1.7	11.7	3.8	4.0
North2	16.9	4.8	2.6	10.1	3.6	5.0
West2	10.7	3.1	1.7	14.3	4.5	5.0
Core3	89.5	25.4	12.0	38.6	14.4	26.0
South3	18.8	5.4	2.5	11.6	4.0	6.0
East3	11.9	3.4	1.6	11.4	3.7	4.0
North3	18.8	5.4	2.5	12.0	4.1	6.0
West3	11.9	3.4	1.6	15.3	4.8	5.0

These two methods of estimating heat pump sizes formed the starting point for a sizing study using the actual HAMBASE model. For each zone, a range of heat pump sizes were chosen and simulated for one year. The amount of time (unmet hours) each zone was unable to meet the thermostat setpoint was then tabulated. The results for the first floor zones are shown in Figure 6.13. Floors two and three had results consistent with the first floor for all zones except the core (the first floor core has the elevator load).

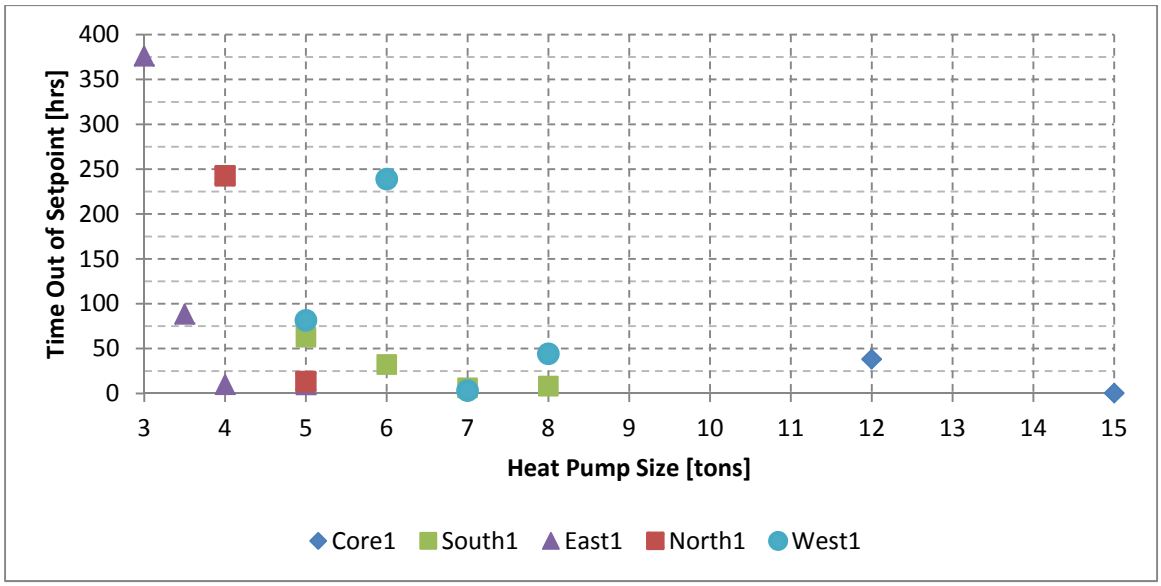

Figure 6.13: Results of heat pump sizing study

Based on the sizing study results, the final heat pump sizes used in the HAMBASE simulation are shown in Table 6.14.

Table 6.14: Heat Pump Sizes used in the HAMBASE Model

Floor	Heat Capacity by Zones (tons)				
	South	East	North	West	Core
Floor 1	7	4	5	5	15
Floor 2	7	4	5	5	10
Floor 3	7	4	5	5	10

Ground loop sizing was performed using GLHEPRO and the Peak Load Analysis Tool that accompanies GLHEPRO. The Peak Load Analysis Tool takes hourly cooling and heating loads for a building and converts them into a table of values that can be used as inputs to GLHEPRO. The table of values includes total heating, total cooling, peak heating and peak cooling for the building by month. The maximum heat pump EWTs were chosen to be 32.2°C (90°F). Note that the residential building design used the heat pump shutoff temperature as the maximum heat pump EWT; this temperature was too high for the commercial office building application.

To generate the hourly loads, the HAMBASE model was simulated without a ground loop. The hourly heating and cooling loads for all zones were combined, and the resulting hourly building totals were used in the Peak Load Analysis Tool to generate the data shown in Tables 6.15a (SI) and 6.15b (BI).

Table 6.15a: HAMBASE Building Loads used as GLHEPRO Inputs

	Total Loads [kW-h]		Peak Loads [kW]	
Month	Heating	Cooling	Heating	Cooling
January	15721	8606	235	164
February	6515	9275	190	184
March	3328	25620	160	246
April	239	48769	84	285
May	82	66723	27	309
June	0	87865	0	319
July	0	100035	0	326
August	0	94823	0	333
September	41	68741	19	307
October	131	53613	53	317
November	2087	25253	95	275
December	15494	11964	256	193
Duration of Peak Load (hrs)			3	9

Table 6.15b: HAMBASE Building Loads (BI units) used as GLHEPRO Inputs

	Total Loads [kBtu]		Peak Loads [kBtu/hr]	
Month	Heating	Cooling	Heating	Cooling
January	53639	29363	801	560
February	22230	31646	649	629
March	11356	87415	546	841
April	815	166399	287	972
May	280	227660	91	1054
June	0	299794	0	1089
July	0	341319	0	1112
August	0	323535	0	1135
September	141	234544	66	1049
October	448	182926	181	1080
November	7122	86164	323	940
December	52866	40821	874	658
	Duration of Peak Load [hrs]		3	9

With the heat pump loads incorporated into GLHEPRO, the remaining inputs were material properties for the ground soil, circulating fluid and bore field geometry. A summary of all of the properties used in the GLHEPRO sizing are shown in Table 6.16.

Table 6.16: Ground Loop Properties used for the Base Model in GLHEPRO

Geometry Properties				
Dimension	SI Value	Units	BI Value	Units
Bore Field Shape	Rectangle	-		
Bore Field Size	10 x 16	bores		
Depth	171	m	561.1	ft
Total GHEX Length	27363.8	m	89776.2	ft
Borehole Spacing	6.1	m	20	ft
Borehole Diameter	127	mm	5	in
Shank Spacing	25.4	mm	1	in
U-Tube Inner Diameter	35.1	mm	1.38	in
U-Tube Outer Diameter	42.3	mm	1.666	in
Thermal Properties				
Dimension	SI Value	Units	BI Value	Units
U-Tube Conductivity	0.39	W/(m·°K)	0.225	Btu/(hr·ft^2·°F)
U-Tube Capacitance	1542	kJ/(m^3·°K)	22.99	Btu/(ft^3·°F)
Grout Conductivity	1.7	W/(m·°K)	1	Btu/(hr·ft^2·°F)
Grout Capacitance	3901	kJ/(m^3·°K)	58.17	Btu/(ft^3·°F)
Ground Conductivity	2.1	W/(m·°K)	1.2	Btu/(hr·ft^2·°F)
Ground Capacitance	2343	kJ/(m^3·°K)	34.94	Btu/(ft^3·°F)
Undisturbed Ground Temp.	22	°C	72	°F
Fluid Properties				
Dimension	SI Value	Units	BI Value	Units
Antifreeze	None			
Convection Coefficient	1534	W/(m^2·°K)	270.2	Btu/(hr·ft^2·°F)
Fluid Factor	1	-		
Flow Rate per Borehole	0.126	L/s	2	gal/min
Total Flow Rate	20.2	L/s	320	gal/min
Simulation Properties				
Dimension	SI Value	Units	BI Value	Units
Borehole Resistance	0.103	(°K·m)/W	0.1775	(°F·hr·ft)/Btu
Max HP Entering Water Temp.	32.2	°C	90	°F
Min HP Entering Water Temp.	-6.7	°C	20	°F
Duration of Sizing	180	months		

6.3 IBL-GHP BASE CASE COMMERCIAL OFFICE BUILDING VALIDATION

The office building was based on a generic medium office building created by DoE's Commercial Reference Building Models [US DoE, 2010]. The DoE implementation exists in

EnergyPlus. EnergyPlus and HAMBASE make different simplifying assumptions, requiring a robust validation process that can isolate the effects of these differences.

In addition to some differences in the underlying physics governing the processes, the EnergyPlus and HAMBASE models use different HVAC systems to provide cooling and heating to the zones. The EnergyPlus implementation uses three variable air volume (VAV) HVAC systems; each floor has a single direct expansion cooling coil to provide cooling and a natural gas furnace for heating. Reheat coils in each zone are then used to adjust the main supply temperature to an appropriate zone supply temperature. The HAMBASE implementation uses an individual heat pump to provide heating and cooling for each conditioned zone. In order to validate the HAMBASE implementation, it was necessary to eliminate the effects of the HVAC system and instead focus on open-loop system responses (e.g. operation with no HVAC system). Closed-loop response (e.g. operation with the HVAC system operational) will still be used in validation, but only to confirm order of magnitude values due to the differences in the HVAC systems.

6.3.1 Test Overview

The results in this section will compare EnergyPlus and HAMBASE simulation results using open-loop and closed-loop tests. The open-loop tests are designed to compare the underlying fundamental models that EnergyPlus and HAMBASE employ for heat transfer and moisture transfer by removing the HVAC system and allowing the temperature and humidity within each zone to float freely. Within these tests there are two general inputs: external weather and internal loads. The closed-loop tests are designed to give order of magnitude comparisons for heating and cooling requirements in the zones.

6.3.2 Testing Standard

The use of the term validation in this section does not imply that EnergyPlus results are the standard; a review of ASHRAE's 140-2007 standard shows that using eight different widely-used building load models results in a large range of responses to standardized building and weather inputs [ASHRAE, 2007]. The ranges found in ASHRAE 140-2007 will be used as the testing standard in this validation.

6.3.1.1 Standards for Open-Loop Temperature Tests

A summary of results from ASHRAE Standard 140-2007 for open-loop (free-floating temperature) tests is shown in Table 6.17. These tests turn off the HVAC system (no heating or cooling), and as a result, the temperatures of the zones can float to equilibrium positions. Comparing the energy analysis computer programs that generated the maximum and minimum floating temperatures for a category gives an upper-bound for "acceptable" free-floating temperature deviations. The eight computer programs had a maximum range of 5°C (9°F) when comparing the maximum annual hourly zone temperatures, a maximum range of 4.8°C (8.6°F) when comparing minimum annual hourly zone temperatures, and a maximum range of 1.7°C (3.1°F) when comparing the average annual hourly zone temperatures. The benchmark used for these tests will be the average of the maximum ranges, or 3.3°C (5.9°F), which is approximately a 7% difference.

Table 6.17: Free-floating Temperature Results from ASHRAE 140-2007

Maximum Annual Hourly Zone Temperature [C°]					
Case	Min	Max	Mean	Max-Min	(Max-Min)/Min
600FF	64.9	69.5	65.2	4.6	7%
900FF	41.8	44.8	43.1	3.0	7%
650FF	63.2	68.2	64.7	5.0	8%
950FF	35.5	38.5	36.5	3.0	8%
Minimum Annual Hourly Zone Temperature [C°]					
Case	Min	Max	Mean	Max-Min	(Max-Min)/Min
600FF	-18.8	-15.6	-17.6	3.2	-17%
900FF	-6.4	-1.6	-4.2	4.8	-75%
650FF	-23	-21.6	-22.7	1.4	-6%
950FF	-20.2	-18.6	-19.6	1.6	-8%
Average Annual Hourly Zone Temperature [C°]					
Case	Min	Max	Mean	Max-Min	(Max-Min)/Min
600FF	24.2	25.9	25.1	1.7	7%
900FF	24.5	25.9	25.2	1.4	6%
650FF	18.0	19.6	18.7	1.6	9%
950FF	14.0	15.0	14.4	1.0	7%

6.3.1.2 Standards for Closed-Loop Temperature Tests

A summary of heating and cooling results from ASHRAE Standard 140-2007 for closed-loop (HVAC is on) tests are shown in Table 6.18 and Table 6.19 These tests have both a heating set-point and a cooling set-point in place so that the zone temperatures are controlled to within a specified range.

Table 6.18: Closed-loop Annual Heating & Cooling Results from ASHRAE 140-2007

Annual Heating [MWh]					
Case	Min	Max	Mean	Max-Min	(Max-Min)/Min
610-600	0.021	0.098	0.057	0.1	367%
620-600	0.138	0.682	0.318	0.5	394%
630-620	0.267	0.551	0.421	0.3	106%
640-600	-2.166	-1.545	-1.882	0.6	-29%
900-600	-3.837	-3.126	-3.344	0.7	-19%
910-900	0.179	0.442	0.321	0.3	147%
920-900	2.07	2.505	2.227	0.4	21%
930-920	0.595	1.08	0.819	0.5	82%
Annual Sensible Cooling [MWh]					
Case	Min	Max	Mean	Max-Min	(Max-Min)/Min
610-600	-2.227	-1.272	-1.867	1.0	-43%
620-600	-2.96	-2.341	-2.614	0.6	-21%
630-620	-1.845	-0.984	-1.367	0.9	-47%
640-600	-0.32	-0.153	-0.24	0.2	-52%
900-600	-4.624	-3.833	-4.154	0.8	-17%
910-900	-1.561	-0.832	-1.231	0.7	-47%
920-900	-0.323	0.016	-0.125	0.3	-105%
930-920	-1.174	-0.682	-0.9	0.5	-42%

The difference in annual heating energy (shown in Table 6.18) between the computer programs with the largest and smallest annual values was 0.7MWh, and the difference in annual cooling was 0.9MWh. The average of all heating and cooling ranges was 0.5MWh. If the HAMBASE implementation used an identical HVAC system as the EnergyPlus implementation, 0.5MWh would be the benchmark used for comparing annual heating and cooling.

The difference in peak heating rate (shown in Table 6.19) between the computer programs with the largest and smallest peak values was 1.1kW, and the difference in peak cooling was 0.8kW. The average of all peak heating and cooling ranges was 0.4kW. If the HAMBASE implementation used an identical HVAC system as the EnergyPlus implementation, 0.4kW would be the benchmark used for comparing peak heating and cooling.

Table 6.19: Closed-loop Peak Heating & Cooling Results from ASHRAE 140-2007

Peak Heating [KW]					
Case	Min	Max	Mean	Max-Min	(Max-Min)/Min
610-600	-0.011	0.001	-0.003	0.0	-109%
620-600	-0.008	0.24	0.062	0.2	-3100%
630-620	-0.021	0.003	-0.003	0.0	-114%
640-600	1.546	2.6	2.03	1.1	68%
900-600	-0.587	-0.414	-0.494	0.2	-29%
910-900	0.003	0.019	0.008	0.0	533%
920-900	0.192	0.458	0.298	0.3	139%
930-920	0.027	0.047	0.034	0.0	74%
Peak Sensible Cooling [KW]					
Case	Min	Max	Mean	Max-Min	(Max-Min)/Min
610-600	-0.811	-0.116	-0.472	0.7	-86%
620-600	-2.56	-1.716	-2.118	0.8	-33%
630-620	-0.842	-0.371	-0.592	0.5	-56%
640-600	-0.08	-0.033	-0.051	0.0	-59%
900-600	-3.355	-2.81	-3.071	0.5	-16%
910-900	-1.122	-0.31	-0.714	0.8	-72%
920-900	-0.517	0.048	-0.313	0.6	-109%
930-920	-0.721	-0.387	-0.527	0.3	-46%

6.3.3 **Open-Loop Tests of HAMBASE Building Load Model**

A variety of open-loop tests were used to compare the HAMBASE and EnergyPlus implementations of the building model. A summary of the tests is shown in Table 6.20 and Table 6.21. The tests in Table 6.20 are covered in detail in the following sections. The tests in Table 6.21 are referenced in the following sections, but the supporting graphs and data can be found in Blair [Blair, 2013].

Table 6.20: Summary of Open-loop Validation Tests

Test Set	Internal Loads	Weather Input	Objective
1	None	Constant weather	Compare non-excited steady-state values
2	None	Temperature-step	Compare time constants
3	None	Relative Humidity (RH)-step	Compare time constants
4	None	Temp, RH, DNI, DHI-sine wave	Compare DC offset, phase shift and amplitude
5	None	Actual weather	Compare max and min free-floating temperatures
6	All	Constant weather	Compare max and min free-floating temperatures
7	All	Actual weather	Compare max and min free-floating temperatures

Table 6.21: Summary of Supplementary Open-loop Validation Tests

Test Set	Internal Loads	Weather Input	Objective
8	None	Temperature and RH-sine wave	Compare DC offset, phase shift and amplitude
9	None	DNI (Direct Normal Irradiance)-sine wave	Compare DC offset, phase shift and amplitude
10	None	DHI (Diffuse Horizontal Irradiance)-sine wave	Compare DC offset, phase shift and amplitude
11	People	Constant weather	Compare steady-state values
12	Lighting	Constant weather	Compare steady-state values
13	Equipment	Constant weather	Compare steady-state values

Tests 1, 2, 3, 4, 5, 8, 9 and 10 assessed the material properties of the building's construction by eliminating all internal loads and applying various external weather files. The weather file was modified to create different excitations of temperature, relative humidity and solar radiation. The input excitations used were constant, ramp, step and sinusoidal. For all of these tests the HVAC system was turned off, and ventilation was set to zero. Infiltration was

kept constant throughout the tests with unique value for each zone based on the external surface area of the zone.

Tests 6, 7, 11, 12 and 13 confirmed that the effects of sensible, latent, radiant and convective internal loads were consistent between EnergyPlus and HAMBASE.

6.3.3.1 Test Set 1: Open-Loop, Constant Weather, No Internal Loads

An external weather file was created with constant dry bulb temperature, humidity, wind speed and cloud cover, as listed in Table 6.22. Direct radiation and diffuse radiation were set to zero. Recall that the HVAC system was turned off and internal loads and ventilation were set to zero. The test was intended to measure the zonal responses of the HAMBASE and EnergyPlus building envelopes to constant external weather inputs.

Table 6.22: Open-loop constant weather inputs

Input Variable	Constant Value
Direct normal solar irradiance [W/m^2]	0
Diffuse horizontal solar irradiance [W/m^2]	0
Cloud cover [0 – 10]	10
Dry bulb temperature [°C]	22
Relative Humidity [%]	50
Wind direction [degrees north]	0
Wind velocity [m/s]	0

The temperature and relative humidity responses for Core1 for both EnergyPlus and HAMBASE are shown in Figure 6.14 for a 15-day period. The data show a steady-state temperature difference of 0.70°C (1.3°F). The percent error from the expected value of 22°C (71.6°F) was +0.5% for EnergyPlus compared to -1.5% for HAMBASE. The steady-state relative humidity difference was 0.6 percentage points. The percent error from the expected value of 50% relative humidity was -0.9% for EnergyPlus and +0.3% for HAMBASE. Similar responses and % differences were found for all 18 zones in the office building.

While the steady-state errors of HAMBASE and EnergyPlus were of the same magnitude, HAMBASE showed a transient temperature response during the first 24 hours of simulation. HAMBASE has no built-in warm up period to eliminate start-up transience, where EnergyPlus pre-simulates three days of operation before beginning to collect data. Pre-simulation allows the model time to reach equilibrium, resulting in the slow monotonic response toward 22°C (71.6°F) during first 24 hours of the EnergyPlus response. HAMBASE lacks a built-in warm-up period, and as a result, it has a transient period before ultimately moving into a monotonic trend toward 22°C (71.6°F). The transient period was most pronounced in first-floor zones, as shown by the responses of East2 in Figure 6.15 and South3 in Figure 6.16.

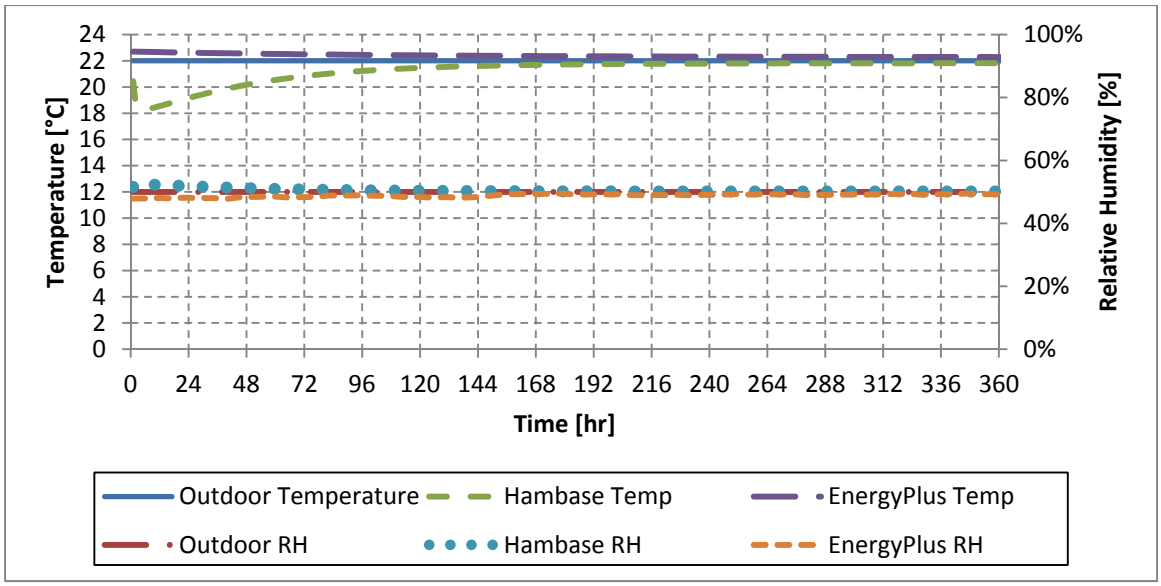

Figure 6.14: Open-loop responses of Core1 to constant weather inputs

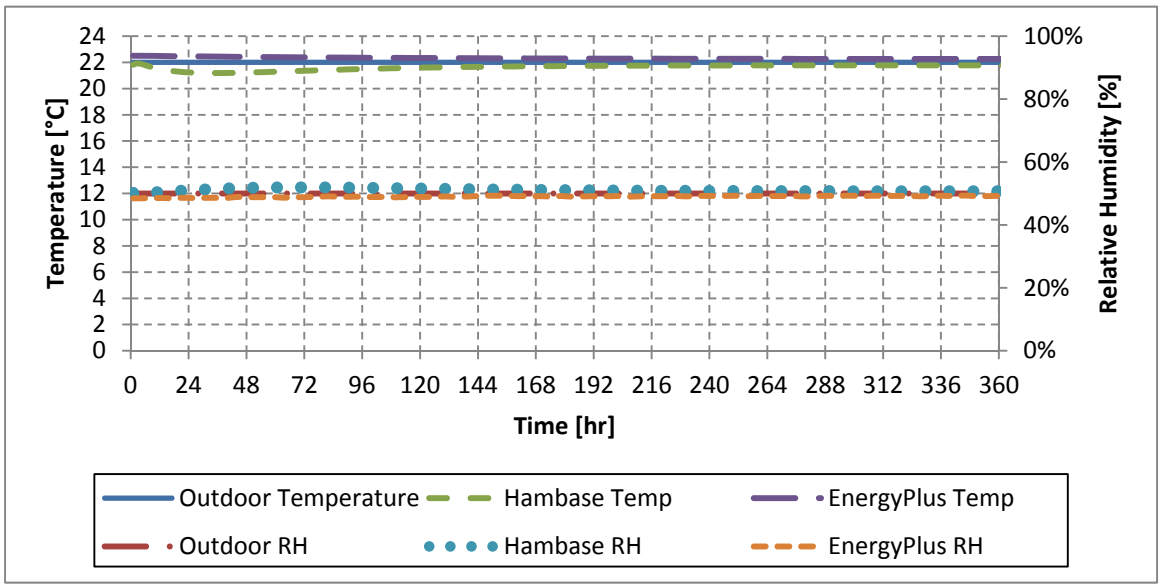

Figure 6.15: Open-loop responses of East2 to constant weather inputs

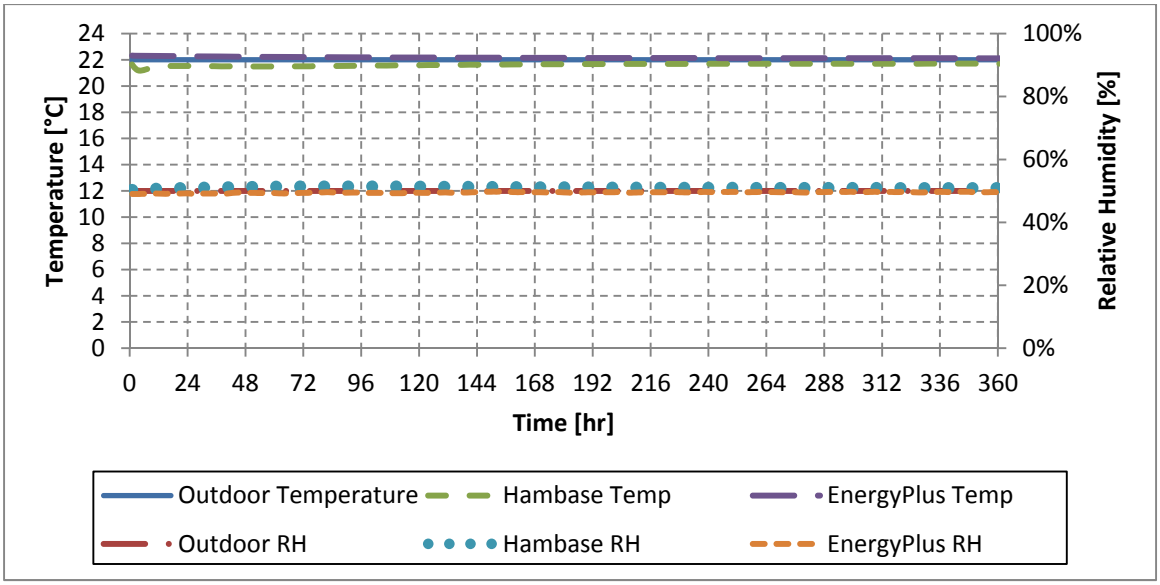

Figure 6.16: Open-loop responses of South3 to constant weather inputs

The average steady-state temperature of all 18 zones is shown in Table 6.23. For all zones the HAMBASE model showed a steady-state temperature less than ambient temperature of 22°C (71.6°F), while the EnergyPlus model showed a steady-state temperature greater than ambient temperature for all zones except the four first-floor perimeter zones. On average, a zone by zone comparison shows the HAMBASE zone temperatures to be 0.44°C (0.8°F) lower than EnergyPlus temperatures.

Table 6.23: Average Temperature of All Zones

Temperature	HAMBASE	EnergyPlus
Average steady-state temperature [°C]	21.76	22.20
Difference from expected value [°C]	-0.24	0.20
Steady-state temperature error	-1.11%	0.89%

The average steady-state relative humidity of the building's 18 zones is shown in Table 6.24. For all zones the HAMBASE model showed a steady-state relative humidity greater than the ambient relative humidity of 50%, while the EnergyPlus model showed a steady-state relative humidity less than the ambient relative humidity except in the four first-floor perimeter zones. On average, a zone by zone comparison shows the HAMBASE relative humidity to be 1.2 percentage points lower than EnergyPlus relative humidity.

Table 6.24: Average relative humidity of all zones

Relative Humidity	HAMBASE	EnergyPlus
Average steady-state relative humidity [RH%]	50.64%	49.49%
Difference from expected value [RH%]	1.29%	-1.02%
Steady-state relative humidity error	0.64%	-0.51%

The data from the open-loop constant weather input tests show excellent steady-state agreement between HAMBASE and EnergyPlus for both temperature and relative humidity.

6.3.3.2 Test Set 2: Open-Loop, Ambient Temperature-Step, No Internal Loads

The constant weather file was altered to create a temperature-step input with temperature of 22°C (71.6°F) for 7 days before a step decrease to 10°C (50°F). All other weather inputs were held constant to values shown in Table 6.22. Recall, the HVAC system was turned off and internal loads and ventilation were set to zero. Figure 6.17 shows the responses for Core1.

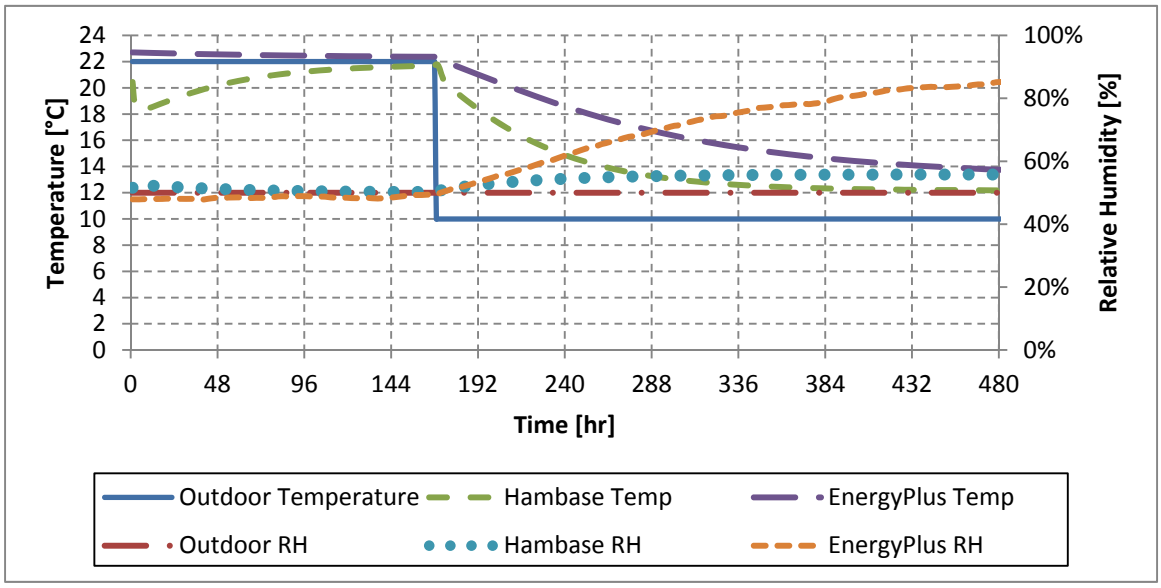

Figure 6.17: Open-loop response of Core1 to ambient temperature-step input

The HAMBASE Core1 temperature response is faster with a time constant of 45.33 hours compared to 88 hours for EnergyPlus. Both HAMBASE and EnergyPlus have a steady-state temperature of approximately 12°C (53.6°F) because the ground temperature remains at 22°C (71.6°F) which provides a warming effect to the zone.

The relative humidity for core zones in EnergyPlus went to 100% due to the absence of moisture transport properties in conjunction with ventilation turned off and no exterior walls to allow infiltration. The ASHRAE psychometric chart shown in Figure 6.18 shows this process using an orange dashed line. The moisture content in the air stays constant while the temperature drops to 10°C (50°F), resulting in a relative humidity of approximately 100%.

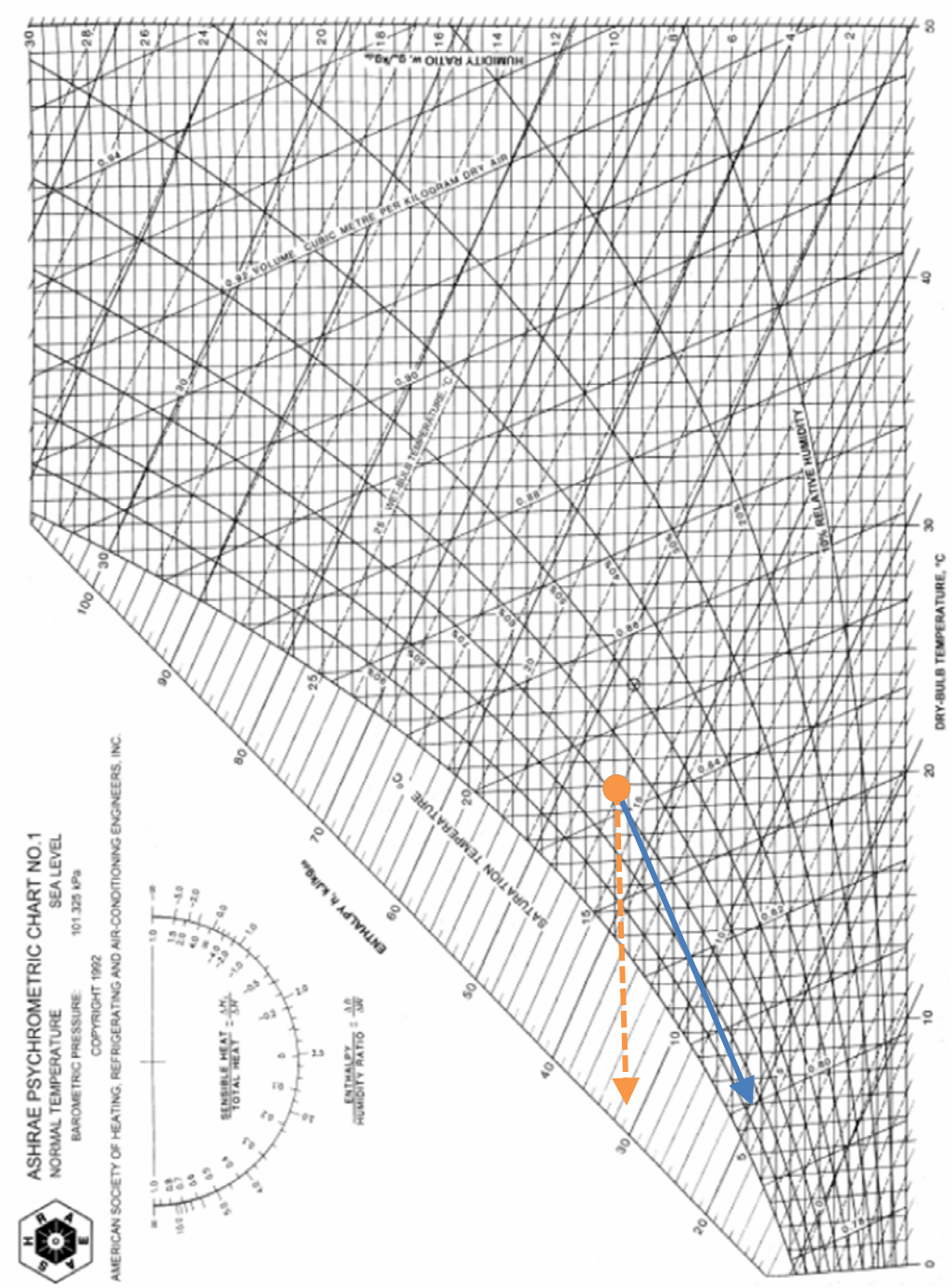

Figure 6.18: ASHRAE psychometric chart showing perimeter zones in blue-solid and core zones in orange-dash for Test Set 2 [ASHRAE, 2009]

The relative humidity response in HAMBASE also increases in the absence of ventilation and infiltration, but it only approaches 60% as opposed to the expected 100%. The results of Test Set 11 in [Blair, 2013] show that the core zone responds with 100% relative humidity to an internal moisture source. This leads to the conclusion that the physics of the core zones in

HAMBASE and EnergyPlus are similarly moisture impenetrable, but HAMBASE is less responsive to changes in relative humidity resulting from temperature change.

Looking at the response of a perimeter zone, as shown in Figure 6.19 and Figure 6.20, reveals the impact of infiltration on the relative humidity response. Where the Core1 zone lacked any external walls and as a result infiltration, the East2 and South3 zones both have one external wall, allowing infiltration to equalize relative humidity in the zone. These responses match the process shown on the psychometric chart by the blue-solid line in Figure 6.18.

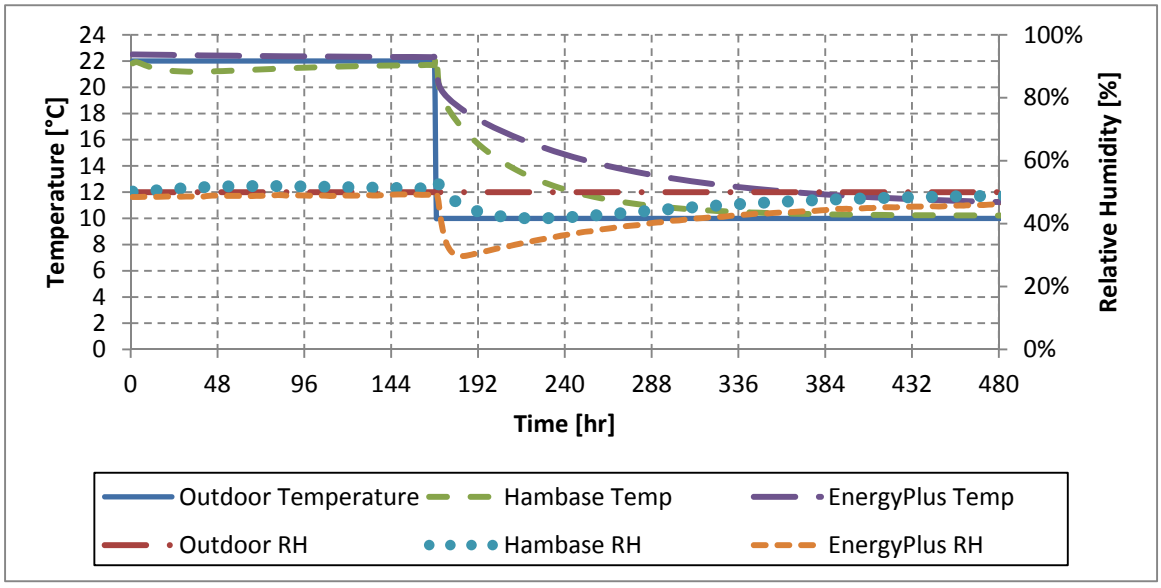

Figure 6.19: Open-loop response of East2 to ambient temperature-step input

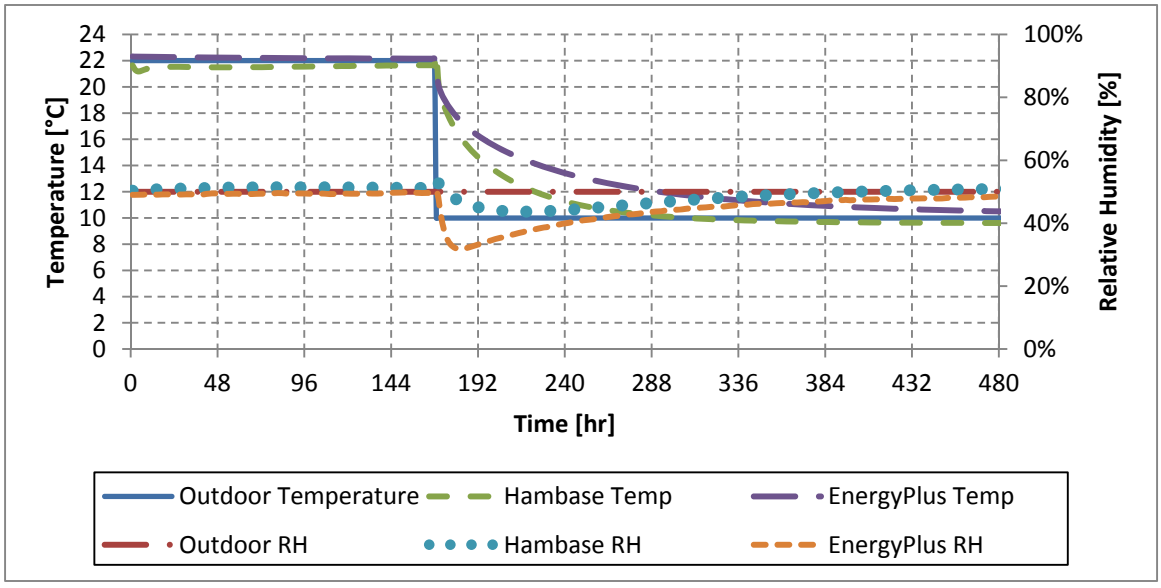

Figure 6.20: Open-loop response of South3 to ambient temperature-step input

The steady-state temperature values for all zones are shown in Table 6.25. The effect of the 22°C (71.6°F) ground temperature is seen in the higher steady-state values for the first-floor zones in both HAMBASE and EnergyPlus. The steady-state values for HAMBASE are lower than EnergyPlus in every zone, which is consistent with the results of Test Set 1. The HAMBASE values for third-floor zones are lower than the outdoor air temperature, implying that the sky temperature for HAMBASE is lower than in EnergyPlus.

Table 6.25: Temperature Results for Open-loop Temperature-step Input

	Steady-State Temperature [°C]		Absolute Error [°C]		Percent Error	
Zone	HB	EP	HB	EP	HB	EP
Core1	12.2	13.6	2.2	3.6	21.7%	36.3%
South1	11.3	12.3	1.3	2.3	13.4%	23.0%
East1	11.3	12.2	1.3	2.2	13.2%	22.3%
North1	11.3	12.3	1.3	2.3	13.4%	23.1%
West1	11.3	12.2	1.3	2.2	13.2%	22.3%
Plenum1	11.1	12.4	1.1	2.4	10.6%	24.2%
Core2	10.4	11.9	0.4	1.9	4.3%	18.5%
South2	10.2	11.2	0.2	1.2	2.1%	12.0%
East2	10.2	11.2	0.2	1.2	2.1%	11.7%
North2	10.2	11.2	0.2	1.2	2.1%	12.1%
West2	10.2	11.2	0.2	1.2	2.1%	11.7%
Plenum2	10.0	11.2	0.0	1.2	-0.2%	12.2%
Core3	9.6	10.8	-0.4	0.8	-3.9%	8.2%
South3	9.6	10.5	-0.4	0.5	-3.9%	4.5%
East3	9.6	10.4	-0.4	0.4	-3.9%	4.4%
North3	9.6	10.5	-0.4	0.5	-3.9%	4.6%
West3	9.6	10.4	-0.4	0.4	-3.9%	4.4%
Plenum3	9.3	10.3	-0.7	0.3	-7.0%	2.6%
Average	10.4	11.4	0.7	1.4	6.9%	14.3%

Comparing the time constants for a given model across different zones shows consistency between HAMBASE and EnergyPlus, as seen in Table 6.26. Both programs show the largest time constant value (slowest response) for the first-floor zones and smallest value (fastest response) for the third-floor zones, which is consistent with their distance from the ground heat-source. On a given floor, both programs show the core zones responded approximately 10% slower than the perimeter zones, which is consistent with the zones sizes.

Comparing the time constants between the programs shows HAMBASE responding approximately twice as quickly as EnergyPlus in every zone, as seen in Table 6.26. While this

difference is significant, a time constant standard does not exist. Changing material properties of the HAMBASE model to better match the EnergyPlus response is an option to improve the time constant match, but this approach was rejected in favor of using identical material values between the programs. The faster response exhibited by HAMBASE will result in higher estimates of the annual heating and cooling values.

Table 6.26: EnergyPlus & HAMBASE Time Constant for Ambient Temperature-step Input

Zone	Hambase Time Constant [hr]	EnergyPlus Time Constant [hr]
Core1	54.3	113.0
South1	43.7	94.3
East1	43.3	93.3
North1	43.7	94.3
West1	43.3	93.3
Plenum1	50.0	104.7
Core2	50.7	102.3
South2	44.7	90.7
East2	44.3	89.7
North2	44.7	90.7
West2	44.3	89.7
Plenum2	46.7	94.3
Core3	45.3	88.0
South3	39.7	76.7
East3	39.7	75.7
North3	39.7	76.7
West3	39.7	75.7
Plenum3	38.3	67.7
Average	44.2	89.5

6.3.3.3 Test Set 3: Open-Loop, Ambient Relative Humidity-Step, No Internal Loads

The constant weather file was altered to create a relative humidity-step input with a relative humidity value of 30% for seven days before a step decrease to 80%. All other weather inputs were held constant to values shown in Table 6.22 Recall, the HVAC system was turned off and internal loads and ventilation were set to zero. Figure 6.21 shows the response for Core1.

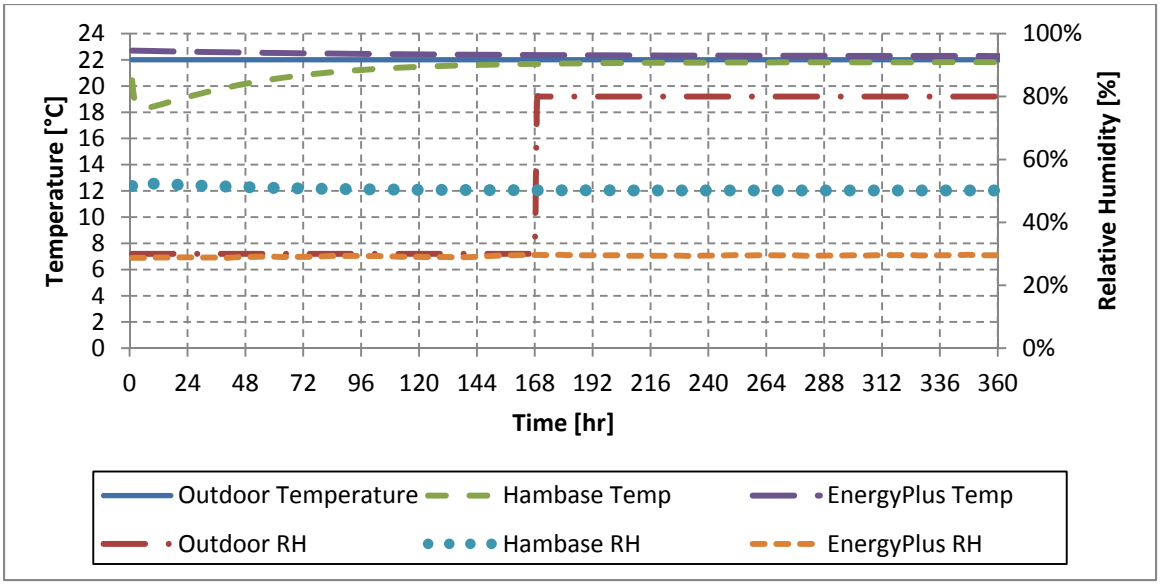

Figure 6.21: Open-loop response of Core1 to ambient relative humidity-step input

Consistent with the results from Test Set 2, no moisture transport occurs in the core zones, so the change in outdoor air moisture does not cause a response in Core1 for either EnergyPlus or HAMBASE. The difference in steady-state relative humidity value results from the warm-up period built into EnergyPlus. The warm-up period changes initial conditions for all the zones, while the initial conditions for HAMBASE remain at 22°C (71.6°F) and 50% relative humidity.

The responses of perimeter zones, as shown in Figure 6.22 and Figure 6.23 show EnergyPlus responding faster than HAMBASE when moisture transport occurs via infiltration. Both programs approach steady-state relative humidity of 80%, as shown in Table 6.27. The HAMBASE values in all zones and the first-floor values from EnergyPlus climb above 80% due to the slightly lower air temperatures in these zones.

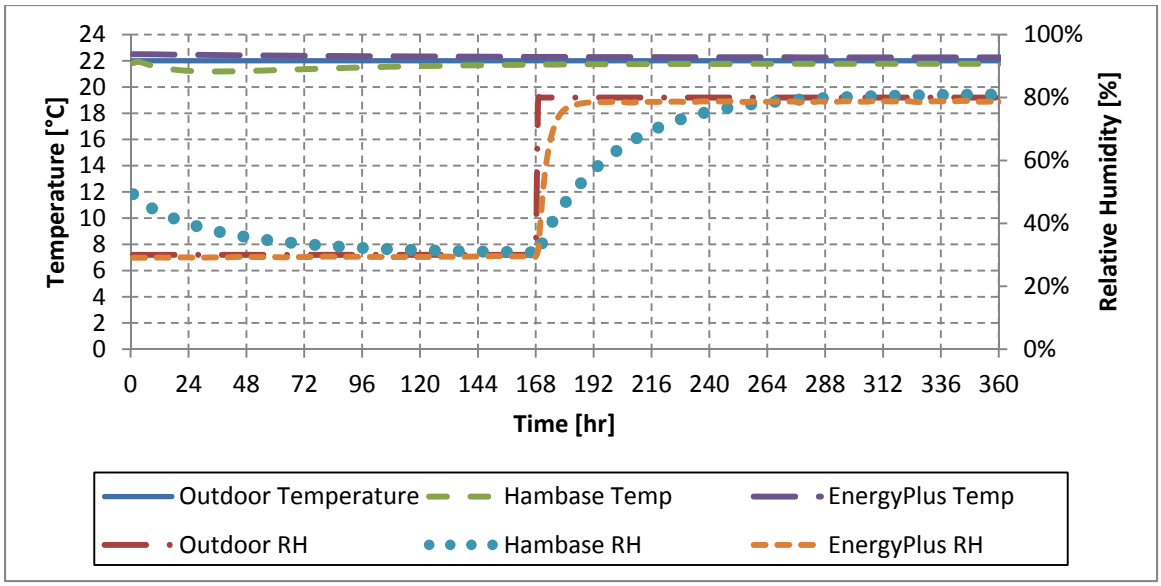

Figure 6.22: Open-loop response of East2 to ambient relative humidity-step input

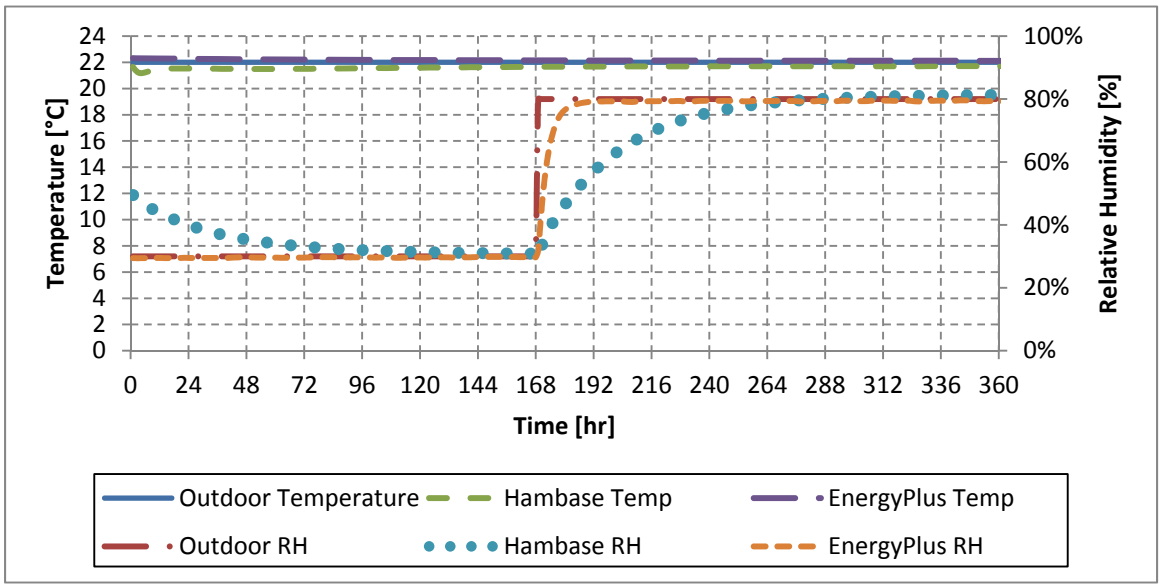

Figure 6.23: Open-loop response of South3 to ambient relative humidity-step input

Table 6.27: Relative Humidity Results for Open-loop RH-step Input

	Steady-State RH [%]		Absolute Error [%]		Percent Error	
Zone	**HB**	**EP**	**HB**	**EP**	**HB**	**EP**
Core1	50.1%	29.9%	N/A	N/A	N/A	N/A
South1	80.8%	80.0%	0.8%	0.0%	1.0%	0.0%
East1	80.8%	80.1%	0.8%	0.1%	1.0%	0.1%
North1	80.8%	80.0%	0.8%	0.0%	1.0%	0.0%
West1	80.8%	80.1%	0.8%	0.1%	1.0%	0.1%
Plenum1	80.7%	77.9%	0.7%	-2.1%	0.8%	-2.6%
Core2	50.1%	29.3%	N/A	N/A	N/A	N/A
South2	81.0%	78.7%	1.0%	-1.3%	1.3%	-1.6%
East2	81.0%	78.7%	1.0%	-1.3%	1.3%	-1.6%
North2	81.0%	78.7%	1.0%	-1.3%	1.3%	-1.7%
West2	81.0%	78.7%	1.0%	-1.3%	1.3%	-1.6%
Plenum2	81.0%	77.7%	1.0%	-2.3%	1.2%	-2.9%
Core3	50.1%	29.7%	N/A	N/A	N/A	N/A
South3	81.4%	79.4%	1.4%	-0.6%	1.7%	-0.8%
East3	81.4%	79.4%	1.4%	-0.6%	1.7%	-0.7%
North3	81.4%	79.3%	1.4%	-0.7%	1.7%	-0.8%
West3	81.4%	79.4%	1.4%	-0.6%	1.7%	-0.7%
Plenum3	82.0%	79.9%	2.0%	-0.1%	2.5%	-0.1%
Average	75.9%	70.9%	0.9%	0.7%	1.2%	0.9%

Time constants for all zones except core zones are listed in Table 6.28. EnergyPlus consistently responds between six and eight times as fast as HAMBASE in all zones. Changing material properties and infiltration rates in HAMBASE could bring the response rates into better agreement, but this option was rejected in favor of using the same properties and rates in both programs.

Table 6.28: EnergyPlus and HAMBASE time constant for ambient RH-step input

Zone	Hambase Time Constant [Hr]	EnergyPlus Time Constant [Hr]
Core1	N/A	N/A
South1	22.33	4.00
East1	22.33	4.00
North1	22.33	4.00
West1	22.33	4.00
Plenum1	63.67	9.67
Core2	N/A	N/A
South2	32.67	4.00
East2	32.33	4.00
North2	32.67	4.00
West2	32.33	4.00
Plenum2	64.00	9.67
Core3	N/A	N/A
South3	33.00	4.00
East3	32.67	4.00
North3	33.00	4.00
West3	32.67	4.00
Plenum3	8.67	1.33

6.3.4 **Test Set 4: Open-Loop, Weather-Sine, No Internal Loads**

The constant weather file was altered to create a combined temperature, relative humidity, DNI and DHI-sine input. The TMY3 weather data was reviewed to find a representative summer day. With the day of August 16 chosen, the weather data was then used for sine-wave curve-fits. The temperature and relative humidity data are shown in Figure 6.24 while the direct normal irradiance (DNI) and diffuse horizontal irradiance (DHI) data are shown in Figure 6.25. The remainder of the constant weather file from Table 6.22 remained unchanged. The temperature and relative humidity data were used independently in Test Set 8, shown in [Blair, 2013]. The DNI and DHI data were used independently in Test Set 9, shown in [Blair, 2013], and Test Set 10, shown in [Blair, 2013].

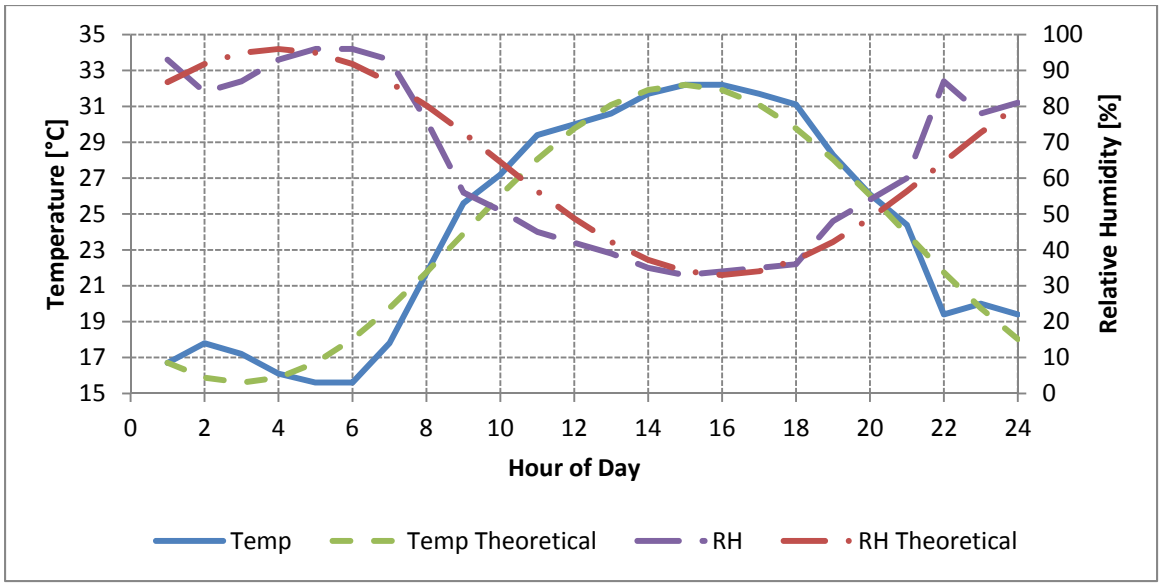

Figure 6.24: Temperature and relative humidity curves for 8/16/2004 used in Test Set 4

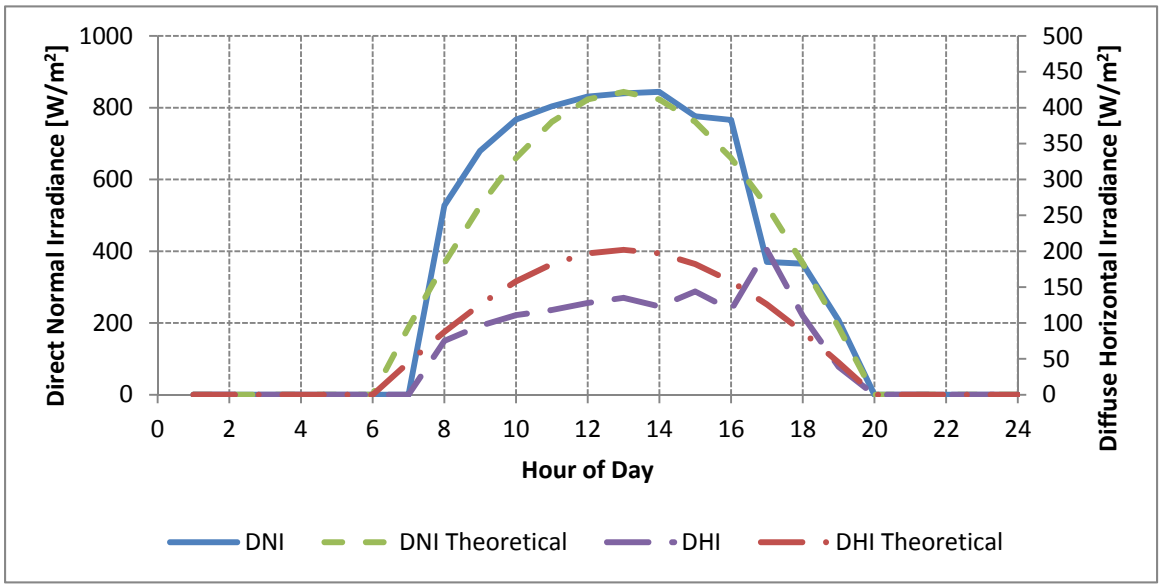

Figure 6.25: Direct and diffuse irradiance curves for 8/16/2004 used in Test Set 4

The complete response of Core1 is shown in Figure 6.26. The faster temperature response of HAMBASE can be seen in the greater amplitude of the Core1 temperature oscillations; 3.4°C (6.1°F) for HAMBASE versus 1.1°C (2.0°F) for EnergyPlus. The lower steady-state temperature value of HAMBASE can be seen in lower center amplitude; 28°C (82.4°F) compared to 30°C (86.0°F) for EnergyPlus. The effect of EnergyPlus' warm-up period and HAMBASE's lack of warm-up period can be seen in the responses over the first six days; 22°C (71.6°F) initial temperature for HAMBASE, 29°C (84.2°F) for EnergyPlus. The frequency of the HAMBASE and

EnergyPlus responses align, as do the locations of the peaks and troughs. The locations of peaks and troughs for the Core zones correspond to a lagged peak outdoor air temperature because of the cores insulation from direct exposure to DNI, DHI and direct outdoor air. A five-day view of steady-state response for Core1 is shown in Figure 6.27.

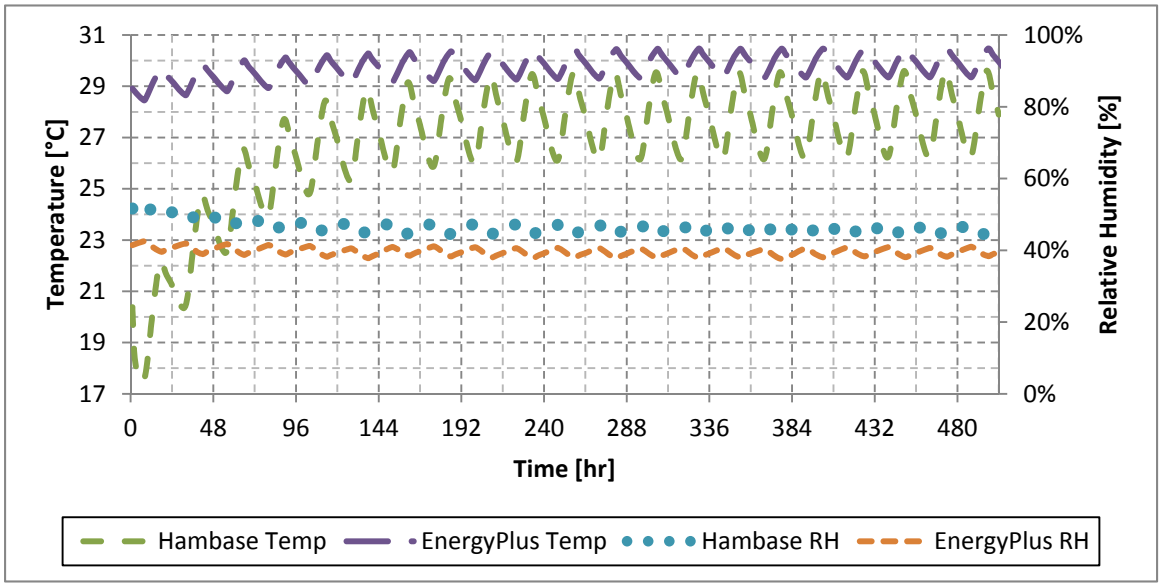

Figure 6.26: Open-loop response of Core1 to weather-sine input

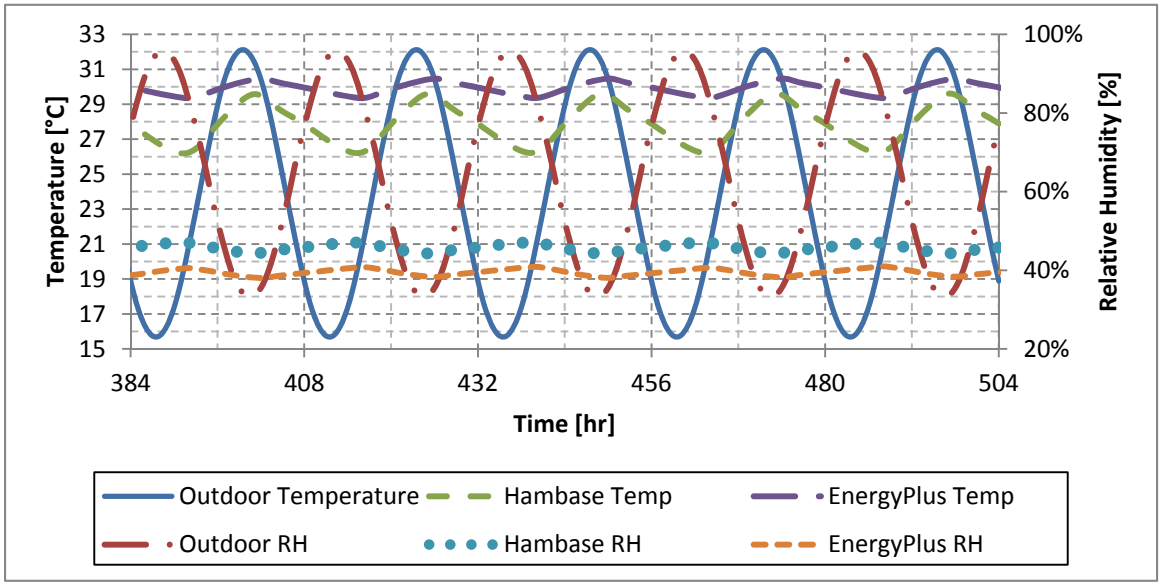

Figure 6.27: Open-loop steady-state response of Core1 to weather-sine input

Five-day steady-state response for East2 and South3 are shown in Figure 6.28 and Figure 6.29, respectively. For both zones, the effect of sun position on DNI can be seen in the altered temperature response. For East2, direct sunlight in the morning causes a bimodal response;

one early in the morning from DNI and a second in early afternoon from high outdoor temperature and high DHI. For South3, the peak temperature response directly aligns with peak temperature, as South3 does not receive significant DNI during summer months.

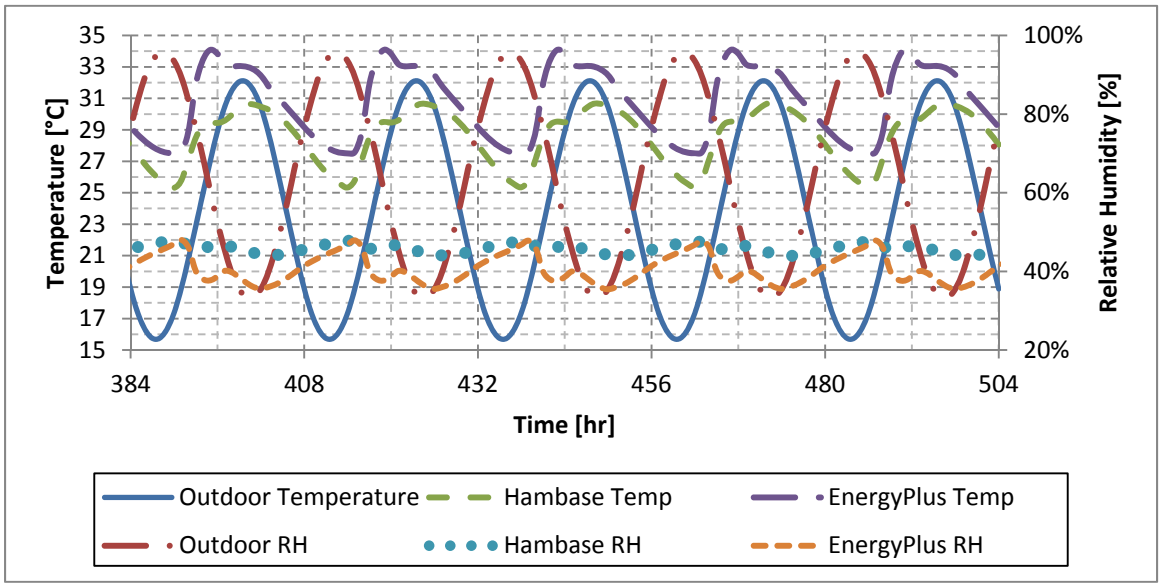

Figure 6.28: Open-loop steady-state response of East2 to weather-sine input

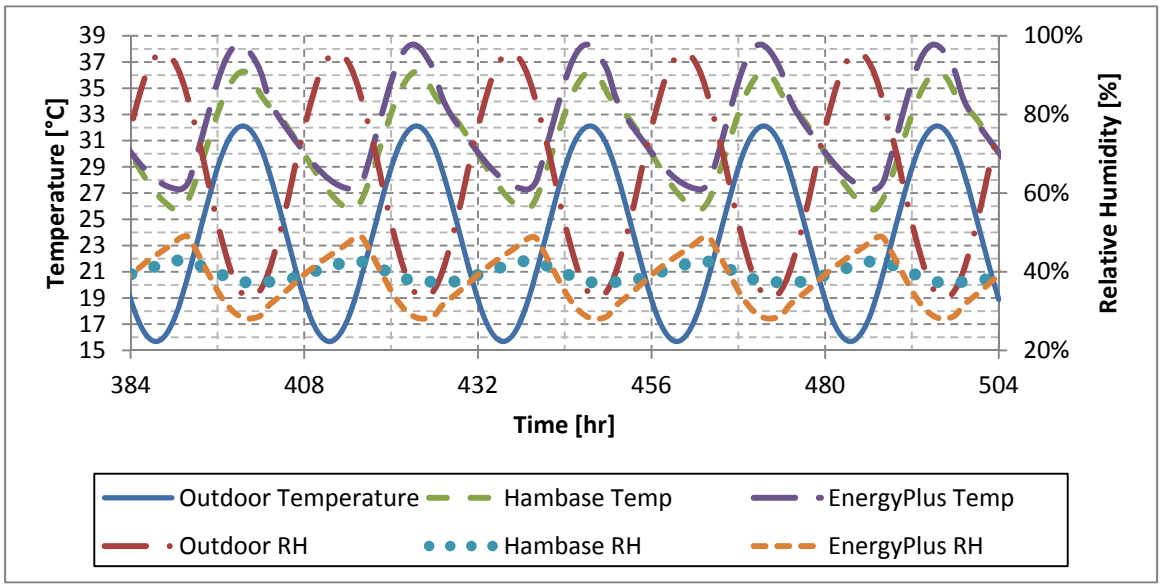

Figure 6.29: Open-loop steady-state response of South3 to weather-sine input

The amplitude of the temperature response for perimeter zones is almost identical between HAMBASE and EnergyPlus, resulting from a greater sensitivity to DNI and DHI by EnergyPlus (DNI and DHI are individually analyzed in [Blair, 2013]. The amplitude of the temperature response for all zones, in addition to the steady-state maximum and minimum temperatures, is

shown in Table 6.29. The steady-state temperatures for HAMBASE are again lower than EnergyPlus, but the increased temperature responsiveness of HAMBASE (seen in the core zones) was approximately balanced by EnergyPlus' sensitivity to solar irradiance (seen in the perimeter zones).

Table 6.29: Temperature Results for Open-loop Weather-sine Input

	Steady-State Max Temperature [°C]		Steady-State Min Temperature [°C]		Steady-State Amplitude (Max-Min) [°C]	
Zone	HB	EP	HB	EP	HB	EP
Core1	29.61	30.48	26.21	29.34	3.40	1.13
South1	24.42	25.04	22.63	23.50	1.79	1.55
East1	23.71	25.37	22.59	23.42	1.13	1.94
North1	23.65	24.36	22.58	23.36	1.07	1.00
West1	25.23	25.65	22.63	23.45	2.60	2.20
Plenum1	23.72	24.60	23.01	24.27	0.71	0.33
Core2	23.58	24.82	23.32	24.61	0.26	0.21
South2	24.25	25.30	22.96	23.87	1.29	1.43
East2	23.70	25.59	22.92	23.80	0.78	1.79
North2	23.64	24.70	22.92	23.81	0.72	0.89
West2	24.76	25.83	22.96	23.83	1.79	1.99
Plenum2	23.84	24.71	23.37	24.39	0.47	0.32
Core3	24.28	24.60	23.42	24.17	0.87	0.43
South3	24.69	25.08	23.05	23.58	1.64	1.50
East3	24.04	25.17	23.01	23.51	1.04	1.66
North3	23.99	24.43	23.00	23.51	0.99	0.91
West3	25.19	25.56	23.03	23.54	2.16	2.03
Plenum3	25.83	24.15	22.83	23.12	2.99	1.03
Average	24.56	25.30	22.95	24.06	1.61	1.24

Results for relative humidity are shown in Table 6.30. Relative humidity response corresponds with results from previous tests.

Table 6.30: Relative Humidity Results for Open-loop Weather-sine Input

	Steady-State Max Temperature [°C]		Steady-State Min Temperature [°C]		Steady-State Amplitude (Max-Min) [°C]	
Zone	HB	EP	HB	Zone	HB	EP
Core1	47%	41%	44%	38%	3%	3%
South1	47%	46%	45%	42%	2%	4%
East1	47%	46%	46%	41%	1%	5%
North1	48%	46%	47%	43%	1%	3%
West1	47%	46%	44%	40%	3%	6%
Plenum1	46%	44%	46%	43%	0%	1%
Core2	49%	43%	49%	42%	0%	1%
South2	46%	45%	45%	41%	1%	4%
East2	47%	45%	46%	40%	1%	5%
North2	47%	45%	46%	42%	1%	3%
West2	46%	45%	45%	40%	1%	5%
Plenum2	46%	43%	45%	42%	0%	1%
Core3	49%	45%	49%	43%	0%	2%
South3	46%	45%	44%	42%	1%	4%
East3	46%	46%	45%	41%	1%	4%
North3	46%	46%	45%	43%	1%	3%
West3	46%	46%	44%	40%	2%	5%
Plenum3	46%	47%	42%	44%	4%	3%
Average	47%	45%	46%	42%	1%	3%

The results of Tests 1-4 show HAMBASE to have faster temperature response based on outdoor air, slower temperature response based on solar irradiance, and slower relative humidity in general.

6.3.3.5 Test Set 5: Open-Loop, Actual Weather, No Internal Loads

In Test Set 5, the actual TMY3 weather file was used. The HVAC system was still turned off and internal loads and ventilation were still set to zero. Figure 6.30 and Figure 6.31 show the temperature and relative humidity response of Core1 for one year and five days, respectively.

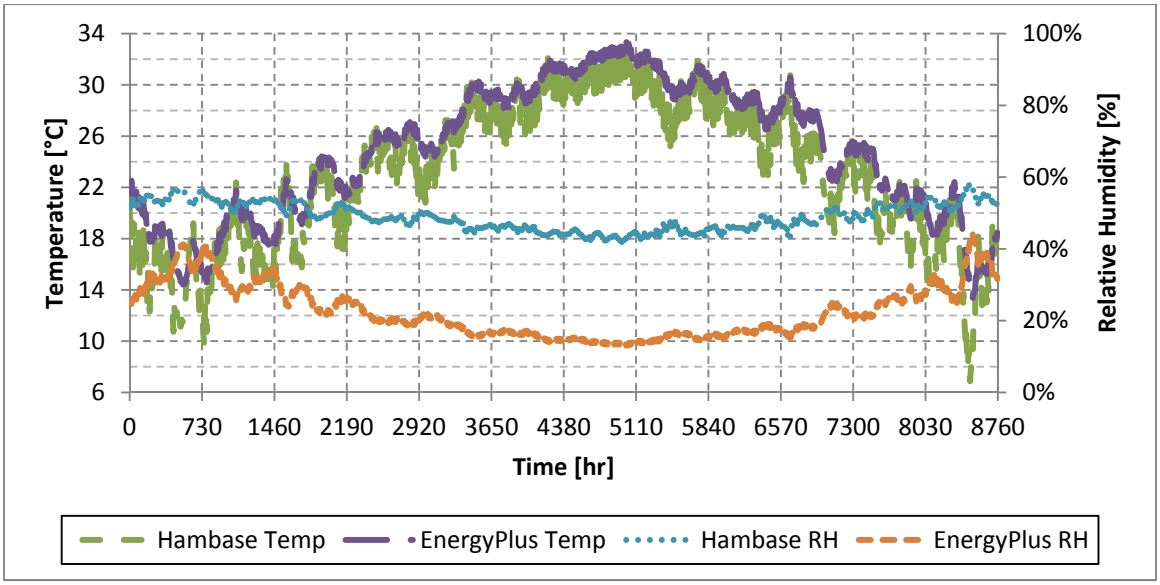

Figure 6.30: Open-loop response of Core1 to actual weather input for one year

The results of Test Sets 1-4 explain the results seen in the core zones. The core zones are not exposed to DNI or DHI, meaning that temperature responds faster in HAMBASE as seen by the thickness (amplitude) of the temperature plot in Figure 6.30. HAMBASE has lower temperatures. Relative humidity in HAMBASE is less responsive and has an initial condition of 50% with no warm-up period, meaning that it starts around 50% RH and basically remains there. The warm-up period in EnergyPlus results in lower initial relative humidity and the greater responsiveness results in a larger range of values. The humidity in core zones does not change rapidly in either program due to the absence of moisture transport.

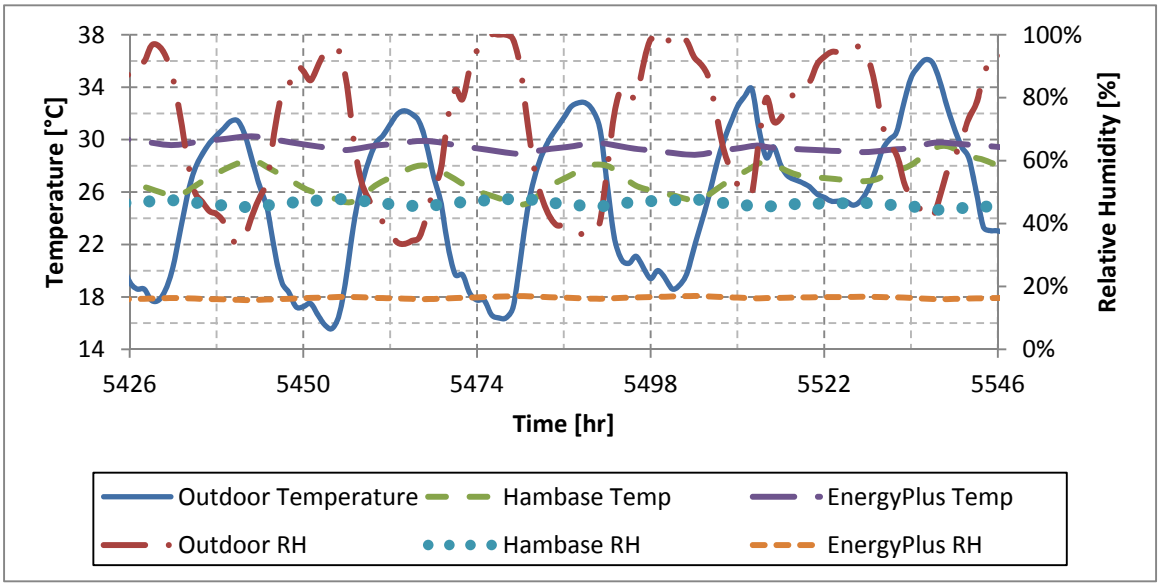

Figure 6.31: Open-loop response of Core1 to actual weather input for Aug 15–19

The results for the perimeter zones, shown in Figures 6.32 through 6.35, again display the effect infiltration and radiation have on the zone responses. The temperature and relative humidity for East2 and South3 are much noisier than Core1.

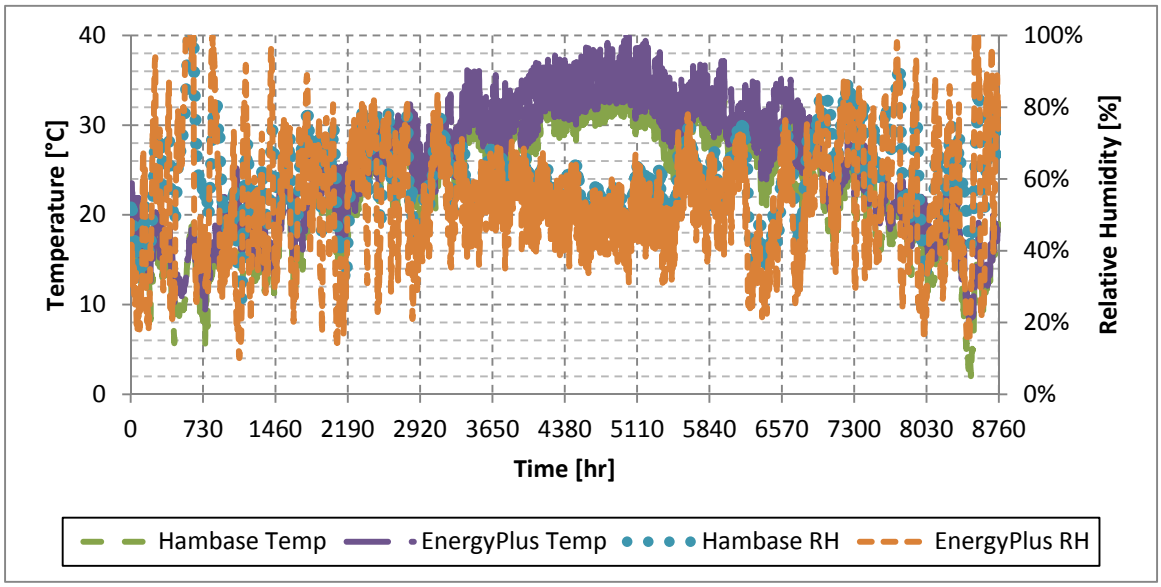

Figure 6.32: Open-loop response of East2 to actual weather input

The temperature responses for the two programs more closely match due to EnergyPlus' sensitivity to solar radiation. East2 again shows bimodal temperature peaks due to early morning DNI and early afternoon DHI and outdoor air temperatures.

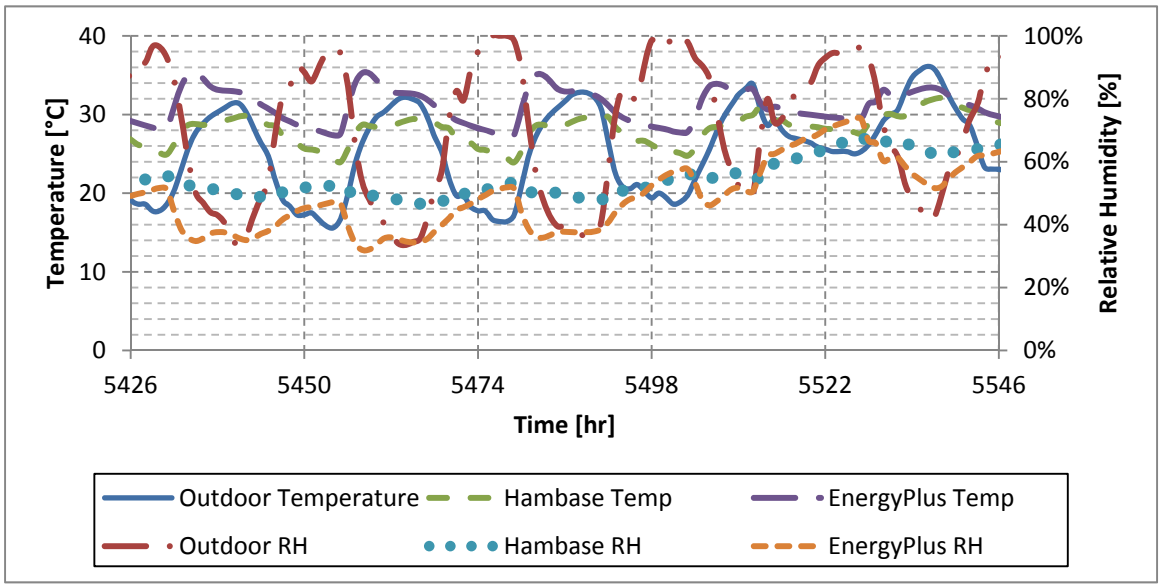

Figure 6.33: Open-loop response of East2 to actual weather input for Aug 15–19

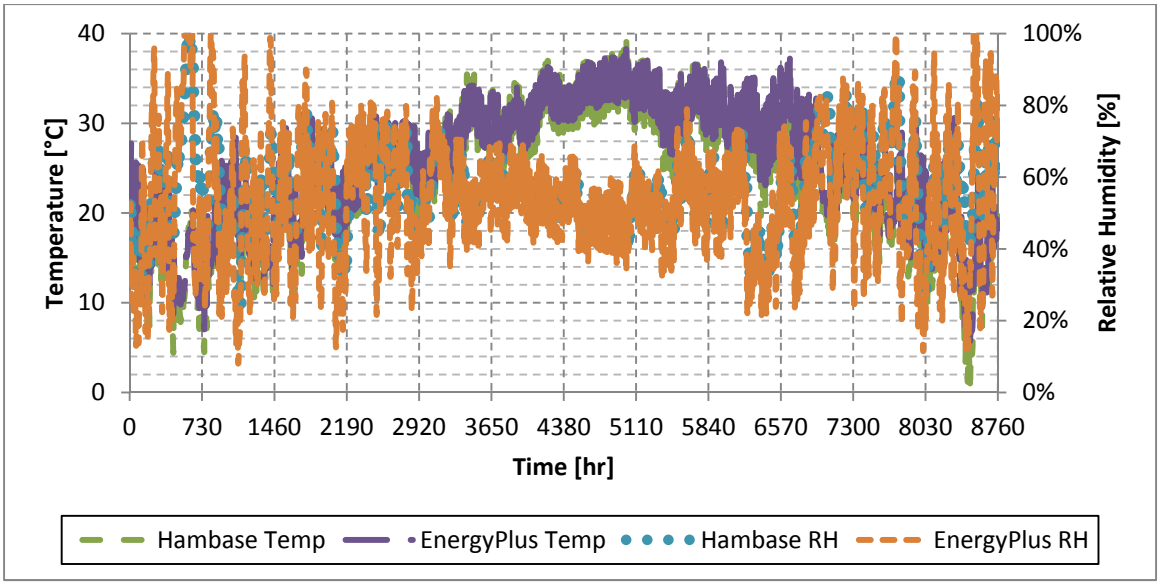

Figure 6.34: Open-loop response of South3 to actual weather input

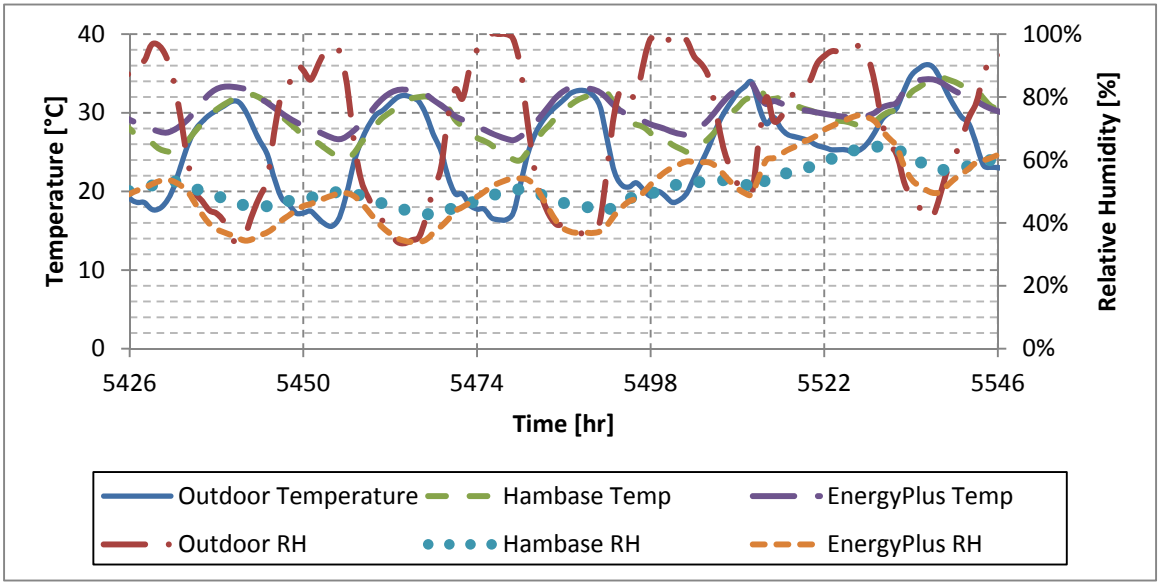

Figure 6.35: Open-loop response of South3 to actual weather input for Aug 15–19

Comparing the annual maximum and minimum temperatures, as seen in Table 6.31, brings together the testing standards and Test Sets. Annual maximum temperatures show close alignment between HAMBASE and EnergyPlus except for the east zones. The east zones represent the extreme case for the temperature sensitivities of HAMBASE and EnergyPlus. HAMBASE is sensitive to outdoor air temperature, but not as sensitive to DNI, so early morning temperatures in east zones will not climb significantly high. EnergyPlus is more sensitive to DNI and less sensitive to air temperatures, so the early morning temperatures will not negate the

morning sun, resulting in higher east zone temperatures. Similarly, annual minimum temperatures for HAMBASE are significantly lower than in EnergyPlus because all minimum temperatures will happen during the night, so the only influence on the zone temperature is the outdoor air temperature, to which HAMBASE is more sensitive.

Table 6.31: Temperature Results for Open-loop Actual Weather Input

	Annual Max. Hourly Temperature [°C]			Annual Min. Hourly Temperature [°C]			Annual Avg. Hourly Temperature [°C]		
Zone	HB	EP	Error	HB	EP	Error	HB	EP	Error
Core1	33.2	33.3	-0.1	6.9	13.2	-6.3	23.0	24.9	-1.8
South1	36.0	36.5	-0.5	3.0	10.2	-7.2	23.1	25.1	-2.0
East1	35.9	39.1	-3.2	2.7	8.9	-6.2	22.7	24.8	-2.1
North1	36.1	35.3	0.8	2.7	8.9	-6.2	22.4	23.9	-1.5
West1	42.4	41.8	0.7	2.8	9.3	-6.5	23.3	25.0	-1.7
Plenum1	34.9	35.3	-0.3	4.6	11.2	-6.7	23.2	25.2	-1.9
Core2	34.7	35.9	-1.2	4.3	10.1	-5.8	23.5	25.5	-2.0
South2	35.8	37.2	-1.4	2.3	8.1	-5.9	23.4	25.4	-2.0
East2	36.1	40.5	-4.4	2.0	7.4	-5.3	23.1	25.2	-2.1
North2	36.2	37.1	-1.0	2.0	7.5	-5.4	22.8	24.5	-1.7
West2	40.9	43.1	-2.2	2.1	7.7	-5.5	23.6	25.4	-1.8
Plenum2	36.3	36.7	-0.4	3.1	8.7	-5.6	23.8	25.3	-1.5
Core3	39.2	37.9	1.3	2.2	6.9	-4.7	24.4	25.2	-0.7
South3	39.2	38.3	0.9	0.8	5.4	-4.6	24.0	25.2	-1.1
East3	39.2	40.3	-1.1	0.6	4.6	-4.1	23.7	25.0	-1.2
North3	39.5	38.6	0.9	0.6	4.7	-4.1	23.5	24.3	-0.8
West3	44.1	44.4	-0.3	0.7	4.9	-4.3	24.2	25.1	-0.9
Plenum3	47.9	41.2	6.7	-0.8	2.6	-3.4	25.1	24.2	1.0
Average	38.2	38.5	-0.3	2.4	7.8	-5.4	23.5	25.0	-1.5

Comparing the building average to the testing standard for open-loop testing shows that the annual maximum hourly temperatures are easily within the range found in the ASHRAE 140-2007 BestTest data, 0.3°C difference for HAMBASE compared to a 5°C difference in BestTest. The annual min hourly temperature was close but ultimately fell outside of the BestTest range, 5.4°C for HAMBASE compared to 4.8°C in BestTest. The annual average hourly temperature fell within the BestTest range, 1.5°C for HAMBASE compared to 1.7°C for BestTest. On a zone-by-zone basis, there are zones that fall outside of the BestTest range on each of the three tests and there are zones that fall inside the BestTest range. Based on these results the two simulations of the model will give similar results on cooling, but different results on heating, with HAMBASE having larger heating values.

Looking at the relative humidity data shown in Table 6.32 gives a similar result. On average there is close alignment between EnergyPlus and HAMBASE, but EnergyPlus has larger extremes due to its greater sensitivity. EnergyPlus has both higher highs and lower lows.

Table 6.32: Relative Humidity Results for Open-loop Actual Weather Input

	Annual Max. Hourly RH [%]			Annual Min. Hourly RH [%]			Annual Avg. Hourly RH [%]		
Zone	HB	EP	Error	HB	EP	Error	HB	EP	Error
Core1	58.3	44.5	13.8	41.4	13.0	28.4	49.0	22.6	26.4
South1	98.5	100.0	-1.5	20.4	7.2	13.2	59.9	54.3	5.6
East1	99.1	100.0	-0.9	22.4	10.0	12.5	61.3	54.9	6.4
North1	99.1	100.0	-0.9	23.4	11.0	12.4	62.4	57.5	4.9
West1	98.8	100.0	-1.2	21.3	7.8	13.5	59.0	54.3	4.7
Plenum1	89.9	100.0	-10.1	33.1	12.2	20.9	59.8	53.8	6.0
Core2	55.6	54.5	1.1	43.1	11.3	31.8	49.0	22.4	26.6
South2	99.9	100.0	-0.1	23.8	7.5	16.3	58.9	53.2	5.8
East2	100.0	100.0	0.0	25.8	10.1	15.7	60.1	53.7	6.4
North2	100.0	100.0	0.0	26.7	10.9	15.8	61.0	55.5	5.5
West2	100.0	100.0	0.0	24.7	8.0	16.8	58.3	53.3	5.0
Plenum2	91.3	100.0	-8.7	33.0	12.5	20.6	57.8	53.3	4.6
Core3	56.1	68.3	-12.2	40.2	10.1	30.0	48.5	23.3	25.1
South3	98.6	100.0	-1.4	23.5	8.0	15.5	56.7	53.9	2.8
East3	99.1	100.0	-0.9	25.5	10.7	14.8	57.9	54.4	3.5
North3	99.2	100.0	-0.8	26.4	11.5	14.9	58.7	56.2	2.5
West3	98.8	100.0	-1.2	24.4	8.4	16.0	56.2	54.1	2.1
Plenum3	100.0	100.0	0.0	12.2	9.6	2.6	53.9	57.1	-3.2
Average	91.2	92.6	-1.4	27.3	10.0	17.3	63.9	82.6	7.8

6.3.3.6 Test Set 6: Open-Loop, Constant Weather, Actual Internal Loads

Test Set 6 shifts the focus from external weather to internal loads. For this test, all of the actual loads, including both their magnitudes and schedules, were used. Detailed description of the loads and schedules can be found in Sections 6.1 and 6.2, and a summary of the internal load profiles found in Section 6.2. The constant weather file described previously in Table 6.22 was used to eliminate weather effects. Similar tests for each type of internal load were also completed and can be found in [Blair, 2013] for people loads, lighting loads and equipment loads.

The temperature and relative humidity response for Core1 is shown in Figure 6.36 with 22 days of data and in Figure 6.37 with 6 days of data. The effect of the warm-up period in EnergyPlus can be seen by the initial zone conditions; 26°C (78.8°F) for EnergyPlus and 22°C

(71.6°F) for HAMBASE. Once the models reach steady-state they behave in a similar periodic manner, with both peaks and troughs matching. The amplitude of the HAMBASE response is larger than EnergyPlus again, just as was found in the weather tests. HAMBASE both gains and loses temperature faster than EnergyPlus.

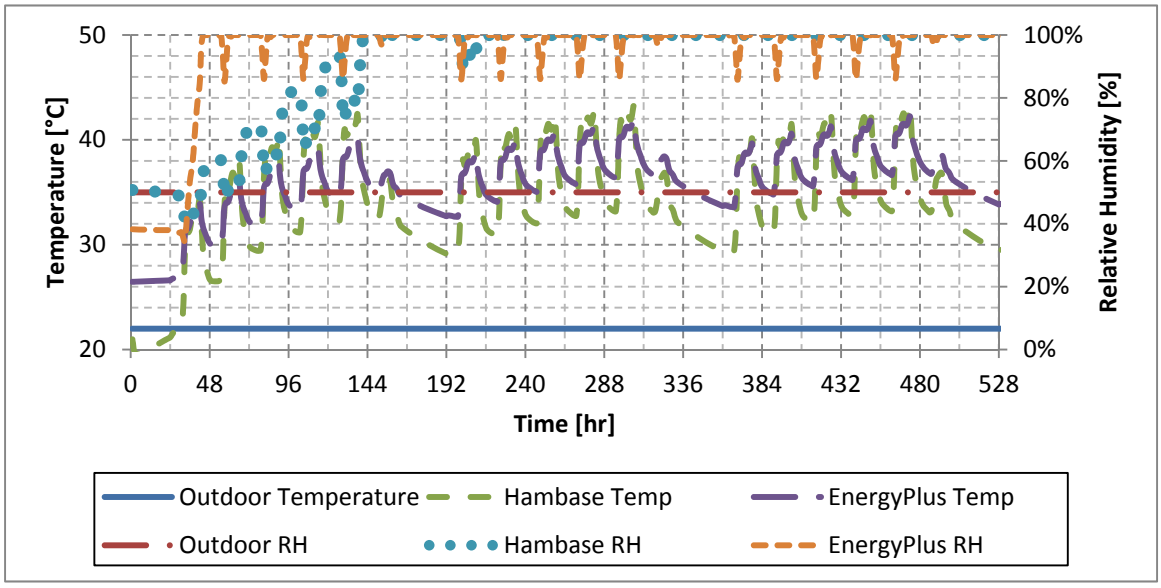

Figure 6.36: Open-loop response of Core1 to actual internal loads

The detailed data in Figure 6.37 further highlights the difference in temperature response, as the HAMBASE zone temperature closely matches the spikes in the load schedule while the EnergyPlus zone temperature is smoother.

The relative humidity response of both EnergyPlus and HAMBASE goes to 100% due to the large latent load from people and the lack of moisture transport in the core zones when ventilation is off.

The responses for perimeter zones East2 and South3 are shown in Figure 6.38 and Figure 6.39, respectively. In these zones, the trends of the HAMBASE temperatures match the trends of the EnergyPlus temperatures in everything but the steady-state value. They have similar periods, similar peaks and troughs and similar amplitudes. The faster temperature response of HAMBASE can still be seen during the Sunday operation in hours 504 to 528. During this period of no internal loads, the HAMBASE temperatures fall-off toward the outdoor air temperature faster than in EnergyPlus.

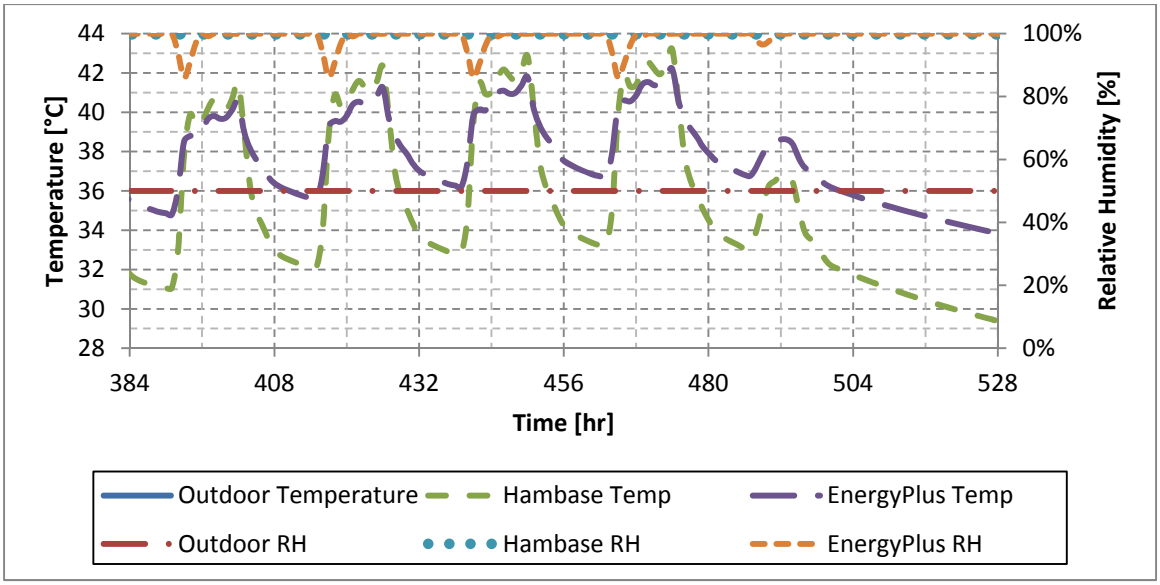

Figure 6.37: Open-loop steady-state response of Core1 to actual internal loads

The relative humidity responses for HAMBASE and EnergyPlus have similar steady-state values, but where the EnergyPlus response oscillates with an amplitude of 10%, the HAMBASE response barely moves. There are three factors contributing to the value of the zone relative humidity: infiltration of outdoor air, internal latent loads and changing indoor air temperature. Based on the lack of sensitivity of HAMBASE to relative humidity in general, this response is reasonable.

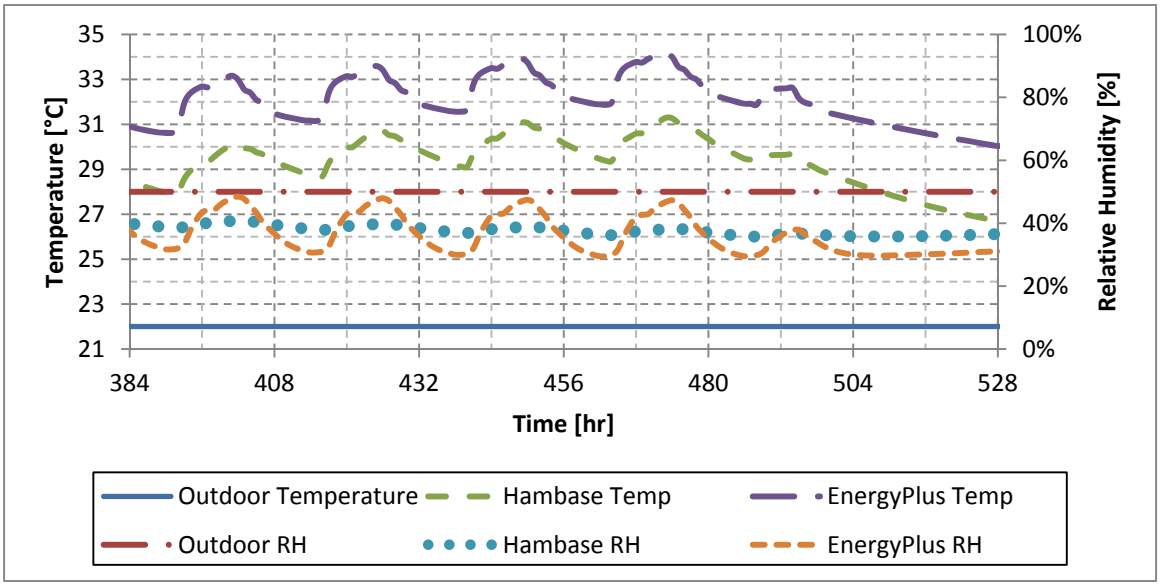

Figure 6.38: Open-loop steady-state response of East2 to actual internal loads

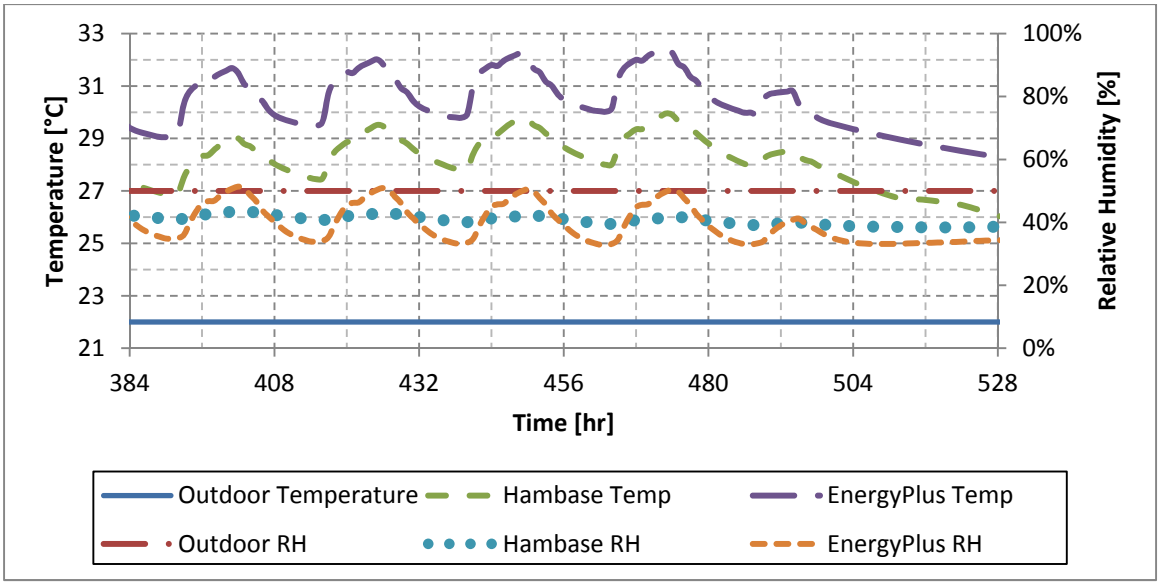

Figure 6.39: Open-loop steady-state response of South3 to actual internal loads

A summary of the temperature results for Test Set 6 are shown in Table 6.33. The maximum and minimum temperatures in EnergyPlus are consistently higher than in HAMBASE, but HAMBASE has slightly greater amplitude. This implies that the two programs have an approximately equivalent sensitivity to internal loads, but the external temperature sensitivity of HAMBASE prevents a closer match.

Table 6.33: Temperature Results for Open-loop, Actual Internal Load Input

	Steady-State Max Temperature [°C]		Steady-State Min Temperature [°C]		Steady-State Amplitude (Max-Min) [°C]	
Zone	HB	EP	HB	EP	HB	EP
Core1	43.19	42.29	29.38	33.71	13.81	8.57
South1	31.99	34.22	26.09	29.55	5.90	4.67
East1	31.73	33.99	26.00	29.37	5.73	4.62
North1	31.99	34.28	26.09	29.58	5.90	4.69
West1	31.73	33.99	26.00	29.37	5.73	4.62
Plenum1	35.48	36.10	27.86	32.06	7.62	4.04
Core2	35.96	38.81	28.87	33.42	7.08	5.39
South2	31.45	34.50	26.60	30.15	4.85	4.35
East2	31.30	34.27	26.54	29.98	4.76	4.29
North2	31.45	34.51	26.60	30.16	4.85	4.35
West2	31.30	34.27	26.54	29.98	4.76	4.29
Plenum2	33.19	34.25	27.50	31.00	5.70	3.24
Core3	33.84	36.02	27.78	30.76	6.06	5.27
South3	29.96	32.52	25.83	28.28	4.13	4.24
East3	29.82	32.31	25.78	28.13	4.04	4.18

North3	29.96	32.51	25.83	28.27	4.13	4.24
West3	29.82	32.31	25.78	28.13	4.04	4.18
Plenum3	30.21	29.78	25.51	26.85	4.70	2.93
Average	32.46	34.50	26.70	29.93	5.76	4.56

A summary of the relative humidity results for Test Set 6 are shown in Table 6.34. The maximum relative humidity values in EnergyPlus are higher, the minimum values are lower and the amplitude values are greater than in HAMBASE.

Table 6.34: Relative Humidity Results for Open-loop, Actual Internal Load Input

	Steady-State Max RH [%]		Steady-State Min RH [%]		Steady-State Amplitude (Max-Min) [%]	
Zone	HB	EP	HB	EP	HB	EP
Core1	100%	100%	100%	86%	0%	14%
South1	42%	50%	36%	30%	5%	19%
East1	42%	49%	37%	30%	5%	19%
North1	42%	50%	36%	30%	5%	19%
West1	42%	49%	37%	30%	5%	19%
Plenum1	31%	28%	25%	22%	6%	6%
Core2	100%	100%	100%	97%	0%	3%
South2	41%	50%	36%	29%	5%	21%
East2	41%	49%	36%	29%	5%	20%
North2	41%	50%	36%	29%	5%	21%
West2	41%	49%	36%	29%	5%	20%
Plenum2	33%	30%	28%	24%	5%	5%
Core3	100%	100%	100%	97%	0%	3%
South3	44%	52%	38%	33%	5%	19%
East3	43%	51%	38%	33%	5%	18%
North3	44%	52%	38%	33%	5%	19%
West3	43%	51%	38%	33%	5%	18%
Plenum3	40%	37%	32%	32%	8%	6%
Average	50%	55%	46%	40%	4%	15%

6.3.3.7 Test Set 7: Open-Loop, Actual Weather, Actual Internal Loads

The final open-loop test uses the actual weather file and the actual internal loads as the inputs to the model. The response of the Core1 zone is shown in Figure 6.40 for a full year of data. Detailed six-day responses during winter conditions and summer conditions are shown in Figure 6.41 and Figure 6.42, respectively.

The responses to Test Set 7 are truly a superposition of the responses found in Test Set 5 and Test Set 6. HAMBASE and EnergyPlus still display different initial conditions resulting from

the warm-up period in EnergyPlus. HAMBASE still displays greater responsiveness to outdoor temperature, as evidenced by the larger amplitude of temperature oscillations and the faster night and weekend temperature fall-off. EnergyPlus still displays greater relative humidity responsiveness, as evidenced by the nightly fluctuations in relative humidity by EnergyPlus.

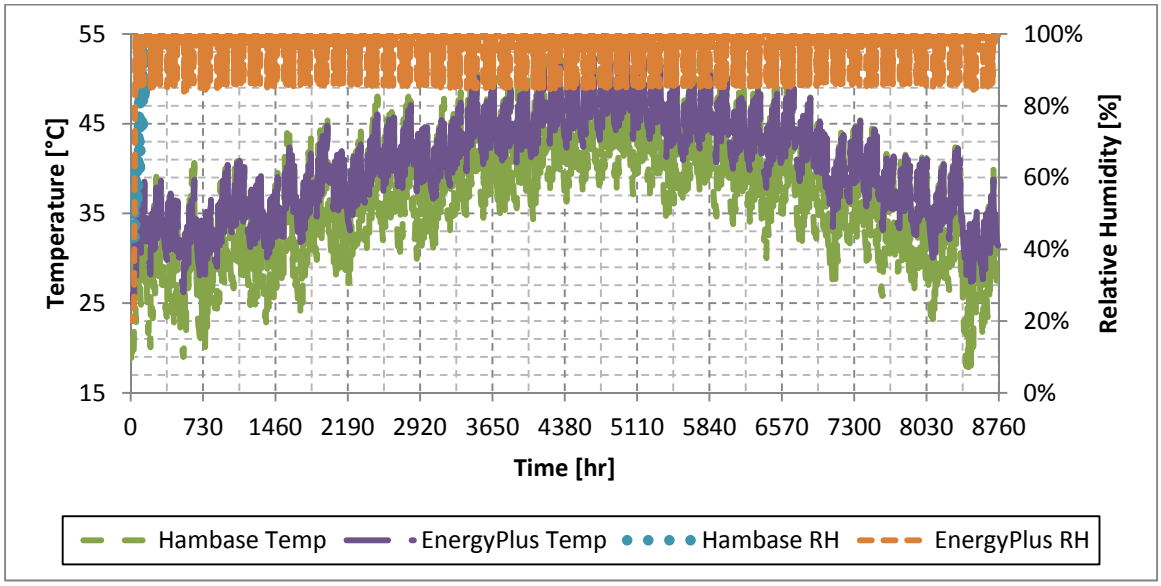

Figure 6.40: Open-loop response of Core1 to actual internal loads and weather

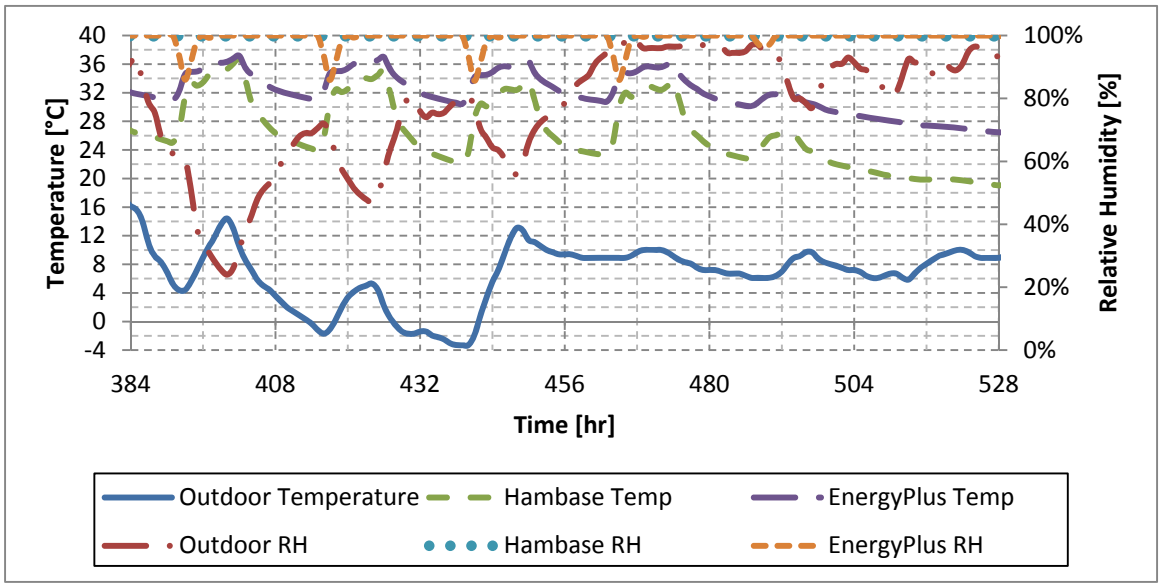

Figure 6.41: Open-loop winter response of Core1 to actual internal loads and weather

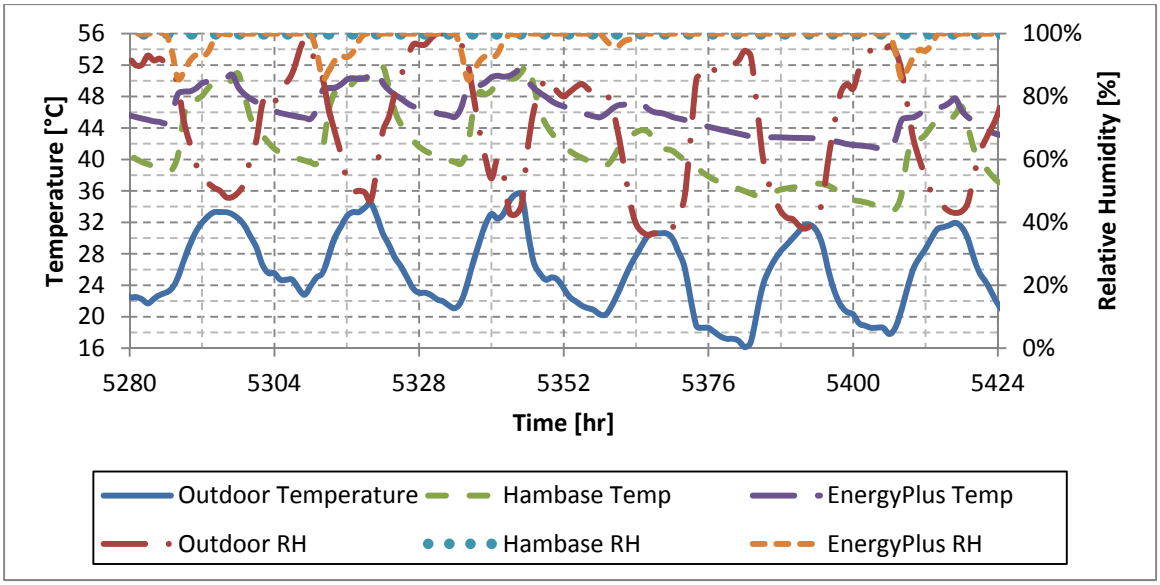

Figure 6.43: Open-loop summer response of Core1 to actual internal loads and weather

Looking at the perimeter zones continues the superposition trend. EnergyPlus' greater sensitivity to DNI can be seen by comparing summer and winter responses in East2 in Figure 6.44 and Figure 6.45. Winter DNI is less than summer DNI, and the EnergyPlus zone temperature amplitude is greater in summer (Figure 6.45) than in winter (6.44) as a result. HAMBASE, with its smaller sensitivity to DNI, has a less pronounced response.

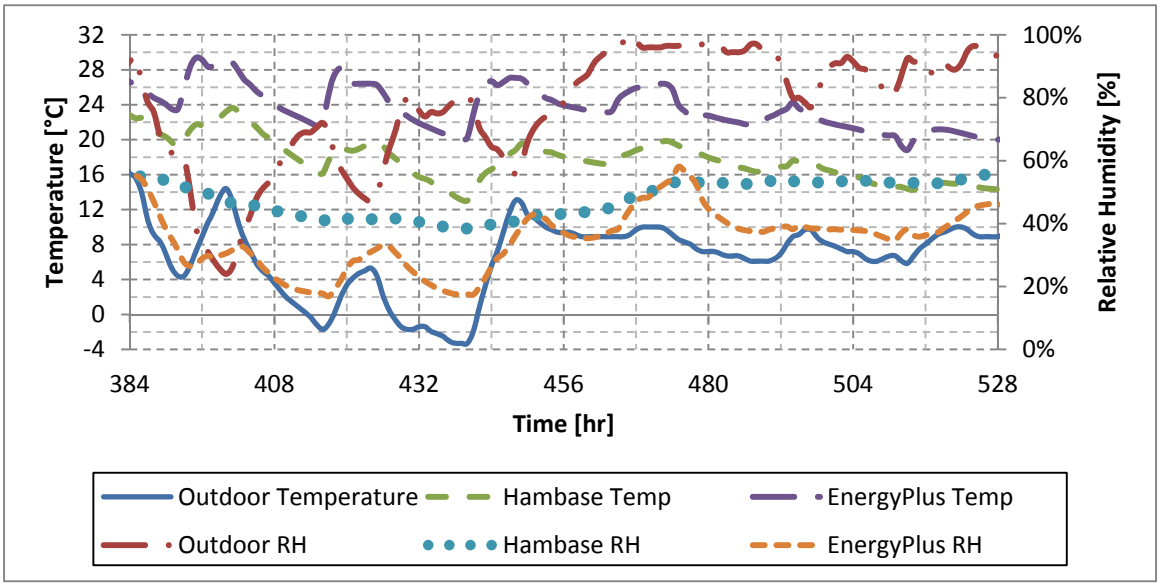

Figure 6.44: Open-loop winter response of East2 to actual internal loads and weather

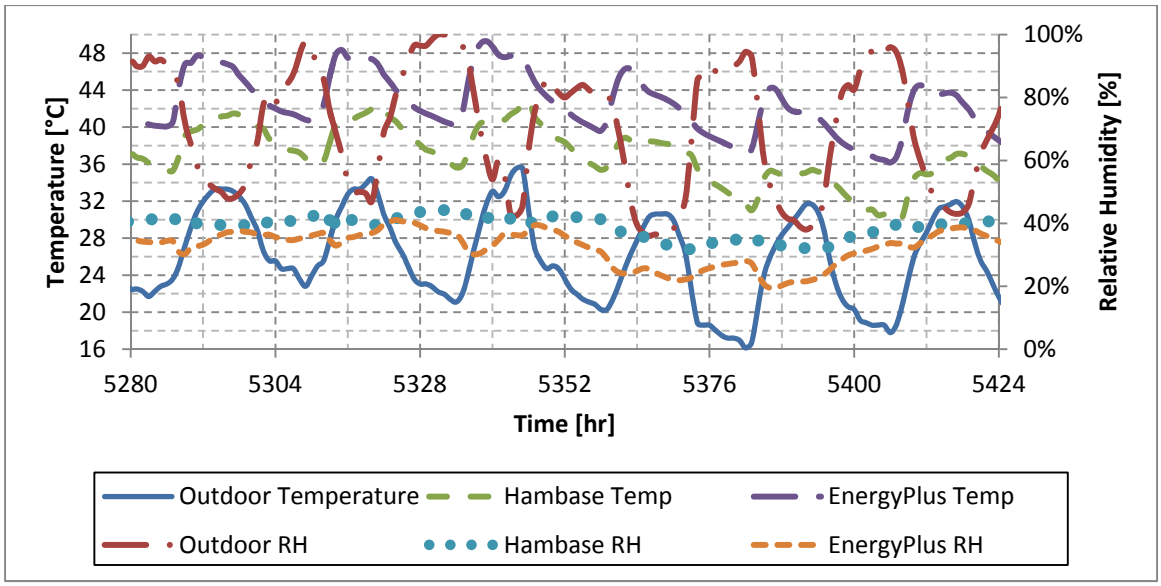

Figure 6.45: Open-loop summer response of East2 to actual internal loads and weather

The response of South3 also shows this effect, seen in Figures 6.46 and 6.47.

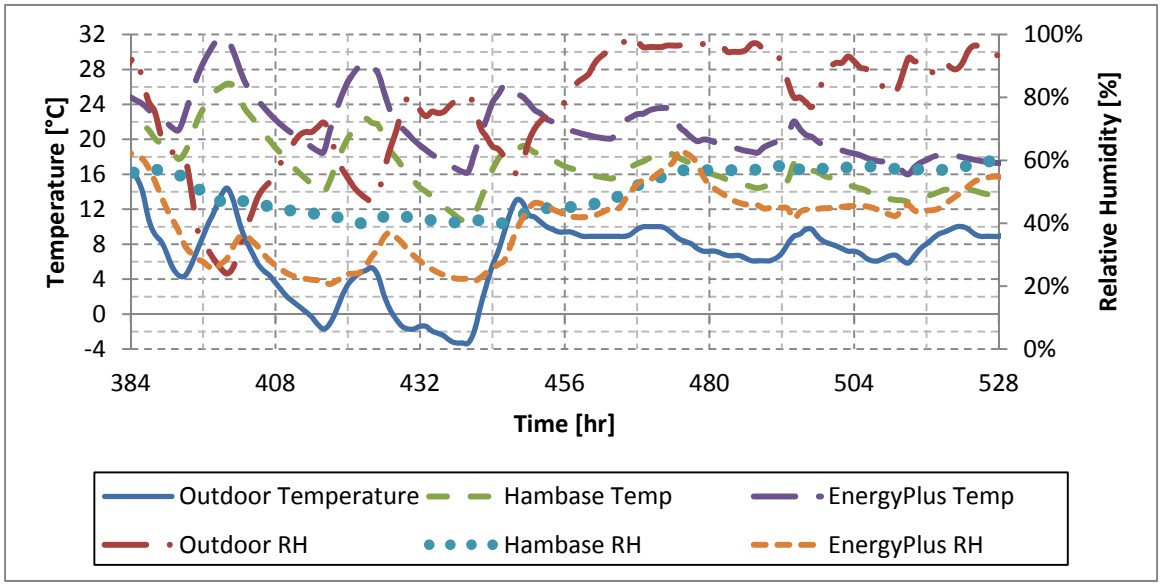

Figure 6.46: Open-loop winter response of South3 to actual internal loads and weather

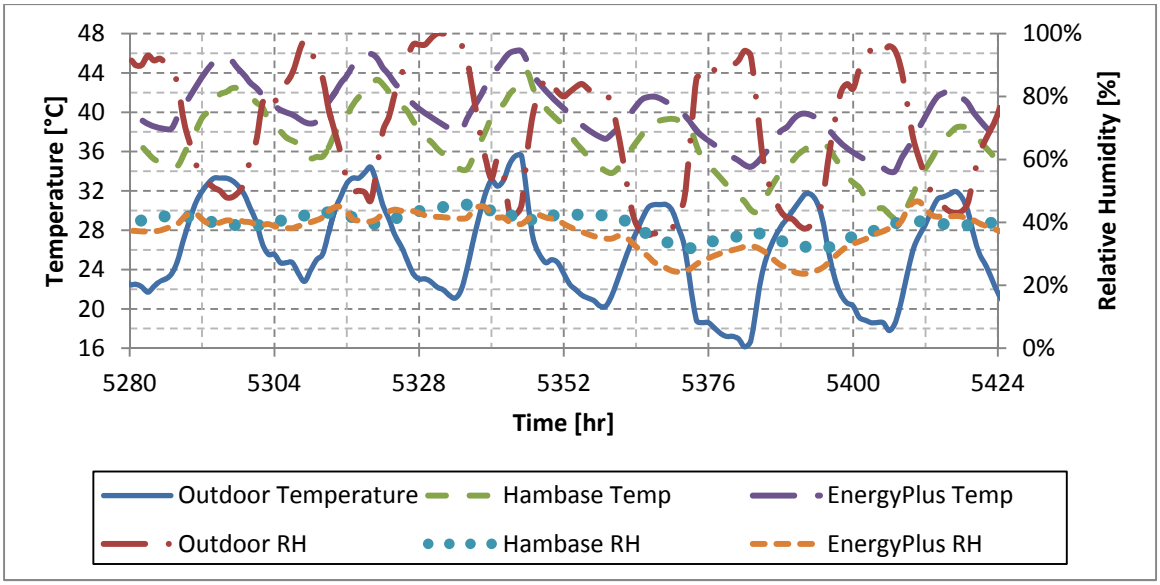

Figure 6.47: Open-loop summer response of South3 to actual internal loads and weather

The south zone only experiences significant DNI during winter. During summer, the sun is too high in the sky to provide significant DNI to a south zone. As a result, the temperature response amplitude for EnergyPlus in the winter is almost identical to the amplitude in summer, even though the summer air temperature is approximately 20°C greater than the winter air temperature. HAMBASE is less responsive to DNI and more responsive to outdoor air temperature, so the summer temperature response amplitude is greater than the winter amplitude.

Summary data for a year of simulation for each zone is shown in Table 6.35 for temperature results and Table 6.36 for relative humidity results.

The maximum temperatures for the two programs are approximately equal, a result of EnergyPlus having a greater sensitivity to DNI while HAMBASE has a greater sensitivity to outdoor air temperatures. HAMBASE shows a much lower minimum temperature, because outdoor air is the only factor affecting the minimum, to which HAMBASE is more responsive. As a result of the lower minimum, HAMBASE also experiences a greater temperature range than EnergyPlus.

The relative humidity results are the opposite of temperature. The greater responsiveness of EnergyPlus causes lower minimum relative humidity values, and as a result, a greater relative humidity range than HAMBASE.

Table 6.35: Temperature Results for Open-loop, Actual Internal Load and Weather Input

	Steady-State Max Temperature [°C]		Steady-State Min Temperature [°C]		Steady-State Amplitude (Max-Min) [°C]	
Zone	HB	EP	HB	EP	HB	EP
Core1	54.47	52.94	17.24	25.06	37.23	27.89
South1	45.56	47.67	9.02	18.75	36.54	28.92
East1	45.15	49.54	8.55	17.52	36.60	32.02
North1	46.12	46.94	8.70	17.89	37.41	29.05
West1	52.22	52.59	8.69	17.91	43.53	34.69
Plenum1	48.55	48.39	13.25	23.31	35.30	25.08
Core2	48.43	51.41	14.73	23.91	33.70	27.50
South2	45.39	49.21	9.15	17.47	36.25	31.75
East2	45.33	51.08	8.92	16.69	36.41	34.38
North2	45.80	48.79	8.81	17.07	36.99	31.72
West2	50.39	53.99	8.81	16.95	41.58	37.04
Plenum2	47.44	48.08	11.40	19.61	36.04	28.47
Core3	50.69	50.52	10.88	17.74	39.81	32.78
South3	47.12	48.28	6.37	12.85	40.76	35.43
East3	47.06	48.99	6.16	12.16	40.90	36.83
North3	47.53	48.18	6.04	12.41	41.49	35.77
West3	52.12	53.47	6.05	12.37	46.07	41.10
Plenum3	56.34	48.59	4.41	8.64	51.93	39.95
Average	48.65	49.93	9.29	17.13	39.36	32.80

Table 6.36: Relative Humidity Results for Open-loop, Actual Internal Load and Weather Input

	Steady-State Max RH [%]		Steady-State Min RH [%]		Steady-State Amplitude (Max-Min) [%]	
Zone	HB	EP	HB	EP	HB	EP
Core1	100%	100%	43%	20%	57%	80%
South1	76%	76%	18%	8%	58%	68%
East1	76%	76%	20%	10%	57%	66%
North1	76%	76%	20%	10%	56%	67%
West1	76%	76%	19%	10%	57%	66%
Plenum1	54%	56%	14%	6%	40%	51%
Core2	100%	100%	49%	20%	51%	80%
South2	76%	78%	19%	8%	57%	70%
East2	76%	78%	20%	9%	56%	69%
North2	76%	79%	21%	10%	55%	69%
West2	76%	78%	20%	10%	56%	69%
Plenum2	56%	62%	16%	6%	41%	56%
Core3	100%	100%	49%	22%	51%	78%
South3	80%	83%	21%	11%	59%	72%
East3	81%	82%	22%	11%	58%	71%
North3	81%	83%	23%	12%	58%	71%
West3	80%	82%	21%	12%	59%	71%
Plenum3	81%	82%	7%	6%	74%	76%
Average	79%	80%	23%	11%	56%	69%

6.4 IBL-GHP BASE CASE COMMERCIAL OFFICE BUILDING SIMULATION RESULTS

The base case model uses a 10x16 borehole field (160 boreholes) on 6.1m (20ft) centers. The ground loop was sized using GLHEPRO using a maximum heat pump EWT of 32.2°C (90°F), resulting in borehole depths of 170.7 meters (560ft) and 3.175cm (1.25in) diameter u-tubes. Recall that the residential building GLHEPRO ground loop sizing was based upon a maximum heat pump EWT of 48.9°C (120°F), the heat pump shutoff temperature, and the GHP system performed as designed. That value of maximum heat pump EWT of 48.9°C was too high for the commercial building case, which further emphasizes the sensitivity of the design parameters on system performance and need for modeling/simulation. Climate Master Tranquility 20 series heat pumps were modeled and Table 6.16 shows the heat pump capacity for each zone in the building

Table 6.16: Heat Pump Capacities by Zone (ClimateMaster Tranquility 20 Series Heat Pumps)

Floor	Heat Capacity by Zones (tons)				
	South	East	North	West	Core
Floor 1	7	4	5	5	15
Floor 2	7	4	5	5	10
Floor 3	7	4	5	5	10

6.4.1 Minute-Time Results

The integrated IBL-GHP model for the commercial building used a time step of 60 seconds for all except the ground loop portion which was updated every 60 minutes, so the range of time scales of simulated data are between 60 seconds and 10-15 years. As an example, Figure 6.25 shows three hours of temperature and humidity data for Core1 on June 30th of the first year of simulation. The data shows the temperature in the zone increasing until it passes the cooling-on setpoint threshold, at which point the temperature decreases due to heat pump operation shown in Figure 6.26. When the heat pump turns on, 54.6 kW of cooling are provided to the zone, lowering the zone air temperature and rejecting heat to the circulating water, resulting in an increase in water temperature. The same behavior is shown for East2 and South3 in the Figures 6.27-6.30.

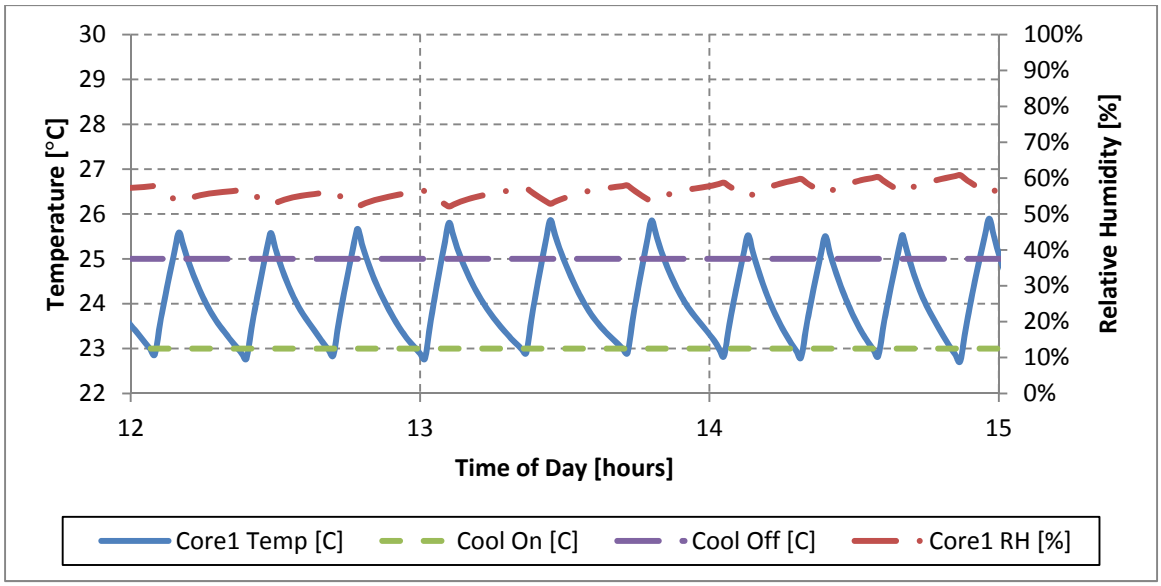

Figure 6.25: Time-step temperature and relative humidity for Core1 for June 30, 12-3pm

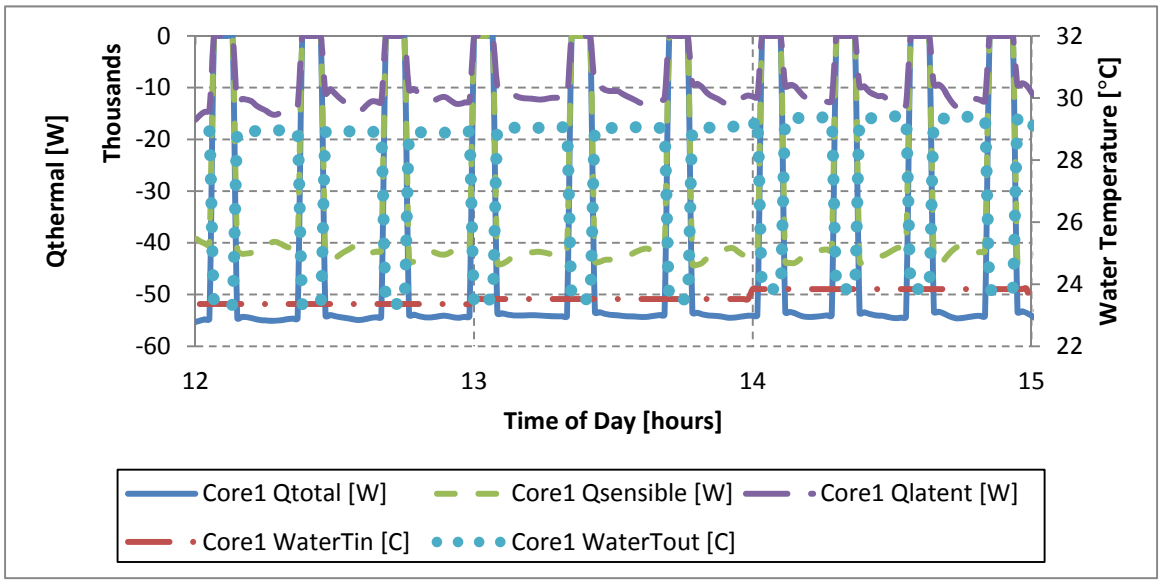

Figure 6.26: Time-step cooling provided and water temperature for Core1 heat pump for June 30, 12-3pm

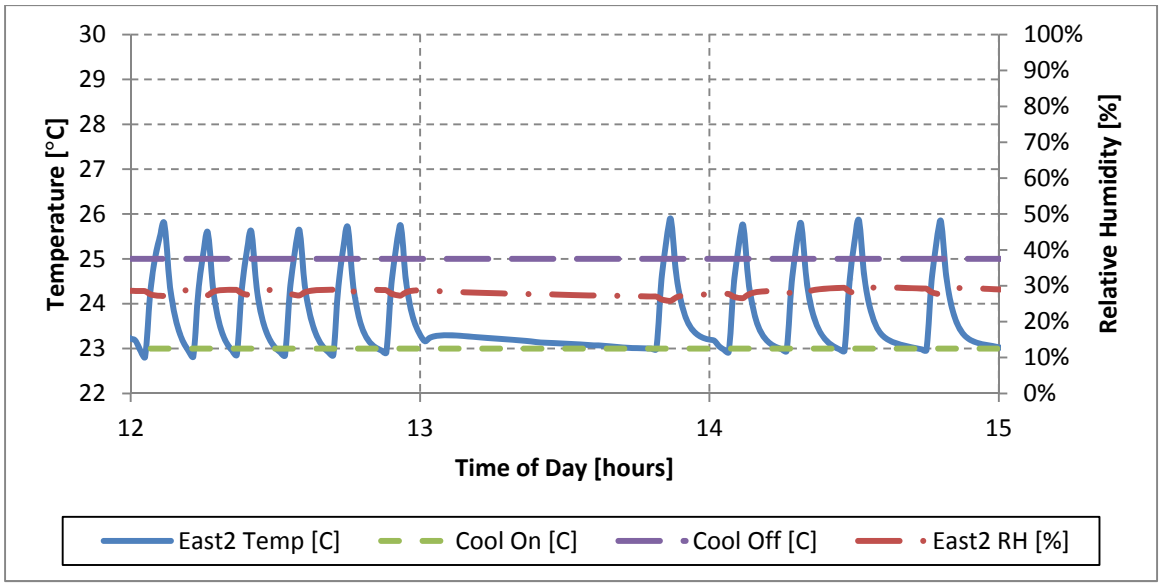

Figure 6.27: Time-step temperature and relative humidity for East2 for June 30, 12-3pm

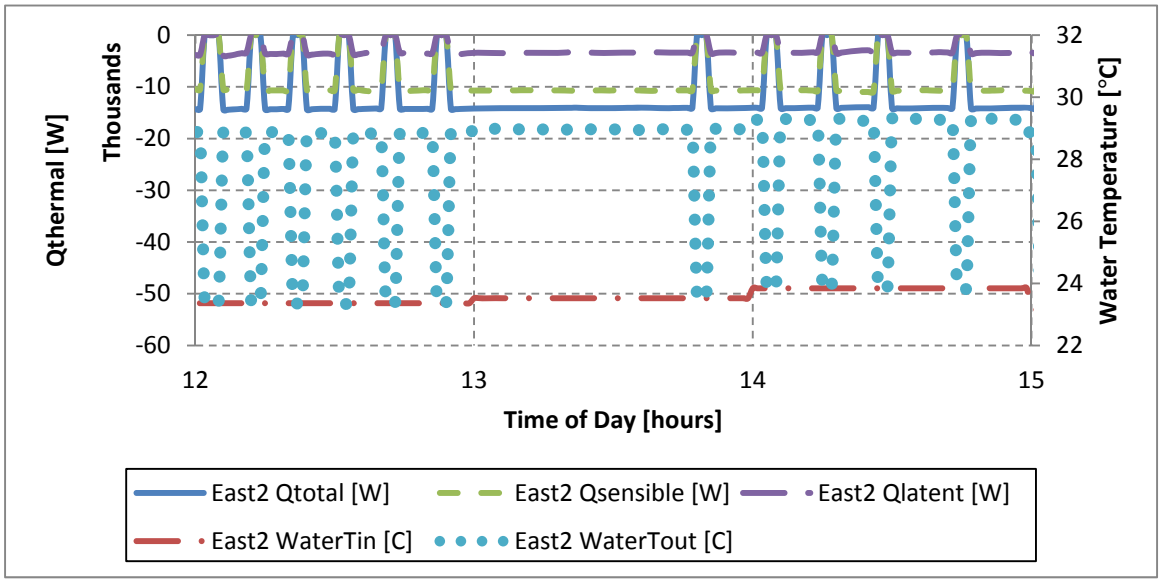

Figure 6.28: Time-step cooling provided and water temperature for East2 heat pump for June 30, 12-3pm

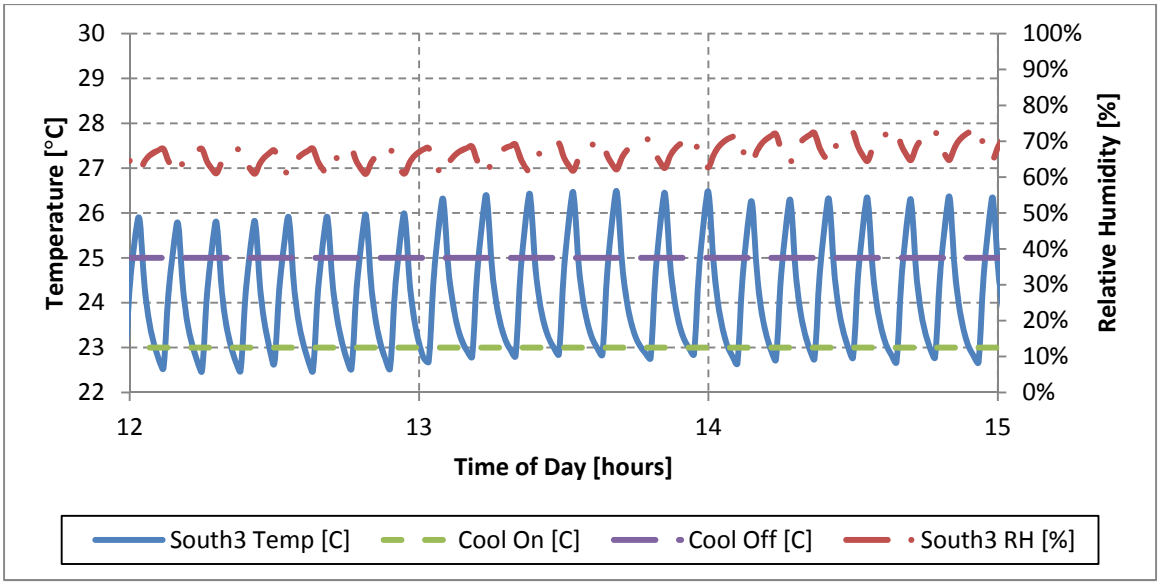

Figure 6.29: Time-step temperature and relative humidity for South3 for June 30, 12-3pm

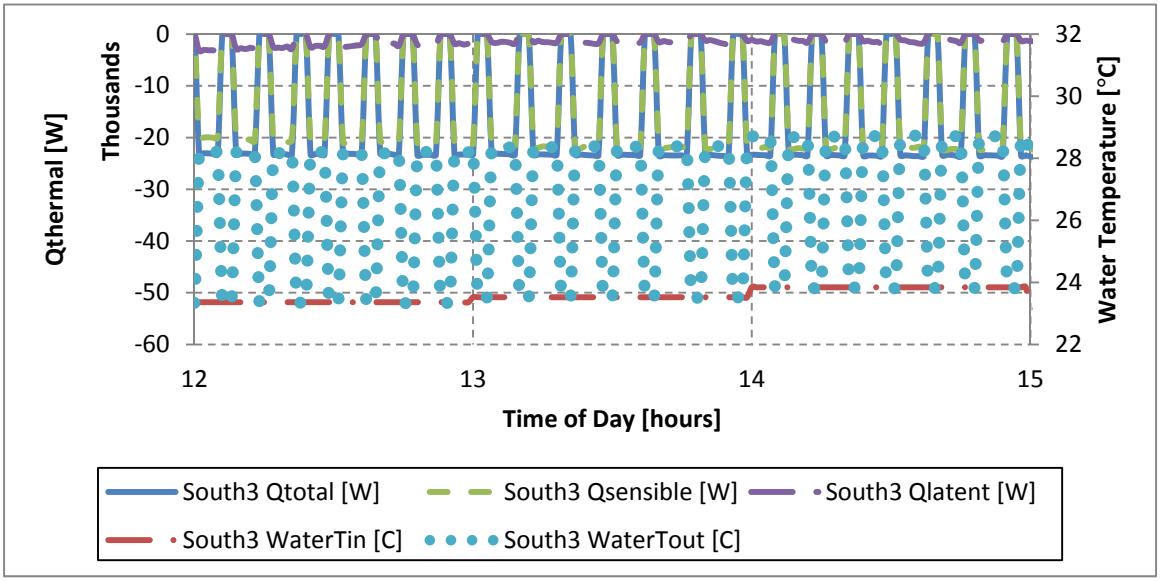

Figure 6.30: Time-step cooling provided and water temperature for South3 heat pump for June 30, 12-3pm

The ground loop operates on a 60-minute time-step due to the significant thermal mass of the ground. As the heat pumps begin to provide cooling, the temperatures of their return water (WaterTout) increases. The return water from all 15 heat pumps mixes in the heat pump header, whose temperature is shown in blue in Figure 6.31. The header temperature fluctuates at 60-second intervals because it is based on the heat pump time-steps. The header temperature is averaged-hourly to form the inlet water temperature to the ground loop, shown in green in

Figure 6.31. The ground loop rejects heat to the ground, and returns cooler water as the inlet to the heat pumps, shown in purple in Figure 6.31.

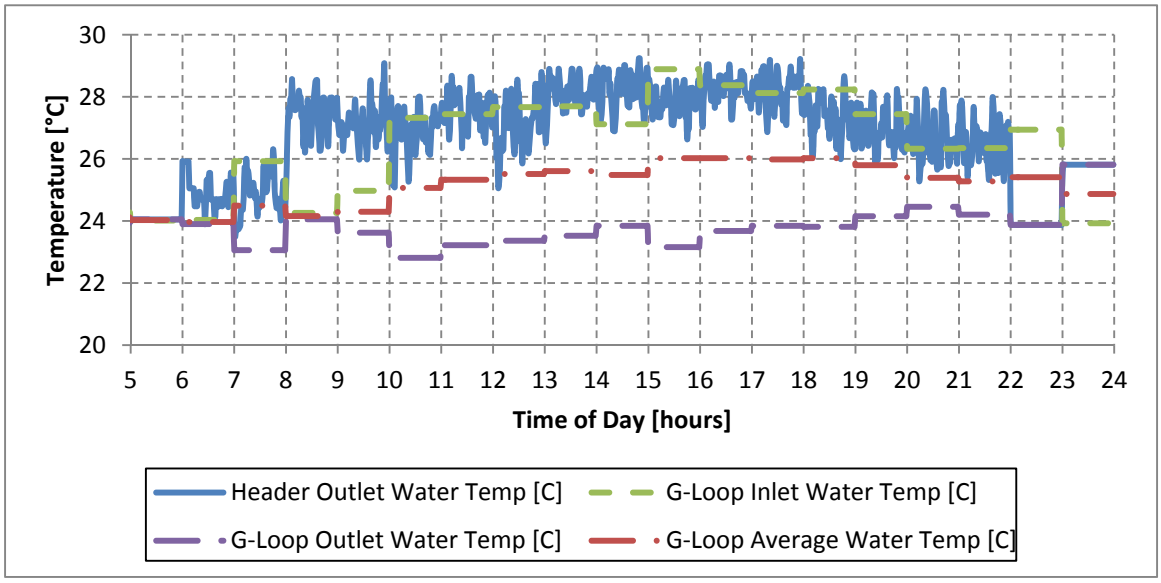

Figure 6.31: Time-step water temperature for the ground loop and heat pump return header for June 30, 5am -12am

6.4.2 Hourly Time Results

This section presents simulation results based on hourly averages for the first year of operation, January 1 through December 31. Hourly averages are the typical way cooling and heating loads are communicated in building load modeling software such as eQuest and EnergyPlus, so converting the data to hourly averages allows easy comparison between models. Hourly averaging also reduces data storage requirements, allowing compressed transfer times and easier storage.

6.4.2.1 Hourly Zonal Temperature Data

Hourly average temperature data for Core1, East2 and South3 are shown in Figure 6.32 - Figure 6.34, respectively. In all three figures, the following temperatures are shown: zone air temperature (blue), the heating setpoint temperature (purple), the cooling setpoint temperature (red), the heating setback temperature (green) and the cooling setback temperature (light blue). During summer operation, Core1 temperature is generally between the cooling setpoint and cooling setback position due to the difficulty maintaining zone temperature when large internal loads are combined with high outdoor temperatures. East2 and South3, in contrast, have smaller internal loads, resulting in lower summer zonal temperatures. The opposite effect can be seen during winter operation. East2 and South3 temperatures regularly fall below the heating

setpoint due to the small internal loads combined with low outdoor temperatures. In contrast, the large internal loads of Core1 maintain temperatures above the heating setpoint except for a few extreme cases.

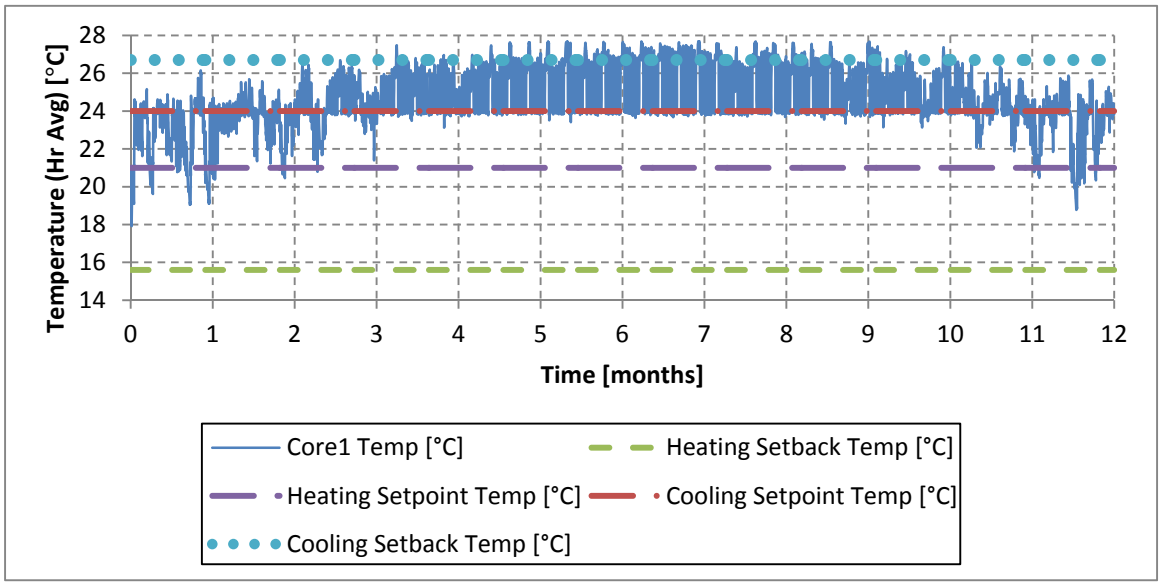

Figure 6.32: Hourly average temperature of Core1 for first 12 months of simulation

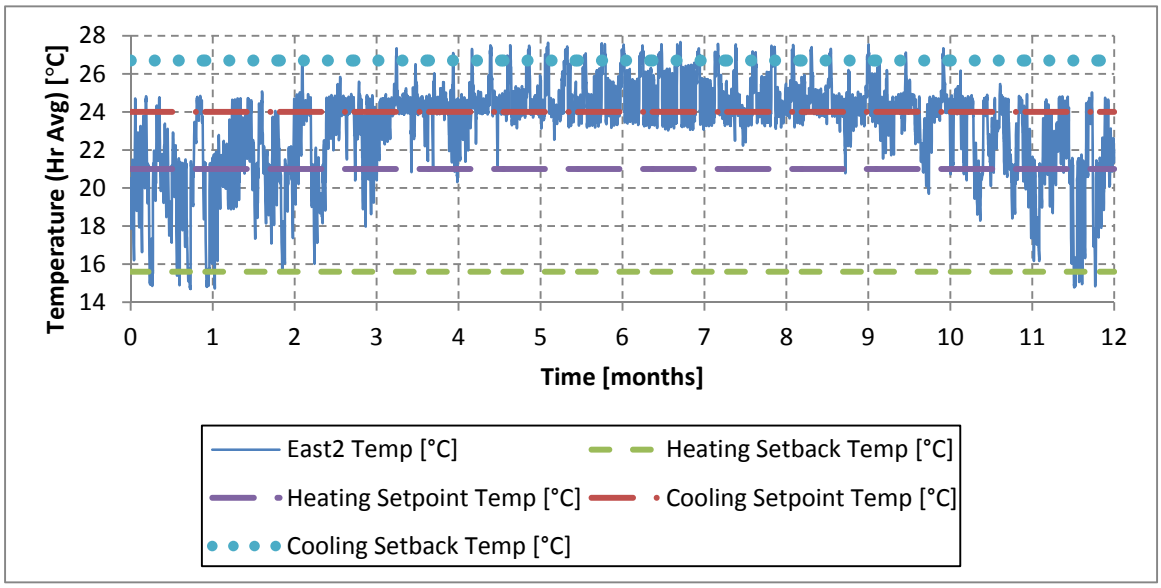

Figure 6.33: Hourly average temperature of East2 for first 12 months of simulation

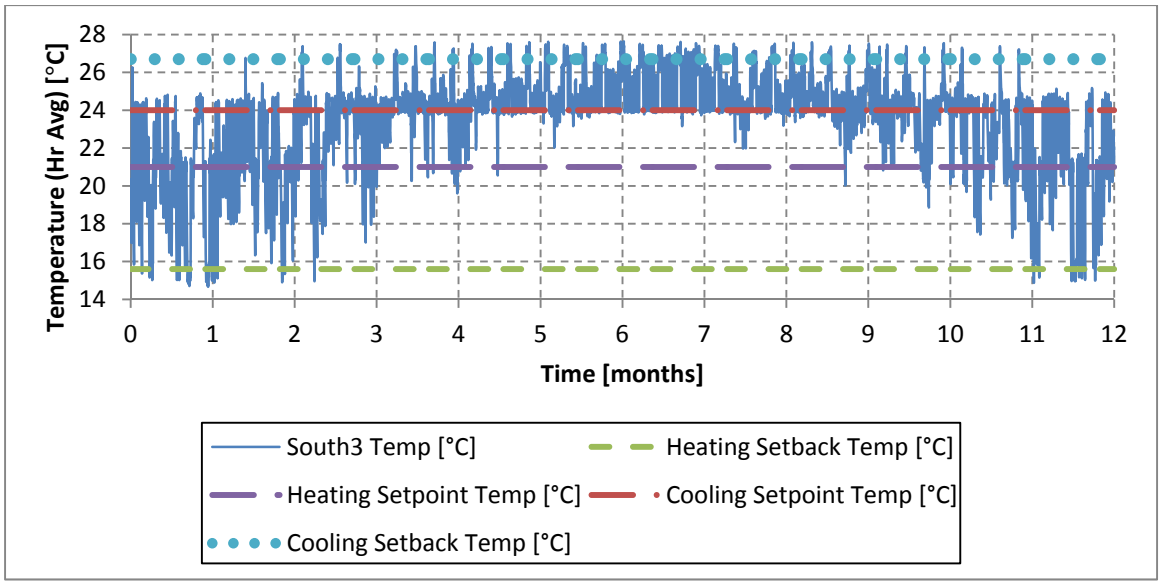

Figure 6.34: Hourly average temperature of South3 for first 12 months of simulation

6.4.2.2. Hourly Heating and Cooling Data

The air temperature in a zone is controlled by heating and cooling added to the zone by the heat pump. Hourly average data for heating and cooling provided to Core1, East2 and South3 are shown in Figures 6.35-6.37, respectively. Cooling is shown as a negative value and heating is shown as a positive value. Comparing the cooling and heating loads for Core1 in Figure 6.35 to the temperature in Figure 6.34 shows the integration between the two systems: when zone temperatures are high, the heat pump provides cooling, when zone temperatures are low, the heat pump provides heating.

Comparing the cooling and heating loads between the zones reveals the effect of heat pump sizing. The 15-ton capacity heat pump in Core1 provides almost 57kW of cooling, compared to 15kW from the 4-ton unit in East2 and 23kW from the 7-ton unit in South3.

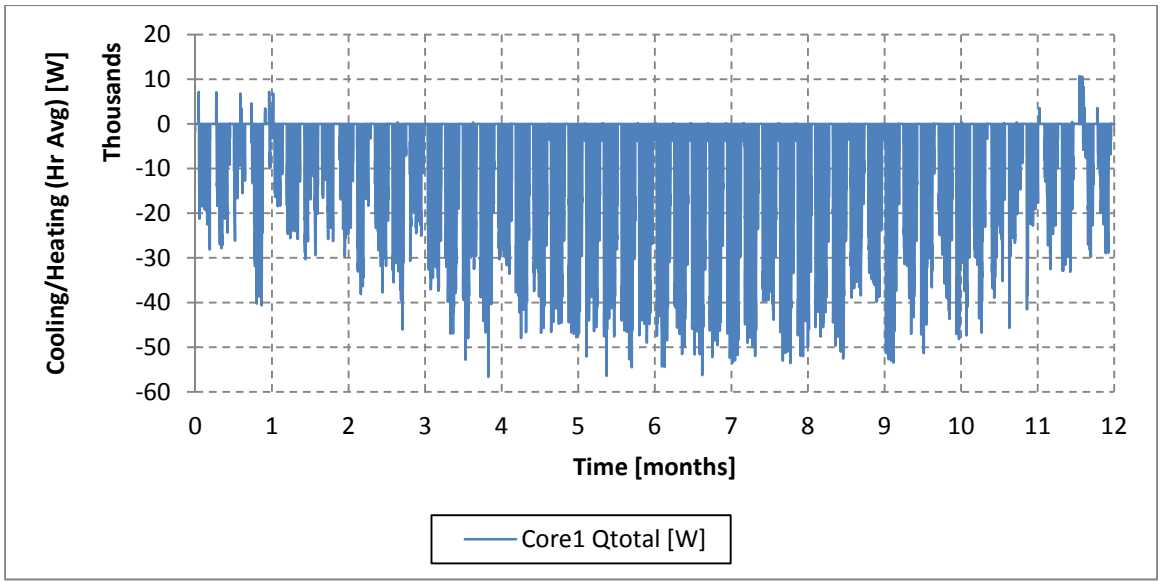

Figure 6.35: Hourly average cooling (negative) and heating (positive) provided by the Core1 heat pump for the first 12 months of simulation

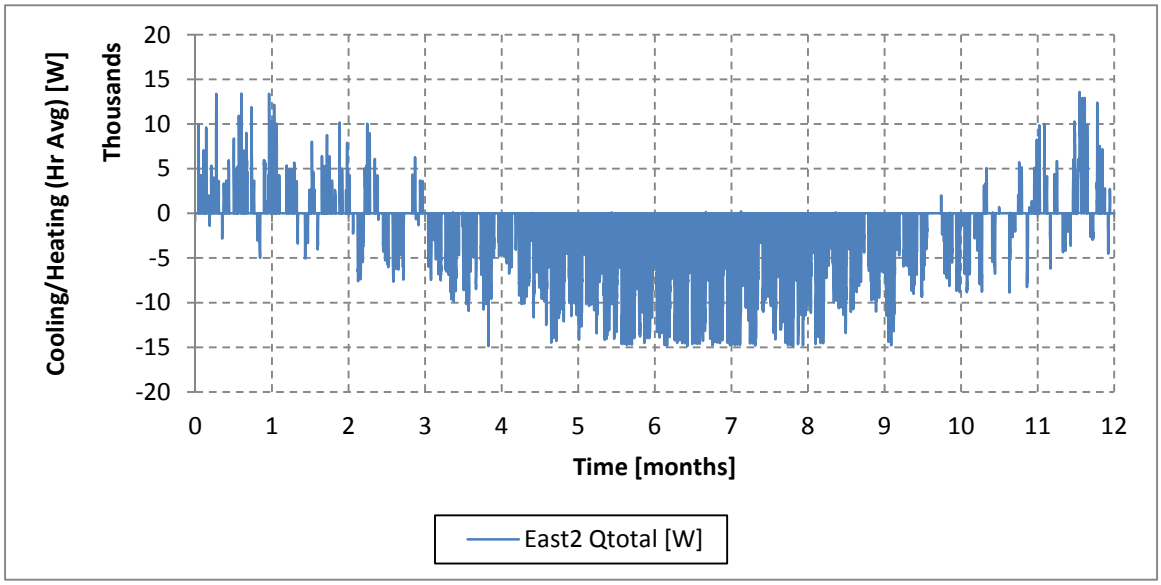

Figure 6.36: Hourly average cooling (negative) and heating (positive) provided by the East2 heat pump for the first 12 months of simulation

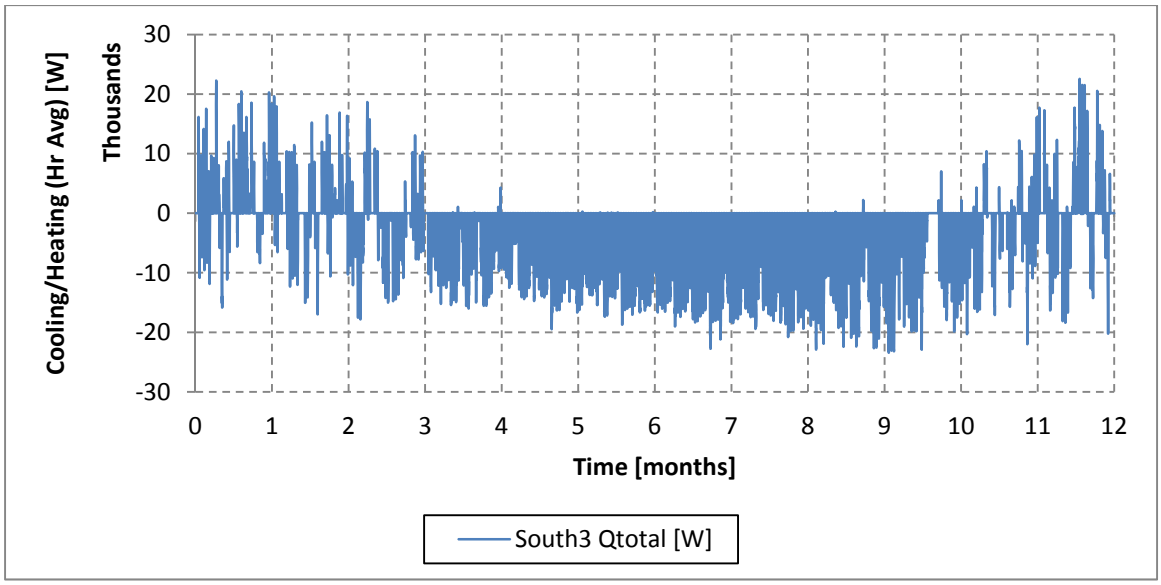

Figure 6.37: Hourly average cooling (negative) and heating (positive) provided by the South3 heat pump for the first 12 months of simulation

6.4.2.3 Hourly Heat Rejection Data

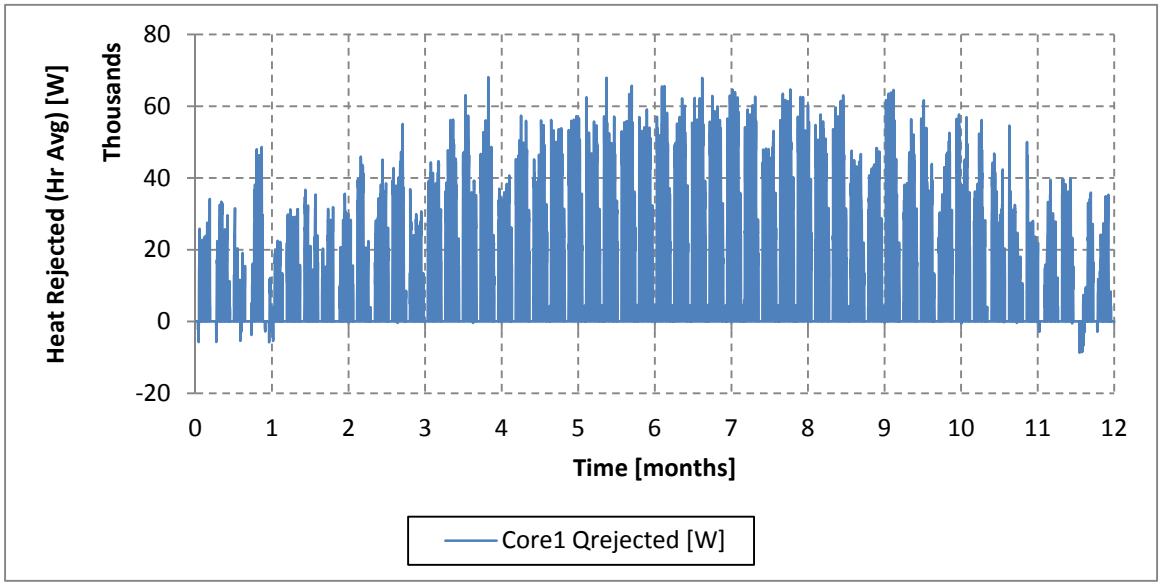

Figure 6.38: Hourly average heat rejected to ground loop water by the Core1 heat pump (cooling is positive) for the first 12 months of simulation

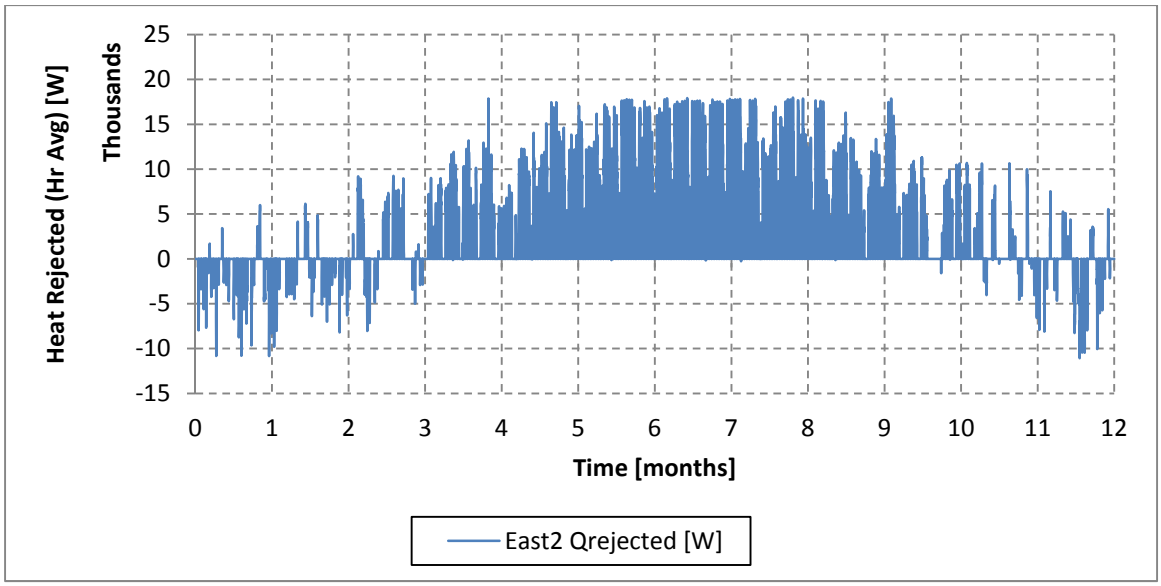

Figure 6.39: Hourly average heat rejected to ground loop water by the East2 heat pump (cooling is positive) for the first 12 months of simulation

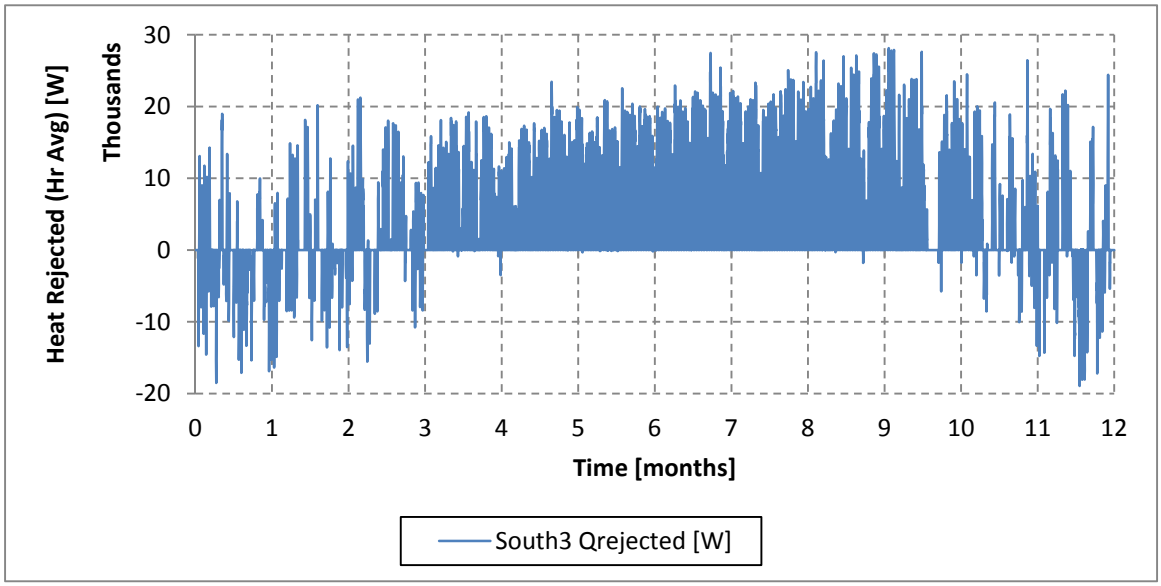

Figure 6.40: Hourly average heat rejected to ground loop water by the South3 heat pump (cooling is positive) for the first 12 months of simulation

6.4.2.4 *Hourly Heat Pump Water Temperature Data*

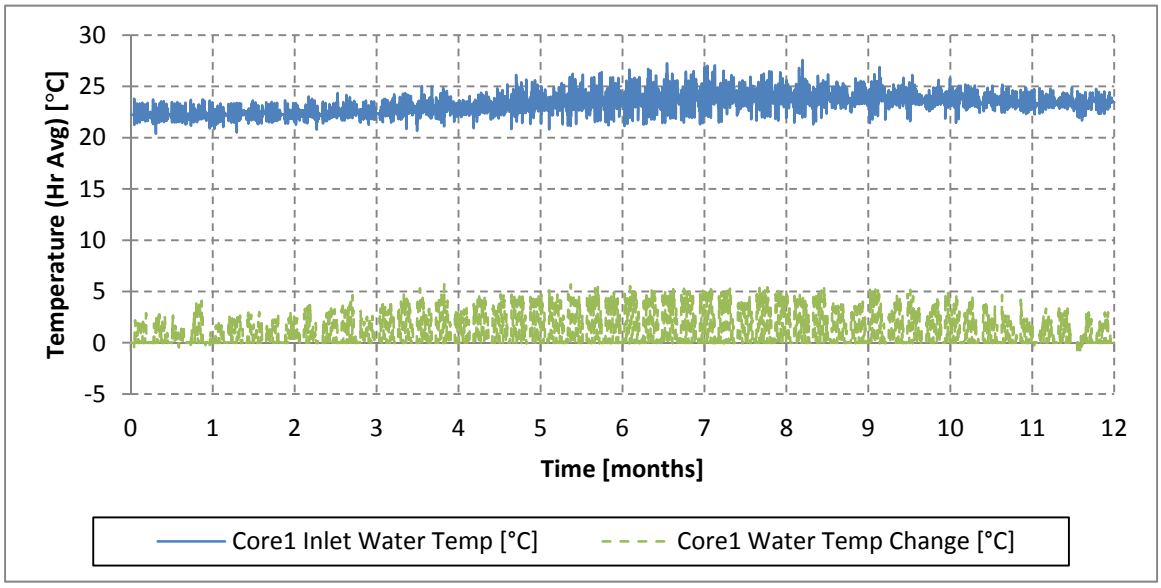

Figure 6.41: Hourly average Core1 heat pump entrance water temperature and temperature change for the first 12 months of simulation

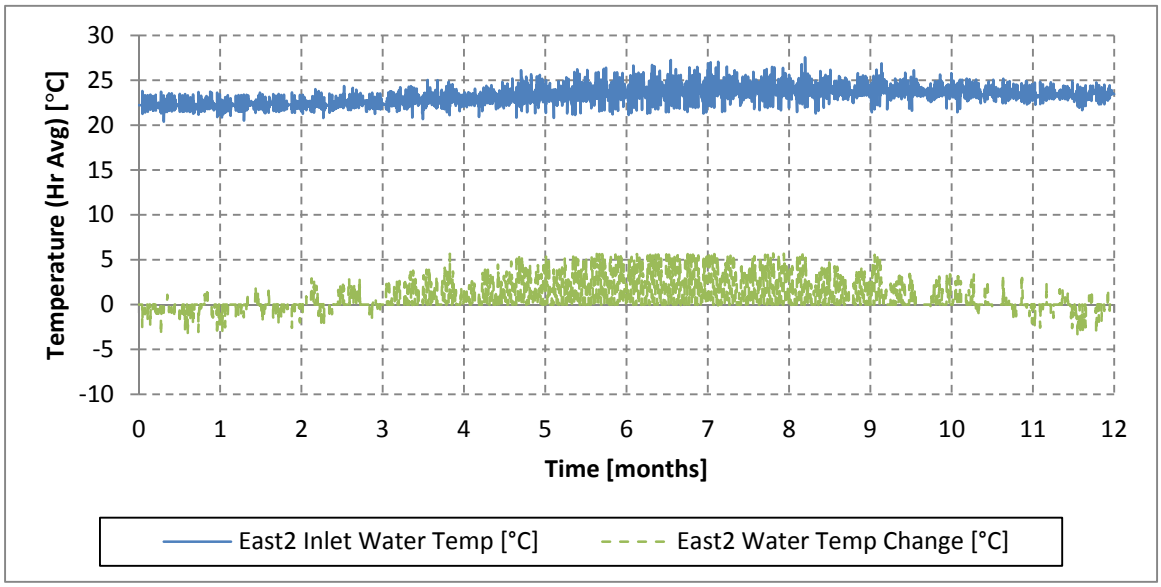

Figure 6.42: Hourly average East2 heat pump entrance water temperature and temperature change for the first 12 months of simulation

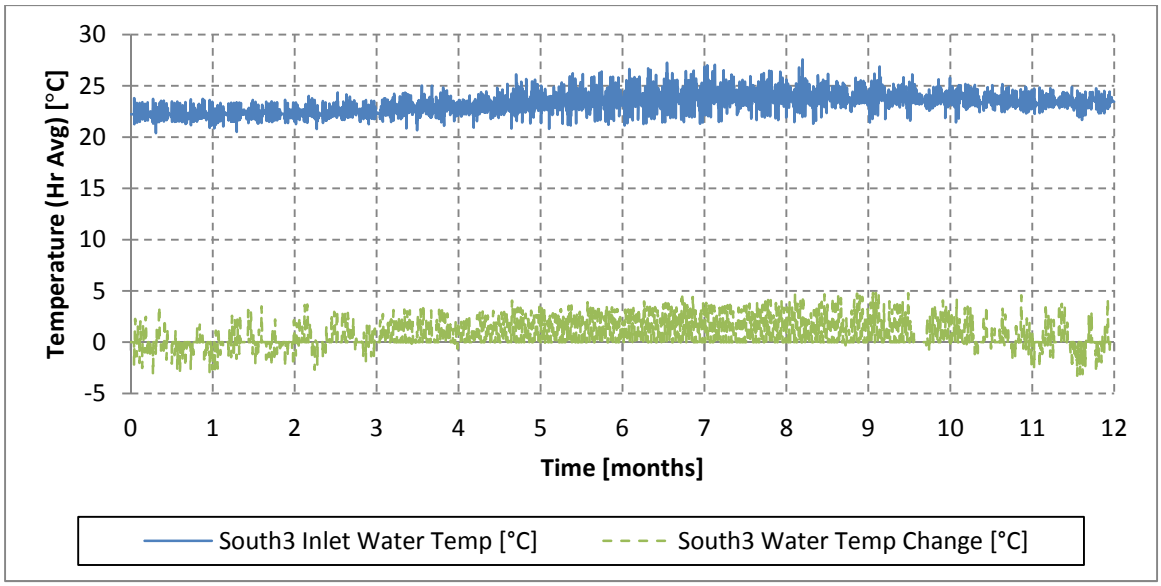

Figure 6.43: Hourly average South3 heat pump entrance water temperature and temperature change for the first 12 months of simulation

6.4.2.5 Hourly Heat Pump Efficiency Data

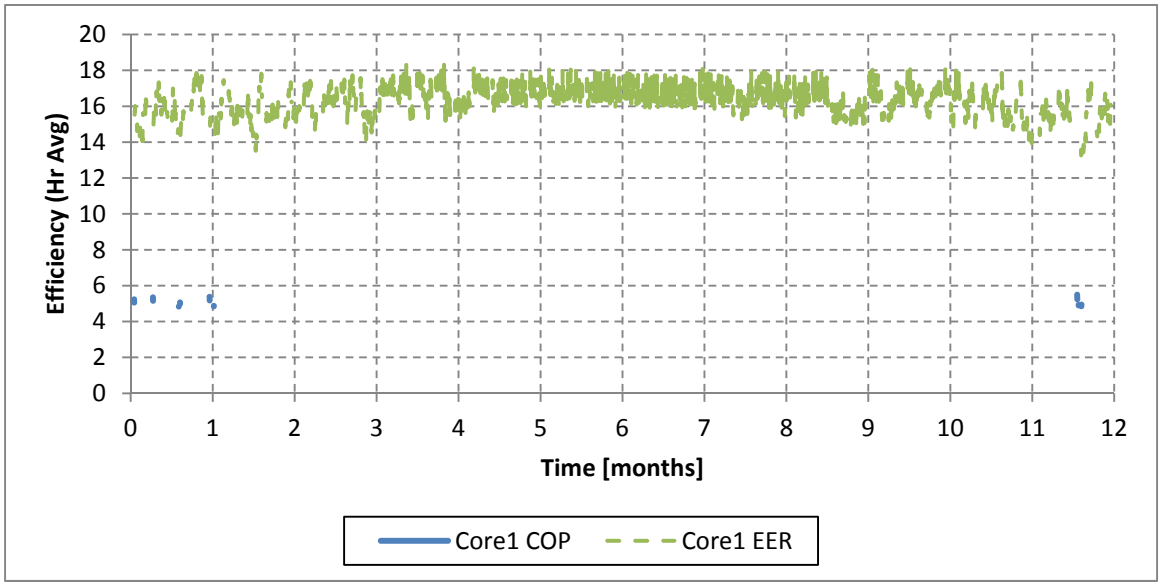

Figure 6.44: Hourly average efficiency ratings for the Core1 heat pump for the first 12 months of simulation (EER: cooling, COP: heating)

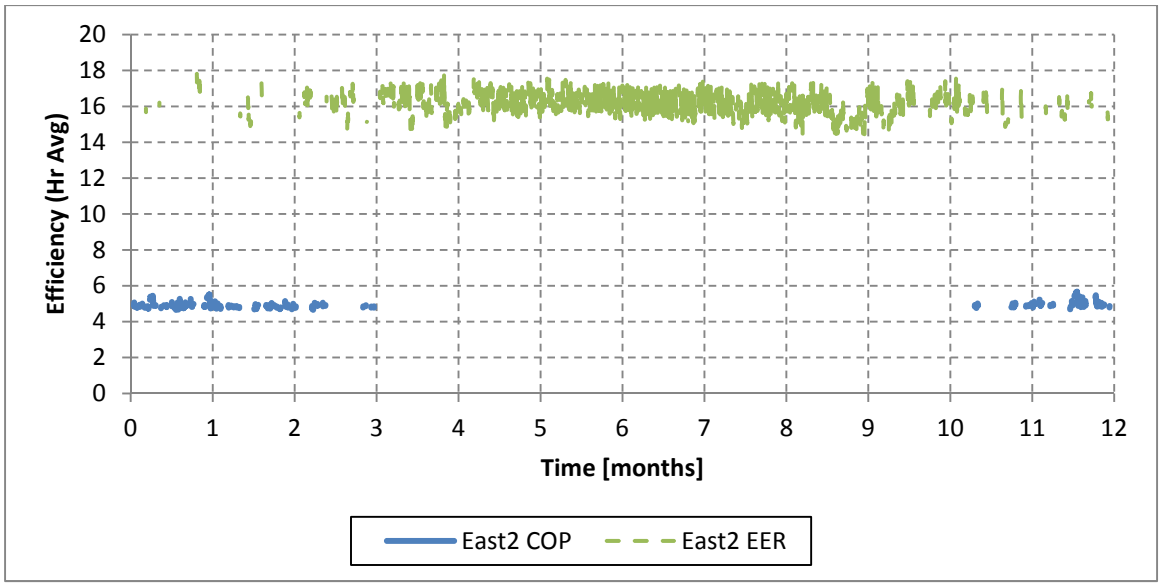

Figure 6.45: Hourly average efficiency ratings for the East2 heat pump for the first 12 months of simulation (EER: cooling, COP: heating)

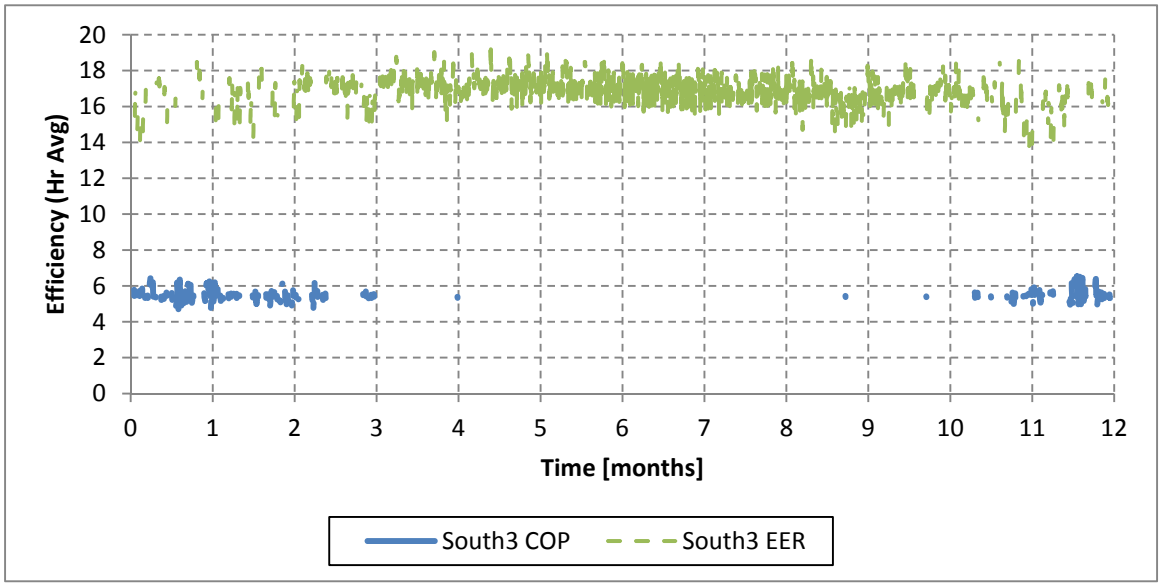

Figure 6.46: Hourly average efficiency ratings for the South3 heat pump for the first 12 months of simulation (EER: cooling, COP: heating)

6.4.2.6 Hourly Ground Loop Water Temperature Data

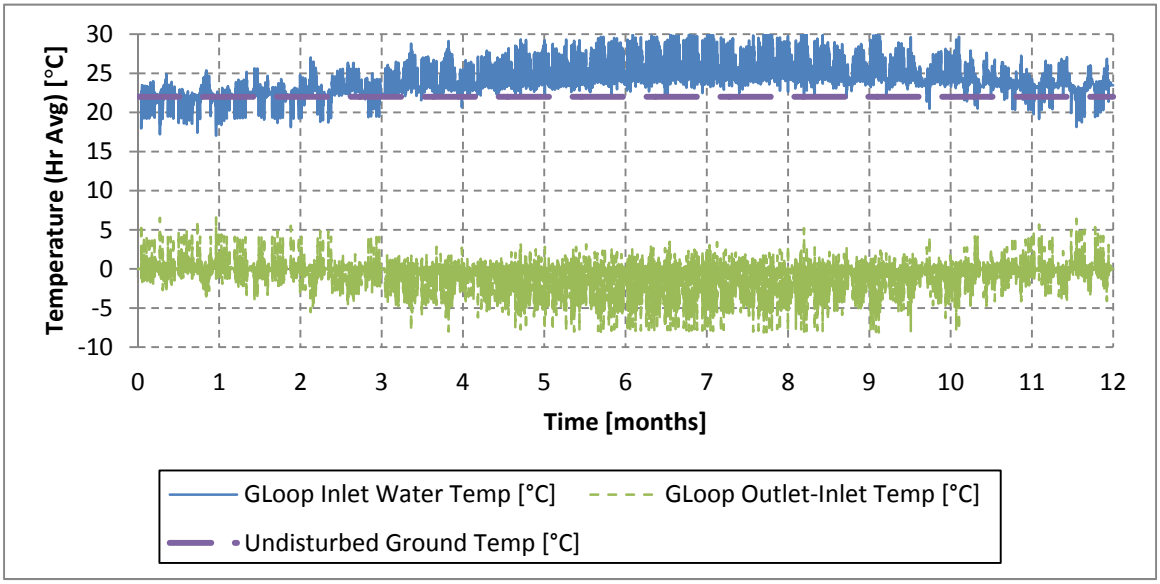

Figure 6.47: Hourly average ground loop entrance water temperature and temperature change for the first 12 months of simulation

6.4.3 Monthly Time Results

Monthly and yearly values are used to examine trends over the duration of the 15-year simulation. Monthly averages, monthly totals, monthly maximum and minimum all serve to smooth the hourly data into a format viewable on a 15-year scale.

Heat pump heating and cooling values for Core1, East2 and South3 are shown in Figure 6.48 as total energy provided (in MWh) and in Figure 6.49 as total operating hours. Data in both figures show consistency from year-to-year in the amount of cooling and heating provided to the zones. These results also show the significant load imbalance in this building. The cooling loads for every zone are significantly larger than the heating loads, as seen in the total energy provided and the total hours of operation for cooling versus heating modes.

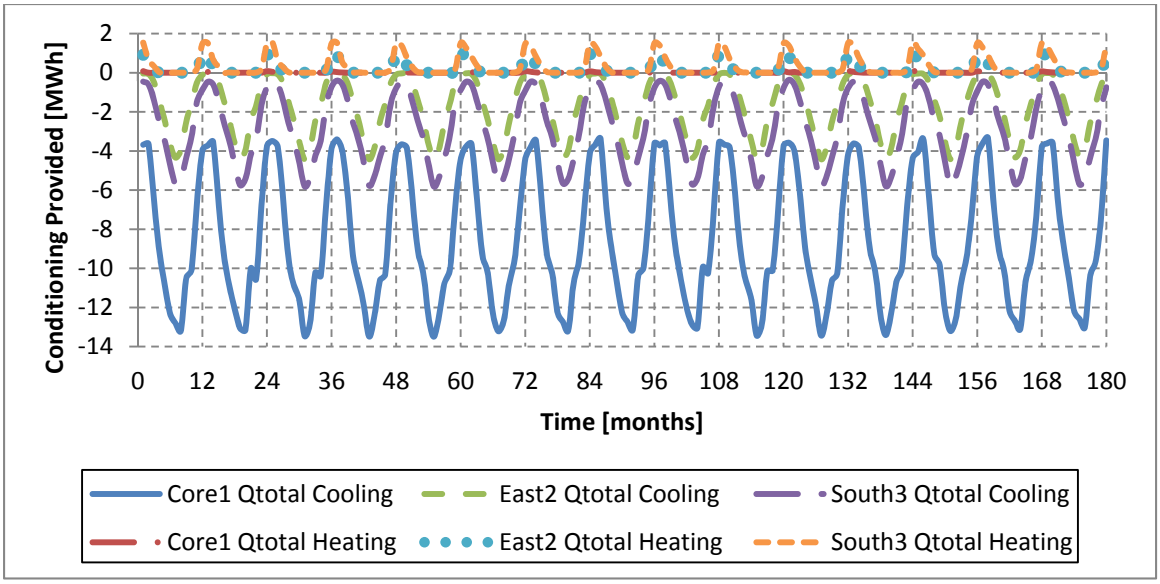

Figure 6.48: Monthly totals for cooling and heating provided in Core1, East2 and South3

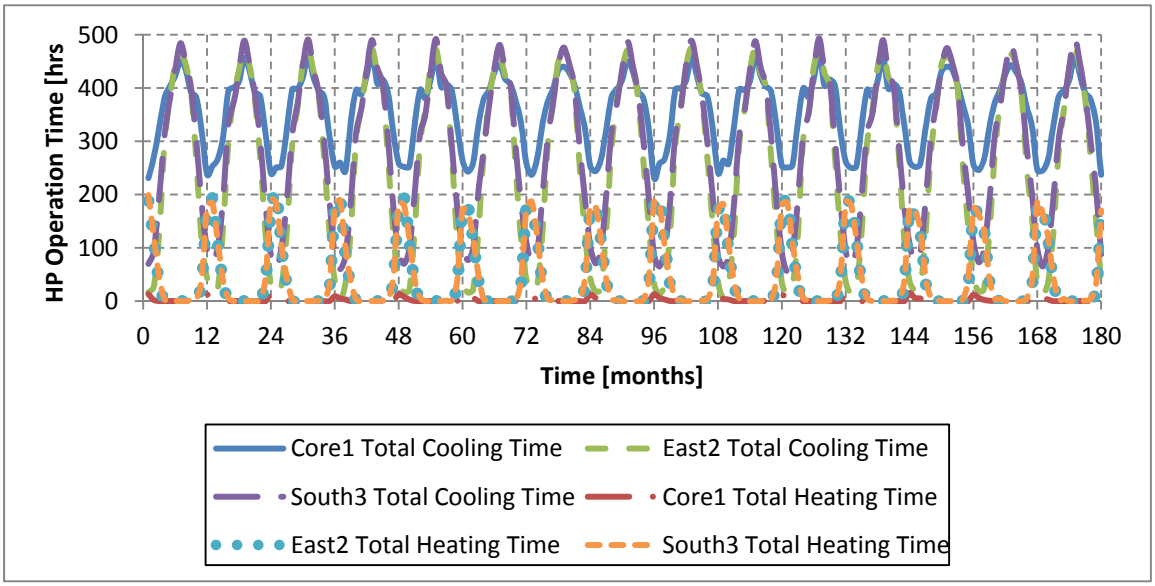

Figure 6.49: Monthly operating times for cooling and heating in Core1, East2 and South3

The total heat rejected to the ground loop by the heat pumps during zone cooling and the total heat absorbed from the ground loop by the heat pumps during zone heating are shown in Figure 6.50. The difference in heat rejection and absorption again emphasize the load imbalance experienced by the ground loop.

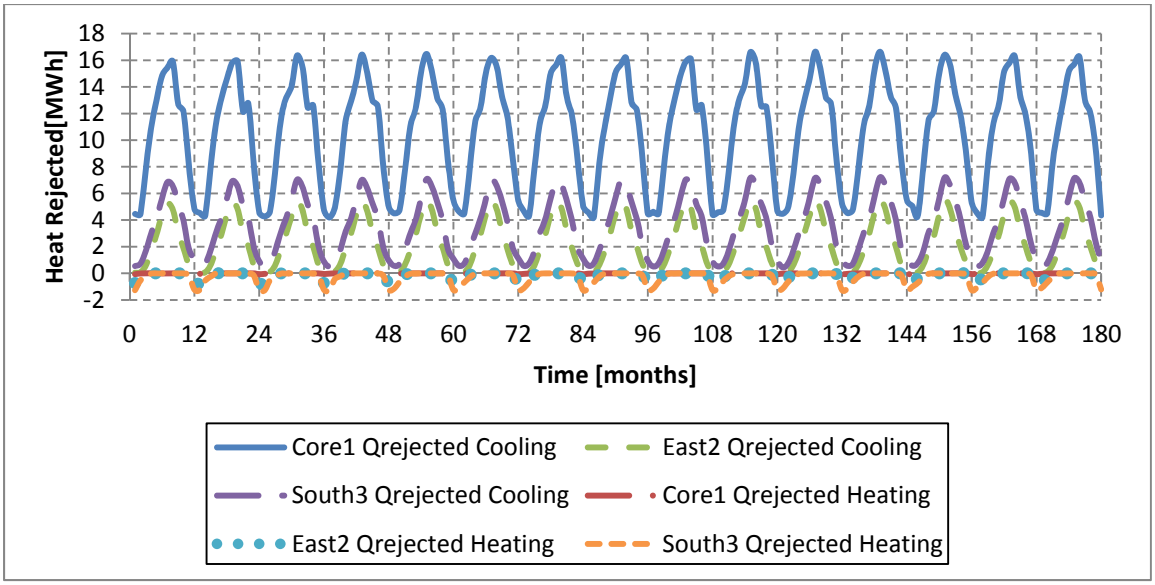

Figure 6.50: Monthly totals for heat rejected and absorbed from Core1, East2 and South3

The load imbalance manifests itself in changes in the ground loop water temperature. Figure 6.51 shows the monthly minimum, maximum and mean temperatures for the ground loop water as it enters the heat pump (heat pump entering water temperature, or HP EWT). The EWT values increase continuously during the 15-year simulation because of the net quantity of heat rejected to the ground.

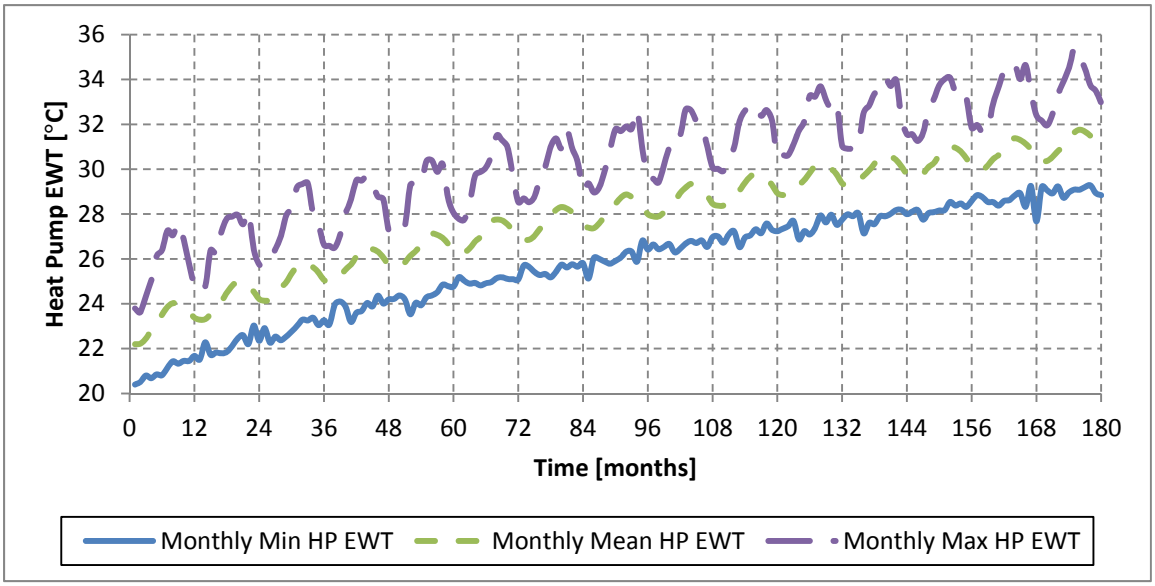

Figure 6.51: Monthly maximum, minimum and mean heat pump entering water temperature

As HP EWT increases, the heat pump compressor needs to work harder to generate a given amount of cooling. Figure 6.52 shows the monthly power usage for Core1, East2 and South3for heating and cooling operation, and Figure 6.53 shows the total power usage for the building. The total power usage resulting from cooling operation increases every year of the 15-year simulation. This means that the cost of cooling this building increases every year because of the significant load imbalance.

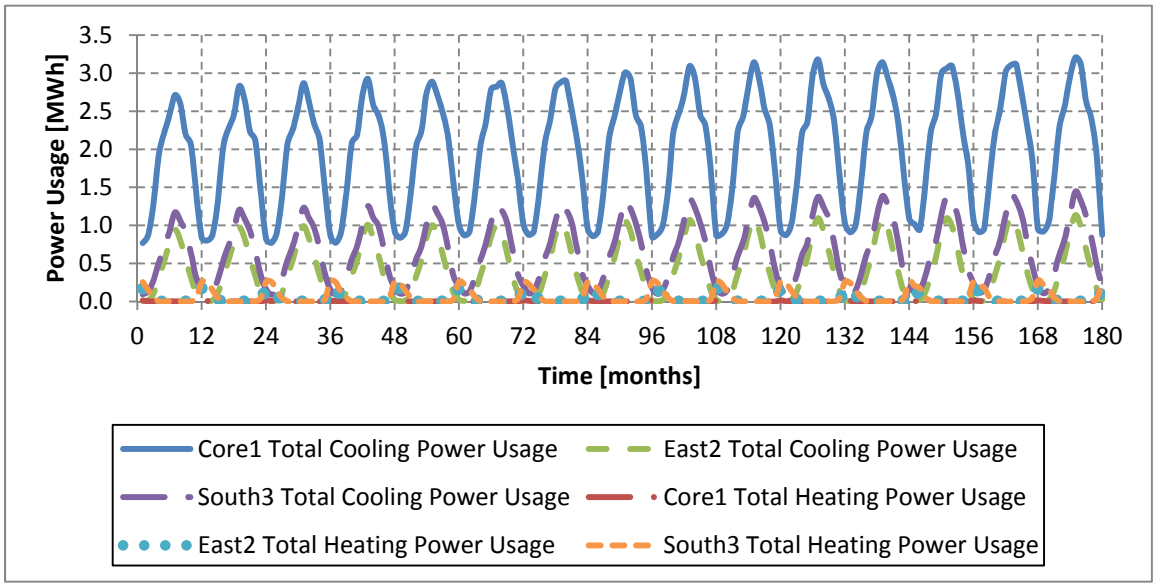

Figure 6.52: Monthly power usage totals in Core1, East2 and South3 for cooling and heating

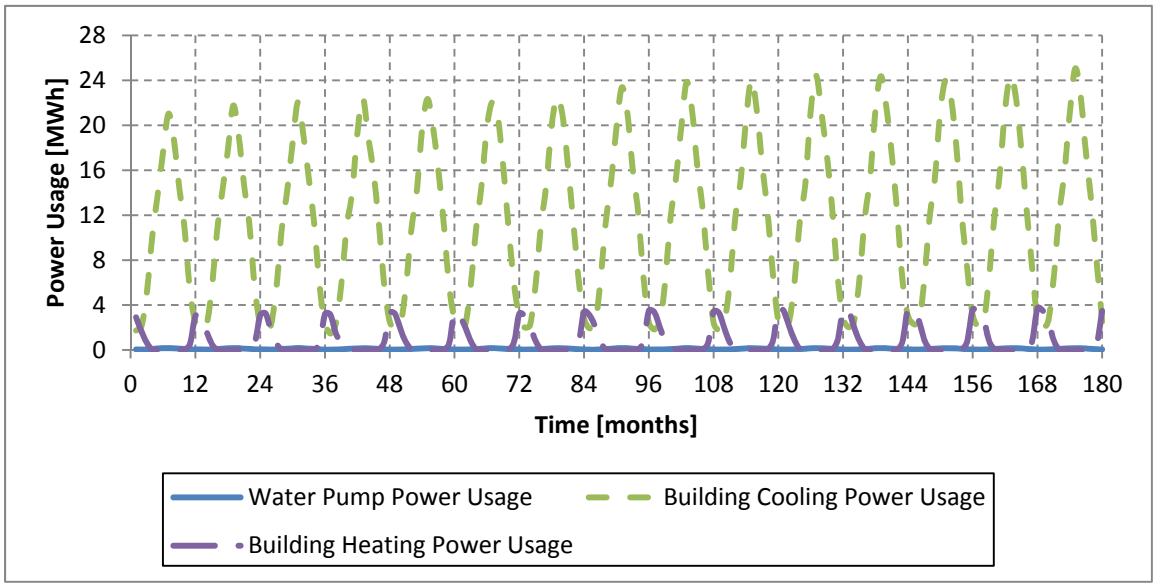

Figure 6.53: Monthly power usage totals for cooling, heating and water pump operation

In addition to increasing the total cost of operation, increasing HP EWT affects the ability of the HVAC system to meet temperature setpoint. The heat pump equipment shuts down to protect itself when entering water temperatures exceed 48.9°C (120°F) during cooling mode and 32.2°C (90°F) during heating mode. During shutdown, the heat pump provides neither heating nor cooling to the zone, resulting in free-floating temperature until the EWT returns to safe conditions. The increasing EWT still affects time out-of-setpoint if EWT values stay below the shutdown threshold. The total cooling capacity of the heat pump is inversely dependent on the entering water temperature, meaning that as the entering water temperature increases the total cooling capacity decreases. The time-out-of setpoint for the model reflect these effects, as shown in Figure 6.54.

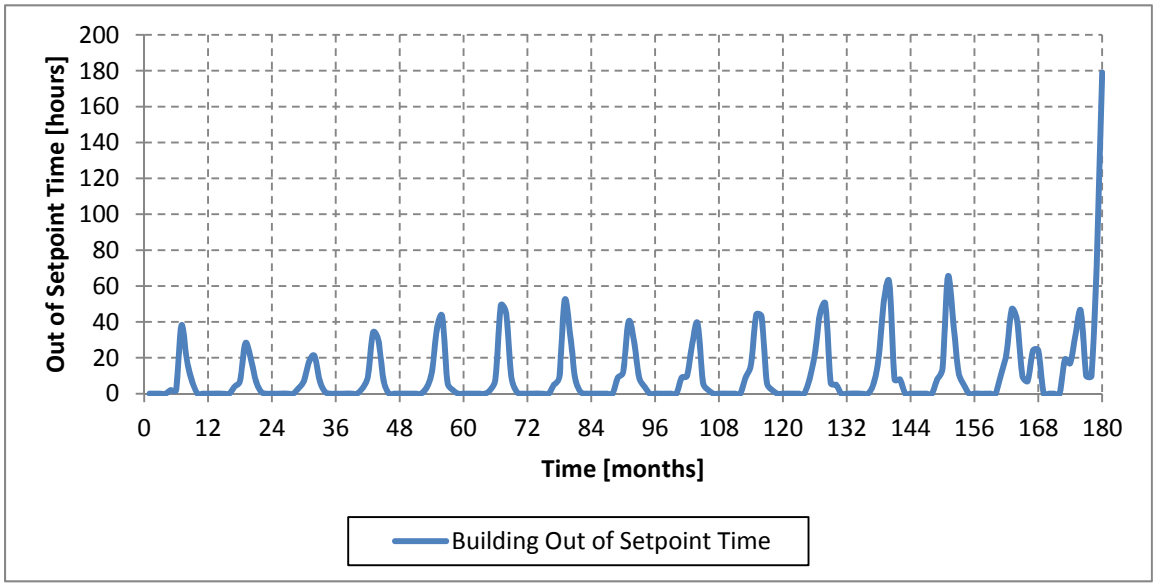

Figure 6.54: Monthly out-of-setpoint times

Another measure of the increasing power usage of the heat pumps is heat pump efficiency. While the amount of cooling and heating provided by the heat pumps hold constant from year-to-year, the increasing amount of power required to run the heat pump results in a decline in cooling efficiency. Cooling and heating efficiency values (EER and COP respectively) are shown in Figures 6.55, 6.56, 6.57 for Core1, East2 and South3, respectively. All three figures show year-over-year declines in cooling efficiency, but they also show the efficiency improvement that results from heating the building.

Heating the building requires the heat pumps to absorb energy from the ground loop, which effectively lowers the ground loop water temperature. As a result, the cooling efficiency values improve in February, March and April (months 14, 15 and 16 for example).

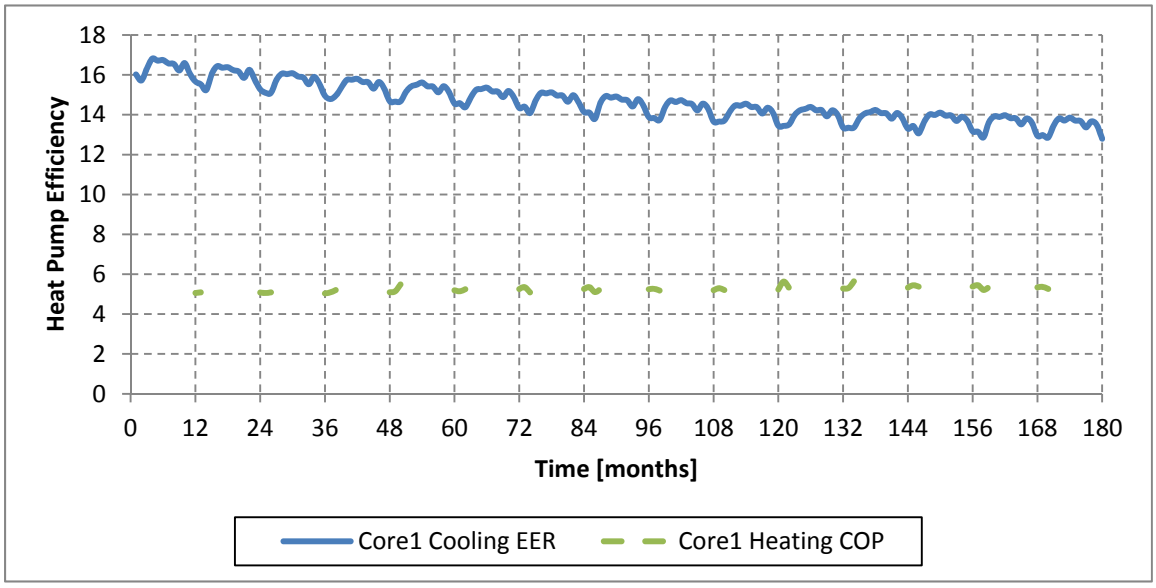

Figure 6.55: Monthly average cooling and heating efficiency for Core1

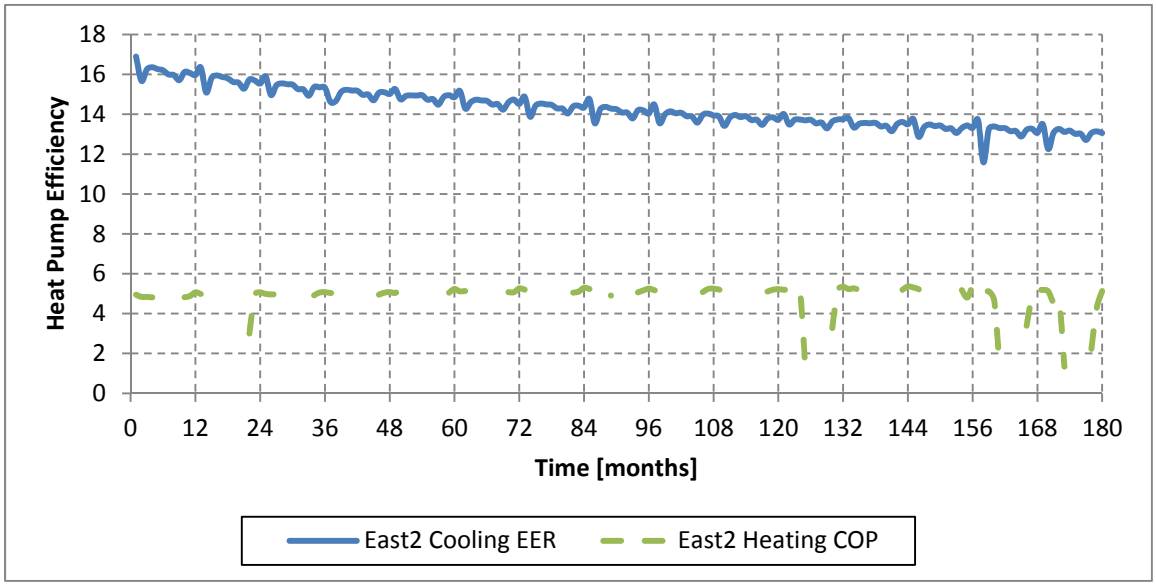

Figure 6.56: Monthly average cooling and heating efficiency for East2

Heating efficiency in all of the zones remains constant during most of the 15-year simulation. In the final years, declines in heating efficiency occur. These declines are an artifact of hourly

averaging. When a zone experiences both heating and cooling in a particular hour, the heating and cooling values cancel each other out in the hourly total, but the total energy usage does not cancel. This process occurs throughout the 15-year simulation, but in the final years the increasing EWT exacerbates it.

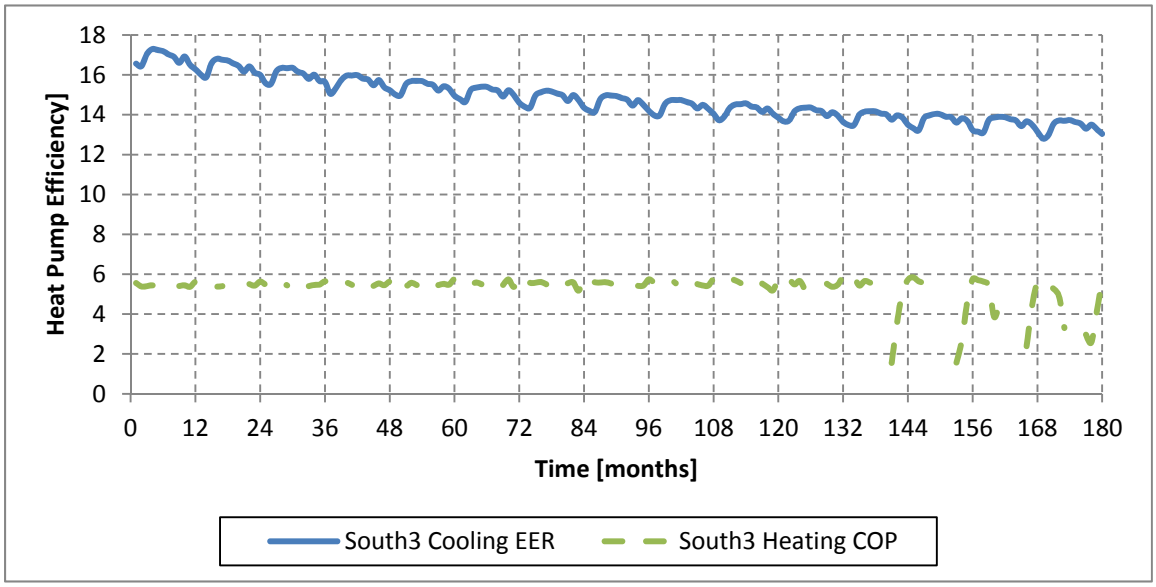

Figure 6.57: Monthly average cooling and heating efficiency for South3

6.4.4 Yearly Time Results

Annual values are used to examine yearly trends over the duration of the 15-year simulation. Annual averages, annual totals, annual maximums and annual minimums all serve to smooth the hourly data into a format viewable on a 15-year scale.

The total cooling energy provided by the building's heat pumps is shown in Figure 6.58. Totals for each floor are also shown. There is a slight decrease in the amount of cooling provided to the building over time, from 600MWh during the first year to 591MWh in year 15. The total hours of heat pump operation spent cooling zones also decreases from 49,671 hours to 49,542 hours during the 15-year simulation, as shown in Figure 6.60. This decline results from the increase in the number of hours when the heat pump is not operating due to high heat pump entering water temperature, as shown Figure 6.62. Annual heating, shown in Figure 5.59 and Figure 6.61, does not decrease over time.

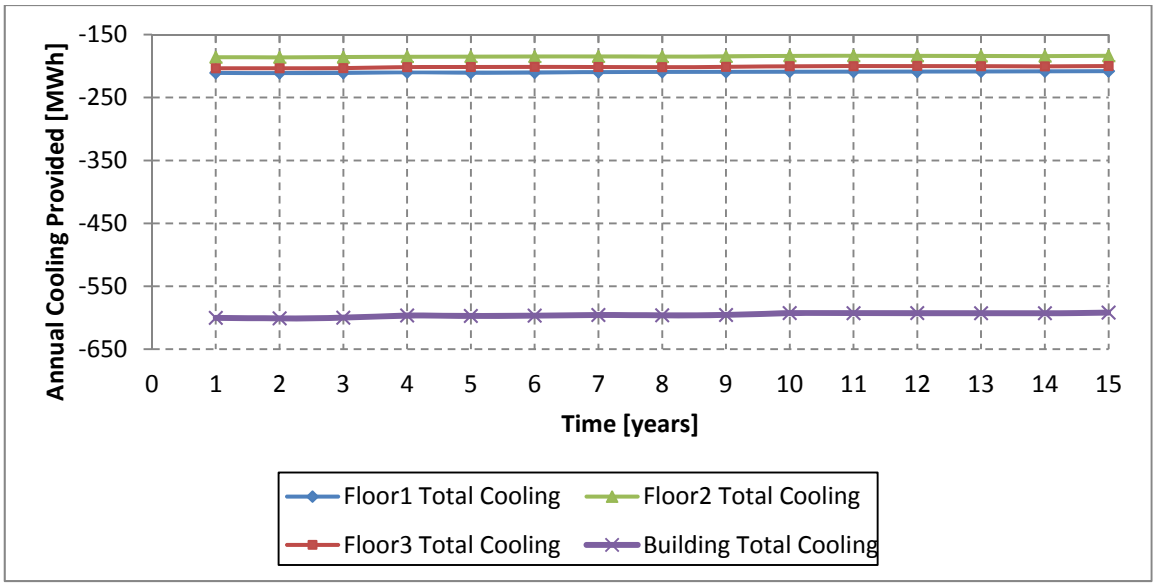

Figure 6.58: Annual total cooling energy provided in the base model

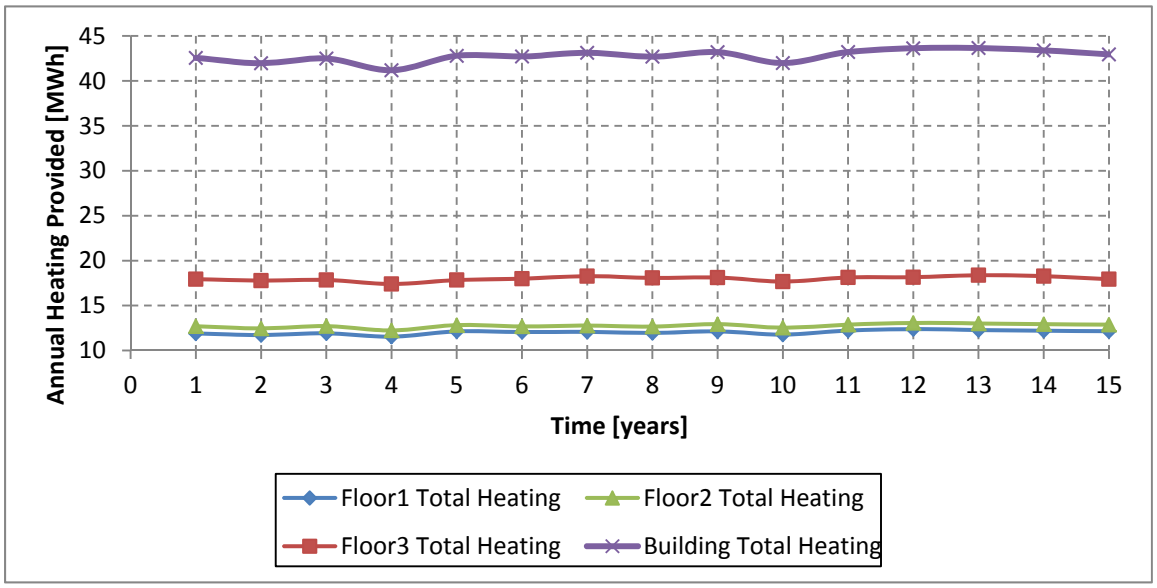

Figure 5.59 Annual total heating energy provided in the base model

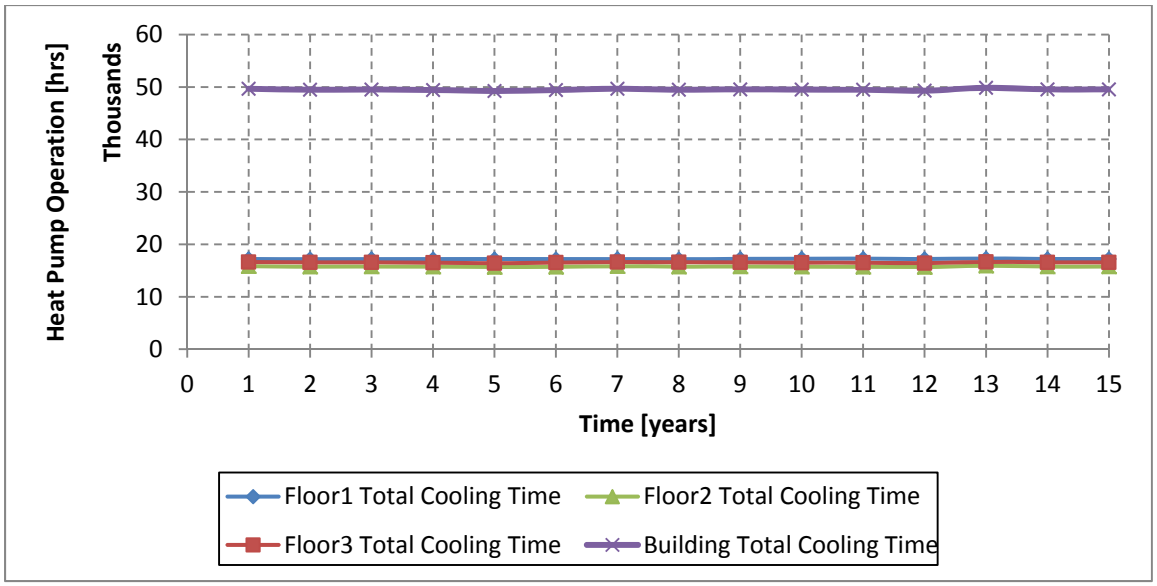

Figure 6.60: Annual hours of heat pump operation providing cooling

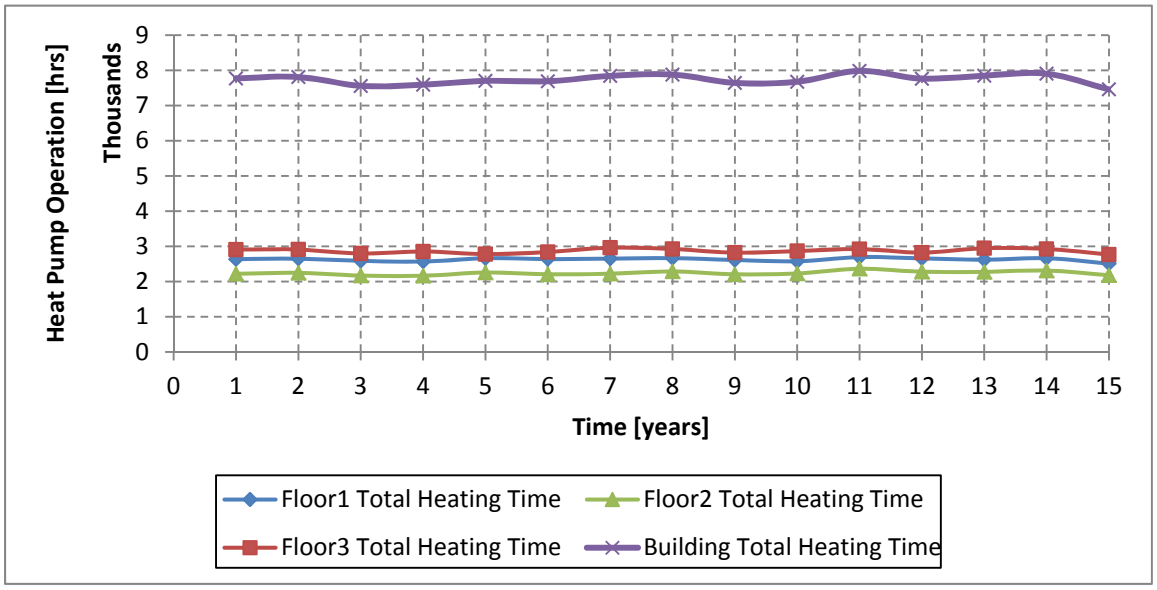

Figure 6.61: Annual hours of heat pump operation providing heating

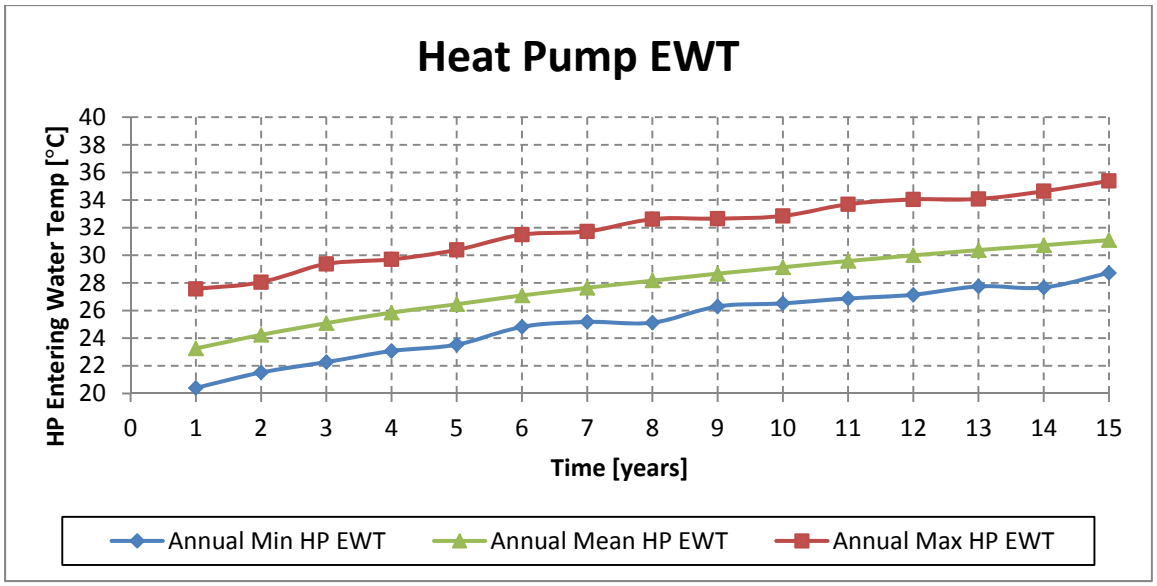

Figure 6.62: Annual extremes for heat pump EWT

The yearly averaged miniumum, mean and maximum heat pump EWTs are shown in Figure 6.62. Over 15 years of operation these temperatures rise approximately 8°C (14°F). The increasing EWTs reduce the total cooling capacity of the heat pumps and increase the amount of energy required to operate the heat pump. The increasing power usage is shown in Figure 6.63. These factors combine with the heat pump shutoff feature to increase the amount of time a heat pump is unable to meet the cooling needs of a zone. Figure 6.64 shows the gradual increase in out-of-setpoint conditions, as well as the rapid increase during the final year of simulation.

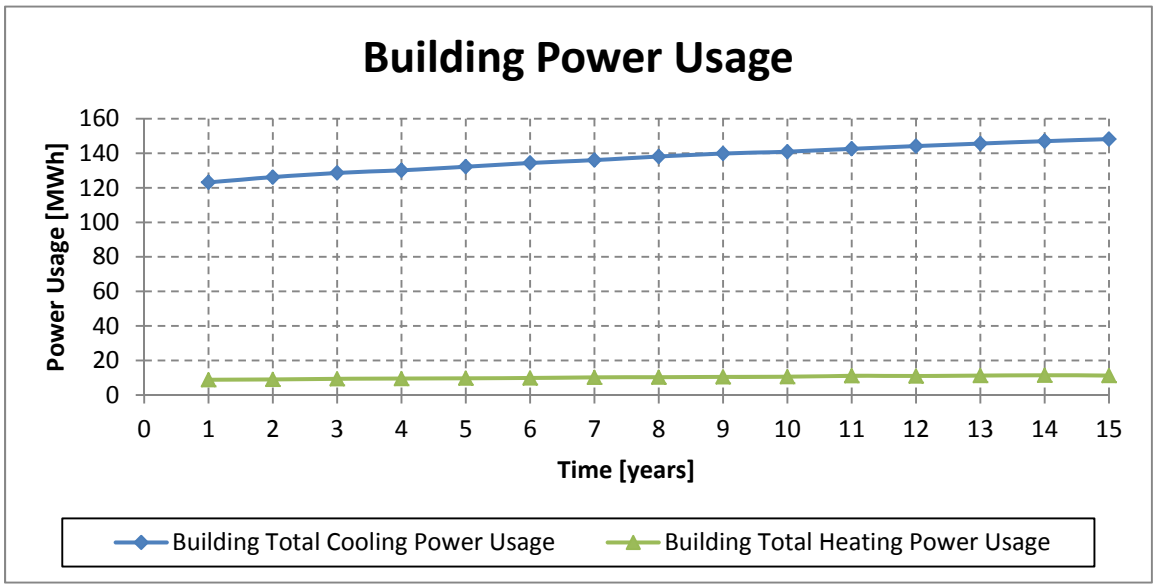

Figure 6.63: Annual power usage for heating and cooling

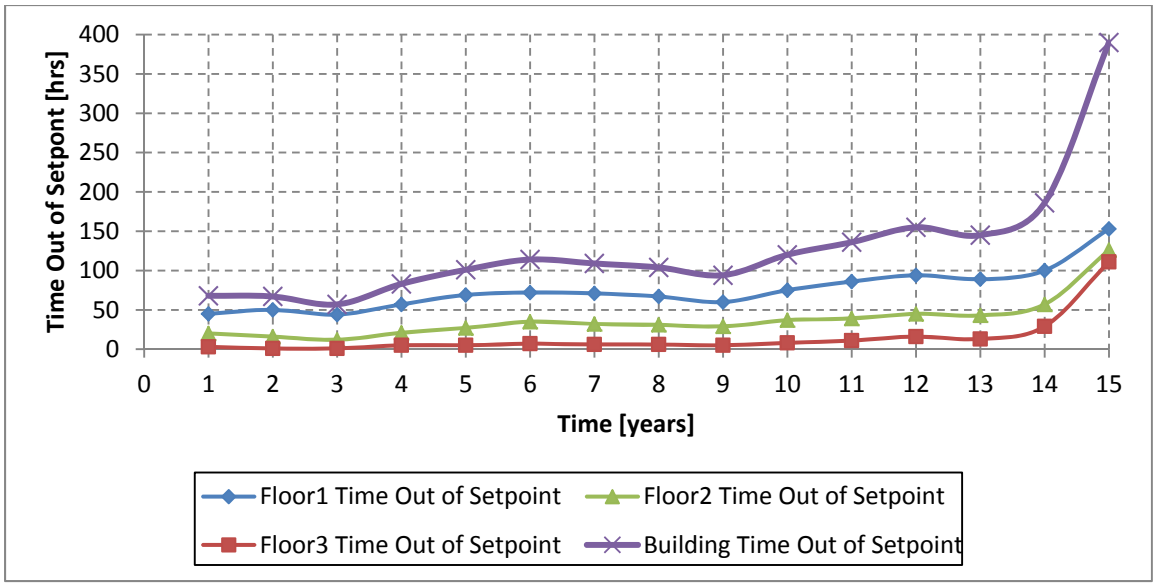

Figure 6.64: Annual total time out-of-setpoint in the base model

The ultimate measure of heat pump operation is efficiency. Cooling efficiency (EER) is shown in Figure 6.65 and heating efficiency (COP) is shown in Figure 6.66. Cooling efficiency declines, for example in Floor 3 from 17 EER to 14 EER, as the EWT increases due to the increasing power usage demands over 15 years of operation. Heating efficiency should increase when heat pump EWT increases, but as the EWT increases there are more hours that experience both heating and cooling. The heating and cooling values cancel each other out in the hourly total, but the total energy usage does not cancel, resulting in lower efficiency. For example, Floor 3, the COP decreased from 5.3 to 4.9.

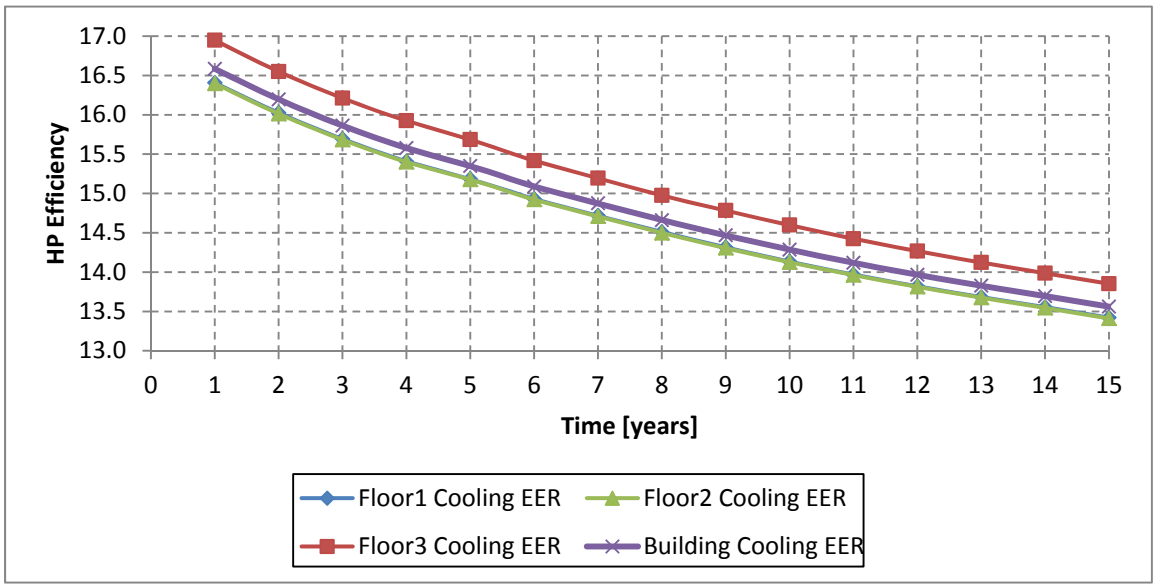

Figure 6.65: Annual average cooling efficiency in the base model

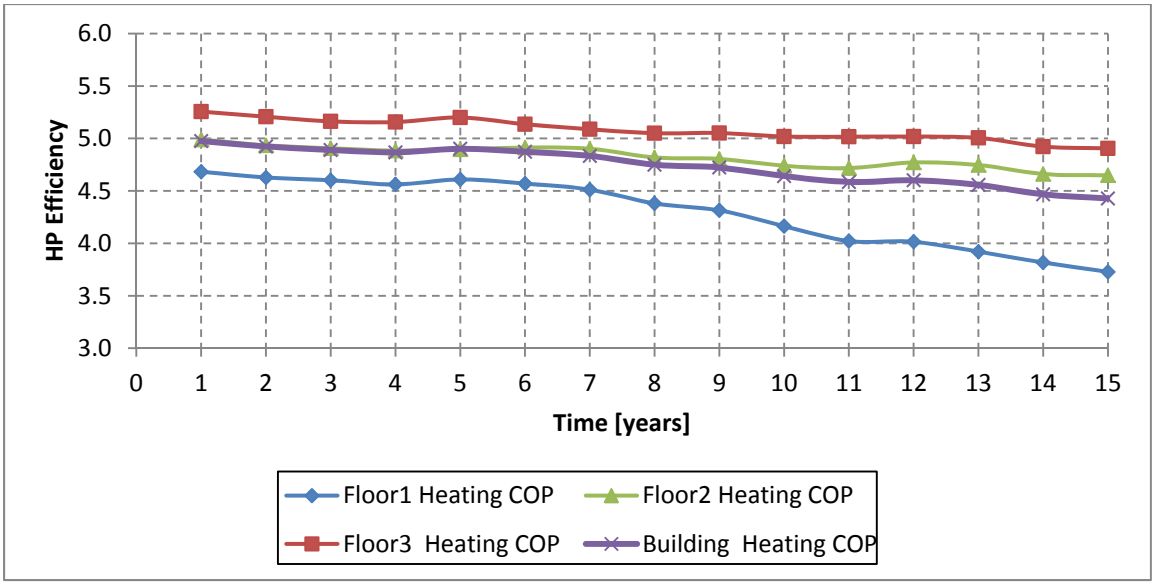

Figure 6.66: Annual average heating efficiency in the base model

6.5 IBL-GHP Base Case Commercial Office Building Sensitivity Study

Perturbations in designer-specified parameter values from the base case were made to determine their effects on the system operating efficiency and cost.

6.5.1 Supplemental Heat Rejection

To reduce the initial cost of installation, hybrid ground loop design approaches have been used. In this section, an ideal, unspecified supplementary heat rejection (SHR) device was included in the ground loop system. This device rejects a percentage of the total load generated by a heat pump during cooling, effectively reducing the total heat entering the ground loop. The actual system or methodology for the SHR device was is the focus of this research, instead, the goal is to decide whether it makes financial sense to find or design an SHR device for use in a ground source heat pump system.

Two different SHR tests are described in the following sections. The first test uses the shutoff heat pump EWT, 48.9°C (120°F), as the maximum heat pump EWT used by GLHEPRO and an extended borehole field centerline spacing of 9.1m (30ft). The use of this EWT should yield the minimum borehole length and minimum heat pump efficiency for the given centerline spacing. Test 1 uses the same GHEX length, 50.3m/borehole (1651ft), for 0%, 10%,and 25% added SHR. Table 6.36 shows the division of heating and cooling loads between the heat pumps and the SHR device.

Table 6.36: Annual Heating and Cooling Loads for SHR Tests

Test	Annual Heating Loads on Heat Pump [kW-h]	Annual Cooling Loads on Heat Pump [kW-h]	Annual Heating Loads on SHR Device [kW-h]	Annual Cooling Loads on SHR device [kW-h]
0% SHR	43,639	601,286	N/A	N/A
10% SHR	43,639	541,157	0	60,129
25% SHR	43,639	451,257	0	150,029

The second test also uses the heat pump shutoff temperature as the maximum heat pump EWT, but uses 10.7m (35ft) spacing. Test 2 resizes the GHEX based on reduced ground loop loads, and so has different GHEX lengths for the 0% SHR, 10% SHR and 25% SHR cases.

6.5.1.1 SHR Test 1: Constant GHEX Depth with 30ft Borehole Spacing

The ground loop system specifications for the first SHR test are shown in Table 6.37. The 0% SHR values reflect using the heat pump shutoff temperature as the maximum EWT used to size the borehole depth that resulted in 50.3m (165ft). That depth is kept constant. In this test, the variable input is the amount of SHR.

The maximum annual EWT for all three SHR conditions is shown in 6.67. The results for the base model are included for comparison. Recall that the base case has 20ft borehole centerline spacing and the borehole sized with maximum heat pump EWT of 32.2°C (90°F). Installation costs were based on a drilling cost of 23$/m (7$/ft) [Hammond, 2011].

Table 6.37: Test 1—Ground Loop Specifications for SHR Test 1 using 30' Borehole Spacing

Test	EWT Cutoff Temp. [°C]	Spacing [m]	Field Length [bores]	Field Width [bores]	Depth [m]	Total Length [m]	Installation Costs [$]
0% SHR	48.9	9.1	10	16	50.3	8,047	184,800
10% SHR	48.9	9.1	10	16	50.3	8,047	184,800
25% SHR	48.9	9.1	10	16	50.3	8,047	184,800
Base Model	32.2	6.1	10	16	170.7	27,310	627,200

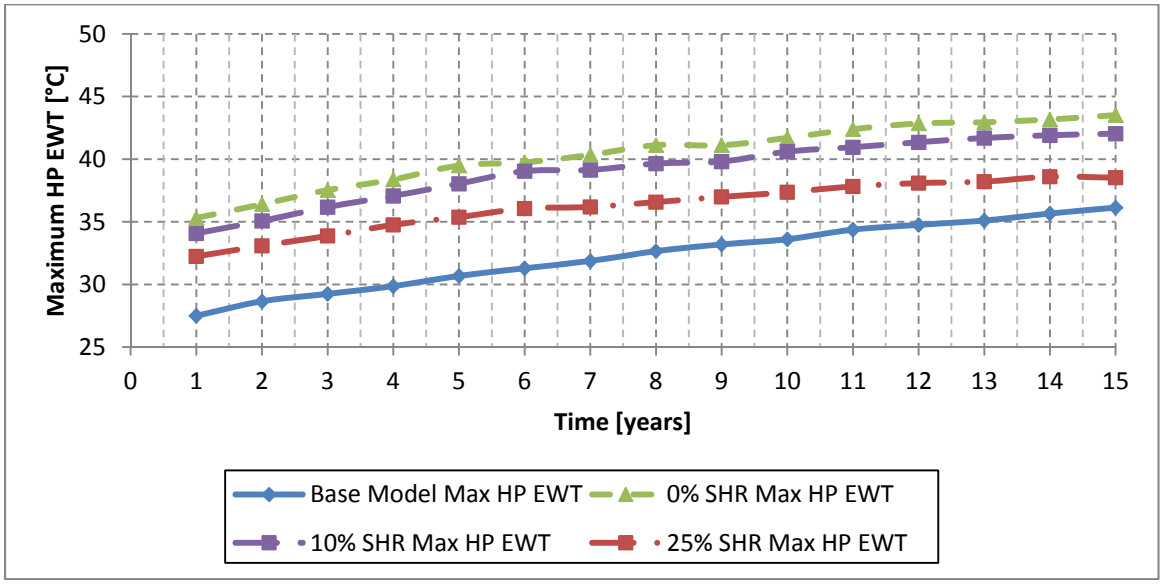

Figure 6.67: Maximum annual heat pump EWT for SHR Test 1

Increasing SHR from 0% to 10% to 25% reduces the maximum heat pump EWT. The initial EWTs for the SHR tests were all greater than that of the base model; the 25% SHR was initially 4.8°C greater than the base model. At the end of the 15-year simulation, this difference was reduced to only 2.4°C, with a total GHEX length 3.4 times shorter. Increasing the SHR allows significantly shorter GHEXs to approach the performance of the base model. The base case results look better because it was designed with a 90°F maximum heat pump EWT.

The performance narrowing effect in heat pump EWT with SHR is also seen in the total cooling provided. Figures 6.68-6.69 show the total cooling and the total heating provided to the zone, respectively. Both figures show that the amount of conditioning provided to the zones by the heat pumps approaches the base case as the SHR increases. In both cooling and heating however, the higher heat pump EWT for the SHR tests reduced cooling capacity and increased time out-of-setpoint for the zone temperature, shown in Figure 6.70.

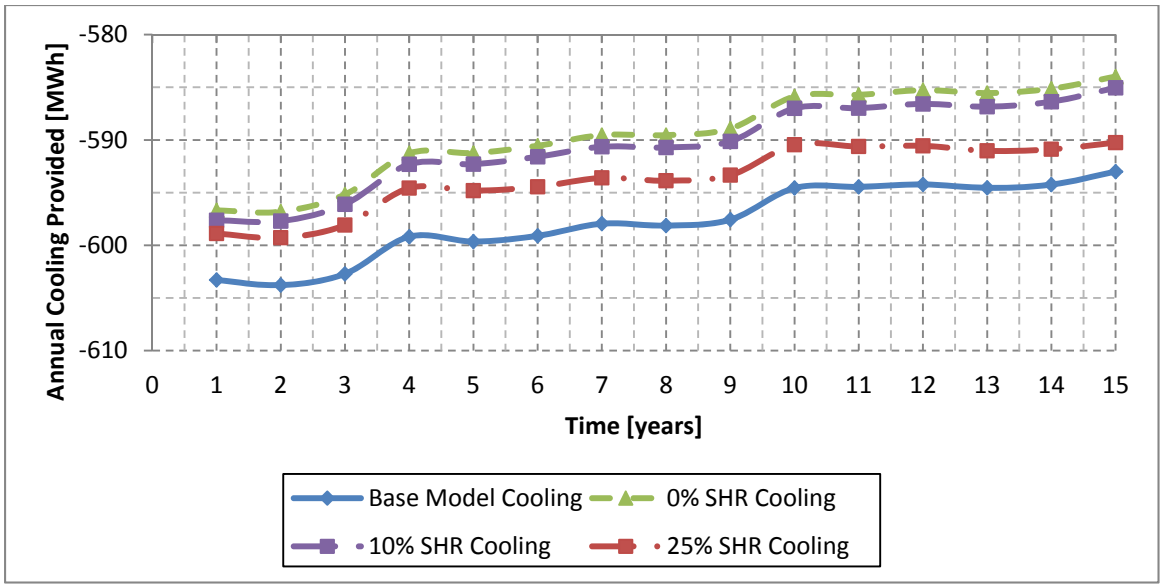

Figure 6.68: Total cooling for SHR Test 1

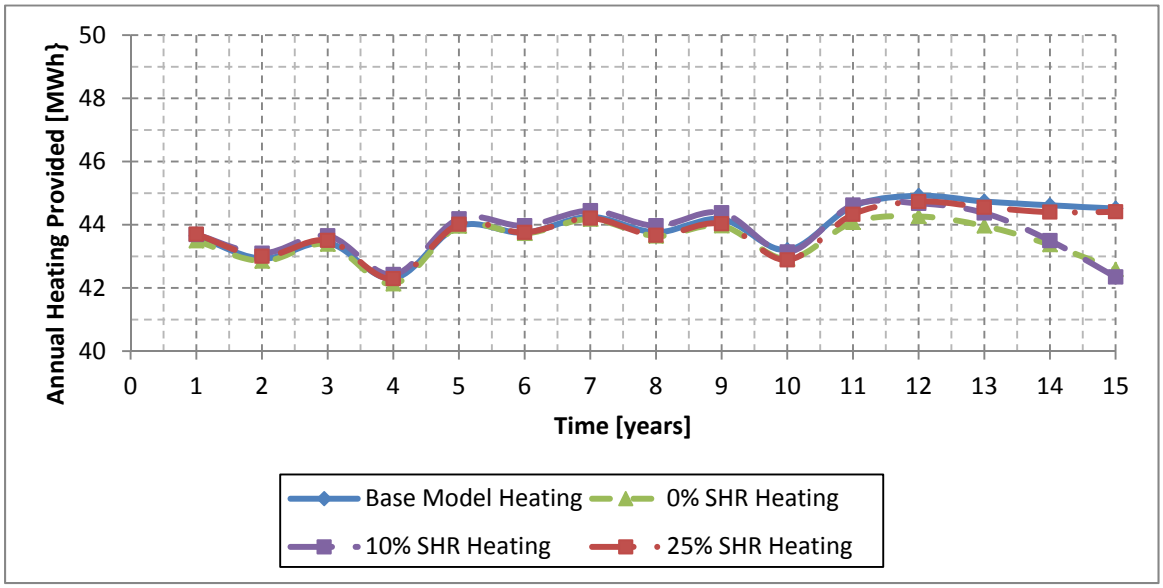

Figure 6.69: Total heating for SHR Test 1

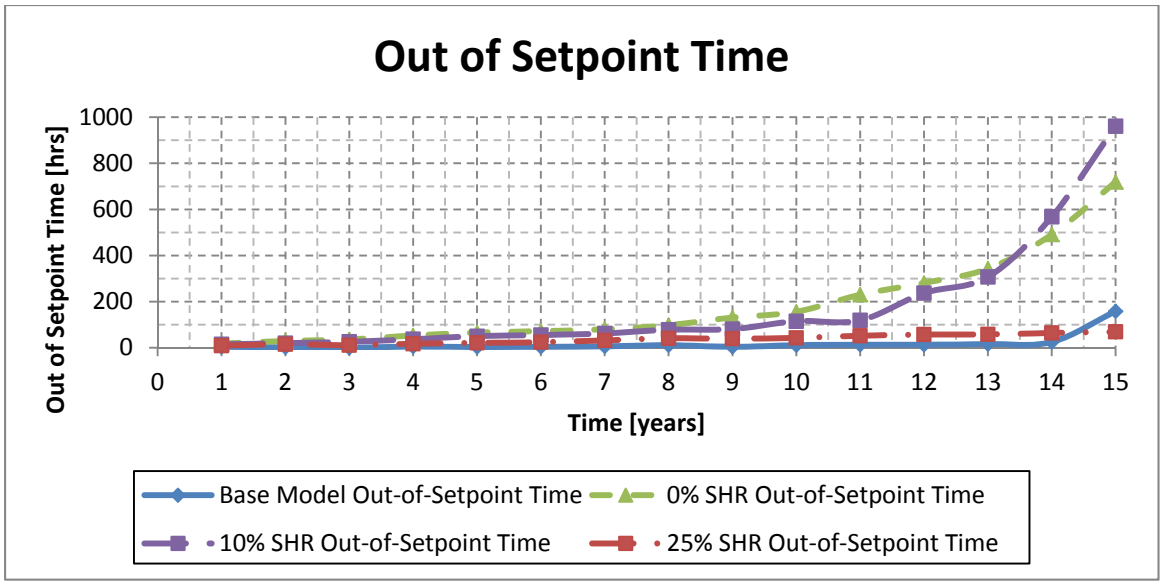

Figure 6.70: Time out-of-setpoint for SHR Test 1

Unlike the base case, the time-out-of-setpoint for the 25% SHR test does increase during year 15. While time-out-of-setpoint gradually increases throughout the simulation for the 25% SHR test, the reduction in heat rejected to the ground loop means that the cooling and heating loads are more in balance. Thus, heating mode operation will do a better job of re-charging the ground, delaying the onset of EWT-induced heat pump shutdown.

This re-charging can be seen in the annual power usage, shown in Figure 6.71 for cooling and Figure 6.72 for heating. For cooling, the power usage for the 25% SHR test is greater than the power usage of the base case, but the rate of change power usage for the 25% SHR test is less. As a result, during the first half of the simulation the base case has a much higher heat pump efficiency during cooling, but the gap between the base case and the 25% SHR test narrows during the second half of the simulation Figure 6.73.

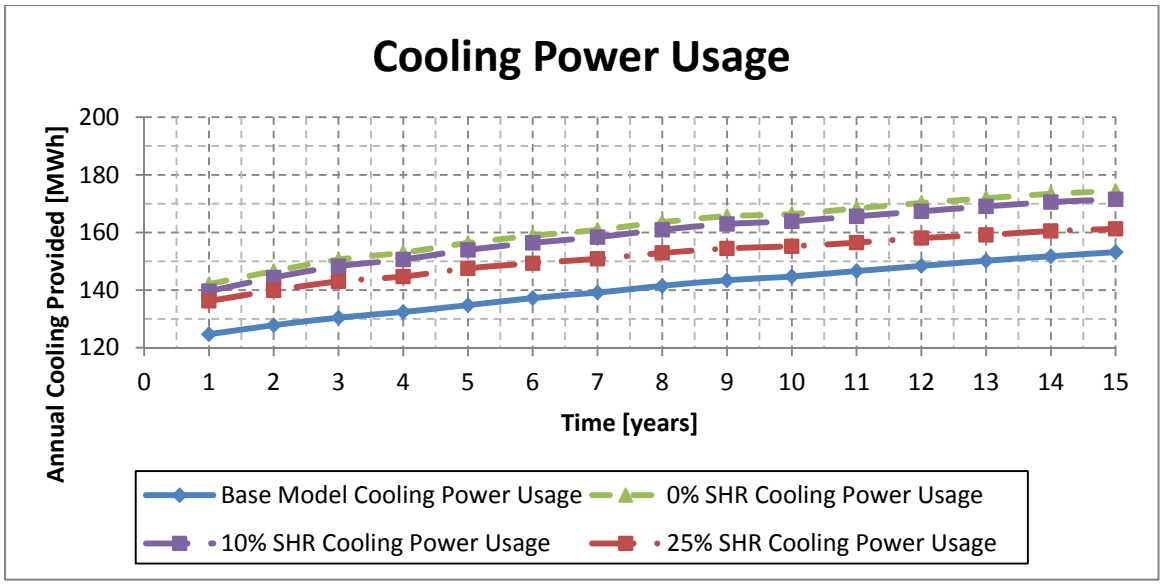

Figure 6.71; Electricity usage required for cooling in SHR test 1

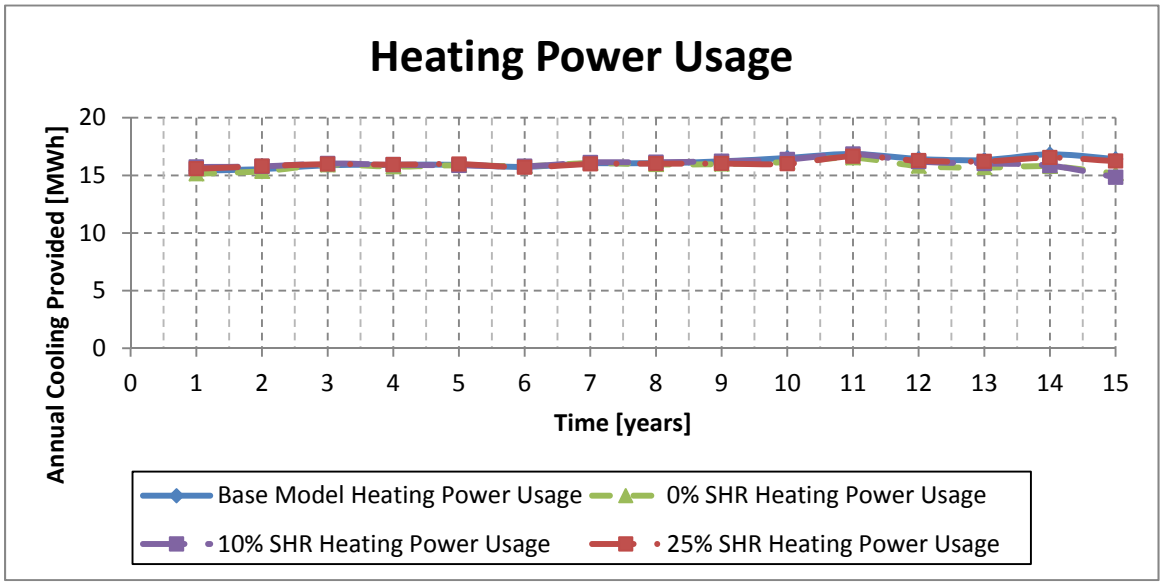

Figure 6.72: Electricity usage required for heating in SHR Test 1

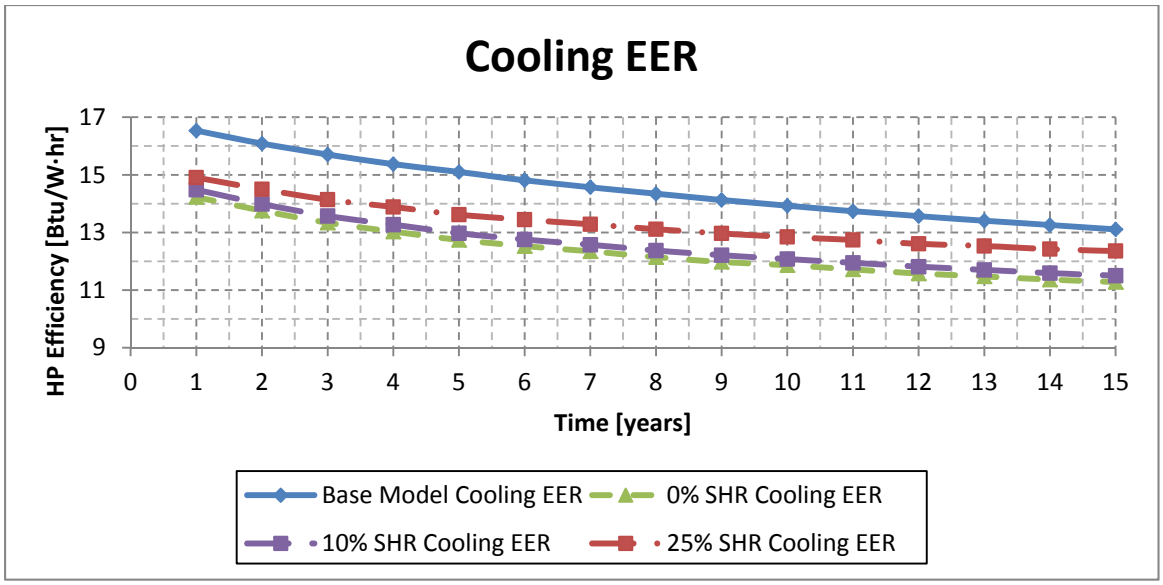

Figure 6.73: Heat pump efficiency during cooling for SHR Test 1

The total power usage of the building was used to calculate operation costs for the HVAC system. Electricity was assumed to be priced at the residential average for the state of Texas, 0.1145$/kWh [US DoE, 2013]. A comparison of the installation costs, 15-year operational costs, total savings and average time out-of-setpoint is shown in Table 6.38. While these results do not include the cost of installation or operation for the SHR system, the difference in installation costs easily provides room to install and operate one while reducing the total cost of ownership.

Table 6.38: Summary of Results for SHR Test 1

Test	Installation Costs [$]	15-Year Operation Costs [$]	15-Year Savings [$]	Max Annual Time Out-of-Setpoint [hrs]
Base Model	627,200	268,885	-	25
0% SHR	184,800	304,482	406,803	491
10% SHR	184,800	300,363	410,922	568
25% SHR	184,800	287,427	423,858	64

6.5.1.2 SHR Test 2: Variable GHEX Depth with 35ft Borehole Spacing

The ground loop system specifications for the second SHR test are shown in Table 6.39. Notice that the depth for each test changes based on the GHEX length specified by GLHEPRO when reduced ground loop loads are used. Installation costs were based on a drilling cost of 23$/m (7$/ft). The results for the base model are included for comparison.

The maximum annual EWT for all three SHR conditions is shown in Figure 6.74. The changing loop lengths for the two SHR cases negate most of the EWT gains that were shown in SHR Test 1. The rate of change of EWT for the 25% SHR case is lower than for the base case, but the difference is not as significant and the initial temperature gap is more pronounced.

Table 6.39: Ground Loop Specifications for SHR Test 2 using 35ft Borehole Spacing

Test	Spacing [m]	Field Length [bores]	Field Width [bores]	Depth [m]	Total Length	Installation Costs [$]
Base Model	6.1	10	16	170.7	27,310	627,200
0% SHR	10.7	10	16	46.0	7,364	169,120
10% SHR	10.7	10	16	41.1	6,584	151,200
25% SHR	10.7	10	16	33.2	5,316	122,080

Results for total cooling (Figure 6.75), total heating (Figure 6.76), out-of-setpoint time (Figure 6.77), electricity usage (Figures 6.78-6.79) and heat pump efficiency (Figure 6.80) are shown on the following pages. All of the results mirror the EWT results: increasing the SHR gives better long-term ground loop response, but the decreased GHEX length largely eliminates the gains found in SHR Test 2.

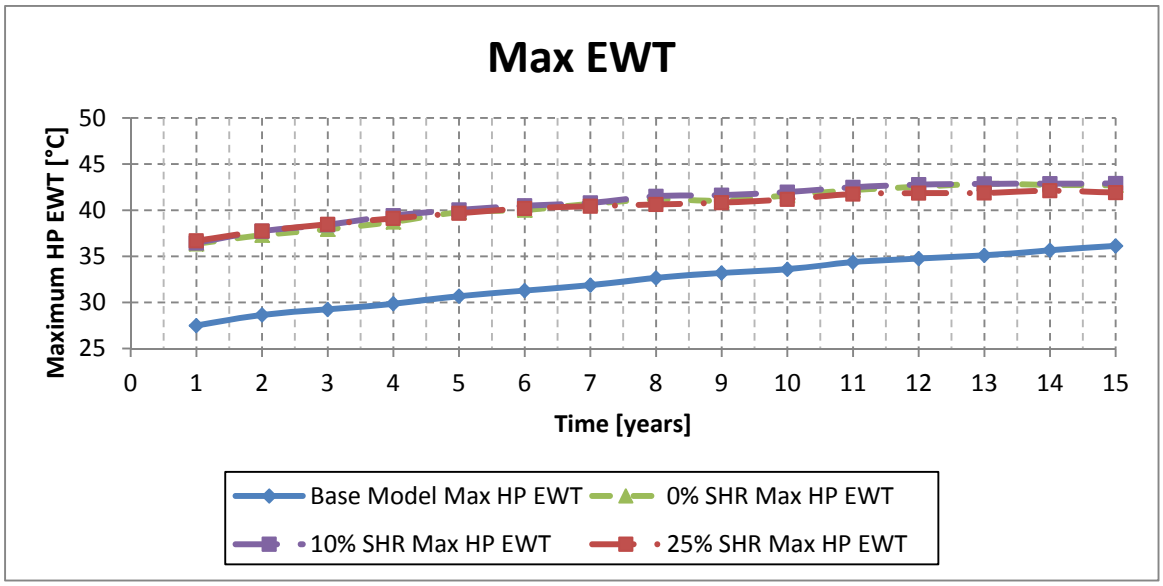

Figure 6.74: Maximum annual heat pump EWT for SHR Test 2

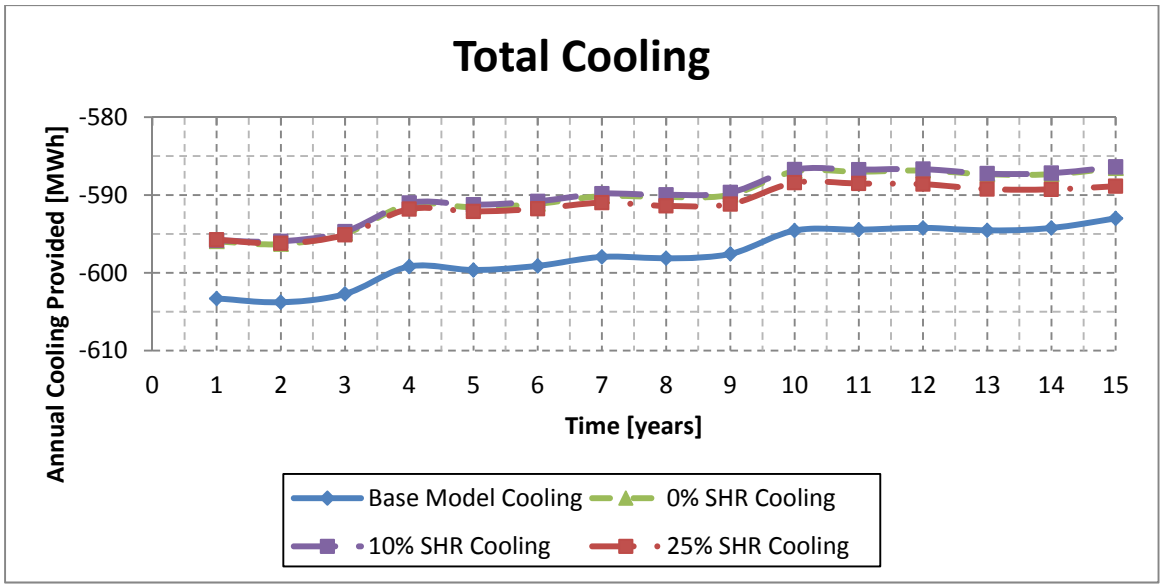

Figure 6.75: Total cooling for SHR Test 2

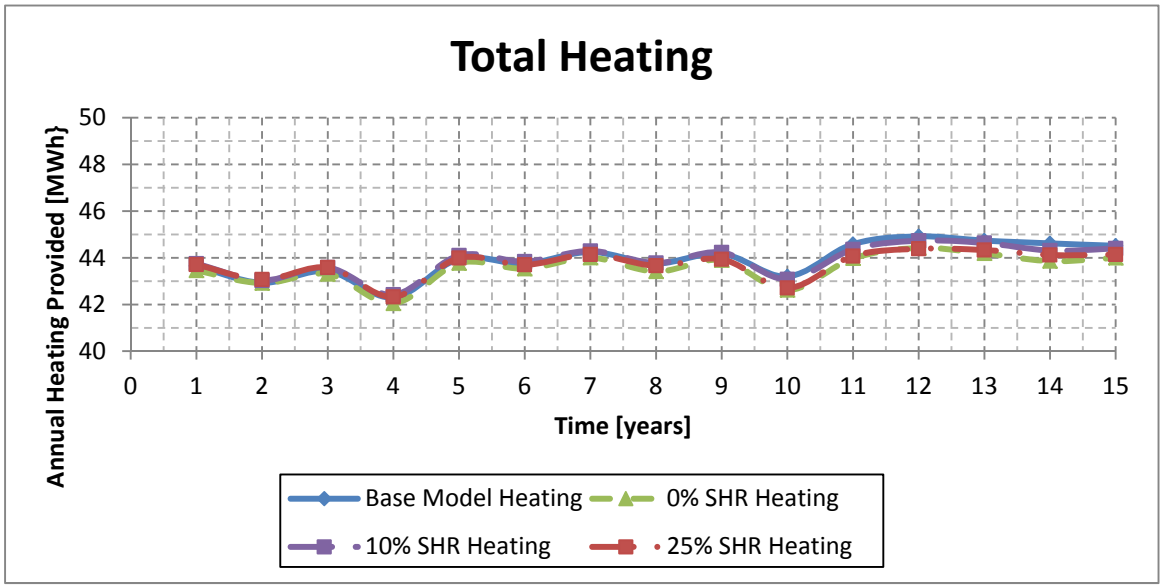

Figure 6.76: Total heating for SHR Test 2

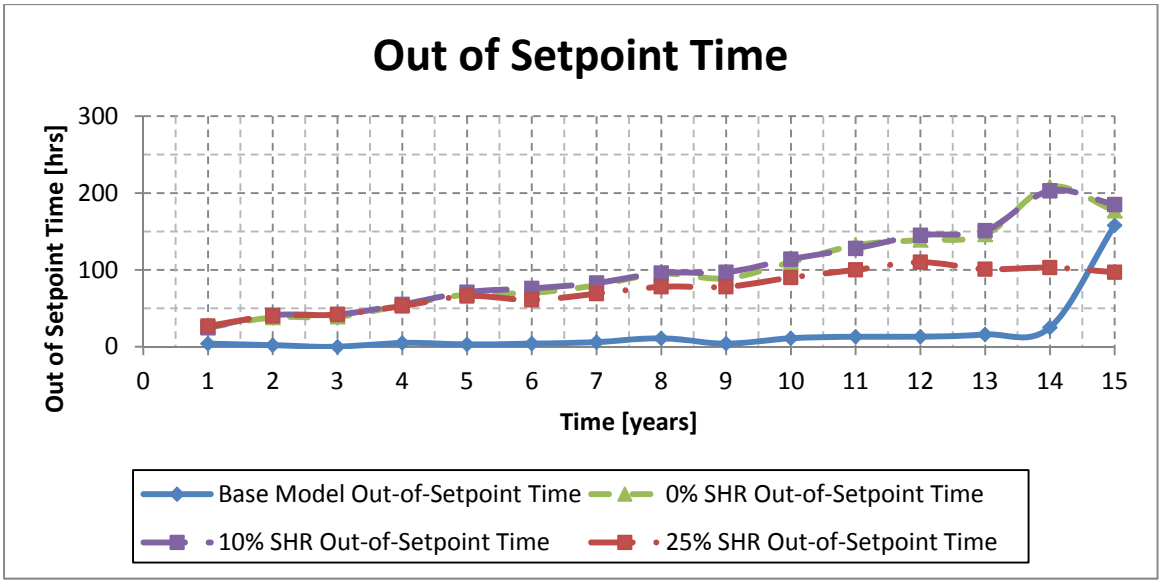

Figure 6.77: Time out-of-setpoint for SHR Test 2

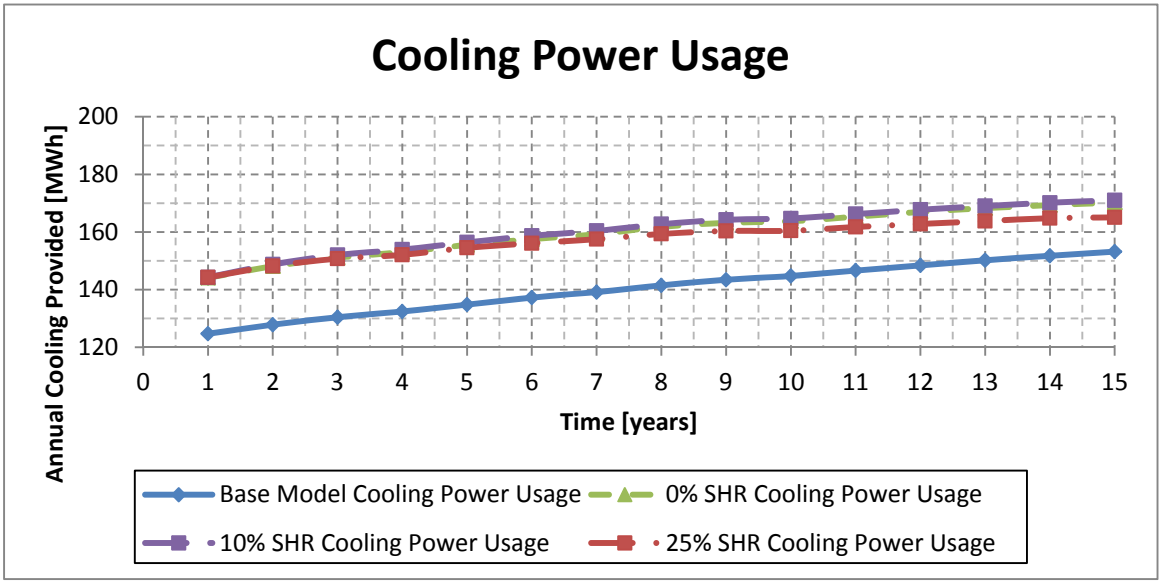

Figure 6.78: Electricity usage required for cooling in SHR Test 2

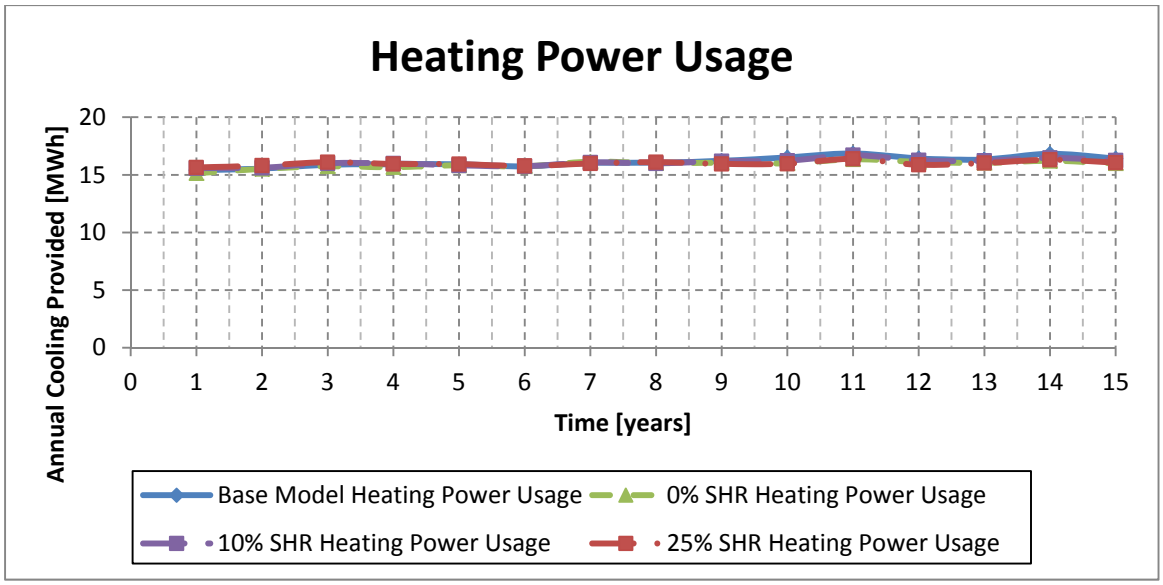

Figure 6.79: Electricity usage required for heating in SHR Test 2

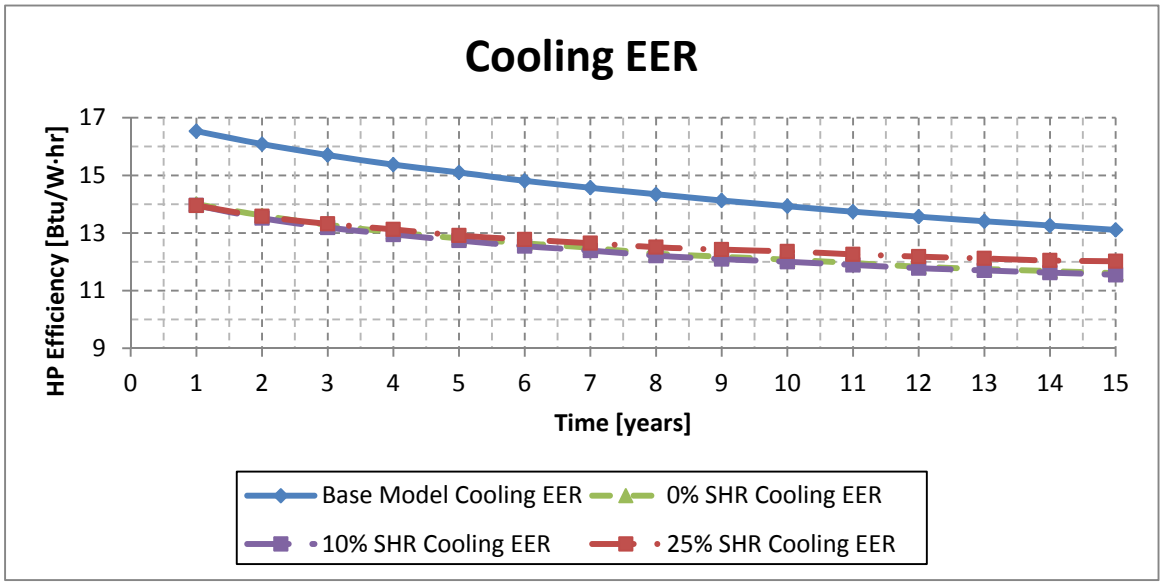

Figure 6.80: Heat pump efficiency during cooling for SHR Test 2

The total power usage of the building was used to calculate operation costs for the HVAC system. Electricity was assumed to be priced at the residential average for the state of Texas, 0.1145$/kWh. A comparison of the installation costs, 15-year operational costs, total savings and average time out-of-setpoint is shown in Table 6.40 These results do not include the cost of installation or operation for the SHR system, but the difference in installation costs still provides room to install and operate one while reducing the total cost of ownership.

Table 6.40: Summary of Results for SHR Test 2

Test	Installation Costs [$]	15-Year Operation Costs [$]	15-Year Savings [$]	Avg. Annual Time Out-of-Setpoint [hrs]
Base Model	627,200	268,885	-	8.4
0% SHR	169,120	301,810	425,155	92.4
10% SHR	151,200	303,566	441,319	94.8
25% SHR	122,080	297,857	476,148	72.7

Blair also reports a sensitivity study varying the maximum heat pump EWT used to size the boreholes from 35^{o}C (95^{o}F) to 48.9^{o}C (120^{o}F) in increments of 5^{o}F [Blair, 2013] with no SHR and 6.1m (20ft) centerline spacing. While increasing EWT decreased installation costs from shorter boreholes and satisfied the zonal temperature control during cooling, each case did not satisfy the heating requirements as the heat pump exceeded the maximum 32.3^{o}C (90^{o}F) during the cooling mode. Heat pump shutoff during the heating mode occurred as early as six years for the 115^{o}F case to approximately 13 years for the 95^{o}F case. Thus the base case of 90^{o}F maximum heat pump EWT was the minimum value that yielded good control for a 10x16 borehole field. Larger borehole fields would not be as restrictive.

7.0 GHP Residential Building Design Study

An original project objective was to develop an interactive web-based program to provide users with design decisions based upon technical GHP/HGHP performance and life-cycle costs, however this task was not accomplished because of the complexity of the IBL-GHP model and long simulation times required for multiyear operation. Instead, a residential building construction design study was performed for three cities representative of the southwest region: Austin, Albuquerque and Phoenix. Using the 195m^2 (2100ft^2) base case residential house (brick exterior, asphalt shingle roof, minimum insulation (per code) in exterior walls/windows) described in Section 4, this study investigated the extent to which the following house construction parameters improve GHP performance.

1) exterior wall type (brick, stone, wood, and cement),
2) roof (shingle and metal),
3) exterior wall insulation (code minimum up to maximum based upon spacing),
4) window fenestration/solar gain (code minimum and maximum thermal insulation effects)—will be referred to as window insulation

Both new construction and retrofit construction cases were considered. In this study, the number of unmet hours was used as a metric to design the GHP systems and compare different construction cases; the ASHRAE Standard 90.1-2007.G3.1.2.2 states that the conditioned space temperature can be outside the setpoint deadband (unmet hours) a maximum of 300 hours based upon hourly averages [ASHRAE, 2007b].

Section 7.1 discusses the building codes and climate/geological properties of the three cities. Section 7.2 lists the material property variations from the base case. Sections 7.3-7.4 provide the results of the new and retrofit construction studies, respectively.

7.1 CITIES, BUILDING LOADS AND BUILDING CODES

7.1.1 Cities

The cities of Austin, Albuquerque, and Phoenix were selected for this study to represent cities in the Southwest region of the US and to illustrate variations in weather and ground properties. Tables 7.1 compares the ground temperatures, ground thermal properties, cooling/heating loads and base case heat pump capacity and ground loop sizing for all three cities. Austin has the best soil thermal properties, Albuquerque has lowest ground temperatures, and Phoenix has the most cooling dominated thermal loads. The loads shown are annual design peak loads, which is 1% of the peak cooling and heating loads. The design peak cooling

loads in Phoenix and Austin are 300% and 25%, respectively, higher than the design peak heating loads. On the other hand, Albuquerque has a slightly higher design peak heating load compared to the design peak cooling load. The uniqueness of each city's weather and geological conditions is reflected in vastly different GHP heat pump capacities and borehole sizing. Albuquerque requires a small heat pump unit (7.71kW/2-ton) because of its lower ground temperature and more balanced heating/cooling loads, In contrast, Phoenix requires a large ground loop (130m/borehole/--425ft/borehole) and a large heat pump capacity (21.9kW/6-ton) because relatively high ground temperatures, relatively low thermal soil properties, and cooling dominated requirements.

Table 7.3: Ground Properties, Design Peak Building Loads, and GHP Sizing for Base Cases in all Three Cities (SI units)

Base Case	Austin	Albuquerque	Phoenix
Ground Temperature °C (^{o}F)	21.7 (71)	15 (59)	22.8 (73)
Soil Thermal Conductivity, W/m*K (BTU/(hr*ft*F))	1.51 (0.87)	0.87 (0.51)	0.87 (0.5)
Soil Heat Capacity MJ/(m^3*K) (BTU/hr)	1.35 (20.1)	1.04 (15.5)	1.21 (18)
Annual Design Peak Cooling Loads kW (kBTU/hr)	7.3 (25000)	6.1 (20700)	10.4 (35500)
Annual Design Peak Heating Loads kW (kBTU/hr)	5.8 (19800)	6.6 (22400)	3.4 (11700)
Heat Pump Unit Size kW (BTU/hr)	14.6 (4)	7.71 (2)	20.7 (6)
Overall Ground Loop Length m (ft)	250 (820)	246 (808)	777 (2550)

7.1.2 Building Loads

Tables 7.2a (SI units) and 7.2b (British units) list the monthly total and peak building loads for the base cases for the 1st year. Austin has cooling loads every month compared to Albuquerque's seven and Phoenix's ten months. Albuquerque has heating loads for eight months, compared to five months for Austin and Phoenix. Furthermore, the differences in the monthly cooling loads are large; Phoenix has a cooling peak load of 11.7kW (40 kBTU/hr) compared to 6.4kW (22 kBTU/hr) for Albuquerque and 8.2kW (28 kBTU/hr) in Austin. The difference in cooling peak loads between Phoenix and Albuquerque is almost 50%. In contrast, Albuquerque has a maximum total monthly heating load of 13939kWhr (13212kBtu), which is about twice the 7619kWhr (7221kBtu) for Austin and three times the 4328kWhr (4102kBtu) for Phoenix.

Table 7.2a: Monthly Building Loads for Austin, Albuquerque, and Phoenix for the Base Cases (SI units)

	Austin				Albuquerque				Phoenix			
Month	Heating Load kWhr	Cooling Load kWhr	Heating Peak Load kW	Cooling Peak Load kW	Heating Load kWhr	Cooling Load kWhr	Heating Peak Load kW	Cooling Peak Load kW	Heating Load kWhr	Cooling Load kWhr	Heating Peak Load kW	Cooling Peak Load kW
Jan	2116	6	10.6	2.1	3847	0	8.8	0.0	1202.2	0.0	10.7	0.0
Feb	1303	47	6.4	2.6	2621	0	6.5	0.0	443.1	267.4	4.5	4.3
Mar	581	486	6.2	4.1	1447	0	5.2	0.0	170.2	548.3	4.1	3.9
Apr	0	1329	0	5.6	281	174	3.2	3.1	29.1	2306.2	2.6	7.5
May	0	2440	0	7.0	40	837	1.6	4.5	0	3668.4	0	8.6
Jun	0	3444	0	7.6	0	2211	0	6.4	0	5622.0	0	11.7
Jul	0	4117	0	8.2	0	3223	0	6.4	0	6508.5	0	11.8
Aug	0	4056	0	7.9	0	2835	0	6.2	0	5645.7	0	11.2
Sep	0	2548	0	6.7	0	1214	0	4.6	0	4234.0	0	9.6
Oct	0	1265	0	6.2	730	212	5.7	3.4	0	2326.5	0	7.2
Nov	382	341	3.8	4.1	2251	0	6.6	0.0	46.9	265.6	2.0	3.0
Dec	1832	10	7.0	2.1	3872	0	7.0	0.0	1180.2	0.0	4.2	0

Table 7.2b: Monthly Building Loads for Austin, Albuquerque, and Phoenix for the Base Cases (British units)

	Austin				Albuquerque				Phoenix			
Month	Heating Load kBTU	Cooling Load kBTU	Heating Peak Load kBTU/hr	Cooling Peak Load kBTU/hr	Heating Load kBTU	Cooling Load kBTU	Heating Peak Load kBTU/hr	Cooling Peak Load kBTU/hr	Heating Load kBTU	Cool-ing Load kBTU	Heating Peak Load kBTU/hr	Cooling Peak Load kBTU/hr
Jan	7221	22	36	7	13126	0	30.1	0	4102	0	36.68	0
Feb	4446	159	22	9	8943	0	22.1	0	1512	912.3	15.24	14.51
Mar	1983	1659	21	14	4936	0	17.6	0	580.7	1871	13.82	13.46
Apr	0	4534	0	19	959	594	10.9	10.7	99.3	7869	8.91	25.69
May	0	8326	0	24	138	2856	5.5	15.4	0	12517	0	29.28
Jun	0	11753	0	26	0	7545	0	21.8	0	19183	0	39.85
Jul	0	14049	0	28	0	10999	0	21.7	0	22208	0	40.36
Aug	0	13838	0	27	0	9674	0	21.0	0	19264	0	38.14
Sep	0	8693	0	23	0	4142	0	15.8	0	14447	0	32.75
Oct	0	4315	0	21	2490	725	19.5	11.5	0	7938.3	0	24.43
Nov	1304	1165	13	14	7681	0	22.4	0	159.9	906.4	6.79	10.36
Dec	6250	34	24	7	13212	0	23.9	0	4027	0	14.25	0

7.1.3 Building Codes

The building codes for the insulation thermal resistance requirements for the three cities are shown in Tables 7.3 and 7.4 below and are established to provide a minimal construction standard based on weather and environmental conditions for those cities.

Table 7.4: Building Code Insulation Requirements [Austin, 2008; Albuquerque, 2007; Phoenix, 2006]

Required Insulation					
City	Fenestration U-factor	Skylight U-factor	Glazed Fenestration SHGC	Ceiling R-value	Wood frame wall R-value
Austin	0.75	0.75	0.4	30	13
Phoenix	0.75	0.75	0.4	30	13
Albuquerque	0.4	0.6	NR	38	13

Table 7.5: Building Code Insulation Requirements [Austin, 2008; Albuquerque, 2007; Phoenix, 2006]

Required Insulation - 2					
City	Mass wall R-value	Floor R-value	Basement wall R-value	Slab R-value and Depth	Crawl Space R-value
Austin	4	13	0	0	0
Phoenix	4	13	0	0	0
Albuquerque	5	19	10 -/-13	10,2ft	10 -/-13

The important parameters for this study are the fenestration U-factor, glazed fenestration SHGC, ceiling R-value, and wood frame R-value. Fenestration and fenestration solar heat gain coefficient (SHGC) will be explained in more detail below. Some of other insulation standards are either not applicable to this study or cannot be implemented without major changes to the model. For example, the modeled house does not have a basement, crawl space, or skylights. Although, this house has a both a floor and a slab, these two parameters will not be considered when conducting the parametric test—the R-value for the slab in two out of the three cities is zero and the floor R-value is easily met with in the existing model.

Albuquerque requires more insulation in the floor and slab, the ceiling, and fenestration. Albuquerque has lower ground temperatures, requiring more insulation from the ground, therefore, the higher floor and slab insulation. Albuquerque is also at a higher elevation than most other cities, ranging from 1490-1950 meters above sea level [PMIUSA, 2011]. Therefore, more insulation is required to minimize the effects of extreme temperatures.

The insulation values that are shown above will be achieved by changing the material thickness to provide the right amount of insulation. To make it easier, this simulation will use an insulation amount that is close to the minimum amount as possible without changing multiple materials for each wall or window. For example, the MinWool Batt insulation used in the external walls has a minimum and maximum thickness that is applied to the walls. Therefore the minimum and maximum MinWool Batt insulation resistance value that gets us closest to the resistance values from the building codes will be used. This will allow a more controlled simulation where only one parameter is being changed at a time. The resistance values of the insulation in the base case house are shown in Table 7.5. Only the exterior walls are closest to the minimum insulation required by the building codes. The rest of the resistance values, which are determined by adding the resistance of the layers of material in each component is higher than the minimum values and is based on the geometry of the house. Only the exterior walls and roof resistance values will be considered for this research.

Table 7.6: Thermal Resistance of Base House Components

Resistance Values – Base Case House		
	R(m^2K/W)	R(h·ft²·°F/Btu)
Exterior Walls	2.64	14.99
Roof	0.63	3.58
Ceiling	6.69	38
Foundation	4.04	22.92

The external wall must meet either the mass wall R-value or the wood frame wall R-value. The International Residential Code defines mass walls as “an above-grade wall made of concrete block, concrete, insulated concrete forms (ICF), masonry cavity, brick, earth, adobe, compressed-earth block, rammed earth, and solid timber/logs [Southface, 2011].” On the other hand, a wood frame wall is a load-bearing wall that carries the weight of the roof and floor all the way down to the foundation. According the 2006 International Energy Conservation Code, in order to use the mass wall R value criteria, 50% of the required insulation R-value must be on the exterior of, or integral, to the wall. Otherwise, the wood frame insulation requirements must be met [Southface, 2011]. In the given house model, the external walls are made out of brick. All of the insulation in the external walls is on the interior of the walls. Therefore, the wood frame insulations are used for the house.

The city code requires that windows maintain a certain fenestration U-factor and SHGC. The fenestration U-factor is a measure how well the window prevents heat from escaping the house,

which is an important factor in minimizing heat loss during the winter. A smaller U-factor means more effective windows. The SHGC is a measure of how well the window blocks sunlight from heating the house, which is an important factor in minimizing the cooling loads during the summer. Again, a smaller solar heat gain factor means more effective windows. Figure 7.1 below illustrates these factors. Both pictures show the inside of the house on the right and the outside on the left. The figure on the left has a higher U-factor and SHGC, which means that more heat will enter the building in the summer, and more heat will escape the building in the winter. The window on the left will not meet the building code fenestration U-factor requirements for any of the cities. Better windows, like the one on the right side of Figure 7.1, are usually double paned with a high SHGC glazing and an air gap in between the two panes. SHGC can be independently controlled by the type of glazing that is applied to the windows. Visible transmission (VT) is an optical property of the window, and refers to the amount of daylight that enters the house. A higher VT is desired to maximize daylight, although it does not affect the thermal properties of the window.

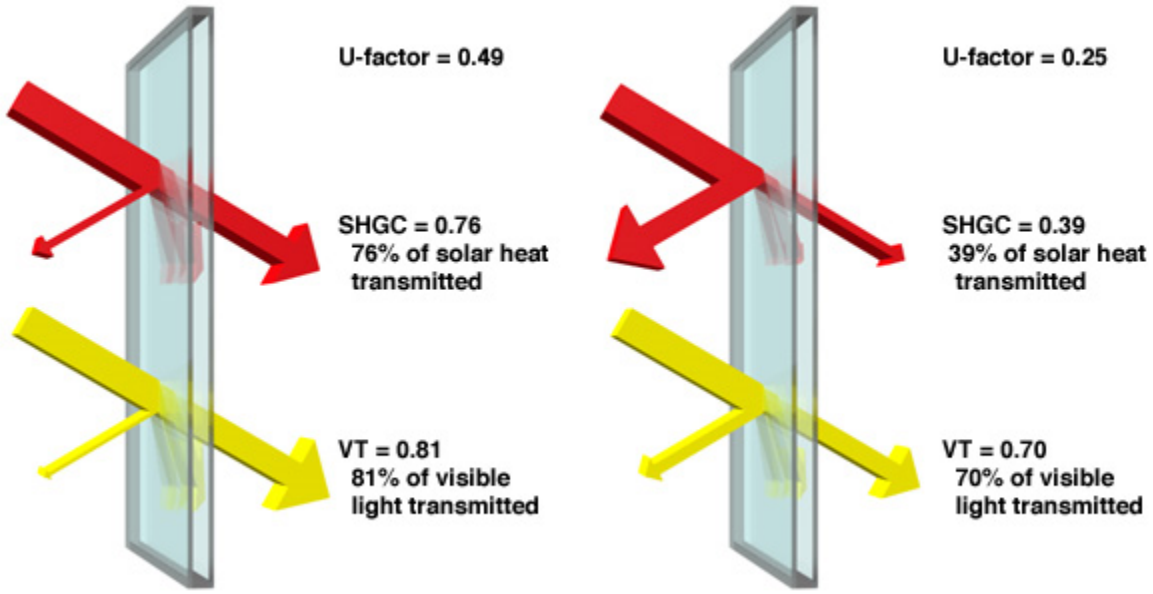

Figure 7.1: Window thermal and transmission properties [Efficient Window Collaborative, 2011]

The modeled house has two different types of glazing on the windows. Most of the windows in the house have low-e, double-paned glazing windows. The built-in windows in the four exterior doors have regular double-paned glazing. All windows have an air fill gap of a quarter of an inch between panes. Furthermore, we assume that there are no solar screens or blinds on the windows, meaning that the fenestration U-factor and solar heat gain factor remains unaffected. When considering the windows, the U-factor and solar gain factor are parameters

that will be changed to compare the performance of a good window to a window that just meets the requirements. The properties of the two types of windows are listed in Table 7.6 below.

Table 7.7: Window Properties in the Residential Base Case

Glazing Type	Fenestration U-Factor	Convection Factor	Fenestration Solar Heat Gain Coeff (SHGC)
Low-e	0.6	0.05	0.72
Regular	0.68	0.05	0.76

When considering the windows, the U-factor and SHGC are parameters that will be changed to compare the performance of a good window to a window that just barely meets the requirements.

7.2 RESIDENTIAL BASE CASE AND VARIATIONS

The base case residential model is 195m^2 (2100ft^2) with 4-inch brick exterior, asphalt shingle roof, minimum insulation (per code) in exterior walls and windows. The house is divided into areas shown in Table 7.7.

Table 7.7: House Component Area

House Component Area	
Component	Area (ft^2)
Ceiling	2124
Doors	100.1
Windows	163.6
Walls, exposed exterior	2322
Walls, garage	0
Floor Area	2124
Floor Perimeter	200
Volume (ft^3)	19116

Table 7.8 shows the material properties used for the base case model for each type of construction sections (listed in order from outside to inside). Refer to Tables 7.3 and 7.4 for minimum resistance values for the exterior walls and windows.

Table 7.8: Materials and Material Properties of Construction Component [eQuest, 2010]

Material	Thickness	Heat Conductivity	Density	Specific Heat Capacity	Resistance	Emissivity	Mu	Ksi(Xi)	Vapor Capacity
	m	W/m K	kg/m^3	J/kg K	m²K/W		Diffusion	Resistance Factor	
External Wall									
Convection Resistance	-	-	-	-	0.12	-	-	-	-
Face Brick 4in	0.101	1.311	2082.4	919.6	0.077	0.9	29	2	0
Insul Bd 1/2 in	0.013	0.055	288.3	1254	0.234	0.9	1.3	1	0
MinWool Batt R24	0.090	0.043	9.61	836	2.086	0.9	1.3	1	0
GypBd 1/2 in	0.013	0.160	800.9	836	0.080	0.9	9	6	0
Convection Resistance	-	-	-	-	0.12	-	-	-	-
Roof									
Convection Resistance	-	-	-	-	0.12				
Blt-Up roof 3/8 in	0.009	0.162	1121.3	1463	0.058	0.9	500	0	0
Bldg Paper Felt	0.038	3.605	1121.3	1463	0.011	0.9	5000	0	0
Plywood 5/8 in	0.016	0.115	544.6	1212.2	0.137	0.9	150	99	0
Roof Cons Mat 4	-	-	-	-	0.044	-	-	-	-
Convection Resistance	-	-	-	-	0.26	-	-	-	-
Ceiling									
Convection Resistance	-	-	-	-	0.12	-	-	-	-
GypBd 3/4in	0.019	0.160	800.9	836	0.119	0.9	9	6	0
MinWool Batt R24	0.274	0.043	9.61	836	6.333	0.9	1.3	1	0
Convection Resistance	-	-	-	-	0.12	-	-	-	-
Foundation									
UFMat	-	-	-	-	3.11	-	-	-	-
Light Soil, Damp 12 in	0.305	0.865	1601.8	1045	0.352	0.9	7.5	2	0
Conc HW 140 lb 6in	0.152	1.730	2242.6	836	0.088	0.9	25	40	0
Carpet and Fiber pad	-	-	-	-	0.366	-	-	-	-
Convection Resistance	-	-	-	-	0.12	-	-	-	-

In this study, the variations in construction properties are exterior wall types, exterior wall insulation, window fenestration (again will be called window insulation), and roof. Table 7.9 lists the material properties for the exterior wall types and maximum exterior wall insulation which is based on the maximum thickness for the MinWool Batt used in the base case. Maximum Window Insulation (Fenestration), shown in Table 7.10, is based on the use of available high end windows. Note that the GHP design followed the same procedure for sizing heat pumps and borehole lengths previously discussed in Section 4.

Table 7.9: Material Properties for Maximum Exterior Wall Insulation and Exterior Wall Types [de Wit, 2008]

Case	Thick-ness	Heat Conducti-vity	Density	Specific Heat Capacity	Resistance	Emissivity	Mu	Ksi(Xi)	Vapor Capa-city
	[m]	[W/mK]	[kg/m^3]	[J/kg K]	[m^{2}K/W]		Diffusion	Resistance Factor	
Maximum Insulation									
MinWool Batt R24	0.246	0.043	9.61	836	5.686	0.9	1.3	1	0
Wood	0.051	0.17	800	1880	0.9	30	40	3.4	0
Stone	0.101	2.3	2750	840	0.9	29	2	0.8	0
Concrete	0.0064	1.86	2500	840	0.9	30	40	3.4	0

The house load model takes into account the orientation of the windows, the type of shading such as awnings, the type of glazing, and shading with blinds or solar screens. The base case house has a total of 16 windows and a front porch shading the four windows in the front and four in the back while the remaining eight windows have awnings. All of the windows have low-e, double-paned glazing with an air gap filled in between the two panes. There are also four doors in the house with a regular, double paned glazing. Five windows and one door face east, six windows and one door face south, five windows and two doors face north. The front of the house faces east.

Table 7.10: Properties of Maximum Window Insulation Case [Home Depot, 2012]

Case	U-factor	Solar Gain Factor
Maximum Window Insulation	0.2	0.25

Another parameter change is from the base case standard asphalt shingle roof to a steel roof. The metal roof will consist of plywood and paper felt similar to the asphalt shingle roof. The paper felt is followed by a layer of aluminum foil to assist in natural convection in the 2-inch air gap that is in between the aluminum foil and the steel roof. There are several benefits of a metal

roof including reduced thermal loads because of the reflective property of metal, as well as low maintenance and long lasting roofs. Specific information about the thickness of each layer of the metal roof is provided in Table 7.11.

Table 7.11: Metal Roof Case Material Properties [de Wit, 2008]

Metal Roof Case	Thickness	Heat Conducti-vity	Density	Specific Heat Capacity	Resistance	Emissivity	Mu	Ksi(Xi)	Vapor Capacity
	[m]	[W/mK]	[kg/m^3]	[J/kgK]	[m^{2}K/W]		Diffusion	Resistance Factor	
Steel	0.0061	46	7800	500	0.68	900000	0	0	0
Air Gap	0.075	0.023	1.2	1000	0.9	1	0	0	0
Aluminum Foil	0.0011	200	2800	880	0.9	3000	0	0	0
Bldg Paper Felt	0.038	3.61	1121	1463	0.01	0.9	5000	0	0
Plywood 5/8 in	0.016	0.115	544.6	1212.2	0.14	0.9	150	99	0
Roof Cons Mat 4	-	-	-	-	0.04	-	-	-	-
Convection Resistance	-	-	-	-	0.26	-	-	-	-

7.3 NEW CONSTRUCTION CASES

The seven new construction cases, listed in Table 7.12 with perturbation from the base case, denoted in *initalics*, illustrates construction material choices available to the homeowner. For example, the Maximum Wall Ins (ulation) case had brick exterior, asphalt shingle roof, minimum window insulation, but with maximum wall insulation. For each case the heat pump capacity and borehole length are resized based upon the heating/cooling loads, heat pump EWT, and borehole life. Therefore, while Table 7.12 only shows one construction parameter change, the borehole lengths and possibly (but not probably because it is based on peak load) heat pump capacity will also change. The cost and GHP performance for each case will be measured.

Table 7.12: New Construction Cases

New Construction Case	Exterior Wall Construction	Roof Type	Exterior Wall Insulation	Window Fenestration
Base	Brick	Shingle	Minimum	Minimum
Max Wall Ins	Brick	Shingle	*Maximum*	Minimum
Max Window Fen	Brick	Shingle	Minimum	*Maximum*
Max Ins/Fen	Brick	Shingle	*Maximum*	*Maximum*
Metal Roof	Brick	*Metal*	Minimum	Minimum
Stone Ext Wall	*Stone*	Shingle	*Maximum*	Minimum
Wood Ext Wall	*Wood*	Shingle	Minimum	*Maximum*
Concrete Ext Wall	*Concrete*	Shingle	*Maximum*	*Maximum*

7.3.1 Austin

Base Case: The base case residential building model for Austin had a 14.6kW (4-ton) heat pump and four in-line boreholes at 61m/borehole (200ft/borehole) on 4.6m (15ft) centerline spacing.

Heat Pump Capacities: All cases required a 4-ton heat pump.

Borehole Lengths: Table 7.13 below shows the peak heating/cooling loads and the length/borehole.

Table 7.13: Ground Loop Length and Peak Cooling and Heating Loads for Each New Construction Cases: Austin

Ground Loop Length and Peak Loads : Austin			
New Construction Case	**Ground Loop Length/Borehole m (ft)**	**Peak Heating Loads kW**	**Peak Cooling Loads kW**
Base	62.8 (206)	10.5	8.1
Max Wall Insulation	61 (200)	10.4	7.8
Max Window Insulation	59.1 (194)	10.5	7.8
Maximum	58.5 (192)	10.2	7.4
Metal Roof	60 (197)	10.7	8.2
Stone	62.8 (206)	10.5	8.4
Wood	62.5 (205)	10.5	8.3
Concrete	62.8 (206)	10.5	8.3

The results show very little changes in the borehole lengths with virtually no difference based on the exterior wall type (brick/stone/wood/concrete). The Maximum Case (maximum window and wall insulation) decreases the length by 4.3m/borehole (14ft/borehole), a 6.8% reduction. This data basically says from the perspective of heat pump capacity and borehole length, there are minimal effects of the new construction options.

Number of Unmet Hours: All cases satisfied the maximum 300 unmet hours (see Table 7.14) at year 15 of operation.

Table 7.14: Number of Unmet Hours Above and Below Setpoint Temperature in the 15th Year: Austin

Number of hours above or below the setpoint temperature in the 15th year: Austin			
Cases	**Unmet Hours Above**	**Unmet Hours below**	**Unmet Hours total**
Base	36	41	77
Max Wall Insulation	40	38	78
Max Window Insulation	54	41	95
Maximum	38	39	77
Metal Roof	45	39	84
Stone Wall	36	41	77
Wood Wall	43	39	82
Concrete Wall	41	44	85

Yearly average water temperature in the ground loop: This value takes the hourly data for the average water temperature in the ground loop and computes the average temperature over the 8760 hours in the year. Figure 7.2 shows less than a degree C variation among all cases, but shows an approximate 4.5°C (8°F) increase in temperature from year 1 to year 15 of operation.

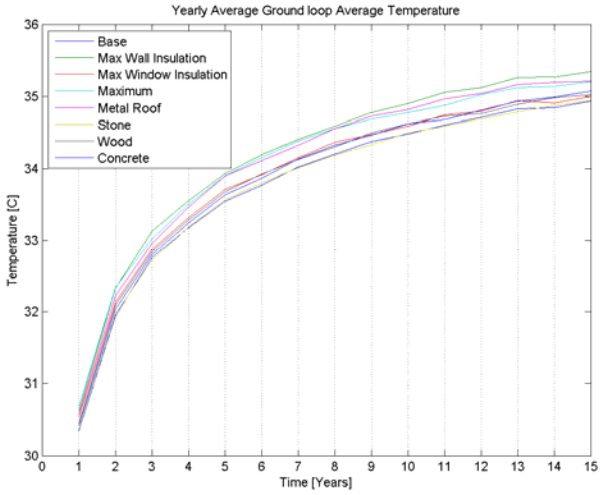

Figure 7.2: Yearly average water temperature in the ground loop: Austin

Electricity Use*:* Figure 7.3 shows the yearly electricity usage for the different new construction cases. The Maximum Case consumes the least electricity, 8.3 MWh in the first year and 9.1 MWh in year 15. On the other hand, the Concrete Case consumes the most electricity, about 8.8 MWh in year 1 and 9.65 MWh in year 15. The second best case is the Metal Roof, followed closely by the Maximum Wall Insulation Case and Maximum Window Insulation Case. The rest of the cases, all with the minimum insulation and different types of external wall material, are

close together and do not vary significantly from one another. The results clear show that increasing the amount of insulation and adding a metal roof are extremely beneficial in reducing the amount of electricity use by the heat pump. There is a 5.6% decrease in the amount of electricity used per year between the best (Maximum) and base case.

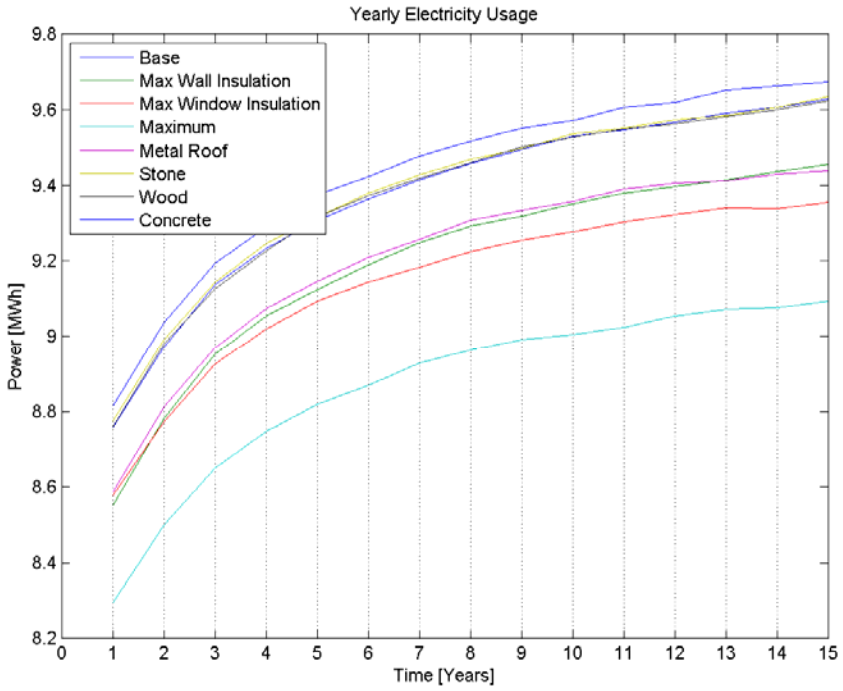

Figure 7.3: Yearly electricity usage for all new house construction cases: Austin

***Cost Analysis**:* Based upon estimates of the cost of associated with different exterior wall materials, roof, windows, insulation, heat pump and ground loops, the biggest differences were in the labor associated with the exterior wall materials and the metal roof. Table 7.15 shows the comparison. Adding more insulation (three maximum cases) reduced electricity and drilling costs but these savings were a little less than the added costs of these improvements, including the Maximum Case.

Table 7.15: GSHP Costs for New House Construction Cases: Austin

15-Year System Cost: Austin									
Case	House Construction Costs				GSHP System				
	Wall	Roof	Window	Wall Insulation	Equipment	Drill	Electricity	Total	Total w/ Rebate
Base	$22,756	$12,187	$3,520	$2,392	$10,000	$8,239	$14,387	$73,480	$68,008
Max Wall Insulation	$22,756	$12,187	$3,520	$3,088	$10,000	$8,012	$14,114	$73,676	$68,273

Max Window Insulation	$22,756	$12,187	$4,640	$2,392	$10,000	$7,779	$14,031	$73,784	$68,451
Maximum	$22,756	$12,187	$4,640	$3,088	$10,000	$7,668	$13,617	$73,955	$68,655
Metal Roof	$22,756	$22,995	$3,520	$2,392	$10,000	$7,760	$14,133	$83,556	$78,228
Stone	$31,928	$12,187	$3,520	$2,392	$10,000	$8,224	$14,399	$82,649	$77,182
Wood	$10,449	$12,187	$3,520	$2,392	$10,000	$8,204	$14,386	$61,137	$55,676
HardieBoard	$11,610	$12,187	$3,520	$2,392	$10,000	$8,223	$14,474	$62,405	$56,939

New Construction Conclusion—Austin: Based solely on GHP performance and associated costs, it appears best to use the cheapest exterior wall construction (wood) with the minimal insulation per code.

7.3.2 Albuquerque

Base Case: The base case residential building model for Albuquerque was 7.71kW (2-ton) heat pump with four in-line boreholes at 61m/borehole (200ft/borehole) on 4.6m (15ft) centerline spacing. The smaller heat pump capacity was due to the low ground temperature and more even heating/cooling building loads. It also turned out that the ground loop was sized on the peak heating load, rather than the peak cooling load.

Heat Pump Capacities: All cases required a 7.71kW (2-ton) heat pump.

Borehole Lengths: Tables 7.16 and 7.17 show the computed lengths/borehole and the heating and cooling loads, respectively, for all cases.

Table 7.16: Ground Loop Lengths for New House Construction Cases: Albuquerque

Ground Loop Length: Albuquerque	
New Construction Case	**Length (ft)**
Base	203
Max Wall Insulation	191
Max Window Insulation	204
Maximum	193
Metal Roof	198
Stone	203
Wood	201
Concrete	203

Table 7.17: Design Peak Heating and Cooling Loads for New House Construction Cases: Albuquerque

Albuquerque Cases	Design Cooling Loads kBtu/hr	Design Heating Loads kBtu/hr	Design Cooling Loads kW	Design Heating Loads kW
Base	20.7	22.4	6.07	6.56
Maximum Insulation	20.3	21.7	5.94	6.35
Maximum Window Insulation	20.6	22.3	6.03	6.53
Maximum	20.0	21.6	5.88	6.32
Metal Roof	20.2	22.0	5.92	6.43
Stone	20.7	22.4	6.07	6.56
Wood	20.7	22.4	6.07	6.56
Concrete	20.8	22.5	6.10	6.58

The results show little change in the borehole length with virtually no difference based on the exterior wall type (brick/stone/wood/concrete). The Maximum Wall Insulation Case had the shortest length. Note that the Maximum Window Case had higher values than the Maximum Wall Insulation Case since the better windows would decrease the heat into the house during winter, thus increasing the heating loads. This data basically says from the perspective of heat pump capacity and borehole lengths, there are minimal effects of the new construction options.

Number of unmet hours: All cases satisfied the maximum 300 unmet hours (see Table 7.18) at year 15 of operation.

Table 7.18: Number of Unmet Hours Above and Below Setpoint Temperature in the 15th Year: Albuquerque

Number of hours above or below the setpoint temperature in the 15th year: Albuquerque			
Cases	**Unmet Hours Above**	**Unmet Hours below**	**Unmet Hours total**
Base	35	164	199
Max Wall Insulation	27	63	90
Max Window Insulation	20	154	174
Maximum	11	48	59
Metal Roof	14	105	119
Stone Wall	35	168	203
Wood Wall	38	162	200
Concrete	56	189	245

Monthly Average Heat Pump EWT: Since the system was sized with the peak heating load, it is oversized for the cooling loads, and the heat pump entering water temperature is not

expected to come close to the maximum heat pump EWT of 48.9°F (120°F) that causes heat pump shut off. Figure 7.4 below shows the ground temperatures for the Base Case and the Maximum Case. The heat pump EWTs are similar for the two cases with maximum EWTs a little below 40°C (104°F), and with a minimum EWT a little below 0°C (32°F). The heat pump will also shut off if the EWT goes below -6.7°C (20°F) and the data shows this situation never occurs. The lower EWTs make the heat pump more efficient during cooling periods.

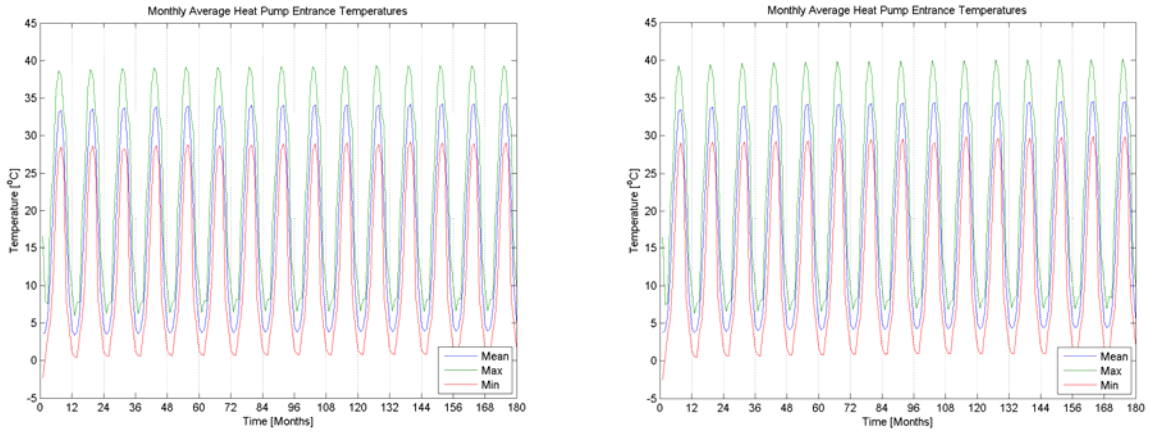

Figure 7.4: Heat pump EWT for Base Case (left) and Maximum Case (Right): Albuquerque

Yearly Average Water Temperature in the Ground Loop: Figure 7.5 shows a plot comparing the monthly averaged water temperature entering the ground loop, average ground loop water temperatures as well as the heat pump EWT for the Base Case.

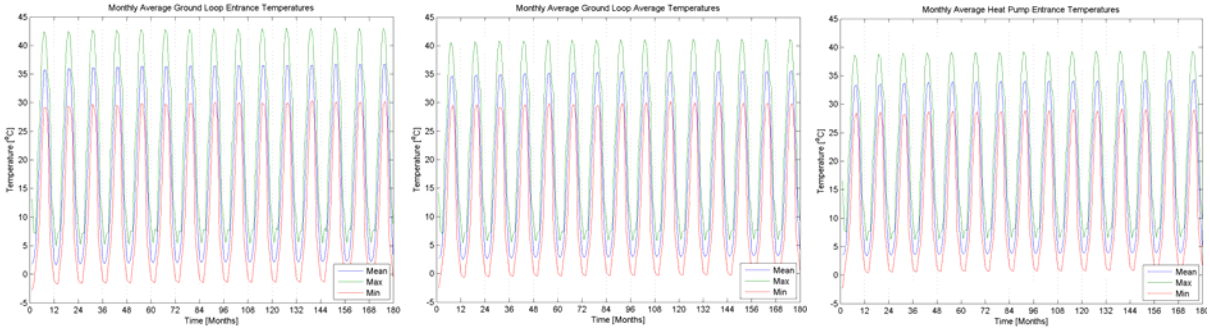

Figure 7.5: Monthly average ground loop entering, ground loop average, and heat pump EWT for Base Case: Albuquerque

In the summer, the water in the ground loop loses heat to the ground and there is a peak 5°C change in temperature between the ground inlet and outlet. In the winter, the water in the ground loop gains heat from the ground and there is a peak 3°C increase water temperature..

Again, since the peak heating, not cooling, load is used to size the ground loop, the yearly average water temperature in the ground loop has a wider range than seen for Austin. The

Maximum Window Insulation Case, with the longest ground loop (refer to Table 7.16), has the minimum ground loop temperatures because this case sees an increase in heating loads (less energy from sunlight enters the conditioned space) and a decrease in cooling loads compared to the Base Case, see Table 7.19.

Table 7.19 Heating and Cooling Loads for Base (left) and Maximum Window Insulation (right) Cases: Albuquerque

Heating Loads (Btu)	Cooling Loads (Btu)	Heating Peak Loads (Btu/hr)	Cooling Peak Loads (Btu/hr)	Month	Heating Loads (Btu)	Cooling Loads (Btu)	Heating Peak Loads (Btu/hr)	Cooling Peak Loads (Btu/hr)
13126	0	30.1	0	Jan	13129	0	30.1	0
8943	0	22.1	0	Feb	8959	0	22.3	0
4936	0	17.6	0	Mar	5047	0	17.5	0
959	594	10.9	10.7	Apr	1035	512	10.9	9.5
138	2856	5.5	15.4	May	153	2628	6.8	14.3
0	7545	0	21.8	Jun	0	7192	0	21.8
0	10999	0	21.7	Jul	0	10621	0	21.7
0	9674	0	21.0	Aug	0	9290	0	20.9
0	4142	0	15.8	Sep	0	3862	0	15.8
2490	725	19.5	11.5	Oct	2569	646	18.9	10.7
7681	0	22.4	0	Nov	7762	0	22.4	0
13212	0	23.9	0	Dec	13206	0	23.6	0

Thus, the amount of heat rejected into the ground will be much less during the cooling months, and is seen by lower ground loop temperatures. On the other hand, the Maximum Wall Insulation Case sees an increase in the cooling loads and a decrease in the heating loads compared to the Base Case. The smaller heating loads result in a smaller ground loop, 58.2m vs. 61.9m (191 vs. 203 ft). Therefore, the larger amount of cooling load must be rejected in a smaller ground loop, effectively increasing the temperature of the ground. Similar justifications can be given for the rest of the cases. Figure 7.6 shows the yearly average heat pump EWT. There is approximately a 1.7^{o}C difference between the maximum and minimum yearly average ground loop temperatures, which will result in dissimilar GSHP system operation times.

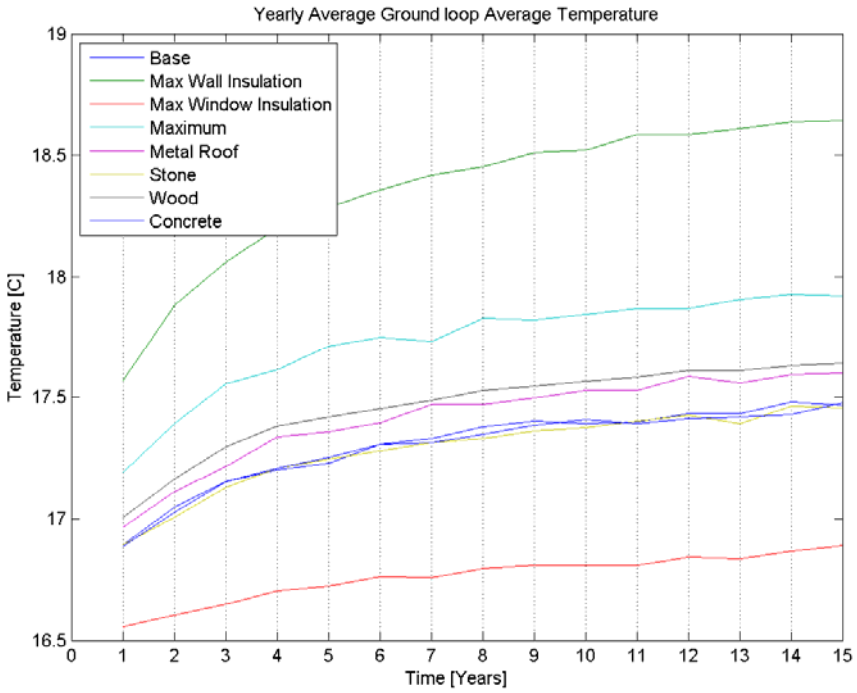

Figure 7.6: Yearly average heat pump EWT: Albuquerque

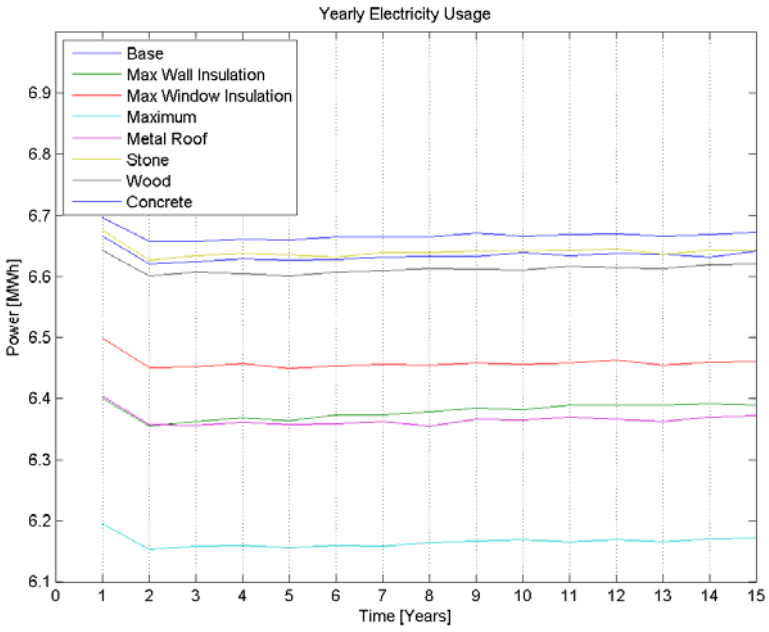

Figure 7.1: Yearly electricity usage for all new construction cases: Albuquerque

***Electricity Use**:* It is interesting to note that electricity use, shown in Figure 7.7, does not appear to be correlated with the ground loop size, and the amount of cooling has a more

significant effect. The reason is that there is a bigger difference in the cooling load power requirements than the heating load power requirements between the different cases is because the system is not sized to meet cooling loads. Thus, different cases with varying cooling loads have different power requirements. The Maximum Case has the least amount of cooling load power requirements because the increased insulation prevents heat from entering the house through the walls and windows. This Maximum Case shows a decrease in electricity usage of 7% from the Base Case. One interesting result is that the Maximum Wall Insulation Case requires less electricity than the Maximum Window Insulation Case. This does not correlate with the amount of cooling load required. Therefore, the increase in the heating loads for the Maximum Window Insulation Case is larger than the increase in cooling loads for the Maximum Wall Insulation Case.

Another point worth mentioning is the spike in electricity use in the first year for all cases. This spike is mainly due to excessive heating required when the system is just starting during winter (0 Time=January 1). The heat pump must work longer to get up to the required temperature from the extremely cold ambient temperatures used as initial conditions. There is about a 0.5MW difference in electricity use for the Maximum Insulation (best) and Concrete (worst) Cases. This represents about a 10% decrease in the electricity used from the worst to the best cases.

***Cost Analysis**:* Based upon estimates of the cost of associated with different exterior wall materials, roof, windows, insulation, heat pump and ground loops, the biggest differences were in the labor associated with the exterior wall materials and the metal roof. Table 7.20 shows the comparison. While the Maximum Case did reduce electricity costs, the savings are very small compared to the construction costs.

Table 7.20: GHP Costs for New House Construction Cases: Albuquerque

System Cost: Albuquerque									
Case	House Construction Costs				GHP System				
	Wall	Roof	Window	Wall Insulation	Equipment	Drill	Electricity	Total	Total w/ Rebate
Base	$22,756	$12,187	$3,520	$2,392	$10,000	$8,239	$14,387	$73,480	$68,008
Max Wall Insulation	$22,756	$12,187	$3,520	$3,088	$10,000	$8,012	$14,114	$73,676	$68,273
Max Window Insulation	$22,756	$12,187	$4,640	$2,392	$10,000	$7,779	$14,031	$73,784	$68,451
Maximum	$22,756	$12,187	$4,640	$3,088	$10,000	$7,668	$13,617	$73,955	$68,655
Metal Roof	$22,756	$22,995	$3,520	$2,392	$10,000	$7,760	$14,133	$83,556	$78,228
Stone	$31,928	$12,187	$3,520	$2,392	$10,000	$8,224	$14,399	$82,649	$77,182
Wood	$10,449	$12,187	$3,520	$2,392	$10,000	$8,204	$14,386	$61,137	$55,676
HardieBoard	$11,610	$12,187	$3,520	$2,392	$10,000	$8,223	$14,474	$62,405	$56,939

New Construction Conclusion—Albuquerque: Based solely on GHP performance and associated costs, it seems best to use the cheapest exterior wall construction (wood) with the minimal insulation per code.

7.3.3 Phoenix

Base Case: Phoenix has the highest ground temperature and lowest ground thermal conductivity of the three cities (see Section 7.1) Moreover, Phoenix has extremely hot summers and relatively warm winters. All these factors require larger heat pumps and longer boreholes. The base case residential building model for Phoenix had a 21.9kW (6-ton) heat pump and six in-line boreholes at 130m/borehole (425ft/borehole) spaced on 4.04m (15ft) centers, based upon GLHEPRO sizing of the building loads and satisfying the maximum number of unmet hours. Table 7.22 shows the monthly building heating/cooling loads for the base case.

Table 7.22: Monthly Building Heating and Cooling Loads for the Base Case: Phoenix

Month	Heating Loads Btu	Cooling Loads Btu	Heating Peak Loads Btu/h	Cooling Peak Loads Btu/h
Jan	4101.7	0	36.68	0
Feb	1512.1	912.25	15.24	14.51
Mar	580.66	1871	13.82	13.46
Apr	99.284	7869	8.91	25.69
May	0	12517	0	29.28
Jun	0	19183	0	39.85
Jul	0	22208	0	40.36
Aug	0	19264	0	38.14
Sep	0	14447	0	32.75
Oct	0	7938.3	0	24.43
Nov	159.9	906.41	6.79	10.36
Dec	4027.1	0	14.25	0

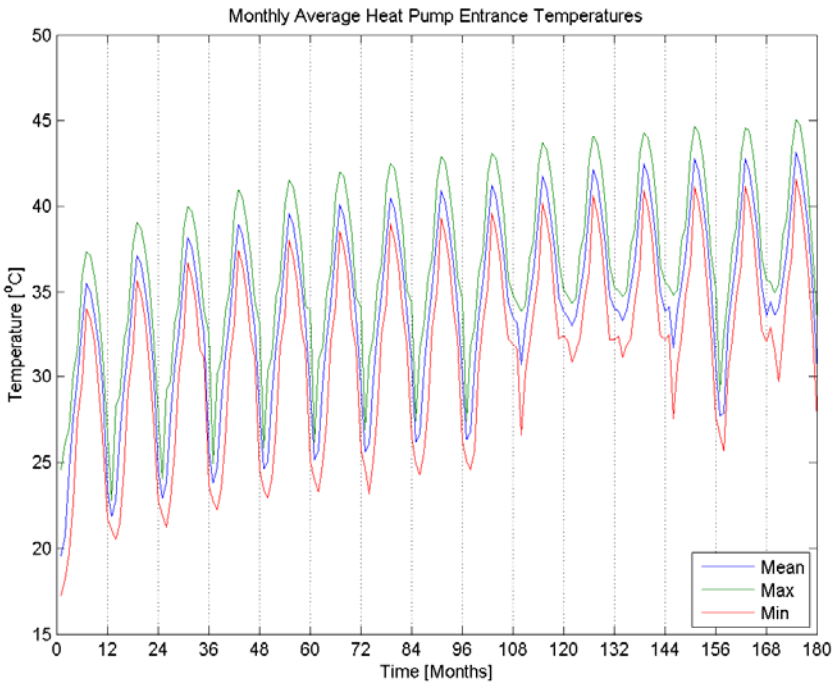

Figure 7.8: Monthly average heat pump EWT for Base Case: Phoenix

Figure 7.8 shows the heat pump EWT for the base case over 15 years of operation. In the first eight years, the mean, minimum, and maximum temperatures increase as expected. After the eighth year, the minimum temperatures are higher than what is expected; in the 120th month, the minimum temperature jumps from 25°C to 31°C which is contrast to the change from 21°C to 22°C seen in the 24th month. The main reason for the non-uniformity in the plot is because Phoenix is highly cooling dominated. Figure 7.9 shows the energy rejected by the ground and the heat pump and sheds some light into this issue. Heat must be extracted from the ground to provide the heating to the house. Notice that in the 108th month, the temperature of the water in the ground loop is higher than the ground temperature, so heat is rejected to the ground rather than extracted from the ground. These higher than expected temperatures are also seen in the heat pump EWT.

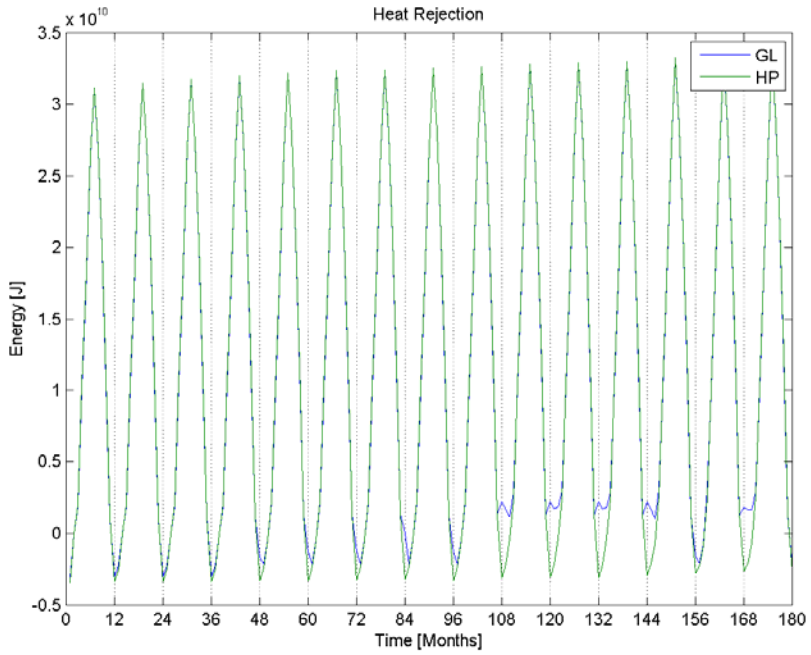

Figure 7.10: Heat rejected to the ground and the heat pump for the Base Case

Heat pump capacities: All cases required a 6-ton heat pump.

Borehole lengths: Table 7.23 shows the length/borehole for each case. The Maximum Case provides the smallest ground loop, followed the Maximum Wall Insulation and Maximum Window Insulation Cases. The Stone Wall Case requires the longest ground loop.

Table 7.23: Ground Loop Length for New House Construction Cases: Phoenix

Borehole Length: Phoenix		
Cases	**Length/Borehole m**	**Length/Borehole ft**
Base	129.5	425
Max Wall Insulation	126.8	416
Max Window Insulation	126.8	416
Maximum	122.8	403
Metal Roof	127.4	418
Stone	132.3	434
Wood	129.8	426
Concrete	130.5	428

The results show very little changes in the borehole length with virtually no difference based on the exterior wall type (brick/stone/wood/concrete) and the maximum window and wall insulation case decreasing the length by only 17m (56 ft) total (6.8%). This data basically says from the perspective of heat pump capacity and borehole lengths, there are minimal effects of the new construction options.

Number of unmet hours: All cases satisfied the maximum 300 unmet hours (see Table 7.24) at year 15 of operation since the ground loop lengths were increased until each case met the requirement.

Table 7.24: Number of Unmet Hours Above and Below Setpoint Temperature in the 15th Year: Phoenix

Number of hours above or below the setpoint temperature in the 15th year: Phoenix			
Case	**Unmet Hours Above**	**Unmet Hours below**	**Unmet Hours total**
Base	0	293	293
Max Wall Insulation	0	278	278
Max Window Insulation	0	249	249
Maximum	0	229	229
Metal Roof	0	212	212
Stone Wall	0	285	285
Wood Wall	0	245	245
Concrete Wall	0	242	242

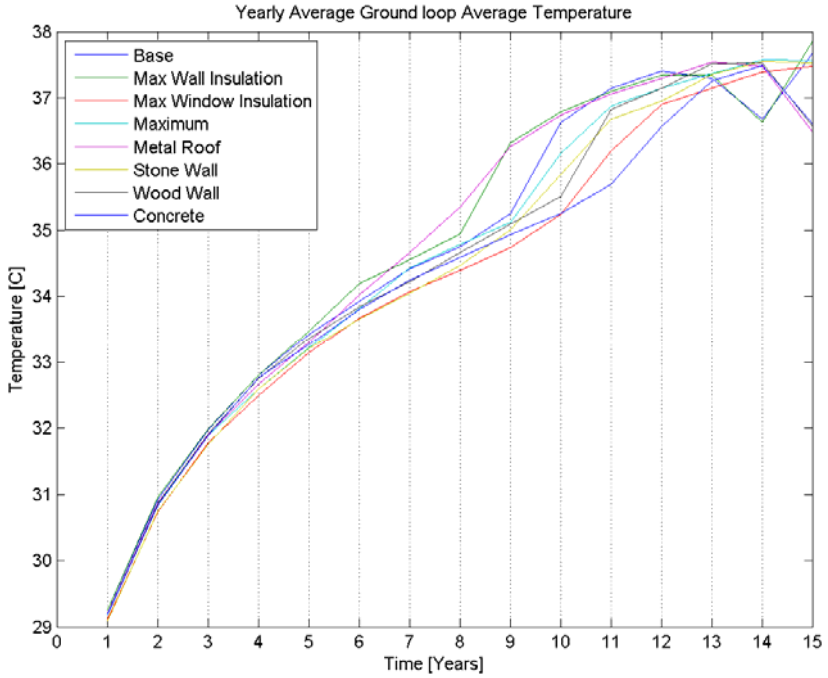

Figure 7.11: Yearly average ground loop average temperature for new construction cases: Phoenix

Yearly Average Water Temperature in the Ground Loop: The ground loop temperatures shown in Figure 7.11 rise from approximately 29°C in the first year to about 37-38°C in the 15th year, a 7-8°C increase over the 15 years. After about eight years, the ground temperatures start

to rise rapidly then some cases started to oscillate after year 12. This is a direct result of the heat rejection plot shown above and this trend occurs for the same reason that the trends seen in the heat pump entering water temperatures. The ground loop average temperatures for the different cases are almost identical, especially in the beginning. This is an interesting result considering the manner in which the ground loops were sized. Instead of being sized exactly by GLHEPRO, a certain amount of length was added to each case to ensure that the sizing constraint of unmet hours was met. Therefore, the results show that the sizing method is consistent for all cases, which allows for a more justified comparison of the different cases.

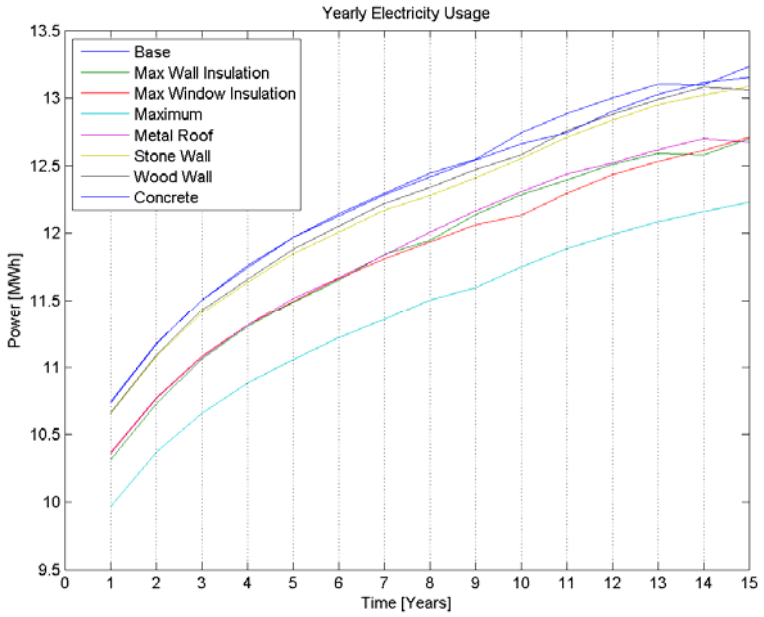

Figure 7.12: Yearly electricity usage for new construction cases: Phoenix

Electricity Use*:* Figure 7.12 shows the yearly electricity usage for the new construction cases. The Maximum Case consumed the least amount of electricity, followed by the Maximum Wall Insulation, Maximum Window Insulation, and Metal Roof Cases. The different exterior wall types and base cases are close to each other and consume the most amount of electricity. The difference in electricity usage between the best and worst case is about 750 kWh, which results in a very small cost saving of about $75/year or $1100 over the course of 15 years.

Cost Analysis: Table 7.25 lists the costs associated with the new construction cases. The biggest differences in costs are attributable to the exterior wall construction cost with wood being the cheapest. The Maximum Case shows the highest electricity savings over the 15 years of operation.

Table 7.25: GSHP Costs for New House Construction Cases: Phoenix

System Cost: Phoenix									
Type	House Construction Costs				GSHP System				
	Wall	Roof	Window	Wall Insulation	Equip-ment	Drill	Electricity	Total	Total w/ Rebate
Base	$22,756	$12,223	$3,520	$2,322	$12,000	$25,500	$16,972	$95,293	$84,043
Max Wall Insulation	$22,756	$12,223	$3,520	$3,042	$12,000	$24,960	$16,321	$94,821	$83,733
Max Window Insulation	$22,756	$12,223	$4,640	$2,322	$12,000	$24,960	$16,293	$95,194	$84,106
Maximum	$22,756	$12,223	$4,640	$3,042	$12,000	$24,180	$15,694	$94,535	$83,681
Metal Roof	$22,756	$23,322	$3,520	$2,322	$12,000	$25,080	$16,359	$105,360	$94,234
Stone	$31,928	$12,223	$3,520	$2,322	$12,000	$26,040	$16,793	$104,830	$93,414
Wood	$10,449	$12,223	$3,520	$2,322	$12,000	$25,560	$16,839	$82,913	$71,645
Concrete	$11,610	$12,223	$3,520	$2,322	$12,000	$25,680	$16,929	$84,284	$72,980

New Construction Conclusion—Phoenix: Based solely on GHP performance and associated costs, it seems best to use the cheapest exterior wall construction (wood) with the maximum wall and window insulation.

7.4 RETROFIT CONSTRUCTION CASES

The four retrofit construction cases, listed in Table 7.26, illustrate construction retrofits with heat pump capacity and borehole length held constant at the base case values. The cost and GHP performance for each case will be measured. It should be expected that all retrofit cases will improve GHP performance over that of the base case, but the economic savings may not warrant the cost of the retrofit.

Table 7.26: Retrofit Construction Cases

Retrofit Construction Case	Exterior Wall Construction	Roof Type	Exterior Wall Insulation	Window Fenestration
Base	Brick	Shingle	Minimum	Minimum
Max Wall Ins	Brick	Shingle	*Maximum*	Minimum
Max Window Fen	Brick	Shingle	Minimum	*Maximum*
Max Ins/Fen	Brick	Shingle	*Maximum*	*Maximum*
Metal Roof	Brick	*Metal*	Minimum	Minimum

7.4.1 Austin

Base Case: The base case residential building model for Austin had a 14.6kW (4-ton) heat pump and four in-line boreholes at 61m/borehole (200ft/borehole) on 4.6m (15ft) centerline spacing., which will remain constant for the retrofit construction cases.

Number of Unmet Hours: It is expected that increased exterior wall and window insulation will improve GHP performance since the existing borehole length would be more than needed (over designed) if the ground loop was resized. The number of unmet hours was decreased almost in half compared to the base case (see Table 7.27) at year 15 of operation.

Table 7.27: Number of Unmet Hours Above and Below Setpoint Temperature in the 15th Year: Austin Retrofit Cases

Number of hours above or below the setpoint temperature in the 15th year: Austin			
Retrofit Cases	**Unmet Hours Above**	**Unmet Hours below**	**Unmet Hours total**
Base	36	41	77
Max Wall Insulation	6	37	43
Max Window Insulation	0	41	41
Maximum	0	38	38
Metal Roof	0	39	39

GHP Performance and Heat Pump EWT: Figure 7.13 shows the yearly averaged heat pump EWT of the Base Case and the Maximum Case. The average and maximum EWTs are lower in the Maximum Case by about 2°C while the minimum EWTs are relatively the same. The maximum temperatures reach 46°C, which is less than 48.3°C (120^{o}F) which automatically shuts off the heat pump. The data shows that the maximum EWT of the Base Case hits 48.3°C at the seventh year, whereas that temperature is never reached in the 15 years of operation in the Maximum Case. Figure 7.14 shows the monthly averaged heat pump EWT temperatures for the Maximum Case over 15 years. Clearly, sizing the GSHP system for the Base Case and retrofitting with the maximum window and wall insulation (Maximum Case) has improved GHP performance.

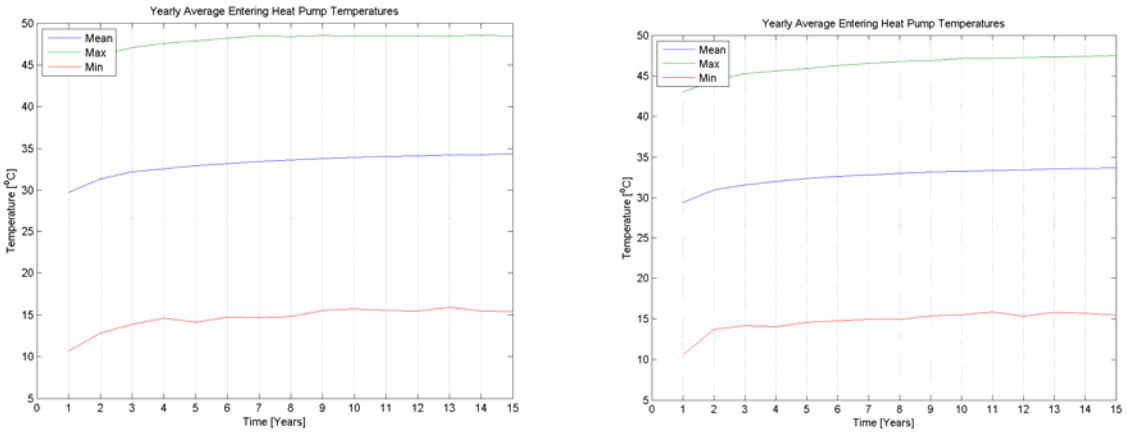

Figure 7.13: Yearly average heat pump EWTs for Base (left) and Maximum (right) Cases: Austin Retrofit

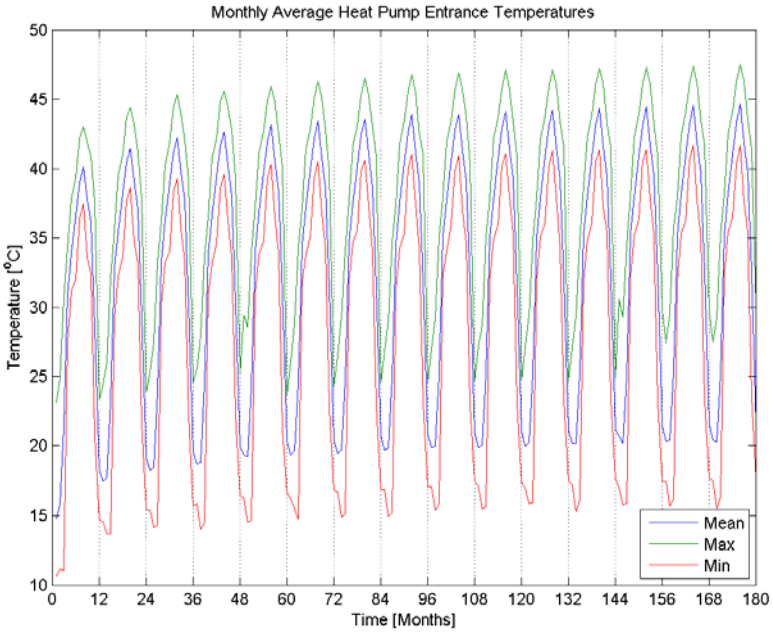

Figure 7.14: Monthly average heat pump EWT for Maximum Case: Austin Retrofit

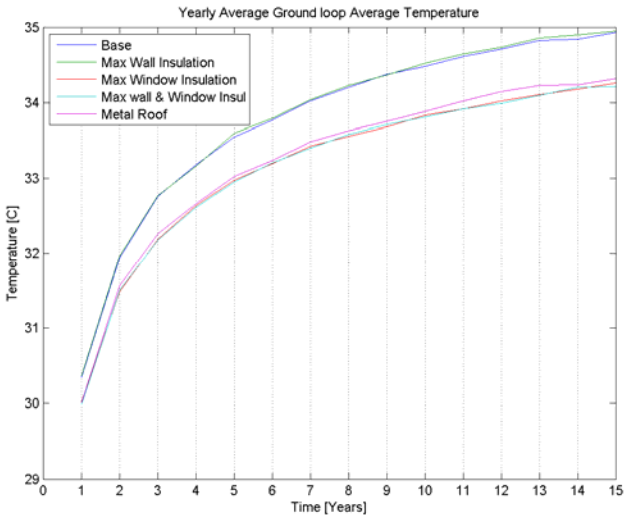

Figure 7.15: Yearly averaged ground loop average water temperatures for all retrofit cases: Austin

Yearly Average Water Temperature in the Ground Loop: Figure 7.15 shows the yearly averaged water temperature in the ground loop increases about 4-5^{o}C over the 15 years of operation. Two distinct groups are seen: group 1 with high temperatures (Base and Maximum Wall Insulation Cases) and group 2 with lower temperatures (Maximum Window Insulation, Maximum, and Metal Roof Cases). The temperature profiles of group 1 are comparable to the cases with the new house construction, reflecting that the amount of ground heating in these cases is similar to the new house construction cases. On the other hand, group 2 shows almost a degree improvement in the ground loop temperatures in the 15th year. This is a significant improvement in the system performance when considering that the total temperature increase over the fifteen years is 4.5^{o}C. The GHP systems in group 2 will have longer operational lives.

Electricity Use*:* The electricity usage is expected be lower for the retrofit cases than the new construction cases because the system is oversized, requiring the heat pump to operate less (more efficiently) to satisfy the cooling and heating loads of the house. Figure 7.16 shows the yearly electricity usage over the 15 years of operation. There is almost a one MWh difference in the electricity usage between the Base Case and the Maximum Case. This reduction is twice the size of the same two cases in the new house construction section. The Maximum Case uses 10% less electricity compared to the Base Case. The other cases, in order of decreased electricity use, are the Metal Roof, Maximum Window Insulation, and Maximum Wall Insulation.

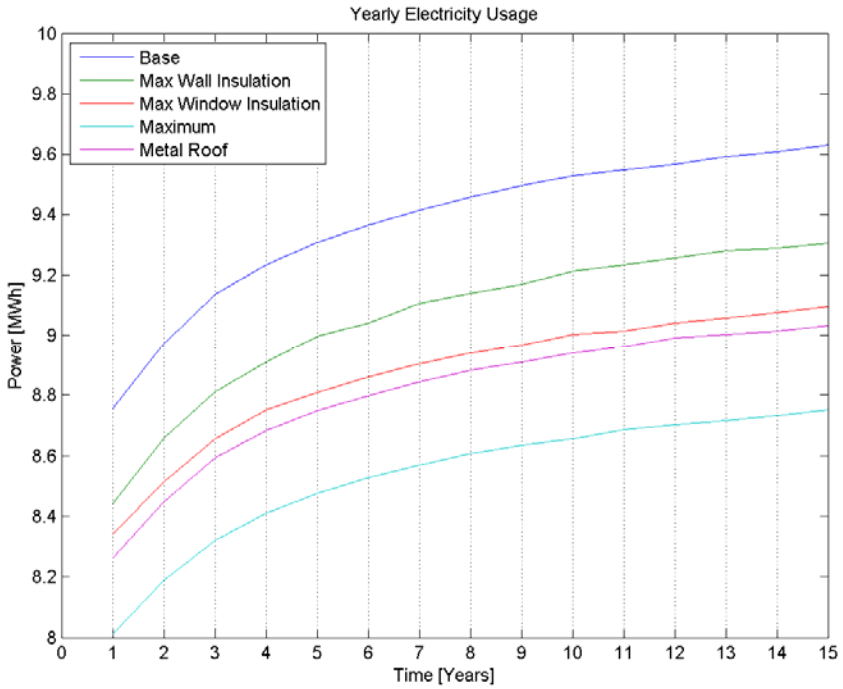

Figure 7.16: Yearly electricity usage for all retrofit cases: Austin

***Cost Analysis**:* Over 15 years, the total cost for every retrofit case is higher than the Base Case; that is, the decreased cost in electricity usage resulting from improved GSHP performance is not sufficient to overcome the retrofit costs. For example, the $3088 cost of installing the maximum wall insulation will only yield a savings of $489 in electricity costs over 15 years of operation. The $8928 cost of installing the maximum insulation in the wall and windows will only yield a savings of $1292 in electricity costs. Table 7.28 shows the cost comparison between different cases, and the data shows that decrease in the electricity cost is less than the retrofit costs. The Metal Roof Case, for example, is sized for a GHP system with the Base Case, which is 11.2m (36ft) longer than the comparable new construction case. The savings in electricity with this additional ground loop length is $322 compared to Metal Roof Case in the new house construction cases.

Table 7.28: GSHP Costs over 15 years for Retrofit Cases: Austin

Retrofit System Cost: Austin									
Retrofit Case	Retrofit House Construction Costs				GSHP System				
	Wall	Roof	Window	Wall Insulation	Equipment	Drill	Electricity	Total	Total w/ Rebate
Base	$22,756	$12,187	$3,520	$2,392	$10,000	$8,239	$14,387	$73,480	$68,008
Max Wall Insulation	$22,756	$12,187	$3,520	$3,088	$10,000	$8,239	$13,898	$73,688	$68,216
Max Window Insulation	$22,756	$12,187	$5,840	$2,392	$10,000	$8,239	$13,612	$75,025	$69,553
Maximum	$22,756	$12,187	$5,840	$3,088	$10,000	$8,223	$13,095	$75,189	$69,722
Metal Roof	$22,756	$27,594	$3,520	$2,392	$10,000	$8,239	$13,811	$88,311	$82,839

Retrofit Construction Conclusion—Austin: Although adding more insulation and/or a metal roof will enhance GHP performance, the savings in electricity over 15 years will not pay for the retrofit costs.

7.4.2 Albuquerque

Base Case: The base case residential building model for Albuquerque was 7.71kW (2-ton) heat pump with four in-line boreholes at 61m/borehole (200ft/borehole) on 4.6m (15ft) centerline spacing, which will remain constant for the retrofit construction cases.

Number of Unmet Hours: Table 7.29 below shows the number of unmet hours in the 1st year. The 1st year is considered because the first year has a spike in the heating requirements resulting in higher unmet hours—this may be artificial due to the initial conditions used in the simulations. Subsequent years showed no time that the set point constraints were violated.

Table 7.29: Number of Unmet Hours Above and Below Setpoint Temperatures in the 1st year: Albuquerque

Number of hours above or below the setpoint temperature in the 1st year: Albuqueque			
Retrofit Case	**Unmet Hours Above**	**Unmet Hours below**	**Unmet Hours total**
Base	35	164	199
Max Wall Insulation	20	43	63
Max Window Insulation	20	161	181
Maximum	8	35	43
Metal Roof	2	6	8

Yearly Average Water Temperature in the Ground Loop: The yearly averaged ground temperatures are shown in Figure 7.17. The data is similar to those for the new house construction cases, with a similar order of performance except that the Metal Roof and Maximum Cases are switched. The reason for this difference can be shown with the heat

rejection plots for the two cases shown in Figure 7.18. There is an increase in both the heat rejected and heat extracted from the Maximum Case compared to the Metal Roof Case, shown in the heat rejected/extracted data. The heat rejection increases slightly more than the heat extracted, thus, the higher ground loop temperatures in the Metal Roof Case.

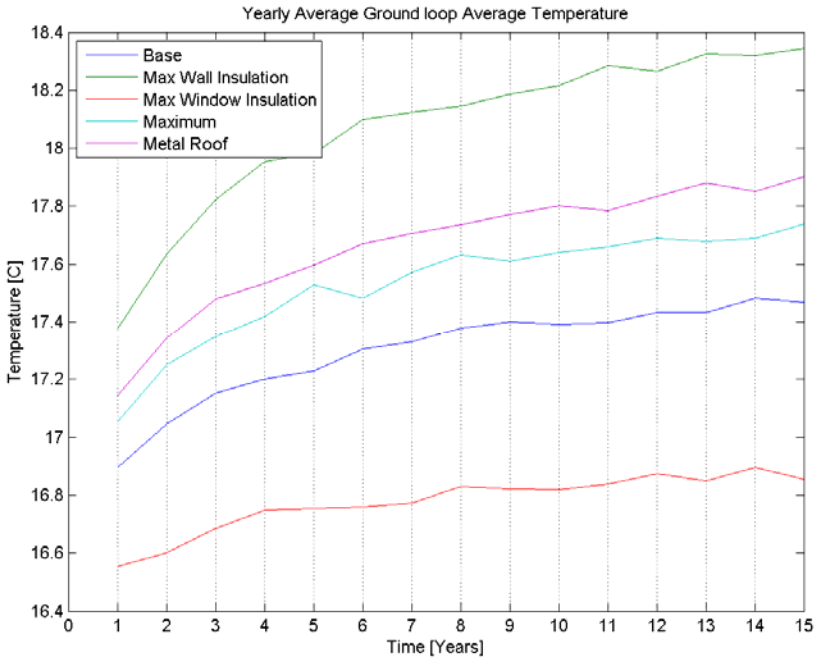

Figure 7.17: Yearly average ground loop average temperatures for all retrofit cases: Albuquerque

Furthermore, the minimum and maximum temperatures are closer together than the new house construction cases. This means that the Maximum Window Insulation Case has temperatures that are a little higher and the Maximum Wall Insulation Case has temperatures that are slightly lower in the retrofit cases. This is due to the fact that in the new construction cases, the ground loop is shorter for the Maximum Window Insulation Case and longer for the Maximum Wall Insulation Case. A shorter ground loop means higher average ground loop temperatures and a longer ground loop means lower average ground loop temperatures.

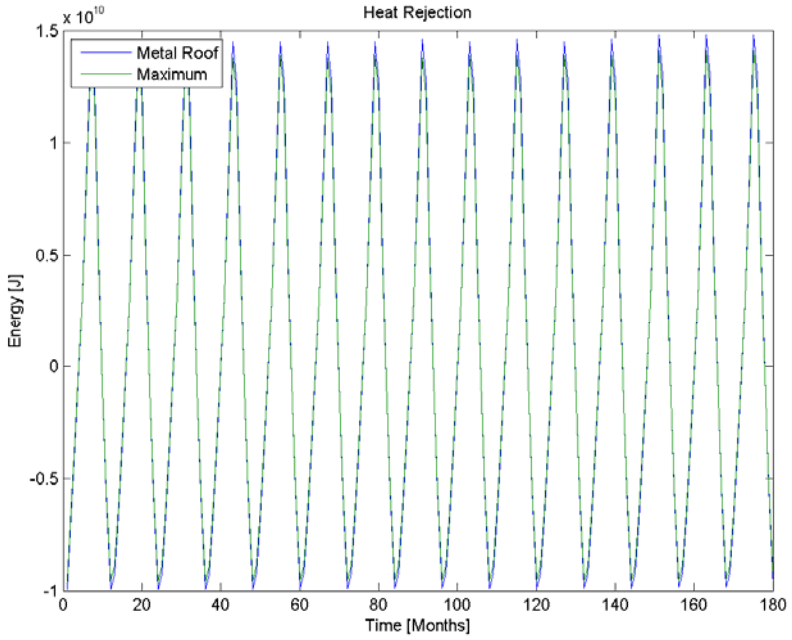

Figure 7.18: Comparing heat rejected to the ground between the Metal Roof and Maximum Cases: Albuquerque Retrofit

***Electricity Use**:* Figure 7.19 shows the electricity use over 15 years. The spike in the first year is present in all cases, and again, is an artificial artifact that is due to the transient effects when the heat pump is first turned on. The Maximum Case consumes the least amount of electricity, which is similar to the new house construction cases. The difference in the electricity usage between the Base Case and the Maximum Case is a little greater than 0.6MW per year, compared to 0.5MW difference for the new house construction case. This increase is expected because the longer retrofit ground loop gives lower heat pump EWTs and the heat pump works less (more efficient) to extract heat from the refrigerant loop. A 0.6 MWh per year difference in electricity translates to a savings of about $50/year. Over the 15 years, without considering the time value of money, the savings is about $750. Based on electricity usage data alone, the recommendation would be to first add more insulation to the walls, followed by insulation to the windows.

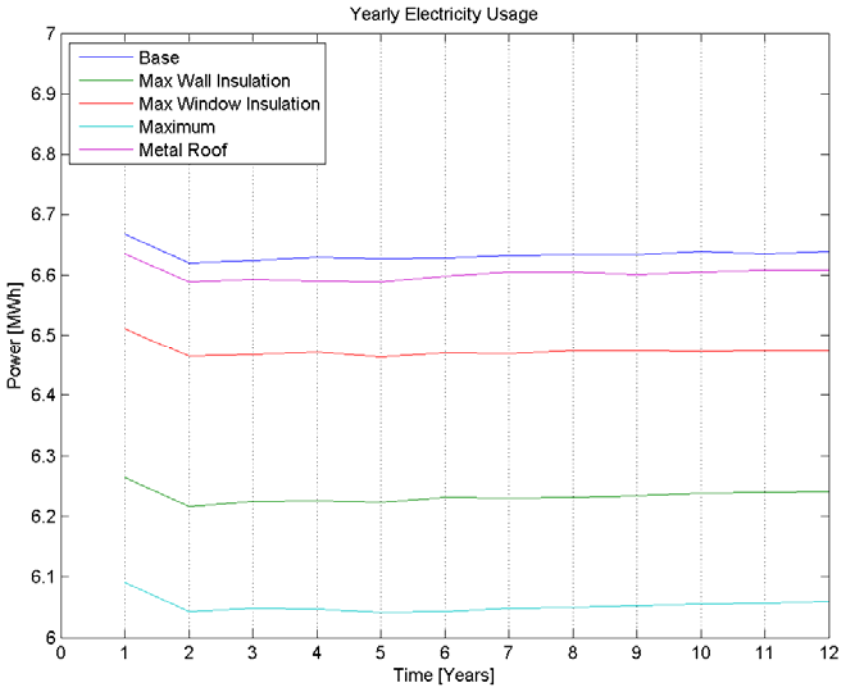

Figure 7.19: Yearly electricity usage for all retrofit cases: Albuquerque

***Cost Analysis**:* Table 7.30 shows that over 15 years of operation, all of the retrofit cases are more expensive than the Base Case, although, the Maximum Wall Insulation Case is only $129 more. This can be compared to an electricity savings of $590 over 15 years. Clearly, after the system runs for a few years, positive payback can be expected for this case. Therefore, the Maximum Insulation Case is recommended over the Base Case. The other cases have too high retrofit costs to overcome the savings in electricity.

Table 7.30: GSHP Costs over 15 years for Retrofit Cases: Albuquerque

Retrofit System Cost: Albuquerque									
Retrofit Case	**Retrofit House Construction Costs**				**GSHP System**				
	Wall	Roof	Window	Wall Insulation	Equip-ment	Drill	Electricity	Total	Total w/ Rebate
Base	$22,756	$12,223	$2,322	$3,520	$7,000	$8,102	$9,779	$65,701	$61,171
Max Wall Insulation	$22,756	$12,223	$3,042	$3,520	$7,000	$8,102	$9,189	$65,831	$61,300
Max Window Insulation	$22,756	$12,223	$2,322	$5,840	$7,000	$8,102	$9,541	$67,784	$63,253
Maximum	$22,756	$12,223	$3,042	$5,840	$7,000	$8,102	$8,921	$67,884	$63,353
Metal Roof	$22,756	$27,986	$2,322	$3,520	$7,000	$8,102	$9,733	$81,419	$76,888

Retrofit Construction Conclusion—Albuquerque: Adding more wall insulation would be cost effective over 15 years of operation.

7.4.3 Phoenix

Base Case: The base case residential building model for Phoenix had a 21.9kW (6-ton) heat pump and six in-line boreholes at 130m/borehole (425ft/borehole) spaced on 4.04m (15ft) centers,), which will remain constant for the retrofit construction cases.

Number of Unmet Hours: Table 7.31 below shows the number of unmet hours in the 15th year. Similar results are seen compared to the new house construction cases where there are only unmet hours below the setpoint temperatures. All of the results show unmet hours below 300, with the Maximum Case showing the lowest number of total hours above and below the setpoint temperature.

Table 7.31: Number of Unmet Hours Above and Below the Setpoint Temperature for the Retrofit Cases in the 15th Year: Phoenix

Number of hours above or below the setpoint temperature in the 15th year: Phoenix			
Retrofit Case	**Unmet Hours Above**	**Unmet Hours below**	**Unmet Hours total**
Base	0	293	293
Max Wall Insulation	0	212	212
Max Window Insulation	0	174	174
Maximum	0	98	98
Metal Roof	0	179	179

Yearly Average Water Temperature in the Ground Loop: Figure 7.20 shows the yearly averaged ground loop temperatures for all retrofit cases. The ground loop average temperatures in the retrofit cases are just slightly lower than the new house construction cases. It is expected that if heat is rejected from a longer ground loop, the average ground loop temperatures should be lower because the heat is spread out in a bigger area. The small difference between the new house construction and the retrofit cases can be attributed to the fact that there is a larger borehole field as well as longer ground loops meaning that the fluctuations in the average temperature with small changes in the length of the ground loop will not be as high.

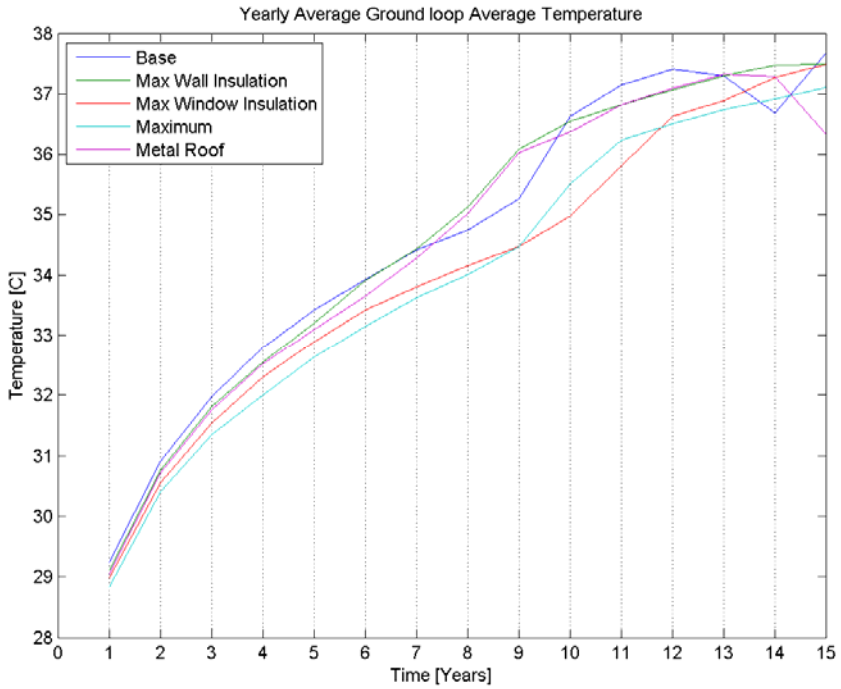

Figure 7.20: Yearly average ground loop average temperatures for retrofit cases: Phoenix

***Electricity Use**:* Figure 7.21 shows a 1 MWh difference in electricity consumed between the best Maximum Case and worst Base Case, amounting to a savings of about $100/year and $1500 over the course of the 15 years. The Metal Roof Case also consumes less energy and provides the same benefits as either the Maximum Wall Insulation or the Maximum Window Insulation Cases.

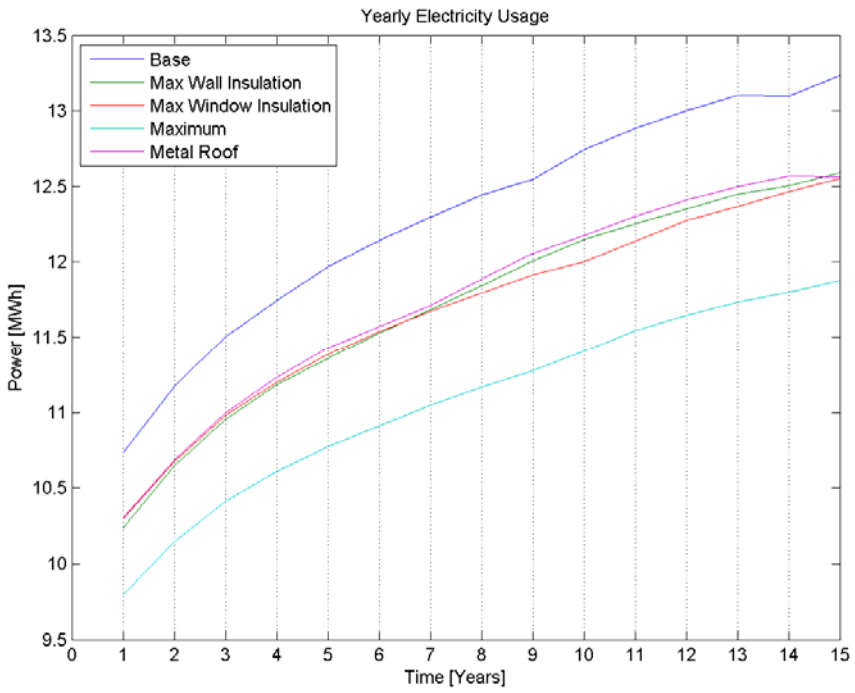

Figure 7.21: Yearly electricity usage for retrofit cases: Phoenix

***Cost Analysis**:* Table 7.32 shows the costs for the retrofit cases. None of the cases lowers the operational cost enough to justify investing in more insulation or a metal roof.

Table 7.32: GSHP Costs over 15 years for Retrofit Cases: Phoenix

Retrofit System Cost: Phoenix									
Retrofit Case	**Retrofit House Construction Costs**				**GSHP System**				
	Wall	Roof	Window	Wall Insulation	Equip-ment	Drill	Electricity	Total	Total w/ Rebate
Base	$22,756	$12,223	$3,520	$2,322	$12,000	$25,500	$16,972	$95,293	$84,043
Max Wall Insulation	$22,756	$12,223	$3,520	$3,042	$12,000	$25,500	$16,155	$95,196	$83,946
Max Window Insulation	$22,756	$12,223	$5,840	$2,322	$12,000	$25,500	$16,115	$96,755	$85,505
Maximum	$22,756	$12,223	$5,840	$3,042	$12,000	$25,500	$15,276	$96,637	$85,387
Metal Roof	$22,756	$27,986	$3,520	$2,322	$12,000	$25,500	$16,216	$110,300	$99,049

Retrofit Construction Conclusion—Phoenix: Retrofit would not provide cost effective changes.

7.5 RESIDENTIAL BUILDING DESIGN STUDY: SUMMARY

GSHP Performance

The heat pump efficiency is highly correlated to its EWT: higher efficiency during cooling at lower EWTs and during heating at higher EWTs. Figure 7.22 provides a graph of the yearly minimum, maximum, and average heat pump EWTs for the Base Case in all three cities.

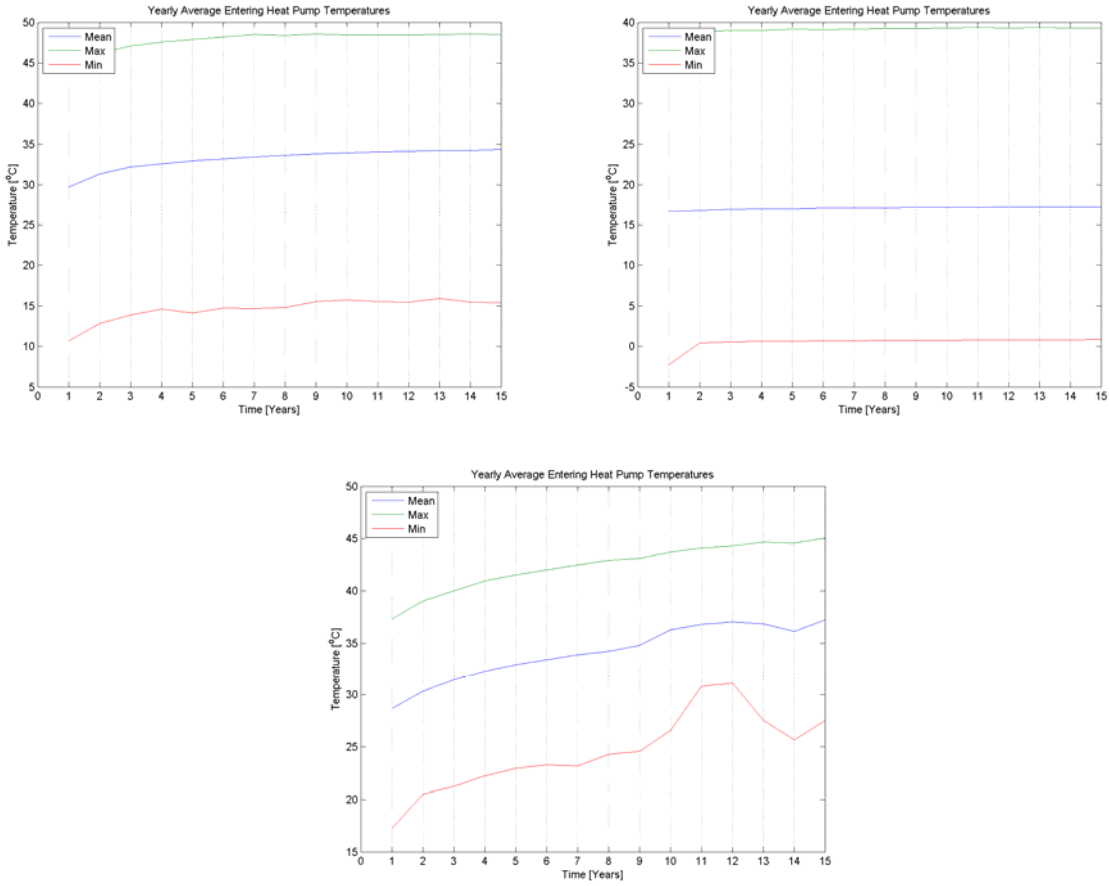

Figure 7.22: Yearly average heat pump EWTs for Base Case in Austin (top left), Albuquerque (top right), and Phoenix (bottom)

Austin is the only city with heat pump EWTs reaching the maximum designed EWT of 48.9°C (120°F), heat pump shutoff temperature. Figure 7.23, shows the heat pump EER and COP ratings over the 15 years. Albuquerque has the highest EER ratings and is the best of the three cities to implement GHPs.

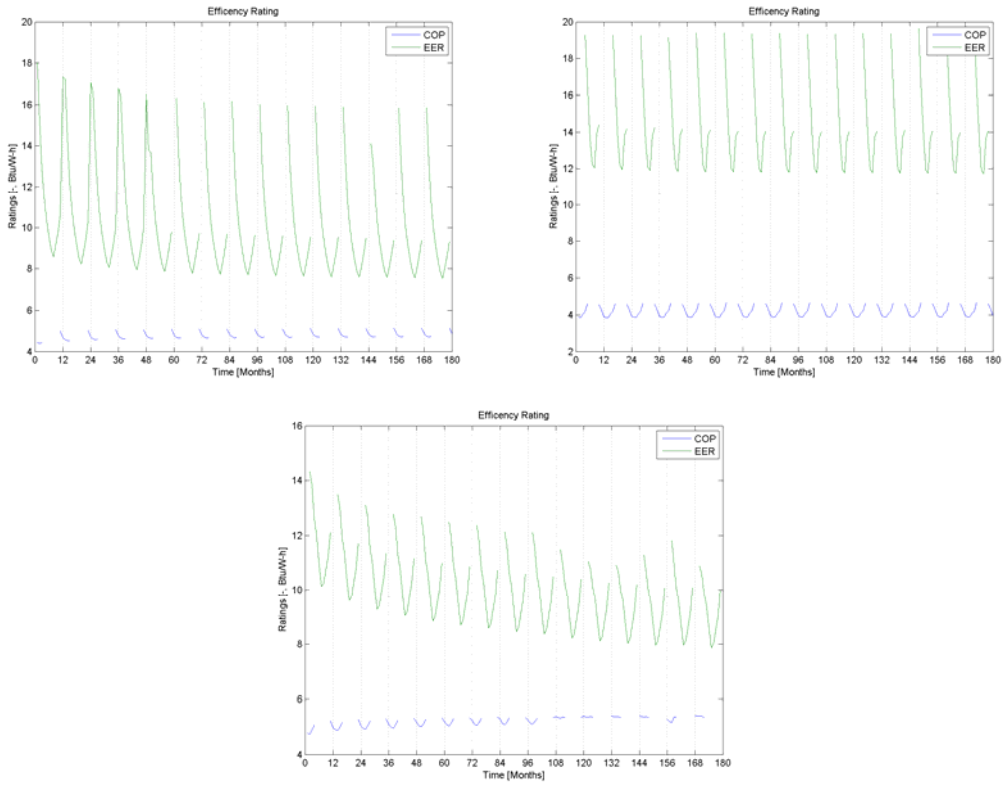

Figure 7.23: Heat pump rating for Base Case in Austin (top left), Albuquerque (top right), and Phoenix (bottom)

Ground Loop Sizes

Ground loops in Austin and Albuquerque were both sized directly using GLHEPRO, while Phoenix was initially sized using GLHEPRO and adjusted until the unmet hour constraint was met. Table 7.33 lists the total borehole lengths for the new construction cases. Albuquerque has the shortest ground loops, but these lengths were nominally the same as in Austin. In Albuquerque, the boreholes were sized on the heating loads, so the Maximum Window Insulation Case increased heating loads and had longer boreholes. The sizing of the ground loop in Phoenix is about three times the sizing of either Austin or Albuquerque. The type of exterior wall material (brick, stone, wood, concrete) made little/no difference in the borehole lengths. In Phoenix, however, the Stone Wall Case had the largest ground loop (higher thermal capacity). The Maximum Wall Insulation, Maximum, and Metal Roof Cases consistently had shorter ground loops. Furthermore, all of the cities show that adding more insulation has more of an effect on the ground loop size than adding a metal roof.

In the retrofit studies, for a constant heat pump capacity and ground loop size, adding maximum insulation in the exterior walls and windows and metal roof increased heat pump efficiency over the Base Case and increased the lifetime of the borehole field.

Table 7.33: Ground Loop Length for Austin, Albuquerque, and Phoenix for New Construction Cases

Ground Loop Length m (ft)			
Cases	**Austin**	**Albuquerque**	**Phoenix**
Base	251 (824)	247 (812)	777 (2550)
Max Wall Insulation	244 (800)	233 (764)	761 (2496)
Max Window Insulation	237 (776)	249 (816)	761 (2496)
Maximum	234 (768)	235 (772)	737 (2418)
Metal Roof	240 (788)	241 (792)	764 (2508)
Stone	251 (824)	247 (812)	794 (2604)
Wood	250 (820)	245 (804)	779 (2556)
Concrete	251 (824)	247 (812)	783 (2568)

Economic Study

Retrofitting with increased exterior wall and window insulation increased the heat pump efficiency, but with the exception of adding wall insulation in Albuquerque, the electricity savings was less than the cost of the retrofits. For new construction cases, for all exterior wall types, adding maximum insulation in the windows and walls increased heat pump efficiency. However, the main difference in total costs over 15 years was the difference in construction costs for the exterior wall types, with wood and concrete being the least expensive option.

Overall Conclusion

Austin, Albuquerque, and Phoenix have very different weather and ground conditions which translate into different GSHP sizing and performance. Austin has good ground thermal properties but relatively high ground temperature, Albuquerque has low ground temperature but poor ground thermal properties, and Phoenix has both high relative ground temperature and poor ground thermal properties. Furthermore, Phoenix is highly cooling dominated and Albuquerque has a more balanced heating/cooling loads. Albuquerque is the best of the three cities for implementing GHPs and it shows the most operational savings and has the lowest overall system costs.

The construction design study for the residential building showed that the exterior wall materials (brick, stone, wood, concrete) had little to no effects on the GHP performance but vastly different costs. Adding wall and window insulation reduced building loads and improved

GHP performance, but in general, the savings in electricity did not justify the added costs of those improvements. It appears that using the most inexpensive exterior wall material (wood or concrete) and installing the maximum wall insulation provided the best cost-performance tradeoff in all three cities.

8.0 PROJECT CONCLUSIONS

The project objective was to develop engineering data, analysis, modeling and decision–support tools to enable the identification, selection, design, specification, and construction of supplementary heat rejection (SHR) systems/devices that, when added to conventional ground–source heat pump (GHP) systems, make the resulting hybrid GHP system technically and economically viable in hot, arid or semiarid climates typical of the southwestern and western United States given: (1) various building types and sizes; (2) historical and predicted installation and maintenance costs; (3) local climate history; (4) building site characteristics; (5) resource availability; (6) various ground resources/designs; and (7) electricity sources along with related costs and greenhouse gas (GHG) emissions. An implicit objective is demonstration that SHR systems/devices are *central* to the viability of GHP systems in these demanding environmental, geological and hydrological conditions, all which have an impact on installation cost and feasibility. An ancillary objective is to develop and distribute web–based information and tools that provide engineering guidance to building owners and designers regarding which SHR–augmented GHP systems offer the best performance at the lowest life–cycle cost.

8.1 INTEGRATED IBL-GHP MODEL FOR RESIDENTIAL AND COMMERCIAL OFFICE BUILDINGS

The major component models of the IBL-GHP system were for the building loads, heat pump (HVAC system), and borehole/ground interactions. For this project, these models are summarized below.

8.1.1 Building Load Model

The HAMBASE building load model was selected from a list of other potential models in Sections 3.1.2 and 3.1.3; its Simulink/MatLab modeling and computational environment provided a flexible and powerful algorithmic platform that easily coupled component models into an integrated system model. HAMBASE inputs industry-standard local climate conditions (TMY data) and geological data for site-specific studies. It is applicable to residential and commercial buildings. HAMBASE residential building simulations compared well with ASHRAE 140-2007 standard studies (Section 3.1.4) and with eQuest results (Section 4.6.4). HAMBASE commercial office building simulations compared well with EnergyPlus simulations in open loop steady-state tests (Section 6.2.2*)*, but HAMBASE transient results showed its time constant to be about half the size of EnergyPlus' time constant.

8.1.2 Heat Pump Model

The air-to-water heat pump model was an empirical model based upon a series of equations that curve fit input/output relations (called performance mapping) to manufacturer's performance data (Section 3.2). While these models lose process physical details, they are computationally efficient, data is available for a wide range of heat pumps, and the results are very accurate when the heat pump operates in the provided data range.

The heat pumps used in this project were ClimateMaster Tranquility 20 Single Stage Series heat pumps of varying capacities. The model was derived so data from other heat pump manufacturers can be used (ANSI/ASHRAE/ARI/ISO 13256-1 standard for rating and testing water source heat pumps). A thermostat model with temperature set points and deadband was implemented to control the heat pump.

8.1.3 Borehole/Ground Loop Model

The vertical borehole-ground loop model computes temperatures inside the borehole tube and the ground outside the borehole. The implemented model utilizes work from Hellstrom, Ekillson, and Xu (Section 3.3.3) using g-functions for accurate short- and long-term time-step computations. GLHEPRO was used to size the ground loop boreholes in all cases. Simulations of the heat pump-ground models for the residential building compared very well with GLHEPRO data (Section 4.6.4).

8.1.4 Simulink Coupling

The component models described above were coupled using Simulink (Section 4.1-4.5) into an integrated Building Load-GHP model (IBL-GHP). Due to the differences in thermal time scales, the residential building model used 30 second time steps for the entire model except for the ground loop model, which is updated every five minutes. The commercial office building model used 60 second time steps for the entire model except for 60 minute time steps for the ground loop model. Simulink's multirate simulation function accommodated the two different update rates.

8.2 RESIDENTIAL BUILDING STUDIES

The IBL-GHP residential building model was applied to a 195m^2 (2100ft^2), single-story residential house using Austin, TX weather and geological data. The building layout, construction data, and scheduled thermal loads were presented in Section 4.6. A ClimateMaster Tranquility 20 Series single speed heat pump with 14kW (4-ton) capacity was selected to satisfy

the building loads. The ground loop was sized using GLHEPRO for a 10-year operation with the maximum heat pump EWT at 48.9^{o}C (120^{o}F), which resulted in four in-line boreholes, spaced on 4.6 meters (15 feet) centerlines and each 68.6m (225ft) deep. The use of the shutoff temperature as the maximum ETW is a limiting case that resulted in the shortest borehole lengths and lowest operating efficiency of the heat pump. The heating and cooling temperature set points were 21^{o}C and 25^{o}C, respectively, with a 1^{o}C deadband. The IBL-GHP residential building model compared well with GLHEPRO data (Section 4.6) to illustrate the validity of the heat pump and ground loop model implementation.

8.2.1 Base Case Simulation Results

Simulations for the base case residential IBL-GHP model ran for up to 15 years of operation. The simulated data illustrated the power of the model to predict system responses from seconds to years (Section 4.7), and it showed the computation and coupling power of the Simulink environment. For the base case, conditioned space temperatures were held to set point except for 63 unmet hours in year 10 (less than 1% of the year and represented 3% of the total cooling time of 2128 hours) and 167 unmet hours in year 15 despite ground heating effects. In other words, the GLHEPRO computed borehole size of 68.6m/borehole using the heat pump shutoff temperature as the upper limit of EWT was sufficient to control the conditioned space temperatures to setpoint. In practice, however, longer boreholes are necessary to compensate for uncertainties in the weather, ground properties, building loads and to keep heat pump EWT below its shutoff temperature for the lifetime of the boreholes.

8.2.2 Sensitivity Studies

A series of sensitivity studies (varying borehole length, borehole configuration and spacing, grout conductivity, and ground temperature) were run and compared to the base case results in Section 4.7. While most of the results are intuitive (e.g. longer borehole lengths decrease heat pump EWT, etc), this report provides quantitative comparisons of performance and costs in Section 4.7. The term ‘under-designed’ is used whenever the parameter perturbation resulted in the number of unmet hours (when the conditioned space temperature was outside the setpoint and deadband ranges) did not satisfy the ASHRAE 90.1 standard of 300 unmet hours. The study showed that any ‘decrease’ in the base case design parameter values resulted in under-designed systems. This result again illustrated that the use of the heat pump shutoff temperature as the maximum heat pump EWT and the resulting GLHEPRO borehole sizing resulted in the minimal acceptable design.

Compared to the base case values, increased borehole length (Section 4.8.1) and grout conductivity (Section 4.8.3) reduced heat pump EWT, increased heat pump efficiency, decreased electricity usage, and increased the lifetime of the borehole field, but with additional installation expense. Decreased ground temperatures (Section 4.8.4), while not controllable, significantly decreased heat pump EWT. One interesting result was increasing ground temperature from the base case caused the heat pump to shutdown during the heating mode when the heat pump EWT exceeded 90^{o}F. The borehole configuration/spacing study (Section 4.8.2) showed that larger centerline spacing improves operating performance, and for a given centerline spacing, the in-line borehole field configuration is superior in performance to a square field configuration.

Sensitivity Study Summary: The parameters varied in this sensitivity study illustrated only a few possible design parameters that could be varied by the IBL-GHP model. All results show that borehole performance is very sensitive to these parameters. The sensitivity study showed that the base case design was a minimal design for the GHP system; any perturbation 'decrease' from the base case parameters resulted in under-designed systems that will not provide adequate control of building temperatures. This result highlights the need to add extra borehole length to account for parameter variations since ground parameters are not typically known to precise values for residential installations. The improved results by adding borehole length have been quantified in this study, as shown by the longer borehole lengths typically used in Austin, TX. With subsidies and tax credits, the longer boreholes are easily justified based on heat pump performance. Of the individual sensitivity studies performed, the most cost effective design parameter that can be addressed by the designer is the borehole configuration and spacing. As expected, placing the boreholes as far apart as possible (and with the largest aspect ratio—in the limit in-line configuration) will significantly increase heat pump efficiency and longer borehole lifetimes. While the results are intuitive, this study showed the quantitative improvements that can be expected.

8.2.3 Building Design Study

The base case residential IBL-GHP model was used to investigated the extent to which variations in the following house construction parameters improved GHP performance and cost in Austin, TX, Albuquerque, NM, and Phoenix, AZ: 1) exterior wall type (brick, stone, wood, and cement), 2) roof (shingle and metal), 3) exterior wall insulation (code minimum up to maximum based upon spacing), and 4) window fenestration/solar gain (code minimum and maximum thermal insulation effects). Both new construction and retrofit construction cases were

considered. The three cities were used as representatives for the southwest region in the US with arid or semi-arid climates. The study used the base case residential building and applied the appropriate building codes, ground and climate conditions for each city (Section 7.3).

Albuquerque was the best of the three cities for implementing GHPs and it showed the most operational savings and had the lowest overall system costs (Sections 7.5 and 7.6). Austin was already shown to provide a good base case design. Phoenix provided the most challenge for GHP design due to its hot summers and resulting cooling-dominated loads.

The construction design study for the residential building showed that the exterior wall materials (brick, stone, wood, concrete) had little to no effects on the GHP performance but vastly different costs. Adding wall and window insulation reduced building loads and improved GHP performance, but in general, the savings in electricity did not justify the added costs of those improvements (Section 7.6). It appears that using the most inexpensive exterior wall material (wood or concrete) and installing the maximum wall insulation provided the best cost-performance tradeoff in all three cities.

8.2.4 SHR Sensitivity Study

Section 4.8.5 described the effects of adding SHR (device/system not specified) to the residential building. The study looked at reductions in heat rejected to the ground from 2%-40% and computed the heat pump efficiencies, electricity used, and savings in shorter borehole lengths. Installation costs was reduced by up to 30%. The basic problem was to identify a SHR device that could remove heat from the relatively low temperature water leaving the heat pump.

8.2.5 SHR-Cooling Tower

In Section 5.1.2, an integrated hybrid IBL-HSHP model was developed using the IBL-GHP model and coupling a model of a 2-ton cooling tower. The use of a 2-ton cooling tower with a 4-ton heat pump may seem unbalanced, but it was the smallest commercially available cooling tower. The tower removed 80% of the total heat that would have been rejected to the ground without the cooling tower. In year 10 of operation the heat pump EWT was reduced by 12^{o}C compared to the GHP-only case. This reduction in temperature increased heat pump efficiency, reduced electricity use and increased the lifetime of the borehole. The HGHP system showed to be very cost effective.

8.3 COMMERCIAL OFFICE BUILDING STUDIES

The IBL-GHP commercial office building model was applied to the Medium Office from the Department of Energy's (DoE) Commercial Reference Building Models [US DoE, 2010]; a 4,982m^2 (53,628ft^2) three-story office building. For each floor, there are five conditioned zones

and one unconditioned plenum (Section 6.1). Each conditioned zone has one ClimateMaster Tranquility 20 Series single speed heat pump of varying capacity to satisfy the heating/cooling loads for that zone. The ground loop was sized using GLHEPRO for a 15-year operation with the maximum heat pump EWT at 32.2^{o}C (90^{o}F) which resulted in a 10x16 borehole filed, spaced on 6.1m (20ft) centerlines and each 171m (561ft) deep. Open-loop comparisons between HAMBASE and EnergyPlus (Section 6.3.3) showed good agreement on steady-state zonal temperatures, but HAMBASE transient responses had time constants approximately half of those from EnergyPlus. Also, the open loop tests showed EnergyPlus to be more responsive in magnitude and time for zonal humidity.

8.3.1 Base Case Simulation Results

Simulations for the base case commercial office building IBL-GHP model ran for 15 years of operation. The simulated data showed good performance and illustrated the power of the model to predict system responses from minutes (Section 6.4.1), hourly (Section 6.4.2), monthly (Section 6.4.3) and yearly (Section 6.4.4), and it showed the computation and coupling power of the Simulink environment to allow multiple time-steps of 1 hour for the ground loop and 1 minute for the balance of the system.

8.3.2 Sensitivity Study

An SHR study, with no device or system specified, on removing 0%, 10%, and 25% of the heat from the water before entering the ground loop investigated the use of the heat pump shutoff temperature as the maximum EWT used to size the boreholes by GLHEPRO. The first case assumed the borehole lengths were constant at the 0% SHR case (Section 6.5.1.1) with 9.1m centerline spacing and the second case resized the boreholes based upon the heat removed (Section 6.5.1.2) with 10.4m centerline spacing. In case 1, only the 25% SHR was able to control the zonal temperatures. In the second case, the SHR decreased installation costs significantly due to shorter borehole lengths (compared to the base case) and each case was able to control the zonal temperatures within ASHRAE constraints.

8.4 SHR STUDY

In this project, two heat rejection strategies were followed: 1) remove heat directly from the water before it enters the ground loops and 2) remove heat from the refrigerant loop of the vapor compression cycle (VCC) of the heat pump so less heat is transferred to the water loop at the condenser of the VCC. Several SHR devices/systems were investigated as discussed in

detail in Section 5 and Appendix D. In the first strategy, the only device that was found to be cost effective was the cooling tower. The temperature of the water loop leaving the heat pump was too low to allow heat exchangers to effectively remove heat. Using the second strategy, optimizing the VCC did not result in sufficient energy to be extracted from the water loop.

9. REFERENCES

Albuquerque. 2007. The Albuquerque energy conservation code, Vol II, 2nd Ed., 2007

American Society of Petroleum Geologists. 1974. Geological maps of Texas. University Press.

ASHRAE. 2007. ANSI/ASHRAE 140-2007 standard method of test for the evaluation of building energy analysis computer programs. ASHRAE - American Society of Heating, Refrigerating and Air-Conditioning Engineers, 2007.

ASHRAE. 2007b, Energy standard for buildings except low-rise residential buildings, standard 90.1, ASHRAE, Atlanta GA, 2007

ASHRAE. 2009. American Society of Heating, Refrigerating and Air-Conditioning Engineers 2009 Fundamentals HandBook, 1791 Tullie Cir, N.E., Atlanta, GA 30329.

Austin. 2008. City of Austin Energy Code Chapter 25-12. Ordinance No. 20071018-088. Reprint.

Austin. 2011. Austin City Water Rates http://www.ci.austin.tx.us/water/downloads/approvedservicerates2011waterretail.pdf

Balasubramanian, Siddharth. 2011. Supplemental heat rejection in ground source heat pumps for residential houses in Texas and other semi-arid regions. Master's thesis, The University of Texas at Austin, 2011.

Balasubramanian, S., Gaspredes, J., Moon, T., and Masada, G. 2012. Cooling towers as supplemental heat rejection systems in ground source heat pumps for residential houses in Texas and other semi-arid regions. ASME 2012 6th Int. Conf. Energy Sustainability, 719, July 2012, pp. 719-729.

Bennet, J., Claesson, J., and Hellstrom, G. 1987. Multipole method to compute the conductive heat flows to and between pipes in a composite cylinder. University of Lund, Department of Building Technology and Mathematical Physics. Lund, Sweden, 1987.

Blair, Jacob. 2013. Simulink-based model of a ground source heat pump system for a commercial office building, MS Thesis, University of Texas at Austin, Dec 2013.

Browder, Lee. 2011. ClimateMaster teleconference meeting, 2011.

ClimateMaster. 2010. Tranquility 20 Single Stage Series Submittial Data. ClimateMaster, Inc., 7300 S.W. 44th Street Oklahoma City, OK 73179.

ClimateMaster. 2011. GeoDesigner. ClimateMaster, Inc., 7300 S.W. 44th Street Oklahoma City, OK 73179.

Copeland. 2011. Copeland Compressors - http://www.emersonclimate.com/en-US/products/compressors/scroll_compressors/copeland_scroll_residential/Pages/Copeland ScrollZRK5Compressor.aspx

Crawley, D., Lawrie, L., Winkelmann, F., Buhl, W., Huang, J., Pedersen, C., Strand, R., Liesen, R., Fisher, D., Witte, M., and Glazer, J. 2001. EnergyPlus: creating a new-generation building energy simulation program. Energy and Buildings, 33:319-331, 2001.

Crawley, D., Hand, J., Kummert, M., and Grifith, B. 2008. Contrasting the capabilities of building energy performance simulation programs. Building and Environment, 43:661-673, 2008.

Cullin, J. and Spitler, J. 2010. Comparison of simulation-based design procedures for hybrid ground source heat pump systems. In 8th International Conference on System Simulation of Buildings, Liege, December 13-15, 2010

de Wit, Martin. 2006. Heat air and moisture model for building and systems evaluation. Technical report, Eindhoven: Technische Universiteit, Eindhoven, The Netherlands, 2006.

Duffy, M., Hiller, M., Bradley, D., Keilholz, W., and Thornton, J. 2009. TRNSYS: features and functionalitity for building simulation 2009 conference. In Building Simulation. IBPSA, July 2009.

Edwards, B.C. et al. 2010. Development of a gluorescent cryocooler, Los Alamos National Laboratory, Ninth Annual American Institute of Astronautics & Aeronautics Utah State University

Elliot, N., Eldridge, M., Shipley, A., Laitner, J., Nadel, S., Silverstein, A., Hedman, B., and Sloan, M. 2007. Potential for energy efficiency, demand response, and onsite renewable energy to meet Texas's growing electricity needs, American Council for an Energy Efficient Economy, 115 pp., March 2007.

Efficient Windows Collaborative Resources. 2011. Solar heat gain factor. http://www.efficientwindows.org/shgc.cfm.

eQuest 3-64. 2010. Lawrence Berkeley National Labs & James J Hirsch & Associates, 2010.

ERCOT. 2011. ERCOT Press Release, August 3, 2011. ERCOT breaks peak demand record third time (Update).

Eskillson, Per. 1987. Thermal analysis of heat extraction boreholes. PhD thesis, University of Lund, 1987.

Field, K., Deru, M., Studer, D., Benne, K., Griffith, B., and Torcellini, P. 2011. U.S. Department of Energy commercial reference building models of the national building stock. Technical report, National Renewable Energy Laboratory, February 2011.

Fisher, D. and Rees, S. 2005. Modeling ground source heat pump systems in a building energy simulation program (EnergyPlus). 9th International IBPSA Conference, pp 311-318, Montreal, Canada, August 2005.

Frontier Associates, LLC. 2008. *Texas Renewable Energy Resource Assessment 2008*, Chapter 7: Geothermal Energy, Texas State Energy Conservation Office, December 2008

Gaspredes, J. 2011. Development of an integrated building load-ground source heat pump model as a test bed to assess short- and long-term heat pump and ground loop performance. M.S. thesis, University of Texas Austin, 2011.

Gaspredes, J., Masada, G., and Moon, T. 2012. Development of an integrated building load-ground source heat pump model as a test bed to assess short- and long-term heat pump and ground loop performance. ASME 2012 6th Int. Conf. Energy Sustainability, 827, July 2012, pp. 827-836.

Gaspredes, J., Masada, G., and Moon, T. 2012b. Effects of ground loop design parameters on short- and long-term operational and economics of ground source heat pumps in hot, semi-arid areas. ASME 2012 6th Int. Conf. Energy Sustainability, 815, July 2012, pp. 815-825.

Hackel, Scott. 2008. Development of design guidelines for hybrid ground-coupled heat pump systems. Master's Thesis, University of Wisconsin, Madison, May 2008

Hackel, S., G. Nellis, and S. Klein. 2009. Optimization of cooling-dominated hybrid ground-coupled heat pump systems. ASHRAE Transactions 115(1): 565-580.

Hammond, Mike. 2011. Meeting ClimateMaster, Nov 2011.

Hasan, A and Siren, K. 2002. Theoretical and computational analysis of closed wet cooling towers and its application in cooling of buildings. Energy and Buildings, 34, pp. 477 – 486

Hellstrom, G. 1991. Ground heat storage: Thermal analyses of duct storage systems. Sweden: Department of Mathematical Physics University of Lund, 1991.

Hirsch, J. 2004. eQuest v3 - overview. Technical report, Energy Design Resources, 2009, Volume 1: DOE-2.2 Basics Manual. Lawrence Berkeley National Labs & James J Hirsch & Associates, 2004.

Home Depot. 2012. Personal Interview. Window and wall costs. 13 Apr. 2012.

Hughes, Patrick. 2008. Geothermal (ground-source) heat pumps: market status, barriers to adoption, and actions to overcome barriers, Technical report ORNL/TM-2008/232, Oak Ridge National Laboratory, December 2008.

IIT Madras. 2011.- NPTEL – http://nptel.iitm.ac.in/courses/Webcourse-contents/IIT%20Kharagpur/Ref%20and%20Air%20Cond/pdf/R&AC%20Lecture%2023.pdf

Incropera, F. and DeWitt, D. 1985. Fundamentals of heat and mass transfer. John Wiley & Sons, 1985.

Jain, N. and Alleyne, A. 2011. Thermodynamics-based optimization and control of vapor-compression cycle operation: optimization criteria. 2011 American Control Conference, June 29 – July 01, 2011.

Jensen, J. and Skogestad, S. 2007. Optimal operation of simple refrigeration cycles: Part 1: Degrees of freedom and optimality of sub-cooling, Computers and Chemical Engineering 31, pp. 712-721, 2007

Kavanaugh, S. 1985. Simulation and experimental verification of vertical ground-coupled heat pump systems. PhD thesis, Oklahoma State University, Stillwater, Oklahoma, 1985.

Kavanaugh, S, Green, M., Mescher, K. 2012. Commercial GSHP performance. ASHRAE Journal, Oct. 2012.

Konopacki, S. and Akbari, H. 2001. Measured energy savings and demand reduction from a reflective roof membrane on a large retail store in Austin. LBNL-47149 Report, pp 22

Larsen, L. and Thybo, C. 2004. Potential energy savings in refrigeration systems using optimal setpoints. IEEE International Conference on Control Applications. Vol. 1, pp. 701-704.

Larsen, L., Thybo, C., Stoustrup, J., and Rasmussen, H. 2004. Control methods utilizing energy optimizing schemes in refrigeration systems. IEEE Control and Decision Conference, Dec 14-16, 2004.

Lee, A. and Jones, J. 1997. Analytical model of a residential desuperheater. Applied Energy, 57(4):271 – 285, 1997

Mac Word. 2011. Allied Thermal Systems - http://www.alliedenergysystems.com/

Mathworks. 2011. Simulink-simulation and model-based design. 2011. URL http: //www.mathworks.com/products/simulink/.

Natural Resources Defense Council and Ceres. 2007. Power to save: an alternative path to meet electric needs in Texas. by Optimal Energy, Inc., January 2007, www.ceres.org/pub/docs/Ceres_texas_power.pdf, Last visited 18 July 2007.

Navigant Consulting. 2009. Ground-source heat pumps: overview of market status, barriers to adoption, and options for overcoming barriers.2009.

Newman, J., Cariste, B., Queiruga, A., Davis, I., Plotnick, B., Gordon, M., and San Martin, S. 2006. Thermoacoustic refrigeration. GSET Research Journall, 2006

NREL. 2008. National Solar Radiation Data Base, 1991-2005 Typical Meterological Year 3

Oklahoma State University. 2007. GLHEPRO 4.0 for Windows

Olszewski, M. and Fontana, E. 1983. Heat pump desuperheaters for supplying domestic hot water – estimation of energy savings and economic viability for residential applications. ORNL/CON-114, 1983

O'Neal, D., Gonzalez, J. and Aldred, W. 1994. A simplified procedure for sizing vertical ground coupled heat pump heat exchangers for residences in Texas. Technical report, Energy Systems Laboratory, Texas A&M University,1994.

Pfafferott, J., Fraunhofer ISE., & Kalz, D., Fraunhofer ISE. 2007. Thermo-active building systems. J. Lang, Ed. (ISSN No. 1610-8302).

Phoenix. 2006. City of Phoenix Amendments to 2006 International Energy Conservation Code.

PMIUSA. 2011. U.S. city elevation chart.

http://www.pmiusa.biz/pdf/US%20City%20Elevation%20Chart.pdf>.

Power Partners Inc. 2009. Submittal Data: ADCM3-125 [Data file]. Retrieved from http://www.eco-maxchillers.com//.pdf

Schmidt, P., Baker, D., Ezekoye, O., and Howell, J. 2006. Thermodynamics: an integrated learning system. Wiley, 2006.

Shiraishi, M., Kikuchi, K., and Yamanishi, T. 1981. Investigation of heat transfer characteristics of a two-phase cosed thermosyphon. In Heat Recovery Systems, 1:287 – 297, 1981

Southface. 2011. Residential energy code FAQ. http://www.southface.org/learning-center/library/res-code-faq.

Spitler J. D., 2000. GLHEPRO – A design tool for commercial building ground loop heat exchangers. Proceedings of the Fourth International Heat Pumps in Cold Climates Conference, Aylmer, Québec.

Texas Is Hot. 2009. TexasIsHot Organizations, *www.texasishot.org,* Last visited 16 July 2009.

TETechnology, 2010. LC-200 Pelier Thermoelectric Liquid Cooler, 1590 Keane Drive, Traverse City, MI.

Turbotec Desuperheaters. 2011.- http://www.turbotecproducts.com/EPspecs.html

USDA. 2009. Soil temperature and moisture regimes of the contiguous United States, US Dept. Agriculture: NRCSW Natural Resources Conservation Service, soils.usda.gov/use/thematic/, Last visited 2 August 2009.

U.S. Dept. of Commerce. 2010. Weather Bureau. Relative humidity and dew point table. http://www.wrh.noaa.gov/sto/rh0-500.pdf.

US DoE. 2001. US DoE Research News—Magnetic refrigerator successfully tested. Ames Laboratory, http://www.eurekalert.org/features/doe/2001-11/dl-mrs062802.php

US DoE. 2001. Assessment of hybrid geothermal heat pump systems. DOE–EE0258, December 2001.

US DoE. 2009. Energy consumption in Texas homes. U.S. DoE EERE, apps1.eere.energy.gov/states/residential.cfm/state=TX, accessed 16 July 2009.

U.S. DoE. 2011. EnergyPlus graphical user interfaces, March 2011. URL http://apps1.eere.energy.gov/buildings/energyplus/ep_interfaces.cfm.

U.S. DoE. 2010). *Commercial Reference Building Initiative*. Retrieved Sept 15, 2011, from U.S. Department of Energy. Sept. 2011 Web site: http://www1.eere.energy.gov/buildings/commercial_initiative/new_construction.html

US DoE. 2011b. Residential electricity prices, August 2011 (cents/kwh), 2011b. URL http://www.eia.gov/state/state-energy-rankings.cfm?keyid=18&orderid=1.

US DoE. 2013. Residential electricity prices, 2013 (cents/kwh), URL http://www.eia.gov/state/state-energy-rankings.cfm?keyid=18&orderid=1.

WaterFurnace. 2010. Legend series specification catalog. WaterFurnace International, Inc., 9000 Conservation Way Fort Wayne, IN 46809, June 2010.

Wikipedia, 2011. Alaska pipeline and thermosyphons.

Xu, Xiaowei. 2007. Simulation and optimal control of hybrid ground source heat pump systems. PhD thesis, Oklahoma State University, 2007.

Yarmark, E. and Phillips, E. 1999. The frozen soil barrier demonstration project, WM'0=99 Conference, February 28-March 4, 1999.

Yavuzturk, Cenk. 1999. Modeling of vertical ground loop heat exchangers for ground source heat pump systems. PhD thesis, Oklahoma State University.

Yavuzturk, C. and J. Spitler. 2000. Comparative study of operating and control strategies for hybrid ground-source heat pump systems using a short time step simulation model. *ASHRAE Transactions* 106 (2) 2000.

Yerba, Fred. 2009. Austin Energy, conference call, August 3, 2009.

Young, Thomas. 2004. Development, verification, and design analysis of the borehole fluid thermal mass model for approximating short term borehole thermal response. Master's thesis, Oklahoma State University.

Zhang, M., Lai, Y., Zhang, J., and Sun, Z. 2011. Numerical study on cooling characteristics of two-phased closed thermosyphon embankment in permafrost regions. Cold Regions and Technology, 65:203-210, 2011

Zeng, H., Diao, N., and Fang, Z. 2003. Efficiency of vertical geothermal heat exchangers in ground source heat pump systems. Thermal Science, 12(1): 77-81, 2003.

APPENDIX A: HAMBASE VALIDATION

Appendix A presents additional validation of the HAMBASE model with the by ASHRAE 140-2007 standard test cases.

Table A.1: Summary of Sensitivity Study Cases

Case	Base Case	Changes	Relevant Figures
610	None	Base case described in Section 4	A.1-A.6
610	610	Add shading over south facing windows	A.7
620	620	Remove the 12m^2 of windows from the south wall and add 6m^2 of shading to the east and west walls	A.8
630	630	Add shading above and around the widows on east and west walls	A.9
640	640	Heater thermostat is setback to 10^{o}C between 2300 and 0700 hrs then at 20^{o}C between 0700 and 2300 hrs	A.10
650	650	Night time ventilation added between 1800 and 0700 hrs, heat is always off and cooling is only provided between 0700 and 1800 hrs	A.11
900	900	Construction materials changed with higher heat capacities	A.12-A.14
910	910	Same as 900	A.15
920	920	Same as 900	A.16
930	930	Same as 900	A.17
940	940	Same as 900	A.18
950	950	Same as 900	A.19
960	960	Add unconditioned sunspace on the south side of house	A.20
600FF	600FF	No heating or cooling provided to the building	A.21
650FF	650FF	Same as 600FF, still has night time ventilation	A.22
900FF	900FF	Same as 600FF	A.23-A.24
950FF	950FF	Same as 600FF, still has night time ventilation	A.25

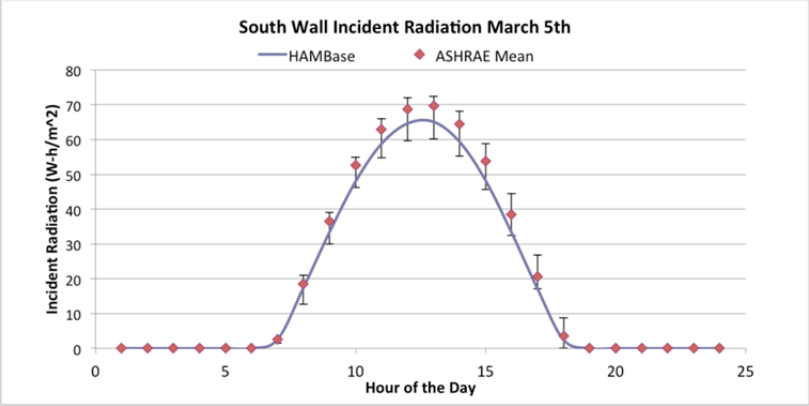

Figure A.1: Comparison of hourly incident radiation on the south wall for March 5th

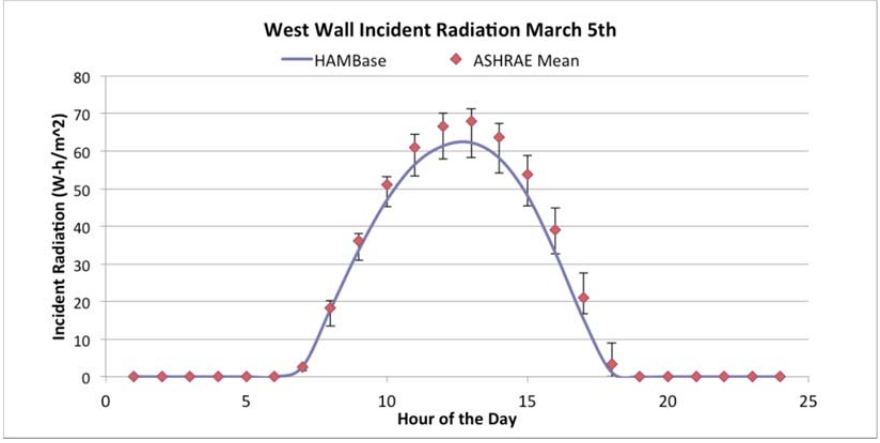

Figure A.2: Comparison of hourly incident radiation on the west wall for March 5th

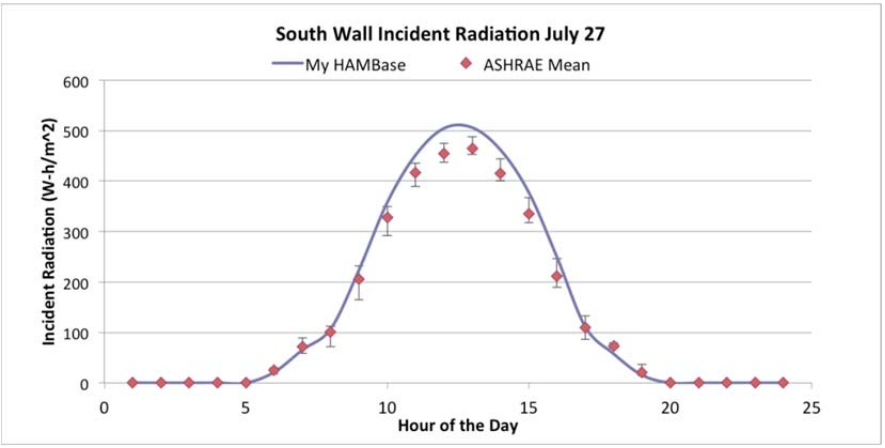

Figure A.3: Comparison of hourly incident radiation on the south wall for July 27th

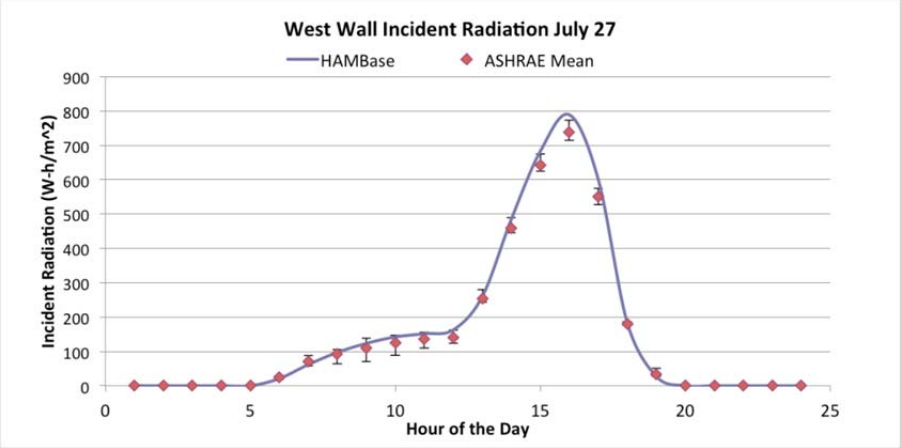

Figure A.4: Comparison of hourly incident radiation on the west wall for July 27th

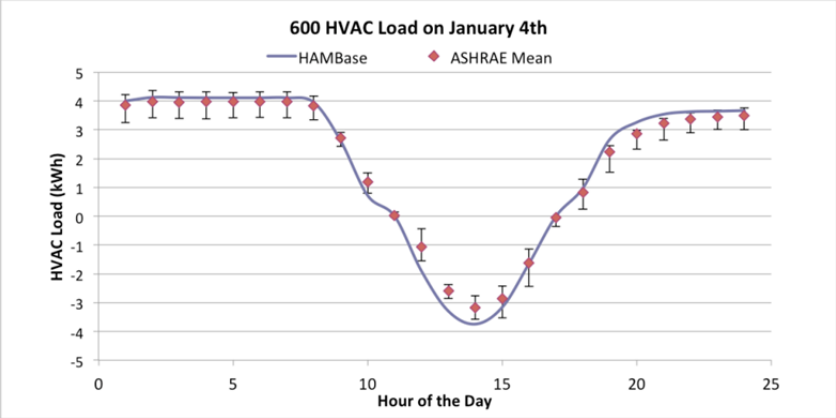

Figure A.5: Comparison of hourly HVAC system loads for case 600 on January 4th

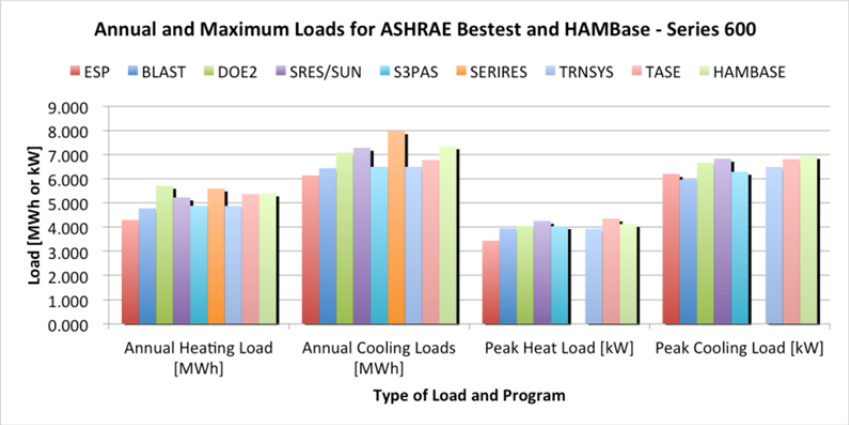

Figure A.6: Comparison of total annual and peak load for case 600

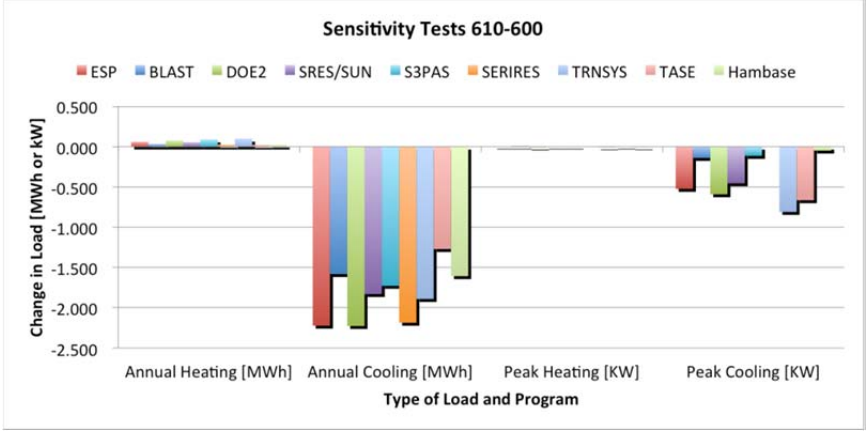

Figure A.7: Comparison of total annual and peak load differences between case 610 and 600. Includes the addition of shading over the south windows

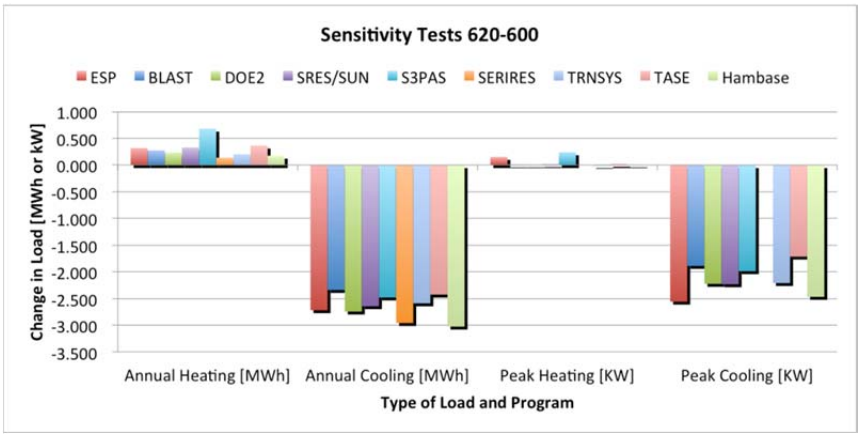

Figure A.8: Comparison of total annual and peak load differences between case 620 and 600. Moves the windows from the south wall to the east and west walls.

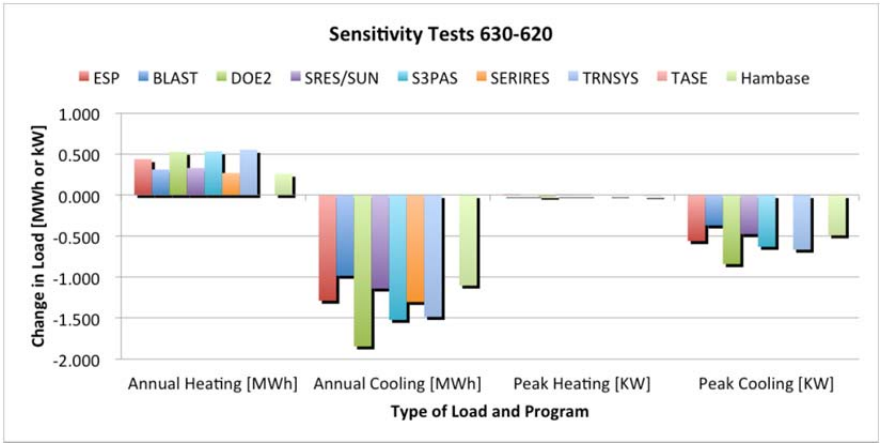

Figure A.9: Comparison of total annual and peak load differences between case 630 and 620. Includes the addition of shading around the windows on the east and west walls

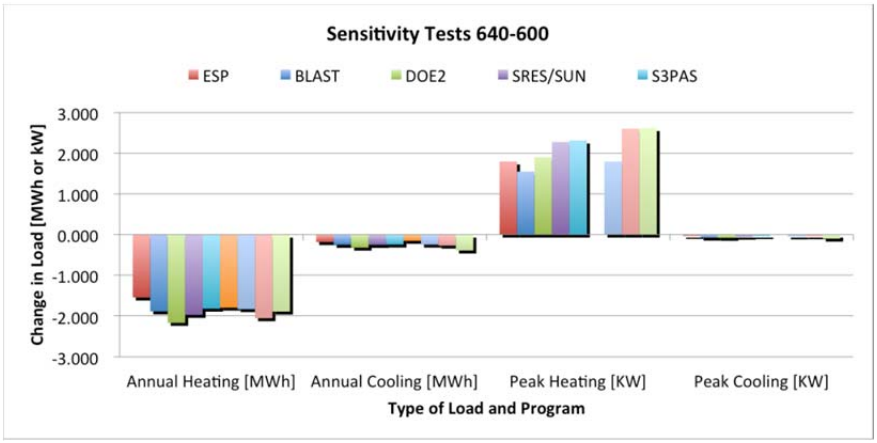

Figure A.10: Comparison of total annual and peak load differences between case 640 and 600. Heater thermostat is setback to $10^{o}C$ at night

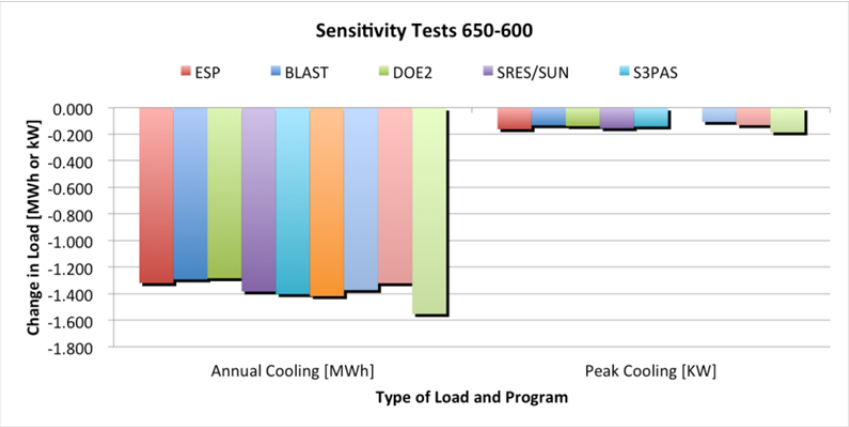

Figure A.11: Comparison of total annual and peak load differences between case 650 and 600. Adds night time ventilation

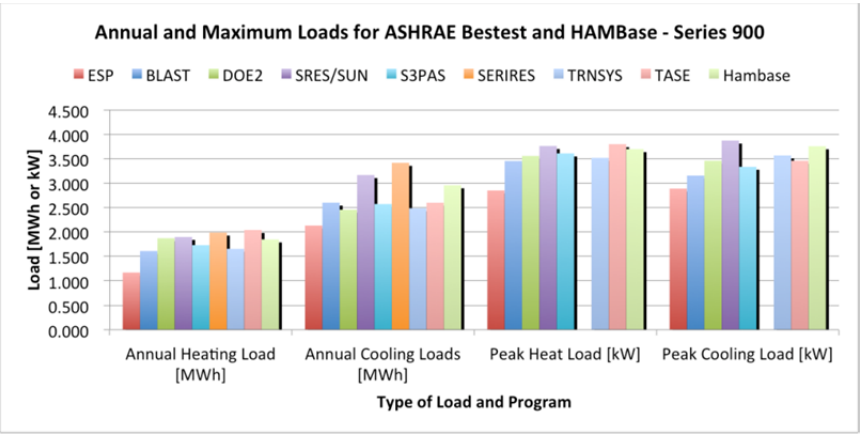

Figure A.12: Comparison of total annual and peak load for case 900

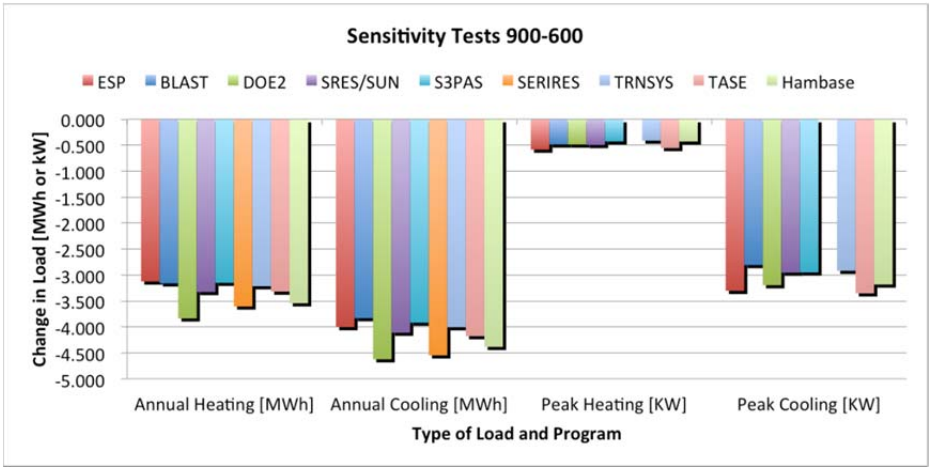

Figure A.13: Comparison of total annual and peak load differences between case 900 and 600. The construction materials properties are changed to have higher volumetric heat capacities

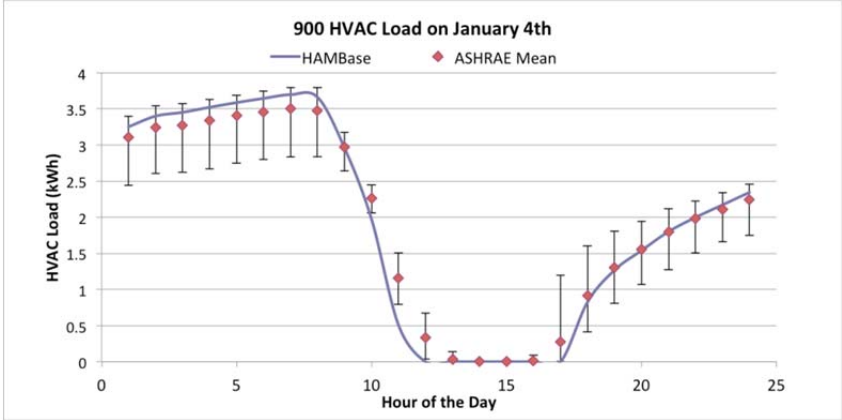

Figure A.14: Comparison of hourly HVAC system loads for case 900 on January 4th

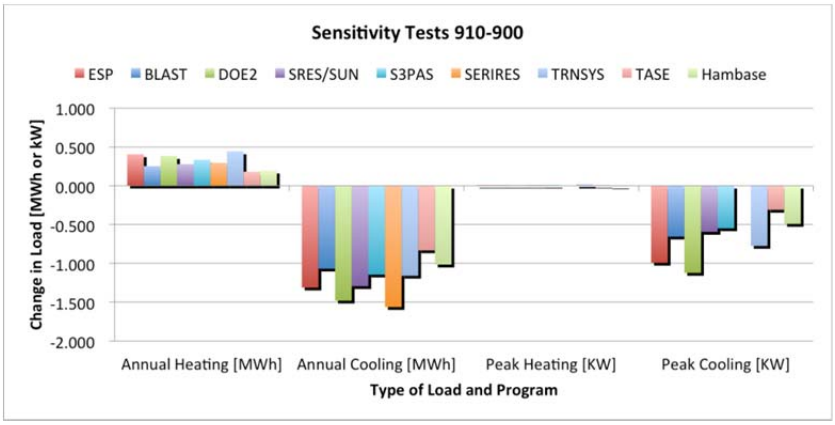

Figure A.15: Comparison of total annual and peak load differences between case 910 and 900. Includes the addition of shading over the south windows

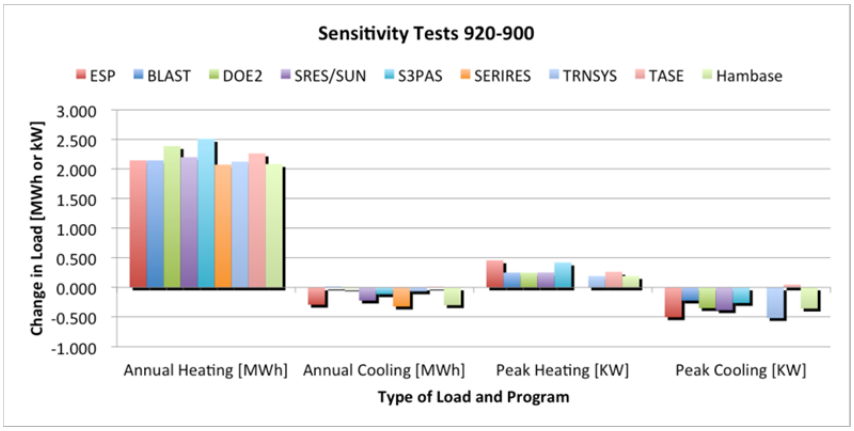

Figure A.16: Comparison of total annual and peak load differences between case 920 and 900. Moves the windows from the south wall to the east and west walls.

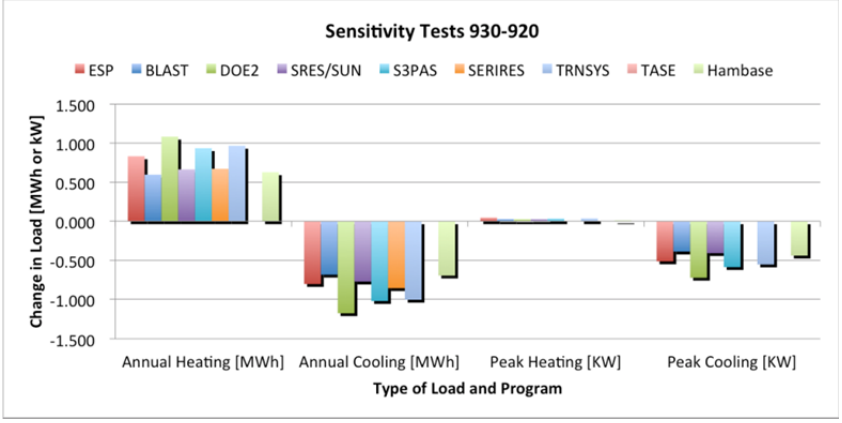

Figure A.17: Comparison of total annual and peak load differences between case 930 and 920. Includes the addition of shading around the windows on the east and west walls

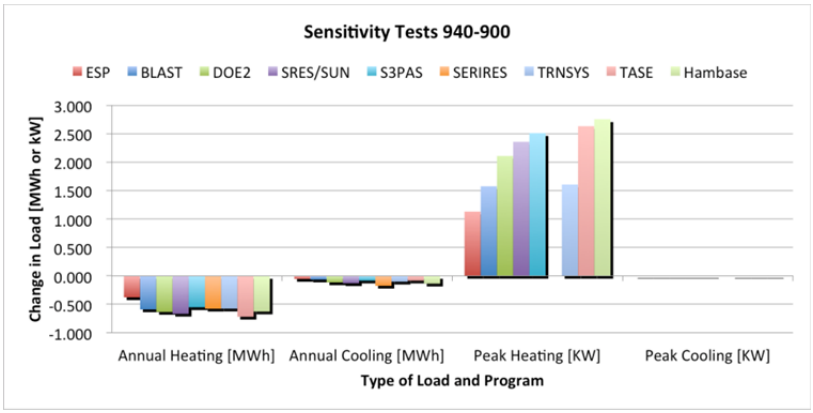

Figure A.18: Comparison of total annual and peak load differences between case 940 and 900. Heater thermostat is setback to 10^{o}C at night

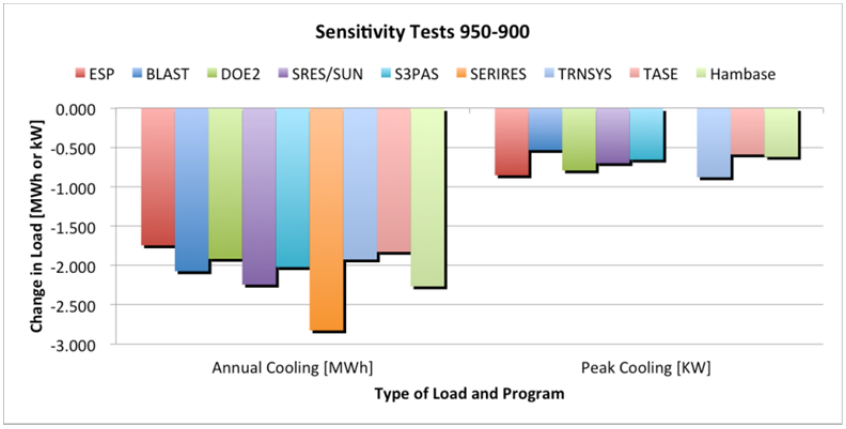

Figure A.19: Comparison of total annual and peak load differences between case 950 and 900. Adds night time ventilation

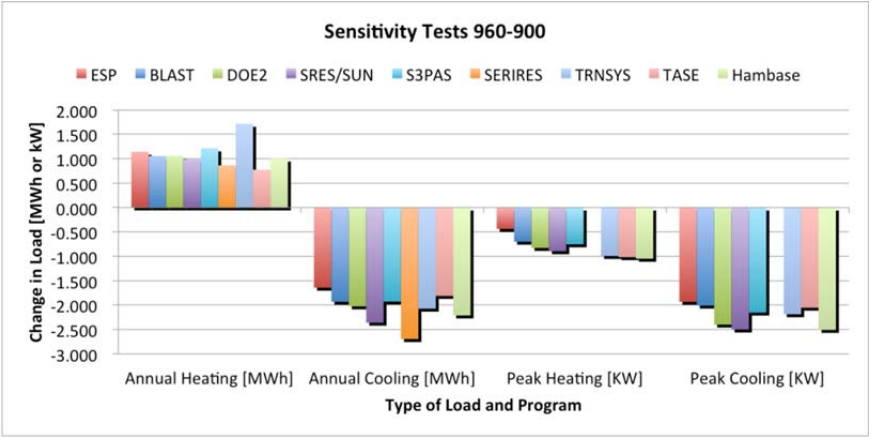

Figure A.20: Comparison of total annual and peak load differences between case 960 and 900. Addition of unconditioned solar space on the south side of the building

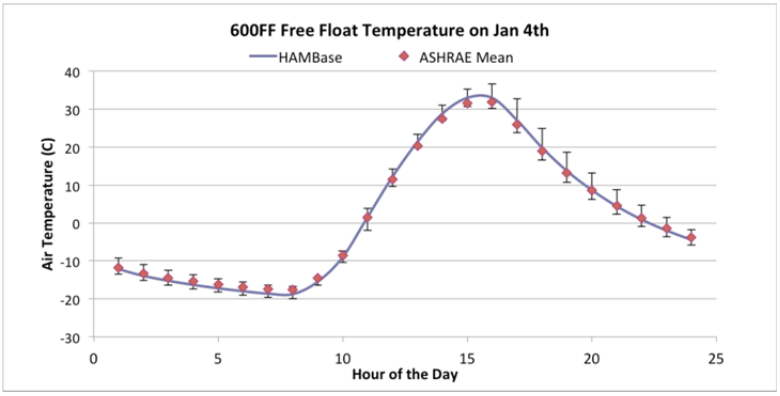

Figure A.21: Hourly temperatures on January 4th for the 600FF case

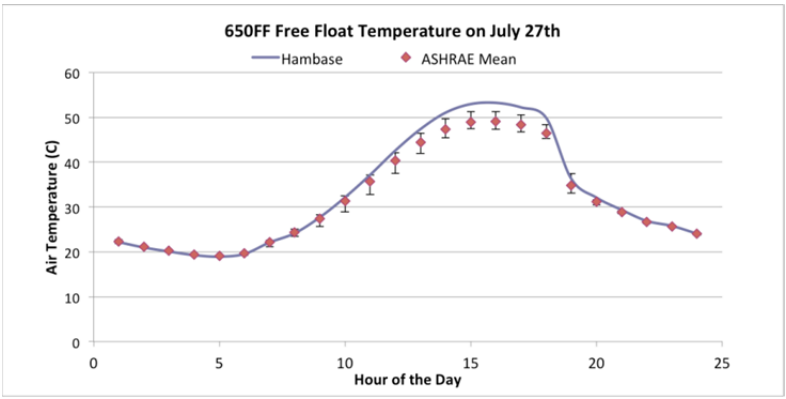

Figure A.22: Hourly temperatures on July 27th for the 650FF case

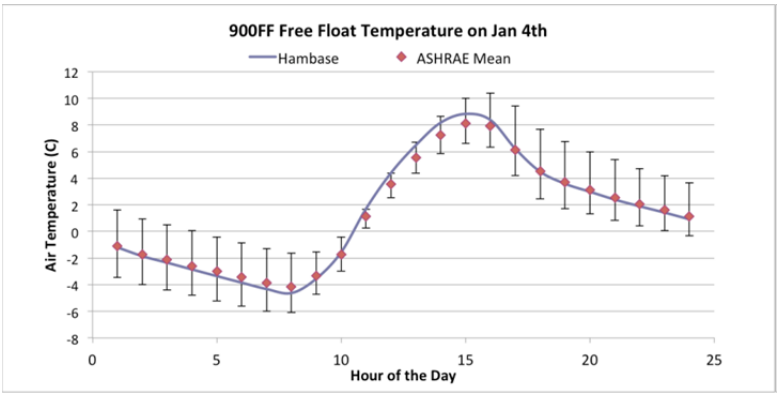

Figure A.23: Hourly temperatures on January 4th for the 900FF case

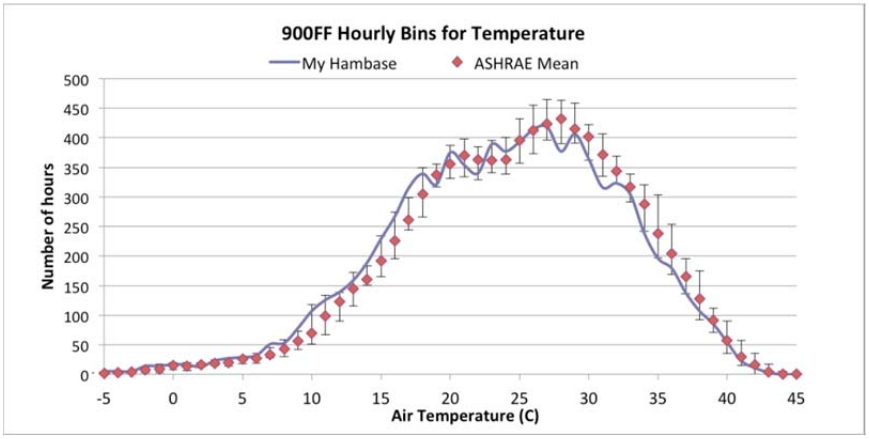

Figure A.24: Histogram of the hourly temperatures for the 900FF case

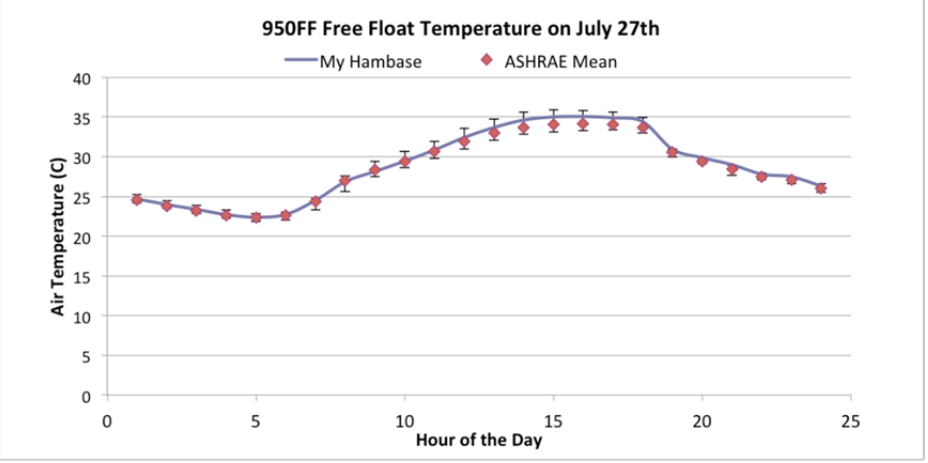

Figure A.25: Hourly temperatures on July 27th for the 950FF case

APPENDIX B: IBL-GHP VALIDATION

Appendix B presents additional validation of the integrated IBL-GHP model with an eQuest model (Section B.1) and with GLHEPRO (Section B.2).

B.1 RESIDENTIAL BUILDING MODEL AND EQUEST VALIDATION

Table B.1: Comparison between Simulink Model and eQuest Residential Building Load Results –Full Internal Load Case

	eQuest	Simulink	Difference	%Diifference
Total Cooling (kBtu)	131801.02	127553.16	-4247.86	-3.2%
Total Heating (kBtu)	0.19	4644.79	4644.61	2508436.3%
Monthly Cooling (kBtu)				
January	5830.78	1247.35	-4583.43	-78.6%
February	5528.83	1840.98	-3687.86	-66.7%
March	8127.50	6332.78	-1794.73	-22.1%
April	10718.38	11052.40	334.02	3.1%
May	12979.23	15129.03	2149.80	16.6%
June	14524.40	18185.60	3661.20	25.2%
July	16225.85	20613.06	4387.21	27.0%
August	16167.55	20295.00	4127.45	25.5%
September	13794.97	15102.13	1307.16	9.5%
October	12423.88	11017.86	-1406.01	-11.3%
November	9194.27	5527.95	-3666.32	-39.9%
December	6285.38	1209.03	-5076.35	-80.8%
Monthly Heating (kBtu)				
January	0.16	2112.91	2112.75	1362073.2%
February	0.00	774.86	774.86	
March	0.00	337.25	337.25	
April	0.00	0.00	0.00	
May	0.00	0.00	0.00	
June	0.00	0.00	0.00	
July	0.00	0.00	0.00	
August	0.00	0.00	0.00	
September	0.00	0.00	0.00	
October	0.00	0.00	0.00	
November	0.00	0.00	0.00	
December	0.03	1419.77	1419.74	4725155.9%

Table B.2: Comparison between Simulink Model and eQuest Residential Building Load Results –No Internal Load

	eQuest	Simulink	Dfference	% Difference
Total Cooling (kBtu)	62892.85	50190.02	-12702.83	-20.2%
Total Heating (kBtu)	761.88	27163.32	26401.43	3465.3%
Monthly Cooling (Btu)				
January	819.57	0.00	-819.57	-100.0%
February	1027.13	27.45	-999.68	-97.3%
March	2566.58	591.12	-1975.46	-77.0%
April	4637.24	2649.84	-1987.41	-42.9%
May	6740.74	5900.19	-840.55	-12.5%
June	8557.49	9395.40	837.91	9.8%
July	10130.18	11531.14	1400.97	13.8%
August	10056.82	11201.90	1145.08	11.4%
September	7782.40	6264.84	-1517.56	-19.5%
October	6119.44	2227.25	-3892.18	-63.6%
November	3302.56	400.87	-2901.69	-87.9%
December	1152.71	0.00	-1152.71	-100.0%
Monthly Heating (Btu)				
January	130.58	8692.30	8561.73	6556.9%
February	193.90	5714.18	5520.	28 2847.0%
March	209.14	2663.09	2453.95	1173.4%
April	0.05	55.71	55.66	116820.2%
May	0.00	0.00	0.00	
June	0.00	0.00	0.00	
July	0.00	0.00	0.00	
August	0.00	0.00	0.00	
September	0.00	0.00	0.00	
October	0.01	51.18	51.17	401615.1%
November	0.07	2159.59	2159.52	2937452.8%
December	228.14	7827.25	7599.12	3330.9%

Table B.3: Comparison between Residential Simulink and eQuest Models Ground Loop Heat Rejection Results—Full Internal Loads

	eQuest			Simulink				
	Q Reject	Q Extract	Net	Q Reject	Q Extract	Net	Difference	Difference
	kBtu	kBtu	kBtu	kBtu	kBtu	kBtu	kBtu	Percent
Total	156151.30	0.08	156151.22	171783.03	3683.07	168099.97	-11948.67	-7.65%
Jan	6842.78	-0.01	6842.79	1562.57	1660.14	-97.57	6940.35	101.43%
Feb	6508.15	0.00	6508.15	2322.34	614.49	1707.85	4800.30	73.76%
Mar	9557.52	0.00	9557.52	8119.07	268.65	7850.42	1707.10	17.86%
Apr	12620.65	0.00	12620.65	14349.17	0.00	14349.17	-1728.52	-13.70%
May	15290.49	0.00	15290.49	19997.24	0.00	19997.24	-4706.75	-30.78%

Jun	17188.25	0.00	17188.25	24636.81	0.00	24636.81	-7448.56	-43.34%
Jul	19249.45	0.00	19249.45	28427.66	0.00	28427.66	-9178.20	-47.68%
Aug	19223.14	0.00	19223.14	28209.49	0.00	28209.49	-8986.35	-46.75%
Sep	16415.56	0.00	16415.56	20592.98	0.00	20592.98	-4177.42	-25.45%
Oct	14817.58	0.00	14817.58	14713.80	0.00	14713.80	103.78	0.70%
Nov	10957.93	0.00	10957.93	7300.80	0.00	7300.80	3657.13	33.37%
Dec	7479.79	0.09	7479.70	1551.10	1139.79	411.32	7068.48	94.50%

Table B.4: Comparison between Residential Simulink and eQuest Models Ground Loop Heat Rejection Results—No Internal Loads

	eQuest			Simulink				
	Q Reject	Q Extract	Net	Q Reject	Q Extract	Net	Difference	Difference
	kBtu	kBtu	kBtu	kBtu	kBtu	kBtu	kBtu	Percent
Total	73844.80	-593.25	74438.05	64778.98	21244.19	43534.79	30310.01	41.05%
Jan	958.20	-99.35	1057.55	0.00	6776.15	-6776.15	7734.35	807.18%
Feb	1203.55	-151.10	1354.65	33.48	4449.03	-4415.55	5619.10	466.88%
Mar	3001.22	-164.04	3165.26	729.07	2074.67	-1345.61	4346.82	144.84%
Apr	5419.85	0.08	5419.77	3340.12	44.45	3295.67	2124.18	39.19%
May	7877.06	0.00	7877.06	7534.96	0.00	7534.96	342.10	4.34%
Jun	10022.90	0.00	10022.90	12106.72	0.00	12106.72	-2083.82	-20.79%
Jul	11888.16	0.00	11888.16	14961.58	0.00	14961.58	-3073.41	-25.85%
Aug	11828.63	0.00	11828.63	14585.83	0.00	14585.83	-2757.20	-23.31%
Sep	9159.76	0.00	9159.76	8117.56	0.00	8117.56	1042.20	11.38%
Oct	7231.61	0.11	7231.50	2865.19	41.33	2823.85	4407.76	60.95%
Nov	3901.88	0.17	3901.70	504.49	1717.26	-1212.78	5114.65	131.08%
Dec	1351.99	-179.11	1531.09	0.00	6141.28	-6141.28	7493.27	554.24%

B.2 RESIDENTIAL HEAT PUMP-GROUND LOOP AND GLHEPRO VALIDATION

Table B.5: Residential Ground Loop Validation Results -Full eQuest Internal Loads

	Heat Rejected			Average HP Entrance Temps			Average GL Entrance Temps		
Time	Glhepro	Simulink	Diff	Glhepro	Simulink	Diff	Glhepro	Simulink	Diff
Month	W/m	W/m	%	°C	°C	%	°C	°C	%
1	0.019	0.014	27.7%	21.56	20.47	5.0%	21.53	20.46	5.0%
2	-0.176	-0.182	-3.3%	22.75	23.39	-2.8%	22.97	23.63	-2.9%
3	-0.745	-0.759	-1.9%	26.37	28.04	-6.4%	27.29	29.03	-6.3%
4	-1.427	-1.456	-2.0%	30.97	31.64	-2.1%	32.75	33.49	-2.3%
5	-1.935	-1.986	-2.7%	34.77	34.58	0.6%	37.18	37.08	0.3%
6	-2.467	-2.543	-3.1%	38.84	38.44	1.0%	41.92	41.64	0.7%

7	-2.758	-2.839	-3.0%	41.53	41.11	1.0%	44.97	44.68	0.7%
8	-2.728	-2.819	-3.3%	42.23	42.15	0.2%	45.62	45.69	-0.2%
9	-2.047	-2.118	-3.5%	38.71	39.19	-1.2%	41.26	41.86	-1.5%
10	-1.410	-1.442	-2.2%	34.98	36.33	-3.8%	36.74	38.17	-3.9%
11	-0.712	-0.723	-1.5%	30.57	34.90	-14.2%	31.46	35.85	-14.0%
12	-0.033	-0.038	-15.6%	25.99	27.08	-4.2%	26.03	27.13	-4.2%

Table B.6: Residential Ground Loop Validation Results - No Internal Loads

	Heat Rejected			Average HP Entrance Temps			Average GL Entrance Temps		
Time	Glhepro	Simulink	Diff	Glhepro	Simulink	Diff	Glhepro	Simulink	Diff
Month	W/m	W/m	%	°C	°C	%	°C	°C	%
1	0.681	0.669	1.8%	17.47	16.52	5.4%	16.62	15.68	5.7%
2	0.493	0.475	3.6%	18.24	16.62	8.9%	17.63	16.01	9.2%
3	0.140	0.136	3.4%	20.26	19.37	4.4%	20.09	19.20	4.4%
4	-0.324	-0.311	4.2%	23.18	25.48	-9.9%	23.59	25.91	-9.8%
5	-0.717	-0.713	0.7%	25.91	28.62	-10.5%	26.80	29.56	-10.3%
6	-1.202	-1.212	-0.8%	29.31	30.41	-3.8%	30.81	31.97	-3.8%
7	-1.445	-1.469	-1.7%	31.38	31.86	-1.5%	33.18	33.73	-1.7%
8	-1.406	-1.429	-1.7%	31.71	32.51	-2.5%	33.46	34.33	-2.6%
9	-0.798	-0.796	0.2%	28.38	31.34	-10.5%	29.37	32.39	-10.3%
10	-0.265	-0.261	1.6%	25.09	29.71	-18.4%	25.42	30.07	-18.3%
11	0.129	0.118	7.9%	22.41	24.30	-8.4%	22.25	24.15	-8.5%
12	0.616	0.598	3.0%	19.04	17.99	5.6%	18.27	17.22	5.7%

APPENDIX C: RESIDENTIAL SENSITIVITY STUDY DATA

Appendix C presents the data presented in the sensitivity study (Section 4.8) of the residential base case model.

Borehole Length Sensitivity

Table C.1: Maximum Yearly Heat Pump EWT in ^{o}C, Based on Hourly Averages, Basis for Figure 4.28

Year	80%	90%	95%	100%	105%	110%	120%
1	48.84	47.57	46.15	44.51	43.17	41.95	39.84
2	49.16	48.53	47.93	46.25	44.91	43.54	41.28
3	49.26	48.70	48.48	47.31	45.88	44.57	42.08
4	49.21	48.83	48.68	47.95	46.54	45.04	42.71
5	49.55	48.91	48.66	48.28	47.09	45.51	43.12
6	49.50	49.11	48.62	48.32	47.39	45.95	43.42
7	49.46	49.09	48.78	48.50	47.74	46.22	43.68
8	49.44	49.02	48.77	48.49	47.97	46.43	43.91
9	49.50	49.11	48.82	48.61	48.12	46.60	44.12
10	49.47	49.04	48.89	48.62	48.25	46.82	44.36
11	49.70	49.21	48.92	48.55	48.35	47.07	44.41
12	49.47	49.05	49.06	48.55	48.36	47.24	44.59
13	49.55	49.24	48.94	48.53	48.45	47.41	44.72
14	49.72	49.31	49.07	48.62	48.43	47.44	44.82
15	49.51	49.13	49.01	48.62	48.47	47.54	44.95

Table C.2: Total Annual Cooling in MWh for Borehole Lengths Tested over 15 years, Basis for Figure 4.29

Year	80%	90%	95%	100%	105%	110%	120%
1	258.0	259.3	259.5	259.4	259.3	259.5	259.5
2	253.8	259.2	259.4	259.2	259.4	259.5	259.5
3	250.2	258.4	259.2	259.4	259.5	259.5	259.2
4	247.6	257.6	259.1	259.4	259.3	259.4	259.4
5	246.4	256.9	258.8	259.5	259.5	259.4	259.6
6	244.6	255.8	258.4	259.4	259.3	259.4	259.4
7	243.0	255.1	258.2	259.2	259.3	259.4	259.3
8	241.7	254.2	257.6	259.1	259.3	259.3	259.5
9	240.8	253.6	257.4	259.0	259.3	259.4	259.4
10	240.0	252.8	257.1	258.9	259.3	259.3	259.3
11	238.9	252.1	256.7	258.7	259.3	259.3	259.4
12	238.3	251.6	256.3	258.7	259.1	259.3	259.3
13	237.9	251.3	256.1	258.7	259.5	259.6	259.7
14	237.3	250.7	255.6	258.4	259.1	259.4	259.4
15	236.7	250.2	255.3	258.2	259.1	259.2	259.4

Table C.3: Total Annual Electricity Use in kWh for the Bore Lengths Tested, Basis for Figure 4.30

Year	80%	90%	95%	100%	105%	110%	120%
1	10225	9609	9331	9068	8858	8658	8325
2	10368	10001	9695	9388	9168	8927	8547
3	10316	10202	9938	9622	9382	9121	8707
4	10288	10310	10090	9775	9514	9254	8834
5	10280	10374	10175	9890	9632	9360	8929
6	10243	10391	10247	9981	9707	9433	8990
7	10205	10406	10306	10054	9782	9505	9045
8	10159	10403	10330	10105	9843	9557	9110
9	10138	10404	10363	10150	9898	9614	9150
10	10115	10398	10380	10183	9938	9652	9182
11	10089	10385	10398	10220	9991	9698	9217
12	10046	10366	10414	10251	10008	9727	9244
13	10040	10364	10414	10280	10065	9763	9283
14	10019	10340	10423	10298	10078	9789	9302
15	10001	10333	10418	10317	10106	9809	9325

Borehole Configuration and Spacing Sensitivity

Table C.4: Total Annual Cooling in MWh for the Borehole Configurations Tested over 15 years, Basis for Figure 4.32

Year	1x4x10	1x4x15	1x4x20	1x4x25	2x2x10	2x2x15	2x2x20	2x2x25
1	259.4	259.4	259.4	259.3	259.2	259.4	259.5	259.4
2	259.4	259.2	259.3	259.3	259.1	259.4	259.3	259.5
3	259.2	259.4	259.4	259.4	258.0	259.3	259.4	259.3
4	258.7	259.4	259.3	259.3	256.6	259.1	259.4	259.2
5	258.4	259.5	259.4	259.4	255.5	259.1	259.5	259.5
6	258.1	259.4	259.4	259.3	254.2	258.7	259.3	259.2
7	257.4	259.2	259.2	259.3	253.2	258.3	259.2	259.2
8	256.9	259.1	259.3	259.3	252.2	258.1	259.1	259.2
9	256.4	259.0	259.2	259.2	251.5	257.9	259.1	259.4
10	255.7	258.9	259.3	259.4	250.8	257.4	259.0	259.3
11	255.4	258.7	259.4	259.3	250.0	257.2	258.8	259.3
12	254.8	258.7	259.1	259.3	249.3	256.8	258.9	259.1
13	254.8	258.7	259.5	259.5	248.8	256.7	259.0	259.5
14	254.0	258.4	259.1	259.4	248.0	256.1	258.5	259.1
15	253.7	258.2	259.4	259.4	248.2	255.8	258.5	259.1

Table C.5: Total Annual Electricity Use in kWh for the Borehole Configurations Tested, Basis for Figure 4.33

Year	1x4x10	1x4x15	1x4x20	1x4x25	2x2x10	2x2x15	2x2x20	2x2x25
1	9293	9068	8962	8909	9478	9159	8992	8911
2	9712	9388	9217	9122	9975	9570	9321	9198
3	9964	9622	9418	9293	10186	9832	9573	9406
4	10119	9775	9551	9413	10248	9998	9746	9556
5	10199	9890	9661	9510	10272	10116	9862	9680
6	10276	9981	9736	9586	10278	10197	9951	9756
7	10300	10054	9801	9644	10273	10252	10027	9838
8	10325	10105	9862	9703	10123	10293	10093	9905
9	10341	10150	9914	9743	10081	10328	10141	9965
10	10337	10183	9964	9801	10051	10342	10189	10006
11	10356	10220	10008	9838	9990	10364	10216	10056
12	10337	10251	10031	9873	9965	10381	10257	10087
13	10357	10280	10072	9904	9957	10387	10290	10135
14	10341	10298	10103	9942	9944	10394	10305	10152
15	10339	10317	10139	9957	9956	10389	10331	10178

Table C.6: Total Annual Time in Hours that Zone 1 Air Temperature is Above Cooling Setpoint for the Borehole Configurations Tested, Basis for Figure 4.34

Year	1x4x10	1x4x15	1x4x20	1x4x25	2x2x10	2x2x15	2x2x20	2x2x25
1	0	0	0	0	0	0	0	0
2	0	0	0	0	53	0	0	0
3	27	0	0	0	185	1	0	0
4	72	0	0	0	346	23	0	0
5	135	2	0	0	466	50	0	0
6	212	10	0	0	601	77	4	0
7	268	27	0	0	714	129	15	0
8	335	37	0	0	798	177	27	0
9	380	48	2	0	925	220	37	2
10	428	63	4	0	1004	259	51	7
11	473	76	11	0	1055	290	69	14
12	525	103	20	0	1115	334	89	20
13	567	129	25	1	1121	353	101	28
14	613	154	29	1	1168	393	120	34
15	649	167	33	2	1263	424	140	44

Grout Conductivity Sensitivity

Table C.7: Mean Yearly Heat Pump EWT in ^{o}C, Based on Hourly Averages, Basis for Figure 4.35

Year	0.500	0.744	1.000	1.333	1.500
1	31.37	30.38	29.81	29.45	29.32
2	33.31	32.26	31.69	31.30	31.19
3	34.23	33.21	32.64	32.19	32.09
4	34.87	33.80	33.21	32.81	32.68
5	35.36	34.28	33.69	33.29	33.13
6	35.61	34.62	34.08	33.60	33.46
7	35.87	34.96	34.35	33.88	33.79
8	36.13	35.17	34.58	34.13	33.96
9	36.27	35.36	34.77	34.31	34.19
10	36.40	35.52	34.95	34.53	34.43
11	36.55	35.69	35.17	34.72	34.61
12	36.68	35.84	35.31	34.91	34.73
13	36.87	36.07	35.53	35.10	34.95
14	36.87	36.10	35.59	35.19	35.04
15	37.01	36.26	35.71	35.28	35.14

Table C.8: Maximum Yearly Heat Pump EWT in ^{o}C, Based on Hourly Averages, Basis for Figure 4.36

Year	0.500	0.744	1.000	1.333	1.500
1	47.55	44.51	42.86	41.70	41.30
2	48.63	46.25	44.62	43.44	42.97
3	48.62	47.31	45.55	44.40	43.94
4	48.86	47.95	46.36	45.04	44.60
5	48.85	48.28	46.74	45.52	45.10
6	48.91	48.32	47.13	45.89	45.46
7	48.94	48.50	47.44	46.25	45.78
8	48.92	48.49	47.78	46.49	46.08
9	48.97	48.61	47.95	46.77	46.27
10	49.04	48.62	48.05	46.97	46.47
11	48.96	48.55	48.25	47.11	46.69
12	49.19	48.55	48.29	47.35	46.85
13	48.99	48.53	48.31	47.56	46.99
14	48.96	48.62	48.51	47.57	47.17
15	49.10	48.62	48.38	47.74	47.24

Table C.9: Total Annual Cooling in MWh for the Grout Conductivities Tested over 15 years, Basis for Figure 4.37

Year	0.500	0.744	1.000	1.333	1.500
1	259.3	259.4	259.4	259.5	259.5
2	259.1	259.2	259.3	259.5	259.4
3	258.9	259.4	259.3	259.4	259.2
4	258.2	259.4	259.4	259.3	259.4
5	257.7	259.5	259.4	259.4	259.4
6	257.0	259.4	259.2	259.3	259.3
7	256.5	259.2	259.3	259.3	259.3
8	256.0	259.1	259.3	259.3	259.3
9	255.0	258.9	259.3	259.4	259.2
11	254.3	258.7	259.3	259.4	259.4
12	253.9	258.7	259.2	259.2	259.4
13	253.8	258.7	259.6	259.6	259.7
14	253.0	258.4	259.2	259.3	259.4
15	252.6	258.2	259.1	259.3	259.2

Table C.10: Total Annual Electricity Use in kWh for the Grout Conductivities Tested, Basis for Figure 4.38

Year	0.500	0.744	1.000	1.333	1.500
1	9571	9068	8810	8636	8576
2	9910	9388	9117	8928	8866
3	10125	9622	9340	9136	9072
4	10233	9775	9484	9283	9221
5	10310	9890	9598	9391	9317
6	10349	9981	9687	9475	9395
7	10379	10054	9760	9545	9476
8	10406	10105	9823	9604	9534
9	10404	10150	9879	9654	9588
10	10415	10183	9925	9708	9630
11	10410	10220	9966	9753	9676
12	10411	10251	10004	9786	9711
13	10416	10280	10050	9825	9755
14	10398	10298	10072	9852	9783
15	10402	10317	10090	9884	9806

Ground Temperature Sensitivity

Table C.11: Mean Yearly Heat Pump EWT in ^{o}C, Based on Hourly Averages, Basis for Figure 4.39

Year	17.3	18.8	20.3	21.8	23.3	24.8	25.3
1	25.91	27.44	28.98	30.45	32.01	33.58	35.13
2	27.77	29.30	30.86	32.37	33.95	35.54	37.12
3	28.65	30.18	31.77	33.32	34.88	36.47	38.33
4	29.27	30.81	32.36	33.94	35.53	37.09	39.12
5	29.71	31.29	32.88	34.43	36.02	37.58	39.60
6	30.03	31.58	33.18	34.74	36.39	37.86	39.89
7	30.29	31.87	33.45	35.05	36.65	38.37	40.14
8	30.55	32.12	33.68	35.35	36.89	38.79	41.74
9	30.73	32.33	33.90	35.51	37.09	39.12	42.05
10	30.92	32.49	34.08	35.71	37.29	39.34	42.24
11	31.09	32.65	34.23	35.88	37.42	39.50	42.41
12	31.25	32.78	34.37	36.00	37.57	39.64	42.51
13	31.42	33.00	34.57	36.19	37.74	39.76	42.64
14	31.49	33.10	34.67	36.24	37.80	39.82	42.71
15	31.59	33.17	34.80	36.40	37.87	39.90	42.79

Table C.12: Maximum Yearly Heat Pump EWT in ^{o}C, Based on Hourly Averages, Basis for Figure 4.40

Year	17.3	18.8	20.3	21.8	23.3	24.8	25.3
1	39.33	41.05	42.85	44.64	46.41 4	8.11	48.56
2	41.00	42.84	44.59	46.48	48.07	48.60	49.07
3	41.95	43.79	45.61	47.41	48.56	48.79	49.04
4	42.65	44.47	46.21	47.98	48.61	48.95	49.28
5	43.04	44.93	46.74	48.33	48.64	49.08	49.24
6	43.46	45.36	47.12	48.55	48.65	49.01	49.27
7	43.85	45.68	47.43	48.48	48.71	49.00	49.39
8	44.08	45.90	47.79	48.64	49.29	49.08	49.60
9	44.37	46.09	48.08	48.52	48.92	49.22	49.66
10	44.59	46.39	48.13	48.61	48.96	49.33	49.66
11	44.72	46.61	48.20	48.58	48.98	49.13	49.71
12	44.87	46.77	48.29	48.65	49.04	49.14	49.65
13	44.99	46.88	48.41	48.78	49.03	49.24	49.64
14	45.07	46.90	48.57	48.72	49.04	49.28	49.64
15	45.29	47.04	48.43	48.68	49.02	49.31	49.90

Table C.13: Total Annual Cooling in MWh for the Ground Temperatures Tested over 15 years, Basis for Figure 4.41

Year	17.3	18.8	20.3	21.8	23.3	24.8	25.3
1	259.6	259.5	259.5	259.3	259.4	259.2	258.8
2	259.6	259.5	259.5	259.4	259.2	258.8	256.3
3	259.4	259.4	259.3	259.3	259.2	257.7	253.4
4	259.5	259.3	259.3	259.3	258.9	256.3	250.2
5	259.5	259.6	259.4	259.3	258.5	255.3	248.5
6	259.3	259.4	259.2	259.2	258.0	254.0	247.2
7	259.5	259.4	259.3	259.1	257.5	252.9	245.9
8	259.3	259.4	259.4	259.1	257.0	251.6	243.6
9	259.4	259.4	259.3	259.0	256.6	250.5	242.0
10	259.4	259.4	259.2	258.9	256.1	249.6	240.4
11	259.5	259.4	259.2	258.9	255.7	248.9	239.0
12	259.4	259.3	259.3	258.5	255.2	248.3	238.1
13	259.7	259.7	259.7	258.6	255.2	247.7	237.7
14	259.3	259.4	259.2	258.0	254.4	247.0	236.5
15	259.4	259.5	259.2	257.9	254.1	246.9	235.7

Table C.14: Total Annual Time in Hours that Zone 1 Air Temperature is Above Cooling Setpoint for the Ground Temperatures Tested, Basis for Figure 4.42

Year	17.3	18.8	20.3	21.8	23.3	24.8	25.3
1	0	0	0	0	0	0	70
2	0	0	0	0	0	70	378
3	0	0	0	0	29	226	702
4	0	0	0	0	71	355	1000
5	0	0	0	5	125	495	1224
6	0	0	0	16	194	622	1362
7	0	0	0	37	252	756	1398
8	0	0	0	49	299	860	1621
9	0	0	0	68	343	981	1795
10	0	0	1	83	401	1110	1814
11	0	0	2	108	442	1184	1766
12	0	0	6	135	497	1229	1825
13	0	0	6	154	550	1246	1861
14	0	0	13	176	587	1273	1896
15	0	0	20	192	625	1363	1935

Table C.15: Average Annual Energy Efficiency Ratio (EER) in Btu/Wh for the Ground Temperatures Tested, Basis for Figure 4.43

Year	17.3	18.8	20.3	21.8	23.3	24.8	25.3
1	10.96	10.46	9.98	9.53	9.08	8.67	8.28
2	10.42	9.94	9.48	9.03	8.62	8.23	7.92
3	10.16	9.68	9.21	8.79	8.39	8.04	7.78
4	9.97	9.50	9.05	8.63	8.24	7.92	7.72
5	9.84	9.38	8.93	8.52	8.14	7.84	7.67
6	9.74	9.28	8.84	8.43	8.06	7.79	7.64
7	9.66	9.20	8.76	8.36	8.01	7.77	7.60
8	9.59	9.13	8.70	8.29	7.96	7.73	7.53
9	9.53	9.06	8.65	8.25	7.92	7.71	7.52
10	9.47	9.02	8.60	8.20	7.88	7.70	7.50
11	9.42	8.98	8.55	8.16	7.86	7.69	7.49
12	9.38	8.94	8.52	8.13	7.84	7.67	7.49
13	9.34	8.90	8.48	8.11	7.83	7.65	7.48
14	9.31	8.86	8.45	8.08	7.81	7.64	7.47
15	9.28	8.84	8.41	8.05	7.79	7.63	7.47

Table C.16: Total Annual Electricity Use in kWh for the Ground Temperatures Tested, Basis for Figure 4.44

Year	17.3	18.8	20.3	21.8	23.3	24.8	25.3
1	8106	8415	8744	9088	9469	9855	10222
2	8353	8685	9051	9428	9815	10192	10389
3	8528	8883	9263	9654	10047	10340	10202
4	8661	9024	9403	9808	10189	10393	10023
5	8754	9129	9515	9915	10269	10407	9995
6	8831	9208	9600	10006	10331	10405	9981
7	8902	9279	9679	10074	10364	10203	9973
8	8953	9337	9733	10144	10377	10100	9431
9	9001	9395	9788	10182	10402	10042	9375
10	9045	9434	9835	10227	10418	10009	9335
11	9088	9473	9878	10262	10424	9994	9302
12	9120	9507	9915	10285	10423	9991	9269
13	9161	9555	9966	10302	10418	9982	9263
14	9174	9578	9986	10312	10406	9968	9231
15	9211	9606	10018	10334	10408	9974	9201

APPENDIX D: OTHER SHR DEVICES/SYSTEMS

D.1 THERMOSYPHONS

Thermosyphons are vertical, two-phase heat pipes that absorb heat from an external source and vaporizes a working fluid at one end of the pipe, moves the working fluid via natural convection to the other end of the pipe, where heat is rejected by convection to an external sink medium, and the working fluid condenses back to the bottom of the pipe. The working fluid is typically a refrigerant (usually ammonia or carbon-dioxide). The pipe is either pressurized or depressurized to keep the refrigerant at its saturated state, and hence constantly evaporating and condensing. There are three parts to a thermosyphon: 1) evaporator, the lowest part of the thermosyphon in contact with the heat source, 2) adaiabtic region, the middle part, and 3) condenser, which is the top part of the thermosyphon.

Thermosyphons rely on the temperature difference between the source temperature and atmospheric sink temperature. Heat absorbed in the evaporator from the external source evaporates the refrigerant. Once it evaporates, the refrigerant's density is decreased and the it rises due to natural convection. Heat transfer occurs throughout the length of the evaporator. The adiabatic section is at the middle of the thermosyphon and no heat transfer is assumed to occur across this section. As the gaseous refrigerant moves upward, it comes in contact with the condenser wall, whose outer wall is at atmospheric temperature asssuming the thermosyphon top is outdoors. The cylindrical fins around the condenser section remove heat by forced convection with the blowing wind. The gaseous refrigerant then condenses into liquid. This condensate attaches itself to the wall and due to its higher density, it slowly flows downward back to the pool of refrigerant in the evaporator.

Thermosyphons are widely used in Alaska and Tibet to keep the soil (permafrost) below freezing temperatures during the winter so that during warmer periods, the soil will remain frozen and still support structures, such as oil pipelines, antennas, and railroad rails. To maintain the structural stability, thermosyphons are installed along the entire length of the structure; see Figure D.1.

Figure D.1: Thermosyphons installed next to the trans-Alaska Pipeline [Wikipedia, 2011]

Thermosyphons can be used in warmer climates. A technology called Frozen Barrier Technology [Yarmark & Phillips, 1999] was tested by DoE to use themosyphons to freeze the ground and create a solid enclosed barrier under the soil to contain radioactive materials. A series of fifty, 30 ft (9.14 m) long thermopiles were installed and to freeze the ground, however, due to the warm ambient climate, refrigeration systems were deployed to remove heat from the condenser sections. Two separate refrigeration units were used to each drive 25 thermopiles and consumed a total of 288kWh (982.7 Btu) per day. A 3.66m (12ft) thick frozen soil was ultimately established. This section of the reports attempts to analyze the use thermosyphons to extract heat from the superheat portion of the vapor compression cycle, and recognizing the high ambient temperatures, both passive and active operations were investigated to determine the feasibility of using such devices.

The design criteria for selecting a thermosyphon depends on the following variables: quantity of heat to be transferred, the temperatures of the source and sink, temperature difference between the evaporator and the condenser and the wind speed in the region. The thermosyphon must be designed to operate at a pressure such that the refrigerant vaporizes for the amount of heat transferred from the heat source. Forced convection is the main mode of removing heat from the condenser, hence fins are attached around the condenser to maximize the heat transfer. Further, the length of the thermosyphon is important to allow the cycle to operate properly.

D.1.1 Objective

The objective of using themosyphons as a SHR device is to extract heat from the superheat region of the refrigerant loop at the discharge of the compressor. By coiling the refrigerant loop around the evaporator of the thermosyphon or passing the refrigerant loop though a high conducting liquid in contact with the evaporator, heat can be transferred from the refrigerant to the working fluid inside the thermosyphon. Depending on the ambient air and wind conditions, this heat can be rejected from the condenser by either passive or active mode (natural or forced convection). As computed in Section 5 on cooling towers, a 5kW SHR capacity is needed for a residential building with a 4-ton cooling load. Hence, our goal is to design a thermosyphon that can extract up to 5kW of power from the refrigerant loop.

D.1.2 Literature Review: Experiments by Shiraishi et al.

Shiraishi et al. performed an experiment to investigate the heat transfer characteristics of a two-phase thermosyphon to remove exhaust heat (temperatures < 60℃/140℉), which is very common in industrial processes [Shiraishi et al., 1981]. The experiment was performed to investigate the temperature variation of the working fluid inside the thermosyphon, the wall, and the effect of filling ratio on the temperature profiles. Results of these experiments were used to verify a mathematical model they also developed.

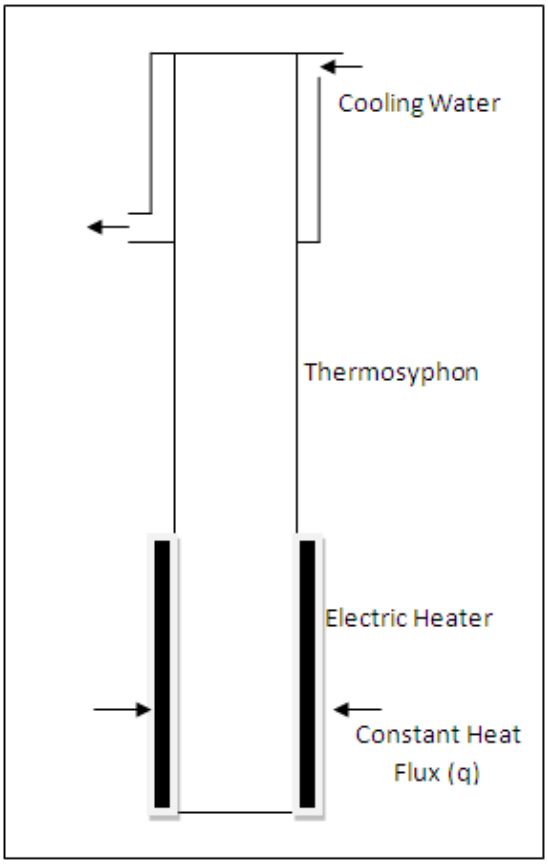

Figure D.2: Experimental setup

The thermosyphon used in the experiment Figure D.2 was made of copper tubing of inner diameter 37mm (1.41in) and outer diameter 45mm (1.77in) and a total length of 1230mm (48.43in). Of this length, the evaporator, adiabatic, and condenser sections were L_e=280mm (11 in), L_a=500mm (19.7in), and L_c=450mm (17.7in) long, respectively. An electric resistance heater, insulated with magnesia to fit in special grooves outside the evaporator, provided a constant heat flux condition to replicate an industrial process, where the exhaust gases provide a constant heat flux. The heat sink (condenser) was fitted with circulating water to condense the refrigerant inside the thermosyphon. The working fluid inside the thermosyphon was water, which has a vapor state at 45℃ and at a pressure of 9.6 kPa.

The amount of working fluid inside the thermosyphon was varied to determine its effect on performance. A quantity called the filling ratio (F), defined as the ratio of the volume of the working fluid to that of the evaporator volume, is given by:

$$F = \frac{\Pi r^2 L_p}{\Pi r^2 L_e} = \frac{L_p}{L_e} \qquad \text{(D.1)}$$

where L_p is the height of water pool in the thermosyphon, L_e is the height of the evaporator and *r* radius of the thermosyphon.

This quantity is introduced for the following reason. The heat exchange process taking place in the portion filled with water ($0 \leq x \leq L_p$) is due to boiling, and for the region above the working fluid ($L_e \leq x \leq L_p$) evaporation takes place in the liquid film of the condensate above the pool of water. The filling ratio indicates the ratio of the amount of heat transferred due to boiling to the amount of heat transferred by evaporation of the fluid.

Heat Transfer Coefficients

Heat transfer in the Condenser

The working fluid (water) is assumed to be saturated vapor by the time it reaches the condenser, and hence the fluid is in single phase. Then heat transfer is purely to condense the water vapor. The condensate which flows back down along the pipe is assumed to be in laminar flow with respect to the radius of the thermosyphon. Using Nusselt's film condensation theory for a flat plate [Incropera and Dewit, 1985], the condensation heat transfer coefficient h_c is given by

$$h_c \frac{(\nu^2/g)^{1/3}}{k} = (4/3)^{1/3} Re_c^{-1/3} \tag{D.2}$$

$$Re_c = \frac{4 q_c L_c}{\lambda \mu} \tag{D.3}$$

where ν is the kinematic viscosity of water, g is the acceleration due to gravity, k is the thermal conductivity of water, λ is latent heat of vaporization, μ is the dynamic viscosity of water (all in SI units).

Heat transfer in the liquid pool of the Evaporator

The heat transfer in the evaporator liquid pool is described as pool boiling. It is different from nucleate boiling since it takes place in closed system where the formation of vapor bubbles has a greater effect on the heat transfer. The empirically-formulated pool boiling heat transfer coefficient h_p is given by Shiraishi et al. (1981):

$$h_p = 0.32 \frac{\rho^{0.65} k^{0.3} C_p^{0.7} g^{0.2}}{\rho_v^{0.25} \lambda^{0.4} \mu^{0.1}} \left(\frac{P}{P_a}\right)^{0.23} q_e^{0.4} \tag{D.4}$$

where ρ is the density of liquid water, ρ_v is the density of water vapor, P is the pressure inside the thermosyphon fluid pool, $P_a$is the atmospheric pressure, C_p is the heat capacity at constant pressure, ν is the kinematic viscosity of water, g is the acceleration due to gravity, k is the thermal conductivity of water, λ is latent heat of vaporization, μ is the dynamic viscosity of water (all in SI units).

Heat Transfer in the liquid film of the Evaporator

The heat transfer process of the falling liquid film is complex and depends on the magnitude of the heat flux applied at the evaporator. At a low evaporative heat flux a continuous liquid film is observed, a phenomena that is well described by Nusselt's condensation theory (Incropera and Dewitt). At a high evaporative heat flux, the film breaks down into droplets which start boiling and leads to a two phase fluid formed on the wall of the condenser. For the latter case, an empirical formulation for the heat transfer coefficient is:

$$h_f \frac{(\nu^2/g)^{1/3}}{k} = (4/3)^{1/3} Re_f^{-1/3} \quad \text{(D.5)}$$

$$Re_f = \frac{4q_e x}{\lambda \mu} \quad \text{(D.6)}$$

$$x = L_p + (\frac{1}{2})L_f \quad \text{(D.7)}$$

where x is the distance measured from the bottom of the thermosyphon, L_f is the distance from the top of the pool level to the top of the evaporator section, $q_e$is the heat flux at the evaporator and all fluid properties are that of saturated water at 45°C/113°F)

D.1.3 Implementation of Shiraishi's Model

The following assumptions are made:

- The axial conduction along the length of the tube is negligible
- Constant heat flux is supplied uniformly to the evaporator
- Steady state operation is assumed and all the heat added to the evaporator is taken away from the condenser section.
- The liquid pool level in the evaporator is assumed to be constant, implying that the rate of evaporation is equal to the rate of condensation.
- The saturation pressure - temperature relationship is used in the liquid pool and the vapor just above the pool. It is expressed as:

$$T = f_s(P) \quad \text{(D.8)}$$

The primary variables affecting the experiment are the heat flux and the vapor temperature inside the thermosyphon. Although the vapor is at its saturated pressure, the pressure varies along the height of the pool. The pressure at any point at a distance x from the bottom is given by:

$$P(x) = P_v + \rho g(L_p - x) \tag{D.9}$$

Once pressure is known, the temperatures can be determined by the saturation temperature – pressure relation.

$$T_i(x) = f_s\big(P(x)\big) \quad , \quad 0 \leq x \leq L_p \tag{D.10}$$

$$T_i(x) = f_s(P_v) \quad , \quad L_p \leq x \tag{D.11}$$

Since all heat added to the evaporator is taken away at the condenser (e.g. steady-state assumption), the heat flux at the condenser is calculated by:

$$q_c = q_e * (\frac{L_e}{L_c}) \tag{D.12}$$

The heat transfer coefficients for different regions of the thermosyphon are calculated using equations (D.2), (D.4) and (D.5). Using the computed coefficients, the temperature profiles of the inner wall $T_w(x)$ are calculated using the following relations:

$$T_w(x) = T_i(x) + \frac{q_e}{h_p} \quad , \quad 0 \leq x \leq L_p \tag{D.13}$$

$$T_w(x) = T_i(x) + \frac{q_e}{h_f} \quad , \quad L_p \leq x \leq L_e \tag{D.14}$$

$$T_w(x) = T_i(x) \, , \; L_e \leq x \leq L_e + L_a \tag{D.15}$$

$$T_w(x) = T_i(x) - \frac{q_c}{h_c} \quad , \quad L_e + L_a < x \tag{D.16}$$

Knowing the thickness of the wall and conduction across it, the outer wall temperatures are also calculated.

D.1.4 Model Validation

Shiraishi's model was implemented and validated with experimental data. It was run for two cases of filling ratios: 1 (entire evaporator section filled with water) and 0.5. In both cases, a vapor temperature of the working fluid (water) of 45℃/113℉ (9.6kPa/0.145psi) was used to mimic the experimental conditions. A heat flux of $3.4*10^4 W/m^2$ was applied along the entire length of the evaporator and the wall and working fluid temperature profiles along the length of the thermosyphon were calculated. In the following figures, the y axis represents distance along the 1.23m (4 ft) length, with the evaporator, adiabatic, and condenser sections represented by 0 - 0.28m (0 - 0.92ft), 0.28m - 0.78m (0.92 - 2.56ft) and 0.78m - 1.23m (2.56 – 4ft), respectively.

Figure D.3 shows the temperatures for a filling ratio F= 1. The red line shows the temperature profile of the working fluid inside the thermopsyphon; it is in saturated vapor form at 45℃/113℉ in both the adiabatic and the condenser section. Since for a filling ratio of 1 the entire evaporator is filled with water, pressure of water increases with the depth, which in turn leads to a higher temperature down the length of the evaporator; this is shown clearly by the linearly increasing temperature from height 0.28m to 0m (0.92 - 0 ft) (bottom of the evaporator). It can be seen from the figure that the model agrees well with the experiments.

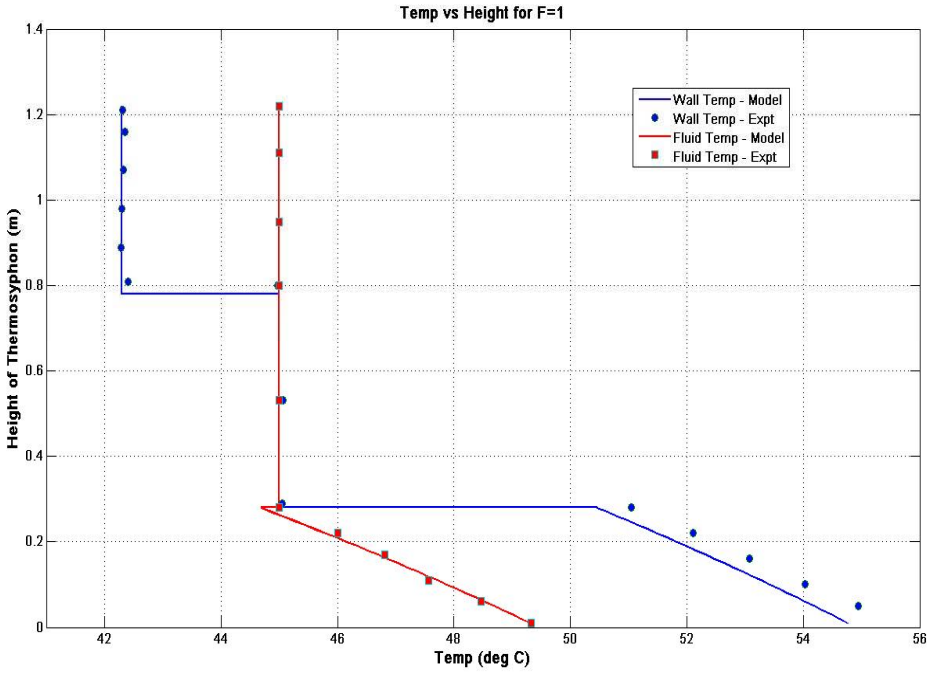

Figure D.3: Temperature profile of working fluid and wall for F =1

The blue line corresponds to the wall temperatures. From the bottom of the thermosyphon to the point where the pool ends, the temperature decreases due to a reduction in saturation pressure. The working fluid above the pool is in saturated vapor state, and hence is at a temperature of 45℃ (9.6 kPa) throughout the rest of the thermosyphon. Since the temperature of the water in the pool decreases with height, the wall temperature also decreases with height to accommodate the heat flux that is supplied. Although, the temperature difference between the pool and wall temperature appear constant from the figure, it is actually not. This is due to the varying value of the heat transfer coefficient in the water pool.

The adiabatic section is assumed to have zero heat transfer, hence the temperature difference between the wall and the working fluid should be zero. The experimental data confirms this assumption. At the condenser section, the heat is transferred from the vapor to the wall, and then to the water outside the thermosyphon. The wall temperature must be lower than the vapor temperature, and experimental data confirms this condition. From the assumptions of steady-state operation and constant heat flux applied at the evaporator section, the heat flux at the condenser was also constant. This led to a uniform wall temperature as can be seen from the experiment too. Figure D.3 shows excellent agreement between the model and experiment.

Figure D.4 shows the results for the case of 0.5 filling ratio. The fluid and wall temperature profile in the pool is similar to that of the previous case.

However, just above the pool and still within the evaporator section (from H=0.14m - 0.28m/ 0.46 – 0.92 ft) the wall temperature increases while the vapor temperature remains constant, even though the heat flux is a constant. The reason for this is the varying heat transfer coefficient just above the pool region.

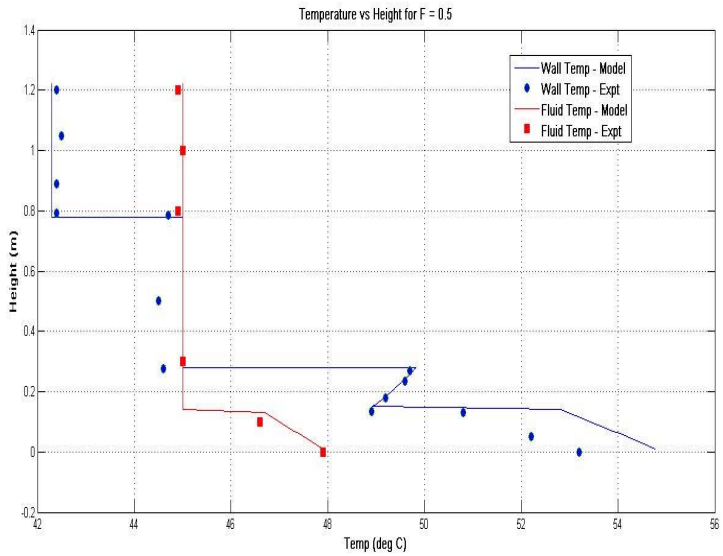

Figure D.4: Temperature profile of working fluid and wall for F =0.5

D.1.5 Model Development for Thermosyphon as SHR System

To use a thermosyphon as a SHR device, the refrigerant loop can either be designed to coil around the evaporator of the thermosyphon or it can be immersed in a liquid which transfers heat uniformly to the evaporator . The subsequent model assumes that the design of the interaction between the refrigerant loop and the thermosyphon is ideal and provides constant heat flux. The refrigerant at the compressor discharge has temperatures in the range of 40–70℃ (104 -158℉) (Refer to Section 5.3 on Desuperheater). The working fluid in the thermosyphon is ammonia and is pressurized to 1468.3 kPa (212 psi), corresponding to a vaporization temperature of 38.8℃/101.8℉. This temperature was chosen low enough to always allow heat transfer between the refrigerant, which is at temperatures greater than 40℃ (104℉), and the ammonia in the thermosyphon. Since the heat is ultimately dissipated into the atmosphere by convection, the ambient temperature must be less than 38.8℃ (101.8℉), and preferably much less than that value for higher heat transfer rates. To improve the effectiveness of convection across the condenser, fins are designed around the condenser (Figure D.5). In summary, the refrigerant from the VCC is assumed to provide an almost constant heat flux to the evaporator and heat is removed at the condenser by either natural or forced convection.

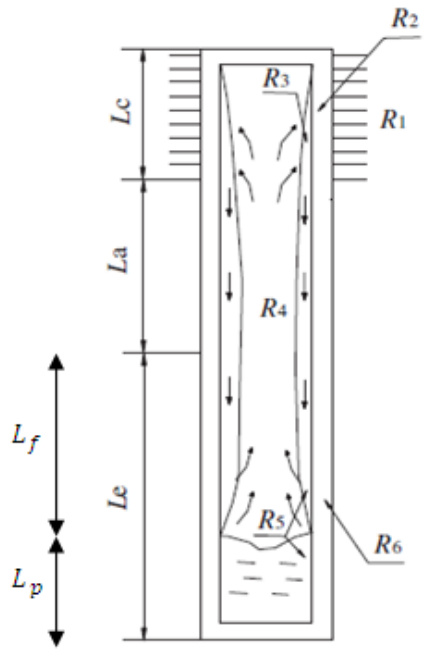

Figure D.5: Schematic of thermosyphon [Zhang et al., 2011]

In Shiraishi et al.'s experiment, a known constant heat flux was supplied at the evaporator, and the heat was removed by external cooling water at the condenser. In our case, the value of heat flux at the evaporator is unknown. Hence, we use the heat transferred at the condenser by convection to determine the heat that must be added at the evaporator. At the condenser, there are three modes of heat transfer: convection across the vapor condensing along the condenser walls, conduction through the wall of the thermosyphon and convection across the fins to the outside air. The heat transfer can be written as:

$$Q = \frac{T_v - T_a}{R_1 + R_2 + R_3} \tag{D.17}$$

where, T_v is the temperature of vapor ammonia at 38.8℃ (101.8℉), $T_a$is the ambient air temperature, $R_3$is the thermal resistance across condensing ammonia vapor, $R_2$is thermal resistance across thermosyphon wall and R_1 is the thermal resistance across condenser fins. The thermal resistances are given by:

$$R_3 = \frac{1}{\pi D_i L_e h_c} \tag{D.18}$$

where $D_i$is the internal diameter of the themosyphon, $L_e$is the length of evaporator and h_c is the heat transfer coefficient given by Eq (4.2).

$$R_2 = \frac{1}{2\pi k_t L_c}\log\left(\frac{D_o}{D_i}\right) \quad \text{(D.19)}$$

where $D_o$is the outer diameter of the thermosyphon, L_c is the length of the condenser, k_t is the thermal conductivity of copper.

$$R_1 = \frac{1}{h_a^e \pi D_o L_c} \quad \text{(D.20)}$$

(D.21)

where $h_a^e = h_a \frac{D_c(L_c - n\delta) + [\,2n(r_2^2 - r_1^2) + 2nr_2\delta\,]\eta}{L_c D_c}$

$$h_a = 0.1378\frac{\lambda_a}{D_c} Re_a^{0.718} Pr_a^{1/3} \left(\frac{S_n}{b_n}\right)^{0.296} \quad \text{(D.22)}$$

$$Re_a = \frac{VD_c}{\nu} \quad \text{(D.23)}$$

where $\boldsymbol{\lambda}$ is the thermal conductivity of air, b_n is the fin height, $s_n$is the fin spacing, $\boldsymbol{\delta}$ is the fin thickness, r_2 is the outer radius of circular fin, r_1 is the inner radius of circular fin, *n* is the number of fins, *Pr* is the Prandtl Number and *η* is the fin efficiency.

The building that was investigated was a 2,100 ft^2 (195 m^2) building located in Austin, Texas. It had a 4 ton unit heat pump installed to provide cooling and heating. The building loads were generated for every two minute time steps to cover the entire year (Jonathan Gaspredes, 2011). From the building load data, it was found that the heat pump was in the cooling mode for 2022 hrs and in the heating mode for 227 hrs of the year. The total time the heat pump was operating during a year was 2,249 hrs. The thermosyphon is operated only when the heat pump is in the cooling mode. Further, since the ammonia vapor inside the thermosyphon is at 38.8℃ (101.84℉), the heat will be rejected from the condenser only if the ambient temperature is less than 38.8℃ (101.84℉). The model is implemented is as follows. For each time step the mode – heating or cooling – of the heat pump is determined. If the heat pump is in the cooling mode, the ambient temperature of air is taken. For ambient temperatures less than 38.8℃ (101.84℉), Equation (D.23) is used to determine the heat removed from the thermosyphon. The heat removed during the heating mode is zero. Once this is done for all the times steps, the heat dissipated is averaged over every hour and results are plotted.

Table D.1 shows two thermosyphons manufactured by Arctic Foundations. The heat that can be removed by these thermosyphons for a temperature difference of 20℃ (between the

vapor and the air) were in the range 1 – 2.5 kW. Hence appropriately-sized units were used in our analysis. Model 170 SF has a larger condenser section (5.2m) and model 70 SF has a smaller condenser section (2.4m/7.9 ft). The evaporator section length for both is 5m (16.4 ft).

Table D.1: Thermosyphon Models by Arctic Foundation Inc [Yarmark, Arctic Foundations]

Model	Diameter D_o (mm/in)	Length (m/ft)	Condenser Length L_c (m/ft)	Price ($)	Weight (lbs/kg)	Capacity $\frac{W}{m^2}$ / $\frac{Btu}{ft^2}$
70 SF	152/6.0	7.4/24.3	2.4/7.9	2,700	310/140.6	1000/292
170 SF	152/6.0	15.2/	5.2/17.0	3,600	625/283.5	2500/730

D.1.6 Passive Condenser Case: Natural Convection

The thermosyphon can be operated in a passive mode, where natural convection of the air dissipates heat at the condenser, or in an active mode, where fans are employed to dissipate heat by forced convection. For the passive case, data for average wind speeds blowing across the terrace of residential buildings in Austin are used for this study, as shown in Table D.2.

Table D.2: Average Wind Speeds in (m/s) / (ft/min) for Different Months [Konopacki & Akbari, 2001]

Jan	Feb	Mar	Apr	May	Jun	Jul	Aug	Sep	Oct	Nov	Dec
1.75/ 344.4	2.88/ 566.8	2.76/ 543.2	3.00/ 590.4	2.80/ 551	2.50/ 491	2.30/ 452.6	1.84/ 362.1	1.94/ 381.8	2.20/ 433	2.23/ 439	3.01/ 592

Figure shows the power dissipated by the thermosyphon condenser (170 SF model) in the passive case for different days of the year. Again, the thermosyphon was switched on whenever the heat pump was in the cooling mode when SHR was necessary. The average power rejected by one thermosyphon is 0.52 kW (1.77 kBtu/h). Hence to achieve at least 5 kW (17.1 kBtu/h) of supplemental power rejection 10 units are needed at a total cost of $ 36,000.

It is interesting to note that more heat is rejected during the summer than during winter, although the ambient temperatures are much lower during the winter. This is due to the fact that the thermosyphon is switched on only during the cooling mode of the heat pump, which happens mostly in summer.

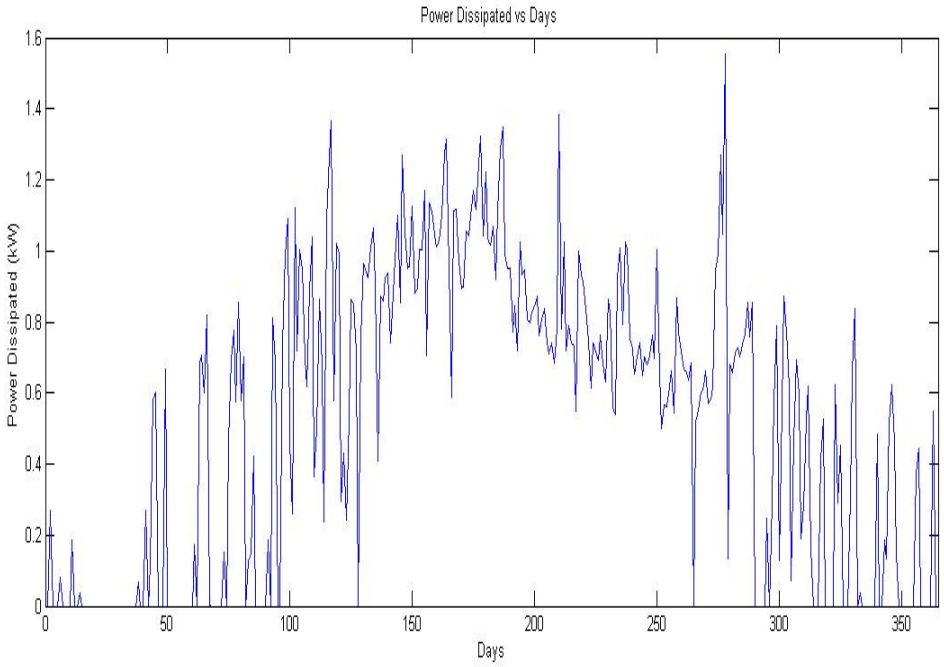

Figure D.7: Power rejected vs days for thermosyphon model 170 SF

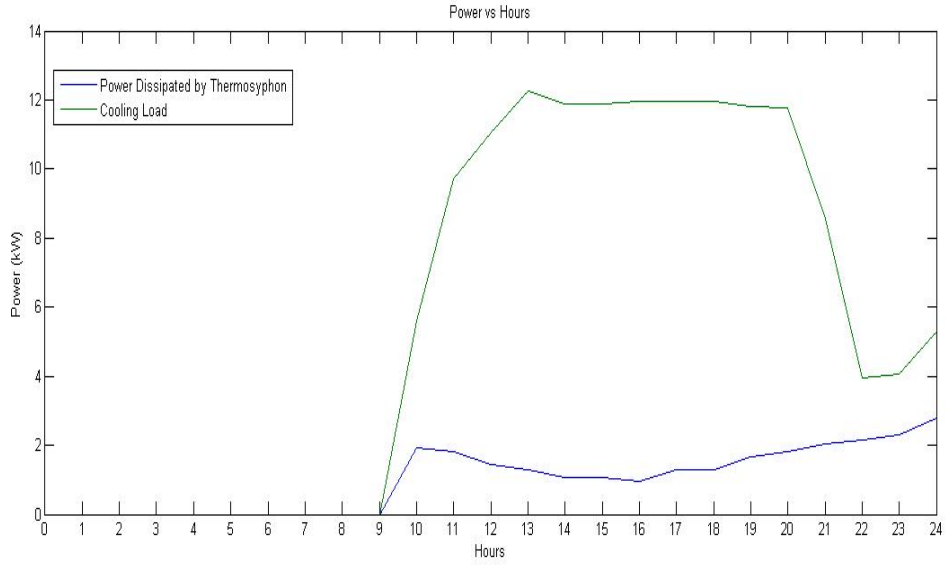

Figure D.8: Power rejected by on July 1 (Model 170 SF)

Figure D.8 shows the power rejected by the thermosyphon for a single summer day (July 1). It also shows the cooling load for that particular day. It can be seen that the thermosyphon

rejects heat only when the heat pump is in the cooling mode. The two profiles don't match each other since other factors like temperature and wind speeds also play a role in the heat rejection.

Figure D.9 shows the power dissipated by the thermosyphon condenser (70 SF model) in the passive case for different days of the year. Again, the thermosyphon was switched on whenever the heat pump was in the cooling mode when SHR was necessary. The average power rejected by one thermosyphon is 0.38 kW (1.3 kBtu/h). Hence to achieve at least 5 kW (17.1 kBtu/h) of supplemental power rejection 13 units are needed at a total cost of $ 33,800 (13* $ 2,600).

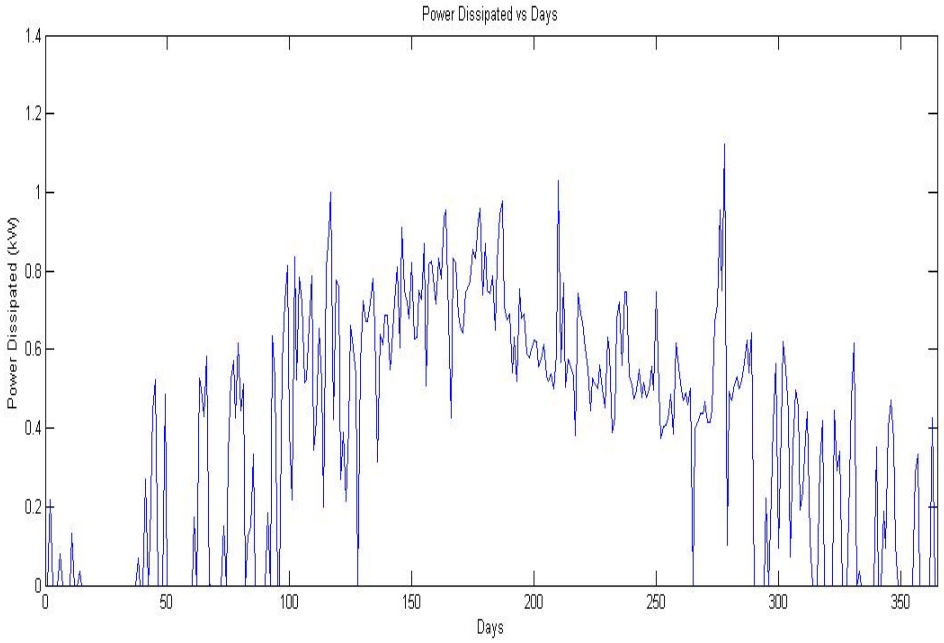

Figure D.9: Power rejected vs days for thermosyphon model 70 SF

D.1.7 Active Condenser Case: Forced Convection

The active case has fans blowing air across the condenser section to increase heat dissipation. Figure D.10 shows the power dissipation for the Model 170 SF run with a Climate Control Model WSS 049 fan (10,000 cfm with 1/3 HP consumption-cost $8422). Average power dissipation during cooling mode is 0.68kW (2.32kBtu/h), which is slightly higher compared to the 0.52kW (1.77kBtu/h) for the passive case. Hence, to achieve 5kW (17.1kBtu/h) of heat rejection nine thermosyphons are required, compared to the 10 required for the passive case. The total cost in this forced convection case is the sum cost of the thermosyphons, fans and the operating electric cost, and it is given as:

Total Cost = Cost of Thermosyphon + Cost of Fan + Operating Cost

= $ 3,600*9 + 8,422 + $ 119 (per year) = $ 32,408 + $ 82 (per year)

Operating Electric Cost = Fan Power * Number of Hours * Cost per kWhr = 0.24867*(1977)*$ 0.1082 = $ 54 per year

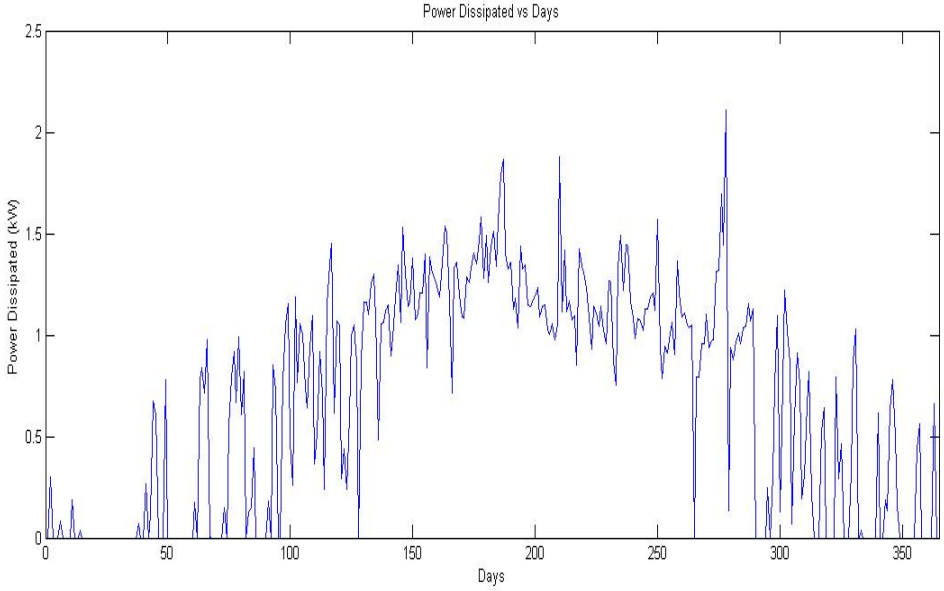

Figure D.10: Power rejected by thermosyphon (170 SF model) with fans

D.1.8 Conclusion

The analysis in this chapter shows that it is prohibitively expensive to install and operate a thermosyphon of the sizes needed to reject 5 kW (17.1 kBtu/h); $33,800 for the passive case and $ 32,408 for the forced convection case. Further, these types of device have never been deployed or tested for a residential house in a warm climate. The thermosyphons currently used in cold regions like Alaska and Tibet. Hence, the practical feasibility of operation in warm climates is unknown. Another difficulty is the design associated with transferring heat from the refrigerant loop to the thermosyphon. Special piping/coils or liquid pools must be designed for the refrigeration loop at the thermosyphon evaporator, which will add to the total cost. Taking into all these factors into account, it can be concluded that use of thermosyphons as SHR devices is not practical in Texas climates.

D.1.9 Thermosyphon Properties

Thermosyphon Working Fluid Properties

$T_v = 38^{\circ}C$
$P_{sat} = 1.468\ MPa$
$P_{atm} = 101.325\ kPa$
$\rho_l = 582.96\ kg/m^3$

$\rho_v = 11.36\ kg/m^3$
$Latent\ Heat = 1108.3\ kJ/kg$
$k_l = 0.4517\ W/mK$
$\mu_l = 124.74 * 10^6\ kg/m\ s$
$C_{pl} = 4920.5\ J/kgK$

Thermosyphon Fin Dimensions
$k_t = 401\ W/mK$
$b_n = .01\ m$
$s_n = 0.02\ m$
$\delta = 0.02\ m$
$r_2 = 0.15\ m$
$r_1 = 0.1\ m$
$\eta = 0.6$
$n = 50$

Air Properties
$k_a = .0257\ W/mK$
$\mathrm{Pr} = 0.72$

D.2 EVAPORATIVE COOLER WITH SHELL AND TUBE HEAT EXCHANGER

Evaporative coolers cool air by evaporation of water; a fan blows air across moist pads continuously supplied with water by a small pump from a collection sump. The air cools and gains humidity as it evaporates water from the pads. It is typically used in low humidity climates, such as in Arizona, Nevada, and New Mexico.

Figure D.11 shows the proposed design that uses a shell and tube heat exchanger between the evaporative cooler and GSHP water before it enters the ground loop. The following were assumed for the analyses to follow: the outlet air from the evaporator is fully saturated (100 % relative humidity—$\emptyset_{out} = 1$, the mass flow rate of air through the evaporator is steady, the mass flow rate of hot water exiting the heat exchanger and entering the evaporative cooler, $\dot{m}_{hw,in}$, is equal to the mass flow rate of cold water exiting the evaporative cooler and entering the heat exchanger, $\dot{m}_{cw,out}$, and to maintain constant water sump volume, the mass flow rate of make-up water into the evaporative cooler, $\dot{m}_{mw,in}$, is equal the mass flow rate of hot water lost through evaporation.

Energy balances for the evaporative cooler heat exchanger are given in Equations D.24 and D.25, respectively.

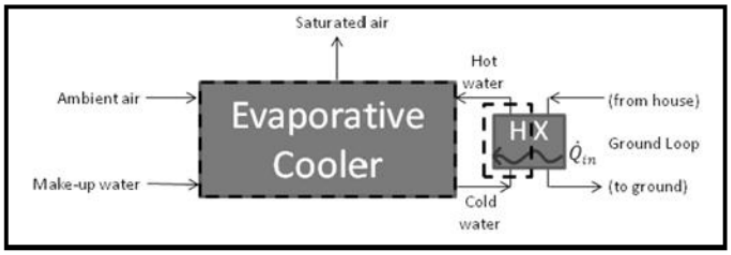

Figure D.11: Evaporative cooler with shell and tube heat exchanger

$$(\dot{m}h)_{hw,in} + (\dot{m}h)_{aair,in} + (\dot{m}h)_{mw,in} = (\dot{m}h)_{cw,out} + (\dot{m}h)_{sair,out} \quad \text{(D.24)}$$

$$(\dot{m}h)_{cw,out} + \dot{Q}_{in} = (\dot{m}h)_{hw,in} \quad \text{(D.25)}$$

where $\dot{m}$ is the mass flow rate, h is the enthalpy, and $\dot{Q}_{in}$ is the heat rate out of the ground loop water and into the evaporative cooler. Subscripts hw is hot water, aair is ambient air, mw is makeup water, cw is cold water, and sair is saturated air.

Combining to get the energy balance across the heat exchanger:

$$(\dot{m}h)_{mw,in} + (\dot{m}h)_{aair,in} + \dot{Q}_{in} = (\dot{m}h)_{sair,out} \quad \text{(D.26)}$$

Equation D.26 states that the energy from the makeup water, inlet air and the heat from the ground loop water are dissipated into the saturated outlet air. Since the air flow is steady, the mass flow rate of make-up water can be represented by:

$$\dot{m}_{mw,in} = \dot{m}_{da}(\omega_{out-}\omega_{in}) \quad \text{(D.27)}$$

where ω is the humidity ratio and subscript da is dry air.

The analysis was applied for the average inlet air properties associated with the months of May and August to represent the worst operating conditions for Austin, TX. May has the highest monthly average relative humidity and August has the highest monthly average dry bulb temperature. Changes in ground loop water temperatures of 5°F and 10°F were assumed and a ground loop flow rate of 3gpm per ton of cooling. The parameter values used for this study were:

Molecular weight of air:	MW_{air}=28.97 kg/kmol
Air pressure:	$P_{in}=P_{out}$=101.325kPa
Heat removed from ground loop water:	2.183kW<$\dot{Q}_{in}$<4.336kW
Average Aug dry bulb temperature:	$T_{db,in,Aug}$=302.5K (84.8°F)
Average May dry bulb temperature:	$T_{db,in,May}$=297.4K (75.6°F)
Makeup water temperature:	$T_{mw,in}$=62.6°F
Average Aug humidity ratio:	$\phi_{in,Aug}$=69.5%
Average May humidity ratio:	$\phi_{in,May}$=75.5%
Outlet air humidity ratio:	ϕ_{out}=100%

Note that the heat removed from the ground loop water reflects the 5°F and 10°F temperature reductions.

For a commercially available evaporative cooler from Essick Air Products/Champion Cooler, and for the outlet air temperature to be close to room temperature, Table D.3 shows the required flow rates and power required to achieve the two cases of 5°F and 10°F decreases in water temperature in the ground loop for 3gpm flow rate. To see a more detailed description of our analysis and a derivation of the values presented in Table 8.

Table D.3: Evaporative Cooler Analysis Summary (3gpm water flow rate)

Engineering Analysis Summary				
Month	May		August	
Average Ambient Air Temperature [°F]	75.6		84.8	
Average Ambient Air Relative Humidity [%]	75.5		69.5	
Ground Loop Temperature Drop [°F]	5	10	5	10
Water Input [gal/min]	0.01641	0.02738	0.02835	0.05395
Air Flow Rate [ft^3/min]	350	500	1100	2000
Outlet Air Temperature [°F]	76.55	77.81	78.22	78.40
Power Input [kW]	0.2400	0.3795	0.4428	0.6325

The proposed system used a 35 Series shell and tube heat exchanger (made by Exergy, LLC Miniature Heat Exchangers, 20gpm capacity, and priced at $2,250), a PE-2.5F pump (made by Little Giant Pump Company, 8gpm capacity, and priced at $130), and an evaporative cooler (made by Essick Air Products/Champion Cooler and priced depending upon ground loop temperature drop—see below). Table D.4 shows the total upfront costs for equipment based upon 3gpm water flow rate.

Table D.4: Evaporative Cooler Upfront Cost Summary (based on 3gpm water flow)

Upfront Cost Summary			
Month	Group Loop Temperature Drop, °F	Evaporative Cooler Cost, $	Total Cost, $
May	5	200	2580
	10	160	2540
August	5	250	2630
	10	340	2720

The operational cost summary for various runtimes, shown in Table D.5, lists the costs of electricity of the evaporative cooler and pump, make-water, and general maintenance for 3gpm water flow rate. Electricity costs were based on equipment specification sheets and a rate of $0.10 per kWh. The make-up water cost was based on a rate of $3.50 per 1,000 gallons water. The maintenance cost was based on a $35 cooler pad replacement fee performed once per year of use.

Table D.5: Evaporative Cooler Operational Cost Summary (based on 3gpm water flow)

Operating Cost Summary								
Month	Group Loop Temperature Drop [°F]	Make-up Water Input [gal/min]	Power Input [kW]	Runtime [%]	25	50	75	100
				[Hours/year]	2190	4380	6570	8760
					Annual Cost [$/year]			
May	5	0.01641	0.3200		86	173	259	346
	10	0.02738	0.4595		122	244	366	488
August	5	0.02835	0.5228		136	273	409	545
	10	0.05395	0.7125		190	379	569	723

D.3 ADSORPTION CHILLER

An adsorption chiller is a device driven by hot water to produce chilled water. Its advantages include having no moving parts and low energy consumption. Adsorption chillers are used in commercial applications where low temperature heat is recovered, therefore reducing the cost of energy.

Adsorption is a process where atoms or molecules accumulate on the surface of a material. Common solids used for adsorption are silica gel and activated carbon because of their high surface area. Silica gel does not produce chemical waste, and its high porosity allows for a large capacity to hold water (40% by weight), thus silica gel and water vapor are the preferred materials in the industry. During adsorption, water vapor accumulates on the surface of silica gel producing heat. In the reverse process, desorption, water vapor is released using heat. A cycle where adsorption and desorption occurs drives the system to chill water. Regeneration temperatures to produce desorption once silica gel is saturated with water vapor are around 150ºC (302ºF), however, lower temperatures of 45ºC (113ºF) are possible to achieve.

Adsorption chillers use low temperature waste heat, solar energy or conventional heating to satisfy water temperature requirements. An adsorption chiller is capable of operating within a range of temperatures, but for optimal performance, the hot water should be at 194^0F, the

cooling water at about 75^0F to 85^0F and the output cold water at 38^0F to 40^0F. When the inlet hot water temperature is below the required hot temperature, water vapor is not released from the silica gel and no desorption process takes place. Consequently, heat is not removed.

A closed loop system that comprises the ground loop and the hot fluid circuit of the adsorption chiller is seen in Figure D.12.

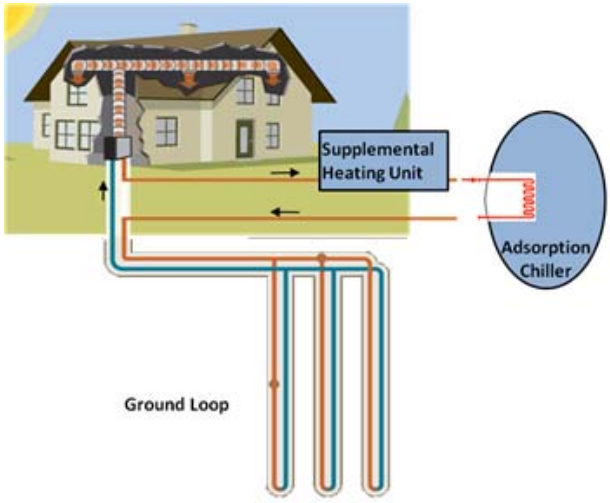

Figure D.12: Closed loop comprising ground loop and hot water circuit

Table D.5 lists the operating range temperatures for a commercial adsorption chiller Power Plant, 2009]. The hot water temperature from the heat pump is not within the chiller's operating range of hot water temperature. The heat pump EWT is in the range of 90°-120°F and with a typical 10°F temperature increase across the heat pump, the heat pump water exit temperatures are too low to be used for adsorption coolers.

Table D.5: Chiller Operating Temperature Ranges

Chilled water	38 °F to 68 °F
Hot water	125 °F to 200 °F
Condenser water	50 °F to 102 °F

D.4 PELTIER THERMOELECTRIC LIQUID COOLER

The LC-200 Peltier Thermoelectric Liquid Cooler by TETechnology, Inc. utilizes conductive heat transfer in conjunction with the Peltier effect to extract heat from a fluid [TET, 2010]. The Peltier effect works on the phenomenon that the passage of an electric current through the junction of two dissimilar metals cools or heats the junction. The LC-200 includes an eight-pass liquid loop and six thermoelectric modules. TETechnology provides a performance chart of the LC-200 on their website that shows the amount of heat the LC-200 can extract from the water

for a specified flow rate. The performance chart was valid for all flow rates exhibiting a turbulent flow.

Assuming the product is placed indoors, the ambient temperature can be estimated at 25°C average room temperature. The inlet water temperature can be approximated to be 32.2°C (90°F). Based on the performance graph, the LC-200 can extract heat at a rate of 210W from the water. In order to determine output temperature of the LC-200, as well as the output temperature if multiple units were run in parallel, the heat rate to be extracted is computed by:

$$Q = \dot{m}C_p(T_{in} - T_{out}) \quad \text{(D.28)}$$

Table D.6 illustrates the economic results that were obtained based on the residential case. Net present values are shown for the new GHP owners and retrofit cases. The data shows the net present value for both retrofitting and reducing the ground loop size of the system is a poor investment.

Table D.6: Economic Analysis of Multiple Liquid Coolers

GHP Water Temperature Drop (°F)	Units	Cost	Ground Loop Savings	NPV of Increased Efficiency Savings	NPV Ground Loop Savings	NPV of Retrofit
0.16	1	$616	$90	$68	($526)	($548)
0.79	5	$3,080	$443	$337	($2,637)	($2,743)
1.59	10	$6,000	$892	$679	($5,108)	($5,321)
2.38	15	$9,000	$1,335	$1,016	($7,665)	($7,984)
3.17	20	$12,000	$1,779	$1,353	($10,221)	($10,647)

The maximum number of units one can purchase of the TETechnology Liquid Cooler is 20. Splitting the flow any further would no longer result in turbulent flow and the performance diagram specified by TETechology is no longer valid. The maximum performance of the LC-200 requires an upfront cost of $12,000 for a 3.17°F temperature drop. Without taking into considering the additional cost in pump power due to the pressure drop in the pipe, as well as the electric power required to run each liquid cooler (approximately $2000/yr), the cost and performance of the LC-200 in large-scale applications did not meet the requirements and constraints, and was deemed not feasible as an SHR device.

D.5 CONCRETE CORE TEMPERATURE CONTROL (CCTC)

Concrete Core Temperature Control (CCTC) is a thermo-active building system (TABS) that utilizes water and a building's structure to store thermal energy. CCTC systems are combined with GHPs to take part of the heat from the building load during the day and release it at night. Water pipes are installed inside concrete slabs in the floors or ceilings to transfer the heat. There are three main phases of cooling using CCTC. During the charging phase, floor slabs are charged with heating/cooling energy. Heat transfer can be actively controlled by varying the supply temperature, mass flow rate and charging time. Due to the thermal inertia of the system, concrete slabs behave as a thermal damper. Consequently, the system goes through a storage phase where thermally activated slabs bridge the time gap between energy supply and energy demand, and partially shift the thermal loads to the night. The last phase involves discharging the energy stored. Room conditioning occurs by means of two methods of heat transfer (radiation and convection) which run in parallel. 60% of the heat/cold stored in the concrete core is transferred to the room via radiation, and 40% via convection. The energy from the concrete is dissipated in a passive manner. In steady state, cooling capacities of 30-40W/m^2 are achieved [Pfafferott et al., 2007]. The cooling capacity is determined by the indoor air temperature dew point because condensation may form on the ceiling.

CCTC has proven to effectively reduce a building load in Germany where high temperatures (30-40°C) are reached during the summer. However, these systems need to be further analyzed to account for climate conditions in Texas. Local temperatures and humidity ratios may require additional cooling during the summer.

D.6 Others

Thermomagnetic: Thermomagnetic cooling is based on the magneto-caloric effect, a phenomenon that causes a change in temperature in a material by exposing it to a changing magnetic field. When a magneto-caloric material with a disoriented magnetic domain is exposed to a magnetic field, causing the material's domain to align with the magnetic field, the material heats up. A heat sink can then be introduced to remove this heat. The final step is the removal of the magnetic field, causing the material to return to its original disoriented state. This requires internal energy and results in a temperature drop for the material [US DoE, 2011]. This is an adiabatic process, also called adiabatic demagnetization. This technology has been prototyped, but no commercially devices are available.

Thermoacoustics: Thermoacoustic cooling uses waste heat to generate sound. A resonance tube is filled with pressurized gases. At one end of the tube, heat is transferred to gas molecules as kinetic energy that causes them to accelerate towards the cooler end of the tube, creating an

area of relatively low pressure in the heated end of the tube. Upon reaching the other end of the tube, the molecules cool and accelerate back towards the hot/low pressure end. This cycle of thermal and pressure oscillation produces sound waves. The sound waves can either be dissipated to the environment, or converted to electricity using a piezoelectric sensor [Newman et al., 2006]. This technology has been prototyped, but no commercially devices are available.

Optical: Optical cooling is based on the principle of anti-Stokes fluorescence, the "phenomena in which a substance that is excited by radiation at one wavelength fluoresces at a shorter wavelength…[that] results in more energy being radiated than is absorbed for each photon" [Edwards et al., 1995]. This net energy loss means a cooler final temperature for the material. This method is also referred to as laser cooling, because it involves a laser shooting photons at a material. This technology is only at the research stage.

Reservoirs: Tanks, swimming pools and greenhouses were analyzed to determine their application as SHR devices. The design of a holding tank with submerged ground loop water coils depended upon tank capacity and water temperatures, ground loop water temperatures, and operating times. The analyses showed that the cost of the holding tank and the operating costs of water replenishment and pump power were not cost effective. For a 7^{o}F reduction in ground loop water temperature, a 2500 gallon tank with water temperature at 60^{o}F running 75% of the time, the costs were approximately $4000 in upfront costs and $2400/year in water costs.

For the cases of using swimming pools and greenhouses during the summers, radiative heating was more than needed to keep the pools/greenhouses heated. The analyses did not look into running the ground loop water during winter to heat the water/air while decreasing the loop temperatures at the same time.

APPENDIX E

COOLING TOWER MODEL PARAMETERS

Parameters used in Cooling Tower Model

$C_a = 1.006\ kJ/kgK$

$C_w = 4.186\ kJ/kgK$

Table E.1: Yearly Power Rejection by Cooling Tower and Heat Pump, Operational Hours, and Quantity of Make-up Water Consumed.

Year	Energy Rejected/Yr kWhr		Total Energy Rejected/Yr kWhr	Ratio Cooling Tower/Heat Pump	Operational Hours hrs		Make up Water/Year gal
	Cooling Tower	Ground Loop			Cooling Tower	Ground Loop	
1	23,099	5,609	28,708	80.5	1,891	1,839	7,101
2	23,236	5,478	28,714	80.9	1,892	1,843	7,143
3	23,294	5,414	28,708	81.1	1,892	1,845	7,161
4	23,329	5,381	28,709	81.3	1,892	1,846	7,172
5	23,359	5,372	28,731	81.3	1,894	1,847	7,180
6	23,379	5,353	28,732	81.4	1,894	1,848	7,186
7	23,366	5,346	28,712	81.4	1,893	1,846	7,182
8	23,383	5,339	28,722	81.4	1,894	1,848	7,187
9	23,398	5,326	28,724	81.5	1,893	1,848	7,192
10	23,403	5,326	28,729	81.5	1,894	1,848	7,193

Table E2: City of Austin, TX Water Utility Rates: 2011

Quantity, gal	Cost, $
0-2000	1.17
2,0001-9,000	3.08
9,001-15,000	7.92
15,001-25,000	10.95
25,0001-over	12.19

APPENDIX F

VCC OPTIMIZATION

Operating Points of Heat Pump TT 049 [Climate Master]

EWT °F/°C	Suction Pressure kPa/psi	Discharge Pressure kPa/psi	Suction Superheat °F/°C	Condenser Subcooling °F/°C
70/21.1	937.9/136.1	1896.6/272.3	11.5/6.4	7.5/4.2
90/32.2	972.4/141.1	2496.6/362.3	9.5/5.3	6.5/3.6
110/43.3	1013.8/147.1	3151.7/457.4	9.5/5.3	5.5/3.1

Load kW/(kBtu/h)	T_3 °F/°C	T_{3sat} °F/°C	T_{2sat} °F/°C	T_2 °F/°C
15.75 /53.74	79.1/26.18	86.7/30.38	86.7/30.38	138.8/59.34
14.06 / 47.9	100.2 /37.84	106.6/41.44	106.6/41.44	161.8/72.10
12.13 / 41.3	119 /48.31	124.5/51.41	124.5/51.41	188.8/87.10

Load kW/(kBtu/h)	T_{w3} °F/°C	T_{w3sat} °F/°C	T_{w2sat} °F/°C	T_{w2} °F/°C
15.75 /53.74	70/21.10	70.3/21.30	78.9/26.05	80.7/27.03
14.06 / 47.9	90/32.20	90.3/32.38	97.9/36.61	100/37.75
12.13 / 41.3	110/43.30	110/43.47	116.6/47.01	119.2/48.45

Pinch Point = $T_w - T_{w3}$ = 5℃ (9℉)